UNIVERSITE MATIERE BRETAGNE MOLECULES LOIRE ET MATERIAUX

IMT Atlantique
Bretagne-Pays de la Loire
École Mines-Télécom

THESE DE DOCTORAT DE

L'ÉCOLE NATIONALE SUPERIEURE MINES-TELECOM ATLANTIQUE
BRETAGNE PAYS DE LA LOIRE - IMT ATLANTIQUE
COMUE UNIVERSITE BRETAGNE LOIRE

ECOLE DOCTORALE N° 596
Matière, Molécules, Matériaux
Spécialité : Sciences des Matériaux

Par
Sathya NARAYANASAMY

Influence of composition on vapor hydration of AVM nuclear glasses

Thèse présentée et soutenue à Marcoule, le 20/11/2019
Unité de recherche : CEA Marcoule
Thèse N° : 2019IMTA0159

Rapporteurs avant soutenance :

Jérôme STERPENICH	Professeur, Université de Lorraine
Stéphanie ROSSANO	Professeure, Université Paris-Est Marne-la-Vallée

Composition du Jury :

Rapporteurs :	Jérôme STERPENICH	Professeur, Université de Lorraine
	Stéphanie ROSSANO	Professeure, Université Paris-Est Marne-la-Vallée
Président :	André AYRAL	Professeur, Université de Montpellier
Examinateurs :	Nadia PELLERIN	Maître de Conférences HDR, Université d'Orléans
	Aurélie VERNEY-CARRON	Maître de Conférences, Université Paris-Est Créteil
Dir. de thèse :	Abdesselam ABDELOUAS	Professeur, SUBATECH, Institut Mines-Télécom
Encadrant :	Patrick JOLLIVET	Ingénieur, CEA Marcoule
Co-encadrante :	Nicole GODON	Ingénieur-chercheur, CEA Marcoule

Invité :

Florent TOCINO	Ingénieur-chercheur, EDF-R&D

INFLUENCE OF COMPOSITION ON VAPOR HYDRATION OF AVM NUCLEAR GLASSES

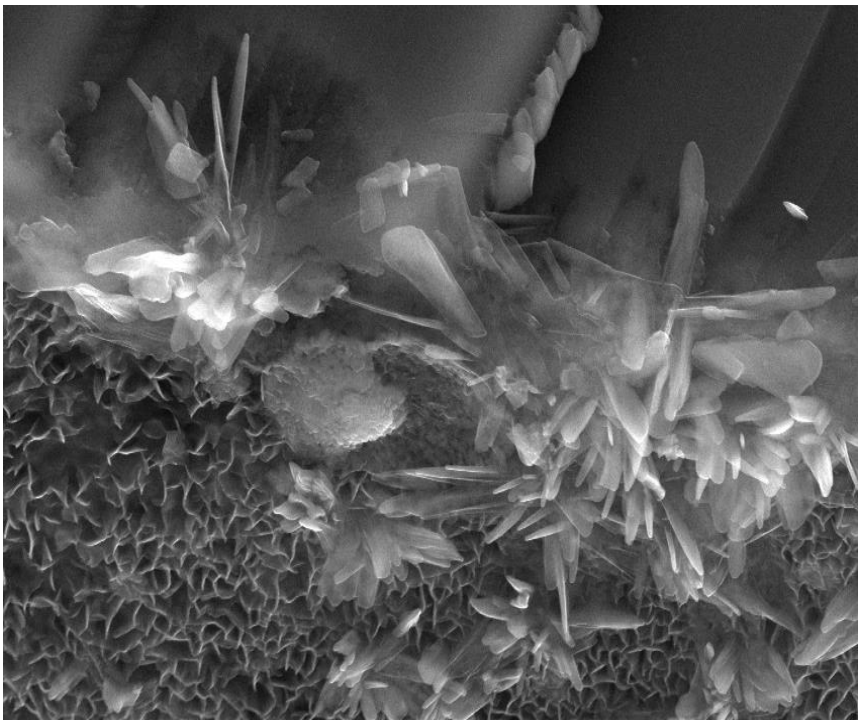

Sathya Narayanasamy

(Nov 2016 - Nov 2019)

Supervised by: Patrick Jollivet
Co-supervised by: Nicole Godon
Thesis Director: Abdesselam Abdelouas

Thesis co-financed by "Commissariat à l'Energie Atomique et aux Energies Alternatives" (CEA) and "Electricité De France" (EDF), and carried out within the "Laboratoire d'études de Comportement Long Terme des matériaux de conditionnement des déchets nucléaires" (LCLT) in CEA Marcoule (DEN/MAR/DE2D/SEVT/LCLT)

Table of Contents

Dedication

Maybe that was the definition of life everlasting;

The belief that the next generation would carry your work forward.

-Ann Patchett

My loving and doting father taught me virtues, showed me the important things in life, set me on a path of constant self-improvement, shared his life experiences with me, told me stories from classical works, sang and danced for me. He is indeed the best Appa in the world. I dedicate this thesis to my late father Mr. S. Narayanasamy, a noble soul.

Acknowledgements

Tout d'abord je veux remercier mon encadrant de thèse Patrick JOLLIVET. Patrick, merci mille fois pour ta pédagogie, gentillesse, patience, honnêteté, tes calculs de tête hyperrapides et pour ta classe. Merci de m'avoir appris à faire de la recherche. Sachant que c'était toi mon encadrant, je ne me suis jamais inquiétée à propos de ma thèse. Merci de m'avoir soutenue jusqu'au bout, même si tu n'étais pas obligé. C'était mon privilège d'être ta thésarde (la dernière en plus !).

Merci également à ma co-encadrante Nicole GODON. Merci Nicole, pour ta présence bienveillante parmi nous chaque matin pendant la pause-café. Merci de m'avoir accueillie chaque fois que je venais sans prévenir pour te poser des questions scientifiques ; et aussi de m'avoir déposée chez moi quand je voulais travailler au-delà des horaires de bus ; et de m'avoir prêtée les livres d'Harry Potter ; et pour beaucoup d'autres choses. Tu as ajouté beaucoup de valeur à mes trois ans passés au LCLT et merci pour tout ça.

Un grand merci à mon directeur de thèse Abdesselam Abdelouas. Merci Abdel pour votre confiance en moi et votre soutien au cours de ces trois ans. Merci également d'avoir montré un petit côté gastronomique de Nantes à Patrick et moi en Mai 2019.

Je remercie le Commissariat à l'Energie Atomique et aux énergies alternatives et Electricité de France pour le financement de cette thèse. Merci à Florent TOCINO et Hélène SCHNEIDER de EDF et Fabien FRIZON du CEA d'avoir suivi ce travail et pour leur intérêt porté à cette thèse. Je remercie Florence BART et Bruno LORRAIN du Service d'Etudes de Vitrification et procédés hautes Températures.

Je remercie tous les membres du Jury. Je remercie les rapporteurs Jérôme STERPENICH et Stéphanie ROSSANO pour la relecture de ce manuscrit, leurs commentaires encourageants et leurs critiques constructives. Merci aussi aux examinateurs André AYRAL, Nadia PELLERIN et Aurélie VERNEY-CARRON pour leur évaluation de mes travaux. Je remercie aussi Aurélie pour les échanges fructueux que nous avons eus avec le LISA. A ce propos, un grand merci à notre star de DGG-USTV 2019, Loryelle SESSEGOLO pour les expériences qu'elle a faites pour cette thèse, et merci également pour les moments amicaux passés ensembles lors en plusieurs occasions et les échanges d'emails humoristiques.

Je remercie Frédéric ANGELI, le chef du Laboratoire d'étude du Comportement à Long Terme des matériaux de conditionnement des déchets nucléaires, de m'avoir accueilli dans son laboratoire. Je le remercie aussi chaleureusement pour ses apports à cette thèse par rapport à l'étude de la structure du gel par RMN, pour ses commentaires pertinents et ses encouragements sur chaque présentation et rapport que j'ai fait au cours de ces trois ans et aussi pour sa gentillesse habituelle.

Un grand merci à Thibault CHARPENTIER, sans qui les études sur la structure du gel par RMN auraient été impossibles. Je le remercie d'avoir patiemment répondu à mes questions sur les résultats de RMN, de m'avoir aidé à rédiger l'article et pour ses contributions scientifiques pour l'étude. Merci aussi à Mélanie MOSKURA pour les expériences RMN et le petit tour extrêmement intéressant du CEA SACLAY.

Je remercie Stéphane GIN pour ses commentaires sur le progrès de la thèse et ses suggestions pour améliorer la qualité du travail. Entre autre, je le remercie particulièrement d'avoir fait le sacrifice de manger à Starbucks pour pouvoir m'aider sur ma présentation à la conférence Goldschmidt2019.

Merci à Laurent DUFFOURS de PrimeVerre pour la préparation des monolithes et des poudres de verres pour mes expériences. Merci à Laurent DUPUY, Elodie CHAUVET et Yves DE PUYDT de Tescan analytics pour les profils ToF-SIMS. Merci beaucoup à Julien CAMBEDOUZOU de l'ICSM pour les caractérisations des échantillons par SAXS et pour son aide avec le traitement de données. Merci également à Jeremy CAUSSE de l'ICSM pour la même raison. Un énorme merci à Martiane CABIE du CP2M, de l'Université Aix-Marseille pour les nombreuses images et analyses MET. Merci également à Corentin LE GUILLOU de l'Université de Lille pour les images et analyses MET.

Merci à Isabelle BIRON, Odile MAJERUS et Fanny ALLOTEAU du C2RMF et de Chimie Paris pour notre collaboration sur les études sur l'altération atmosphérique des verres et de m'avoir donné l'opportunité de présenter dans le « International Symposium of Glass Degradation » au C2MRF à Paris et de publier dans un livre de conference proceedings.

Je remercie très chaleureusement Chistine ALMUNIA du DSV au CEA Marcoule de m'avoir aidé avec les essais de détermination du pH du gel en utilisant les fluorophores sensibles au pH et le microscope confocal. Merci d'avoir passé autant de temps avec moi sur cette nouvelle idée, j'ai apprécié ton enthousiasme contagieux.

Je dois beaucoup de remerciements aux membres fabuleux du LCLT pour leur contribution à mon travail ainsi que pour avoir rendu ma vie quotidienne au CEA belle et agréable. Merci Jean-Pierre pour les nombreuses images MEB de haute qualité, et aussi pour tes blagues et ta bonne humeur habituelle. Merci aussi à Marie pour les images MEB. Je dois te dire que j'ai toujours apprécié ta présence dans la salle café les matins qui a ajouté une certaine vivacité aux discussions. Pierre, en plus de ta personnalité splendidement amicale, je te remercie aussi pour tes appréciations et encouragements au cours de ces trois ans. Ça compte beaucoup pour moi. Merci Myriam pour ton aide précieuse avec la DRX et tes délicieux gâteaux. Merci Géraldine, Emmanuelle et Frédéric pour les nombreuses analyses ICP et pour votre fiabilité. Merci beaucoup Christophe, pour toutes les discussions sur l'altération du verre en phase vapeur. Merci Florence pour ton aide avec le spectromètre infrarouge et de m'avoir aidée chaque fois que j'en avais besoin pour les manips. Et Céline, ton sens de l'humour et ton visage toujours souriant me remonte le moral à chaque fois et ça va me manquer ne plus voir Patrick te taquiner. Merci beaucoup Loïc d'avoir pris le temps de me montrer une méthode de traitement de données de ToF-SIMS. Merci Manon et Pierrette, vous êtes formidable. Merci Yves pour tes barres de chocolat, tes chansons, ton enthousiasme et bien sûr pour tes connaissances sur des sujets divers qui surpasse Wikipédia. Merci Olivier de m'avoir initiée à la course d'orientation.

Merci Muriel NEYRET, Julia AGULLO, Lionel CAMPAYO, Nicolas MASSONI, Elise REGNIER, Jean-Marc DELAYE, Sylvain PEUGET, Magaly TRIBET et tous nos collègues du LDMC, LMPA, LPTI et LDPV. Un merci spécial à Sophie SCHULLER ☺. Merci aussi à Fabienne DELABAUDIERE pour son superbe efficacité.

Chers et chères membres privilégiés du « Weekend au shiit », vous êtes dans une grande partie responsable des bons souvenirs que j'ai accumulés au cours de ces trois ans et j'en suis éternellement reconnaissante. Marie, mille fois merci, cœur, cœur, cœur et surtout, youghoughou. Mais sérieusement, tu es un amour. Maxime, en commençant par mon premier jour à Bagnols-sur-Cèze, quand tu m'as récupérée à la gare, je te dois beaucoup de remerciements. Tu es quelqu'un d'très bien et je te souhaite beaucoup de bonheur. Mathilde, tu es une adorable personne et une amie à envier, merci aussi pour ton travail formidable pendant ton stage. C'était un plaisir de travailler avec toi. Leila, tu m'as soutenue pendant les moments les plus durs et merci pour tout. Tu es intelligente, courageuse et je te souhaite beaucoup de réussite dans la vie. Merci Thibault, Céline et Trilce, vous êtes très cools et je vous adore. Nicolas et Mélanie, je garde de très bons souvenirs avec vous cette dernière année et ça me

manque de ne plus vous voir tous les jours. Merci aussi Nicolas pour tes calculs de NBO pour les verres complexes et autres discussions sur le comportement des verres AVM.

Cloé, j'ai beaucoup apprécié ta compagnie, tu es géniale. Merci pour tous les jours où tu m'as ramenée chez moi après les horaires de bus. Sinon, il m'aurait fallu deux mois de plus pour terminer ma thèse. Hélène, tu es adorable et je te remercie très chaleureusement pour ta bienveillance.

Un merci spéciale à Paul ESTEVENON pour son aide au début de cette thèse avec les mesures infrarouges, la bibliographie et toutes les discussions sur le sujet passionnant de l'altération du verre en phase vapeur. Merci Léa, c'était un plaisir de te côtoyer, même si c'était pour une très courte durée. Merci Raphaël et Kamlesh, et bonne chance pour la thèse.

Merci aussi à Sophie, Anne, Luiz, Thomas DUCASSE, Mathieu, Erik, Birsen, Judith, Thomas CHARPIN, Boris, Anne-Lise, Dylan, Célia, Valentin ; et les stagiaires Benjamin (mon grand Benjamin/l'insolent), Pierre ASPLANATO, Robin, Marion, Léa HIPPOLYTE, Léna, Jonathan, Vito, Julie, Elise…

Nadine, merci de nous avoir ouvert ton cœur et ta maison à Amreen et moi. Ton amitié était l'un des meilleurs cadeaux de mon aventure en France. Maria, merci beaucoup pour ton amitié, ton soutien, tes mots d'encouragements et toutes nos discussions. Norma et Raphaël, votre amitié est quelque chose que je chérirai. Thank you Ruwaid and Mohan. I am glad that we finally decided to get to know each other.

Amreen, thank you from the bottom of my heart for practically living with me through the highs and lows that I experienced these three years. I was appreciated for the mental strength that I displayed during the difficult times. You gave me a lot of that strength. I cannot thank you enough. Maitreyi, thanks a lot for being almost a sister to me and helping me to feel at home in France. Anupreethi and Subbhashree, time and distance could not drift us apart. Thank you for all these years of love.

My gratitude for my family goes beyond measure. But, I just want to say this. Appa, you taught me to dream, aim high, and be self-critical and ambitious. My dear Ravi, thank you for not accepting mediocrity. Amma, you are my rock, my person. Together, you add meaning to my success.

Résumé en français

Influence de la composition des verres nucléaires AVM sur leur altération en phase vapeur

Contexte de l'étude :

Les déchets radioactifs issus du retraitement des combustibles nucléaires usés pour extraire l'uranium et le plutonium contiennent des actinides et des produits de fission qui peuvent être hautement radioactifs pendant très longtemps (radioactivité supérieure à 10^9Bq/g avec une demi-vie supérieure à 31 ans). L'option retenue par la France pour le confinement de ces déchets nucléaire de haute-activité vie-longue (HA-VL) est la vitrification où les déchets nucléaires sont incorporés dans un réseau vitreux. Le colis de verre nucléaire est constitué d'un bloc de verre dans un conteneur en acier inoxydable entouré par un sur-conteneur en acier. L'Agence Nationale pour le gestion et stockage des Dechets RadioActif (ANDRA) travail sur le projet Cigéo (Centre industriel de stockage géologique) pour le stockage géologique de ces colis HA-VL. Il est possible que pendant le stockage des colis, le verre soit exposé à un milieu insaturé dû à la corrosion des sur-conteneurs plus les matériaux de construction conduisent à la libération d'hydrogène qui ralentit la pénétration de l'eau souterraine dans le site du stockage. Dans ce contexte, l'altération du verre en phase vapeur a été étudiée dans cette thèse en se focalisant sur l'influence de la composition du verre.

Choix des verres :

Les verres étudiés dans cette thèse sont des verres de type AVM (*Atelier de Vitrification de Marcoule*). Les verres AVM industriels sont des verres borosilicates complexes contenant plus de 20 oxydes dont des produits de fission et des actinides provenant des réacteurs UNGG (Uranium naturel Graphite-Gaz) de Marcoule. Le verre AVM6 dont la vitesse résiduelle d'altération en milieu aqueux (eau pure) à 50 °C est la plus élevée, le verre AVM10 dont la vitesse résiduelle d'altération est la plus basse et le verre AVMV4, qui représente une composition moyenne des verres AVM sont les trois verres complexes simulants inactifs choisis dans le domaine des verres AVM. Les verres AVM sont des verres riches en Mg, un élément connu pour augmenter l'altération du verre en milieu aqueux, et sont dépourvus de Ca, un élément connu pour améliorer la résistance du verre à l'altération aqueuse. Par conséquent, il

était aussi nécessaire d'étudier le rôle des éléments alcalino-terreux tels que Ca et Mg sur l'hydratation en phase vapeur. Donc, trois verres simplifiés Q, QCa et QMg ont été préparés sur la base de la stœchiométrie Si/Al du verre AVMV4. Ainsi, AVM6 (49.3 SiO_2, 18.6 B_2O_3, 16.7 Na_2O, 5.9 Al_2O_3, 6.3 MgO, …), AVM10 (43.5 SiO_2, 16.3 B_2O_3, 16.4 Na_2O, 8.3 Al_2O_3, 10.4 MgO, …), AVMV4 (48.2 SiO_2, 16.7 B_2O_3, 18.6 Na_2O, 7.2 Al_2O_3, 7.2 MgO, …), Q (57.5 SiO_2, 15.3 B_2O_3, 19.2 Na_2O, 8.1 Al_2O_3), QCa (52.7 SiO_2, 14.6 B_2O_3, 19 Na_2O, 7.5 Al_2O_3, 6.2 CaO) et QMg (52.6 SiO_2, 15 B_2O_3, 18.8 Na_2O, 7.7 Al_2O_3, 5.8 MgO) sont les six verres de cette étude (%molaire).

Étude de l'influence de la composition de verre sur son hydratation en phase vapeur

Les six verres ont été altérés dans une enceinte climatique à 50 °C et 95 % d'humidité relative (HR) pendant 6 mois et 18 mois, afin d'étudier l'influence de la composition du verre sur les vitesses et les mécanismes d'hydratation en phase vapeur. En plus de la caractérisation d'échantillons altérés après 6 mois et 18 mois par MEB, MET, DRX, ToF-SIMS et SAXS, la cinétique de l'hydratation a également été étudiée jusqu'à 18 mois par spectroscopie infrarouge (FTIR).

Les résultats ont mis en évidence la sensibilité élevée des vitesses d'hydratation en phase vapeur aux variations mineures de compositions des verres. Les verres AVM6 et AVM10 s'altérèrent 10-20 fois plus vite que le verre AVMV4. L'analyse des résultats a suggéré que la teneur en aluminium par rapport à celle des alcalino-terreux joue un rôle clé dans la durabilité du verre. Lorsque le rapport molaire Al_2O_3/MgO<1, ce qui est le cas pour les verres AVM6 et AVM10, la vitesse d'hydratation en phase vapeur de ces deux verres est 10 à 20 fois plus élevée que celle du verre AVMV4, ceci s'expliquant par la formations de précipités riches en Mg.

Les vitesses d'hydratation des trois verres simplifiés, dont le rapport molaire Si/Al était basé sur le verre AVMV4, étaient dans le même ordre de grandeur que le verre AVMV4. L'un de ces verres ne contenait pas d'alcalino-terreux (Q) et les deux autres verres contenaient plus de Al_2O_3 que de CaO (QCa) ou de MgO (QMg). La quantité de phases secondaires formées sur les quatre verres les plus durables (AVMV4, Q, QCa et QMg) était très faible par rapport aux deux verres moins durables (AVM6 et AVM10).

La figure rf. 1 montre un schéma de la morphologie des six verres hydratés en phase vapeur. Les six verres ont une couche de gel de quelques dizaines de nm d'épaisseur. Dans le cas des deux verres moins durables, leur altération plus importante s'est manifestée par des zones de forme irrégulière et très poreuse de quelques centaines de nm à quelques µm de profondeur qui étaient ponctuellement présentes sous la couche de gel.

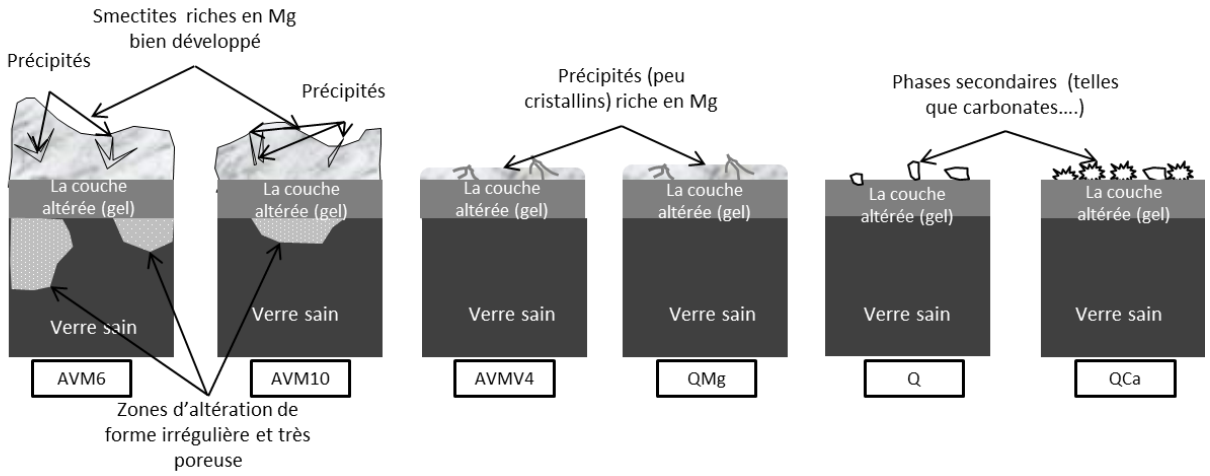

Figure rf. 1 Représentation schématique de la morphologie des couches altérées en phase vapeur des six verres (50°C, 95% HR durée 6 mois et 18 mois)

Après une comparaison de l'épaisseur de la couche de gel formée sur les verres plus durables après six mois d'hydratation avec la fraction d'oxygènes non-pontantes (ONP) du verre sain, l'hydrolyse du réseau vitreux a été identifiée comme le mécanisme contrôlant la vitesse d'hydratation en phase vapeur. La dépendance de la durabilité du verre avec le rapport Al_2O_3/(MgO ou CaO) soutient également l'idée que l'hydrolyse du réseau vitreux doit être le mécanisme prédominant d'hydratation en phase vapeur, au moins jusqu'à six mois d'hydratation à basse température (50°C).

L'étude de la cinétique d'hydratation en phase vapeur jusqu'à 18 mois montre une inflexion de l'augmentation de la quantité de SiOH dans le verre altéré avec le temps après 120-200 jours d'hydratation pour les six verres. Cette inflexion suggère que la vitesse d'hydratation doit avoir chuté d'un facteur 5 à 15 après 120-200 jours. Cela suggère la présence d'un mécanisme de passivation par le gel formé en phase vapeur. Une comparaison du facteur de chute de vitesse avec la rétention des éléments dans le gel suggère qu'après environ six mois, le mécanisme prédominant d'hydratation en phase vapeur (hydrolyse du réseau vitreux) devient la diffusion des molécules d'eau à travers la couche de gel vers le verre sain.

Études complémentaires sur l'hydratation des verres en phase vapeur

Pour approfondir nos connaissances et compréhension de l'hydratation des verres en phase vapeur, un sujet qui est relativement récent en France dans le domaine des verres nucléaires, des études complémentaires ont été effectuées.

Effet de la température :

Pour étudier l'effet de la température sur l'influence de la composition des verres, les trois verres simplifiés ont été hydratés pendant 3 trois mois en phase vapeur à 95% HR et deux températures différentes (90°C et 120°C). L'effet de température a aussi été étudié sur AVM6, le verre le plus réactif parmi nos six verres étudiés. AVM6 a été hydraté en phase vapeur pendant 1 an à 97% HR et températures 70°C et 90°C. Les verres altérés ont été caractérisés par MEB, DRX et ToF-SIMS et les résultats ont été comparés avec ceux obtenus à 50°C.

L'étude de l'effet de la température sur l'influence de la composition du verre a montré que pour certains verres, le mécanisme prépondérant d'hydratation en phase vapeur a changé avec la température (probablement entre l'hydrolyse du réseau vitreux et la précipitation des phases secondaires) et, par conséquent, l'influence de Ca et de Mg a également varié.

L'étude de l'effet de la température sur le verre AVM6 a montré qu'avec la température, la nature des phases secondaires a varié, et par conséquent, le comportement des éléments dans le gel a également changé. Cependant, la morphologie du verre altéré était similaire pour les trois températures. Alors qu'en général la vitesse d'hydratation en phase vapeur augmente avec la température, seulement deux des quatre verres suivent une loi d'Arrhenius pour la dépendance à la température.

Effet de l'humidité relative :

Le verre AVM6 a été altéré pendant un an à 50°C et quatre HR différentes (55%, 76%, 83% et 95%). Les échantillons altérés ont été caractérisés par MEB, DRX et ToF-SIMS. Les résultats ont montré que la vitesse d'hydratation en phase vapeur a également augmenté de façon exponentielle avec l'humidité relative. Certaines phases secondaires comportant des métaux de transition et des terres rares n'ont été identifiées qu'à de faibles valeurs d'humidité relative. La diminution du pH dans la couche altérée avec l'augmentation de l'humidité relative est l'hypothèse la plus probable pour expliquer les différences de comportement des éléments dans le gel et la précipitation des phases secondaires avec l'évolution de l'humidité relative.

Étude des mécanismes d'hydratation en phase vapeur avec des traceurs isotopiques

Les verres AVM6, AVM10, QCa et QMg ont été hydratés en phase vapeur pendant un an à 20°C et 91% HR où la phase vapeur était imposée par une solution saline enrichie en isotopes traceurs (90% D_2O + 10% $H_2{}^{18}O$). Les échantillons altérés ont été caractérisés par DRX et par ToF-SIMS, pour déterminer les profils de pénétration des isotopes provenant de la vapeur dans l'échantillon altéré. Les résultats ont suggéré que le mécanisme contrôlant l'hydratation en phase vapeur a également changé en fonction de la composition du verre (interdiffusion ou hydrolyse du réseau vitreux) ainsi que de la température.

Étude comparative de la structure des gels formés en phase vapeur et en milieu aqueux

Pour la première fois, ^{17}O, qui est un noyau qui permet de sonder la structure globale du gel et du verre sain, a été utilisé pour étudier la structure des gels formés en phase vapeur. Les verres Q et QCa ont été hydratés en phase vapeur à 90°C et 98% HR pendant 213 jours. La phase vapeur a été contrôlée par une solution saline enrichie en ^{17}O (40%). Ces verres ont aussi été altérés en milieux aqueux (eau pure enrichie à 40% en ^{17}O) à très fort rapport S/V (~500000 m^{-1}) et à 90°C pendant 59 jours (Q) ou 213 jours (QCa) selon le verre. La structure des gels a été étudiée par spectroscopie RMN en sondant les noyaux ^{17}O, ^{11}B, ^{29}Si, ^{27}Al and ^{23}Na.

Les résultats ont montré pour la première fois la recondensation du bore avec des oxygènes provenant de la phase vapeur. Dans le milieu aqueux, même si du bore est présent dans le gel en raison du rapport S/V extrêmement élevé, il n'y a pas d'évidence de la recondensation du bore avec ^{17}O provenant du milieu d'altération. Les résultats suggèrent également que les liaisons Al en phase vapeur semblent moins hydrolysables que dans le milieu aqueux, ce qui suggère que l'hydrolyse du réseau vitreux est un phénomène plus sélectif/local en phase vapeur qu'en milieu aqueux.

Altération aqueuse des verres

Dans une première partie, les verres hydratés en phase vapeur à 50°C et 95% HR pendant six mois et 18 mois ont été mis en contact avec de l'eau pure à 50°C et 20 m^{-1} pendant 28 jours pour étudier (i) les effets de la couche formée en phase vapeur pendant l'altération aqueuse subséquente et (ii) les conséquences de l'altération aqueuse sur les produits d'hydratation en phase vapeur tels que le gel et les phases secondaires.

Les résultats montrent que le gel formé en phase vapeur n'a pas de propriétés passivantes vis-à-vis de l'altération du verre en milieu aqueux. Le mécanisme de passivation lié au gel qui a été

discuté plus tôt est seulement présent pendant l''hydratation en phase vapeur et il n'a aucun effet en milieu aqueux. Certaines des phases secondaires formées lors de l'hydratation en phase vapeur étaient également facilement solubles lorsqu'elles étaient immergées dans l'eau. Les résultats semblent également indiquer que la couche de gel elle-même pourrait être soluble/instable.

Dans une deuxième partie, l'altération aqueuse des verres simplifiés Q, QCa et QMg à très fort S/V (~200000 m^{-1}) et à 50°C pendant 3 mois a été comparée avec l'hydratation en phase vapeur à 50°C et 95% HR pendant 6 mois. Le but de cette comparaison est d'étudier si l'altération en phase vapeur est équivalente à l'altération aqueuse des verres à très fort rapport S/V. L'analyse des études cinétiques et structurales montrent clairement que l'hydratation des verres en phase vapeur n'est pas comparable à une altération en milieu aqueux à très fort rapport S/V.

Introduction

Context of the study

More than 70% of the electricity produced in France is supplied by nuclear power plants. The processes involved in the nuclear fuel cycle, such as uranium mining for nuclear fuel, the operation of a nuclear power reactor and the reprocessing of spent fuel to recover uranium and plutonium, result in radioactive waste production. The resulting waste from spent nuclear fuel reprocessing contains actinides and fission products, which are mostly transition metals. The radioactivity of some of these radionuclides exceeds 10^9Bq/g bringing them under the category of high-level activity nuclear waste (HLW). The half-life of some of the radioactive elements in the HLW exceeds 31 years, which is the threshold beyond which the waste is classified as long-lived (LL) radioactive waste. This includes elements whose half-life is in the range of 1.5 million (^{93}Zr) – 80 million years (^{244}Pu). This necessitates a long-term disposal solution of these HLW. Several countries (France, USA, UK, Japan, Russia, India etc.) decided to immobilize the HLW in a vitreous matrix which can be isolated by disposing them in underground repositories with engineered barriers from the surrounding environment. Glass was the chosen matrix for two principal reasons. Firstly, the glass network is capable of homogeneously incorporating a wide variety of radioactive elements in its structure. Secondly, it has been proven to be a stable solid waste form for thousands of years based on geological and archeological evidence. The HLW is calcined, mixed with glass frit, melted, poured into stainless-steel containers and cooled (figure 1)[1].

ANDRA[2], the French radioactive waste management agency, is currently working on the project CIGÉO, which is a geological repository for the long term disposal of HLW glass packages among other types of radioactive waste. The repository will be constructed in Callovo-Oxfordian clay medium 500 m beneath the earth's surface. The HLW glass package (glass in stainless steel canister encased in a steel over-pack) would be placed in specially designed alveoli of the repository.

[1] ANDRA, *Dossier 2005 Argile - Tome Architecture et Gestion du Stockage Géologique*, ANDRA, Editor. 2005. p. 1-497.
[2] *Site internet de l'ANDRA*. Available from: http://www.andra.fr/

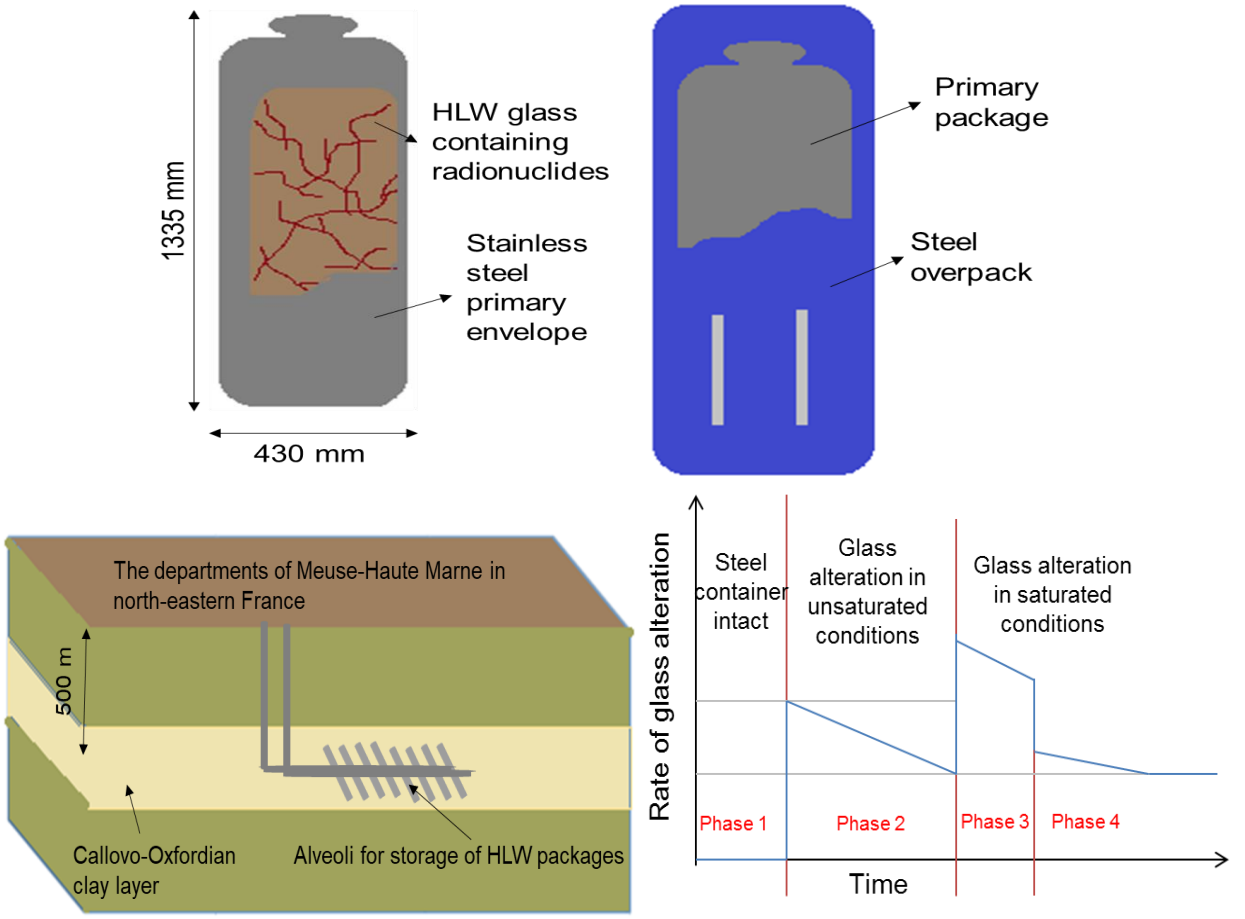

Figure 1 (Top-left) Schematic representation of the HLW nuclear waste glass (with fissures and cracks) encased in a stainless steel canister. (Top-right)Schematic representation of steel over-packs encasing the primary glass package. (Bottom-left) Approximate schematic representation of the deep geological repository envisaged by ANDRA, which is planned to be built 500 m beneath the earth's surface. (Bottom-right) the evolution of glass alteration rate with time depending on the different phases of glass alteration; The top and bottom left images were drawn based on the references given in footnotes 1, 2 and 3; the bottom-right image is based on an image provided in the reference given in footnote 3.

The production of H_2 in the repository, principally due to the anoxic corrosion of steel from the glass packages and the surrounding construction material, will slow-down the saturation of the repository by the surrounding ground water. This may result in the exposure of the HLW glasses to an unsaturated "transitory" environment for a period that could reach up to tens of thousands of years before being completely immersed in aqueous ground water[3]. The bottom-right image in figure 1 represents the 4 phases defined by ANDRA for glass alteration. Phase 1 corresponds to the phase when the surrounding stainless steel canister is intact and therefore there is no glass alteration. Phase 2 corresponds to the period where the steel container has corroded exposing the glass to unsaturated conditions. Phase 3 corresponds to

[3] ANDRA-Collectif, *Dossier d'options de sûreté - Partie après fermeture (DOS-AF)*. 2016, ANDRA. p. 1-467.

the initial dissolution rate (forward dissolution rate) at the initial contact with the ground water that saturates the repository. Phase 4 corresponds to a lower & steady alteration rate regime (residual rate). The decrease in the glass alteration rate in each phase is related to the decrease in temperature of the radioactive glass packages and alveoli over time.

Alteration of nuclear waste glasses in an unsaturated medium was also a possibility in the scenario projected by the Yucca mountain project for nuclear waste disposal[4]. Therefore, several studies on the vapor hydration of American nuclear waste glasses have been published since 1982. Research on the topic of vapor hydration of the French nuclear waste glasses was started fairly recently since 2008. The information gathered from these various studies have been presented in the first chapter of this manuscript, which is dedicated to summarizing the results of various studies on the vapor hydration of the nuclear waste glasses. It is to be noted that the research conducted on the alteration of glasses in vapor phase or unsaturated medium is rather limited in comparison to the number of studies conducted on glass alteration in aqueous medium (fully immersed conditions).

The work carried out during this thesis

The study conducted for this thesis, focuses on the AVM (*Atelier de Vitrification de Marcoule)* glasses. The AVM glasses are complex borosilicate glasses containing more than 20 oxides including fission products and actinides issued from the first generation UNGG (Uranium naturel Graphite-Gaz) reactor at Marcoule.

Studies on the effect of temperature, relative humidity and pH of the vapor phase on SON68[5], ISG[6] and CSD-B[7] glasses have been carried out in France. A comprehensive study of the effect of glass composition on glass durability during vapor hydration of French glasses has not yet been carried out. Additionally, the vapor hydration of AVM glasses has never been investigated before. The range in AVM glasses composition is extensive due to the variation in the composition of the fission products solution. For these reasons, the influence of glass composition of the AVM glasses was investigated by using inactive surrogates and simplified glass compositions and presented in chapter 2 of this manuscript. Six glasses were chosen for

[4] Bates, J.K., M.G. Seitz, and M.J. Steindler, *The relevance of vapor phase hydration aging to nuclear waste isolation.* Nuclear and Chemical Waste Management, 1984. **5**: p. 63-73.
[5] Inactive simulant of the French reference nuclear waste glass R7T7
[6] International Standard Glass- A simplified glass with only six oxides based on the glass composition of the complex SON68
[7] Inactive simulant of the intermediate-level long lived waste glass

the study. The AVM6 glass that alters with the highest residual glass alteration rate in aqueous medium (pure water) at 50°C, the AVM10 glass that alters at the lowest residual glass alteration rate and the AVMV4 glass, which represents an average glass composition of AVM glasses are the three chosen complex glasses. AVM glasses are Mg rich glasses, an element known to increase glass alteration in aqueous medium, and also contain only trace amounts of Ca, an element known to improve glass resistance to aqueous alteration. Therefore, it was necessary to investigate the role of the alkaline-earth elements such as Ca and Mg on vapor hydration of glasses as well. It is difficult to identify their specific influence in a complex glass with several oxides due to possible interference and synergies between other elements. The use of simplified glass compositions helps to understand the role of specific element on glass durability. Therefore, three simplified glasses Q, QCa and QMg were prepared based on the Si/Al stoichiometry of AVMV4 glass to study the influence of Ca and Mg. The fission products loading of AVM glasses suggest that the temperature of the glass packages during the expected time of exposure to water vapor will be around 50°C. The relative humidity (RH) was chosen to be 95% since the conditions expected in the repository are close to saturation[8]. The results presented in chapter 2 helped to identify the influence of glass composition and especially glass stoichiometry. The various solid characterization techniques also helped to identify the rate-controlling vapor hydration mechanism at 50°C.

It is suspected based on literature review that the rate-controlling vapor hydration mechanism, and consequently the influence of glass composition too could vary with temperature. Therefore, the influence of temperature on the influence of glass composition was investigated by altering the three simplified glasses Q, QCa and QMg in vapor phase at temperatures 90 & 120 °C at 95% RH and the results were compared with the alteration of these glasses at 50°C. These results are discussed in chapter 3. Literature survey also suggests that the response of each glass to temperature and humidity could be composition dependent too. The effect of temperature and relative humidity on the AVM6 glass, the most reactive AVM glass, was also investigated. These results also are discussed in chapter 3. Chapter 3 also discusses an isotopic tracer study (using D & ^{18}O isotopes) conducted at 20°C and 90% RH on four of our six glasses, which is the result of an academic collaboration between CEA and Laboratoire Interuniversiaire des Systèmes Atmosphériques (LISA).

[8] Collectif, *Référentiel du comportement des colis de déchets HA-MAVL - Tome 2 - Déchets vitrifiés*, ANDRA and CEA, Editors. 2012. p. 1-548.

While various solid characterization techniques such as SEM, TEM, and ToF-SIMS were used to study the morphology of the altered layer in chapters 2 & 3, the structure of the glasses altered in vapor phase was so far not investigated in this thesis. NMR spectroscopy was used to investigate the structure of the gel layer formed on the Q and QCa glasses altered in vapor phase at 90°C and 98% RH and the results are presented in chapter 4. Very few studies on the NMR spectroscopy characterization of the structure of the gel layer formed in vapor phase exist in literature and this is the first study that uses vapor phase enriched in ^{17}O to probe the global structure of gel layer formed in vapor phase and pristine glass.

A question that often arises while discussing glass alteration in water (either saturated or unsaturated conditions) is that whether glass alteration in vapor phase is equivalent to glass alteration in aqueous medium (immersed conditions) at a very high surface area of glass to solution volume (SA/V) ratio. This question has been pursued with a special interest in this thesis work. NMR spectroscopy was used to structurally characterize the gel layer formed in aqueous medium at a very high SA/V ratio at 90°C as well. The results presented in chapter 4 are basically a comparison of the structure of the gel layers formed in these two media (saturated and unsaturated with water).

The validity of equating glass alteration in vapor phase to glass alteration in aqueous medium at a very high SA/V ratio has been addressed a little further in chapter 5 as well by comparing vapor hydration results of the Q, QCa and QMg glasses presented in chapter 2 with an aqueous alteration experiment conducted at 50°C and a very high SA/V ratio.

Another question that is important from the point of view of geological disposal of the HLW glass packages is the effect and fate of the gel layer formed during vapor phase hydration during subsequent aqueous alteration of the glasses. This question has been addressed for the six vapor hydrated glasses discussed in chapter 2 by immersing these vapor hydrated glasses in aqueous medium at 50°C. The results are discussed in detail in chapter 5. Experiments help us to understand the basic reactions/alteration products and get insights on the short term glass alteration rates. But geochemical modelling of these processes will be a necessary step to be able to predict the long term behavior of glass in the repository conditions. The small attempt that has been made to identify a suitable approach for the modelling of glass alteration in vapor phase is discussed at the end of chapter 5.

Chapter 1 Bibliographic study

1.1 Introduction

This chapter summarizes the knowledge acquired from the different studies conducted on the vapor hydration of nuclear glasses available in literature. Insights from the studies on the atmospheric corrosion of decorative, historic glasses and natural archeological glasses such as basaltic and obsidian glasses are also borrowed.

One of the earlier researches on the vapor hydration of glasses was conducted to develop new dating methods of archeological and geological sites based on the presence of obsidian glasses [1]. Obsidian (or volcanic) glasses, that were exposed to atmosphere, absorbed water to form hydrated layers on their surface. The thicknesses of these hydrated layers were correlated with the age of the sample. The correlations became more complicated as it was identified that hydration of glasses are dependent on a number of parameters such as relative humidity, temperature, glass compositions, weather patterns etc. The research on hydration dating of rhyolitic volcanic glasses continues to evolve over the course of the years [2-7].

The vapor hydration phenomenon of nuclear glasses was of interest to the laboratories associated with the Department of Energy in the USA, since the scenario projected by the Yucca mountain project for nuclear waste disposal involved exposure of nuclear waste glasses to an unsaturated environment before being altered by groundwater that fills the repository [8, 9]. As a result many publications have dealt with this phenomenon since 1982 [10-20]. Studies that draw analogies between the vapor hydration of nuclear glasses and the natural atmospheric corrosion of archeological or volcanic glasses for thousands of years to predict the long-term behavior of glass in an unsaturated environment have also been published [21-23]. Research on the vapor hydration of the French nuclear waste glasses was conducted in France in the laboratories of SUBATECH since 2008 and in CEA Marcoule since 2015 [24-29]. The research was started due to the recent reports of ANDRA, which projected a scenario of vapor hydration of nuclear waste glasses for tens of thousands of years before saturation of repository by groundwater.

Atmospheric alteration of medieval, historic glasses, stained glass-windows of Cathedrals and glass artefacts in museums has been studied in order to understand the phenomenon and preserve these glasses from further degradation [30-35].

These studies have helped to identify the basic glass-vapor reaction mechanisms, alteration products, intrinsic and extrinsic parameters affecting the kinetics and mechanisms and the effect

of aqueous leaching of a glass that was pre-hydrated in vapor phase. Several authors have also discussed in detail about possible alteration mechanisms in unsaturated medium, although inconclusively.

1.2 Glass structure

Glass was the chosen matrix for the immobilization of High Level Activity (HLA) nuclear wastes because this non-crystalline, amorphous material can incorporate homogeneously a variety of elements in different stoichiometry, which is the case of reprocessing spent fuel solutions. The well-known physical and chemical durability of glass for several thousand years also played an important role in the choice of glass matrix for the immobilization of HLW [23, 36].

The elements present in the glass can be either a network former (forms covalent bonds with O atoms) such as Si, Al, B (in 3 or 4 coordination number), Zr (in 6 coordination number), P etc. or a network modifier (linked to O atoms via ionic bonds thereby depolymerizing the glass network) such as alkali and alkaline-earth elements. There are also intermediate elements that are capable of playing both roles depending on glass composition like transition metals and rare-earth elements.

Glass is composed of a disordered network exhibiting short-range order formed by tetrahedra of Si, Al and B, trigonal sites of B and (or) octahedra of Zr. The alkali and alkaline-earth elements can either act as charge compensating atom for $[AlO_4]^-$, $[BO_4]^-$ or $[ZrO_6]^{2-}$ units or as network modifiers, which results in the formation of non-bridging oxygen (NBO) atoms that depolymerize the glass network. The degree of polymerization of the glass has been shown to play an important role in glass durability in aqueous medium [37]. The fraction of NBO in the glass can be calculated using the equations 1.2.1 and 1.2.2 that are given below:

$$NBO = \frac{2*(mol\ fr.\ of\ oxides\ of\ modifer\ cations - mol\ fr.of\ oxides\ of\ network\ formers\ requiring\ charge\ compensation)}{N(O)} \quad \text{Equation 1.2.1}$$

$$N(O) = \sum(no.of\ oxygen\ atoms\ in\ 1\ molecule\ of\ oxide * mol\ fr.of\ oxide) \quad \text{Equation 1.2.2}$$

1.3 Glass-water and glass-vapor reaction mechanisms

The reactions occurring between water molecules and glass network are the same during alteration in aqueous medium and in vapor phase. Water molecules can diffuse into the glass

network through voids at the surface, if the ring sizes are sufficiently large to permit penetration of molecular water. This may result in the formation of hydrated layer. Water molecules that are adsorbed on the glass surface can progressively penetrate into the glass network to form a hydrated layer called as “gel” by a de-alkalization (inter-diffusion) step (equation 1.3.1) and (or) or a matrix dissolution (hydrolysis) step (equation 1.3.2) [38].

$$((\equiv Si - O^- M^+)_{glass} + H^+_{water} \rightarrow (\equiv Si - OH)_{glass} + M^+_{water}) \quad \text{Equation 1.3.1}$$

$$((\equiv Si - O - Si \equiv)_{glass} + H_2O \rightarrow 2\,(\equiv Si - OH)_{glass}) \quad \text{Equation 1.3.2}$$

Localized dissolution-precipitation or condensation mechanisms and re-organization of the gel layer have also been discussed in literature [29, 33]. The elements that are released from the glass into the water may form secondary precipitates. In certain cases, a phenomenon called as etching takes place, where the glass is completely dissolved locally, leaving behind pits (equation 1.3.3) [14].

$$((\equiv Si - O - Si(OH)_3)_{glass} + OH^- \rightarrow (\equiv Si - O^-) + (H_4SiO_4)_{aq}) \quad \text{Equation 1.3.3}$$

Even though the reactions between glass and water are same in both cases (aqueous alteration and vapor hydration), the importance of each of the above mentioned reactions and the rate-controlling mechanisms are different in both mediums. The behavior of elements in the gel layer is also different in both mediums. For example, in recent literature, during the vapor hydration of an alkali aluminosilicate glass, Na^+ was retained in the gel layer formed during vapor hydration. Whereas, Na^+ ions are retained to a much lesser extent in the gel layers formed in aqueous medium. After gel characterization, it was suggested that the Na^+ ions in a gel formed in vapor phase participated in a gel depolymerisation reaction as shown in equation 1.3.4 & equation 1.3.5 [33].

$$H_2O + \equiv Si - O^- Na^+_{(glass)} \rightarrow \equiv Si - OH_{(glass)} + Na^+OH^- \quad \text{Equation 1.3.4}$$

$$Na^+ + OH^- + \equiv Si - O - Si \equiv_{(glass)} \rightarrow \equiv Si - OH_{(glass)} + \equiv Si - O^- Na^+_{(glass)} \quad \text{Equation 1.3.5}$$

A significant amount of research has been conducted on the long term alteration of nuclear waste glass in water [39-47]. A generalized evolution of glass alteration in aqueous medium over time is given in figure 1- 1. This evolution was constructed based on a number of experiments and regroups all the possible different regimes of alteration. In general, glass alters by means of inter-diffusion at the initial contact with water, rapidly followed by hydrolysis

reactions [38]. This rate is known as the initial or forward glass dissolution rate r_0 during stage 1. At the premier instants, it is considered that glass dissolves congruently. After the initial hydrolysis reactions, concentration of glass elements in the solution increases and they re-condense or precipitate to form an alteration layer called “gel” layer. This gel layer has been shown to have passivating properties that reduce the diffusion coefficient of water through the gel layer to the pristine glass [48, 49]. This passivating effect by the gel layer, along with the reduction in the chemical affinity for the dissolution of Si, results in a drop in the glass alteration rate until it attains a steady state. The alteration rate during this steady state is called the residual alteration rate r_r and this phase of alteration is designated as stage 2 of glass alteration. At this stage, diffusion of ionic species and water through the gel and secondary phase precipitation are the rate-controlling mechanisms. It is assumed that the glass alteration in water will progress at the same order of magnitude of r_r for the long term. In certain cases, a resumption of alteration after stage 2 has been noticed. This resumption (stage 3) is associated with the precipitation of stable secondary phases such as zeolites and C-S-Hs (Calcium Silicate Hydrates)[9] and occurs at conditions of high alkali glasses, high pH (>10.5), temperature (>90°C) and high SA/V ratio [50].

In the vapor hydration phenomenon of glass, on the other hand, such a generalized profile of evolution of vapor hydration rate over time has not yet been established. One study conducted at temperatures ranging between 75°C and 240°C suggested that vapor hydration kinetics (increase in thickness of “hydrated layer” with time) was described by a parabolic rate law, but this was true only for some American nuclear waste glasses [14]. In some studies, an incubation period at the beginning of the experiment during which vapor hydration was almost absent was reported. After this incubation period, a linear increase in the gel layer thickness was observed. Different explanations were given by authors for this period of delay in the beginning of alteration, that included, limitations in the amount of water adsorbed on the glass surface [18], time taken for the diffusion of water into the bulk glass [51], the time taken for elemental concentrations in the water layer to reach a value favorable for reaction to occur [11] and the time taken for secondary precipitates to form [19]. The duration of the delay has been shown to be a function of both glass composition and temperature [52]. In certain cases, an acceleration of vapor hydration rate after precipitation of CSHs has been reported [14]. But this type of sudden acceleration is not always reproducible because of the relatively extreme

[9] Table A1- 2 in appendix 1 lists the chemical formulae of all the phases mentioned in this chapter

thermodynamic conditions required to precipitate these phases (T>150-200°C, $pH_{200°C}$>10 and 100% RH).

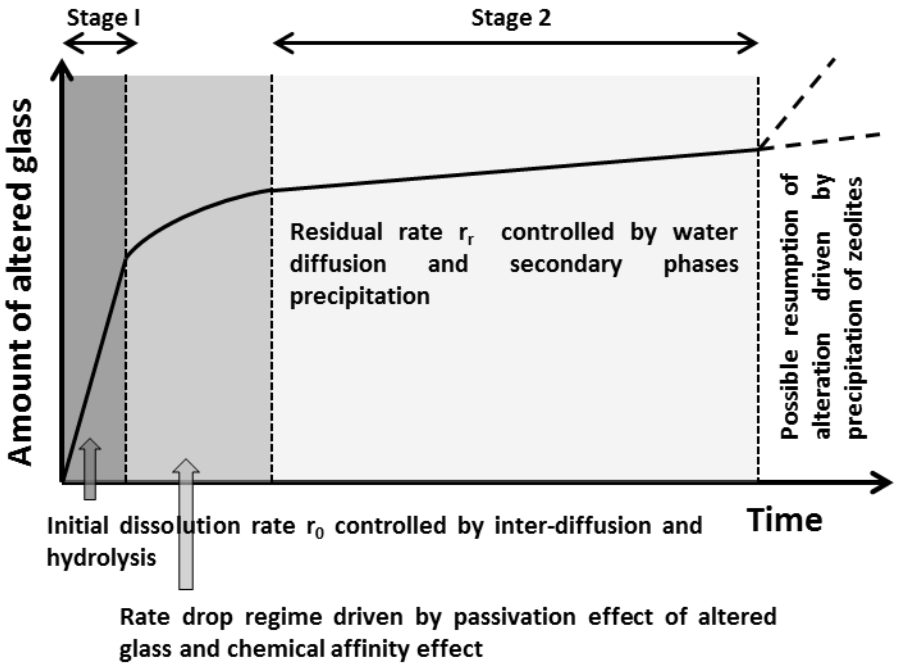

Figure 1- 1 The generalized evolution of alteration of borosilicate glass in water with time and the different stages of alteration (Based on reference [47])

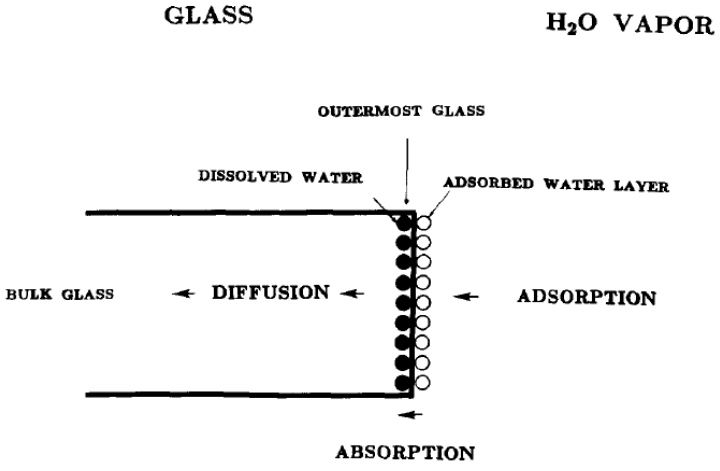

Figure 1- 2 Basic schema for the reaction of glass with water vapor [14]

In some experiments, an inflexion in the vapor hydration rate after 100-200 days of alteration has also been noticed [27, 53]. In recent vapor hydration experimental work conducted on alkali-aluminosilicate glass at 40°C and 80°C (85% RH), a “self-acceleration” of the vapor hydration kinetics was reported and it was suggested that this self-acceleration was a result of

increase in the pH of the very small volume of solution during the premier instants of vapor hydration, promoting network hydrolysis [54].

Figure 1- 2 shows the basic schema for the reaction of water vapor with glass, as described by Abrajano et al. [14]. Water that is adsorbed on the glass surface diffuses into the glass by means of diffusion as water molecules, ion-exchange with network modifier elements and glass network hydrolysis. One can imagine that this is a dynamic process. i.e. the layer of adsorbed water gets renewed with time.

Certain studies have identified vapor hydration as a transport controlled process, where molecular water diffusion and ion exchange occur in parallel. The formation of hydrated layer was said to be controlled by the faster process among the two [14]. The possibility of formation of a hydrated layer without accompanying de-alkalization was also suggested. A study on hydration of silicate glasses in steam atmosphere reported that both molecular water and silanol groups were present in the hydrated layer, although mostly molecular water [55]. A study conducted on an alumino-borosilicate glass at 100% RH and temperatures ranging from 90°C - 210°C concluded that a hydrogenated altered layer was formed by an inter-diffusion mechanism based on experiments conducted in the presence of ^{18}O isotopic tracer [56]. The theory of formation of altered/hydrated layer by inter-diffusion mechanism was also supported by the work conducted by Sessegolo et al. [32]. Other studies conducted on different glass compositions propose that network-hydrolysis is responsible for the formation of the vapor hydrated 'gel' layer [29, 38, 57]. Some studies affirm the occurrence of both inter-diffusion and network-hydrolysis mechanisms during vapor hydration [33, 58]. Localized dissolution-precipitation or condensation mechanisms and re-organization of the gel layer have also been discussed in literature [29, 33].

1.4 Altered layer

1.4.1 Morphology of the altered layer

The glass alteration reactions described in the earlier section results in the formation of an altered layer called as "gel" that grows from the glass surface towards the bulk glass. The layer is usually visually distinguishable from the pristine glass through optical microscope or SEM/TEM images. Depending on intrinsic and extrinsic parameters, this layer may consist of a 2-3 sublayers.

(i) In some cases, a hydration front between the glass and gel layer is present, which is highlighted in TEM images (figure 1- 3 center).

(ii) The amorphous gel layer that is formed due to inter-diffusion and hydrolysis reactions of water with glass matrix is the most common result of vapor hydration reactions. When the thickness of this altered layer is sufficiently large (>2 µm), scaling might occur, where the altered layer is peeled off from the surface [33, 58].

(iii) In some glasses, a poorly crystalline layer of precipitated phyllosilicates is formed on top of the gel layer (figure 1- 3 left).

(iv) Crystalline secondary phases such as carbonates, zeolites and Calcium-Silicate-Hydrates (CSH) are found on the surface of the altered glass (figure 1- 3 right).

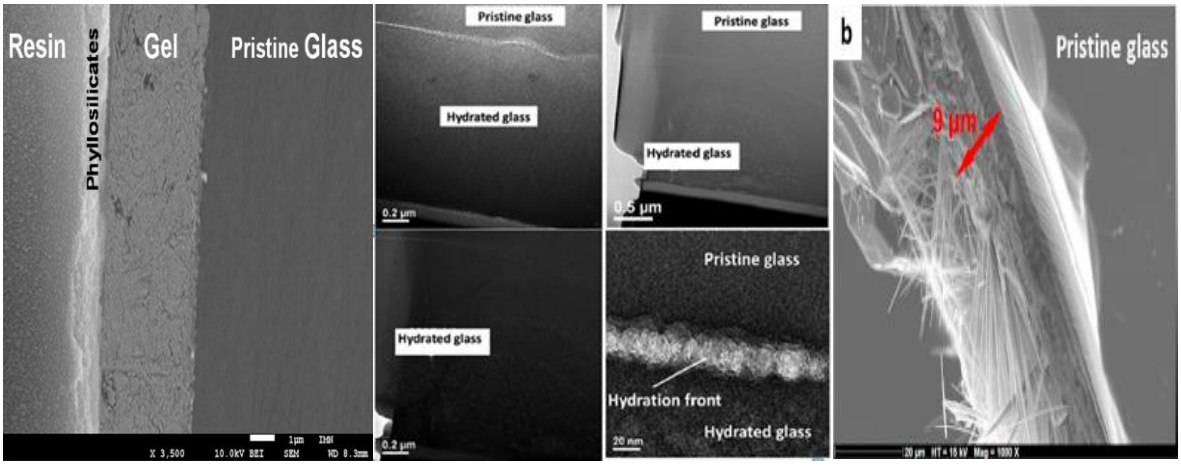

Figure 1- 3 (left) SEM image of SON68 glass hydrated at 125°C, 95 %RH for 593 days [29]; (center)TEM photographs of CSD-B glass hydrated for 365 days at 90°C and 95% RH [27]; (right) SON68 hydrated at 175°C and 98%RH for 290 days under Argon atmosphere [25]

In order to study the evolution of surface layers during the altered layer formation of glass corrosion, SON68[10] glass was altered in water vapor at 200°C and 100% RH for durations ranging between 22 days to 1021 days [59]. These altered glasses were studied using Analytical Electron Microscopy (AEM)/Scanning Electron Microscopy (SEM)/Transmission Electron Microscopy (TEM) to characterize the surface layer formed. Based on this study, six zones in the surface of the altered layer were identified. Figure 1- 4 (right) shows the different zones that are morphologically distinguishable from one another. The layer closest to the pristine glass is designated as zone 6. It is a layer of hydrated glass, where the nucleation of smectites begins. Above this layer, the zones 4 & 5 are present. These amorphous zones comprise the majority of the altered layer and distinguishable from one another by the larger porosity in the zone 4. Zone 3, which is a thin layer, rests above zone 4 and consists of very small grains of poorly crystalline smectites. Zone 2 constitutes a well crystallized honey combed structure of smectites and zone

[10] Table A1- 3 in appendix 1 lists the composition in weight % of all the glasses mentioned in this chapter

1 is the surface of the altered layer where crystalline secondary phases cover the glass surface. It is to be noted that this study was conducted on SON68 hydrated at 200°C. Based on the effect of temperature on vapor hydration rate, which is discussed later in section 1.5.1.1, the dominant vapor hydration mechanism of glass may not be the same at temperatures below 90°C. Therefore, the morphology of the altered layer formed at low temperatures may also vary. A study conducted by Biwer et al. on the hydrated layer using AEM concluded that the altered layer development was significantly affected by small differences in glass composition [15].

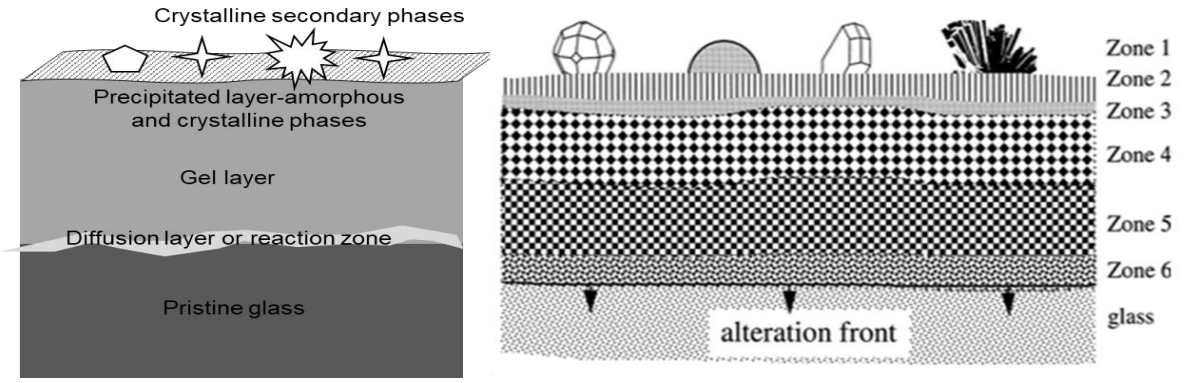

Figure 1- 4 (left) Schematic describing the different layers of altered glass formed during alteration in aqueous medium drawn based on reference [60]; (right) Schematic describing the different zones of the altered surface layers based on hydration of SON68 glass in steam at 200°C [59]

The gel layer formed is not always of uniform thickness as shown in the examples above. Irregularly altered zones where the thickness of the irregularly shaped altered layer is larger in certain areas of the sample have been noticed in literature [30, 61-63], especially in atmospheric alteration studies. The formation of a heterogeneous altered layer and craters are often attributed to a localized chemical attack due to surface defaults such as cracks/scratches/fissures or deposit of dust particles/matter from exposure to atmosphere or formation of hygroscopic salts locally on the surface or preferential/irregular water condensation [14, 64, 65].

1.4.2 Behavior of elements in the altered layer

Based on observations from different vapor hydration experiments conducted at high temperature and saturated water vapor conditions, the gel layer is often enriched in network forming elements, alkaline-earth elements, transition metals and rare earth elements (Si, Al, Ca, Ti, Mn, Mg, Ni, Fe, Zn, Zr, La, Th) and is depleted in alkalis such as Li, B, Na, K, Cs and Mo. Elements such as Si, Al, Ca, Mg, Fe, Zn, Zr may also be depleted in the gel in certain cases

depending on the precipitation of secondary phases that consume these elements. The layer of secondary precipitates made of phyllosilicates and crystalline phases retained mineral forming elements such as Si, Al, Ca and Mg [9, 14, 15, 19, 22, 25, 59, 66-68]. The elemental behavior in the altered layer discussed above was summarized from experiments mostly conducted in saturated water vapor conditions and high temperatures. There is difference to be noted in the behavior of alkalis and alkaline earth elements in the altered layer between these experiments and the experiments described below, which were conducted in unsaturated water vapor and high temperatures.

Detailed analysis of the elemental profile in the altered layer was performed using TOF-SIMS on SON68 altered at (125°C, 95%RH, and 593 days) and (150°C, 92%RH, and 100 days) [51, 53, 69]. Although there were some differences for certain elements in the three different experiments, an overall pattern of elemental distribution is notable. Specifically, alkalis were only slightly depleted with an almost constant profile and alkaline-earth elements were more depleted from the gel layer. Boron was depleted from the gel layer in all cases. Cs and the alkaline-earths seemed slightly retained in the phyllosilicate layer. The transition elements and the rare-earth elements were generally retained in the gel layer and depleted in the phyllosilicate layer. In one specific case (150°C, 92%RH, 101 days), La and Pr were well retained in the phyllosilicate layer.

Retention of alkali elements such as Na in the gel layer was also observed during the atmospheric alteration experiments of a mixed alkali lime silicate glasses (at 80°C and 85% RH [33] and 20°C and 90% RH [70]). This was surprising since several µm thickness of altered layer was formed in the glass surface, which was enriched in O content. Their retention in the gel is indicative of the absence of water condensation and surface run-off rather than absence of inter-diffusion reactions. In the cited study [33], a reorganization of the gel network due to the de-polymerization of ≡Si-O-Si≡ bonds to form a higher quantity of ≡Si-O^-Na^+ species was identified, which indicates the liberation of Na^+ due to inter-diffusion mechanism, which in turn participates in the reorganization of the gel network (equations 1.3.3 and 1.3.4).

The behavior of elements in the altered layer provides information about the alteration mechanisms. Depletion of alkalis from the gel layer in certain cases suggests ion-exchange mechanism. Ideally in vapor hydration experiments, alkali should not be significantly depleted in the altered layer, unless an alkali consuming secondary precipitate is formed. The depletion of B suggests glass dissolution by network hydrolysis. The depleted B and alkalis from the altered layer must normally be present in the precipitates. If these elements are absent in the

precipitates as well, the only explanation is that the elements have been washed away by water that condenses on glass surface and runs-off. This will result in an increase in the hydration rate and prevent the glass alteration to attain steady-state conditions. This case does not exactly represent an actual scenario involving alteration in unsaturated vapor, where the reaction occurs with the molecules of water that adsorb on the glass surface.

1.4.3 Secondary precipitates

Precipitation of secondary phases is an important aspect to study during vapor hydration of glasses because they form much more rapidly in vapor phase than during aqueous alteration of glasses notably due to high SA/V ratios. The very small amount of water available for glass dissolution in vapor phase gets saturated very quickly by glass elements and hence attains conditions that are thermodynamically favorable for the precipitation of secondary phases. In some vapor hydration studies, their precipitation is a mere consequence of liberation of modifier cations from glass network [33, 53]. This is especially true for salts such as carbonates of alkali and alkaline-earth elements formed during low temperature experiments (< 90°C). In other cases, the precipitation of Si or Al consuming phases such as zeolites (analcime) and C-S-Hs (tobermorite) are suspected to act as a driving force for the acceleration of vapor hydration kinetics [14, 19]. This phenomenon has only been observed during vapor hydration experiments at very high temperatures (>150°C). The phases that precipitate during vapor hydration of glasses strongly depends on glass composition and temperature [53]. A recent study [54] explained how higher temperatures (>80°C) activate hydrolysis mechanism much quicker than inter-diffusion mechanism and as a result, the alkali and alkaline-earth elements are not completely solvated out from the gel layer (due to insufficient and “bound” character of water molecules). This resulted in the absence of formation of carbonates of calcium and sodium during vapor hydration at 80°C, which formed rather extensively during vapor hydration at 40°C.

Another reason that they are of specific concern is that these phases might incorporate actinides and other radioactive fission products. During eventual contact with aqueous medium following aging in unsaturated media, these actinides may dissolve or form colloids that get detached from the glass surface and become mobile in the water, posing environmental threat [11].

The commonly reported phases in various vapor hydration studies of nuclear waste glasses apart from analcime are tobermorite, calcite, apatite and gyrolite (which are the major Ca consuming phases). On the experiments conducted on radioactive glasses, U is mostly present

in secondary phases such as Na,K-weeksite, uranyl silicate phases, haiweeite, soddyite etc [66, 67]. Recently a new uranium containing phase was also observed called KNAURSI. It was discovered that since the apparition of this phase, the quantity of weeksite reduced steadily. This new phase is capable of incorporating actinides such as Np [71]. Other actinides such as Pu and Am and fission products such as ^{99}Tc were not detected in the altered layer or the secondary precipitates. Probably their concentration in the altered layer was below detectable limits of SEM/EDS [67]. Other commonly observed phases are phillipsite, lithium phosphate, powellite etc. Poorly crystalline phyllosilicate precipitates such as smectites are also observed in multiple experiments beneath the layer of crystalline precipitates and above the gel layer [14, 15, 19, 20, 53]. The table A1-1 in appendix 1 provides information on the different articles on vapor hydration experiments with the experimental conditions, the altered layer thickness formed, and the secondary phases identified and the elemental enrichment/depletion in the altered layer that has been reported.

Since it was discovered that the precipitation of crystalline secondary phases (zeolites, CSHs) during aqueous alteration may result in a resumption of alteration as described in section 1.3, attempts to predict the secondary phases that will precipitate have been undertaken. It was considered that vapor hydration at high temperatures (150-200°C) and 100% RH were similar to long-term alteration in aqueous medium at high SA/V and that the phases that precipitated during these experiments were representative of the phases that would precipitate during long term aqueous alteration of glasses. This assumption was based on the coherence between the phases that precipitated during the vapor hydration experiments on nuclear glasses and the phases that were observed on the natural analogue basaltic glasses of nuclear waste that were altered in the environment for thousands to millions of years [22, 72].

1.5 Hydration kinetics

The rate of hydration is measured as the thickness of altered layer formed over time. SEM/TEM and optical microscopy help to visually identify the altered layer thickness based on the distinguishable change in the physical structure of the altered layer from the bulk glass. Recent works have also utilized FTIR spectroscopy to follow hydration kinetics based on the infrared absorbance of the SiOH and free and bound H_2O molecules [24, 27, 53, 68]. In the cited vapor hydration studies of SON68 and ISG glasses, an increase of 0.09-0.1 absorbance units in the band of SiOH corresponded to approximately 1 µm thickness of altered layer formed. ToF-SIMS permits to identify the thickness of the altered layer by profiling the enrichment or depletion of elements relative to the pristine glass.

1.5.1 Factors influencing hydration kinetics

1.5.1.1 Temperature

Experiments conducted at different laboratories under similar conditions but different temperatures have shown that the alteration rate increases as a function of temperature. For example, in the experiment conducted on CSD-B glass at 95% RH, the hydration rate during the first 30 days was 9.5 times greater at 90°C than at 50°C [27]. Therefore, high temperatures have been applied to accelerate alteration and predict the glass long term behavior. However, the vapor hydration of SON68 at high temperatures (90-200°C, activation energy (Ea)=43-47 KJ/mol) [26] and lower temperatures (35-90°C, Ea=34±0.4 KJ/mol) [29] suggests that the rate-controlling mechanisms may depend on temperature. Figure 1- 5 shows the Arrhenius plot drawn by Neeway for temperatures between 125-200°C [68]. The hydration rate predicted by this plot for reaction rate at 90°C is an order of magnitude higher than experimental measurements.

It has been observed that more secondary precipitates form at higher temperatures during short time period, than at ambient temperatures during long time periods. The difference in the hydration mechanism at higher temperatures may be due to the precipitation of secondary phases such as analcime, which result in an increase in the alteration rate. These secondary phases consume Si and Al, thus increasing their release from the glass matrix due to chemical affinity.

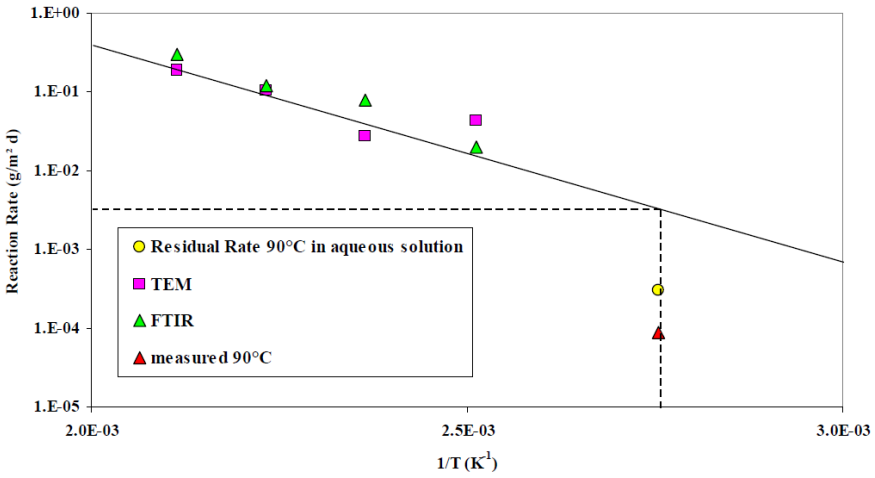

Figure 1- 5 Arrhenius plot of the hydration of glass at temperatures (90-200°C) measured using TEM and FTIR *[68]*

There are also other studies that report non-Arrhenius temperature dependence of vapor hydration rate between temperatures 20°C and 50°C [70] and 40°C and 80°C [54]. It was supposed that the reason for this non-Arrhenius behavior is that different glass-water reactions

are more strongly activated than others at different temperatures. (i.e.) At 20°C, inter-diffusion mechanism is predominant [70] and at 80°C network-hydrolysis mechanism is predominant [54].

1.5.1.2 *Relative humidity*

The relative humidity plays a very important role in the quantity of water adsorbed on the glass surface. The sorption isotherm of SRL165 nuclear waste glass at 23°C [73] resembles closely to the type III of the IUPAC sorption isotherm classification [74]. This type is obtained on a non-porous or macro-porous surface with weak gas adsorption. It corresponds well since the experiment was conducted on pristine glass powders of 30-45 µm. The evolution of mass of water retained on glass surface as a function of relative humidity of SON68 monolith samples are shown in figure 1- 6 [53], which also corresponds well to the same adsorption isotherm type.

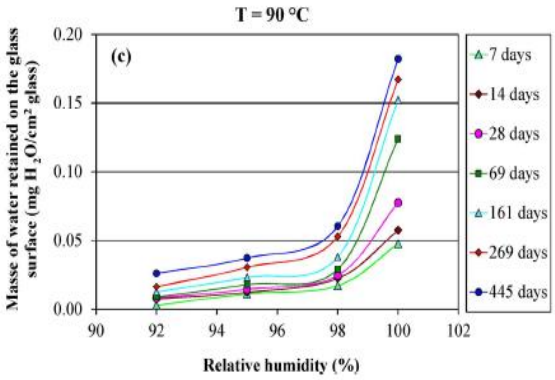

Figure 1- 6 (right) Mass of water retained on the glass surface of SON68 vapor hydrated at 90°C as a function of RH at different durations of alteration [29]

According to the sorption isotherm pf SRL165 glass, up until a relative humidity of 85%, the increase in the number of monolayers adsorbed is low, but after 85%, the increase is exponential [73]. Consequently, the alteration of glasses under vapor phase hydration is negligible below 60% RH and the thickness of hydrated layer increases for higher relative humidity. A critical humidity below which hydration rates are insignificant was identified in earlier publications (very low values below 70% RH at 202°C for SRL 131 glass) [14, 70, 75]. The figure 1- 6 shows that the exponential increase in mass of water retained on glass surface occurs between 98% and 100% of RH. At low relative humidity, where only one monolayer of water is adsorbed on the glass surface, it is characteristic of a Van der Waals' force linking the hydrophilic groups on glass surface and water molecules. The state of water molecules is "solid-like". With the increase in humidity, the isotherm is linear and the number of monolayers of water adsorbed on glass surface increases. In this stage, the water is in an intermediary state between

solid and liquid. In the final part of the isotherm, the thickness of the water layer is sufficiently high for water to be present in liquid state. If the material had micro or mesopores, the water could have condensed in the pores in liquid state [76]. The absence of a hysteresis in the desorption isotherm of the SRL165 glass shows that there are no micropores/mesopores on the glass surface studied [73]. Similar isotherm experiments conducted on altered glass powders could exhibit different type of sorption isotherms because of the mesopores present in the gel layer or better/poorer interaction between porous altered grains and water vapor (most likely Type IV or II) [77]. This means that depending on the nature of the sample (monolith or powder) the same processes may not be taking place at the same relative humidity. It may even be sensitive to the surface area of the glass powders. The quantity of water adsorbed is also sensitive to glass composition [78]. Other factors that increase the quantity of water adsorbed with increasing relative humidity are surface defects and modifier cations [79].

The dependence of alteration rate on RH has been confirmed for several glass compositions [14, 15, 24, 27, 53, 68].

1.5.1.3 pH of the vapor phase

Chaou et al. studied the influence of the pH of the vapor phase on the glass alteration rate [25, 28]. Table 1-1 lists the different conditions of SON68 glass alteration and the corresponding alteration rate and secondary phases. Under acidic pH conditions, crystalline secondary phases couldn't be detected on the sample. The precipitation of Si and Al consuming phases such as analcime at neutral and basic pH conditions were considered to drive the higher vapor hydration rates. The quantity of hydrated glass formed under acidic pH conditions of the vapor phase was lower than that under basic pH conditions as shown in figure 1-7 [25]. The authors also remarked that the hydration rate dropped significantly with time. The presence of reactive gases in the vapor phase could also influence the morphology of the altered layer and the nature of the alteration products [14]. Carbonate and sulphate salts formed on altered glass surface thanks to the interaction of mobile modifier cations with atmospheric species [33].

1.5.1.4 Glass composition

Glass composition influences vapor hydration rate in three ways. (i) As mentioned in section 1.5.1.2, it can influence the quantity of water adsorbed on the glass surface. The release of alkali by initial ion-exchange reactions decreases the vapor pressure of water adsorbed on the surface of the glass and promotes additional water vapor condensation [80]. The dependence of adsorbed water quantity on the alkali content was demonstrated in the work done on an Obsidian glass and SRL165 glass [73].

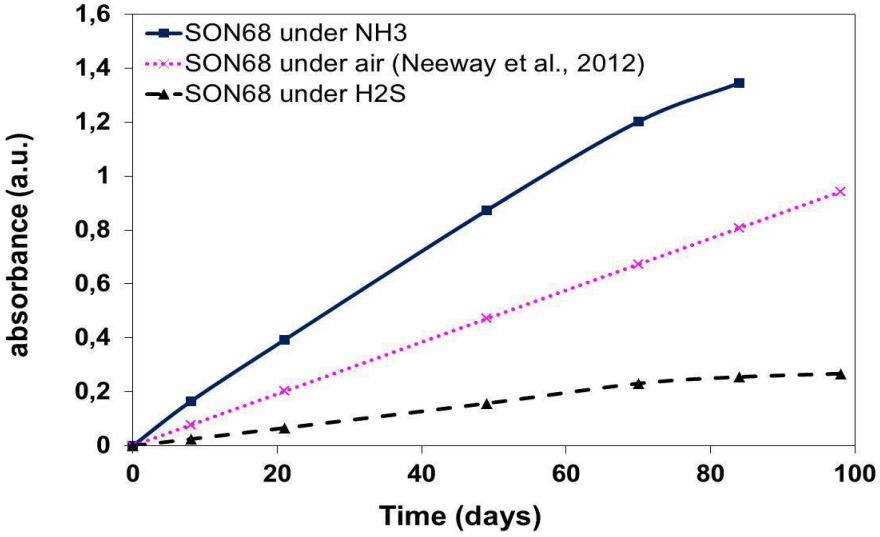

Figure 1- 7 Increase in the difference in absorbance of SiOH between pristine glass and altered glass as a function of the duration of the vapor hydration [25]

Table 1- 1 Vapor hydration study of SON68 glass under different atmospheric pH conditions [25, 28, 68]

T, °C	RH, %	Atmosphere	Duration, days	Average rate calculated over total duration, µm/day	Phases precipitated
175	98	H_2S 1%/Ar (pH- 4,91)	365	0.011	-
175	98	NH_3 8%/Ar (pH- 9,09)	98	0.152	Analcime, tobermorite, phyllosilicates, gyrolite, apatite
175	98	Argon (pH - 5,65)	290	0.031	Gyrolite, tobermorite, analcime, apatite
175	98	CO_2 60%/Ar (pH-4,47)	365	0.016	Clay like phase, Ca-carbonates
175	95	Air	99	0.087	Tobermorite, analcime, Fe-rich phase, Powellite, Calcite

(ii) The second way that the glass composition can influence the vapor hydration kinetics is by playing a role in the resistance of the glass to network-hydrolysis reactions. A higher number of modifier cations depolymerize the glass network by increasing the number of non-bridging oxygen (NBO) atoms. Na^+ ions have a more negative effect than Ca^{2+} or Mg^{2+} modifier cation because the former is ionically bonded to only one ≡Si-O^- unit while the latter are ionically bonded to two ≡Si-O^- units. In a study of the penetration rate of water in the glass, different glass compositions (Na_2O-SiO_2, Na_2O-MO-SiO_2, Na_2O-M'_2O_3-SiO_2, Na_2O-MgO-M'_2O_3-SiO_2, where M & M' are divalent and trivalent elements respectively) were placed in steam at 100-180°C for 3-72 hours. The authors have concluded that the calculated penetration rate of water clearly increases with an increasing amount of Na_2O. They also noted that the penetration rate decreased with the increase of MgO at a fixed temperature and was lower in a glass containing Al_2O_3 rather than B_2O_3 [55]. In a study conducted by Diebold and Bates (1987) an increase in the Na_2O content from 10-12% in the SRL 131 glass composition increased the hydration rate by four times [14]. The addition of Al, Zr and Zn can be expected to increase glass durability [61] since ≡Si-O-Al≡, ≡Si-O-Zr≡ and ≡Si-O-Zn≡ bonds are less soluble during network hydrolysis reactions than ≡Si-O-B≡ or ≡Si-O-Si≡ bonds [37, 81].

(iii) The third way through which the glass composition can influence vapor hydration kinetics is through its major role in the nature of secondary phases that precipitate. For example, in the vapor hydration tests conducted on some American nuclear waste glasses, the presence of Al seems to have a detrimental effect on the glass durability. Four complex glasses with more than 15 oxides (WVCM44, WVCM 50, SRL 165, and SRL 202) were altered in steam at 200°C for up to 80 days [18]. Although the comparison of their alteration rates does not permit to specifically identify the influence of a particular element, it is noteworthy that the most durable glass had the lowest mass% of Al_2O_3 and vice versa. In the experiment conducted on PNNL 76-68 in steam at 200°C for up to 15 days, the very low alteration rate (altered layer thickness immeasurable by SEM) was in fact attributed to the trace amounts of Al present in the glass. The presence of Al in the glass leads to the precipitation of secondary phases such as analcime; analcime consumes Na, thereby increasing the solubility of this element from the glass matrix. The lack of Al in PNNL 76-68 glass prevents the precipitation of this phase, eliminating the sink for Na [14]. Analcime also consumes Si, thus contributing in the increase of glass alteration.

The above paragraph highlights the possible dual effect of elements such as Al depending on the vapor hydration mechanism. Most of the experiments in vapor phase have been conducted at relatively high temperatures from 90 to 200°C, which makes the alteration conditions thermodynamically favorable for the precipitation of secondary phases. Based on the Arrhenius activation energy values calculated for vapor phase experiments conducted at low (35-90°C) and high (90-200°C) temperatures, the mechanism of glass hydration may not be the same in these temperature ranges [53, 68]. At ambient temperatures, there may be an absence of secondary phase precipitation, at least for short alteration time (a few years) and the glass durability may even be enhanced by the presence of Al_2O_3 in the glass, as observed in aqueous alteration.

1.5.1.5 ***Other factors affecting hydration kinetics***

(a) Radioactivity: The number of studies to evaluate the effect of radioactivity on the vapor hydration rates are extremely limited [66, 67, 82, 83]. These few studies have however shown a significant effect of radioactivity on increasing the vapor hydration rate. These few studies also showed that radioactivity could influence the secondary phases that precipitate. However, it is important to note than these experiments were conducted in the presence of air in the heated vessel containing the radioactive samples. In such a system, the production of nitric acid is enhanced and results in an increased effect of radioactivity. In the absence of oxygen or nitrous oxide, the production of nitric acid with only N_2 and water vapor will not be facilitated. The nuclear waste is planned to be buried in an anoxic environment, where the production of nitric acid is not envisaged.

(b) Glass inhomogeneity: A study on low-activity American nuclear waste glasses compared vapor hydration test (200°C, 100% RH, time < 24 days) results of same glasses fabricated by two different vitrification processes (canister centerline cooling (CCC) vs. quenched) and noticed significant differences. The CCC glasses altered 2-10 times faster. This is attributed to the higher crystallinity of the CCC treated glass. A large variability in the altered layer thickness for the CCC treated samples is linked to the non-reproducibility of the crystallinity of the glasses [84].

(c) Fractures: The effect of stress on hydration rate was investigated by altering fractured glasses and 'fractured and annealed' glasses polished to 320, 600 and 2000 grit of surface roughness in steam at 200°C for 6-24 hours [85]. The authors noticed that the 'fractured and annealed' glasses exhibited a $t^{1/2}$ dependence on the hydration layer thickness, indicating a diffusive mechanism of glass alteration whereas the fractured

glasses altered at a rate proportional to t. The difference in the hydration rate is 75% in the first 15 hours and increases to up to 200% by 20 hours. Stress was identified as the rate accelerating parameter. The fractured surfaces also generally showed more developed secondary phases. Photomicrographs showed that the alteration progressed preferentially along cracks and striations. The authors discussed that diffusion was the dominant alteration mechanism in the 'fractured and annealed' glass and network hydrolysis must be the dominant alteration mechanism in the fractured glasses. A study on the stress corrosion of vitreous silica concluded that the mechanical strength of many glasses decreases with time due to exposure to ambient conditions. The authors linked this loss to the slow growth of cracks due to a stress-corrosion process. The crack growth is explained by a decrease in the energy barrier to the rupture of the Si-O-Si bond at the crack tip [86]. This study suggests that the extent of glass alteration by vapor hydration is specifically enhanced at the region of the fractures.

(d) Redox state: The glass processing environment and added agents may control the oxidation state (and consequently the coordination number) of the elements commonly affected by the redox state such as Fe, Mn, Ce and actinides. The effect of the redox state of Fe in the glass was verified on Hanford low activity waste glasses. Two glasses, AMOG-01 (Fe (II)/Fe = 0.87) and AMOG-02 (Fe (II)/Fe = 0.4) were altered in steam at 200°C for up to 28 days. The calculated mass loss for AMOG-02 at the end of 28 days was twice that of AMOG-01 [87].

1.6 Hydration of natural analogues of nuclear waste glasses

Some of the natural glasses that are studied for the purpose of drawing analogies to long term alteration of glasses are tektites, rhyolitic (obsidian) glasses and basaltic glasses. Basaltic glasses contain 50 weight% SiO_2. Tektites and rhyolitic glasses have approximately 70 weight % SiO_2 and low alkali metal contents. The age of these glasses dates back up to millions of years old. They are useful as nuclear waste glass analogues because they occur naturally and are weathered for geological periods of time in atmosphere, soil and water. Two types of studies can be conducted on natural analogues: characterization of naturally occurring glasses to identify the alteration products and mechanism; and conducting experiments on natural glasses or their synthetic homologues to identify the glass dissolution mechanism and verify if the same alteration products can be produced in the laboratory [23]. These natural glasses are found in sea-bed, sub-aerial conditions or buried in soil for geological time scales. Natural glasses that alter in subaerial conditions are subjected to cycles of rain, humidity and high and low

temperatures. These variations in the environmental conditions cannot be known for such a long period of time.

However, vapor hydration experiments conducted in the laboratory have been capable of reproducing the type of altered layer and secondary phases identified on natural analogues [1, 22, 88]. Many studies found that the depth of the hydrated layer was proportional to the square-root of time, which implied that vapor hydration is a diffusion controlled process [1, 89]. Some studies found evidence for water diffusion, hydrolysis and secondary phases precipitation on naturally altered tektites, but not de-alkalization [21, 90].

1.7 Aqueous leaching of a glass pre-hydrated in vapor phase

Since, an aged nuclear waste glass that was subjected to vapor hydration will eventually come in contact with water upon the saturation of the disposal site, immersion studies of vapor hydrated samples were carried out. The objective was to verify the integrity of the altered layer formed during vapor hydration, possible passivation properties and chemical affinity effect to reduce the dissolution rate in water.

In two different sets of vapor hydration experiments conducted on SON68 glass, with parameters ranging from 35°C- 200°C and 80-99% RH, the vapor hydrated samples were immersed in de-ionized water or Callovo-Oxfordian (COx) clay porewater at 50°C. In both experiments, the pH of the leachate increased since the first day. The leach rate of hydrated samples seemed to be higher than that of the pristine glass. It was considered that this increase was due to the dissolution of secondary precipitates such as powellite and probably Li-containing analcime. The initial increase in the glass tracer elements concentration was also attributed to the release of these elements from the gel layer. In the experiment conducted by Bouakkaz, these rates stabilized after 29 days [53]. SEM analysis of the altered layers formed during vapor hydration showed that they were slightly detached and appeared more porous after leaching [53, 68]. Table 1-2 lists the tests conducted on American borosilicate nuclear waste glasses doped with actinides and fission products. In summary, the initial radioactivity released by an aged glass is much higher than a fresh glass. Precipitated solid phases containing radionuclides from the aged glass appear to easily detach and settle at the bottom of the reactor during subsequent leaching [11, 91].

Table 1- 2 Immersion studies of vapor hydrated samples of American nuclear waste glasses [11, 91]

Glass	Hydration temperature	RH	Time	Leaching conditions	Radioactivity released
PNL76-68	340 °C	100%	17 days	Basaltic groundwater-dynamic leaching 0,5 mL/h- 90 °C	Pu concentration 70 times higher; Np, U, Cs, Eu concentrations higher from the hydrated glass
SRL131	202 °C	100%	4 days	Leached for up to 28 days (static leaching)	Np and Ba released at a rate similar to fresh glass; Cs at a lower rate; ^{239}Pu, ^{241}Am, ^{152}Eu at a considerably higher rate
SRL composition WV glass composition	90-200 °C	100%	Up to 180 days	Leached at 90 °C for 28 days (static leaching)	Glass with thicker vapor hydrated layer → higher leachate pH; Np, Pu, Am released 10, 300, 300-500 times higher release rate for SRL glass; 3, 10, 4-10 times higher for WV glass

1.8 Differences between alteration in aqueous medium and vapor phase

Is vapor hydration of glass equivalent to aqueous alteration at a very high SA/V ratio? When glass is altered at a high SA/V ratio, smaller volume of glass needs to be dissolved to saturate the smaller volume of water available for glass dissolution. The pH of the leaching solution is also rapidly increased to values ≥9. This could influence the dominant mechanism of glass alteration (matrix dissolution at high pH vs. ion-exchange at low pH) [92]. It may also favor the precipitation of zeolites and CSHs after the residual rate of alteration has been reached, resulting in a resumption of glass alteration [50].

For the SON68 glass, it was concluded that the principal effect of SA/V is that the residual rate is attained more quickly with an increase in the SA/V ratio [93] (i.e. lesser quantity of glass altered to reach steady state conditions). Following this trend, the quantity of glass altered must be even lower during vapor hydration of SON68. In contrast, the alteration of SON68 in water at high SA/V and in vapor phase has shown that the glass alters at a higher rate in the vapor phase for the same temperature and duration. The altered layer thickness (calculated as equivalent layer thickness) formed on SON68 glass altered in deionized water (S/V 2000 m^{-1}) at 90°C for 5000 days is around 220 nm [93]. Whereas, approximately 1.5 µm

thick altered layer was formed on a SON68 glass hydrated at 90°C and 92%RH for 750 days [53]. In another experiment where SON68 was hydrated at 90°C and 92%RH for 272 days, an altered layer of 1.4 µm thickness was obtained [51], value similar to that obtained at 750 days.

The possible reason could be that vapor hydration can be considered as more of a dynamic process in comparison with the static high SA/V experiments. i.e. the water monolayers could get renewed with time by the adsorption of new molecules of water from the vapor phase onto the altered glass surface.

However, in certain other experiments, the thickness of altered layer formed in vapor phase is negligible in comparison to the thickness of altered layer formed during aqueous alteration for the same temperature and duration. The examples of such cases can be found in the comparative study conducted by Abrajano et al. [13]. A glass that is more durable in aqueous medium is not necessarily durable in vapor phase. For example, among the glasses SRL131 SRL211 and PNL 76-68, PNL 76-68 is more reactive than the other two in aqueous alteration. However, in vapor hydration, this glass has shown very little alteration even in extreme conditions. Similarly, WVCM44 glass, which is more reactive than WVCM50 glass in aqueous medium, is less reactive during vapor hydration [94].

All these studies suggests that even though the same reactions occur between glass and water molecules, the importance of each reaction with respect to the progress of reaction and the rate-controlling reaction mechanisms differ depending on whether the glass is altered in vapor phase or aqueous medium. Therefore, one cannot simply extrapolate glass alteration at a high SA/V ratio to predict vapor hydration rates. However, it could be possible to explain the differences between aqueous alteration and vapor hydration of glasses based on effects of pH and secondary phases that are susceptible to form under given conditions.

The behavior of elements in the gel layer is also different between samples altered in vapor phase and aqueous medium. Alkali elements are poorly retained in the gel layer formed during aqueous alteration and alkaline-earth elements are retained to a higher extent, while it is usually vice-versa in the samples altered in vapor phase. In vapor phase, the quantity of water is insufficient to leach alkali elements from the gel layer and the formation of carbonates is favored depleting alkaline-earth elements from the gel layer. This is suggestive of a difference in the passivation properties of the gel layer formed in the two different mediums.

1.9 Conclusion

This chapter summarizes many vapor hydration experiments conducted on the American and French nuclear waste glasses and the knowledge obtained from their results.

From the experimental results so far, it can be understood that the reactions occurring between glass and water are the same for alteration in aqueous medium and unsaturated water vapor. However, the rate controlling reaction mechanism and the driving force for alteration is different in both cases. The difference largely arises due to the changes in the water chemistry (pH, ionic strength etc.) as a result of the extremely small volume of water available for reaction in vapor phase hydration.

The precipitation of secondary phases seems to be the strongest driving force for alteration in vapor phase at high temperature. Some of the phases that are commonly observed are smectites, zeolites, calcium-silicate-hydrates, calcite, powellite, phosphates etc. These phases begin to appear within the first few days of alteration during vapor hydration at high temperature for several glasses, while in aqueous alteration these phases appear only during long term alteration. At high temperatures and low solution volume that gets saturated rapidly, the conditions are thermodynamically favorable for the precipitation kinetics of these phases. More studies need to be conducted on vapor hydration of glasses at low temperature over a long duration to verify if the secondary phase precipitation kinetics is favored in low temperatures as well. Few studies conducted at ambient temperatures have suggested that the rate controlling mechanism of vapor hydration at high temperatures (125-200°C) and low temperatures (35-90°C) are not the same.

Aqueous leaching of glasses that were pre-hydrated in vapor phase seems to result in dissolution of some of the secondary phases formed during vapor hydration. Due to this, release of radioactive elements is increased when compared to the aqueous alteration of a pristine glass.

Note: It is to be noted that this manuscript does not contain a dedicated chapter to explain the various experiments / materials and methods discussed / used in this chapter. This decision was made since each chapter from chapter 2 describes a particular experiment designed to answer specific questions. The table of experiments described below lists the different experiments described in each chapter along with the aim of the experiment, the glasses studied, the alteration conditions, the duration of the experiment and the characterization techniques used. From chapter 2 to chapter 5, each chapter contains its own experiments section and the characterization parameters for SEM, TEM, XRD and ToF-SIMS analyses are also explained in Appendix A. The principle and data treatment of the SAXS characterization technique is provided in Appendix 2. For the FTIR spectroscopy and NMR spectroscopy, the data acquisition parameters are provided within the chapters 2 and 4 respectively.

Table 1 Table of experiments

Chapter	Parameter studied	Glasses studied	Temperature	Relative humidity (or) SA/V ratio	Duration	Characterization techniques
2	Influence of glass composition	AVM6 AVM10 AVMV4 Q QCa QMg	50°C	95% RH (RH controlled by climatic chamber)	181 days (6 months) and 557 days (18 months)	SEM TEM ToF-SIMS XRD SAXS FTIR
3	Effect of temperature	AVM6	70°C and 90°C	97% RH (RH controlled by NaCl)	1 year	SEM XRD ToF-SIMS
		Q QCa QMg	90°C and 120°C	95% RH (RH controlled by NaCl)	91 days	SEM XRD ToF-SIMS
	Effect of relative humidity	AVM6	50°C	55%, 76%, 83% and 95% RH (controlled by $MgNO_3$, NaCl, KNO_3 and K_2SO_4 respectively)	1 year	SEM XRD ToF-SIMS
	Mechanism of glass alteration	AVM6 AVM10 QCa QMg	20°C	91±3% RH (RH controlled by K_2SO_4 enriched 90% D_2O and 10% in $H_2{}^{18}O$)	1 year	XRD ToF-SIMS
		AVM6 AVM10 QCa QMg	20°C	90% RH (controlled by NaCl)		

Chapter	Parameter studied	Glasses studied	Temperature	Relative humidity (or) SA/V ratio	Duration	Characterization techniques
4	Structure of the gel layer, mechanism of glass alteration	Q QCa	90°C	98% RH (controlled by NaCl enriched 40% in $H_2{}^{17}O$)	213 days	NMR spectroscopy SEM XRD ToF-SIMS
				(aqueous medium) 570438 m^{-1} (Q) and 563708 m^{-1} (QCa) SA/V ratio in DI water enriched 40% in $H_2{}^{17}O$	59 days (Q) and 213 days (QCa)	NMR spectroscopy ICP-OES analysis of leachate at the end of the experiment, XRD
				(aqueous medium) duplicate experiment in DI water of natural abundance around 600000 m^{-1} SA/V ratio	59 days (Q) and 213 days (QCa)	Periodic ICP-OES analysis of leachate to follow hydration kinetics, XRD
5	Study of aqueous alteration of vapor hydrated glasses	AVM6 AVM10 AVMV4 Q QCa QMg (after vapor hydration according to parameters described in chapter 2)	50°C	(aqueous alteration) 19.4 m^{-1} SA/V ratio in DI water	28 days	Periodic ICP-OES analysis of leachate to follow hydration kinetics, SEM
	Comparison of aqueous alteration of glasses at a very high SA/V ratio with vapor hydration of glasses	Q QCa QMg	50°C	(aqueous alteration) 193186 m^{-1} 189533 m^{-1} 198876 m^{-1} SA/V ratio respectively in DI water	91 days	Periodic ICP-OES analysis of leachate to follow hydration kinetics

Chapter 2 Influence of composition of nuclear waste glasses on vapor phase hydration

This chapter has been published as an article in the journal of nuclear materials. Apart from a few changes in the introduction to avoid redundancy, the text of the rest of the chapter has been extracted from the article.

Narayanasamy, S., Jollivet, P., Godon, N., Angeli, F., Gin, S., Cabié, M., . . . Abdelouas, A. (2019). Influence of composition of nuclear waste glasses on vapor phase hydration. *Journal of Nuclear Materials, 525*, 53-71. doi:https://doi.org/10.1016/j.jnucmat.2019.07.015

2.1 Introduction

This chapter focusses on the study of the influence of glass composition on the vapor hydration of nuclear waste glasses. As described earlier in the introduction, a study exclusively dedicated to understand the influence of composition of the French nuclear waste glasses on vapor hydration kinetics has not been conducted so far. However, through various vapor hydration studies, it can be clearly understood that glass composition has a non-negligible effect. The different ways by which glass composition may affect vapor hydration kinetics was already discussed in section 1.5.1.4. Through literature survey, it is noted that the ISG glass alters faster than the SON68 glass at 175°C and 98% RH until 60 days [24] and CSD-B glass alters faster than SON68 glass at 90°C and 92% RH until 32 days [27]. The thicknesses of the hydrated layer formed on SRL202U and SRL131U glasses were several times higher than that of SON68 glass during vapor hydration at 200°C and 100% RH [59]. Since all these glasses contain multiple oxides in varying stoichiometry, it is difficult to understand how the glass composition plays a role in the chemical durability of these glasses. In this work, the effect of stoichiometry as well as the specific influence of elements has been investigated.

Choice of glasses for this thesis work:

AVM glasses are of specific interest in this thesis. These are complex (>20 oxides) borosilicate glasses that contain a significant amount of Mg. These glasses are produced by COGEMA in the Marcoule vitrification facility and their composition is specifically adjusted to incorporate HLW radioactive waste from the fission product solutions from reprocessed Uranium Naturel Graphite-Gaz (UNGG) reactor. The fission product loading in these glasses is between

5-15%, which is lower than that of the R7T7 glass (around 20%), which is the French reference nuclear waste glass for incorporation of HLW issued from light water reactors using UOx fuels [95]. The chemical durability of these glasses can be investigated through inactive surrogates. The range in the AVM glasses composition is extensive due to the variation in the composition of fission products solution. More than 25 AVM glass (inactive) compositions exist. Years of research on the chemical durability of these glasses during aqueous alteration at 50°C and 5500 m^{-1} in initially pure water were analyzed and summarized in the thesis work of Bruno Thien (2010) [96]. From this work, it was identified that among the many inactive surrogates, the AVM6 glass was the most altered and the AVM10 glass was the least altered glass [97]. We decided to study these two glasses in vapor phase for this thesis work, thus focusing on the two extremes of glass durability identified in aqueous medium. In the cited thesis work [96], a new glass composition, AVMV4, was formulated to be referenced as an "average" or "representative" composition of the AVM glasses. The AVMV4 glass was also studied in vapor phase along with the other two glasses. A comparison of the vapor hydration of the three chosen AVM glasses would permit to study the influence of glass stoichiometry. The specific influence of alkaline-earth elements such as Mg and Ca was investigated, since AVM glasses contain a significant amount of Mg and very little Ca and the effects of these elements on glass alteration rate in aqueous medium are relatively well-known [98-102]. Based on literature review, it is expected that these elements would be detrimental to glass durability in unsaturated medium due to their tendency to form secondary precipitates. The study of their specific influence cannot be carried out using a complex glass with several oxides due to possible interference and synergies between other elements. Therefore, three simplified glasses (Q, QCa and QMg) were prepared based on the Si/Al stoichiometry of AVMV4. The use of simplified glass compositions helps to understand the role of specific element on glass durability [37, 47, 103, 104].

Choice of temperature and relative humidity: The fission product loading of AVM glasses suggests that the temperature of the glass packages during the expected time of exposure to water vapor will be around 50°C. Therefore, it was decided to conduct our experiments at 50°C. The relative humidity (RH) was chosen to be 95% since the conditions expected in the repository are close to saturation [105].

2.2 Materials and methods

2.2.1 Sample preparation

The synthesis of the AVM glasses has already been described by Thien [97]. The glass samples for this study were retrieved from the same batch. Q, QCa and QMg were prepared using the oxide precursors (SiO_2, H_3BO_3, Na_2CO_3, Al_2O_3, CaO (for QCa) and MgO (for QMg)). The mixtures were put in a Pt-Rh crucible and heated during 3 h at 1450°C. They were then annealed at 620°C during 1 h in a graphite crucible. Afterwards, the temperature of the furnace was decreased at a rate of 0.5°C/min until 300°C and then it was turned off. The compositions of the glasses after dissolution in acid solution were determined by Inductively Coupled Plasma-Optical Emission Spectroscopy (ICP-OES). The data in mol% oxides are provided in table 2-1. The error percentage associated with the measured values is 3%. The fraction of Non-Bridging Oxygen (NBO) atoms in the glass network was theoretically calculated based on equation 2.2.1.1 and equation 2.2.1.2. ^{11}B NMR spectra (Appendix 4, Figures A4-8, 9, 10, 11 shows images only for the glasses Q and QCa) were collected on a Bruker Avance II 500WB spectrometer. The calculated NBO values and the fraction of $B^{(IV)}$ for each glass are provided in table 2-1. The error associated varies between 3 to 8%.

$$NBO = \frac{2*(mol\ fr.\ of\ oxides\ of\ modifer\ cations - mol\ fr.of\ oxides\ of\ network\ former\ requiring\ charge\ compensation)}{N(O)} \quad \text{Equation 2.2.1.1}$$

$$N(O) = \sum(no.of\ oxygen\ atoms\ in\ 1\ molecule\ of\ oxide * mol\ fr.of\ oxide) \quad \text{Equation 2.2.1.2}$$

For all glasses, the NBO values are similar despite their differences in compositions (except Q). The percentage of $B^{(IV)}$ in each glass shows that Mg is less efficient to compensate $[BO_4]^-$ entities than Ca.

For each glass, two monoliths of dimensions (2.5x2.5x0.1 cm^3) were prepared for vapor hydration during 180 days and 557 days, respectively. These monoliths were cut from the glass bars and polished to optical finish (surface roughness <<1 µm) on both faces. Similarly, one polished monolith for each glass was also prepared with dimensions (2.5x2.5x0.08 cm^3) for the purpose of studying hydration kinetics using Fourier Transform Infrared (FTIR) spectroscopy. All the glass monoliths were washed in ultra-pure acetone and absolute ethanol under ultrasonic agitation and dried for a few hours in an oven at 50°C before starting the experiment. Powder

samples of each glass were prepared by crushing glass pieces using Retsch MM400 ball-mill apparatus equipped with tungsten carbide balls. The size fraction of 2 – 5 µm were separated using pure acetone solvent and the application of Stokes law, for Small Angle X-ray Scattering (SAXS) measurement.

Table 2- 1 Glass compositions (mol% of oxides) (measured by ICP) (error 3%) and fraction of Non-Bridging Oxygen atoms (NBO) and percent of boron in 4-coordiantion (^{IV}B) (error 3-8%)

	AVMV4	AVM6	AVM10	Q	QCa	QMg
SiO_2	48.16	49.29	43.39	57.48	52.67	52.6
Al_2O_3	7.15	5.88	8.30	8.07	7.49	7.74
B_2O_3	16.71	18.64	16.29	15.28	14.6	15.02
Na_2O	18.61	16.65	16.39	19.17	19.01	18.83
CaO	0.04	0.24	0.24	0	6.23	0
MgO	7.15	6.28	10.38	0	0	5.81
Li_2O	0.05	0.89	0.91	0	0	0
ZrO_2	0.22	0.10	0.29	0	0	0
Fe_2O_3	0.38	0.79	0.81	0	0	0
NiO	0.13	0.27	0.27	0	0	0
Cr_2O_3	0.09	0.20	0.20	0	0	0
P_2O_5	0.08	0.00	0.81	0	0	0
SrO	0.06	0.03	0.08	0	0	0
Y_2O_3	0.02	0.01	0.02	0	0	0
MoO_3	0.29	0.13	0.39	0	0	0
MnO	0.10	0.05	0.13	0	0	0
Ag_2O	0.02	0.01	0.03	0	0	0
CdO	0.05	0.26	0.26	0	0	0
TeO_2	0.03	0.01	0.03	0	0	0
Cs_2O	0.07	0.03	0.09	0	0	0
BaO	0.06	0.03	0.08	0	0	0
La_2O_3	0.05	0.02	0.06	0	0	0
Ce_2O_3	0.05	0.02	0.07	0	0	0
Pr_2O_3	0.02	0.01	0.03	0	0	0
Nd_2O_3	0.14	0.04	0.10	0	0	0
RuO_2	0.17	0.08	0.22	0	0	0
PdO	0.11	0.05	0.15	0	0	0
Fraction of NBO	0.134	0.158	0.162	0.036	0.111	0.115
Percent of ^{IV}B	39	20	27	48.5	46.5	37

2.2.2 Alteration protocol

A WEISS WKL64 climatic chamber was used to hydrate the samples at 50°C and 95% RH. The apparatus continuously monitors and displays the temperature and RH in the test zone. De-mineralized water is used to produce steam and then de-humidified to have the programmed RH in the test zone. The monolithic glass samples are placed horizontally in a curved grid Teflon basket that allows the sample to be exposed to vapor on both faces. The glass powders were dispersed in plastic petri dishes. Similar protocol for vapor hydration of glasses has been used before in literature [33].

2.2.3 Experiments

Hydration kinetics

A glass monolith of dimensions (2.5 x 2.5 x 0.08 cm^3) was placed in the climatic chamber at 50°C and 95% RH. The sample was removed periodically (approximately once a month) for a short duration (≈10 minutes) and analyzed in transmission mode using a Vertex 70 FTIR spectrometer. It was then replaced in the chamber to continue hydration. Five spectra at different regions of the monolith were recorded and averaged. The diameter of the diaphragm was set to 6 mm. The spectra were recorded from 4000 to 400 cm^{-1}. The deconvolution of the spectra from 4000 to 2600 cm^{-1} into five Gaussian bands was attributed to the vibration of the OH stretching mode in SiOH molecules (≈3595-3605 cm^{-1}), bound water-silanol groups (≈3515-3518 cm^{-1} & ~3170-3185 cm^{-1}), symmetrical OH stretching mode in the free water molecule (≈3400-3415 cm^{-1}) and the glass matrix (≈2700 cm^{-1}). This type of deconvolution is based on the protocol used to follow vapor hydration kinetics using infrared spectroscopy in recent literature [24, 27, 53, 68]. The hydration kinetics was followed by studying the evolution of the increase in absorbance of the band attributed to the OH stretching mode in SiOH molecules over time.

Calculation of error in the increase in absorbance values: With every deconvolution, the standard error associated with the increase in the area of the Gaussian is calculated by Origin software. The error values for the Gaussian fit are less than 2%. However, while measuring the FTIR spectrum at 5 different places for the same sample, the sample compartment is opened and closed. Due to this the background that was earlier measured is disturbed. Therefore, several backgrounds were measured throughout the day of the FTIR analysis, and the standard deviation among the absorbance values in the range of wavenumbers 3595-3605 cm^{-1} was used to calculate the error value. After error propagation calculation, 0.02 (a.u.) was calculated as the absolute error value.

Characterization of altered glasses

For each composition, two glass monoliths of dimensions (2.5 x 2.5 x 0.1 cm^3) and the glass powders were placed in the climatic chamber at 50°C and 95% RH for a period of 180 days and 557 days respectively. Afterwards, the monoliths were removed from the chamber and cut into dimensions of (1x1x0.1 cm^3) approximately for characterization by Scanning Electron Microscope (SEM), Transmission Electron Microscope (TEM), X-Ray Diffraction (XRD) and Time-of-Flight Secondary Ion Mass Spectrometry (ToF-SIMS). The glass powders were characterized by Small Angle X-ray Scattering (SAXS) to probe the porosity and the pore-size of the gel layer.

For the purpose of studying the evolution of pore characteristics of the gel layer with time, the powdered samples of AVM6 were altered for 11 days, 31 days and 90 days at 50°C and 95% RH, in addition to the standard alteration time of 180 days and 557 days. These samples were characterized by SAXS.

2.2.4 Characterization techniques

The details of the apparatuses used (SEM, TEM, XRD, ToF-SIMS) and analytical parameters are detailed in Appendix A of this manuscript.

It is to be noted that depth profiles of secondary positive ions on the altered glass surfaces were obtained from ToF-SIMS analysis. The normalization of the ToF-SIMS profiles (of each element with respect to the intensity of Si and the intensity of each element in the pristine glass zone) to be able to clearly identify zones of enrichment and depletion were carried out using the formula given in equation AA-1 in Appendix A. In literature, the most immobile element in the glass network is used for normalization of ToF-SIMS profiles to avoid matrix effects, which could be either Si or Zr [106, 107]. In our experiments, Si can be considered immobile. This is valid after verification that Si bearing phases are in relatively small quantity. It was chosen as the element for normalization since it is present in a sufficiently large quantity in the glass, such that the precipitation of secondary phases on the glass surface will not result in depletion of a large fraction of this element.

The altered layer depth was calculated based on boron depletion in the gel layer (using equation AA-2 in Appendix A). Boron is a good tracer for glass alteration in aqueous medium since it is neither retained in the gel layer nor forms secondary phases. In vapor phase it would be logical to expect that the retention of boron in the gel layer is much higher since the quantity of water available to leach boron is highly limited. However, the ToF-SIMS profiles indicate that

the retention of boron in the gel layers is very limited (< 20%). Therefore, boron is used as a tracer to measure altered layer thickness in the vapor hydration phenomenon as well. The thickness of the zone of interface between gel layer and pristine glass measured by ToF-SIMS could be influenced by sample artefacts such as surface roughness of the sample due to precipitates or due to the heterogeneity of the altered layer.

The altered glass powders were characterized by SAXS in order to study the pore characteristics of the gel layer. The analytical parameters of the experiment and the SAXS principle & raw data treatment to obtain the porosity, pore size and specific surface area of the pores are described in section 1 of Appendix 2. The data treatment was based on previous works [108-110].

2.3 Results

The solid characterization of the altered glass has given insights into the morphology of the altered layer, behavior of elements in the altered layer, porosity of the altered layer and the vapor hydration kinetics. In each subsection, the results of all six glasses have been presented. An overall analysis of the results showed that the behavior of the altered glasses AVM6 and AVM10 is similar and that of AVMV4 and QMg is similar. For this reason, the results of these two couples of glasses have been presented together in section 2.3.1 and section 2.3.3. The Q and QCa glasses, which do not contain Mg, are also presented following the four above mentioned Mg-containing glasses.

2.3.1 Morphology of the altered layer (SEM/TEM images)

2.3.1.1 AVM6 and AVM10

The SEM images showed that the alteration of these two glasses is similar in the following accounts:

(i) Irregular alteration: SEM images of cross-sections showed that both glasses had altered in a heterogeneous manner. Figure 2-1 shows the SEM and TEM cross-sections of AVM6 and AVM10 altered for 180 days and 557 days (denoted hereafter as AVM6-180, AVM6-557, AVM10-180 and AVM10-557). The altered surface was punctuated with low density altered zones in the shape of irregular cups whose widths and depths varied from a few hundred nm to a few µm (figure 2-1 (a) and (c) and Appendix 2-figure A2- 1). They were formed on both faces. TEM images of micro-sections showed that in both glasses, these irregular zones were highly porous. This was the case for all four samples. According to STEM-EDX analysis (Appendix 2-

section 3, figures A2- 6, A2- 7 and A2- 8), the porous zone is depleted in Mg, Fe and enriched in Ca.

An attempt to calculate a statistical average thickness of the altered layer of the AVM10-180 sample was made. Ten cross-section SEM images on both faces of AVM10-180 were taken. These images spanned a width of approx. 10 µm each and were taken at a distance of approx. 500 µm apart from one another. From these images, 334 measurements of the irregular altered zone thicknesses were calculated using GIMP image processing software. The average of these measurements for the AVM10 glass is around 659 nm. The minimum thickness measured is 78 nm and the maximum thickness measured is 1.9 µm. The same process could not be repeated for other samples due to technical difficulties.

(ii) Precipitation of Mg-rich phyllosilicates and other secondary precipitates: Both glass surfaces were covered by secondary precipitates. SEM images showed well-developed leafy precipitates on both AVM6-180 and AVM6-557 (figure 2-2(a) and figure 2-1(b)). Needle shaped precipitates were present sporadically on the altered surface (figure 2-2(a)). In AVM6-557, these needle-shaped phases were much more developed and formed clusters. As shown in figure 2-2(c) and 2-2(d), curiously, these clusters formed in straight lines. It seems as though these phases preferentially formed along surface defects created during sample preparation (polishing). TEM images also showed the presence of a layer of phyllosilicates on the surface of the micro-sections that measured approx. 70 nm in AVM6-180 (Figure 2-2(b)) and approx. 200-250 nm in AVM6-557 (figure 2-1 (b)). TEM-EDX analysis and EDS mapping of an altered zone also indicated that the phyllosilicates were enriched in Mg, Fe and Na in addition to Si and they were depleted in Al with respect to the pristine glass composition (Appendix 2 –section 3, figure A2- 6 and A2- 7). Figure A2-4 in Appendix 2 shows the enrichment of Mg in the phyllosilicate layer.

The leafy precipitates in AVM10-180 seemed to be under-developed and visually different in comparison to AVM6. In AVM10-557, they were better developed than AVM10-180, as can be seen in figure 2-2(f) in comparison to 2-2(e). This can also be affirmed by the SEM & TEM images provided in the Appendix 2-section 2, figure A2- 3. The quantity of the needle shaped crystalline phases also seem lower than that on the AVM6 samples and the AVM10-557 samples seem to contain more of them than AVM10-180 samples (Appendix 2- figure A2- 2). The TEM images show a phyllosilicate layer of approx. 300 nm thickness for AVM10-180 and approximately 70 nm thick phyllosilicate layer for AVM10-557 (figures 2-2(e) and 2-2(f)). It is to

be noted here that it is not the overall layer thickness, but just the thickness of the phyllosilicate section.

(iii) The third similarity between AVM6 and AVM10 samples is the presence of a dense homogeneous gel layer beneath the phyllosilicate layer but above the porous irregularly altered zones. This gel layer is approximately 50 nm thick in AVM6-180 (figure 2-2(b)) and 70 nm thick in AVM6-557 (figure 2-1(b)). It is approx. 30 nm thick in AVM10-180 and AVM10-557 (figures 2-2(e) and 2-2(f) respectively). This layer is enriched in Mg, Si and Ca, and sometimes slightly depleted in Al (Appendix 2- figures A2- 5, A2- 6, A2- 7 and A2- 9).

To summarize, under the tested conditions, AVM6 and AVM10 glasses alter similarly, which is not the case for aqueous alteration of these glasses at the same temperature. The altered surface is composed of a phyllosilicate layer at the top (few tens to a few hundreds of nm thick) that is composed of Si, Al, Mg, Fe, Ca and Na. Underneath the phyllosilicates, TEM images have revealed a uniform gel layer of a few tens of nm thickness that seems enriched in Mg and Si and depleted in Al, with respect to the pristine glass. Porous irregularly altered zones are present in a heterogeneous/discontinuous manner beneath the gel layer.

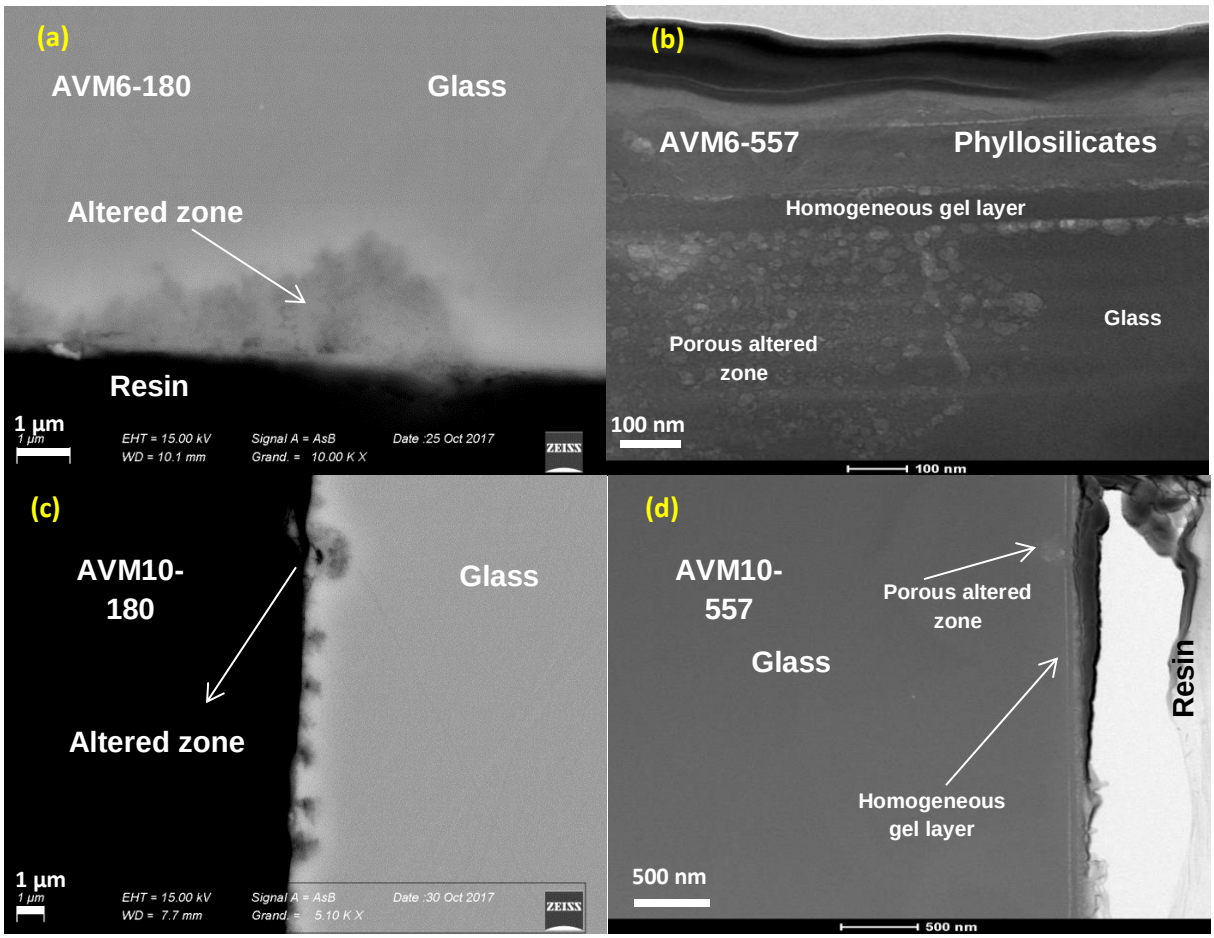

Figure 2- 1 (a) SEM image (cross-section) of AVM6 (altered for 180 days at 50°C and 95%RH) showing an irregularly altered zone; (b) TEM image of AVM6 (cross-section) (altered for 557 days) showing a porous irregularly altered zone on the left side of the image and an unaltered zone adjacent to it. (from top) the resin, the layer of phyllosilicates of approx. 200-250 nm thickness, a homogeneous gel layer of approx. 70 nm thickness and the very porous altered zone. The pores visible beneath the homogeneous gel layer on the right side of the image were enlarged due to exposure to electron beam; but this clearly shows the presence of the homogeneous gel layer even in zones where irregular altered zone is not present; (c) SEM image of AVM10 (cross-section) (altered for 180 days) showing an irregularly altered zone; (d) STEM-BF image of AVM10 (cross-section) (altered for 557 days). This micro-section shows one irregularly altered zone spanning approx. 230 nm and the presence of a uniform approx. 30 nm thick gel layer throughout the micro-section

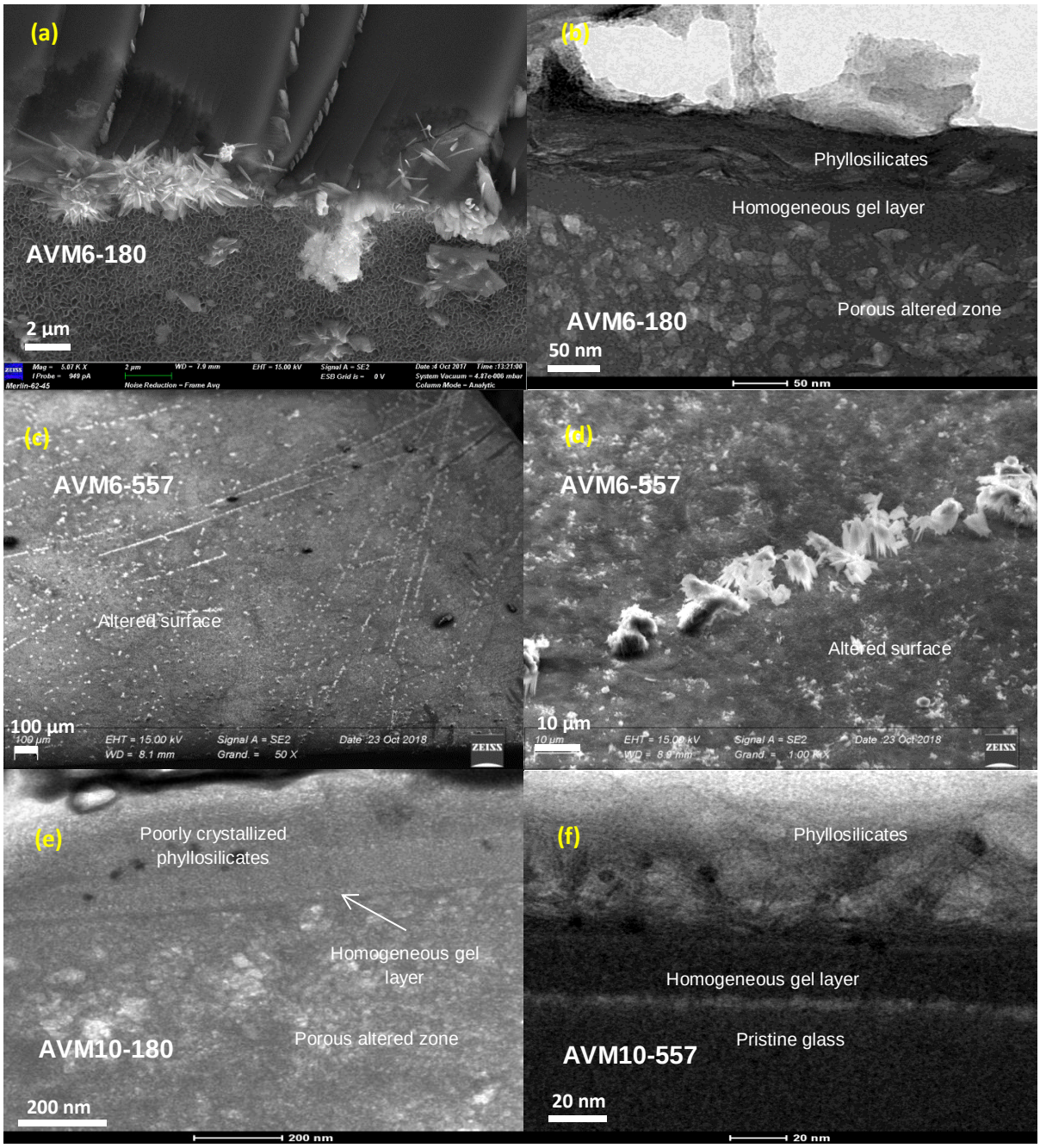

Figure 2- 2 (a) SEM image of AVM6 (altered for 180 days at 50°C and 95% RH) showing leafy precipitates and needle shaped crystalline phases; (b) TEM image of AVM6 (cross-section) (altered for 180 days) showing a 70 nm thick layer of phyllosilicates above an approx. 50 nm thick homogeneous gel layer. The porous irregularly altered zone is present beneath the homogeneous gel layer; (c) SEM image of AVM6 (altered for 557 days) - Formation of crystalline precipitates along straight lines assumed to be surface defects created while polishing; (d) Closer look at image (c) – Cluster of needle shape precipitates; (e) TEM image of AVM10 (cross-section) (altered for 180 days) - The image shows the presence of poorly crystallized phyllosilicates of approx. 330 nm thickness at the surface; the black circular spots are precipitates rich in Ag, Mo and P. Beneath the precipitates, a uniform gel layer of 15-30 nm is present. A very porous altered zone is present beneath the homogeneous gel layer; (f) TEM image of AVM10 (cross-section) (altered for 557 days) – The image shows the presence of well-developed approx. 70 nm thick phyllosilicate layer containing precipitates rich in Ag, Mo and P (circular spots). Underneath, an approx. 27 nm thick uniform gel layer is present. The porosity visible at the gel-glass interface is an artificial enlargement of pores due to exposure to electron beam.

Identification of secondary precipitates

The compositions of the phyllosilicates were analyzed using STEM-EDX. It is to be noted that the Na concentration was not constant throughout the analysis. The Na atoms migrated under the beam towards the resin. It was verified that the concentration of other major elements were not affected due to long exposure to electron beam. The stoichiometry of elements (excluding Na) in the phyllosilicate layer, calculated from the STEM-EDX analysis, for the four samples described in section 2.3.1.1 are provided in table 2-2 (the estimated uncertainty is around 12% relative error).

It can be noted that the composition of phyllosilicates is variable during the alteration of different glasses. No correlation could be identified with pristine glass compositions (Si/Al ratio for example) as was previously suggested [111]. The phyllosilicates formed on AVM6-180 and AVM6-557 have a very similar composition. The stoichiometric ratio of Si/Mg suggests that the composition of the phyllosilicates formed on AVM6 glass is similar to that of a di-octahedral smectite such as montmorillonite-$((Na,Ca)_{0.33}(Al,Fe,Mg)_2(Si_4O_{10})(OH)_2 \cdot nH_2O)$, with slight variations in the composition based on the different transition metal substitutes available. The quantity of Al and other elements capable of occupying octahedral sites in the smectite (Mg, Fe) is not sufficient to envisage a tri-octahedral smectite.

The XRD patterns of the AVM6 samples showed an intense peak corresponding to (001) reflection at 15 Å (Appendix 2- figure A2-10), which can be associated with montmorillonites [112]. Other peaks, if present, were not clearly distinguishable from the background noise. Apart from the composition given by EDX analyses, the other method to distinguish di-octahedral smectites from tri-octahedral smectites is the appearance of the (060) reflection between 1.49 and 1.51 Å [113, 114]. It is difficult to distinguish the peaks around 1.51Å in the XRD patterns from the background noise. The physical magnitude represented by the (001) and (060) lines have different orientations. Therefore, it is possible that the intensity of one of the two peaks increases preferentially than the other. However, these results seem to suggest the formation of a di-octahedral smectite (montmorillonite) on the glass surface during vapor phase hydration in this study.

The composition of the phyllosilicates formed on AVM10-180 and AVM10-557 seem to differ, notably in Mg and O content. AVM10-180 sample has higher Mg and O contents. It is reasonable to suggest that the excess Mg and O in the AVM10-180 sample may be due to the presence of brucite ($Mg(OH)_2$), which is a well-known precursor of Mg-rich smectites [115-117]. No peaks were distinguishable in the XRD pattern, although the TEM images (figure 2-2(f) and

Appendix 2-figure A2- 3) clearly show the presence of a sheet-type mineral. The stoichiometric ratios suggest the possibility of either a di-octahedral smectite or a tri-octahedral smectite, depending on the incorporation of Al in tetrahedral sites or octahedral sites, respectively.

At this stage the exact composition of the smectite formed on AVM10 samples in this study cannot be affirmed with the available information. However, a possible smectite composition is proposed based on the EDX analyses of AVM10-557 (table 2-2) and the generic formula for tri-octahedral smectites proposed by Joly et al. [118]. This generic formula shown in equation 2.3.1.1 was earlier used by Arena et al. for identification of a phyllosilicate formed on nuclear waste glass simulant ISG in the presence of Fe and Mg (aqueous alteration, SA/V 20000 m^{-1}, 50°C, 511 days) [99]. "X" in equation 2.3.1.1 corresponds to cations other than Al that may occupy octahedral sites, such as Mg or Fe. The proposed composition is $[(Si_{3.85}Al_{0.15})((Mg, Fe)_{2.13}Al_{0.87})O_{10}(OH)_2]^{0.72+}[Na_{0.1}Ca_{0.1}]^{0.3+}$.

$[Si_{(4-a)}Al_a)(X_{(3-b)}Al_b)O_{10}(OH)_2]^{(a+b)-}[X_cNa_dCa_e]^{(2c+d+2e)+}$ (Equation 2.3.1.1)

Table 2- 2 Composition (normalized to 4 moles of Si) of phyllosilicates measured by STEM-EDX analyses (around 12% relative error)

	O	Mg	Al	Si	Ca	Cr	Fe	Nd	
AVM6-180	13.60	1.51	0.18	4.00	0.07	0.01	0.18	0.01	
AVM6-557	15.62	1.72	0.20	4.00	0.06	0.03	0.16	0.00	
	O	**Mg**	**Al**	**Si**	**P**	**Ca**	**Cr**	**Fe**	**Nd**
AVM10-180	35.00	3.44	1.09	4.00	0.21	0.10	0.00	0.27	0.08
AVM10-557	20.82	2.01	1.06	4.00	0.17	0.16	0.01	0.23	0.00

2.3.1.2 AVMV4 and QMg

The Si/Al ratio of the glass QMg is the same as the glass AVMV4. The SEM images of both the Mg-containing glasses showed some similarities (i) The altered surface showed the presence of thread-like carpet of precipitates along with µm sized cluster of fibrous precipitates in the SEM images of samples altered for 180 days (AVMV4-180 and QMg-180) (figure 2-3(c) and 2-3(a) respectively). The altered surface of the samples altered for 557 days (AVMV4-557 and QMg-557) showed the presence of holes of 400-500 nm in diameter and a gnawed appearance, with pit size of a few hundred nm, respectively (figure 2-3(d) and 2-3(b) respectively) (ii) The altered layers of all four samples were not visible in SEM, indicating that their thickness must be less than 100 nm. Irregularly altered zones were also not observed in the SEM images. TEM images of cross-section of AVMV4-557 show the presence of a gel layer of

approximately 80 nm thickness (figure 2-3(e) & (f) and Appendix 2, figure A2-11). Above this apparently homogeneous gel layer, a mixture of amorphous and crystalline phases is distributed across the 5 µm cross-section in varying thicknesses (200 nm to 20 nm). STEM image of QMg-180 showed an altered layer next to the pristine glass that appears homogeneous and is between 40-60 nm in thickness (figure 2-4(a)). On the surface of the altered layer, a layer of fibrous precipitates of 30-40 nm in thickness is present. The electron diffraction patterns obtained from TEM imaging did not show any fringes in the zone of precipitates, indicating that the precipitates are probably amorphous. The STEM-EDX analysis indicated that the amorphous precipitates and the gel layer in the surface are enriched in Mg and Na and depleted in Al, with respect to pristine glass (Appendix 2-figure A2- 12). Similar gel layer morphology was also observed on QMg-557 (figure 2-4(c)).

2.3.1.3 Q

SEM images of Q altered for 180 days and 557 days (Q-180 & Q-557) do not show any recognizable secondary precipitates. TEM image of a micro-section of Q-180 shows the presence of a seemingly homogeneous altered layer of approx. 40 nm thickness (figure 2-4(b)). The pores that are visible on the altered layer-pristine glass interface were formed / enlarged during exposure of the sample to the electron beam. TEM image of a micro-section of Q-557 also showed a similar homogeneous gel layer of approximately 80 nm thickness (figure 2-4(d)).

2.3.1.4 QCa

SEM images of QCa altered for 180 days (QCa-180) show a few unidentified scattered precipitates on the surface. TEM image of QCa-180 shows the presence of an apparently homogeneous altered layer of approximately 80 nm (figure 2-5(a)). The difference in density between the pristine glass and gel layer seems to be higher than other glasses observed.

Figure 2- 5(b) shows the SEM image of QCa altered for 557 days (QCa-557). The sample surface contained significantly more surface precipitates than QCa-180. There seems to be two types of secondary phases; clusters of pointed needle-like secondary phases and cuboid precipitates. Figure 2-5(c) shows the SEM image of sample cross-section. An altered layer of approx. 110-150 nm thickness is distinguishable due to the contrast difference between the layer and the pristine glass. Calcite was identified by XRD patterns on QCa-180 and QCa-557 (figure A2-10).

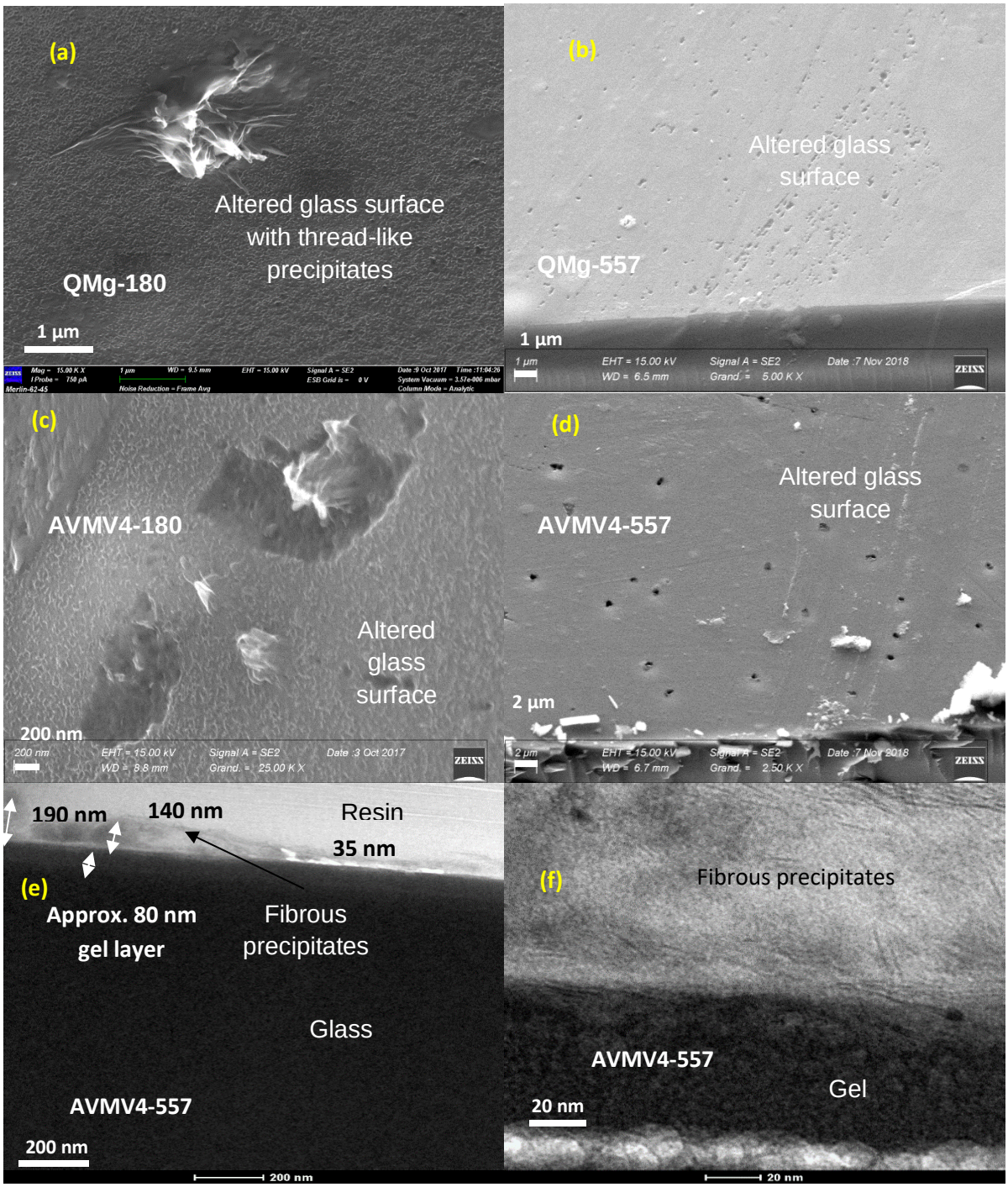

Figure 2- 3 (a) SEM image of QMg (altered for 180 days at 50°C and 95% RH) showing a carpet of thread-like precipitate and fibrous cluster of secondary precipitates; (b) SEM image of QMg (altered for 557 days) showing a gnawed appearance at the altered sample surface; (c) SEM image of AVMV4 (altered for 180 days) showing a similar altered surface to QMg altered for the same duration; (d) SEM image of AVMV4 (altered for 557 days) showing holes/pits of size 400-500 nm; (e) TEM image of AVMV4-557 (cross-section) showing a layer of phyllosilicates of varying thickness on altered glass surface and a uniform homogeneous gel layer of approx. 80 nm thickness; (f) A zoom of image (e), showing the homogeneous gel layer with a mixture of amorphous and crystalline precipitates on the altered surface. There appear to be more crystallized precipitates towards the surface and at the interface of gel-layer precipitate-layer

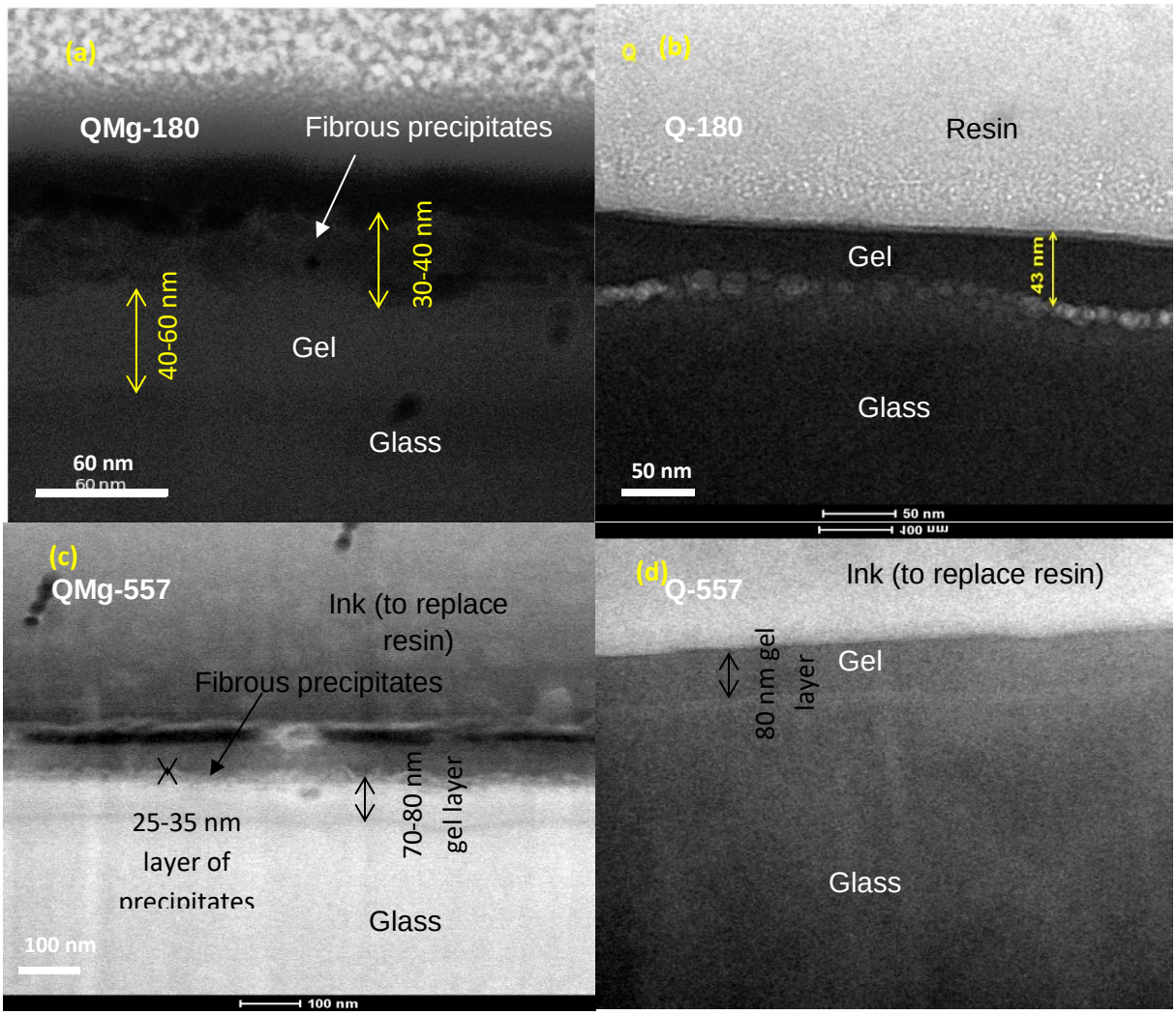

Figure 2- 4 (a) STEM image of QMg (cross-section) (altered for 180 days at 50°C and 95% RH); (b) TEM image of Q (cross-section) (altered for 180 days); (c) STEM (DF) image of QMg (cross-section) (altered for 557 days); (d) TEM image of Q (cross-section) (altered for 557 days)

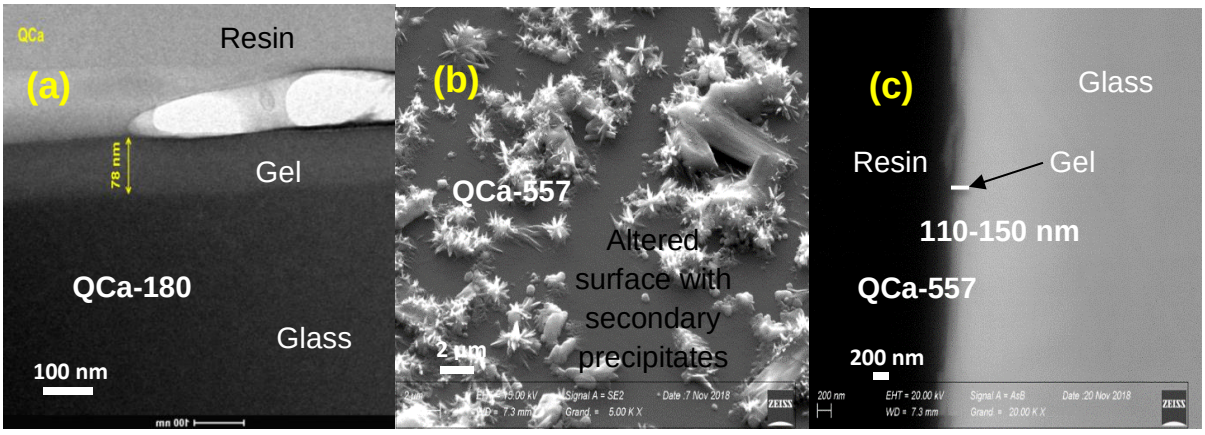

Figure 2- 5(a) TEM image of QCa (cross-section) altered for 180 days at 50°C and 95% RH; (b) SEM image of QCa altered for 557 days at 50°C and 95% RH; (c) SEM image of cross-section of QCa altered for 557 days

2.3.2 Behavior of elements in the altered layers (ToF-SIMS profiles)

Among all the characterization techniques presented in this study, ToF-SIMS and FTIR analyze the largest surface area of the sample in a uniform manner for all six samples. Therefore, it is considered to be the most suitable method for inter-comparison and the most representative in terms of element behavior in the altered layer and the average depth of altered zone. Table 2-3 summarizes and compares the thicknesses of the altered layers measured using ToF-SIMS and TEM images. The uncertainties of the given values could not be calculated. The percent error associated with ToF-SIMS measures is generally considered to be less than 3% [119]. Other factors contributing to the uncertainty are surface irregularity due to precipitates, constant speed of abrasion used for the entire zone of analysis and irregular/discontinuous altered zones. However, based on the coherence between the results of ToF-SIMS and other characterization techniques, it can be presumed that the uncertainty associated with the altered layer thicknesses can be overlooked.

Figure 2-6 presents the normalized ToF-SIMS profiles of the major elements present in the six glasses altered for 180 days. The normalized ToF-SIMS profiles of all the elements present in all six samples altered for 180 days and 557 days are presented in appendix 2 (figures A2-13 to A2-19).

As observed in section 2.3.1, a similarity in the behavior of elements of the glasses AVM6 / AVM10 and AVMV4 / QMg is noticeable. The striking similarity in the behavior of H, B, Al, Na and Mg in the glasses AVMV4 and QMg are presented in appendix 2 (figure A2-20). Globally, for each glass, the behavior of elements in the altered layer is remarkably similar among the two different samples altered for two different durations.

The four Mg-containing glasses show the presence of a layer of precipitates towards the surface of the altered layer. As in SEM images, the thickness of this precipitate layer is much higher in AVM6 (250-300 nm) and AVM10 (150-250 nm) than the AVMV4 and QMg glasses (<10 nm). This precipitate layer mainly contains Mg, Na, Li, Cs and Fe (in addition to Si).

The altered layer-pristine glass interface is rather sharp for the samples AVMV4, Q, QCa and QMg, unlike for the AVM6 and AVM10 samples. This apparently broad interface of AVM6 and AVM10 samples is due to the irregular and discontinuous altered zones observed in SEM images. Therefore the thickness estimated for these two glasses is considered as an average

thickness of the analyzed zone. Based on the ToF-SIMS thickness (boron) from table 2-3, the glasses AVM6 and AVM10 alter 10-30 times faster than the other four glasses.

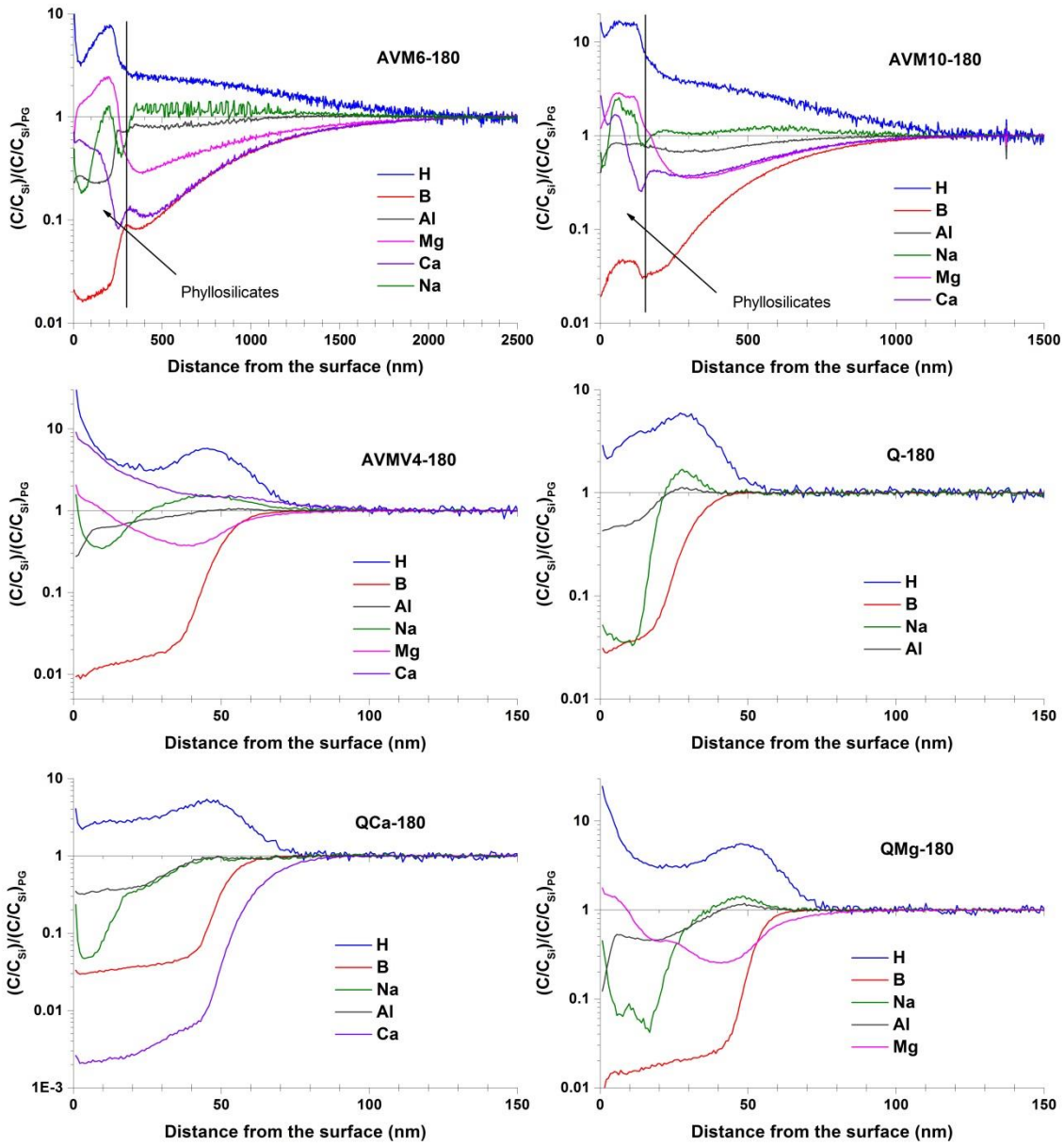

Figure 2- 6 ToF-SIMS profiles of all six glasses altered at 50°C and 95% RH for 180 days; The profiles of only the major elements of the AVM glasses are shown here

Among the samples altered for 180 days, AVMV4, QCa and QMg alter 1.7 times faster than the glass Q. Among the samples altered for 557 days, QCa alters almost twice that of AVMV4, QMg and Q. In testing two samples of each glass for durations of 180 and 557 days, we

considered that the rate of alteration would be similar. However, the increase in the thickness of altered layer from 180 days to 557 days suggests that the vapor hydration rate has decreased by a factor of 9.1 for AVMV4, 8.5 for QMg, 1.9 for Q and 1.6 for QCa after 180 days of alteration (considering that the vapor hydration rate is constant between 0-180 days and between 180-557 days).

Table 2- 3 Thickness (in nm) of the altered layer (altered at 50°C and 95% RH for 180 days and 557 days each); (ToF-SIMS) is measured from equation AA-2 in appendix 2; (TEM) is measured based on the density difference between pristine glass and gel layer in TEM images

Duration of alteration	**180 days**		**557 days**	
	(ToF-SIMS)	**(TEM)**	**(ToF-SIMS)**	**(TEM)**
AVM6	1060	(70 nm homogeneous layer + Irregular alteration + surface precipitates)	900	(70 nm homogeneous layer + Irregular alteration + surface precipitates)
AVM10	630	(~30 nm homogeneous layer + Irregular alteration + surface precipitates)	905	(~30 nm homogeneous layer + Irregular alteration+ surface precipitates)
AVMV4	52	-	64	(~80 nm homogeneous altered layer + surface precipitates)
Q	31	~43 nm homogeneous altered layer	66	~76 nm homogeneous altered layer
QCa	52	~78 nm homogeneous altered layer	121	110-150 nm homogeneous altered layer (SEM)
QMg	53	(~60 nm altered layer + ~30 nm fibrous precipitates)	66	(~76 nm homogeneous altered layer + surface precipitates)

Generalizing the behavior of elements in the four Mg containing glasses, a large fraction of boron is lost from the gel layer formed in vapor phase (retention varies from ~5-20%). The Mg-containing glasses develop a continuous layer of phyllosilicates on the surface, which is distinguishable in the ToF-SIMS profiles through the enriched profiles of alkali (Li[11], Cs[11] and Na to a lower extent), alkaline-earth elements (particularly Mg), and transition metals[11] (except Zr, Pd). This precipitate zone in the ToF-SIMS profiles is usually depleted in Al, Zr[11] and rare-earth

[11] Only in the case of the AVM glasses

elements[11], suggesting that these elements do not participate in the formation of the layer of phyllosilicates. The gel layer, present beneath the phyllosilicate layer, is depleted in elements that are enriched in the phyllosilicate layer (such as Li, Cs, Mg and transition metals). The retention of the elements that are scarcely present in the phyllosilicate layer (Al, Zr and rare-earth elements) is almost 100% in the gel layer. Surprisingly, Na is also well-retained in the gel layer.

In coherence with the STEM-EDX results, Al is depleted in the zone of surface precipitates of the Mg-containing glasses, indicating that the Si/Al ratio is higher in the phyllosilicate layer than the glass.

In case of the Q and QCa glasses, boron is significantly depleted in the gel layer. Na is depleted in the part of the gel layer that is close to the surface. The retention of Al is between 70-90% in the gel layer. In the QCa glass, the depletion of Ca is deeper than that of B and the retention factor is also lower than that of B.

The ToF-SIMS profiles, which have been normalized to Si and to PG, might give an impression that many elements are depleted from the gel layer, even though not as extensively as boron. It seems likely that this depletion is due to a migration of the elements towards the surface to form precipitates. In the zone of precipitates, the depletion of elements such as Zr, rare-earths and Al is because they are almost absent in the precipitate layer, towards the surface. The elements which are really depleted (absent in gel layer and precipitate layer) are boron, Ca in QCa and Na from the surface of Q and QCa. The retention of Ca is < 3% in the gel layer of QCa (in both QCa-180 and QCa-557).

The gel layer composition can be calculated from the ToF-SIMS profiles. Normalized ToF-SIMS profiles give access the retention factors (fraction of number of atoms of elements present in the gel layer with respect to the number of atoms present in the pristine glass) of elements in the gel layers. The gel composition can be obtained by applying this retention factor to the mole fraction of elements in the pristine glass.

Tables A2-2 and A2-5 in appendix 2 (section 10) give the retention factors of all elements in the gel layers formed during vapor hydration for 180 days and 557 days respectively. Tables A2-4 and A2-7 provide the calculated gel layer composition in mole percent of oxides for the gel layer formed during vapor hydration for 180 days and 557 days respectively.

2.3.3 Porosity of the altered layer (SAXS)

The porosity, pore-size and specific surface area values reported in this paper were calculated by considering that the pores of the gel layer are filled with water. This assumption will be discussed later in section 2.4.3. The data treatment was based on previous works [108-110] and is explained in detail in the appendix 2 (section1). q is the scattering vector in nm^{-1} and I_{corr} (cm^{-1}), calculated from equation A2-9 in appendix 2, separates the scattering intensity in the high q domain by the pores in the gel layer from the scattering in the low q domain by the grain envelopes.

AVM6 and AVM10: The plots of $I_{corr}\ vs.\ q$ of these two glasses show a porod regime ($I_{corr}\ \alpha\ q^{-4}$). The SAXS spectra of these glasses are provided in figure A2- 21 (appendix 2). In both glasses, the high q porod regime shifts to higher q values with time. However, porod's law cannot be used to calculate the porosity and specific surface area of pores for these two glasses, since the SEM images of the monolith samples indicate that these glass surfaces are covered with phyllosilicates. Therefore, the SAXS diagram contains information regarding both the porosity of the gel layer and the inter-layer spacing of the phyllosilicates and they cannot be deconvoluted.

AVM6 glass powders of particle size 2-5 µm that were prepared as described in section 2.2.1 were altered at 50°C and 95% RH for 11 days, 31 days and 90 days, for the purpose of characterization by SAXS and identification of possible trends in the evolution of the gel layer. These samples are referred to as AVM6-11, AVM6-31 and AVM6-90. The $I_{corr}\ vs.\ q$ plots of these glasses are shown in figure A2- 22 (appendix 2). Porod's law is respected at higher q values for all three samples including the sample altered for only 11 days. The quantity of secondary phases on these samples altered for a short duration is negligible (TEM images (Figure A2-24 in appendix 2) of AVM6 samples altered for 90 days at 50°C and 95% RH show that the surface precipitates are visually much less denser than the AVM6-180 samples). Therefore, the porosity, pore-size and specific surface area of the gel layer can be calculated. The porosity, pore diameter and specific surface area of AVM6-11 are 66%, 4.4 nm and 328 m^2/g respectively; that of AVM6-31 are 47%, 4.5 nm and 235 m^2/g respectively; and that of AVM6-90 are 11%, 4.8 nm and 58.2 m^2/g. These values are recapitulated in table 2-4. It can be noticed that porosity decreases with time, while pore size increases. The $I_{corr}\ vs.\ q$ plot of AVM6-11 is distinctly different than that of the other AVM6 samples. The shoulder corresponding to the highest intensity is at a higher q for the AVM6-11 sample. This translates to a smaller

average pore size than the other glasses [120]. However, the porod regimes of the AVM6 samples altered for larger duration is shifted towards much higher q. This suggests the presence of smaller pores in the samples that were altered for a duration longer than 11 days, even though the average pore-size increases with increase in duration of alteration.

AVMV4 and QMg: $I_{corr}\ vs.q$ plot of these two glasses are similar in the sense that, neither of them display a porod's regime. The plots are shown in figure A2-22 (appendix 2). The exponent D ($I(Corr) \propto q^{-D}$) decreases with increase in duration of alteration, suggesting an increase in the roughness of the pore-interface. It can be considered that the reason for the absence of a porod's regime in the SAXS diagram is the interference of poorly crystallized precipitates. This means that the D value, which varies between 3.4 and 2.6, is not representative of a rough pore-interface in the gel layer, but rather a distortion of signal due to the presence of almost equal proportions of gel layer and poorly crystalline precipitates.

Q and QCa: The $I_{corr}\ vs.q$ plot of these two glasses exhibit a porod's regime (figure2- 7). The absence of a substantial amount of secondary precipitates on the SEM and TEM images of the monolith samples validate the use of these measurements to calculate the porosity, pore size and specific surface area of pores. The porosity of Q-180 is 65% and decreases to 44% in the Q-557 sample. The pore diameter increases from 4.3 nm in the Q-180 sample to 5 nm in the Q-557 nm. The surface area of pores also decreases from 451 m^2/g (in the Q-180 sample) to 264 m^2/g (in the Q-557 sample). The porosity of QCa-180 is 27%, which decreases to 9% in the QCa-557 sample. The pore diameter increases from 5.1 nm in QCa-180 to 7.5 nm in QCa-557. The surface area of pores decrease from 158 m^2/g in QCa-180 to 37.6 m^2/g in QCa-557. These calculated values are presented in table 2-4. Contrary to AVM6 and AVM10 samples altered for 180 days and 557 days each, the high q porod's regime shift towards lower q at longer duration of alteration. This indicates an increase in the average pore size with time. The higher pore sizes of the QCa sample than the Q sample and the factor of increase in pore-size with time correspond well with the magnitude of the shift in high-q porod's regime to lower q values for these samples as shown in figure 2-7.

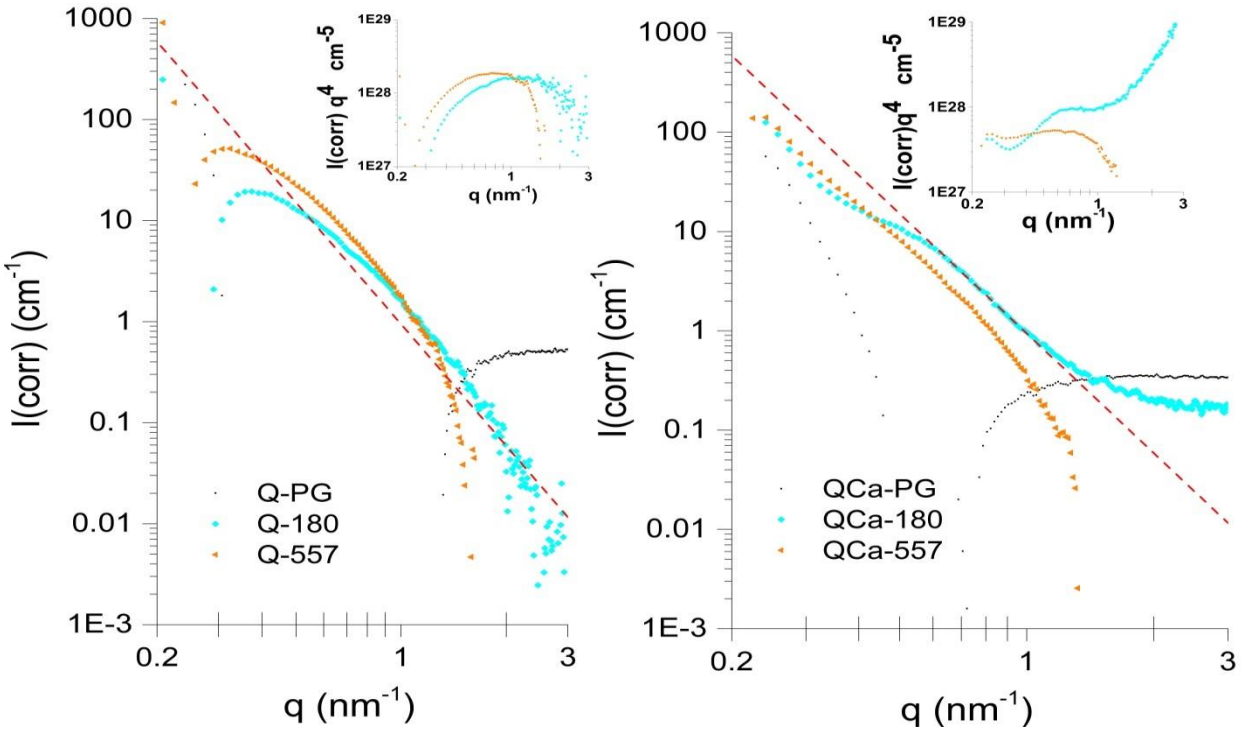

Figure 2- 7 SAXS spectra of the glasses (a) Q and (b) QCa that were unaltered (black squares), altered for 180 days (blue circles) and 557 days (orange triangles); The red dotted lines represent I α q^{-4}; The inset graphs show the plot of (I(corr)*q^4) vs. q highlighting the shift of the porod regime towards lower q with increasing duration of alteration; I(corr) is a result of data treatment to separate the intensity scattered by grain envelopes and the inner pores of the gel layer

Table 2- 4 Porosity, pore-size and surface area of gel calculated from SAXS data; $Ø_{gel}$ corresponds to the volume fraction of gel calculated from ToF-SIMS profiles of monoliths that were used to calculate the porosity of the gel formed on glass powders

	Time (days)	Porosity (%)	pore diameter, nm	Surface area of pores, m^2/g	$Ø_{gel}$
Q	180	65	4.3	451	0.05
	557	44	5	264	0.1
QCa	180	27	5.1	158	0.08
	557	9	7.5	37.6	0.19
AVM6	11	66	4.4	328	0.06
	31	47	4.5	235	0.15
	90	11	4.8	58.2	0.64

2.3.4 Hydration kinetics

2.3.4.1 FTIR spectroscopy

Figure A2-25 in appendix 2 shows the infrared spectra of the AVM6 sample vapor hydrated for various durations up to 557 days (only the infrared spectra of AVM6 sample is shown to serve as an example). Figure A2-26 shows an example of deconvolution of the infrared spectra into five Gaussian bands. The centroid value of each Gaussian band varies slightly because of varying glass composition. The centroid values for all five Gaussian bands for all six glasses are provided in table A2-8 in Appendix 2. The hydration kinetics is followed by studying the evolution of the increase in the absorbance of the band attributed to the OH stretching mode in SiOH molecules. For this, the absorbance around 3600 cm^{-1} (OH stretching) measured at a given time of alteration (A) is reduced by the absorbance for the pristine glass (A_0). Figure 2-8 shows the increase of ($A-A_0$) over time for all the six glasses until 557 days of alteration. Figure 2-8(a) shows the difference in the increase of ($A-A_0$) versus time according to the glass stoichiometry. The increase in absorbance of AVM6 glass is approximately twice that of AVM10, 10 times that of QCa and 15 times that of AVMV4, Q and QMg. By correlating the increase in the absorbance of the SiOH band to the thickness of altered layer formed and the vapor hydration rate, it seems that there is an inflexion in the vapor hydration rate of all six glasses around approximately 6 months in the given conditions. For the AVM10 glass, it seems that this inflexion occurs at 4 months. In figure 2-8(d), it seems that there is acceleration in the vapor hydration rate between 60 and 120 days of alteration, followed by a strong slowdown of the vapor hydration rate. Figures 2-8(c) shows the strikingly similar behavior of the AVMV4 and QMg glasses. The inflexion seems to occur around 120 days of alteration. There also seems to be a decrease in the absorbance after approximately 380 days of alteration. Figure 2-8(b) shows the evolution of ($A-A_0$) vs. time of the glasses Q and QCa. The inflexion seems to occur approximately around 180 days for the samples Q, QCa and AVM6. The factor by which the rate of increase of ($A-A_0$) drops after six months vary from 7.5 (AVM6) to 15 (AVM10). Figures A2-27-29 in appendix 2 show the evolution of the increase in absorbance of the Gaussian bands associated with the other water related species. The trend of evolution with time is very similar to the evolution of the increase in absorbance associated with the SiOH molecules that were discussed above.

2.3.4.2 Alteration kinetics based on the different measurements of thickness

The measurements of the thickness of the altered layers formed by ToF-SIMS and SEM/TEM images after 180 days and 557 days of vapor hydration of the six glasses are presented in table 2-3. It can be noticed that the thickness measured by ToF-SIMS is lower than the thickness measured by SEM/TEM images for four of the six glasses (AVMV4, Q, QCa and QMg). This is likely due to the fact that in ToF-SIMS, the layer of precipitates and the gel layer might get abraded faster than the pristine sample due to the difference in composition and their lower density. But the same speed of abrasion was used whatever the layer considered. As a result, the thicknesses of the altered layers, which are a combination of the gel layers and precipitate layers, are underestimated. Nevertheless, the thicknesses measured by ToF-SIMS and TEM images are in the same order of magnitude. A second similarity between the thicknesses measured by both techniques is that the sample Q has the smallest thickness among the four samples altered for 180 days and the thickness of the samples Q, QMg and AVMV4 are similar among the samples altered for 557 days. Therefore, it can be stated that the two techniques corroborate each other. In the case of the glasses AVM6 and AVM10, which have an irregular alteration, ToF-SIMS provides an average altered layer thickness in a relatively larger zone (50x50 μm^2) and the SEM/TEM images have shown that the thickness could vary from a few tens of nm to a few µm. The average thickness provided by ToF-SIMS is useful to identify the relative durability of glasses. In addition, according to the FTIR results, the glasses AVM6 and AVM10 alter 10-20 times faster than the other four glasses. This result is very well corroborated by the ToF-SIMS results. While studying the alteration kinetics based on ToF-SIMS and SEM/TEM images, the rate of formation of altered layer (in nm/day) after 180 days and 557 days calculated by assuming linear alteration kinetics shows that the rate has decreased between 180 days and 557 days of vapor hydration. This result is also explained very well by the FTIR spectroscopy, which shows an inflexion in the rate of increase in ($A-A_0$) with time after about 120-200 days of alteration. Thus the alteration kinetics measured by three different techniques are coherent.

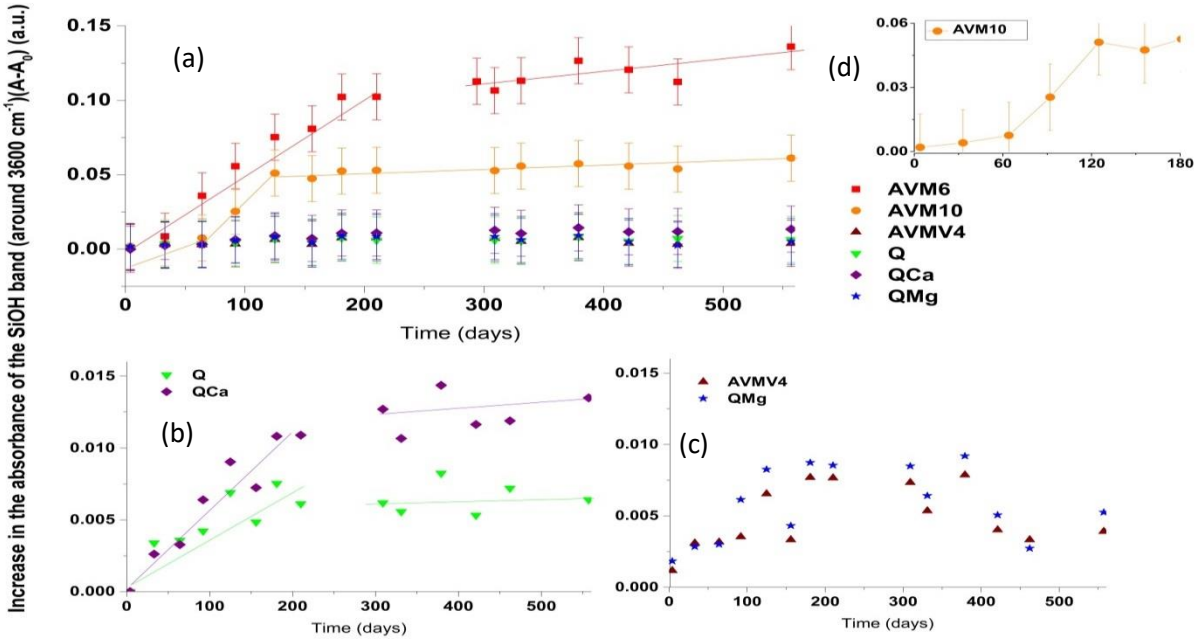

Figure 2- 8 Evolution of ($A-A_0$) with time; (i. e.) The increase in the absorbance of the SiOH band at 3600 cm^{-1} of deconvoluted FTIR spectra of glasses altered at 50°C and 95% RH until 557 days (A) with respect to the absorbance of the SiOH band of the deconvoluted FTIR spectrum of the unaltered glass monolith (A_0). (a) Evolution of ($A-A_0$) for all six glasses; (b) Evolution of ($A-A_0$) of the glasses Q and QCa; (c) Evolution of ($A-A_0$) of the glasses AVMV4 and QMg; (d) A zoom of image (a) to observe closely the evolution of ($A-A_0$) of AVM10 glass until 180 days

2.4 Discussion

2.4.1 Morphology of the altered layer

Figure 2-9 shows a schematic description of the different morphologies of the altered layer for all six glasses altered under the same conditions. All six glasses present a homogeneous gel layer of tens of nm thickness adjacent to the pristine glass. AVM6 and AVM10 present irregularly shaped, discontinuous and more porous altered zones beneath the continuous gel layer. These two glasses contain significant amount of well-developed Mg-rich smectites and needle-shaped precipitates (AVM6 has more of it than AVM10). AVMV4 and QMg also present a layer of poorly-crystalline Mg-rich layer of precipitates on the surface above the gel layer. However, the SEM images have shown that they are present in a much lesser quantity than in AVM6 and AVM10. SEM images have not revealed any irregularly altered zones in these glasses. Q and QCa glasses also contain precipitates on the surface of the gel layer, but unlike in the Mg-containing glasses, they do not cover the glass surface. They are rather present in the form of crystals, which are either isolated or in clusters.

The morphology of AVM6 and AVM10 altered samples is rather surprising, particularly because of the presence of porous irregular altered zones beneath the homogeneous gel layer. Irregular alteration has been noticed in literature [30, 61-63], especially in atmospheric alteration studies. The formation of a heterogeneous altered layer and craters are often attributed to a localized chemical attack due to surface defaults such as cracks/scratches/fissures or deposit of dust particles/matter from exposure to atmosphere or formation of hygroscopic salts locally on the surface or preferential/irregular water condensation [14, 64, 65]. The unexpected part was the presence of the uniform and continuous gel layer in-between phyllosilicates and irregular more porous discontinuous altered zones. A similar dense gel layer formed in-between phyllosilicates and irregular porous zones could not be found in literature. The closest analogy found was the gel layer formed during the aqueous alteration of a Si-B-Na-Ca-Zr glass. In the cited studies, a dense gel layer was present on the altered surface and above a porous gel layer. This denser gel layer was associated with pore-closure with time and passivating effect of the gel layer [121-123]. However, in literature, a denser gel layer close to the unaltered glass and a porous gel layer towards the glass surface and beneath secondary phases have been noticed [124]. Two possibilities can be imagined in our study: (i) The hydration front is irregular; the pore closure due to reorganization of the gel occurs at the surface in the region of the "oldest" gel, as suggested in the above mentioned example [123]. (ii) The denser gel layer and the irregular, more porous, discontinuous altered zones were formed or driven by two different mechanisms. The second assumption seems more likely and is discussed further in section 2.4.5.

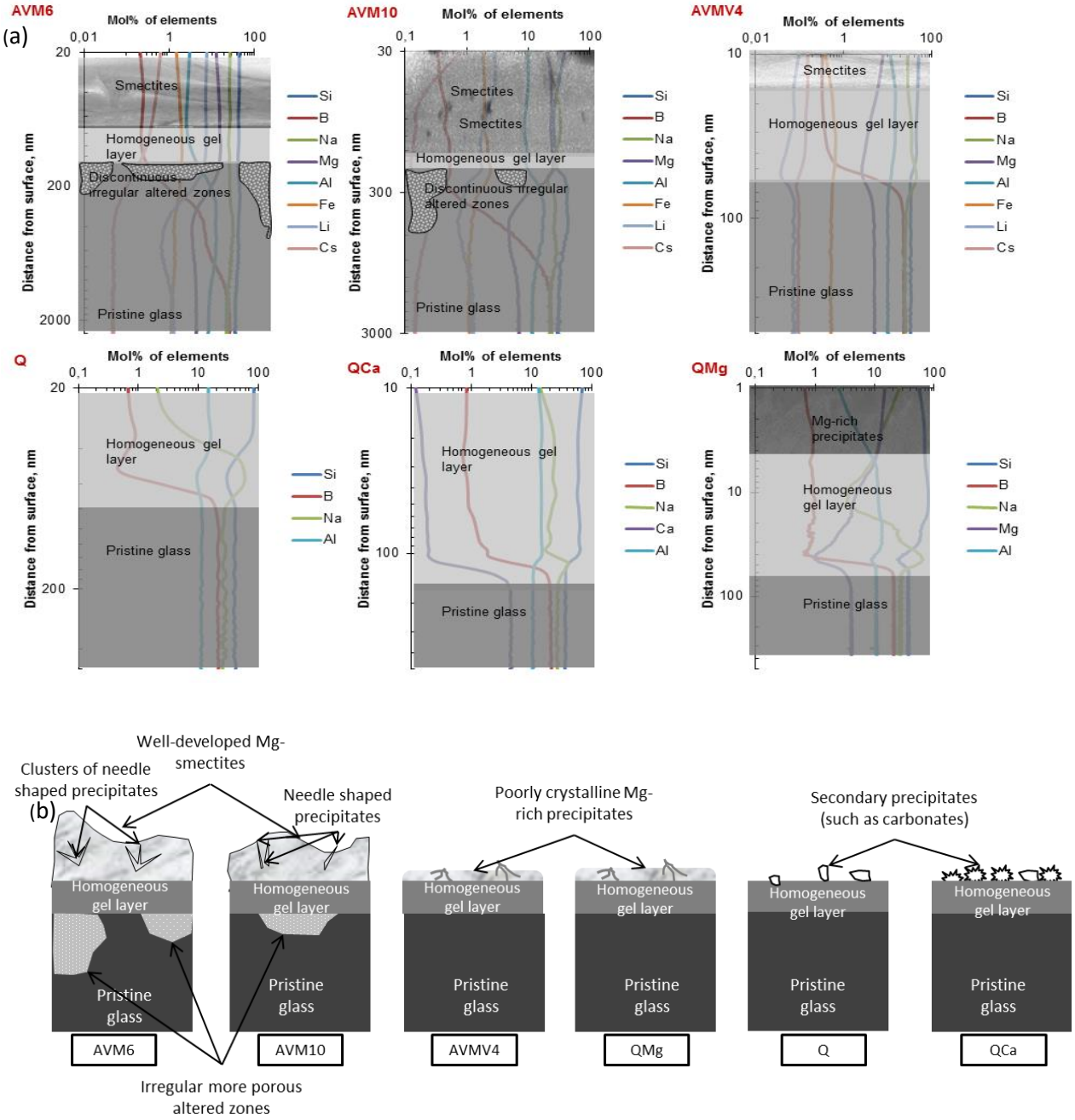

Figure 2- 9 (a) Description of the altered layer morphology of the six glasses that were vapor hydrated at 50°C and 95%RH for 180 days and 557 days; This description was constructed based on TEM images and ToF-SIMS profiles at 557 days; X-axis is the mol% of elements (without considering O) calculated from ToF-SIMS intensities; y-axis is the distance from the surface in nm; The portions of the ToF-SIMS profiles that correspond to pristine glass, homogeneous gel layer and smectites were chosen approximatively by a combined analysis of TEM images and ToF-SIMS profiles; (b) Schematic description of the morphology of the altered glasses

2.4.2 Behavior of elements in the altered zone

Boron is depleted in the gel layer of all six glasses (less than 20% retention). Although it is useful to estimate the altered layer thicknesses from ToF-SIMS profiles, its depletion is puzzling. It would be logical to expect that elements are not lost from the altered layer during vapor phase hydration. The depletion could mean that there is water condensation on glass surface followed by run-off. If this is the case, the loss of other soluble elements such as Na and Li can be expected as well. However, Na is retained to a higher extent than boron as can be seen in figure 2-6. The profiles of B, Na and Li do not resemble each other. Therefore, the possibility of evaporation of boric acid species at 50°C and 95% RH should also be investigated [125, 126].

Hence, a vapor hydration experiment was conducted with 0.6 g of borosilicate glass (QMg) powder of particle size 20-40 µm (90°C, 98% RH, 153 days) using the protocol previously used on glass monoliths by Neeway et al. [26]. The glass powder was placed in a cup inside the reactor above NaCl solution that was used to impose relative humidity. The set-up was arranged in such a way that the water that condenses on glass powders in the cup cannot run-off. Despite the set-up, 0.7±0.1 mg of boron was present in the NaCl solution at the end of the experiment. The vapor hydration rate of QMg at 90°C was estimated based on unpublished results and using this value, it was estimated that 27±6% of boron from the altered layer was lost by evaporation. This experiment shows the possibility of evaporation of boron/boric acid species and indicates that at 50°C, probably only a small fraction of boron escapes due to volatility and a large fraction must be lost due to condensation and run-off.

Ca is depleted to a higher extent than boron in the QCa glass (<2% retention). It can be justified by the formation of calcite crystals on the surface of the glass, which may adhere poorly. For a glass that has only 52 nm thick altered layer, sufficient quantity of calcite had precipitated to be identified in XRD pattern. The depletion of Na towards the surface of the Q glass could probably be due to formation of carbonates (although undetected). In the other glasses, Na is well retained in the gel layer. In figure 2-6, a certain similarity can be observed in the profile of Na and H for all glasses. This suggests that Na is reactive and might be linked to inter-diffusion reaction. Despite being probably released from the glass network, Na is still well retained in the gel layer (except in Q). It may be present in porewater, form precipitates or may participate in the hydrolysis of ≡Si-O-Si≡ bonds to form ≡Si-O^-…Na^+ bonds, as suggested in literature [33].

2.4.3 Porosity of the altered layer

During the SAXS data treatment, it was assumed that the pores in the gel layer are filled with water. This assumption is supported by the calculation of the threshold pore-size by Kelvin's equation (equation 2.4.3.1) [127], below which, water is expected to condense in pores due to capillary effect. This threshold pore-radius was calculated to be 9.2 nm at 50°C and 95% RH from equation 2.4.3.1. The maximum value of the pore-radius measured through SAXS is <4 nm. Therefore, it seems highly probable that the pores are filled with water. The porosity of the gels was also calculated by considering that the pores are filled with air, but in this case, the calculated porosity values were unrealistic. This further reinforces our assumption that the pores are filled with water. However, a certain uncertainty is associated with this assumption. Even if it is considered that the pores are indeed filled with water during the experiment, it is unclear if the water stays in the pores during characterization or it evaporates/escapes into the atmosphere once the sample is removed from the humid and hot atmosphere (95% RH & 50°C). Data analysis has been carried out despite this uncertainty by considering that water remains inside the pores, since the samples were not exposed to high temperatures or desiccators during storage until characterization. Specific studies to carefully assess the impact of this uncertainty on data treatment are a necessary perspective.

$$\ln\frac{P}{P_0} = -\frac{2H\gamma V_l}{RT}$$ Equation 2.4.3.1

The values of the porosity, specific surface area of the pores and the pore-radiuses are in the same order of magnitude as those observed in published aqueous alteration experiments of borosilicate glasses [109, 128, 129]. 66% porosity of the gel layer of Q-180 and AVM6-11 (table 2-4) seem relatively high, especially while comparing with TEM images of Q-180, which do not show a very porous altered layer. This means that either the porosity measured by SAXS is overestimated or there is some other unknown mechanism that could explain such high porosity values, which needs further investigation of the gel layer formed on these glasses. This porosity value may be overestimated due to the volume fraction of gel used in data treatment, which is reasonably assumed based on altered layer thicknesses of the gel layer formed on monoliths. This being said, such high porosity values have also been reported during aqueous alteration of glasses [109, 129].

From table 2-4, all three glasses show a decrease in porosity and surface area of pores with time and an increase in the average pore size with time. This evolution in our vapor hydration study is similar to the results of an aqueous alteration study conducted by Girard et al.,

who altered glasses containing Si, B, Na, Ca and Zr in aqueous medium at an SA/V (surface area of glass/solution volume) ratio of 3000 m^{-1} at 90°C for time periods up to 96 h [129]. According to their results, the porosity, depending on composition, increased rapidly to a maximum value within a few hours of glass alteration. After reaching maxima, the porosity and specific surface area of pores decreased with increasing time of alteration, probably due to a shrinking gel and the pore-size increased due to either coalescence of pores or further dissolution at the pore walls. The initially high porosity after a few hours of glass leaching was attributed to leaching of Si from the solution without re-condensation until the solution becomes saturated with respect to Si. This theory was based on the calculation of an estimated porosity from leachate composition. In this study, the leachate cannot be sampled since it is a vapor phase alteration. Therefore, an acceptable estimated porosity cannot be calculated using the leached fraction of soluble elements such as B and Na, as was done in literature [129]. However, an estimated porosity was calculated based on the retention factor R of elements in the gel layer calculated from ToF-SIMS profiles of monoliths and the volume fraction occupied by oxides $\emptyset_i$ as shown in section 8 of the appendix 2.

The estimated porosity values thus calculated vary between 14% and 25% (table A2-1-appendix 2). For all six glasses, the estimated porosity value at 557 days is less than the estimated porosity value at 180 days. This decrease in this estimated porosity is coherent with the SAXS results. Nevertheless, the values of porosity calculated by SAXS for the glass Q is 3.2 to 3.9 times higher than the hypothetical values estimated by depleted elements (based on ToF-SIMS results). It can be supposed that the porosity estimated by retention of elements in the gel layer calculated based on ToF-SIMS analysis is probably underestimated, because it considers that the elements present in the porewater of the gel layer are a part of the gel layer network. There is the possibility of overestimation of porosity values by SAXS as well. In the cases in which the SAXS porosity is lower than the porosity estimated from SIMS data, different hypotheses such as a shrinking gel or precipitation of colloids or secondary phases (calcite) in the pores could be proposed based on literature [129, 130].

2.4.4 Hydration Kinetics

Overall, the relative durability of the glasses identified by the increase in absorbance of the SiOH molecules in FTIR spectra are coherent with that measured by other characterization techniques. These results reinforce the argument that FTIR spectroscopy is a good method to follow vapor hydration kinetics, in the absence of sampling techniques to determine soluble element concentrations in the leachate. All glasses showed an inflexion in the vapor hydration

kinetics after 120 or 180 days of alteration. The cause for this inflexion has not yet been investigated. But such inflexion has been observed earlier in literature, notably in the experiments conducted on CSD-B (inactive simulant of intermediate-level long lived waste glass) and SON68 glasses after about 100-200 days of alteration (at 35-90°C) [27, 53].

2.4.5 Influence of glass composition and insights into vapor hydration mechanisms

The difference in the vapor hydration kinetics of AVM6, AVM10 and AVMV4 is an indication of the significant effect of glass composition on glass hydration. The effect of stoichiometry on the relative durability of AVM glasses in aqueous medium was already investigated [96, 97]. According to these studies, the three major parameters affecting glass durability in water under a given condition were pH, Mg and Al concentration. When $pH_{50°C}$>9, alteration rates increase due to precipitation of Mg-aluminosilicates. Moreover, AVM glasses contain very little Ca. Therefore, it is considered that the role of charge compensating atoms of $[AlO_4]^-$ units is preferentially occupied by Mg (the preference in gels decreases in the order Ca^{2+}>Mg^{2+}>Na^+). Thus, a higher quantity of Al in the gel layer probably retains higher quantity of Mg in the gel, thereby, increasing the passivation properties of the gel layer [96, 97]. This interpretation was used to explain the highest relative durability of AVM10 glass in aqueous medium, since it contains the highest Al concentration among the three glasses.

In our vapor hydration study, AVM10 glass is one of the two least durable glasses. Therefore, the glass durability is not simply linearly dependent on Al concentration. The reason for this could be that the AVM10 glass contains higher MgO molar concentration than Al_2O_3 (i.e. molar ratio of Al_2O_3/MgO<1). Therefore, as an extreme case, if it is considered that all the $[AlO_4]^-$ units in the gel layer are charge compensated by Mg^{2+} ions, there is still an excess of Mg that can saturate the molecular water layers/porewater to form Mg-silicates, thus driving the glass alteration. The difference in the relative durability of AVM10 between aqueous medium and vapor phase could be due to the possibly higher pH of the very small volume of water in vapor phase, thereby promoting the precipitation of Mg-silicates during vapor hydration and not as much during aqueous alteration.

The lower durability of AVM6 glass in this vapor hydration study can also be explained using the same interpretation (i.e. molar ratio of Al_2O_3/MgO<1). The extensive alteration of AVM6 and AVM10, which is manifested as irregularly altered zones, could be driven by the precipitation of a significant amount of Mg-silicates. On the other hand, this ratio is equal to 1 for AVMV4 and is greater than 1 for QMg, suggesting that, Mg could be principally occupying the

role of charge compensating atom and therefore be less available for participation in the formation of secondary phases. As a result, the vapor hydration of these two glasses may not be accelerated due to the precipitation of Mg-silicates.

The lack of structural study to support this assumption definitely needs to be acknowledged. The distribution of coordination number of Al in the gel layer was not studied. Incidentally, recent publications have shown that due to the high cation field strength of Mg, the presence of this element in the glass network increases the fraction of $^{(v)}$Al and $^{(vi)}$Al and $^{(iii)}$B, and thus contributes to glass depolymerisation [131, 132]. As a matter of fact, the fraction of $^{(iv)}$B in the Mg containing glasses in our study were lower than that in the glasses Q and QCa (section 2.2.1). It is also suggested that some of the Mg could be acting as a network former [132]. Therefore, there is a need to better understand the role of Mg in the glass as well as in the gel, its impact on the gel structure and especially the competition between ions to compensate the charge of $[AlO_4]^-$ units.

In order to understand the specific effect of Ca and Mg on vapor hydration of glasses, the results of the simplified glasses Q, QCa and QMg need to be focused upon. Table 2-3 shows that QCa and QMg alter 1.6 to 1.7 times faster than Q, among the samples altered for 180 days. This can be construed to be a negative effect of Ca and Mg, due to the precipitation of calcite and Mg-rich precipitates. However, the NBO fraction (table 2-1) indicates that these two glasses have higher fraction of NBOs than the glass Q. From figure A2-23 in appendix 2, it can be seen that, among the glasses altered for 180 days, the higher the NBO fraction, the higher the thickness of the altered layer formed. This relation seems to be linear for the glasses AVMV4, Q, QCa and QMg and a sharp rise is noted for the glasses AVM6 and AVM10, which have undergone extensive alteration due to secondary phases precipitation. Therefore, the slightly higher altered layer thicknesses of the glasses QCa and QMg in comparison to Q could be due to the lower resistance to network hydrolysis and not a negative effect of Ca or Mg. This suggests that network-hydrolysis could be the rate limiting mechanism of formation of the uniform gel layer.

Among the samples altered for 557 days, the altered layer thickness of QCa is twice that of Q and QMg. This change in the relative durability of glasses with a longer duration can be explained by considering the presence of a passivating altered layer. The SAXS results also hint at a reorganization of the homogeneous gel layer, at least in the case of Q, QCa and AVM6. The inflexion in the vapor hydration kinetics (FTIR spectroscopy) after 180 days approximately strongly suggests the presence of a passivation mechanism of the gel layer in all six glasses. After six months, the altered layer of QMg (and AVMV4) could have become more passivating

than that of Q and QCa. This presumption is based on ToF-SIMS profiles, which show that the retention of Ca in the gel layer is less than 1% and Na is less retained in the gel layer of Q. The gel layer of QMg (and AVMV4) retains a higher quantity of Mg. It has already been shown that the retention of Mg increases the passivation properties of the gel layer [97]. This implies that the rate-limiting vapor hydration mechanism changes, probably to diffusion of species through the gel layer, after the inflexion of vapor hydration rate due to the formation of a passivating altered layer. This is in agreement with the structure discussion above for AVMV4 and QMg.

In brief, the specific effect of Ca or Mg could not be seen in this vapor hydration study because the excessive concentration of Al (molar ratio of Al_2O_3/(MgO or CaO) ≥ 1) has masked the possible negative effect that Ca or Mg could have due to secondary phase precipitation. The presence of Al in the glass increases its resistance to network hydrolysis since ≡Si-O-Al≡ bonds require more energy to be broken than ≡Si-O-B- or ≡Si-O-Si≡ bonds [37, 133].

The interpretation of the results suggests that the rate-limiting mechanism of formation of the gel layer in vapor hydration is network hydrolysis in this study. This conclusion is reinforced by the fact that AVM10, which has the highest Al content in the pristine glass, has the lowest thickness of the homogeneous gel layer (15-30 nm in TEM), even if the overall alteration layers cumulate to larger thickness after secondary phases form.

The formation of irregularly shaped (few tens of nm to few µm thick), discontinuous, more porous altered zones behind the homogeneous gel layer in AVM6 and AVM10 glasses seem to be driven by precipitation of significant quantities of Mg-silicates. During vapor hydration, extensive alteration due to secondary phase precipitation is naturally local (and hence irregular). Thus, it is possible that in AVM6 and AVM10, the two types of altered zones were formed by two parallel mechanisms.

The precipitated secondary phases found at the surface in the other four glasses (AVMV4, Q, QCa and QMg) are probably a consequence of the release of alkaline-earth elements from glass network and do not drive the formation of their homogeneous gel layer.

2.4.6 Vapor hydration vs. aqueous alteration

Glass AVM6 was found to be the glass of lowest durability of the series in aqueous leaching and in the present vapor phase alterations. However, a reversal of glass durability in vapor phase and aqueous medium has been observed between the glasses AVM10 and AVMV4. The residual alteration rates of the three complex glasses in aqueous medium (initially pure water, 50°C, SA/V=5500 m^{-1}, values measured between 5-10 years of alteration) are: AVM6- 5.1×10^{-4} g/m^2/day; AVM10- 9×10^{-5} g/m^2/day; [97]; AVMV4- 5.6×10^{-4} g/m^2/day (personal

communication-value estimated based on a statistic interpolation model). The difference may be due to changes in the solution chemistry of the very low volume of water available for glass dissolution in vapor phase. This small volume of water may get rapidly saturated with respect to secondary phases that are clearly different than those that precipitate during aqueous alteration.

The smectites formed during vapor hydration, as identified through STEM-EDX analyses (see sub-section 2.3.1.1), seem to be different than those that form during aqueous alteration of the same glasses. A tri-octahedral smectite was identified on AVM6 altered in aqueous medium [97], while a di-octahedral smectite (type montmorillonite) was identified during this vapor hydration study of AVM6. The phyllosilicate formed in vapor phase contained 75% lower Al, 40% lower Mg and 10 times higher Fe content.

The phyllosilicate composition obtained on AVM10 in this study was compared with the phyllosilicate composition obtained during the aqueous alteration of AVM10 in the study conducted by Thien et al. (SA/V 5500 m^{-1}, 50°C, 2500 days, initially pure water and 400 mg/L of $MgCl_2.6H_2O$ added after 114 days) [134]. The concentration of Al in the phyllosilicate of our study was 25% lower than the Al concentration in the smectite identified by Thien et al [134]. Similarly, the concentration of Mg was 30% lower and the concentration of Fe was three times higher.

This shows that caution needs to be taken while extrapolating aqueous alteration results to vapor hydration by considering that vapor hydration is equivalent to aqueous alteration at a very high SA/V ratio. Certain studies conducted vapor hydration tests in extreme conditions (150-200°C, 100% RH) to predict the secondary phases that would form during long-term aqueous alteration of glasses [19]. Here, it is clearly shown that the same phases do not precipitate in both media. However, in a recent aqueous alteration study conducted in CEA on the three AVM glasses in a solution known as S3 (rich in Ca, SO_4, Na, Si, Cl etc.), it was also observed that the residual glass alteration rate of the AVM10 glass was higher than the AVMV4 glass [135]. This shows that the relative glass durability can be reversed even among different aqueous alteration experiments depending on the experimental conditions.

One similarity between aqueous alteration and vapor hydration studies of glasses is the texture of the gel layer. SAXS data indicated that the porosity, pore-size and specific surface area values are in the same order of magnitude and evolve similarly with time in the two glasses of different compositions and in different alteration conditions [128, 136]. This could imply a similar mechanism of formation of the gel layer.

2.5 Conclusion

In order to study the influence of glass composition on vapor hydration kinetics, three complex glasses (>20 oxides) and three simplified glasses (4 or 5 oxides) were altered in vapor phase (at 50°C and 95% RH) for a period of 180 days and 557 days. Based on the analysis of the characterization results of the altered samples, it seems that network hydrolysis is the rate limiting mechanism of formation of the gel layer during vapor hydration of these glasses. Under conditions that are favorable for the precipitation of secondary phases, it seems that the vapor hydration kinetics is accelerated in a localized manner, leading to the formation of irregularly shaped, discontinuous altered zones that could be up to a few µm thick. The presence of alkaline-earth elements (such as Mg or Ca) seems to make the glass more reactive, since they actively participate in the formation of secondary phases. However, the negative effect of these elements is attenuated by the presence of Al, since Al increases the resistance to hydrolysis of glass network and its presence in the gel layer retains alkaline-earth elements to compensate $[AlO_4]^-$ entities. Therefore, when the molar ratio of Al_2O_3/(MgO or CaO)≥1, the positive effect of Al prevails over the expected negative effect of Ca or Mg and therefore the glass is relatively more durable. When the ratio is <1, the negative effect of Ca or Mg prevails. For this reason no specific effect of Ca or Mg on vapor hydration of the three simplified glasses could be seen (molar ratio of Al_2O_3/(MgO or CaO)≥1).

Apart from this principal result, two types of altered layer morphologies have been identified. The porous texture of the gel layer of a vapor hydrated glass has been investigated using SAXS. The measured pore-diameters vary between 4.3-7.5 nm, similar to the pore-sizes found in the gel layer formed on various similar glasses during aqueous alteration.

It has been shown that the vapor hydration mechanism changes with glass composition and time. The rate of vapor hydration evaluated in FTIR showed a decrease between 180 days and 300 days, which validate the formation of a passivating layer.

Chapter 3 Complementary studies to gain insights into vapor hydration mechanisms

3.1 Introduction

The effects of temperature and relative humidity on vapor hydration of glasses are relatively well-known [26, 29, 56]. In general, glass hydration rate increases both with temperature and relative humidity. Glass hydration rate may follow an Arrhenius law for temperature dependence and the diffusion rate of water can increase exponentially with increasing relative humidity. But studies have shown that glass response to these parameters can vary depending on the glass composition. For example, in a study conducted on an alkali-aluminosilicate glass, a thicker hydrated layer was formed on the glass altered at 20°C and 70% RH for 3 months (350 nm) than at 50°C and 76% RH for 4 months (230 nm) [70]. This highlights the need to specifically study the response of each glass composition to these variable parameters to predict with good accuracy the glass alteration rates of the nuclear waste glasses in the geological repository. The influence of these parameters can also affect the influence of glass composition on vapor hydration. It is likely that this will be the case for the effect of temperature on the influence of glass composition since temperature and secondary phase precipitation kinetics are closely associated.

As can be seen from the conclusions of chapter 2, a specific effect of Ca or Mg could not be identified at 50°C and 95% RH due to the presence of Al, which suppressed the suspected negative effect of Ca or Mg. From literature review it is also strongly suspected that the rate-controlling vapor hydration mechanism is different at low temperatures (35°C-90°C) and high temperatures (120°C-200°C) [53]. For this reason, it was decided to investigate the effect of temperature on the vapor hydration of the glasses AVM6, Q, QCa and QMg and also to observe if the influence of glass composition varied with temperature. The section 3.2 discusses the effect of temperature on these four glasses.

The effect of relative humidity was studied at 50°C on AVM6 glass. The choice of the glass was based on the fact that this glass would alter relatively quickly at a short duration. This is discussed in section 3.3.

In recent literature, the use of isotopes such as ^{18}O, D, ^{29}Si etc. to identify the mechanisms of formation of the gel layer has proved to be very useful [32, 137, 138]. As an

exploitation of a valuable opportunity presented to us due to inter-laboratory collaboration with Laboratoire Interuniversitaire des Systèmes Atmosphériques (LISA), the mechanisms of formation of the gel layer was investigated on four out of the six glasses in this thesis. The chosen glasses were altered in vapor phase that was isotopically enriched in D and ^{18}O at 20°C and 90%RH at LISA. These results are discussed in section 3.4.

3.2 Effect of temperature

3.2.1 Experiment

1. The three simplified glasses Q, QCa and QMg were altered in vapor phase at two different temperatures (90°C and 120°C) and 95% RH for 91 days. The protocol of alteration is described in figure 3-1. Glass monoliths of dimensions (2.5x2.5x0.1 cm^3) were placed vertically in a Teflon walled stainless steel autoclave above 8 wt% NaCl solution, which imposes the 95% RH relative humidity [139]. The autoclave is placed inside an aluminum cylinder to prevent rapid heating and cooling cycles, which might induce water condensation on the glass monoliths. The setup was then placed in an oven at 90°C or 120°C.

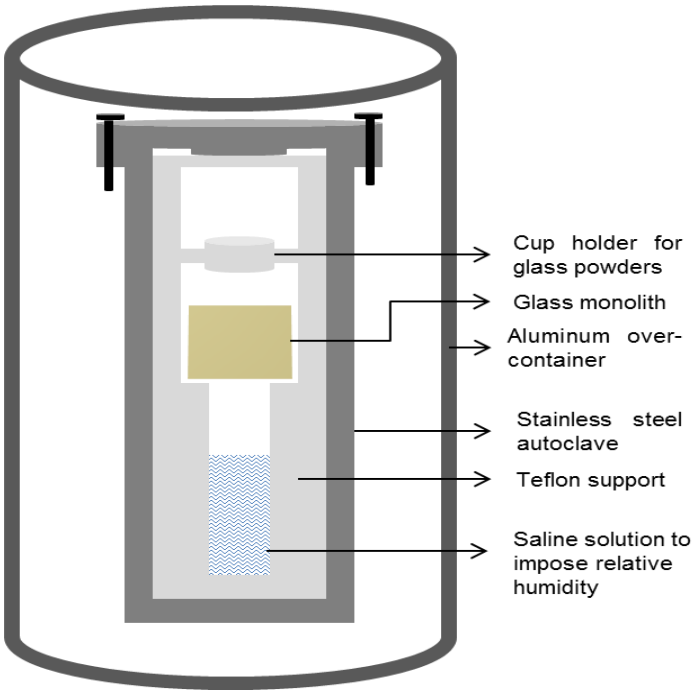

Figure 3- 1 Protocol used for glass alteration in vapor phase; Schematic description based on reference ([68])

At the end of three months, the reactors were removed from the oven, allowed to cool to ambient temperature and then the monoliths were stored in ambient conditions until

characterization. The altered surfaces were characterized using Scanning Electron Microscope (SEM), X-Ray Diffraction (XRD) and Time-of-Flight-Secondary Ion Mass Spectrometry (ToF-SIMS). Refer to Appendix A for information on characterization techniques.

2. The AVM6 glass was altered in vapor phase at 70°C and 90°C for a period of 1 year. The same protocol of glass alteration in vapor phase that is described above was used for the AVM6 glasses as well. 5.25 wt.% NaCl solution was used to impose a relative humidity of 97%. At the end of the experiment, the monoliths were characterized using SEM, XRD and ToF-SIMS.

The glass compositions and preparation of samples have already been described in chapter 2, section 2.2.1.

3.2.2 Results

3.2.2.1 Simplified glasses (altered at 90°C & 120°C)

SEM images

Figure 3-2 shows the SEM images of the altered surface of the Q, QCa and QMg glasses after vapor hydration for 91 days at 95% RH and 90°C/120°C. In all cases, the surface was covered with secondary precipitates. The type of secondary phases varied with both temperature and glass composition. Since the vapor hydration protocol used NaCl to control the relative humidity, NaCl crystals had precipitated on the surface of all three glasses altered at 120°C (XRD patterns), but was not detected on the glasses altered at 90°C. Carbonates of sodium were identified through SEM on the altered surface of the glasses Q and QCa altered at 90°C, but were not detected by XRD patterns. Ca-carbonate was also identified on the QCa glass altered at 90°C. The surface of the Q glass altered at 120°C only showed NaCl crystals. The SEM image of QCa glass altered at 120°C shown in figure 3-2 shows the presence of few fibrous precipitates, but they could not be identified. The QMg glasses altered at both temperatures did not show any carbonates. But the type of secondary precipitates varied with temperature. The QMg glass altered at 90°C showed the presence of leafy precipitates clustered in a circular form, whereas the QMg glass altered at 120°C did not show any circular precipitates, but instead showed the presence of secondary precipitates of a dendritic morphology and some NaCl crystals.

Figures A3-1, 2 & 3 shown in Appendix 3 shows the SEM images of cross-sections of the three glasses altered in two temperatures. The thicknesses of the altered layers that could be measured from these images are provided in table 3-1. EDS analysis of pristine glasses and gel

layers show that the gel layers of all glasses altered at both temperatures are strongly enriched in carbon (figures A3-1, 2 and 3).

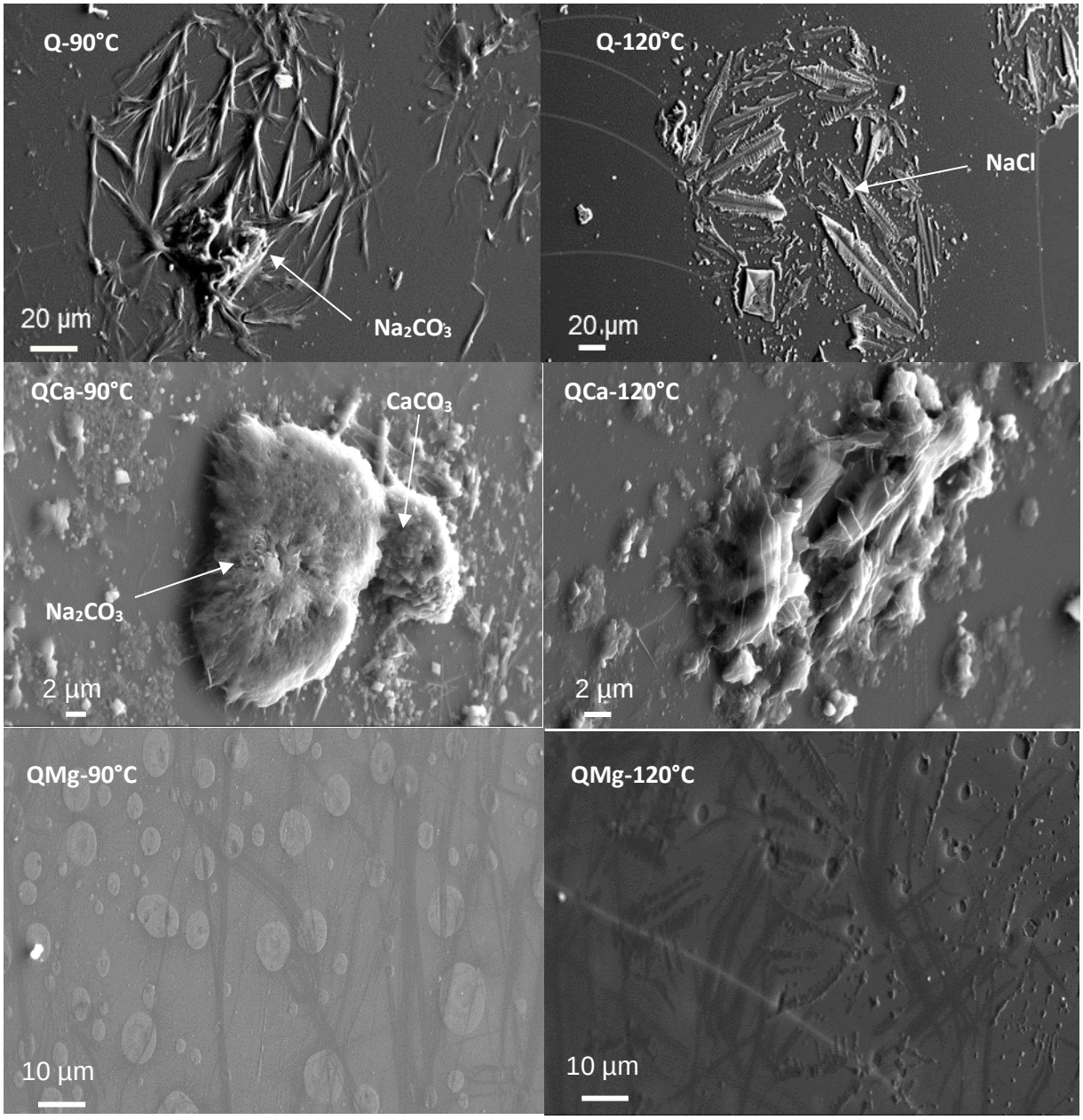

Figure 3- 2 SEM images of the three simplified glasses Q (top), QCa (center) and QMg (bottom) altered in vapor phase at 95% RH and 90°C (left) and 120°C (right) for 91 days

XRD patterns

The XRD pattern of the Q glass (figure 3-3) altered at 90°C showed the presence of peaks that could be attributed to aluminosilicate hydroxides. The XRD pattern of the QCa glass

altered at 90°C confirmed the presence of calcite and indicated the presence of chlorite ($Al_{4,5}(Al_{0.8}Si_{3,2})O_{10}(OH)_8$). Although the SEM images of QMg altered at 90°C showed the presence of secondary precipitates, no peaks were present in the XRD pattern. This could be due to either low quantity of secondary phases or poor crystallinity. The XRD patterns of the Q and QCa glasses altered at 120°C show only intense peaks for NaCl. The XRD pattern of the QMg glass altered at 120°C shows the presence of aluminosilicates in addition to NaCl.

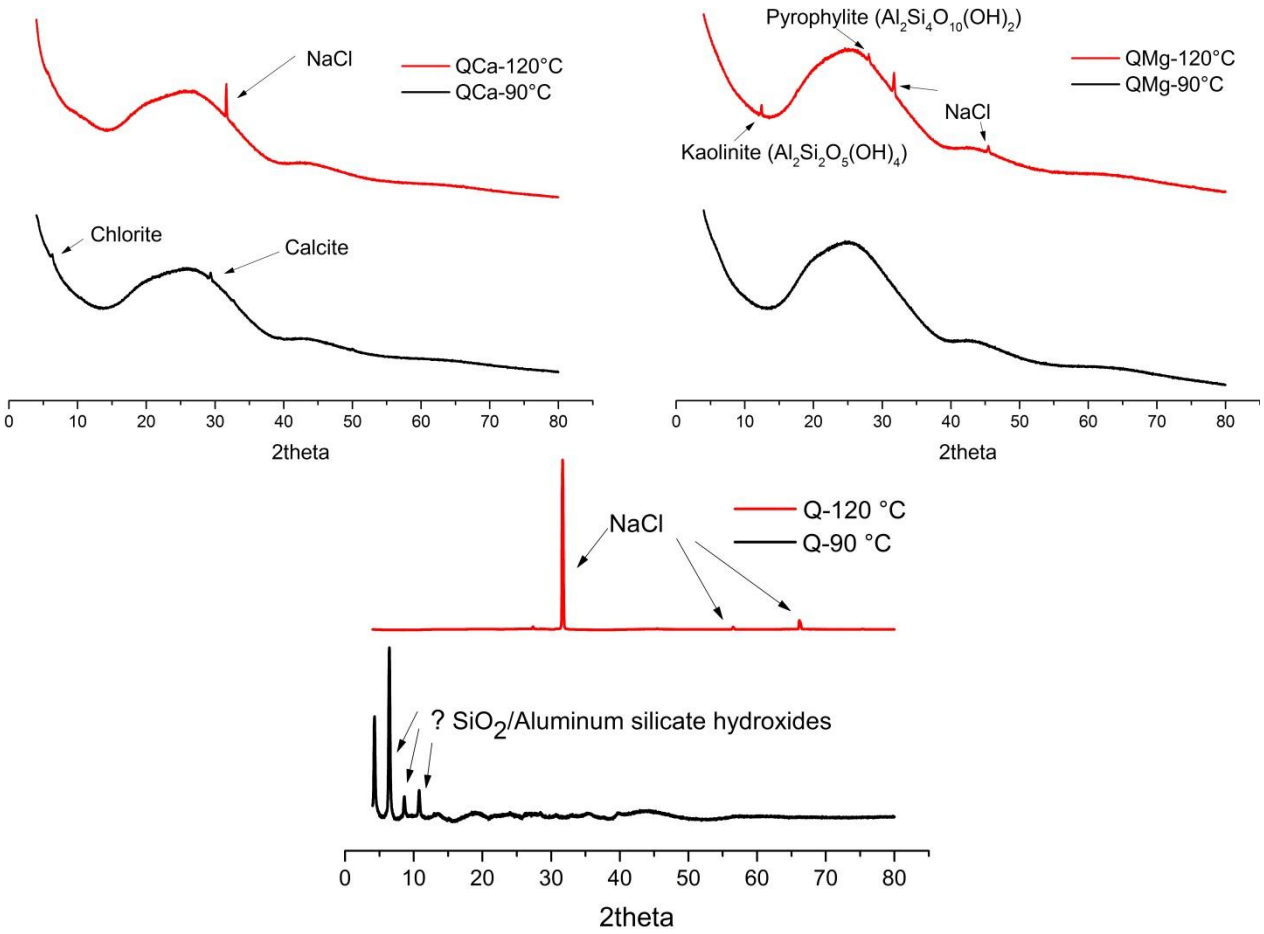

Figure 3- 3 XRD patterns of the Q, QCa and QMg glasses altered at 95% RH and 90°C and 120°C for 91 days

ToF-SIMS profiles

Figure 3-4 shows the ToF-SIMS profiles of Q, QCa and QMg glasses altered at 90°C and 120°C. The thickness of the gel layer is identified through the depletion of boron. This thickness is only slightly lower than the thickness of hydrogen penetration. The boron depletion in the glasses Q, QCa and QMg altered at 90°C is more uniform throughout the gel layer (90-98% depletion), whereas the boron depletion is higher towards the surface than the gel-glass interface in the gel layers formed on the glasses altered at 120°C (80-99% depletion). The gel

layer-pristine glass interface identified through boron depletion is quite sharp, suggesting that the gel layers are homogeneous in thickness. This has also been verified from SEM images. Table 3-1 compares the thicknesses of the gel layer measured by SEM images and ToF-SIMS profiles and shows that they are in same order of magnitude and within error associated with thicknesses that can be expected from ToF-SIMS measurements, except QMg glass altered at 120°C.

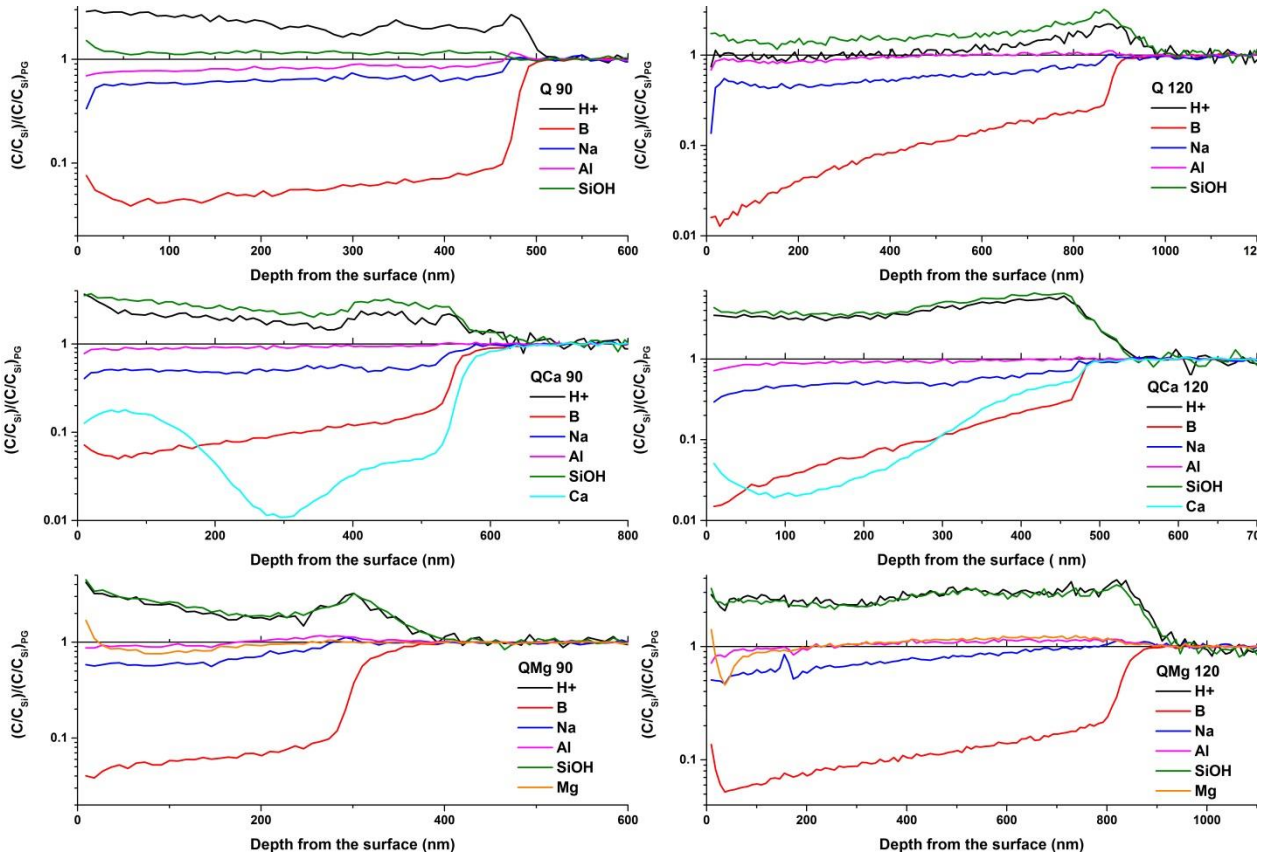

Figure 3- 4 ToF-SIMS profiles (normalized with respect to the intensity of Si and pristine glass) for the glasses Q (top), QCa (center) and QMg (bottom) altered in vapor phase at 95%RH and 90°C (left) and 120°C (right) for 91 days

Table 3- 1 Thicknesses of the gel layers formed during vapor hydration of Q, QCa and QMg at 95% RH and 90°C and 120°C for 91 days as measured from SEM images and ToF-SIMS profiles; (The ToF-SIMS thicknesses are based on the depth of boron depletion)

	90°C		**120°C**	
	Thickness (SEM), nm	**Thickness (ToF-SIMS), nm**	**Thickness (SEM), nm**	**Thickness (ToF-SIMS), nm**
Q	620	480	960	880
QCa	585	550	500	470
QMg	310	310	1200	830

For the Q and QCa glasses altered at 90°C and 120°C, the Na profiles indicated that the gel layer was uniformly depleted in Na (by ~50%). For the QMg glasses altered at 90°C and 120°C, Na was more depleted towards the surface of the gel layer than the gel-pristine glass interface (~40-50% depletion). Globally, Al seemed to be well-retained in the gel layer in all glasses altered at both temperatures. The behaviors of the alkaline-earth elements (Ca or Mg) vary in the glasses QCa and QMg. While Ca is significantly depleted in the gel layer of the QCa glass altered at 90°C and 120°C, Mg is well retained (almost 100%) in the gel layers formed on the QMg glasses altered at both temperatures. For the QCa glass altered at 90°C, Ca is more depleted than boron (96-99% depletion) in the part of the gel layer close to the gel-glass interface and is depleted to a lesser extent towards the surface of the gel layer (90% depletion). One of the reasons for this type of profile for Ca could be the migration of Ca towards the surface to form precipitates (calcite). In the QCa glass altered at 120°C, Ca was less depleted than boron in the gel-glass interface. Based on XRD patterns and ToF-SIMS profiles, it does not seem that Mg in the QMg glasses is involved in secondary phase precipitation.

3.2.2.2 AVM6 glass (altered at 70°C and 90°C)

SEM images

The SEM images of the AVM6 glass altered at 97% RH and 70°C and 90°C are shown in figure 3-5. The surface of AVM6 glass altered at 70°C was covered with clusters/carpets of leafy secondary phases that were of an amoeboid shape. On the other hand, the surface of AVM6 glass altered at 90°C was covered entirely with a carpet of leafy secondary phases. The leafy precipitates on the surface of the sample altered at 90°C visually seems better developed than the leafy precipitates on the surface of the sample altered at 70°C. The altered surface of both samples seemed to be covered with holes of a few hundred nm in size. The AVM6 glass altered at 90°C seemed to have more of these holes. The SEM image of the cross section of the AVM6 glass altered at 70°C shows a homogeneous gel layer of 290-350 nm thickness. In the zone characterized by SEM, no holes were identified in the cross-sections. The SEM images of cross-sections of the AVM6 sample altered at 90°C shows the presence of numerous mushroom shaped holes that are a few µm deep and wide (also see figure A3-5 in appendix 3). Above these holes, the surface was covered with a gel layer of homogeneous thickness of about 1 µm.

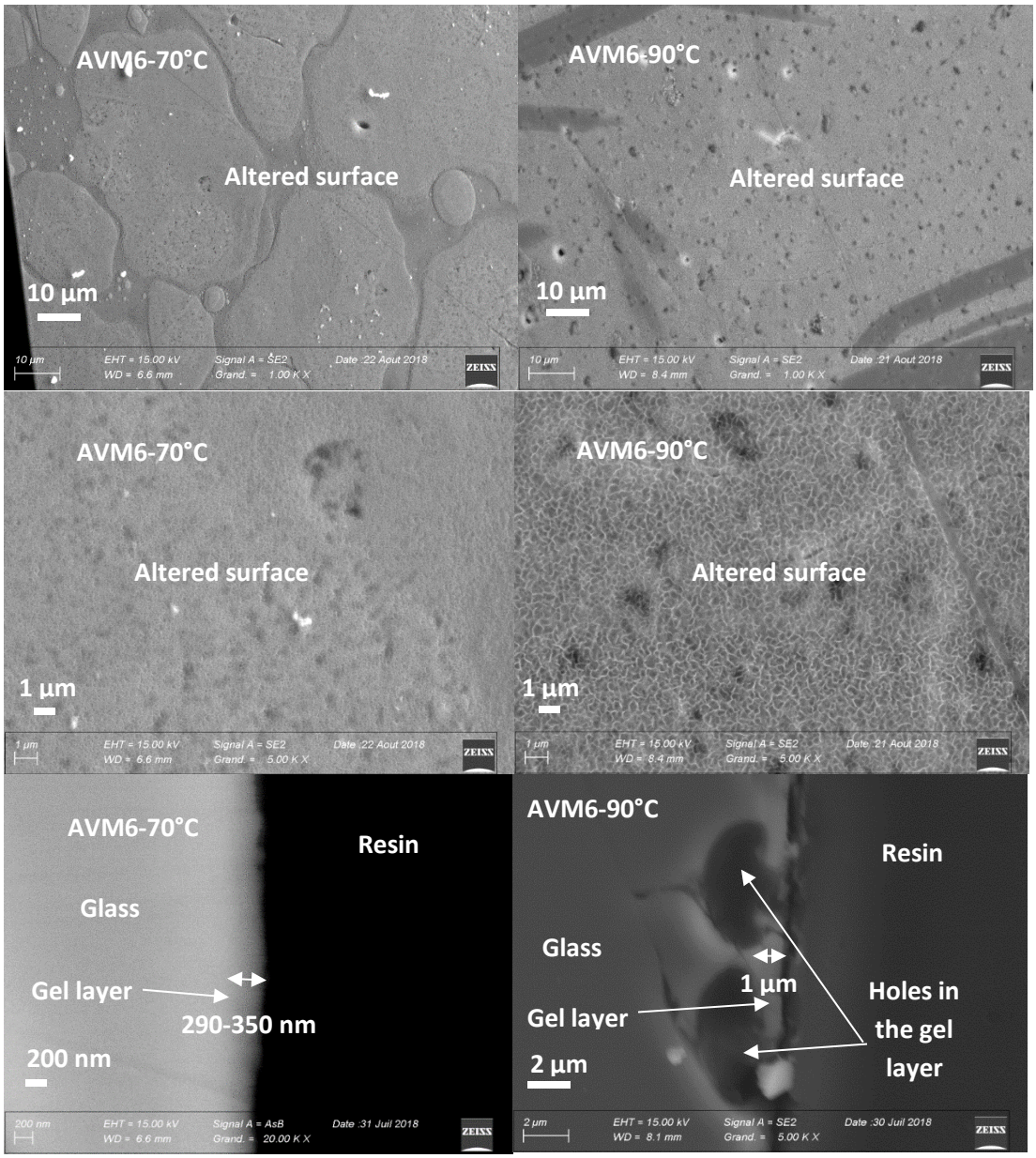

Figure 3- 5 SEM images of AVM6 glass altered in vapor phase at 70°C (left) and 90°C (right) and 97% RH for 1 year. The top and middle images are direct observations of the altered surface while the bottom images show the cross-sections of the altered samples

XRD patterns

The XRD patterns of the AVM6 glasses altered at 70°C and 90°C are provided in figure 3-6. Although the protocol used for vapor hydration at 70°C and 90°C used NaCl to impose relative humidity, no peaks to indicate the presence of NaCl were identified. The sample altered at 90°C showed the presence of a small peak around 20° (2θ) (around 4.5 Å in d-scale) and 24.5° (2θ) (around 3.6 Å in d-scale) that indicates the presence of alumino silicates. The AVM6

glass altered at 70°C did not show any peaks other than RuO_2 (platinoids that did not get incorporated in the network during glass preparation). However, the background subtracted XRD pattern seemed to contain peaks merged with the background noise around the same region (20° and 24.5° (2θ)) (see figureA3-6 in appendix 3).

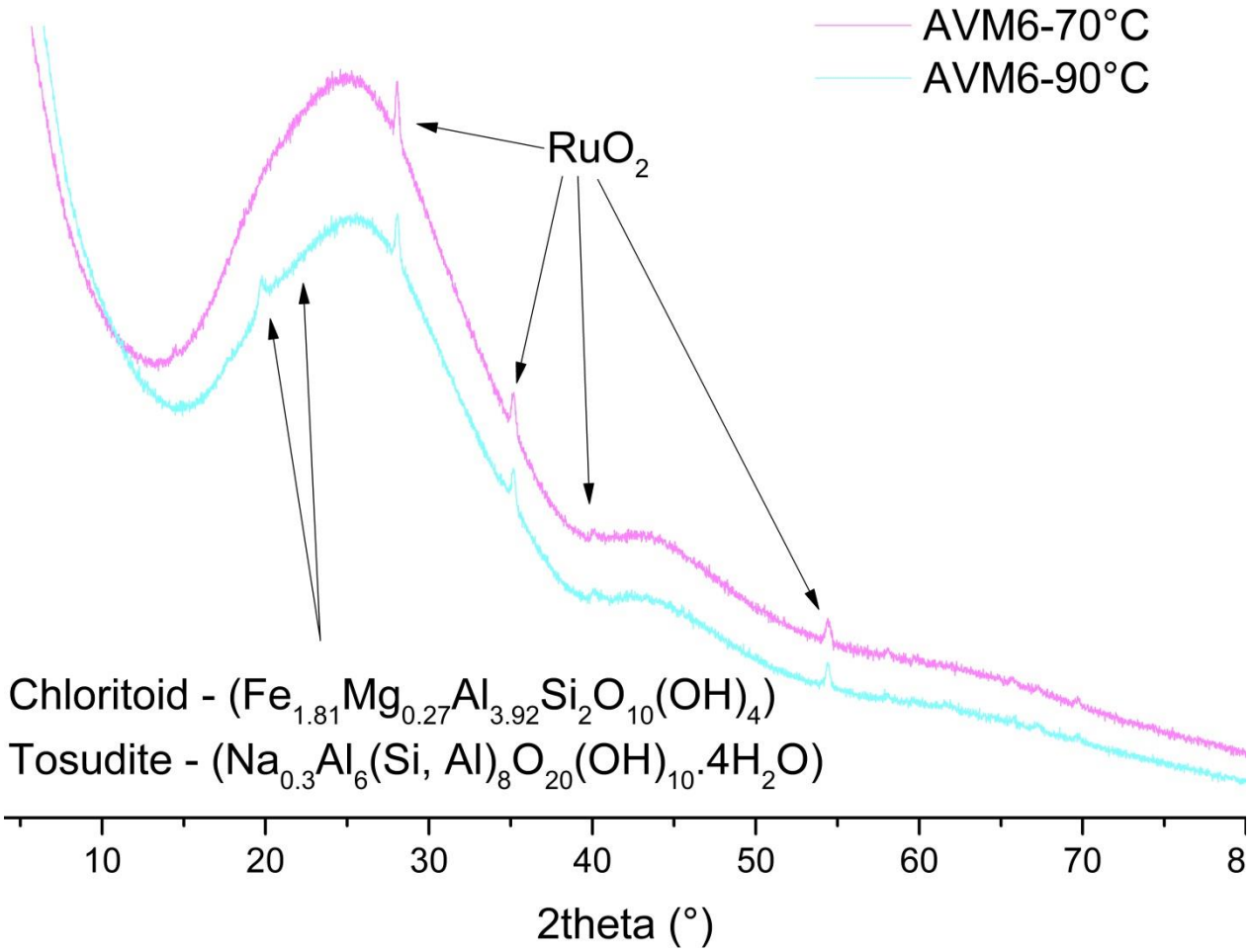

Figure 3- 6 XRD patterns of the AVM6 glass altered at 70°C & 90°C and 97% RH for 1 year

ToF-SIMS profiles

The ToF-SIMS profiles of the AVM6 sample altered at 70°C and 90°C are provided in figures 3-7 and 3-8 respectively. The thicknesses of the altered layers measured by the depths of boron depletion are provided in table 3-2.

The ToF-SIMS profiles of the AVM6 glass vapor hydrated at 70°C show that (figure 3-7), apart from hydrogen penetration, formation of SiOH and boron depletion, the alkali and alkaline-earth elements are very mobile in the gel layer. It seems that these elements have migrated

towards the surface of the gel layer probably to form secondary precipitates. From these profiles, it looks like the first 40 nm in the ToF-SIMS profiles are secondary precipitates. The migration of alkali and alkaline-earth elements has resulted in a depletion of these elements in the gel layer close to the gel-glass interface. The depletion of rare-earth elements and transition metals towards the surface of the altered sample could be due to the presence of a layer of precipitates close to the surface that does not incorporate these elements. (See figure A3-10 in appendix 3 for un-normalized ToF-SIMS profiles which also show this depletion). This means that the alkali and alkaline-earth elements migrate towards the surface to form precipitates and that there is no real loss of rare-earth elements and transition metals.

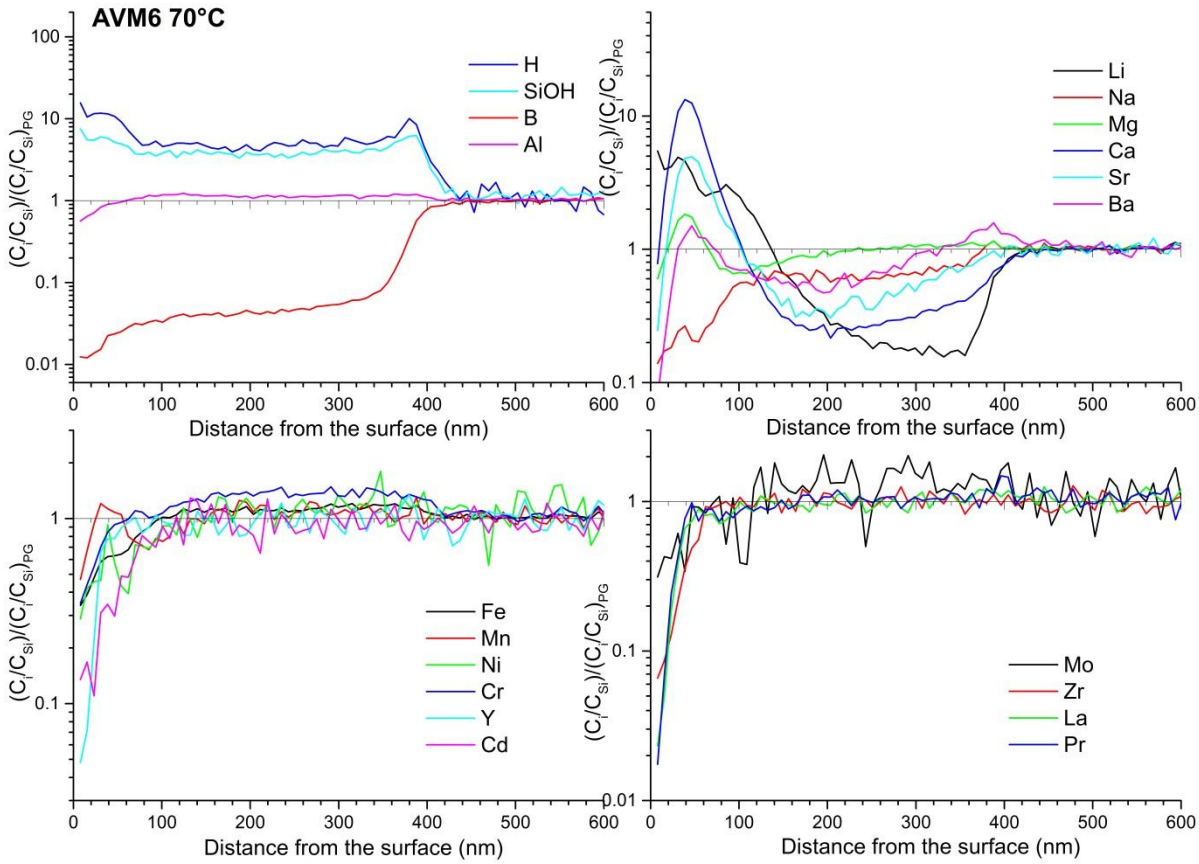

Figure 3- 7 ToF-SIMS profiles (normalized with respect to the intensity of Si and pristine glass) for the glass AVM6 altered in vapor phase at 70°C and 97% RH for 1 year

The ToF-SIMS profiles of all the elements in the gel layer of AVM6 glass altered at 90°C (figure 3-8) resembles that of the AVM6 glass altered at 70°C, except, the thickness of the altered layer is 1 µm and the thickness of the layer of secondary precipitates (based on the depth of depletion of rare-earth elements and transition metals and the mobility of alkali and alkaline-earth elements) is around 250 nm.

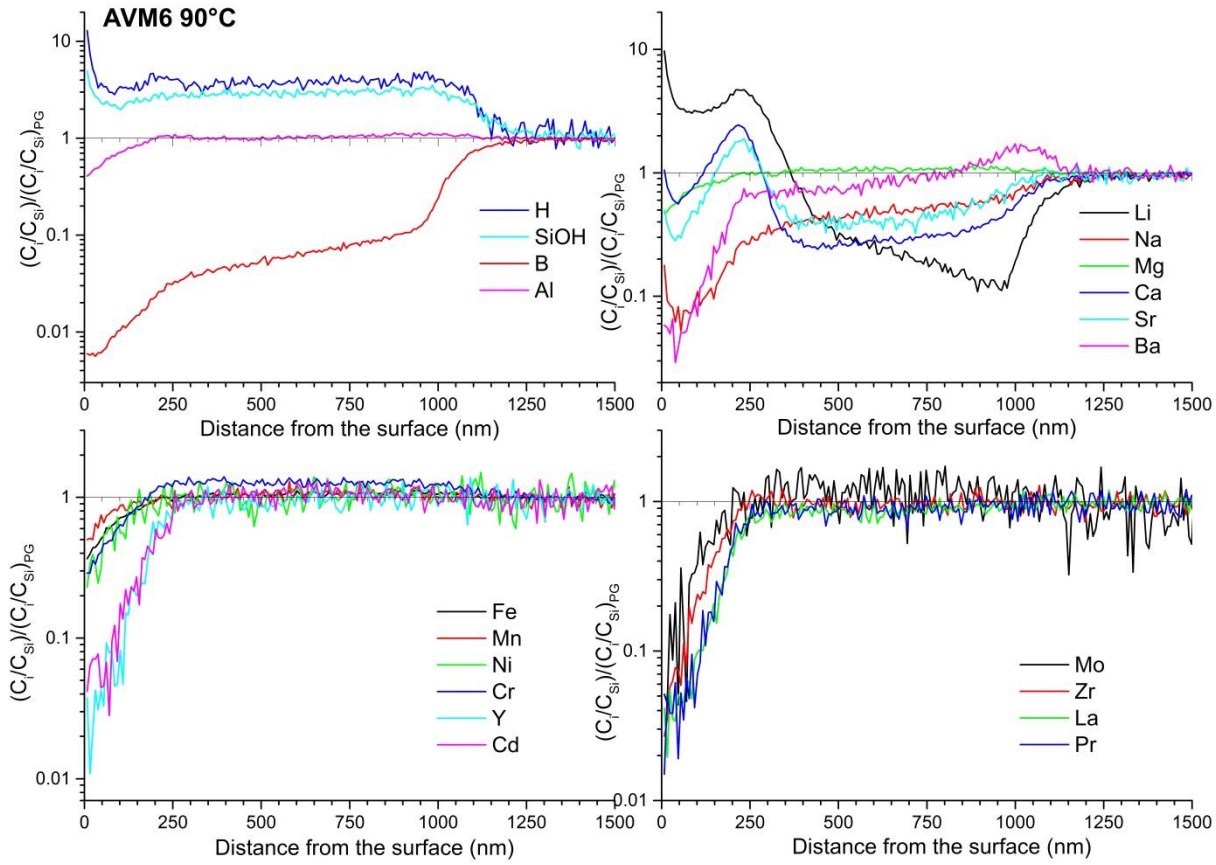

Figure 3- 8 ToF-SIMS profiles (normalized with respect to the intensity of Si and pristine glass) for the glass AVM6 altered in vapor phase at 90°C and 97% RH for 1 year

Table 3- 2 Thickness of the gel layer formed during vapor hydration of AVM6 glass at 70°C and 90°C at 97% RH; (The ToF-SIMS thicknesses are based on the depth of boron depletion)

	Thickness (SEM), nm	**Thickness (ToF-SIMS), nm**
AVM6- 70°C	300	390
AVM6- 90°C	1000	1050

3.2.3 Discussion

3.2.3.1 Effect of temperature

Glass alteration in aqueous medium is a thermally activated process. Several studies have shown that the dependence of the overall glass dissolution rate (k) on temperature follows Arrhenius law ($k = A_0 e^{\frac{-E_a}{RT}}$) [140, 141]. When the Arrhenius law is valid in a given temperature range, it means that glass alters by the same mechanism in that range [140]. The term "overall glass dissolution rate" was used because all the reactions resulting in glass alteration such as water diffusion, ion-exchange and network hydrolysis are thermally activated. Therefore, it is difficult to identify the activation energy of individual reactions in the glass alteration process. Nevertheless, the experiments in the literature have permitted to estimate that an activation energy of around 65-75 KJ/mol suggests that glass alteration occurs mostly by network hydrolysis [141, 142]. An activation energy below 50 KJ/mol suggests that inter-diffusion is the predominant glass alteration mechanism [140]. It is usually considered that activation energies in-between these two ranges indicate glass alteration by both network hydrolysis and inter-diffusion mechanisms.

The vapor hydration of glasses is also a thermally activated process. Literature survey has shown that the dependence of vapor hydration rate (V_H) on temperature in a given range follows Arrhenius law only for certain glass compositions. For example, in the study conducted on vapor hydration of alkali/alkaline-earth-silicate glasses in the temperatures 20°C and 50°C in one case [70] and 40°C and 80°C in another case [61], the vapor hydration rate did not follow Arrhenius law for temperature dependence. On the other hand, the vapor hydration rate of the SON68 glass follows Arrhenius law for temperature dependence in range 125-200°C with an activation energy of 43-47 KJ/mol [68] and an activation energy of 34±4 KJ/mol [29] in the temperature range 35-90°C. This difference in activation energy suggests that the rate-controlling vapor hydration mechanism is different between these two temperature ranges. Activation energies measured in other studies in various conditions vary from 34 KJ/mol to 137 KJ/mol [4, 14, 56, 57].

In our study, we attempt to verify the temperature dependence on Arrhenius law for the simplified glasses and the AVM6 glass. To do this, we calculate the vapor hydration rate in m/day (by dividing the thickness measured by ToF-SIMS by the duration of alteration) and multiply it by the glass density to obtain the vapor hydration rate in g/m^{2}day (V_H which is considered equivalent to K in the equation given above). For the simplified glasses, this vapor hydration rate at 90°C and 120°C over 3 months is calculated by considering that the vapor

hydration rate is constant during this time duration (thickness/time). This is compared with the vapor hydration rate at 50°C. Using the thickness of the altered layer (ToF-SIMS) formed on these simplified glasses at 50°C and 95% RH for 6 months (chapter 2), and the linear regression of evolution of hydration kinetics (increase in absorbance of SiOH molecules over time in FTIR spectrum- chapter 2, section 2.3.4), the vapor hydration rate at 50°C over 3 months is calculated.

In case of the AVM6 sample, the Arrhenius law for the temperature dependence of the vapor hydration rate is verified by comparing the vapor hydration rate (V_H) in g/m^{2}day after 1 year of alteration. While, the thicknesses of the altered layer formed after 1 year were measured by ToF-SIMS for the temperatures 70°C and 90°C (this chapter section 3.2.2.2), the thickness of the altered layer formed on the AVM6 sample altered at 50°C after 1 year was calculated by using the thickness of the layer formed after 6 months of alteration (TEM images, chapter 2) and the linear regression of the evolution of hydration kinetics (chapter 2, section 2.3.4). The calculated V_H values are provided in table 3-3.

Simplified glasses (Q, QCa, QMg):

In figure 3-9, plots of ln(V_H) vs. 1/T (K^{-1}) for the four glasses of this study, Q, QCa, QMg and AVM6 are presented. It was assumed that the vapor hydration rate was constant until three months in the case of glasses altered at 50°C (based on FTIR analysis in chapter 2), 90°C and 120°C. The assumption that the vapor hydration rate is constant for three months is reasonable because, studies conducted on SON68 glass and CSD-B glass have shown that, higher the temperature, longer the time taken for an inflexion in vapor hydration rate [27, 29]. Therefore, the vapor hydration rate must be constant for 3 months for the glasses altered at temperatures higher than 50°C.

Based on the plots shown in figure 3-9, the vapor hydration rate of the glasses Q and QCa show a deviation from Arrhenius law for temperature dependence between the ranges 50°C to 120°C, whereas the vapor hydration rate of the QMg glass follows Arrhenius law for temperature dependence with an activation energy of 58±8 KJ/mol. In the glasses Q and QCa, the factor of increase of the vapor hydration rate between 50°C and 90°C (37 and 22 times respectively) is higher than that of the glass QMg (15 times). On the other hand, the factor of increase of the vapor hydration rate at 90°C and at 120°C in the glasses Q and QCa (1.8 and 0.9 times) is lower than that of the glass QMg (2.7 times).

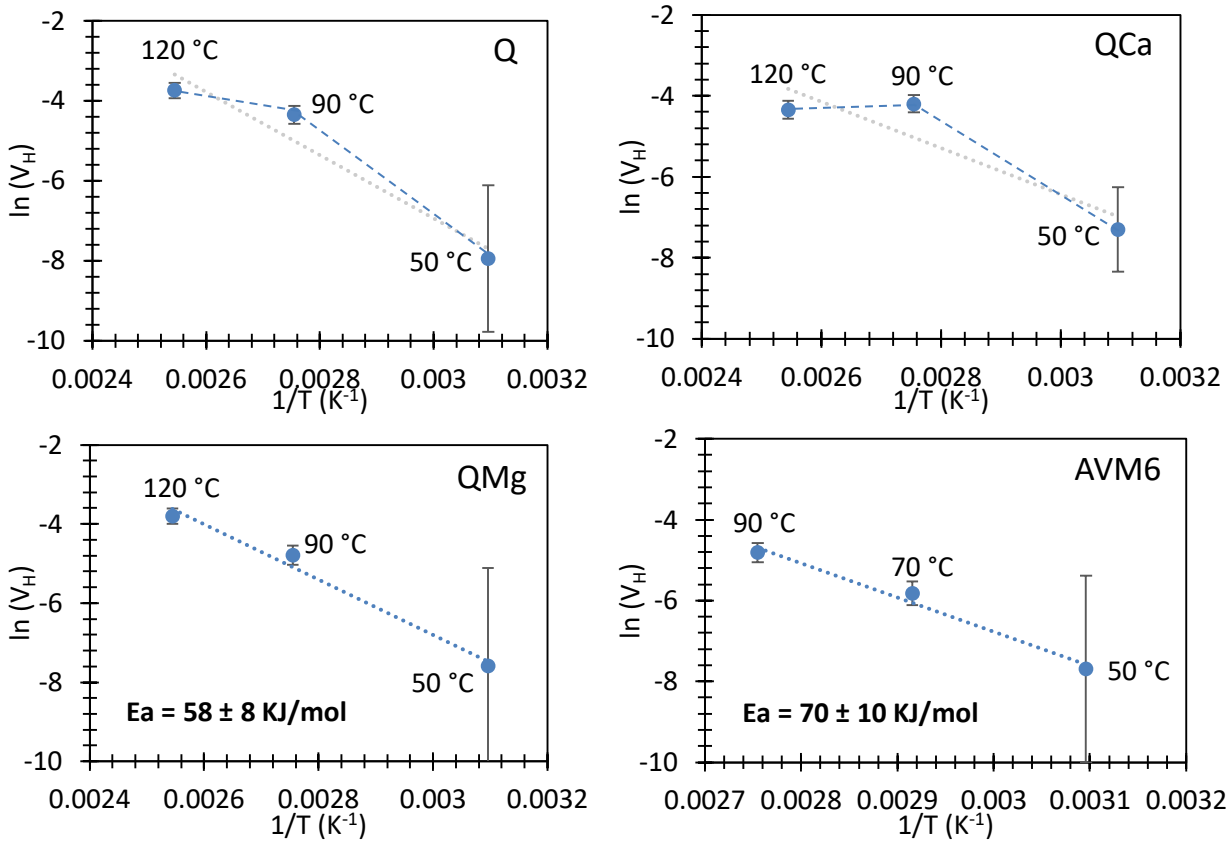

Figure 3- 9 Plots of ln(V_H) vs 1/T (K^{-1}) for the glasses Q (top-left), QCa(top-right) , QMg(bottom-left) and AVM6 (bottom right) altered in vapor phase in the temperature ranges 50°C to 120°C; V_H represents the vapor hydration rate measured in g/m^2day;

Table 3- 3 calculated vapor hydration rates (V_H) used to study if the temperature dependence follows Arrhenius law

	V_H (g/m^2day)*		
	50°C	**90°C**	**120°C**
Q	3.53×10^{-4}	128.7×10^{-4}	236.6×10^{-4}
QCa	6.75×10^{-4}	150.5×10^{-4}	129.7×10^{-4}
QMg	5.06×10^{-4}	83.12×10^{-4}	222.3×10^{-4}
	V_H (g/m^2day)**		
	50°C	**70°C**	**90°C**
AVM6	4.56×10^{-4}	29.6×10^{-4}	80.78×10^{-4}

*Vapor hydration rate calculated for 3 months

**Vapor hydration rate calculated for 1 year. It should also be kept in mind that this vapor hydration rate is calculated only for the thickness of the homogeneous gel layer formed on the surface and does not include the irregular heterogeneously altered porous zones

In chapter 2, it was concluded that the formation rate of the gel layer in vapor phase was controlled by a network hydrolysis mechanism in the three simplified glasses Q, QCa and QMg at 50°C and 95% RH. For the QMg glass, the vapor hydration rate must be controlled by network hydrolysis even at 90°C and 120°C since the vapor hydration rate follows an Arrhenius law for temperature dependence.

From the XRD patterns given in figure 3-3, the Q and QCa glasses altered at 90°C contain peaks for aluminosilicate hydrates, whereas, these glasses altered at 120°C contain only peaks for NaCl. The precipitation of the aluminosilicate phases at 90°C could be one of the reasons that resulted in a slight increase in alteration rate, thereby changing the rate-controlling mechanism between 50°C and 90°C.

While temperature clearly seems to have an effect on vapor hydration rate and the secondary phases that precipitate, the morphology of the gel layer is homogeneous in all three temperatures. The behavior of elements in the gel layer does seem to vary with temperature. Figure A3-12 shows the ToF-SIMS profiles of Mg in the QMg glass as a function of temperature. While Mg seems more mobile in the gel layer at 50°C, with depletion close to gel-glass interface and enrichment close to the surface, the retention of Mg is almost 100% in the gel-glass interface and in most of the gel layer for the QMg glasses altered at 90°C and 120°C. The enrichment of Mg in the surface of the QMg glasses altered at 90°C and 120°C is lower than the enrichment in the QMg glass altered at 50°C. One explanation for this difference in behavior with temperature could be that at 50°C, the formation of a Mg-containing precipitate could be favored and at higher temperatures it may not be. In the case of the behavior of Ca in the QCa glass altered at 50°C, 90°C and 120°C, as the temperature of vapor hydration increases, more Ca is retained in the gel layer (figure A3-12). Figure A3-13 shows the behavior of Na in each glass at different temperatures. Similar to Mg, Na is also very mobile and has a sinusoidal profile in the gel layer of the Q, QCa and QMg glasses altered at 50°C. But in contrast to Mg, Na is enriched in gel-glass interface and depleted in the part of the gel layer that is close to the surface. In the case of the glasses altered at 90°C and 120°C, the profile of Na is uniform throughout the gel layer (about 50% retention). At these two temperatures, the behavior of Na is similar in all three glasses.

The difference in behavior of elements with temperature seems to be linked to the precipitation of secondary phases at each temperature. This type of behavior with temperature where higher fraction of alkali and alkaline-earth elements ($M^{+/2+}$) are retained in the gel layer with increasing temperature was also observed in a recent study on the effect of temperature on

the atmospheric alteration of a mixed-alkali lime silicate glass. In the cited study, it was argued that the reason for higher retention of $M^{+/2+}$ cations at higher temperatures could be the engagement of water molecules in network hydrolysis reactions (which is much more strongly thermally activated than inter-diffusion process) rather than solvation of $M^{+/2+}$ cations. Whereas at lower temperatures, water molecules have sufficient time to solvate the $M^{+/2+}$ cations and these cations migrate towards surface to form secondary precipitates. This argument could very well be applied to explain our results as well [54]. There are also a couple of other hypotheses that could be proposed. For example, at high temperatures, as soon as the $M^{+/2+}$ ions are released they could precipitate on site as silicates or carbonates, forbidding its migration towards the surface. Another possibility is that since the solubility of the secondary phases increases with temperature, under the given conditions, sufficient glass may not be dissolved yet to reach the solubility. These hypotheses could be probed further using thermodynamic calculations.

One important aspect that has not been analyzed in our study, but could have significant effect on the nature of the secondary phases that precipitate and solubility of the elements within the gel layer is the pH. While calculating the activation energies using Arrhenius law, it is assumed that the pH is similar at all temperatures. But unfortunately, there are no means to measure this value experimentally. Models need to be developed to verify if the change in local pH within the vapor hydrated gel layer could be the reason for varying solubility of Ca at different temperatures, for example.

AVM6:

There are differences between the behavior of AVM6 glass and the simplified Q, QCa and QMg glasses in vapor phase. As seen earlier in chapter 2, the morphology of the AVM6 glass altered in vapor phase at 50°C and 95% RH was particular since, in addition to the formation of a homogeneous gel layer of ~50 nm thickness on the glass surface after 6 months, very porous and irregularly shaped discontinuous altered zones were present beneath the gel layer. The vapor hydration at 70°C and 90°C seem to have a similar morphology. The SEM images of the glass surface altered at 70°C showed the presence of what seems to be holes beneath the carpet of phyllosilicates (figure 3-5 center-left). However, these holes could not be identified in the SEM images of cross-section of the altered sample. The cross-section images showed a homogeneous gel layer of 290-350 nm thickness (figure A3-4). The SEM images of both, the altered surface and the cross-sections, of the AVM6 sample altered in vapor phase at 90°C showed the presence of numerous holes (figure 3-5 and figure A3-5). As can be seen from figure A3-5 (bottom-right), these mushroom-shaped holes are not completely empty, but seem to

be of very low density based on the contrast in electronic density. At 50°C, what seemed to be highly porous irregular zones might have developed into even more porous cup-shaped zones at 90°C. Based on the SEM observations, figure 3-10 shows a schematic description of the altered layer morphology of AVM6 glass at different temperatures. This type of corrosion seems to morphologically resemble sub-surface pitting corrosion commonly observed in steel alloys due to slight inhomogeneity in the composition of the initial matrix. As discussed in chapter two, it seems that the homogeneous gel layer and the irregular pitting type alteration seem to be two separate processes occurring in parallel. From the thicknesses of the homogeneous gel layer formed at 50°C (60 nm, calculated), 70°C (386 nm, measured from ToF-SIMS) and 90°C (1053 nm, measured from ToF-SIMS), V_H was calculated for the formation of the homogeneous gel layer (note that the irregular pitting type alteration is not included in this). The bottom right image in figure 3-9 shows the evolution of $\ln(V_H)$ vs 1/T (K^{-1}). The dependence of the rate of vapor hydration (only the formation of gel layer, without including the 'pit' type irregular altered porous zones) of the AVM6 glass follows Arrhenius law for temperature dependence with an activation energy of 70±10 KJ/mol. This activation energy is close to the activation energy of the QMg glass in the study. Similar to the QMg glass, the rate of formation of the gel layer must be controlled predominantly by network hydrolysis reactions in the temperature range 50°C to 90°C.

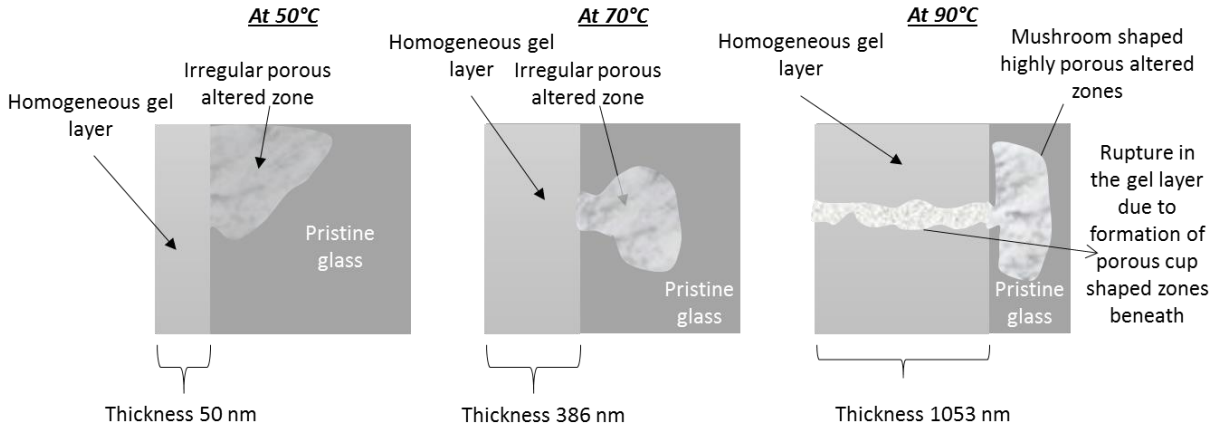

Figure 3- 10 Schematic representation of the evolution of AVM6 glass altered at different temperatures

Despite the similarity in the vapor hydration of AVM6 glass between 50°C and 90°C in terms of altered layer morphology and mechanism of formation of the gel layer, the secondary phases that have precipitated are different. From chapter 2, it was noted that the glass altered at 50°C and 95% RH during 6 months and 18 months had an intense peak around 6° (15 Å) that indicated the presence of a smectite (probably montmorillonite). The glasses altered at 70°C and

90°C however did not have the same secondary phases precipitated on their surfaces. The XRD pattern of the glass altered at 90°C shows two peaks around 20° and 24.5° (2θ) which were identified as phyllosilicates/aluminosilicates. The XRD pattern of the glass altered at 70°C did not show any peaks, but after background subtraction it seems that two small peaks are present at 20° and 24.5° 2θ. As was the case in simplified glasses, the same phases do not precipitate during vapor hydration of AVM6 during different temperatures. Based on the similarity in altered layer morphology and rate controlling gel-layer formation mechanism at three different temperatures, the 'pitting' type corrosion observed in AVM6 glass is a property of the glass and not related to the identity of the secondary phases that precipitate. Since, the surface treatment of all glasses in this thesis is similar, the fact that only certain glasses show 'pitting' type corrosion could mean that there could be slight inhomogeneity in the AVM6 glasses, which favor extensive alteration in a localized manner. Figure A3-29 in appendix 3 confirms the presence of inhomogeneities in the pristine AVM glasses.

3.2.3.2 Effect of temperature on the effect of glass composition

Figure 3-11 shows the ToF-SIMS profiles of boron of all the three simplified glasses altered at three different temperatures. Ca has a negative effect on glass alteration at 50°C since the glass QCa has altered 1.65 times more than the glass Q after 6 months and twice that of glass Q after 18 months. At 90°C, the negative effect of Ca is less pronounced since the glass QCa has altered 1.14 times more than the glass Q. At 120°C however, Ca has a positive effect since the glass Q has altered almost twice that of QCa.

Mg, like Ca at 50°C, has a negative effect on vapor hydration (after 6 months) since the glass QMg has altered 1.65 times more than the glass Q. At 90°C, Mg has a significant positive effect since the glass Q has altered 1.55 times more than the QMg glass. At 120°C, Mg has no visible effect on vapor hydration rate since both Q and QMg glasses had altered to a similar extent.

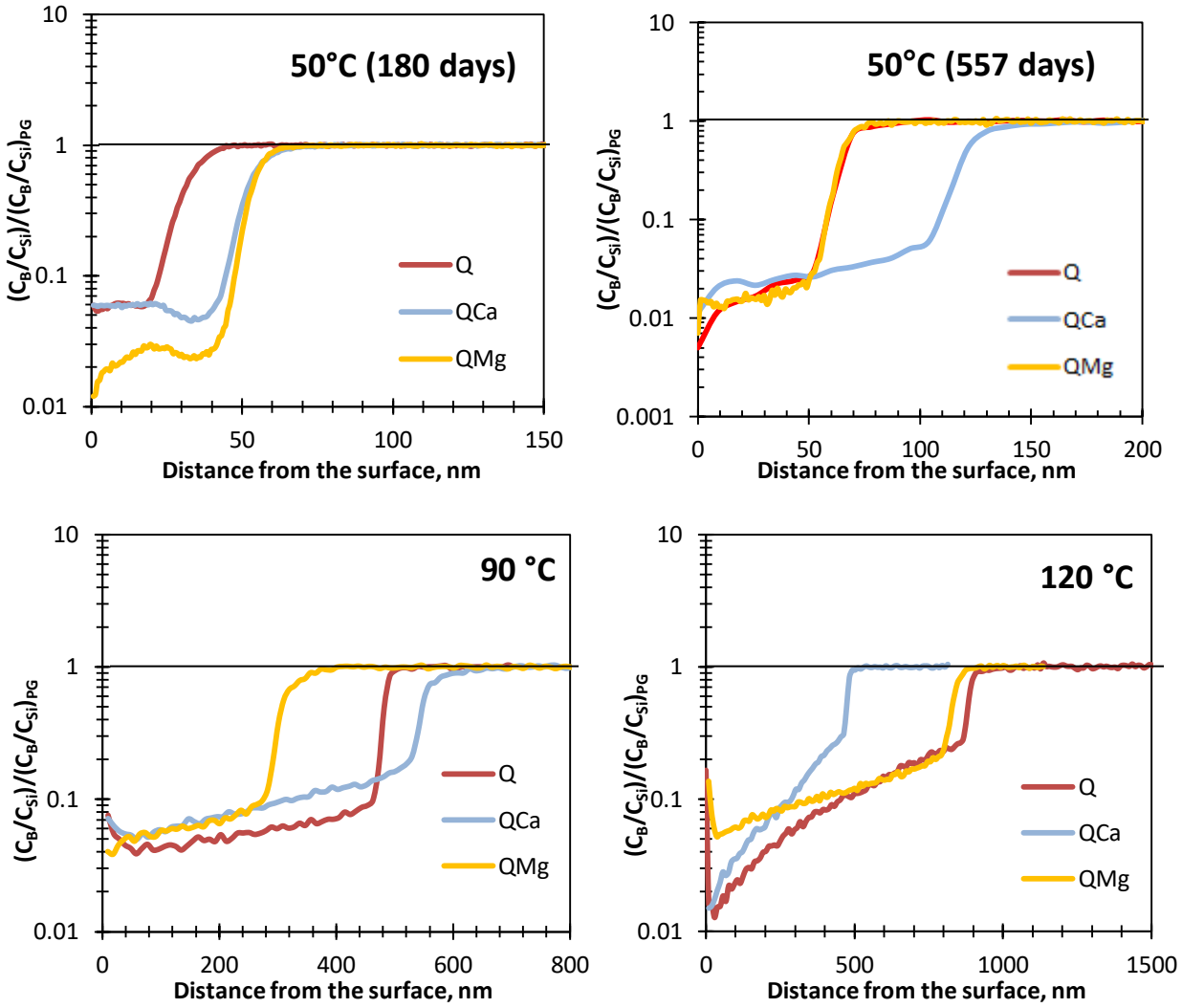

Figure 3- 11 ToF-SIMS profiles (normalized with respect to pristine glass and Si) of boron of the glasses Q, QCa and QMg altered in vapor phase at 95% RH and temperatures of 50°C (top-left) for 180 days, 50°C (top-right) for 557 days, 90°C (top-right) for 91 days and 120°C (bottom) for 91 days

The positive or negative effect of many elements depends on the dominating alteration mechanism and the role played by these elements in the glass structure. Both Ca and Mg play the role of network modifiers in the pristine glass. The pristine Q glass is more polymerized than the QCa and QMg glasses. Since at 50°C, until around 180 days, network hydrolysis is the rate-controlling mechanism in vapor phase, the QCa and QMg glasses have altered at a higher rate. But this is not a direct negative effect of the presence of these elements. At a longer duration (557 days), the glass alteration is no longer controlled by network-hydrolysis. As explained in detail in chapter 2, the vapor hydration rate may be controlled by transport limitations through the gel layer. In this viewpoint, the gel layer of the glass QMg may be the most passivating since it retains more than 50% of the Mg mole fraction in the gel layer. The retention of Mg in the gel

layer is known to increase its passivation properties [97]. The gel layers formed on the glasses Q and QCa must be less passivating since <3% Ca is retained in the gel layer of QCa and the gel layer of Q contains neither Ca nor Mg. Therefore, the factor of rate drop must be lower in Q than in QMg, leading to a similar thickness of alteration in both cases after 557 days.

At 90°C, rate-controlling mechanism of vapor hydration is still network hydrolysis in the QMg glass (based on Arrhenius law, figure 3-9). But the alteration of Q and QCa has been piloted by some other mechanisms. It seems reasonable to suppose that the precipitation of alumino-silicate hydroxides (identified on Q and QCa by XRD pattern but not on QMg, figure 3-3) on the Q and QCa glasses must have resulted in the higher alteration of these glasses than QMg at 90°C.

At 120°C too the vapor hydration of the QMg glass is piloted by network hydrolysis. One of the explanations for the significant positive effects of Ca could be that as the temperature increases, higher quantity of Ca is retained in the gel layer (figure A3-12). In the part of the gel layer close to the gel-glass interface, the retention factor (from ToF-SIMS profiles) of Ca is 30-40% at 120°C and 3-4% at 90°C. It is well known from glass aqueous alteration studies that the retention of Ca in the gel significantly increases its reticulation properties and slows down glass alteration rate [81, 143-146].

It is hard to distinguish if the secondary phase precipitation is a consequence of release of elements from glass network due to glass alteration, or if it acts as a sink and drives vapor hydration (or perhaps both depending on time, especially when Al or Si are involved). Nevertheless, it is clear from this study that the influence of glass composition is sensitive to the temperature. Depending on glass composition, the rate-controlling vapor hydration may or may not change with respect to temperature in the range studied here. It needs to be admitted that unfortunately, the discussion on the temperature effects has been carried out without the knowledge of pH, a parameter that plays a significant role in determining rate-controlling mechanisms, secondary phase precipitation and element solubility/behavior in the gel layer. We do not have access to this parameter and the results do not show any clear behavior indicative of pH values, although it is commonly postulated that pH must be basic due to the very small water volumes.

3.2.4 Conclusion on the effect of temperature

The nature / identity of the secondary phases that form on glass surface during vapor hydration varies with temperature for all four glasses studied in this section. But the altered layer morphology seems to be similar regardless the temperatures. Therefore, it is likely that the altered layer morphology is dependent on the glass properties (most likely homogeneity) and not the nature of secondary phases. Since the behavior of alkali / alkaline-earth elements in the gel layer seems to depend on the secondary phases that precipitate, it also varies with temperature. The retention of both Ca (for QCa) and Mg (for QMg and AVM6) in the gel layer seems to increase with increasing temperature.

The rate of formation of the homogeneous gel layer seems to follow Arrhenius law for temperature dependence for the two Mg-containing glasses among the four glasses studied in temperature ranges 50°C-90°C in one case and 50°C-120°C in another case. For both glasses, the activation energies were similar (taking into account the associated uncertainties), with probably network-hydrolysis as the rate controlling mechanism. In the case of the remaining two glasses that do not follow Arrhenius law for temperature dependence in the range 50°C-120°C, the rate-controlling mechanism varies with increasing temperature. As a result, the effect of glass composition on vapor hydration also varies with temperature.

3.3 Effect of relative humidity

3.3.1 Experiment

AVM6 glass monoliths of dimensions (2.5x2.5x0.1 cm^3) were prepared and sent to Loryelle Sessegolo at "Laboratoire Interuniversitaire des Systèmes Atmosphériques (LISA)", where they were altered in vapor phase at 50°C and four different relative humidity values (55±9%, 76±3%, 83±2% and 95±3%) for 1 year. The vapor hydration protocol is described in detail in the reference [70]. It consists of an air-tight container equipped with a perforated shelf with large holes to hold samples, above a tray to contain the saturated salt solution that will be used to impose the relative humidity in the container. This container was then placed in an oven at 50°C. At 50°C, saturated $MgNO_3$ solution was used to impose 55% RH, saturated NaCl solution was used to impose 76% RH, saturated KNO_3 solution was used to impose 83% RH and saturated K_2SO_4 solution was used to impose 95% RH. The relative humidity was measured using a sensor and the uncertainty in the relative humidity was measured from the standard deviation of the sensor measurements as well as taking into account 2% error associated with the sensor measurements. At the end of one year of experiment, the samples were removed from the containers and placed in a desiccator (14% RH) until characterization, according to the protocol used at LISA.

3.3.2 Characterization of altered samples

The altered surface and morphology of the altered samples were characterized by Scanning Electron Microscope (SEM). The precipitated crystalline secondary phases were identified by X-Ray Diffraction (XRD) and the behavior of elements in the gel layer was studied by Time-of-Flight Secondary Ion Mass Spectrometry (ToF-SIMS). Refer appendix A for information on analytical parameters.

3.3.3 Results

SEM images

Figure 3-12 shows the SEM images of the AVM6 sample vapor hydrated at 95% RH and 83% RH. On the surface of the AVM6 sample vapor hydrated at 95% RH, circular clusters of fibrous secondary precipitates of a few µm diameters are present along with fewer shapeless clusters of fibrous phases. The SEM image of the cross-section of the sample shows an altered layer of approximately 200 nm thickness. In the section of the sample analyzed, many irregularly altered zones could not be identified (in chapter 2, many irregularly altered zones were identified

on the AVM6 glass altered at 50°C and 95% RH in the climatic chamber for 6 months and 18 months).

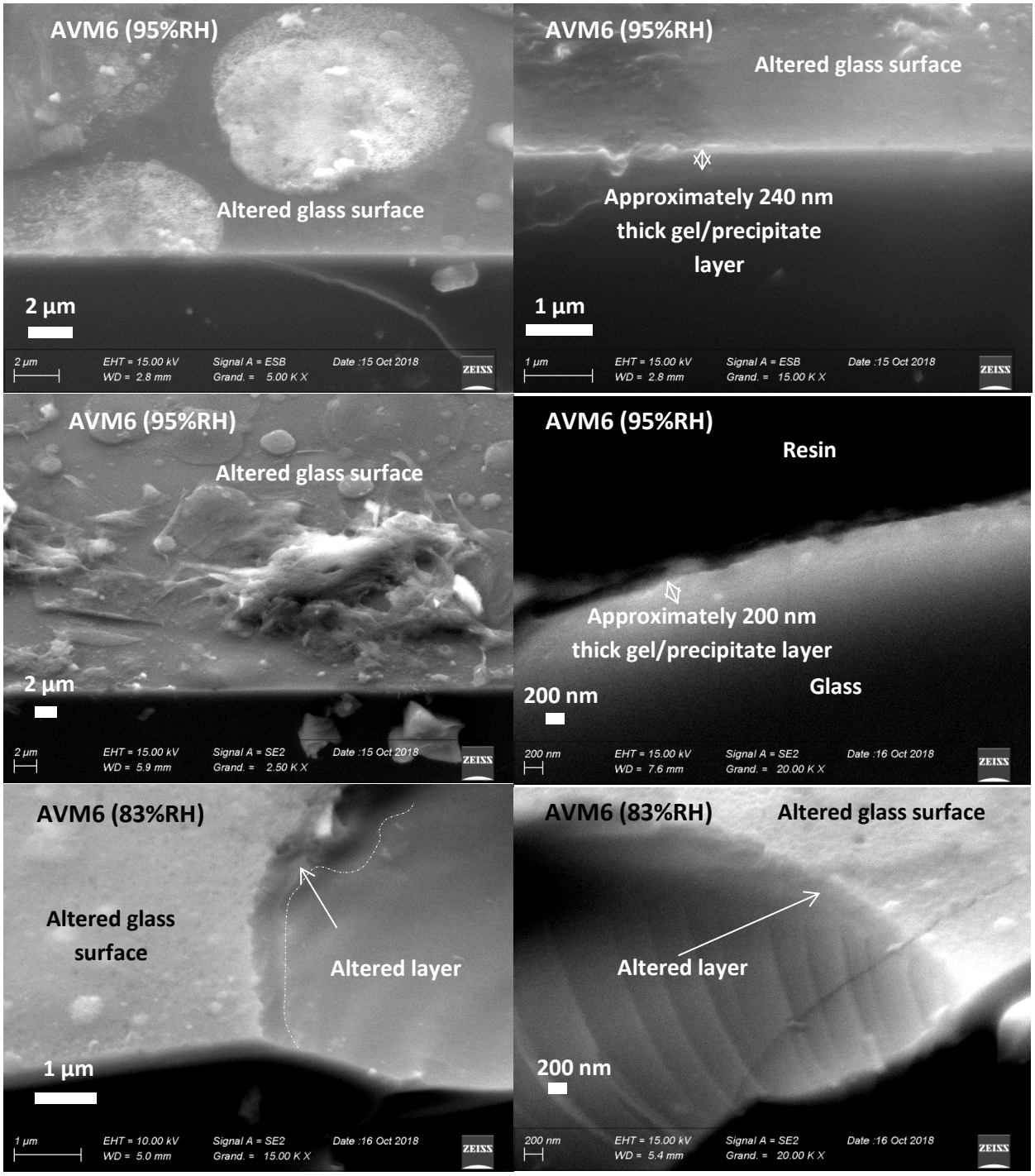

Figure 3- 12 SEM images of AVM6 glass altered at 50°C and 95% RH (top and center) and 83% RH (bottom). The center-right image is the cross-section of the AVM6 sample altered at 95% RH. The remaining images are a direct observation of the altered sample

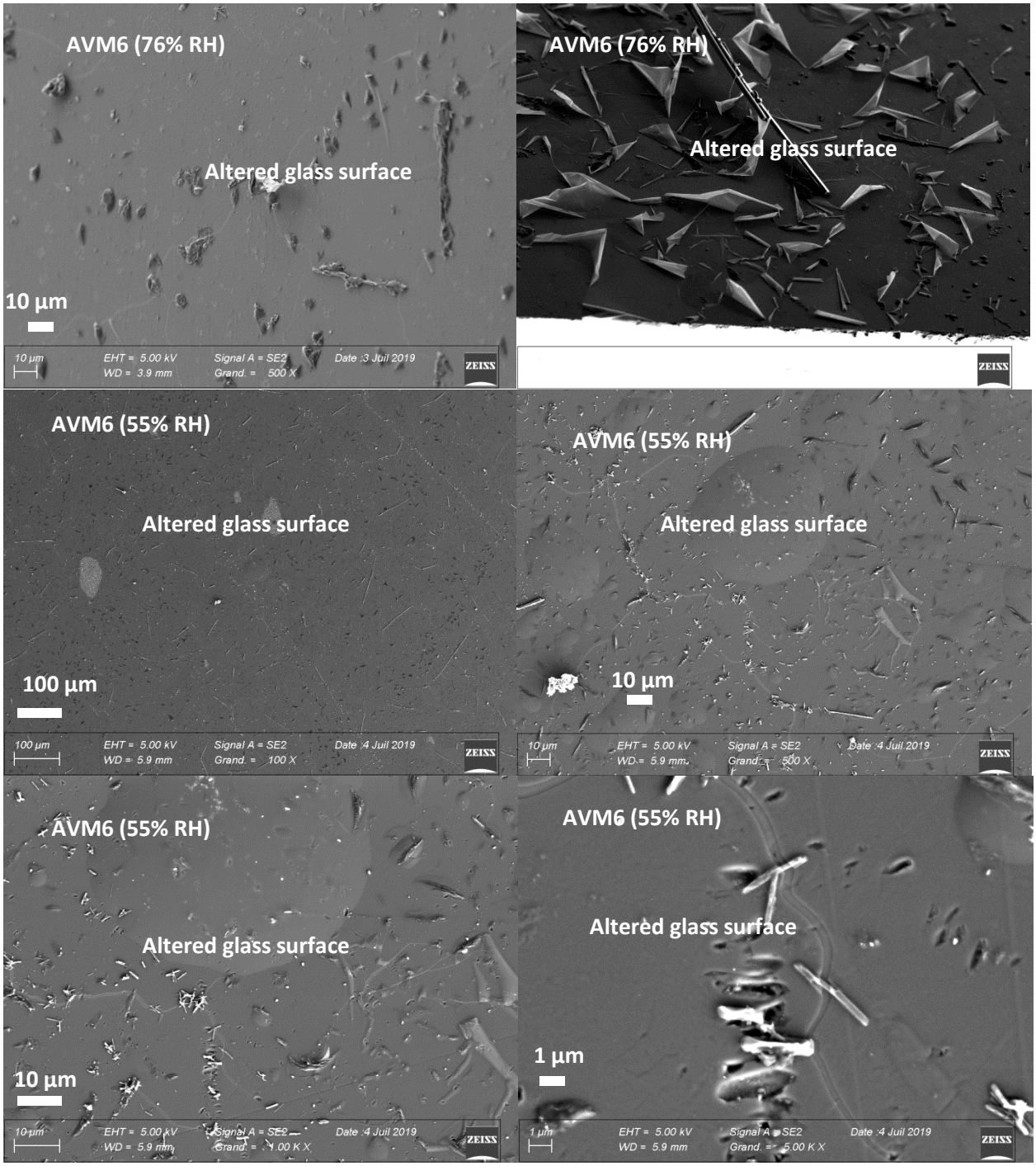

Figure 3- 13 SEM images of AVM6 glass altered at 50°C and 76% RH (top) and 55% RH (center and bottom). All images are a direct observation of the altered sample

The surface of the AVM6 sample vapor hydrated at 83% RH also seemed very similar to the sample vapor hydrated at 95%. The sample also contained irregularly altered zones as shown in the bottom-left image of figure 3-12.

Figure 3-13 shows the SEM images of the AVM6 samples vapor hydrated at 76% RH and 55% RH. Visually these surfaces are different from each other and also are different from the surfaces of the samples altered at the two higher RH values. The top-left and bottom-left images in figure 3-13 show the altered surfaces of AVM6 samples altered at 76% RH and 55% RH respectively at the same magnification. The forms of the secondary phases formed on these surfaces are visually different. The sample altered at 55% RH seems to contain more singular needle-like precipitates and there are circular spots on the altered surface that appear bulged. No such bulged zones are visible on the sample altered at 76% RH. However, the surface looks scaled, as though it is a more advanced stage of the bulged zones that have peeled off. A few singular needle-like precipitates were visible on the sample altered at 76% RH as well.

XRD patterns

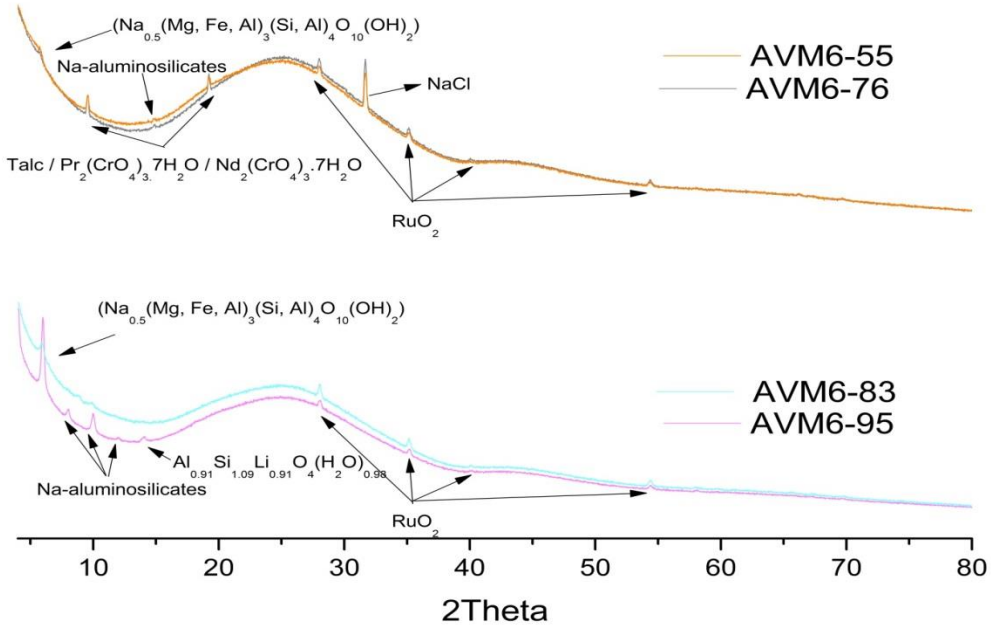

Figure 3- 14 XRD patterns of AVM6 glass altered in vapor phase at 50°C and 55% RH, 76% RH, 83% RH and 95% RH for 1 year

Figure 3-14 shows the XRD patterns of the AVM6 glass altered in all four RH values. At all 4 RH values, a peak around 6° (2θ) (or 15 Å) is present indicating the formation of an aluminosilicate containing Na, Mg and Fe. The intensity of the peak increases with increasing

relative humidity, suggesting that either a higher quantity of this phase had precipitated with increasing relative humidity or that as the relative humidity increases, the crystallinity of the precipitates improve. This peak was present on the AVM6 samples altered at 50°C and 95% RH for 6 months and 18 months in chapter 2 as well.

Only the AVM6 samples altered at lower RH values, 55% and 76% RH, contain peaks at 10° and 19.2° (2θ) (around 9.2 and 4.6 Å in d-scale), which could be $Nd_2(CrO_4)3.7H_2O$ or $Pr_2(CrO_4)3.7H_2O$ (figures A3-15,16). These two samples also contain a peak at 15° (2θ) (around 6 Å in d-scale), which is attributed to sodium aluminosilicate hydrates and a peak at 32° (2θ) (around 2.8 Å in d-scale) which indicates the presence of NaCl. While the presence of NaCl on the AVM6 sample altered at 76% RH was expected since NaCl was used to impose relative humidity, its presence on the AVM6 sample altered at 55% RH is puzzling since $MgNO_3$ was the salt used to impose relative humidity. The peak at 32° (2θ) could also be attributed to Calcium-Silicate-Hydrates (CSHs), but it would be surprising to find CSHs formed only on samples altered at 55% and 76% RH (less altered) and not on samples altered at 83% and 95% RH (more altered).

For the AVM6 samples altered at 83% and 95% RH, in addition to the peak at 6° (2θ), there are also peaks at 8°, 10°, 12° and 14° (2θ) (around 11, 8.8, 7.5 and 6.3 Å in d-scale) that correspond to sodium alumino silicates. Figures A3-15 to A3-21 show the secondary phase analysis by EVA software [147] of the peaks present on the XRD patterns.

ToF-SIMS profiles

Table 3-4 provides the altered layer depths (boron depletion) and the depths of hydrogen penetration through the surface of the AVM6 glasses altered in all 4 RH values. Figure 3-15 presents the ToF-SIMS profiles of the AVM6 sample altered at 55% RH and 50°C for 1 year. The thickness of boron depletion is around 27 nm in the gel layer, which is a little higher than the boron depletion in a pristine AVM6 glass (14 nm). Transition metals and rare-earth elements are depleted in the first 10-20 nm of the gel layer, which was the case in pristine samples as well (figure A3-7). The depletion of Ba, Sr and Li is slightly deeper than the depletion of boron in the AVM6 glass altered at 55% RH. The retention of boron in the first 20 nm of the gel layer is only between 2-10%. It seems as though the gel layer might be heterogeneous since the gel-glass interface of hydrogen penetration is larger than the thickness of gel layer and according to the profile of boron, its concentration is not uniform in the gel layer and the gel-glass interface is also large. However, it cannot be ascertained because large interfaces may also be caused by the

presence of secondary precipitates on the altered surface. The thickness of the layer is smaller than the resolution of SEM, so the assumed heterogeneity of the gel layer cannot be verified.

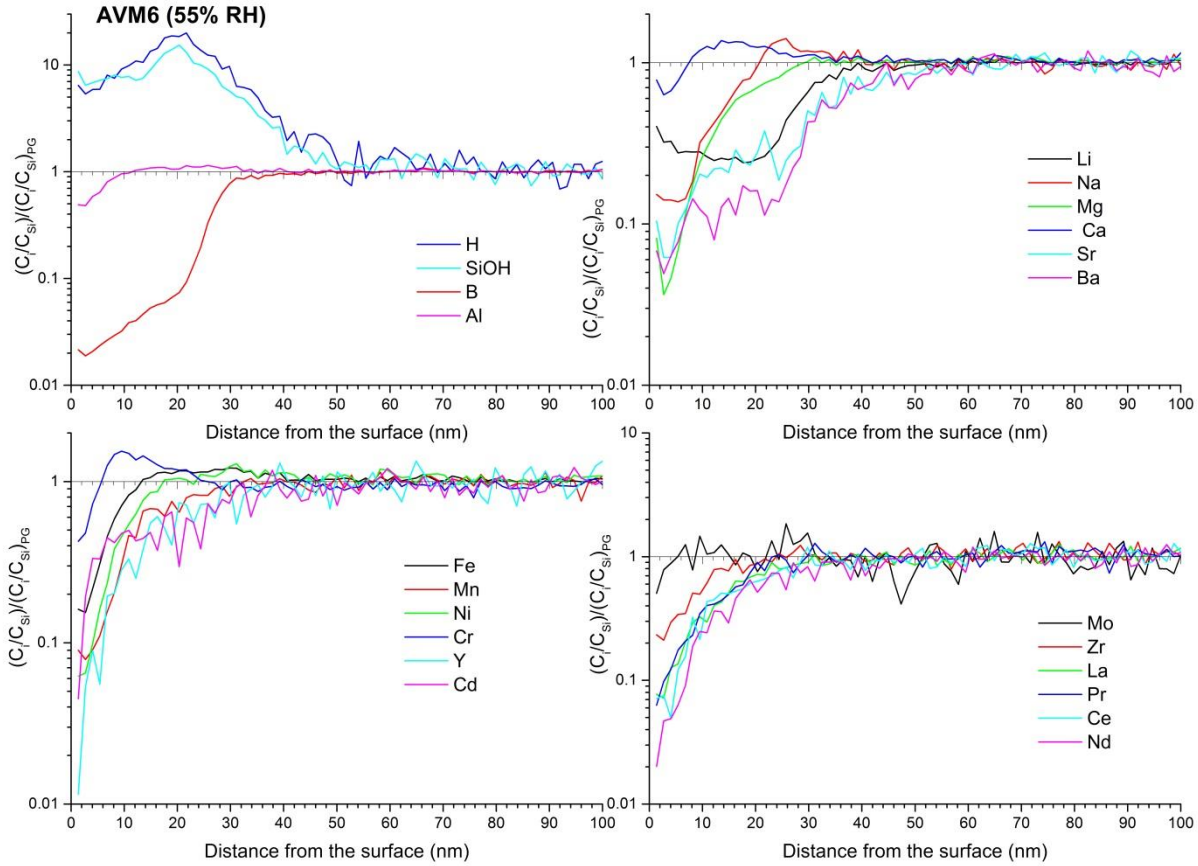

Figure 3- 15 ToF-SIMS profiles (normalized with respect to the intensity of Si and pristine glass) for the glass AVM6 altered in vapor phase at 50°C and 55% RH for 1 year

Figure 3-16 shows the ToF-SIMS profiles of the AVM6 glass altered at 76% RH. The altered layer depth is 190 nm and the thickness of hydrogen penetration is 200 nm. Similar to the AVM6 glass altered at 55% RH, the retention of boron is around 2-10% in the gel layer. The retention of Na in the gel layer is uniform and is around 40%. The other alkali and alkaline-earth elements are depleted in the part of the gel layer that is close to the gel-glass interface and their concentration increases towards the surface of the altered glass. Such a profile suggests that the elements have migrated towards the surface probably to form secondary precipitates. Ba is the most mobile alkaline-earth element, with only 1-4% retention in the gel layer close to the gel-glass interface. The retention factors of Ca, Sr and Li in this region are also only around 10%. The transition metals and the rare-earth elements are depleted in the first 20 nm of the gel layer, except Mn, whose retention factor declines continually in the gel towards the altered surface until it is only 2-3% retained.

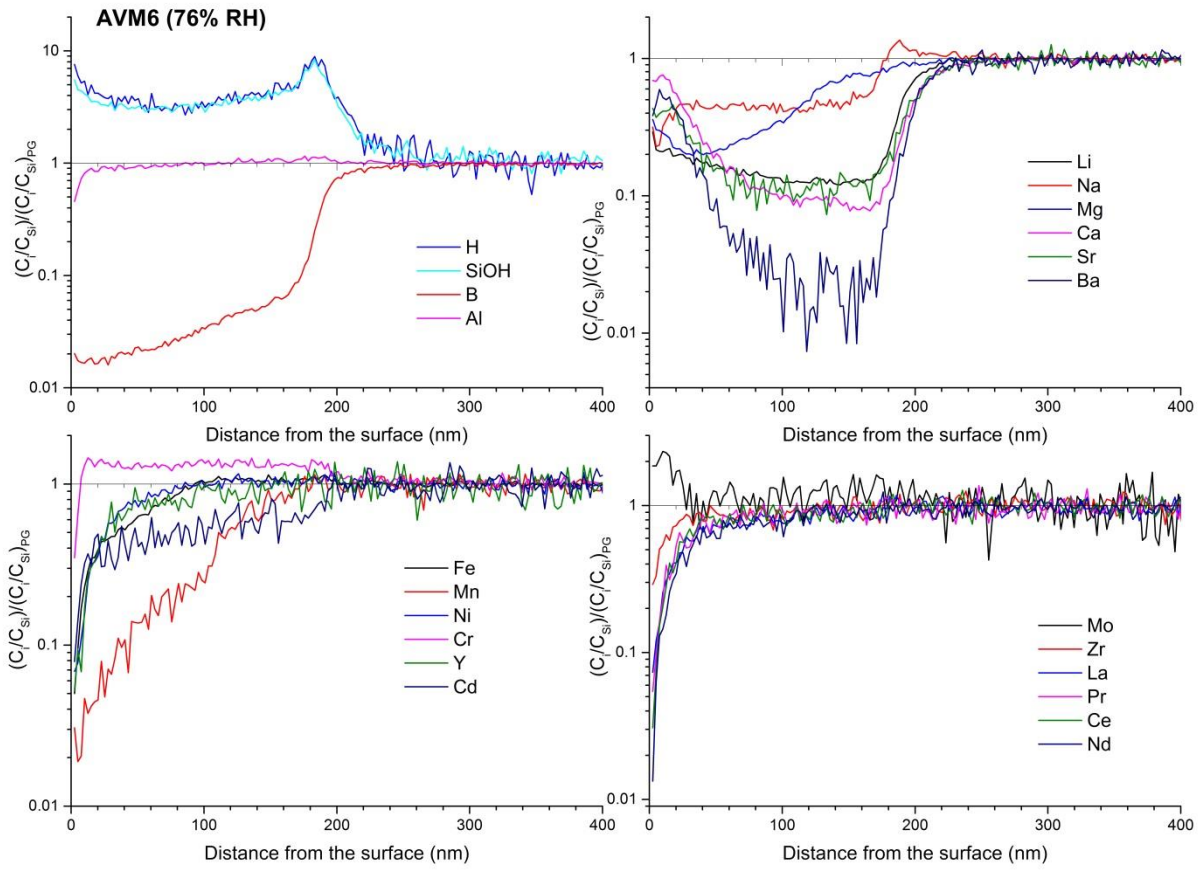

Figure 3- 16 ToF-SIMS profiles (normalized with respect to the intensity of Si and pristine glass) for the glass AVM6 altered in vapor phase at 50°C and 76% RH for 1 year

Figure 3-17 shows the normalized ToF-SIMS profiles of the elements for the AVM6 glass altered at 83% RH. The altered layer thickness is around 124 nm and the thickness of hydrogen penetration is around 129 nm. This thickness value is surprising since it is lower than the altered layer thickness of the AVM6 glass altered at 76% RH for the same temperature and duration. As seen from figure 3-12, the AVM6 glass altered at 83% RH has a heterogeneous altered layer. Therefore, the reason for this unexpectedly low altered layer thickness could be that the ToF-SIMS analysis might have been done in a region with very few irregularly altered zones. Apart from this discrepancy, the behavior of elements in the gel layer is quite similar to that of the AVM6 glass altered at 76% RH in terms of shape of the profiles and the retention factors of elements in the gel layer (except Mn). The Mn behavior in this glass is quite similar to the behavior of other transition metals in the gel layer.

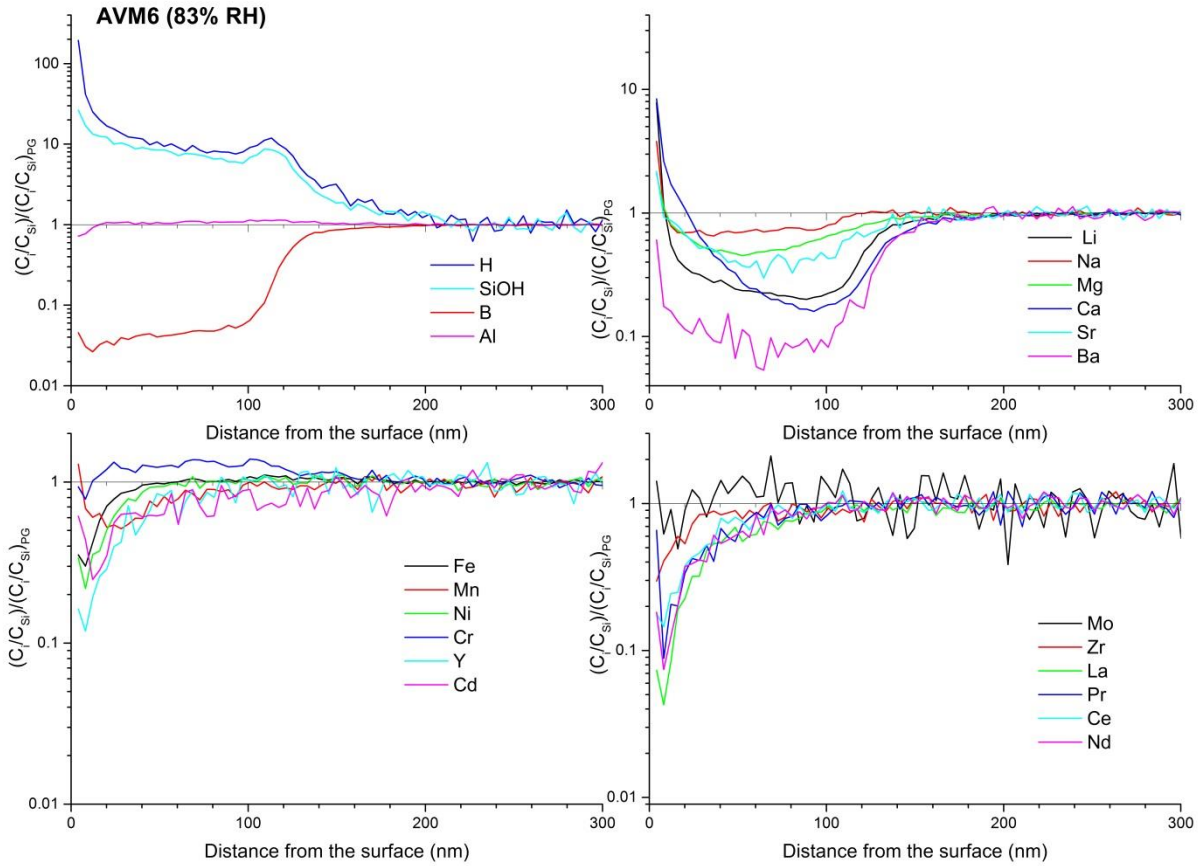

Figure 3- 17 ToF-SIMS profiles (normalized with respect to the intensity of Si and pristine glass) for the glass AVM6 altered in vapor phase at 50°C and 83% RH for 1 year

Figure 3-18 shows the normalized ToF-SIMS profiles of the AVM6 glass altered at 95% RH. The altered layer thickness is around 540 nm and the thickness of hydrogen penetration is around 620 nm. Similar to the AVM6 glass altered at 55% RH, the gel-glass interface is quite large. It seems that the altered layer could be heterogeneous in this case as well, keeping in mind that the heterogeneity could also be caused by surface irregularities (presence of secondary precipitates). The rare-earth elements and the transition metals are immobile in the altered layer except the first 30-50 nm, where they seem to be slightly depleted probably due to the presence of secondary precipitates in this region. Once again, the alkali and the alkaline-earth elements are very mobile in the gel layer. They are depleted in the part of the gel layer close to the gel-glass interface and their concentration increases towards the surface. Na seems to be enriched in the first 250 nm of the gel layer (towards the surface).

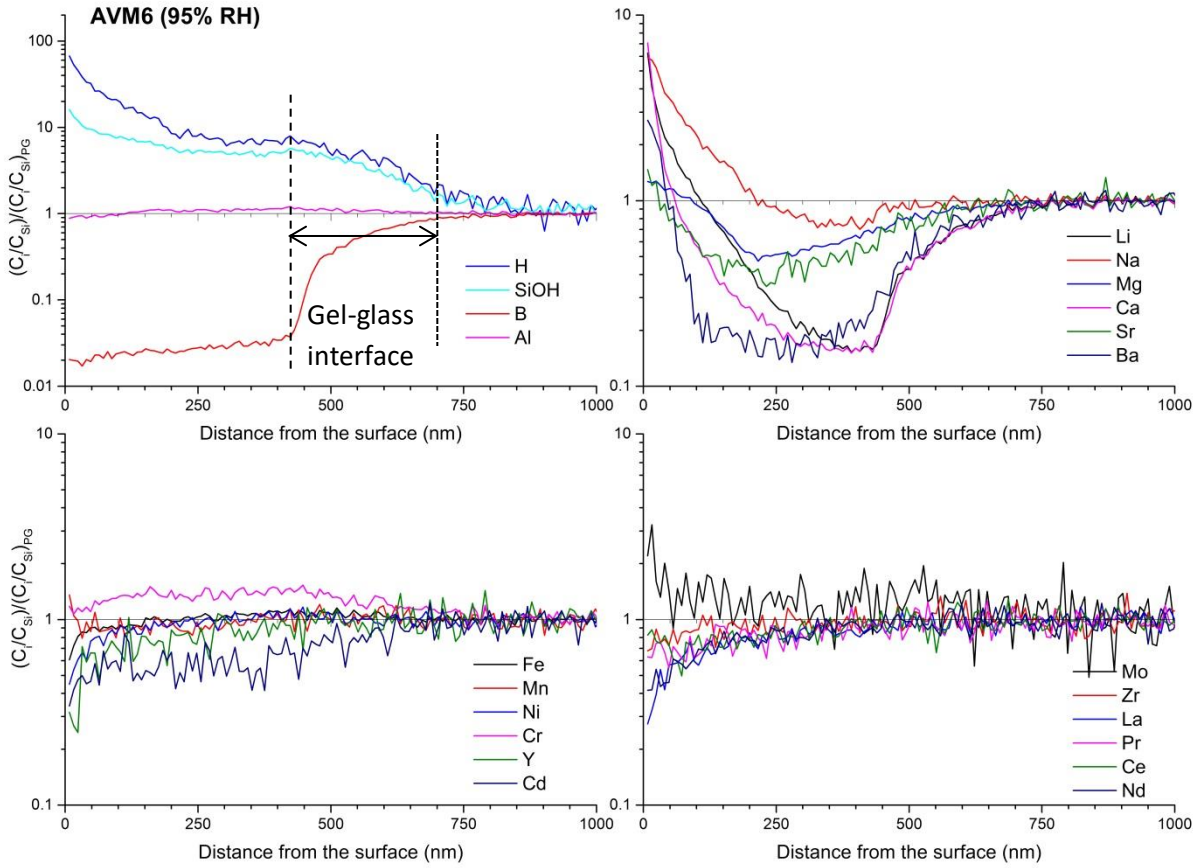

Figure 3- 18 ToF-SIMS profiles (normalized with respect to the intensity of Si and pristine glass) for the glass AVM6 altered in vapor phase at 50°C and 95% RH for 1 year

Table 3- 4 Thickness of the penetration of hydrogen into the surface of the altered glass and the thickness of boron depletion (gel layer thickness) for the AVM6 glass altered in vapor phase at 50°C and x% relative humidity for 1 year. The given values are measured from ToF-SIMS profiles normalized with respect to pristine glass and Si intensity.

Relative humidity, %	Thickness (hydrogen), nm	Thickness (boron), nm
55	31	27
76	200	190
83	129	124
95	620	541

3.3.4 Discussion

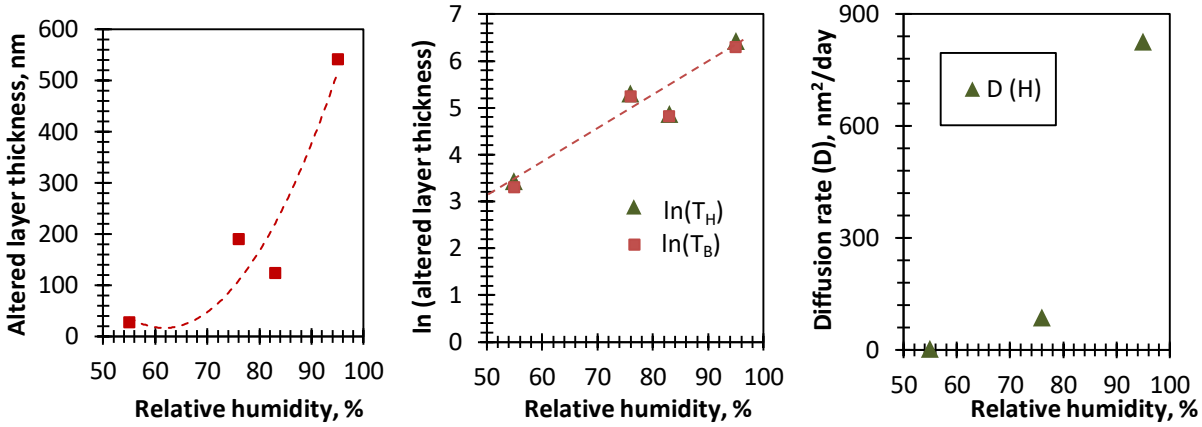

Figure 3- 19 (left) Evolution of the altered layer thickness (measured from the ToF-SIMS profiles of boron) as a function of relative humidity for the AVM6 glass altered in vapor phase at 50°C for 1 year; (center) natural logarithm of the thickness of hydrogen penetration and boron depletion with respect to RH; (right) Evolution of diffusion rate, D, of hydrogen into the altered layer as a function of the RH;

The influence of relative humidity was studied on the AVM6 glass since, among the six glasses studied in this thesis, AVM6 alters at the fastest rate. However, at the time of launching the experiment, it was unknown that the AVM6 glass alters in a heterogeneous manner. Despite the possible heterogeneity of the altered layer, we were able to calculate an altered layer thickness for each AVM6 sample from ToF-SIMS profiles based on equation AA-2. This altered layer thickness is plotted as a function of the relative humidity in figure 3-19. From 55% RH to 95% RH, it can be seen that the altered layer thickness increases more or less exponentially, except the discrepant value at 83% RH.

Even though the alteration of the AVM6 glass is heterogeneous, the altered layer thickness measured by ToF-SIMS is considered to be representative of an average thickness of the altered zones, since the area analyzed by ToF-SIMS is relatively large (50x50 μm^2). Therefore, the lower thickness of AVM6 glass altered at 83% RH than at 76% RH is quite puzzling. The different possibilities that are considered are measurement error of the value at 83% RH or ToF-SIMS analysis in a zone that was relatively less altered.

In literature, some studies have found that glass alteration rate evolves exponentially with increasing relative humidity [7, 14, 70] and other studies have found that the evolution is linear [148, 149]. A few studies have noted a threshold RH value below which glass alteration is negligible and beyond which the alteration rate increases exponentially. This threshold value varies between 60% and 90%, depending on the study (glass composition, temperature) [7, 14, 70].

Table 3-4 gives the depth of hydrogen penetration in the AVM6 glass samples altered at different RH values. Considering this depth as a "diffusion thickness, e", a diffusion coefficient, D can be calculated using the equation $e = 2\sqrt{\frac{Dt}{\pi}}$ based on Fick's law. The diffusion coefficient (calculated in nm^2/day) also evolves exponentially with relative humidity (figure 3-19).

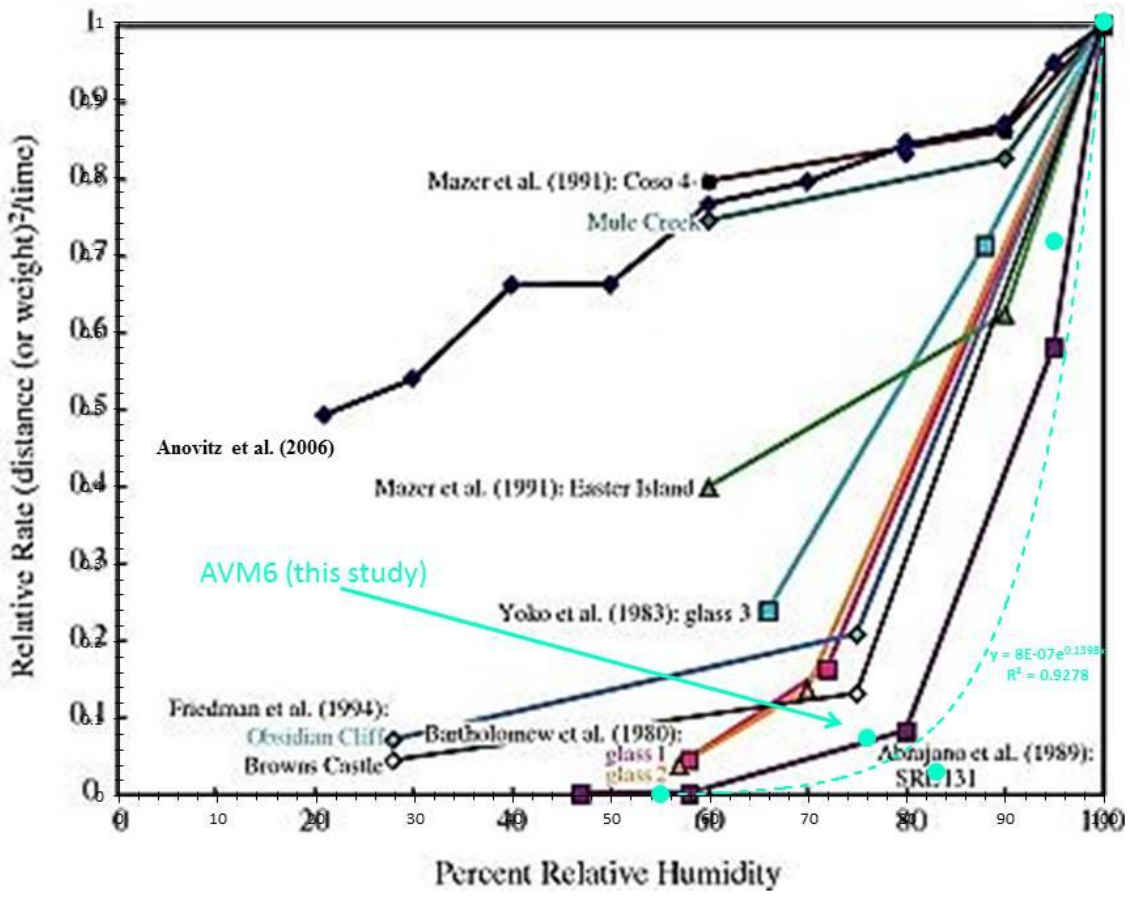

Figure 3- 20 Comparison of evolution of diffusion rate in (distance²/time) as a function of relative humidity in literature [149] and in this study

Figure 3-20 is extracted from literature [149] which compares the normalized diffusion rate as a function of RH for different studies (different compositions and temperature). The figure from literature is superimposed with the results from our study. The evolution of the diffusion rate in our study is very similar to the evolution of the diffusion rate of an SRL131 glass, a borosilicate nuclear waste glass, altered in vapor phase at 202°C [14].

The effect of relative humidity on secondary phase precipitation is also noticeable from our results. The samples altered at 83% and 95% RH have the same precipitates. The peaks in the XRD pattern of AVM6 sample altered at 95% RH are more intense than those for the sample

altered at 83% RH. This is most likely related to the faster alteration of the sample at 95% RH, due to the availability of water molecules. Some of the peaks are only present on the patterns of the AVM6 samples altered at 55% RH and 76% RH. These peaks indicate the presence of NaCl and hydrated oxides of rare-earth and transition elements. These precipitates have been identified despite the relatively low alteration of the AVM6 samples altered at 55% RH.

The ToF-SIMS profiles have not only revealed increasing alteration rate with increasing humidity, but certain elements such as Na, Mg, Al, Zr and other transition metals and rare-earth elements also show increased retention factor in the gel layer with increasing relative humidity. In order to facilitate comparison of the retention of elements in altered layers of different thicknesses, a "percent altered layer" was used for normalization. "Percent altered layer" is calculated as $\frac{x}{x_0} * 100$, where x is any given depth and x_0 is the altered layer depth calculated from equation AA-2 in appendix A. Figure 3-21 shows the normalized intensity of Na, Mg, Zr, Al, Mn, Ni, Fe, Nd and Ca as a function of the "percent altered layer" for all four RH values. These figures show a clear influence of the relative humidity on the retention of different elements. This effect is particularly marked for Na and Mg. At a low RH (55%), the first 40% of the gel layer retains only 10-20% of Na and Mg, whereas at 95% RH, Na is enriched in the gel layer and retention of Mg is 100%. When it comes to the elements Zr and Al, they are almost 100% retained in most of the gel layer for all RH values except at 55% RH, where Zr is depleted up to 80% and Al is depleted up to 50% in the gel near to the surface. Similarly, Nd is also significantly depleted only in the gel layer formed at 55% RH. In case of the transition metals Fe and Mn, they are depleted up to 90% in the gel layers formed at both 55% RH and 76% RH, but almost fully retained in the gel layers formed at higher RH values. The behavior of Ca is inverse to the all the other elements discussed above. In the gel layer formed at 55% RH, Ca is almost 100% retained. In the gel layers formed at higher RH values, the retention of Ca is only around 10% near the gel-glass interface but the enrichment increases towards the surface. The normalized intensity is not 1 even at 100% of the gel layer, meaning that the depletion of Ca is more profound than that of boron.

The reason for the influence of RH on the gel layer composition could be related to the pH of the water film on the surface of glass exposed to relative humidity. The lower the RH, the lower the quantity of water adsorbed on glass surface and consequently the pH may be higher. The solubility of phases such as $Ni(OH)_2$, $La(OH)_3$, zircon etc., increases starting from $pH_{50°C}$ >10 as shown in the figure A3-22. Also at basic pH, the formation of metal complexes is favored [150, 151], which may also favor the departure of these elements from the gel layer. The mobility of the transition metals in the gel layers formed at 55% and 76% RH and their complete retention

in the gel layers formed at higher RH values suggests that in the water film formed at lower RH values (55% and 76%), $pH_{50°C}$ >10 and at higher RH values, $pH_{50°C}$ <10. Here, hypotheses for migration mechanisms of these elements have not been discussed. But one of the suggestions is that the migration of elements towards surface may be facilitated by water condensation in gel porosity. It has already been discussed in chapter two that it is very likely that water condenses in the pores of the gel layer.

The enrichment of Na and Mg towards the surface in the gel layer formed at 95% RH must be due to their incorporation in phyllosilicates formed at the surface, since it was seen from the XRD patterns that the intensity of the peak attributed to phyllosilicates increased with increasing RH. Concerning the inverse behavior of Ca, the solubility of Ca decreases when $pH_{50°C}$>10. Therefore, Ca is only retained in the gel layer formed at 55% RH. This is coherent with the deduction that at 55% RH, $pH_{50°C}$ > 10, based on other element behaviours.

Comparison of vapor hydration in different protocols

The AVM6 sample in this study that was altered at 50°C and 95% RH for 1 year can be compared with the AVM6 samples that were altered at 50°C and 95% RH for 6 months and for 18 months which are described in chapter 2. The AVM6 monolith samples were retrieved from the same batch for both the studies. The difference between the study described in this chapter and the study described in chapter 2 is the alteration protocol (apart from the duration of alteration). In this chapter the AVM6 sample was vapor hydrated at LISA using their protocol, where the sample was placed in an air-tight container above a saturated K_2SO_4 solution to impose the relative humidity. In chapter 2, the AVM6 sample was vapor hydrated in a WEISS WK64L climatic chamber regulated at 50°C and 95% RH. Ideally, the glass alteration in both protocols must be similar since the temperature and relative humidity are the same. But, a few differences are noticeable among the AVM6 samples altered in the two different protocols.

One of the remarkable differences lies in the ToF-SIMS profiles. In the ToF-SIMS profiles of the two samples altered in the climatic chamber, a layer of phyllosilicates of 250-350 nm thickness is distinguishable from the ToF-SIMS profiles through the behavior of all the elements including transition metals and rare-earth elements in the AVM6 glass (figures A2-13 and A2-14).

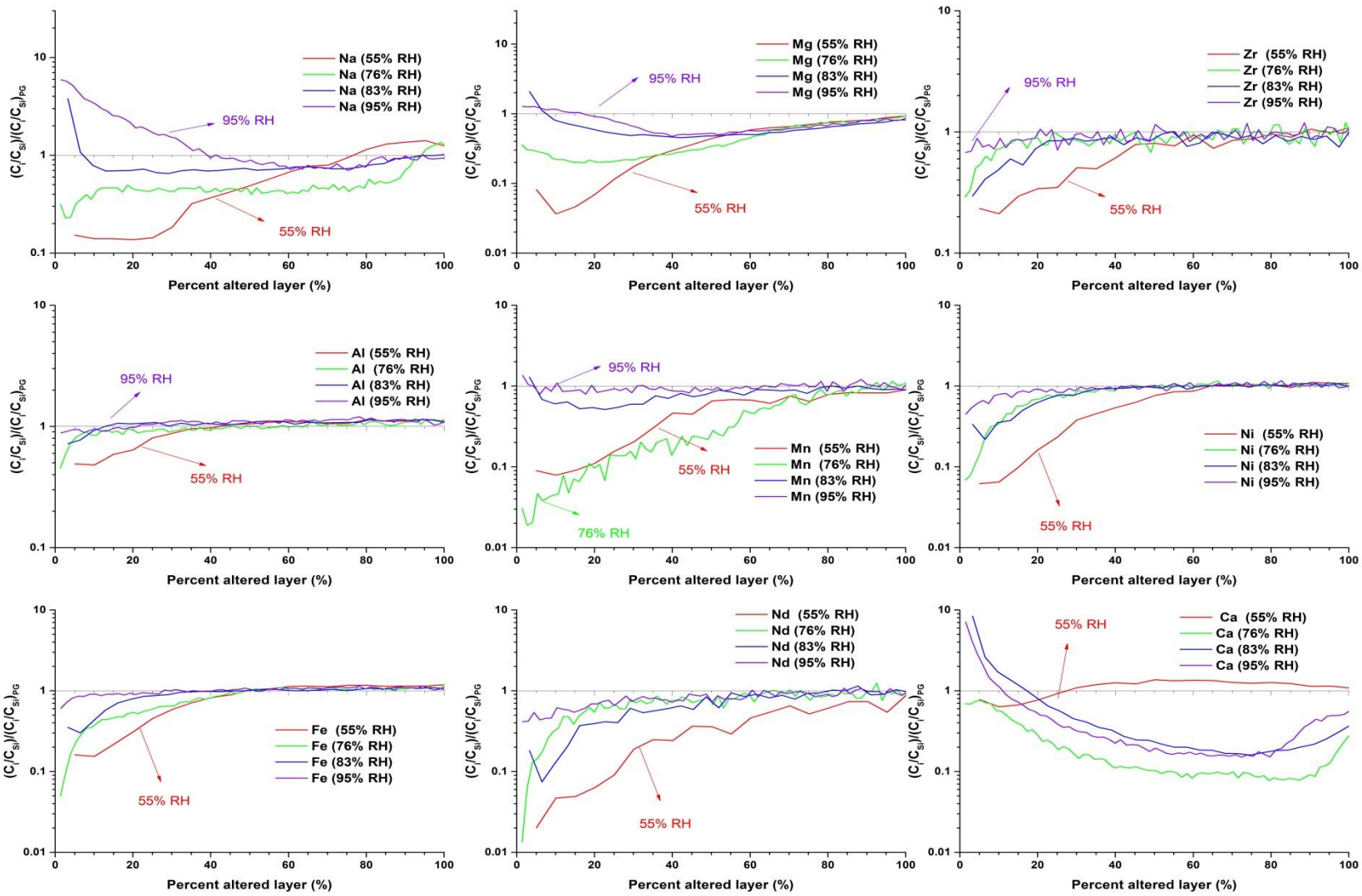

Figure 3- 21 A comparison of the normalized ToF-SIMS profiles of Na, Mg, Zr, Al, Mn, Ni, Fe, Nd and Ca as a function of percent of altered layer for the AVM6 glass altered in vapor phase at 50°C and 4 RH values (100% corresponds to the altered layer depth (gel-pristine glass interface) calculated from B profiles)

In case of the sample altered in LISA, a phyllosilicate layer of around 200 nm can be distinguished from the ToF-SIMS profiles through the profiles of the elements H, Na, Mg, Li and other alkali and alkaline-earth elements. However, aluminum, transition metals and rare-earth elements do not seem to be mobile at all. This could mean that the Si/X (where X is Al, a transition metal or rare-earth element) ratio in the gel layer, phyllosilicate layer and the pristine glass is the same for the sample altered in LISA. Also the interface between the gel-layer and pristine glass is also different between the two samples altered in the climatic chamber and the one sample altered at LISA. The thickness of the altered layer measured using the boron ToF-SIMS profile in the sample altered in the climatic chamber for 6 months is 1060 nm, whereas the thickness measured on the sample altered at LISA for 1 year is 541 nm. It is to be kept in mind that in both cases, the altered layer could be heterogeneous, explaining this variation in the overall altered layer thickness.

Figure A2-2 in appendix 2 shows the SEM images of the AVM6 sample altered in the climatic chamber for 6 months. While comparing them with figure 3-12 in this chapter, small differences in the nature of the secondary phases can be noted. The XRD patterns of all three samples altered in two different protocols show the same peak at 6° (2θ), indicating the presence of an aluminosilicate incorporating Na, Mg and Fe. But, the sample altered at LISA had some additional peaks at 8°, 10°, 12° and 14° (2θ) indicating the presence of other aluminosilicates, which were absent in the sample altered for a longer duration in the climatic chamber.

The differences in the samples due the different vapor hydration protocols used are not drastic, but seem to have affected the nature of some of the secondary precipitates (and thus, the element behavior in the altered layer) and the overall thickness of the altered layer.

3.3.5 Conclusion on the effect of relative humidity

The effect of relative humidity on the vapor hydration of AVM6 glass was studied at four different RH values. The vapor hydration kinetics increased with increasing RH. The factor of increase between 76% RH to 95% RH was higher than that between 55% RH to 76% RH. The increase in the water diffusion coefficient through the gel layer as a function of RH seemed to be exponential and was similar to another American nuclear waste borosilicate glass. SEM characterization revealed that the nature of the secondary phases and the altered layer was different between the samples altered at low RH (55% RH and 76% RH) and high RH (83% RH and 95% RH). Similarly, the XRD pattern also revealed that some of the precipitated phases are different between the low RH experiments and the high RH experiments. Secondary phases containing transition metals and rare-earth elements were identified only at experiments conducted at low RH. These elements were also revealed to be more mobile in the gel layer through ToF-SIMS profiles only at low RH experiments. This is most likely due to a pH effect, which may increase with decreasing RH. This is rather a positive information from the point of view of geological disposal scenario since the RH values expected in the repository are close to saturation. Despite varying RH and alteration protocols, one aluminosilicate phase that incorporates Mg, Na and Fe was identified on all samples, with varying XRD pattern peak intensities depending on the extent of glass alteration.

3.4 Study of vapor hydration mechanisms using isotopic tracers

3.4.1 Experiment

Monolith samples of dimensions (2.5x2.5x0.1 cm^3) of the glasses AVM6, AVM10, QCa and QMg were prepared and sent to LISA, where they were altered in vapor phase at 20°C and 91% RH for one year in the presence of deuterium and ^{18}O isotopes. The alteration protocol that was used is the same that is described in section 3.3.1, except that the saturated K_2SO_4 solution that was used to impose a RH of 91±3% was prepared using water that was 90% enriched in D_2O and 10% enriched in $H_2{}^{18}O$. The saturated K_2SO_4 solution imposed a relative humidity of 95% when prepared with water at natural isotopic abundance, but with isotopic enrichment, the measured relative humidity was around 91%.

A duplicate experiment was conducted with the same glasses of same dimensions at 20°C and 90% RH for 1 year using the protocol described in section 3.2.1 (figure 3-1), where 14 wt.% NaCl salt solution was used to impose the 90% RH. The water used to prepare the salt solution was of natural isotopic abundance. This duplicate experiment was conducted to verify that there was no additional effect of the isotopic tracers on the vapor hydration kinetics and element behavior in the altered layer.

3.4.2 Characterization of the altered samples

After vapor hydration, the altered samples were characterized by XRD and ToF-SIMS. Refer to appendix A for details on analytical parameters of the characterization techniques. It is to be noted here that the depths of penetration of ^{18}O, H and D are calculated using the formula given in equation AA-3 in Appendix A.

3.4.3 Results

This vapor hydration experiment was conducted at an ambient temperature (20-22°C), therefore any alteration that the samples have undergone relative to the pristine samples must be due to the relative humidity (90% RH) which is higher than ambient conditions. Figures A3-7, 8 & 9 in appendix 3 show the ToF-SIMS profiles of pristine samples for the four glasses of this study. These figures show the loss of all glass elements and penetration of H and SiOH in the first 5-20 nm in the pristine samples as well. This very thin depleted layer might have either been created while polishing the samples or during storage in ambient conditions (~20°C and <40% RH). It is to be noted that the penetration of H in the older pristine samples, (i.e. AVM6 and

AVM10) is deeper than the penetration of H in the recently elaborated pristine samples (i.e. QCa and QMg)[12].

Figures 3-22, 3-23 & 3-24 and figure A3-28 in appendix 3 show the normalized ToF-SIMS profiles of the glasses altered in vapor phase with and without isotopic enrichment (left side and right side of the images respectively). These profiles show that the element behavior in the surface of the altered glass is identical in both experiments (enriched and unenriched). Similar to the penetration depth of H, SiOH and the isotopic tracers, all the elements seem only depleted in the first few nm. From table 3-5, we can compare the depth of hydrogen penetration and boron depletion in the pristine sample and the altered samples. These depths are only a few nm deeper than that in the pristine sample. This suggests that the glass alteration is extremely low under the given hydration conditions.

[12] AVM6 and AVM10 samples were fabricated around 2007 whereas QCa and QMg glasses were fabricated in early 2017

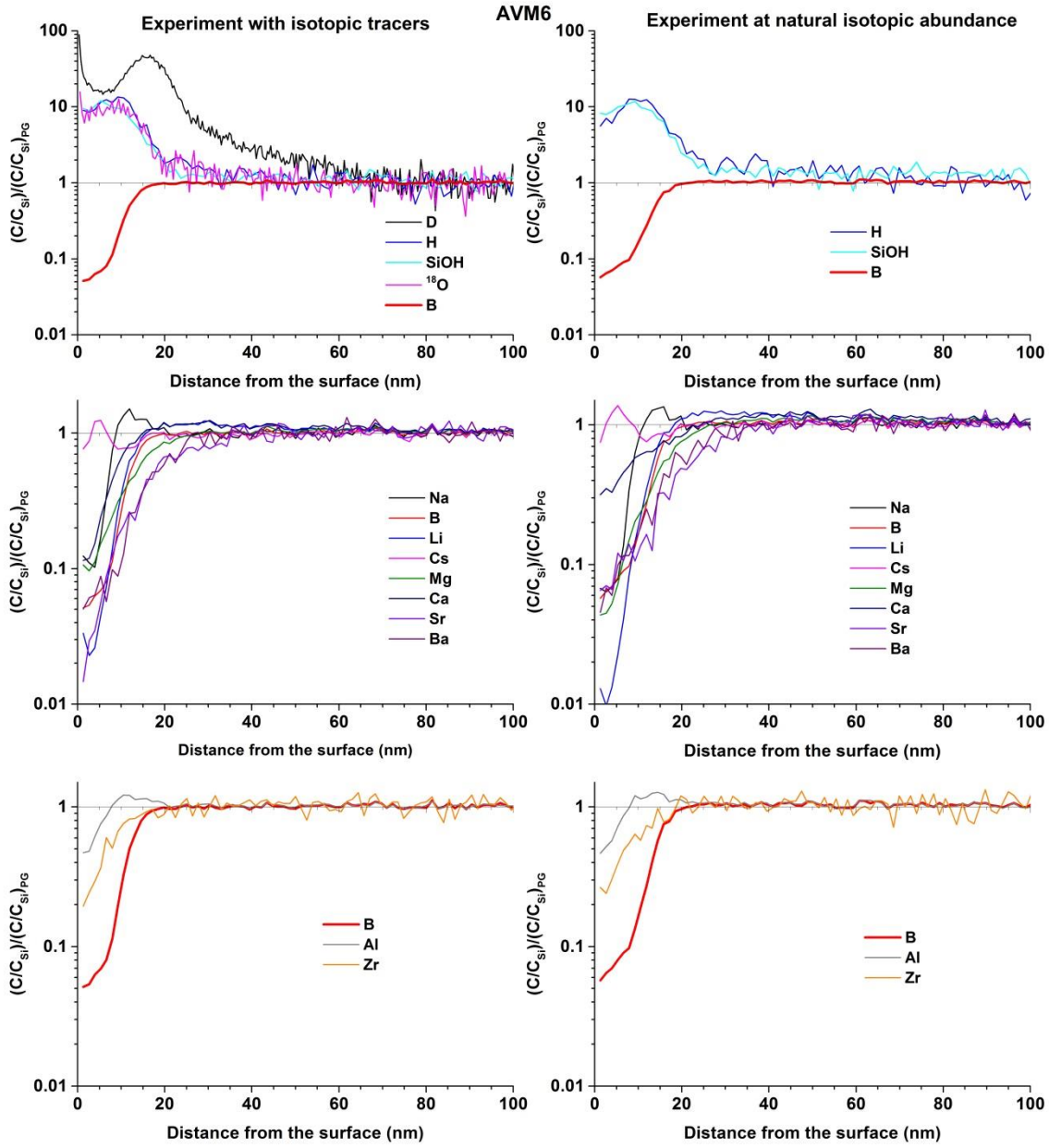

Figure 3- 22 Normalized ToF-SIMS profiles of the network formers, alkali and alkaline-earth elements, hydrated species and tracer isotopes for the AVM6 samples altered in vapor phase at 20°C and 90% RH for 1 year; The profiles on the left side correspond to the experiment conducted with enriched isotopic tracers D and ^{18}O; The profiles on the right side for the same elements correspond to the experiment conducted at natural isotopic abundance.

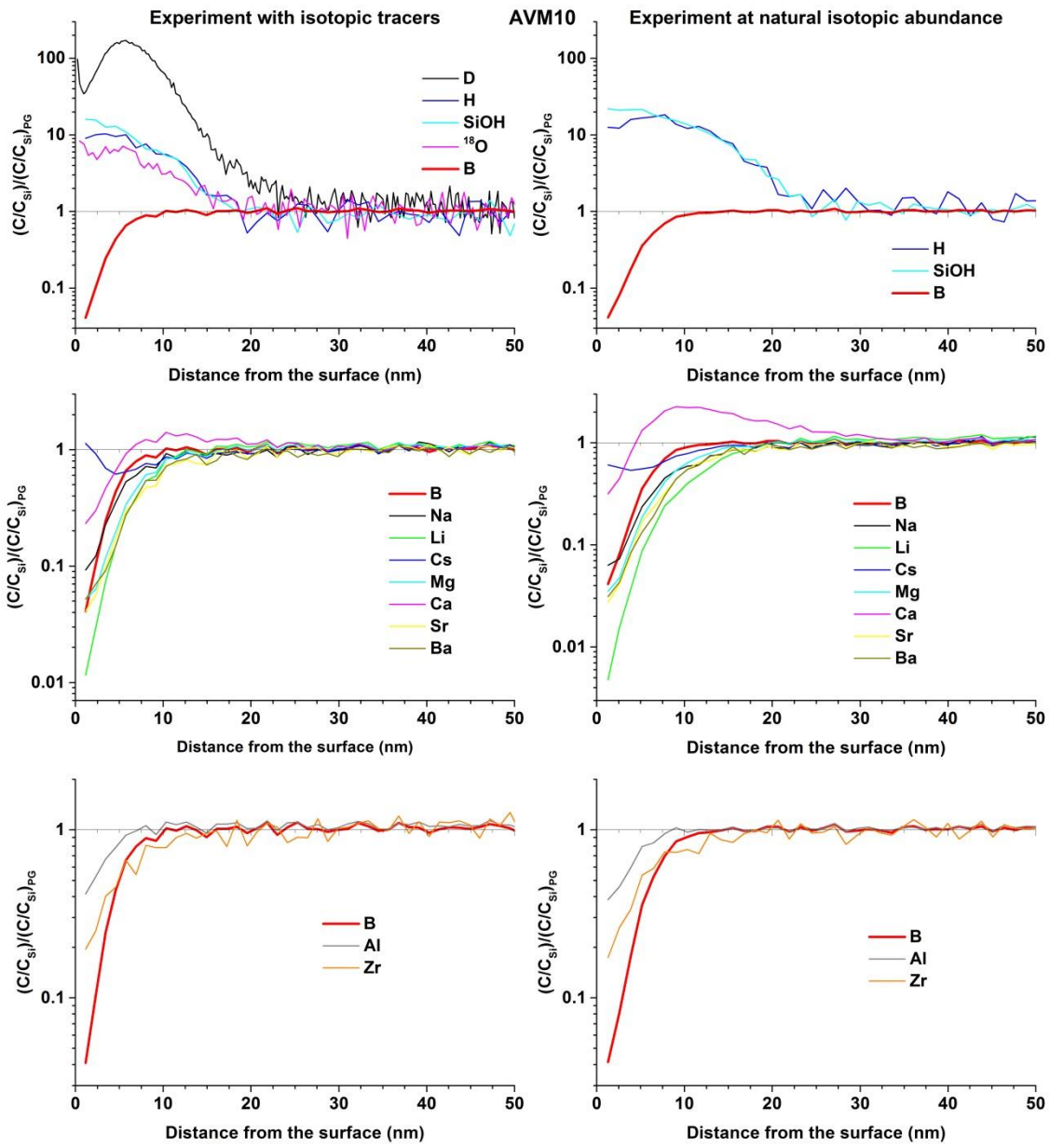

Figure 3- 23 Normalized ToF-SIMS profiles of the network formers, alkali and alkaline-earth elements, hydrated species and tracer isotopes for the AVM10 samples altered in vapor phase at 20°C and 91% RH for 1 year; The profiles on the left side correspond to the experiment conducted with enriched isotopic tracers D and ^{18}O; The profiles on the right side for the same elements correspond to the experiment conducted at natural isotopic abundance.

Despite this very low alteration in vapor phase during 1 year, certain secondary phases have been identified through XRD on some of these vapor hydrated glasses. Figure A3-23 in appendix 3 shows the presence of NaCl on the AVM6 sample altered at natural isotopic abundance (relative humidity imposed using NaCl). The XRD pattern of the AVM10 sample altered in vapor phase that was enriched in isotopic tracers showed peaks that could be Na-alumino silicates or Mg-silicate hydroxides (figure A3-24). The QCa sample altered at natural

isotopic abundance showed several peaks corresponding to Ca-silicates/aluminosilicates (figure A3-26). The QCa glass altered in the presence of isotopic tracers too showed a small peak that was barely distinguishable from the background noise that could be Ca-aluminosilicates (figure A3-25). The QMg glasses altered with and without isotopic tracers showed peaks corresponding to Mg silicates (figure A3-27).

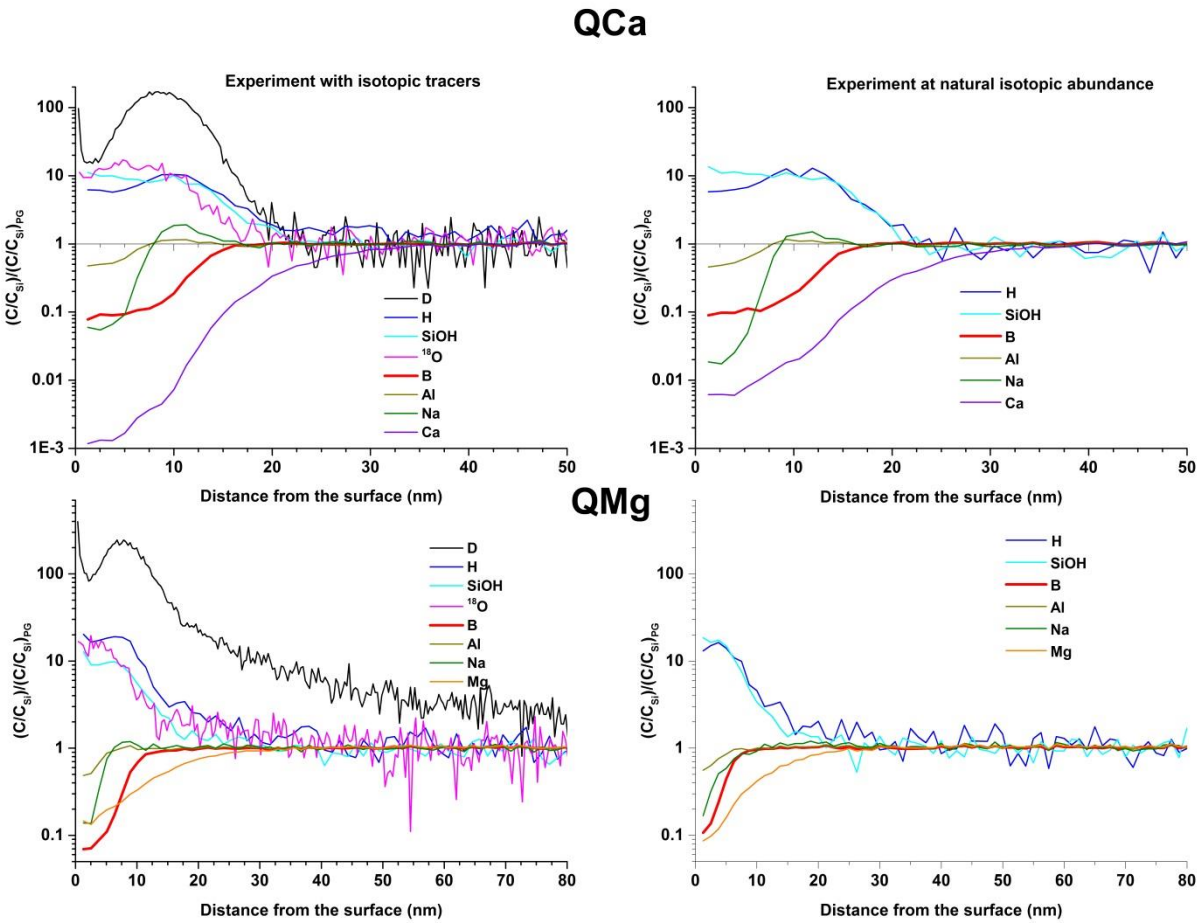

Figure 3- 24 Normalized ToF-SIMS profiles of the QCa (top) and QMg (bottom) samples altered in vapor phase at 20°C and 90% RH for 1 year; The profiles on the left side correspond to the experiment conducted with enriched isotopic tracers D and ^{18}O; The profiles on the right side for the same elements correspond to the experiment conducted at natural isotopic abundance.

Regarding the element behavior in the hydrated layer, boron is not the most depleted element as is the case usually in vapor hydrated glasses. For all glasses, Li is the least retained element towards the altered surface. The depth of depletion of the alkaline-earth and rare-earth elements is greater than the depth of depletion of boron. The depletion of alkali elements such as Na and Cs and the transition metals are lesser than that of boron.

Figure 3-25 presents the D/H and $^{18}O/^{16}O$ ratios (after normalization) through the depth of the altered layer as measured by ToF-SIMS profiles in all four glasses vapor hydrated in the isotopically enriched medium. The behavior of these two isotopes in the gel layer gives the key information on the mechanisms of vapor hydration. The penetration of D without accompanying ^{18}O indicates glass alteration by an ion-exchange/inter-diffusion mechanism. It may or may not be accompanied by the loss of network-modifier elements. The penetration of ^{18}O in the gel layer either indicates network-hydrolysis mechanism. In case of the AVM6 and QMg glasses, the depth of penetration of D is 1.5 & 1.33 times greater than the depth of penetration of ^{18}O molecules respectively. This indicates a pre-dominant interdiffusion mechanism. In case of the glasses, AVM10 and QCa, the depth of penetration of D and ^{18}O is almost similar. This means that network hydrolysis/penetration of water molecules is either equivalent to interdiffusion mechanism or predominates vapor hydration in these glasses.

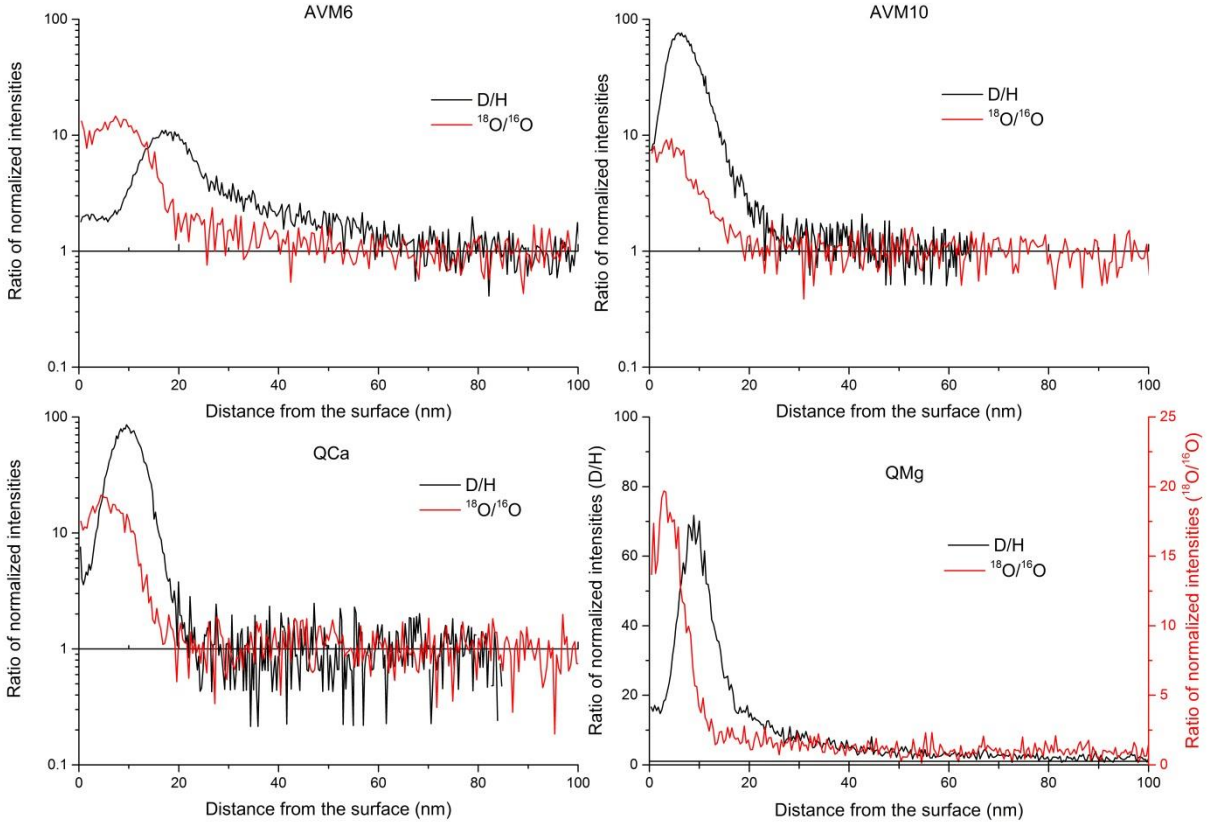

Figure 3- 25 Ratio of the normalized (with respect to Si and pristine glass) intensities of the isotopes D/H and $^{18}O/^{16}O$ measured by ToF-SIMS as a function of the distance from the surface of the samples for the glasses AVM6 (top-left), AVM10 (top-right), QCa (bottom-left) and QMg (bottom-right)

Table 3- 5 Depth of penetration of H (in nm) into the surface of the pristine glasses, glasses altered in vapor phase at 20°C and 91% RH for 1 year with and without isotopic enrichment; Depth of penetration of isotropic tracers D and ^{18}O (in nm) into the surface of the glass samples altered in enriched vapor phase; Depth of depletion of boron (in nm) from the surface of the pristine sample and the samples altered in vapor phase with and without isotopic enrichment (PG: Pristine Glass)

	Depth of penetration, nm					Altered layer depth, nm		
		H			Oxygen-18	(B depletion)		
	PG	Experiment with isotopic tracers		Experiment at natural isotopic abundance	Experiment with isotopic tracers	PG	Experiment with isotopic tracers	Experiment at natural isotopic abundance
		D	H					
AVM6	14	21	16	16	14	14	12	14
AVM10	11	9	11	16	11	4	5	6
QCa	7	12	16	16	11	4	13	13
QMg	7	12	11	8	9	-	8	5

3.4.4 Discussion

At 20°C and 90% RH, the four glasses in this study have altered to an extremely low level, even though the glasses were altered for 1 year. In the absence of elevated temperatures to thermally activate the glass-water reactions, simply an increase in the relative humidity does not result in the formation of a gel layer of a significant thickness. This shows that these borosilicate glasses are more resistant to vapor hydration than other alkali-silicate glasses, especially used as stained glass windows. The alkali-aluminosilicate glass that was altered in exactly the same condition using the same protocol at LISA for similar duration had developed a hydrated layer of about a few hundred nm to a few µm depending on the duration of alteration (a few months to 1 year) [70].

For two of the four glasses studied (AVM6 & QMg), inter-diffusion was identified as the pre-dominant glass alteration mechanism since D penetrates deeper than ^{18}O. The D penetration depth is also deeper than the depletion of alkali-elements. This is usually referred to as glass hydration without accompanying de-alkalization. But this does not mean penetration of water molecules, since if it was the case, then ^{18}O would have also penetrated as deep as D. Therefore, this means that D diffuses inside the glass network by means of ion-exchange, but the modifier element that was exchanged from the glass structure was not immediately leached out and must remain in the interstitial spaces. This is similar to the results in the cited reference where hydrated glass of a 200 nm was formed without accompanying de-alkalization [70]. The depth of ^{18}O penetration (30 nm) in the cited reference is also lower than D penetration depth.

Hydration of the glasses without accompanying de-alkalization was also reported during other vapor hydration studies in literature [14, 57].

In the other two glasses (AVM10 and QCa), the depth of penetration of D and ^{18}O are very close to each other, suggesting that network hydrolysis could predominate vapor hydration. The depletion of alkali/alkaline-earth/rare-earth elements also indicates the occurrence of inter-diffusion mechanism. This shows that at 20°C, the rate controlling vapor hydration mechanism is very sensitive to composition. But with the results in this study, the mechanism by which glass composition influences vapor hydration cannot be ascertained. In literature, it has been suggested that when the glass contains a significant fraction of modifier elements, inter-diffusion mechanism will be favored. In our study, we were not able to make such correlations.

In chapter 2, for the glasses AVM6 and QMg, secondary phase precipitation and network hydrolysis were identified as the rate-controlling vapor hydration mechanisms respectively at 50°C, contrary to inter-diffusion mechanism at 20°C. Once again, in coherence with section 3.2, the temperature dependence of the vapor hydration mechanisms has been demonstrated. Due to the very low extent of alteration and the lower RH value of the experiment at 20°C, it was not verified if Arrhenius law was obeyed between 20°C and the temperatures discussed in section 3.2.

At 20°C, the behavior of elements is different than at other temperatures in general. Li, alkaline-earth and rare-earth elements are more depleted than boron. The XRD pattern identified phases containing Ca and Mg. Therefore, formation of phases containing these elements could be the sink behind the relatively higher depletion of these elements. An unexpected result in our study at 20°C and 90% RH is the identification of silicate secondary phases through XRD patterns. Fewer secondary phases were identified through XRD on the same glasses at 50°C and 95%RH in chapter 2 and at 90°C and 95% RH in section 3.2 of this chapter. However, these phases do not seem to have accelerated the glass alteration at 20°C and 91% RH in any way. They seem to be a consequence of glass alteration. While carbonates are routinely identified during atmospheric alteration studies, formation of silicates is commonly observed only during vapor hydration at higher temperatures. Therefore, the absence of carbonate phases and the formation of silicate phases on 5 out of 8 samples is surprising. Especially since the silicate phases must have been well crystallized in order to be detected by XRD despite their low quantity. In literature, one study showed that more phases had precipitated during vapor hydration (at 85% RH) of an alkali-silicate glass at 40°C than at 80°C [61]. In the study, it was explained that the solvation of alkaline-earth elements was less favored compared to network

hydrolysis at 80°C, due to which these elements could not be mobilized to form secondary precipitates. This result highlights the need to understand better the thermodynamics of the secondary phases that are susceptible to form during vapor hydration at different temperatures and also time durations.

Observing the ToF-SIMS profiles of ^{18}O and H, it can be seen that the highest intensity is towards the surface of the altered samples. In the case of the ToF-SIMS profiles of D however, the highest intensity is close to what seems to be gel-pristine glass interface. It was already observed in previous studies with these isotopic tracers that D very rapidly exchanges with H from the atmosphere once it is removed from the medium enriched in D [152]. It is logically presumed that the original profile of D must have resembled the profile of H. But due to exchange, D must be lost from the gel layer between the time it was removed from the reactor and the time that it was characterized by ToF-SIMS. Nevertheless, we are able to identify the depth of penetration of D due to the peak in the intensity of D in the ToF-SIMS profiles at the interfacial region. The higher intensity of D in the interface could be because they are less easily exchangeable with atmosphere due to transport constraints or they could form stronger bonds at the interface or the water speciation at the interface could be different.

3.4.5 Conclusion on the study of vapor hydration mechanism

At 20°C and 91% RH, the extent of glass alteration is very low even for duration as long as 1 year. Nevertheless, the usage of isotopic tracers D and ^{18}O has helped to identify that the pre-dominant vapor hydration mechanism is inter-diffusion in case of two out of the four glasses and maybe hydrolysis mechanism for the other two glasses. At 20°C, the dependence of vapor hydration mechanism on glass composition was also noted. The temperature dependence of the rate-controlling vapor hydration mechanism was revealed in this study as well. This study has pointed out the need to understand the secondary phase precipitation kinetics at different temperatures. In vapor phase alteration, secondary phases may play a key role from the point of view of retention of radionuclides by the nuclear waste glasses.

3.5 Conclusion

In this chapter, the effect of temperature and relative humidity on the AVM6 glass was studied. It was revealed that while the altered layer morphology was similar at all the temperatures (continuous gel layer of homogeneous thickness along with intermittently present irregularly altered zones), the nature/identity of the secondary phases and the behavior of elements in the gel layer varied with temperature. A difference in some of the precipitated secondary phases and the nature of the altered layer between low RH values (55% & 76%) and high RH values (83% and 95%) was noted. Secondary phases incorporating rare-earth elements and transition metals (which are inactive simulants for radioactive actinides and fission products) precipitated at the sample surface only at low RH experiments. Their mobility in the gel layer was also revealed to be high only at low RH experiments. While it was argued that network hydrolysis is the rate-controlling mechanism for the formation of the homogeneous gel layer at temperatures 50°C-90°C (95-97% RH), isotopic tracer study revealed that inter-diffusion could be the pre-dominant glass alteration mechanism at 20°C and 91% RH for this glass and for QMg as well. However, for AVM10 and QCa, the same isotopic tracer study suggests that network hydrolysis could be the predominant glass alteration mechanism at 20°C and 91% RH.

The effect of temperature between 50°C and 120°C at 95% RH was also investigated on the three simplified glasses Q, QCa and QMg. This study revealed the changing rate-controlling mechanism with temperature and consequently, the changing effect of glass composition.

Despite a very low glass alteration at 20°C and 91% RH, glass composition has an effect on the pre-dominant vapor hydration mechanism. But unfortunately, with the results available, it was not possible to understand how the glass composition plays a determinant role.

These results highlight the very high temperature dependent sensitivity of chemical durability in vapor phase to glass composition. Small changes in composition result in large differences in alteration and differences in the predominance of one rate-controlling vapor hydration mechanism over another.

Chapter 4 NMR investigation of glass alteration in vapor phase and in aqueous medium

4.1 Introduction

The structure of glass determines its physical and chemical properties. The glass composition influences the coordination numbers and the type of bonding of the atoms. Raman spectroscopy, infrared spectroscopy and Nuclear Magnetic Resonance spectroscopy (NMR) are some of the most useful and common tools used to study the structure of glass. These techniques permit to study the coordination numbers and intramolecular bonds in both solids and liquids. Many studies exist on the investigation of glass structure of various compositions using these techniques [153-158].

The added advantage of NMR spectroscopy is its ability to selectively probe the nearest neighboring atoms of specific isotopes of key interest to borosilicate glass structure such as ^{11}B, ^{29}Si, ^{27}Al, ^{23}Na, ^{17}O, etc. Several studies in the past have provided structural insights by correlating isotropic chemical shifts that can be obtained from MAS[13] NMR with coordination number, bond-distance, bond-angle and first and second neighbor populations[159]. NMR spectroscopy studies help to analyze if the alkali and alkaline-earth elements that have been added to the silicate/borosilicate glass are mixed homogeneously. Such studies have pointed out that Na^+ ions are preferred by four coordinated B and Al units for charge compensation [160, 161] and in mixed alkali glasses containing Li (Li/Na and Li/K), the alkali are less randomly mixed [159]. Ca^{2+} and Mg^{2+} ions that have a higher cation field-strength interact much more strongly with NBO[14] than Na^+ and the increase in five coordinated Al units with the increase in Mg^{2+} ions is non-negligible [162]. Similarly, studies have provided information on the effect of concentration of network forming elements on the glass structure. The fraction of five-coordinated Al increases slightly with the increasing fraction of Al in the glass. Increasing Al/Si ratio also decreases the randomness of the Ca/Mg mixing [163]. In a borosilicate glass containing Zr, the charge compensation of the six coordinated Zr entities takes preference over the charge compensation of the four coordinated B entities. As a result, the fraction of three coordinated boron units increases [161].

[13] Magic Angle Spinning
[14] Non-bridging oxygen atoms

Some of the experiments have also studied and linked the gel structure (gel formed during aqueous alteration of glasses) with the pristine glass structure (by techniques other than NMR spectroscopy also for that matter) [106, 107, 133, 164-168]. In a basic media, Si network is remarkably modified from the pristine glass with an increase in the Q^3 and Q^2 species [166]. From ^{1}H DQ[15] experiments and ^{1}H-^{29}Si CP- MAS[16] NMR experiments, silanol groups and molecular water physisorbed to Si sites can be distinguished. In the presence of both Na and Ca, an exchange of the charge compensating atom of the $[AlO_4]^-$ units from Na in the pristine glass to Ca in the gel layer is also observed. Two aluminum environments have also been distinguished through ^{1}H-^{27}Al CP-MAS NMR experiments [133]. Elements such as Zr and Pb have a similar structural configuration in the pristine glass and in the gel [107, 169]. Usually in a sample that is fully altered in aqueous medium (which contains only gel), ^{11}B NMR signals are not detected since the gel layer formed in aqueous medium retains such a low quantity of boron that it is beneath the detection limit of NMR [106].

In case of the gel layer formed during vapor hydration, the number of studies is scarce [33, 61, 170]. The published NMR results on a vapor hydrated (80°C and 85% RH for 72 hours) alkali silicate glass has revealed the close proximity of the SiOH, H_2O and Na^+ species in the gel layer and demonstrated that there is no alkali loss in the gel layer formed in vapor phase, which is unlike the gel layer formed during aqueous alteration [33].

In literature, it has already been discussed that the reactivity of glass in aqueous medium could differ from its reactivity during vapor hydration. Certain glasses could be more reactive in vapor phase than in aqueous medium [29, 33], while glass alters faster in aqueous medium in other cases [13]. Despite these differences, some studies consider that glass alteration in vapor phase is similar to its alteration in aqueous medium at a very high surface area of glass to solution volume (SA/V) ratio [8, 18, 19, 171]. While the effects of SA/V ratio on glass alteration already seem complex [171, 172], it is not clear if the differences observed between glass chemical durability in aqueous medium and in vapor phase can be explained as an effect of SA/V ratio alone. In order to gain more insights into the validity of this comparison, we chose to do a comparative study of the structure of the gel layer formed on two glass compositions altered in vapor phase and in aqueous medium at a very high SA/V ratio.

[15] Double Quantum
[16] Cross Polarization-Magic Angle Spinning

In this chapter, two simplified borosilicate glasses (with natural abundance isotopic composition for oxygen atoms) were altered separately in vapor phase and in aqueous medium at a very high SA/V ratio, where both alteration mediums (the water used to leach glass in aqueous medium and the water used to generate humidity in vapor phase) were enriched in ^{17}O in order to specifically probe the global structure of the alteration layer by ^{17}O NMR. Pristine glasses enriched in ^{17}O were also prepared for comparison with the alteration layer structure. The local chemical environments of ^{17}O, ^{1}H, ^{29}Si, ^{27}Al, ^{23}Na and ^{11}B in the pristine samples and gels formed in both mediums were probed using MAS, CP-MAS and 2D MQMAS[17] NMR spectroscopy in order to compare their structure.

4.2. Materials and methods

4.2.1 Sample preparation

Glass compositions used in this study are the quaternary soda-aluminoborosilicate glass named as “Q” and quinary soda-lime-aluminoborosilicate glasses named as “QCa”. These are the same glasses that were described in chapter 2.

4.2.1.1 Preparation of unenriched glasses

The glass blocks, whose preparation is described in section 2.2.1, was used for this study as well. They were cut to make polished monoliths (surface roughness < 1 µm) of dimensions (2.5x2.5x0.1 cm^3) and the remaining glasses were then crushed with tungsten carbide balls in a Retsch MM400 ball-mill apparatus to obtain glass powder. Glass powders of particle size 0.45 < ø < 2 µm were obtained by applying Stokes’ law for terminal velocity of glass particles of 1 micron radius falling through 99.99% pure acetone solvent and using 0.45 µm pore-size membrane filter.

4.2.1.2 Preparation of glasses enriched in ^{17}O

Two batches (200 mg each) of the Q and QCa glasses were prepared using a sol-gel process. Metal-alkoxide precursors ($Si(C_2H_5O)_4$, $B(C_2H_5O)_3$, $Al(C_2H_5O)_3$, $NaOC_2H_5$ (and $Ca(CH_3O)_2$ for QCa)) were mixed with anhydrous C_2H_5OH and stoichiometric proportion of enriched water (80% ^{17}O) according to equation 4.2.1.1 in one batch and water of natural abundance in the second batch. After hydrolysis reactions (equation 4.2.1.1), wet-gels are formed, which are then dried in oven at 90°C until dry gels are obtained. These well-mixed powdered dry-gels were then melted together in two separate platinum foils in an oven, under argon atmosphere. The temperature of the oven was raised to 160°C at a rate of 4.7°C/min and maintained at this temperature for 30

[17] Multi Quantum Magic Angle Spinning

minutes. Afterwards, the temperature of the oven was raised to 1200°C at a rate of 4.7°C/min and the glasses were melted at this temperature for 25 minutes. The platinum foils are then immediately removed from the oven and glassy masses form almost instantaneously upon rapid cooling. The resulting glasses are crushed in a Retsch MM200 ball-mill apparatus to obtain glass powders. The first batch containing ^{17}O enriched glasses were used for NMR spectroscopy and the second batch containing natural abundance glasses were analyzed for composition using ICP-OES spectroscopy (provided in table 4-1). The differences in composition between the unenriched glasses and the glasses enriched in ^{17}O are discussed further below.

$M\text{-}(O\text{-}R)_n + n\ H_2{}^{17}O \rightarrow M\ (^{17}OH)_n + n\ ROH$ *(M = metal of charge n^+; R = organic group)*

Equation 4.1.2.1

Table 4- 1 Glass composition (analyzed by ICP-OES), glass density measured by He pycnometer and the specific surface area of glass powders measured by BET (0.45-2 µm)

	Q unenriched	Q enriched in ^{17}O	QCa unenriched	QCa enriched in ^{17}O
SiO_2	57.5	64.3	52.7	58.1
B_2O_3	15.3	10.3	14.6	8.3
Na_2O	19.2	16.4	19.0	15.3
Al_2O_3	8.1	9.1	7.5	8.8
CaO			6.2	9.5
ρ (g/m^3)	2.44		2.50	
Specific surface area of glass powders size fraction 0.45 < Ø 2 µm (m^2/g)	5.00		4.64	

4.2.2 Experiment

4.2.2.1 Vapor phase alteration

The protocol used for vapor hydration in this chapter is similar to the protocol that is described in chapter 3 (figure 3-1). Approximately 300 mg of Q and QCa glass powders (0.45 < ø < 2 µm) were each taken in a Teflon cup supported in a Teflon container. 3.25 wt% of NaCl was prepared using 40% $H_2{}^{17}O$ water and added at the bottom of each container to impose 98% relative humidity (RH) at 90°C [139]. A (2.5x2.5x0.1 cm^3) monolith of each glass was also placed above the NaCl solution, to analyze the thickness of the altered layer formed using Scanning

Electron Microscope (SEM) and study the behavior of elements in the gel layer by Time of Flight-Secondary Ion mass Spectrometry (ToF-SIMS). This set-up was placed inside a stainless-steel autoclave, which was in-turn placed inside an aluminum over-container to avoid rapid heating and cooling of the reactor set-up. The entire vapor phase alteration protocol that is described in figure 4-1 is based on the protocol used in the cited references [24-27, 29]. The two reactors, each containing the Q and QCa samples respectively, were placed in an oven at 90°C for 213 days. These durations were adapted to obtain a significant proportion of altered glasses. At the end of the experiment, the reactors were cooled to ambient conditions and the samples were retrieved and stored in aluminum foils / Eppendorf tubes in ambient conditions until characterization.

The monoliths were characterized using SEM, XRD and ToF-SIMS. Details of the analytical parameters are provided in Appendix A.

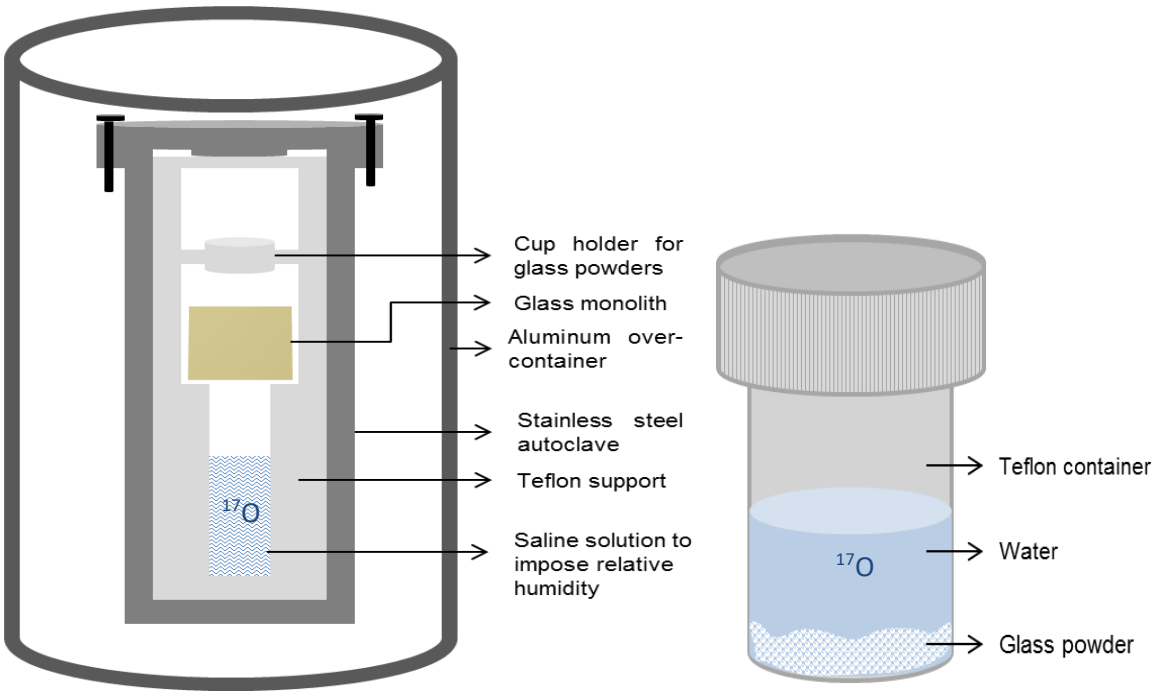

Figure 4- 1 (left) protocol used for alteration of glasses in vapor phase; (right) protocol used for glass alteration in aqueous medium at a very high SA/V ratio

4.2.2.2 Aqueous alteration at a very high SA/V ratio

Approximately, 250 mg of Q and QCa glass powders (0.45 < ø < 2 µm) were leached by 2.22 g and 2.07 g of 40% $H_2{}^{17}O$ enriched DI water respectively in Teflon containers to achieve SA/V ratios of 570438 m^{-1} and 563708 m^{-1} respectively (as shown in figure 4-1). The first Teflon container was placed in a second larger Teflon container with water to minimize water loss. This setup was placed in an oven at 90°C. The glass Q was altered for 59 days and the glass QCa was altered for 213 days. At the end of the experiment, the pH of the solution was measured and the leachate was sampled, ultra-filtered using a 10000 Dalton membrane filter (~2 nm) and diluted in 0.5 N HNO_3 and analyzed using ICP-OES to calculate the altered glass percentage using equation A4-1 in appendix 4 and the gel composition.

A duplicate experiment was carried out for each glass using natural abundance DI water and 100 µL of leachate was periodically sampled to follow alteration kinetics. This precaution was taken to prevent the possible formation of substantial quantity of secondary phases at high SA/V ratio and temperature conditions that may destabilize the gel due to formation of zeolites, as observed in literature [50, 173, 174]. The sampled leachate was analyzed using ICP-OES to calculate the altered glass percentage and normalized mass losses of elements using equations A4-1 and A4-2.

4.2.3 NMR spectroscopy

NMR data were collected on a Bruker 500WB Avance II spectrometer operating at a magnetic field of 11.72T, using a 4-mm Bruker CP-MAS probe at a spinning frequency of 12.5 kHz. For ^{27}Al, ^{23}Na and ^{11}B, a single short pulse excitation of 1 µs in length (tip angle of about 15°) was used to acquire quantitative spectra with a recycle delay of 1s for ^{27}Al, ^{23}Na and 2s for ^{11}B. ^{17}O MAS NMR spectra were acquired using a rotor-synchronized spin echo pulse sequence (i.e., with a spin echo delay of one rotor period and selective pulse on the central transition) in order to minimize the baseline distortion due to the ringing signal. For ^{17}O two-dimensional multiple quantum MAS (MQMAS) spectra, the Z-filter three pulse sequence [175] was used. For ^{11}B MQMAS experiments, Z-filter and RIACT two pulse sequence were used for optimized acquisition of the BO_4 and BO_3 peaks, respectively, as detailed in Ref [161]. ^{29}Si MAS NMR spectra were acquired using a 90° pulse after a presaturation period (composed of a train of about 20 90° pulses with a 2ms delay between the pulses) a recycle delay of 20s (no change in lineshape were observed for longer recycle delay). For spin-echo REDOR experiments selective 90° and 180° pulses (frequency 10-20 KHz; 180° pulse duration of 8-10 µs) were applied on the

central transition (1/2↔1/2) [168, 176, 177]. Chemical shifts are referenced to an external sample of 1M boric acid solution (19.6 ppm), 1M $AlCl_3$ solution (0 ppm), 1M NaCl solution (0 ppm), powder tetrakistrimethylsilane (TKS) with the highest intensity peak situated at -9.9 ppm (from that of TMS) and $H_2{}^{17}O$ (40%, 0 ppm) for ^{11}B, ^{27}Al, ^{23}Na, ^{29}Si and ^{17}O, respectively.

All data were processed and fitted using an in-house software (T. Charpentier) with procedures described in Refs [161, 167, 178].

4.3. Results

When the experiments were stopped after 213 days of alteration in vapor phase, it was noted that a thin film of water was visible on the surface of the glass powders. This suggested that water had condensed onto the surface of the glass powders due to their high surface area. However, this water volume was too small to be sampled. It can also be ascertained that water did not overflow from the cup containing the glass powders.

The glass monolith samples were placed vertically in the same reactor, below the cup containing the powder samples. Water droplets were not visible on its surface when the reactor was opened. But this does not mean that there was no surface condensation and run-off of water molecules.

The alteration kinetics of the glasses that were altered in aqueous medium was followed by periodically sampling and analyzing the leachate of the duplicate experiment conducted with pure water of natural abundance. The pH, normalized mass losses (calculated using equation A4-2) and the altered glass percentage (calculated using equation A4-1) of the two glasses that were altered in unenriched water and water enriched with ^{17}O are provided in table A4-1 in appendix 4. The graphs depicting the evolution of these values with time are provided in figure A4-5 in appendix 4.

While following the alteration kinetics of the aqueous alteration experiment in unenriched water, decrease in the pH of the leachate of the glass Q at 56 days was noted. Therefore, as a precautionary measure, the aqueous alteration experiment of the glass Q in both mediums (unenriched and ^{17}O enriched) was stopped after 59 days due to the risk of precipitation of zeolites under given conditions [174] that may destabilize the gel and affect data interpretation. The decision was also supported by the fact that at 56 days, the Q glass powders had altered to almost 90%, which was judged as a sufficient quantity of gel for characterization by NMR studies. The altered glass percentage of the QCa glass at 56 days was only 50%, due to which its alteration went on up to 213 days.

4.3.1 Solution analyses of the aqueous alteration experiments

The results discussed below are the solution analyses of the duplicate experiment that was conducted in unenriched water (natural abundance of oxygen atoms). The solution analyses of the experiment conducted in water that was enriched in ^{17}O (40%) was conducted only at the end of the experiment. A comparison of the results of the duplicate experiment and the experiment with ^{17}O water on the last day of the experiment gave us information on the similarity between the experiments.

The pH of the leachate of the glass Q (duplicate experiment) was around 9.15 from the very first sampling done after 7 days of leaching and seemed rather steady until 28 days. The pH measured at 56 days was 8.4, but increased up to 9.17 at 59 days. An XRD analysis of the powder after the experiment was stopped did not indicate the formation of crystalline secondary phases. The pH value is consistent with other aqueous alteration experiments conducted at a very high SA/V ratio [179]. The pH of the QCa-leachate was slightly higher than that of Q (around 9.6), which can be explained by the presence of Ca in the leachate.

At such a high SA/V ratio, it is possible that the residual rate regime has already been reached within 7 days, when the first sampling was done. Therefore, the evolution of the NLs of the elements did not increase with time. As is classically observed during aqueous alteration experiments at a high SA/V ratio, the NL of boron in the solution was the highest due to its high solubility. The solubility of $B(OH)_3$ species in water at 90°C is 303800 mg/L, which is two orders of magnitude higher than the boron concentrations in solutions in our experiment. According to thermodynamic calculations using PHREEQC geochemical modelling tool and LLNL geochemical database, the precipitation of $B(OH)_3$ species due to increasing boron concentration is less favored with increasing alkaline pH. According to the standard database used, the only possibility for precipitation of secondary phases containing boron under given pH conditions and temperature is a calcium-containing phase called colemanite ($Ca_2B_6O_{11}.5H_2O$). Due to the lack of detection of this phase, the use of boron as a tracer for glass alteration seems justified. The NL of Na is lower than that of boron suggesting that it is retained in the gel layer, mostly to compensate the charge of $[AlO_4]^-$ units [106]. The retention factor of an element *i* in the altered layer can be calculated by using the formula $(1 - \frac{NL_i}{NL_B})$, assuming that boron is not retained in the altered layer. The retention factor of Na in the gel layer of the glass Q, thus calculated suggests that the retention of Na is 14% excessive of the total mole fraction of Al in the gel, suggesting that it could be playing a role other than charge compensation. The retention of the other elements (Si & Al) in the gel layer varied between 97-100%. The SEM images of the

Q glass powders altered in aqueous medium (figure A4-6 in appendix 4) and the XRD analyses confirm that secondary phases did not precipitate during the alteration of this glass. The pH and concentration of elements in the leachate enriched in ^{17}O in which the glass Q was altered for 59 days was similar to the concentration of elements in the leachate of the duplicate experiment on the same day. The altered glass percentage of the ^{17}O experiment was 84% at the end of the experiment, while it was 90% in the duplicate experiment. Therefore, it can be safely concluded that the alteration of the Q glass in unenriched water and water enriched in ^{17}O is quite similar.

The positive effect of Ca on glass alteration at a basic pH and low reaction progress [101] due to its incorporation in the gel layer and the formation of a passivating layer is evident in this experiment as well. The glass alteration rate seems to have already reached a steady state before 7 days of glass alteration (based on solution analyses of the duplicate experiment); the NL of boron does not increase with time in the case of the glass Q and increases at a very slow rate ($9.6x10^{-5}$ g/m^{2}day) in the case of the glass QCa. However, the altered glass % in QCa is 64% at the end of 213 days while that of the glass Q is 74% on the 7th day and 90% at the end of the experiment. Evidently there is no resumption of glass alteration in the glass QCa, but this does not rule out the possibility of formation of secondary precipitates such as C-S-Hs. As expected, the retention of Na in the gel layer of QCa (32%) was lower than its retention in the gel layer of Q (48%). It has already been proven in literature that Ca^{2+} ions preferentially occupy the role of charge compensators of $[AlO_4]^-$ units in the alteration layer instead of Na. Therefore, if we consider that all of Ca is involved in charge compensation, there is still a deficit of 20% charge compensators, which can be fulfilled by Na^+ ions. There is still 75% excess Na^+ ions retained in the gel layer that could be either playing the role of network modifiers or participate in secondary phase precipitation. Exploring other possibilities, if it is considered that the role played by Na in the gel layer is only charge compensation of $[AlO_4]^-$ units, then 80% of $[AlO_4]^-$ units are charge compensated by Na and 20% by Ca ions. Based on leachate composition, 98% of Ca that was present in the pristine glass is retained in the gel layer. Apart from occupying the role of charge compensators for the remaining 20% of $[AlO_4]^-$ units, there is 76% excess of Ca in the gel layer that may either form secondary precipitates or form bonds with silanol groups in the gel layer, which increase its passivation properties [143, 180]. Based on the XRD analyses of the QCa glass powder altered in unenriched water for 213 days, at least some of the excess Ca has precipitated as calcite on the altered glass powders (figure A4-7 in appendix 4). So, in our case, Na^+ probably compensates the charge of $[AlO_4]^-$ units since Ca precipitates as calcite.

4.3.2 Solid characterization of the vapor hydrated samples

The monoliths placed in the reactor as shown in figure 4-1 were characterized using SEM, XRD and ToF-SIMS in order to gain information on the vapor hydration of the glass powders (which were characterized by NMR spectroscopy) placed in the same reactor. This reasonably assumes that the vapor hydration of glass monoliths and glass powders is similar.

Glass Q: Figure A4-1 in appendix 4 shows the SEM image of a cross section of the Q monolith after vapor hydration at 90°C and 98% RH for 213 days. The image clearly shows the presence of a homogeneous altered layer of uniform thickness that seems cracked and slightly detached from the pristine glass-gel layer interface. The thickness of this layer is ~900 nm – 1 µm. The XRD analysis showed the presence of a very small peak (figure A4-1 in appendix 4) that corresponds to the presence of aluminosilicates such as kaolinite. The ToF-SIMS profiles (normalized with respect to the intensity in the pristine glass and the intensity of Si) are presented in figure A4-2 in the appendix 4. While the profiles indicate that the altered layer is homogeneous, the thickness of the altered layer estimated from the depletion of boron in the gel layer is 277 nm (the depth at which the intensity of boron is 50% of its intensity in the pristine glass). This is not coherent with the thickness of the altered layer estimated by SEM images. During the ToF-SIMS analyses, the same speed of abrasion was used for the gel layer and the pristine glass. If the gel layer is of a lower density than the pristine glass, then it could be abraded at a faster rate than the pristine glass. As a result, the thickness of the gel layer could be underestimated. Usually in glass alteration studies, despite the same speed of abrasion used for both layers, there is a good correspondence between the gel thickness estimated by ToF-SIMS and SEM images. For unknown reasons, this is not the case in our study. Our hypothesis is that the density of the gel layer formed must have been much lower than that of the pristine glass, although this hypothesis clearly needs verification. Some studies in the past have shown that differences in the thicknesses measured by ToF-SIMS and other characterization techniques can be possible due to slight changes in the abrasion speed in the gel layer, layer of crystalline or amorphous precipitates and the pristine glass [181, 182]. Since among the two techniques, the SEM images are more reliable for the estimation of gel layer thickness, we affirm that the thickness of the gel layer formed is around 1 µm. Using this information, it can be stated that the Q glass powders, whose grain diameter is < 2µm, that were vapor hydrated in the same reactor as the monoliths must have been completely altered.

Based on ToF-SIMS profiles that were normalized with respect to Si and pristine glass, the retention of boron in the gel layer is around 13%; the retention of Na is around 72%; and the

retention of Al is around 81% of its mole fraction in the pristine glass. The ToF-SIMS profile of H in figure A4-2 in appendix 4 suggests that the gel layer is more hydrated towards the pristine glass-gel layer interface than towards the surface of the gel layer. The profiles of ^{17}O and ^{18}O show their enrichment with respect to their natural abundance in the glass. Their presence in the gel layer could be explained rather by the formation of the gel layer by hydrolysis of the glass network by water molecules from the atmosphere, than the penetration of water molecules into the glass network. The depletion of boron, which is more significant than the depletion of Na, also supports the argument that the gel layer is rather formed by a network hydrolysis mechanism.

However, the loss of boron from the sample is puzzling and suggests that water condensed on the glass surface and overflowed into the NaCl solution that was placed beneath the monoliths in the reactor. Effectively, when the NaCl solution was analyzed for boron concentration by UV-spectrophotometry at the end of the experiment, 626±63 mg/L of boron was present in the NaCl solution. The amount of boron that could have dripped into the NaCl solution from the gel layer due to the formation of approximately 900 nm – 1 µm gel layer on both sides of the glass monolith is around 92-120 mg/L. The remaining boron present in the NaCl solution must come from the glass powders[18] placed above the monolith. But it has already been established that the water that condenses on the glass powders will remain in the impermeable Teflon cup and not overflow. The only explanation is the volatility of boron species (orthoboric or metaboric acid) which is likely to occur at this higher temperature and relative humidity [125, 126]. The argument of boric acid evaporation is also supported by the significant retention of the soluble Na species in the gel layer, which could have been removed along with boron if boron was indeed lost due to condensation of water molecules on surface and overflow. For the moment, both the explanations for boron loss seem likely.

Glass QCa: The figure A4-3 in appendix 4 shows the SEM image of the cross-section of the vapor hydrated QCa glass monolith. Unlike the Q sample, the altered layer was not clearly distinguishable in this case. A very slight difference in contrast between the surface of the altered sample close to the resin and the pristine glass below suggests that an altered layer of approximately 1.7 µm may be present on this sample. The ToF-SIMS profiles shown in figure

[18] The amount of boron present in 70% altered glass powder of the Q glass is 12.1 mg of B (considering a boron mass fraction of 0.0506). If all of the boron from the gel layer formed on altered glass powders passed into the 6mL NaCl solution, the concentration of boron would be 2024 mg/L of boron. The fraction of boron in the solution that comes from the powders only is around 500 mg/L. This calculation shows that the gel layer formed on glass powders in vapor phase must retain a substantial quantity of boron.

A4-4 (normalized with respect to the intensity of Si and the pristine glass) indicate that the thickness of the gel layer is around 285 nm. This thickness is similar to the thickness of the gel layer measured by ToF-SIMS on the glass Q. It can be supposed that as in Q glass the thickness of the gel layer formed on QCa glass is also underestimated by the ToF-SIMS measurements. According to these profiles, the retention of boron in the gel layer of QCa is ~9% of its mole fraction in the pristine samples; the retention of Na is ~61%; and the retention of Al is ~77%. The profile of Ca is slightly different than the other elements in the sense that it is depleted in the gel layer with slight enrichment towards the surface, likely due to the presence of non-crystalline secondary phases. Its overall retention in the gel layer is around 24%. The loss of Ca from the gel layer could be attributed to the formation of secondary phases, although the presence of neither calcite nor calcium-silicate/calcium alumino-silicate phases were detected through XRD analysis (the XRD pattern without any peaks is shown in figure A4-3). The lack of their detection does not indicate their absence. It is possible that the quantity of secondary phases was insufficient or the phases were not well-crystallized to be detected by XRD analysis.

The summary of the information that is pertinent for the NMR structural analysis of the gel layer formed by aqueous alteration at a very high SA/V ratio and the gel layer formed due to vapor hydration of glasses is that:

(i) In aqueous alteration,

- The glass Q is more altered than the glass QCa. As shown in table A4-1 in appendix 4, 84±4% of the Q glass powders have been altered by water enriched in ^{17}O (40% enrichment) and 55±2% of the QCa glass powders have been altered by ^{17}O enriched water.

- In the gel layer of the glass Q, an excess Na is present with respect to the quantity of mole fraction of Al, suggesting that some of the Na could be present in a role other than charge compensation for $[AlO_4]^-$ units. In the gel layer of the glass QCa, it is likely that both Na^+ and Ca^{2+} ions could be playing a role other than charge compensation such as network modifiers or secondary phase precipitation. Calcite was detected by XRD pattern.

(ii) In vapor hydration,

- According to SEM images, the glass QCa has altered more than the glass Q. Due to the small size of the grains (Ø < 2 µm) of the glass powders of Q and QCa, these samples must have altered completely in vapor phase.

- Taking into account the uncertainty associated with the measurement of the thickness of the altered layer, it is difficult to infer information about the role of Ca in glass hydration but we can suggest that it does not play a protective effect. This is in contrast with the significant positive effect of Ca during aqueous alteration. This point will be discussed further in chapter 5.

- Another difference observed between glass alteration in these two environments is the better retention of Na in the gel layer formed in vapor hydration. This is clearly due to the absence of a large quantity of water to solubilize and remove Na from the gel layer. The quantity of Na retained in the gel layer is excessive of the quantity of Na required for charge compensation of $[AlO_4]^-$ units, suggesting that they could be playing the role of network modifiers or precipitate secondary phases within the gel layer (such as Na_2CO_3).

At 90°C and 98% RH, the QCa sample altered in vapor phase has a higher thickness of the altered layer than the equivalent thickness of the altered layer calculated using boron concentration for the QCa sample altered in aqueous medium after 213 days of alteration. Although the Q sample was altered for different durations in vapor phase (213 days) and in aqueous medium (59 days), based on the trend of evolution of boron concentration as a function of time after 8 days of aqueous alteration (almost no increase), it can be reasonably assumed that in case of the Q glass as well, the Q sample altered in vapor phase for 213 days has a higher altered layer thickness than the Q sample altered in aqueous medium (if the alteration was continued until 213 days).

4.3.3 NMR spectroscopy

4.3.3.1 Pristine glass structure

In order to compare the local environment of oxygen atoms in pristine samples and the gel layer formed in vapor phase and aqueous medium, these glasses were enriched in ^{17}O. Differences in the composition between glasses of natural ^{17}O abundance that were altered in a medium enriched in ^{17}O and the pristine ^{17}O enriched samples were observed, as detailed in table 4-1. This was caused by the evaporation of boron and a small fraction of Na during the elaboration of the ^{17}O enriched samples by the sol-gel method (and thus prepared in very small quantities). Despite these differences, the structural configuration of the principal elements (Si, B, Al, Na) in the two pristine samples were found to be quite similar from the comparison of the NMR spectra. This similarity in structure validates the comparison of the oxygen environments in the pristine glass and altered samples. Figures A4-8 & A4-9 in appendix 4 show the comparison of the ^{11}B, ^{27}Al, ^{23}Na and ^{29}Si MAS spectra of the two samples. Only a very slight difference in the BO_4 and

BO_3 species among the QCa samples, a slightly narrower Full Width Half Maximum (FWHM) of the ^{29}Si of the ^{17}O enriched QCa sample and a very slight shift in the MAS dimension of ^{27}Al between the Q samples can be noticed. These differences are however negligible.

4.3.3.2 ^{11}B MAS NMR spectroscopy of pristine and altered samples

The quantification of the BO_3 and BO_4 in the pristine samples was achieved from ^{11}B MAS NMR spectra fitting. The ^{11}B MQMAS spectra for the pristine Q and QCa (unenriched) glasses are provided in appendix 4 figure A4-10 and A4-11 and were used to extract the NMR parameters to fit the NMR spectra. The resulting percentage of BO_4 in the glass Q is 49% and in glass QCa is 47%.

Figure 4-2 shows the comparison of the ^{11}B MAS spectra of the pristine samples (unenriched pg), samples altered in aqueous medium (AM) and the samples altered in vapor phase (VP) of the glasses Q and QCa[19]. The signal from boron in the altered samples that are shown in figure 4-2 could either be from the boron present in the residual pristine glass in the altered sample or it could be from boron that has condensed in the gel layer. In order to clarify this, $^{11}B\{^1H\}$ Rotational Echo DOuble Resonance (REDOR) experiments were carried out on all four samples (Q-AM, Q-VP, QCa-AM & QCa-VP) to identify the fraction of hydrated boron species in the sample. The principle of the REDOR experiment is to first collect a spin echo decay on ^{11}B (blue curve) and then collect the same echo decay but while irradiating ^1H (red curve), thus reintroducing the ^{11}B-^1H dipolar interactions during the echo decay. This causes a controlled additional decrease of the echo. The extent of decrease is directly dependent on the proximity of these two nuclei. The part of the echo decay that is only due to ^{11}B-^1H dipolar interactions can be extracted by difference (ΔS, green curve). The results are presented in figure 4-3. Thus the renormalized REDOR signal approaches 1 if all the ^{11}B nuclei are (dipolar)-coupled to the ^1H. Once the REDOR curve has stabilized, it can be considered that the residual signal is due to un-coupled nuclei (i.e) non-hydrated boron in our case. This is also confirmed by the figures A4-12 and A4-14 in Appendix 4 showing the REDOR filtered MAS spectrum that is close in shape (not in intensity because of echo filtering) to the MAS NMR spectrum of the glass.

The estimation of ΔS is also a quantitative method of estimating the percent of altered glass in the leached sample. From figure 4-3, it has been estimated that the percent of altered glass is 73% in Q-AM, 65% in QCa-AM, 80% in Q-VP and 87% in QCa-VP.

[19] Just a reminder that the comparison is made between unenriched pristine glasses and unenriched glasses that were altered in an alteration medium enriched in ^{17}O.

These results indicate the presence of hydrated boron species in the gel layer formed in both aqueous medium and vapor phase.

The chemical shift of BO_4 lines is more positive in the altered samples by about 0.8-1.3 ppm when compared to the pristine samples (figure 4-2). This shift could be linked to the change in the first and second neighbors of boron atoms that influence the electronegativity in its environment.

From figure 4-2, it can also be seen that the altered samples have a higher fraction of BO_4 than BO_3. This highlights the fact that BO_3 units are more soluble than BO_4 units and therefore are leached more rapidly [168].

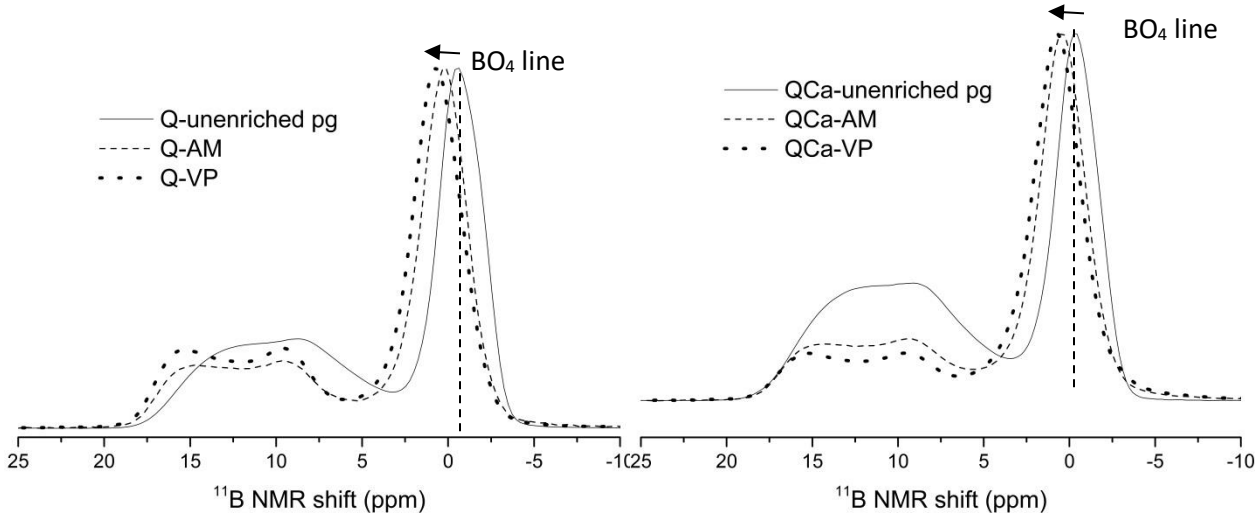

Figure 4- 2 ^{11}B MAS NMR spectra of the pristine samples (called unenriched pg-solid lines), samples altered in aqueous medium at a very high SA/V ratio (called AM-dashed lines) and samples altered in vapor phase (called VP-dotted lines) of the Q glass (left) and the QCa glass (right); The profiles are normalized with respect to the maximum height of the BO_4 line (between isotropic dimensions -0.6 to 0.7 ppm).

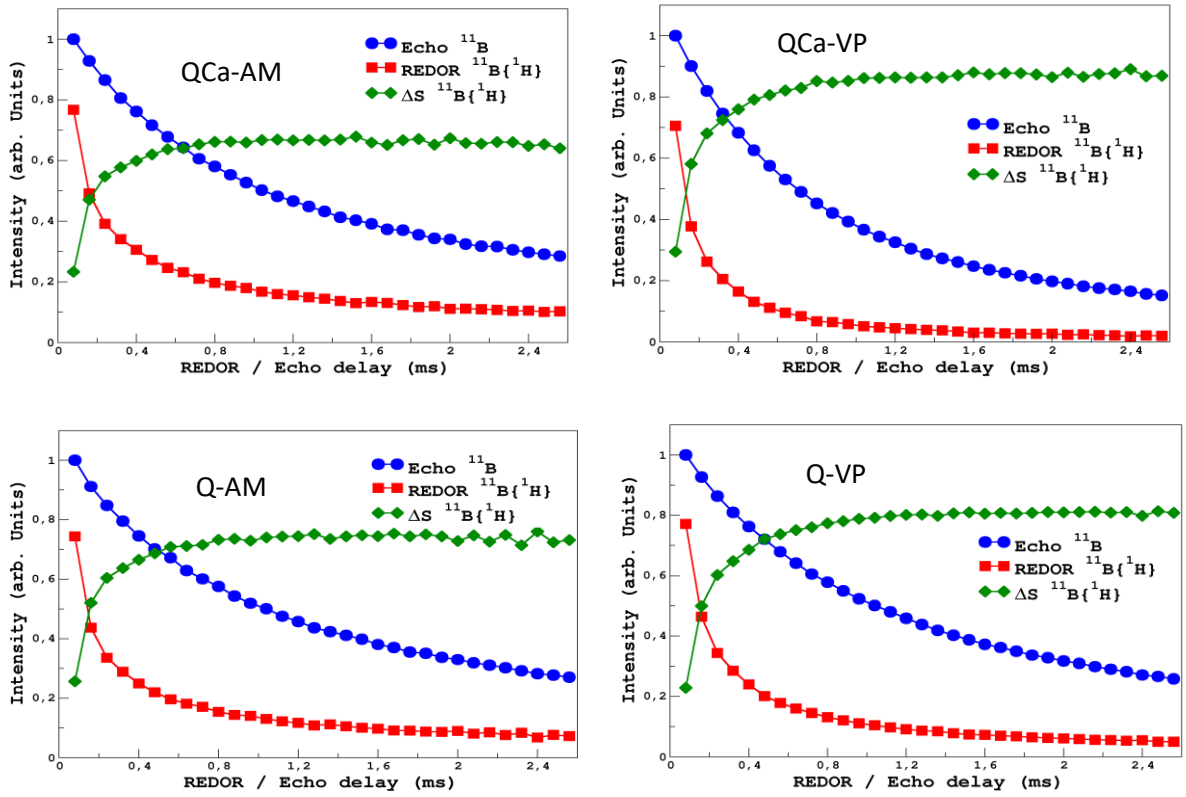

Figure 4- 3 (top-left- for the sample QCa-AM) Blue circles- ^{11}B spin-echo intensity as a function of spin-echo delay; Red circles- ^{11}B{^{1}H} rotational-echo double-resonance (REDOR) intensity as a function of the REDOR time; Green circles (ΔS)- REDOR signal subtracted from the echo, which must be equal to 1 if all of the ^{11}B is close to ^{1}H; (top-right) similar plot for the sample QCa-VP; (bottom-left) Q-AM sample and (bottom-right) Q-VP sample;

4.3.3.3 ^{29}Si MAS NMR spectroscopy of pristine and altered glasses

Figure 4-4 shows the normalized ^{29}Si MAS NMR spectra of the pristine and altered samples of the glass Q. As commonly observed during aqueous alteration experiments, the isotropic chemical shift is slightly more negative in altered glasses [106, 133, 168]. This decrease in chemical shift is associated with either increase in the quantity of bridging oxygens or change in the nearest neighbor effects. The presence of Al and boron tend to increase the chemical shift due to their electronegativity [161, 183]. Since in our case, it is known that at least a fraction of boron has been lost from the gel layer both in the case of vapor phase and aqueous medium, this is most likely the reason for the negative chemical shift. The impact of chemical composition on ^{29}Si MAS chemical shift is complex and this makes it difficult to obtain information on the relative degree of polymerization of one type of gel with another.

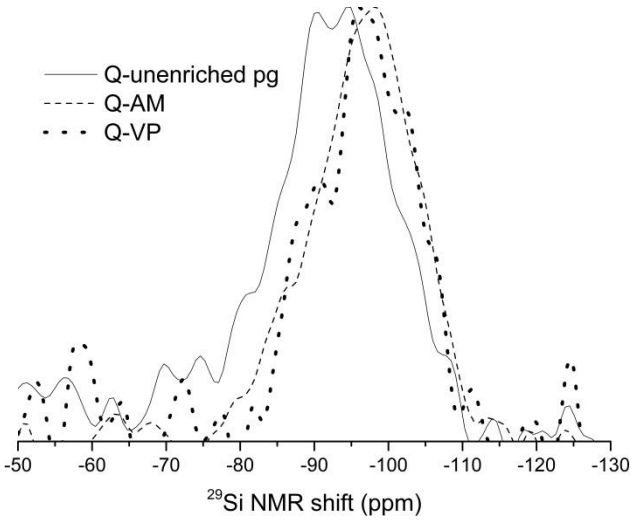

Figure 4- 4 ^{29}Si MAS NMR spectra of the pristine samples (called unenriched pg-solid lines), samples altered in aqueous medium at a very high SA/V ratio (called AM-dashed lines) and samples altered in vapor phase (called VP-dotted lines) of the Q glass

4.3.3.4 ^{27}Al MAS NMR spectroscopy of pristine and altered samples

Figure 4-5 shows the normalized ^{27}Al MAS NMR spectra of the pristine and altered samples of the Q and QCa glasses. The chemical shift for 4-fold coordination state Al (^{IV}Al) is around 55 ppm [183]. The ^{27}Al MAS NMR spectra show that Al is exclusively in 4-fold coordination state. The spectrum of the pristine glass is usually broadened due to quadrupolar interactions in addition to isotropic chemical shift distribution. No peaks are present in the 20 to -10 ppm range associated with ^{VI}Al species [183]. The signal in the range 40 to 30 ppm could either be due to the presence of low quantities of ^{V}Al or it could be the tail part of the ^{IV}Al signal. The altered samples contain ^{IV}Al only. In both cases (Q and QCa), the spectrum is narrower in the altered samples than the pristine samples. This narrowing is also classically observed in the ^{27}Al MAS spectra of glass alteration gels [106, 133] and is usually associated with the presence of water molecules in aluminum surroundings [184]. VP and AM samples show similar ^{27}Al MAS NMR spectra, except for the gel layer formed on the QCa sample altered in vapor phase (QCa-VP) which has a narrower peak than the other three gels. In the QCa gel, the role of charge compensation can be played by Ca^{2+} or Na^{+}, while in the Q sample it can be played only by Na^{+} ions. Angeli et al. showed that charge compensation by Ca^{2+} ions in the gel layer broadened the spectra due to an increase in the quadrupolar interaction with respect to the ^{27}Al spectra of $[AlO_4]^{-}$ units charge compensation by Na^{+} ions [133]. It is possible that in the gel formed on QCa in vapor phase, the aluminum atoms could be mostly charge compensated by Na^{+} ions and the Ca^{2+} ions could be consumed due to formation of secondary phases such as calcite or CSHs (although undetected by XRD analysis, its presence in undetectable quantities is not ruled out).

This could result in a narrower spectrum for QCa-VP. In the gel formed in aqueous medium on the other hand, it is likely that Ca^{2+} are preferentially involved in charge compensation than the more soluble Na^{+} ions [106]. Nevertheless, owing to the fact that three of the four gels (Q-AM, Q-VP & QCa-AM) have very similar ^{27}Al MAS spectra despite possibilities of varying charge compensators suggests that in the QCa-VP gel, the difference in the ^{27}Al MAS spectra must be due to a relatively higher hydration of the gel than the other samples. It was already mentioned in section 4.3.3.2 that QCa-VP is the most altered sample among the four. The δ_{iso} chemical shift of Zeolite NaA is around 59.2 ppm [183], while that of QCa-VP is around 59.8 ppm. However, it is unlikely that the alteration of QCa in vapor phase at 90°C has resulted in the formation of zeolites since the signal shape is not characteristic of crystalline aluminosilicate phases. It is very likely that the narrower ^{27}Al MAS spectra of the QCa-VP sample means that it is the most altered sample and that it is not related to precipitation of secondary phases.

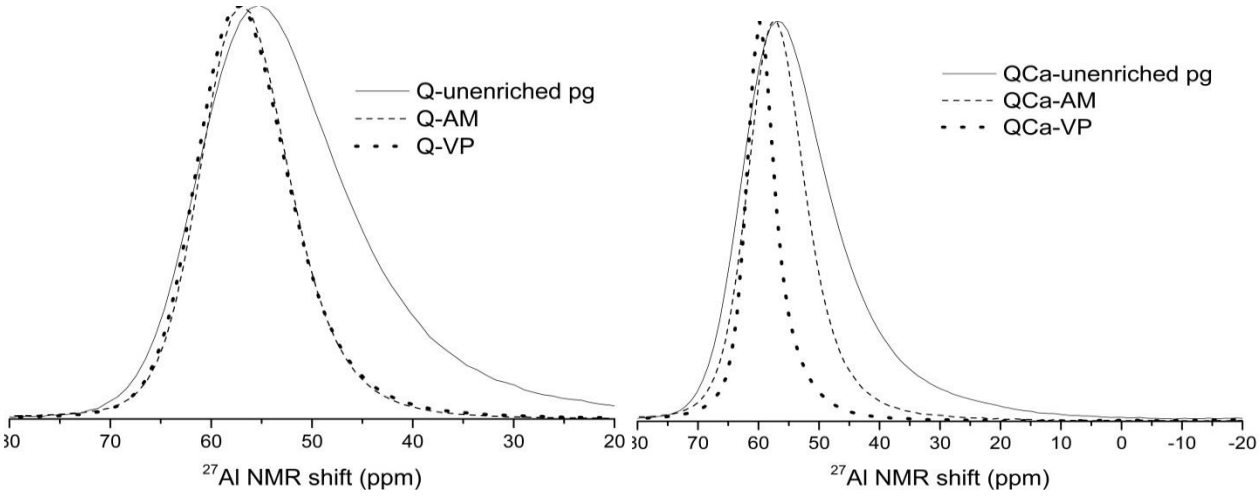

Figure 4- 5 ^{27}Al MAS NMR spectra of the pristine samples (called unenriched pg-solid lines), samples altered in aqueous medium at a very high SA/V ratio (called AM-dashed lines) and samples altered in vapor phase (called VP-dotted lines) of the Q glass (left) and the QCa glass (right)

4.3.3.5 ^{23}Na MAS NMR spectroscopy of pristine and altered samples

Figure 4-6 shows the ^{23}Na MAS NMR spectra of the pristine samples and the samples altered in aqueous medium and vapor phase of the glasses Q and QCa. The spectra of the pristine samples exhibit a single broad peak at around -15 ppm, similar to most soda-silicate glasses [183, 185]. The altered samples exhibit a much narrower peak with a more positive chemical shift. This reduction in linewidth and positive chemical shift is associated with an increase in hydration of the samples [183]. The $Na^{+}(H_2O)_n$ environment is more symmetric than the dehydrated structure in which Na^{+} ions play the role of charge compensators for $[AlO_4]^{-}$ units, leading to a more narrower peak. The positive shift has also been linked to an increase in the

fraction of Na^+ ions that play the role of network modifiers [185]. In the work of Alloteau et al., the increase in the peak symmetry of the ^{23}Na MAS spectra was directly linked with the degree of alteration [33]. Following this line of interpretation, among the two samples altered in aqueous medium, the sample Q has a more symmetrical (narrower) peak than QCa, suggesting that the Q sample is the more altered one (figure A4-13). The opposite is observed for the samples altered in vapor phase, highlighting that the QCa samples have altered more in the vapor phase. This is coherent with the percent of altered glass estimation discussed in section 4.3.3.2 and also with the results of the sample characterization of the duplicate experiments (section 4.3.1 and 4.3.2). This justifies the assumption that the alteration of glass powders and monoliths in vapor phase behaves similarly. The presence of Na_2CO_3 in the gel layer would have resulted in a contribution around -55 ppm of the ^{23}Na MAS spectra, which is absent [186].

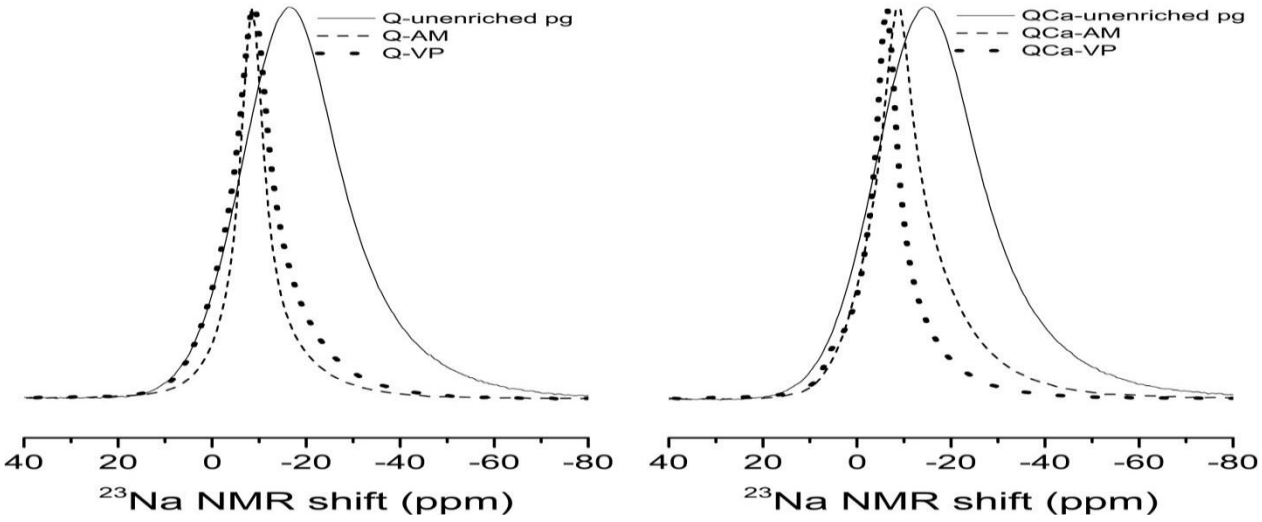

Figure 4- 6 ^{23}Na MAS NMR spectra of the pristine samples (called unenriched pg-solid lines), samples altered in aqueous medium at a very high SA/V ratio (called AM-dashed lines) and samples altered in vapor phase (called VP-dotted lines) of the Q glass (left) and the QCa glass (right)

4.3.3.6 ^{17}O MAS and MQMAS NMR spectroscopy

The ^{17}O MAS NMR spectra of pristine and altered Q and QCa glasses are reported in figure 4-7. A major difference is noted in the 50-100 ppm region. The various oxygen contributions can be resolved from MQMAS NMR spectra, which are given in figure 4-8. Figure 4-9 shows the projection on the isotropic dimension. The key information that is evident from these spectra is the additional contribution around 50-100 ppm in the ^{17}O MAS dimension mainly due to the presence of boron species in the pristine samples and the samples altered in vapor phase [169]. Although a significant quantity of boron has been lost from the gel formed in vapor phase, the remaining boron seems to have re-condensed with ^{17}O coming from the alteration medium

(vapor phase), suggesting a hydrolysis/recondensation mechanism for the formation of the gel layer in vapor phase. $^{17}O\{^{11}B\}$ REDOR experiments on the Q-VP sample, whose results are shown in figure 4-10, confirm the presence of B-^{17}O-B linkages.

The signal around 50-100 ppm is definitely absent in the Q-AM samples. The signal from the QCa-AM was too noisy to make meaningful conclusions. From figure 4-8, the QCa-VP sample contains signals in the range 50-100 ppm suggesting the presence of at least a small fraction of B-^{17}O-B linkages. Therefore from figures 4-7, 4-8, 4-9 and 4-10, two of the four samples (Q-VP, QCa-VP) indicate the formation of B-^{17}O-B and Si-^{17}O-B links in the gel layer, one of the samples (Q-AM) does not and we are not sure in the fourth sample (QCa-AM) (although figure 4-7 shows that QCa-VP sample does not indicate the presence of Si-^{17}O-B or B-^{17}O-B links).

An interesting point to note from figure 4-9 is that in the glass Q, the ratio of Si-^{17}O-Si and Si-^{17}O-Al proportions is similar in the pristine glass and the gel formed in aqueous medium. In the gel formed in vapor phase, the proportion of Si-^{17}O-Si is much higher than Si-^{17}O-Al. The ToF-SIMS profiles do not indicate any loss of Al from the gel layer. One of the hypotheses that can be put forward is that in vapor phase, the $[AlO_4]^-$ entities are less soluble/hydrolysable by the water molecules from the vapor phase than the Si tetrahedral units. As a result, there are lesser Al atoms linked to ^{17}O than Si atoms considering the stoichiometric ratio of Al/Si in the pristine glass.

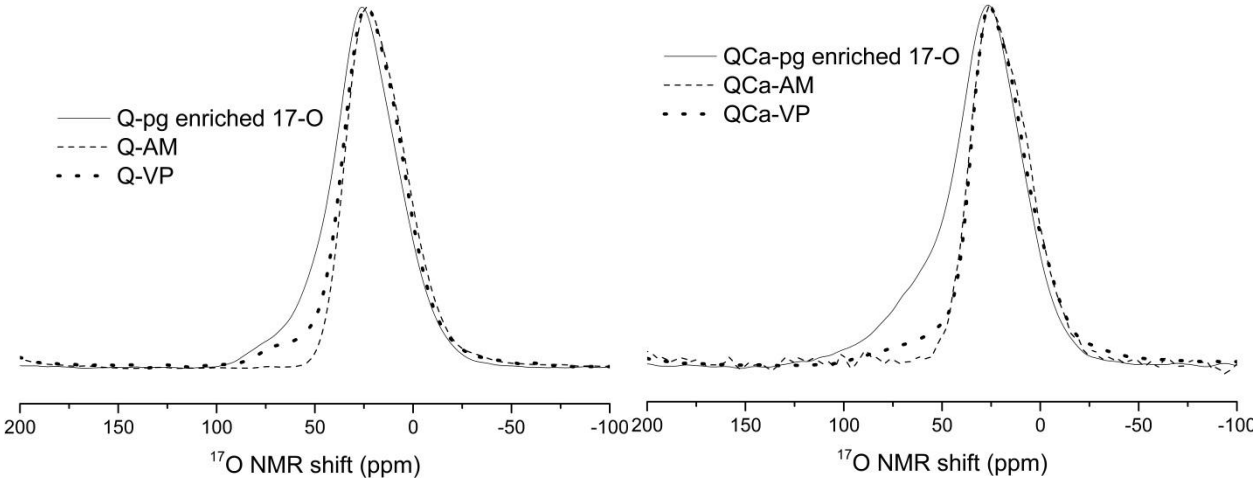

Figure 4- 7 ^{17}O MAS NMR spectra of the pristine samples enriched in ^{17}O (called pg enriched 17-O-solid lines), samples altered in aqueous medium at a very high SA/V ratio (called AM-dashed lines) and samples altered in vapor phase (called VP-dotted lines) of the Q glass (left) and the QCa glass (right)

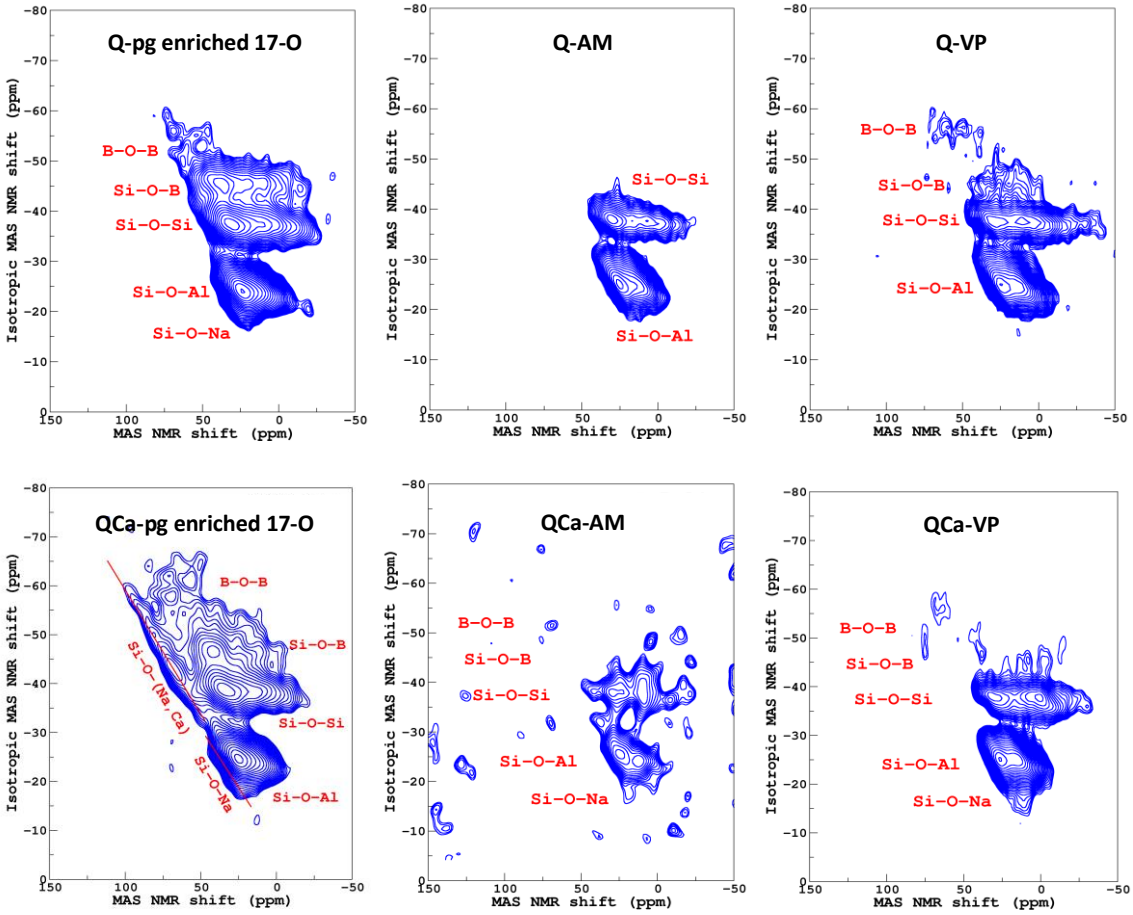

Figure 4- 8 ^{17}O MQMAS NMR spectra of (top left) pristine Q glass enriched in ^{17}O; (top center) Q glass altered in aqueous medium; (top right) Q glass altered in vapor phase; (bottom left) pristine QCa glass enriched in ^{17}O; (bottom center) QCa glass altered in aqueous medium; (bottom right) QCa glass altered in vapor phase

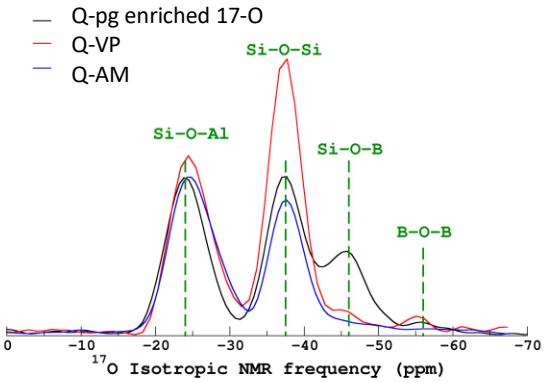

Figure 4- 9 Projections in the isotropic dimension of the ^{17}O MQMAS NMR spectra for the Q samples (pristine, altered in vapor phase and in aqueous medium)

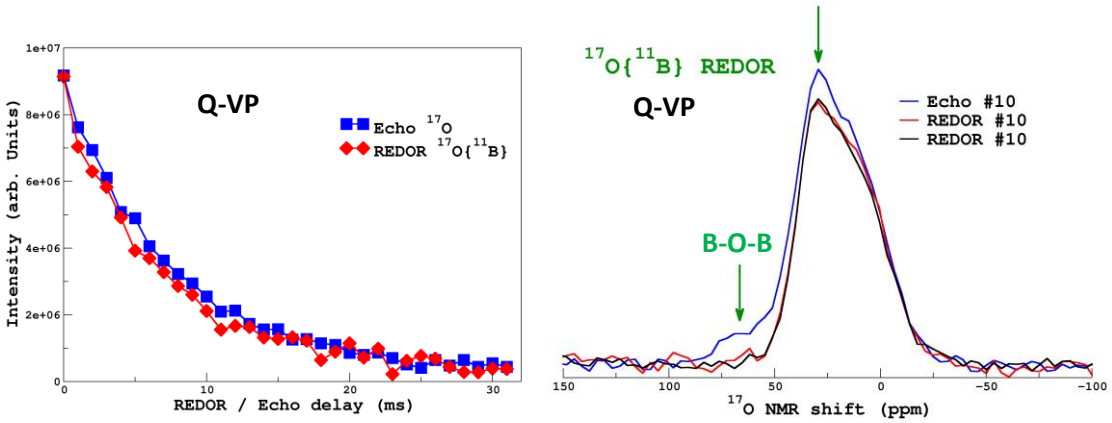

Figure 4- 10 (For the sample Q-VP) (Left) Blue squares- ^{17}O spin-echo intensity as a function of spin-echo delay; Red diamonds- ^{17}O{^{11}B} rotational-echo double-resonance (REDOR) intensity as a function of the REDOR time; (Right) Projection on the isotropic dimension

4.4. Discussion

The structure of the gel layer formed in aqueous medium was compared with that formed in vapor phase using NMR spectroscopy in two different glass compositions.

The solution analyses of the Q and QCa samples altered in aqueous medium, the solid characterization of the samples altered in vapor phase and the ^{11}B{^{1}H} REDOR experiments of all samples have confirmed that at 90°C and 98% RH, the samples have a higher thickness of altered layer in vapor phase than in aqueous medium. The alteration kinetics in aqueous medium suggests that both the glasses altered at a negligible rate after 8 days of immersion in aqueous medium (due to the extremely high SA/V ratio). There is no information on the vapor hydration kinetics for these glasses at 90°C and 98% RH. Therefore, a direct comparison of the alteration rate in these two mediums cannot be made. Nevertheless, taking into account our results and results from literature, it is probable that after 8 days , the vapor hydration rate is higher than the residual rate of these glasses in aqueous medium.

One of the noteworthy results is the presence of ^{11}B MAS NMR signals in the altered samples. It was verified that a major fraction of the signal was from boron in the gel layer which was in close proximity to proton through ^{11}B{^{1}H} REDOR experiments (and also by ^{1}H/^{11}B CPMAS experiments, data not shown). Unexpectedly, hydrated boron species were present in the gel layer formed in aqueous medium as well.

In the case of the samples altered in vapor phase, boron recondensation with ^{17}O (B-^{17}O-B and Si-^{17}O-B linkages) in the gel layer is confirmed for the Q-VP sample through the ^{17}O MQMAS NMR spectra and ^{17}O{^{11}B} REDOR experiments. The ^{17}O MQMAS NMR spectrum of the QCa-

VP sample also indicates the presence of at least a small proportion of B-^{17}O-B and Si-^{17}O-B linkages. The presence of B-^{17}O-B linkages in the samples altered in vapor phase suggests the recondensation of the hydrolyzed boron with ^{17}O from the vapor medium. These results show that in vapor phase, the gel layer forms by a hydrolysis reaction resulting in the formation of hydrated boron species.

Regarding the samples altered in aqueous medium, figures 4-8 and 4-9 show that there are no B-^{17}O-B linkages in the Q-AM sample. In the QCa-AM sample, too much noise prevented any meaningful conclusions on the presence of B-^{17}O-B linkages (although the right image of figure 4-7 seems to strongly suggest their absence). Among the samples altered in aqueous medium, while the presence of hydrated boron species is confirmed, B-^{17}O-B linkages are most likely absent (definitely absent in the case of the Q-AM sample). The hydrated boron species could be due to the presence of BO_3 and BO_4 species which haven't been completely hydrolyzed yet. But, this doesn't mean that boron recondenses in the gel layer as is the case in the gel layer formed in vapor phase. Anyhow, the presence of hydrated ^{11}B signals in the gel layer formed in aqueous medium is still surprising since usually in aqueous alteration experiments, no signal from ^{11}B is detected in the gel layer. This makes us question the use of boron as a tracer for glass alteration in aqueous medium at such a high SA/V ratio.

Despite such a high SA/V ratio that was used to be as close as possible to vapor hydration, differences exist between glass alteration in vapor phase and aqueous medium, notably the influence of Ca, which is different in both mediums. While Ca clearly has a positive effect during aqueous alteration, in vapor phase, its slightly negative effect has been noted through various characterization techniques. The altered glass percentage calculated through ^{11}B{^{1}H} REDOR experiments clearly demonstrate this. In figure A4-13 in appendix 4, ^{23}Na MAS NMR spectra show that in aqueous medium, the Na environment of glass Q is more hydrated than glass QCa (due to narrower peak), while it is inverse in vapor phase. The ^{17}O MAS NMR spectra also show clear differences between alteration in aqueous medium and vapor phase. The signal in the range of 50-100 ppm corresponding to the presence of B-^{17}O-B linkages is present only in the samples altered in vapor phase.

The ^{17}O MQMAS NMR spectra of the Q glass samples have also given information on the differences in the mechanisms of formation of the gel layer between the two alteration mediums. Based on the difference in the proportion of Si-^{17}O-Si and Si-^{17}O-Al linkages between the pristine glass, glass altered in aqueous medium and vapor phase, it can be reasonably hypothesized that in vapor phase, the gel layer forms by a hydrolysis/recondensation phenomenon that is

more selective while in aqueous medium it is seems more congruent with the pristine glass composition. It is well-known that Si-O-Al bonds are more resistant to network hydrolysis than Si-O-Si bonds. It seems that in vapor phase Si-O-Al bonds are more resistant to network hydrolysis than in aqueous medium. One of the hypotheses is that it could be related to the smaller quantity of water available and therefore lower energy to break bonds in vapor phase. Clearly, this theory needs further investigation to concretely discuss the reasons behind the lower fraction of Si-^{17}O-Al linkages in the gel layer formed in vapor phase. Unfortunately, it couldn't be verified if the same phenomenon is observed in the QCa samples due to the noisy ^{17}O MQMAS NMR spectrum of the QCa sample. Another phenomenon supporting the possibility of a higher resistance of Si-O-Al linkages to network hydrolysis in vapor phase than in aqueous medium is that in chapter 2, it was shown that the phyllosilicates that formed on vapor hydrated AVM6 contained 75% lower Al fraction than the phyllosilicates formed on AVM6 altered in aqueous medium. Similarly, in case of the AVM10 glass, the Al fraction in the phyllosilicates formed on vapor hydrated glass was 25% lower than that formed during aqueous alteration (section 2.4.6).

4.5 Conclusion

This chapter presents one of the very few studies conducted on the gel layer formed during vapor hydration of glasses using NMR technique. Since vapor hydration is often considered as aqueous alteration of glasses at a very high SA/V ratio, we decided to compare the structure of gel formed in these two mediums.

The structural analysis by NMR study shows that both in aqueous medium and in vapor phase, glass alteration by water have similar effect on the structure of Al and Na. The environments of both Al and Na become more hydrated, leading to more symmetrical MAS spectra. However, two main differences were noted between glass alterations in these two mediums. (i) Although boron is present in the gel layer formed in both aqueous medium and vapor phase, only the gel layer formed in vapor phase has shown evidence for recondensation of boron in the gel layer with oxygen atoms coming from the alteration medium (presence of B-^{17}O-B and Si-^{17}O-B bonds). In aqueous medium, only hydrated boron species seem to be present in the gel layer. (ii) The second difference clearly observed on one of the glasses is the difference in the Si-^{17}O-Al proportions (with respect to Si-^{17}O-Si proportion) between the gel layer formed in vapor phase and the gel layer formed in aqueous medium. While in aqueous medium this proportion was mostly similar to that of the pristine glass, in vapor phase Si-^{17}O-Al proportion was qualitatively lower. These two differences show that the gel layer forms by a hydrolysis/condensation mechanism in both alteration media at 90°C. But in vapor phase it is a more selective phenomenon, where Si tetrahedral units are preferentially hydrolyzed than Al tetrahedral units.

While this study demonstrates the subtle differences in the structure of the gel layer formed in two different alteration media, it would be of interest to see if/how these structural differences translate into macroscopic gel layer properties.

Chapter 5 Aqueous alteration of glasses

5.1 Introduction

The recent radioactive waste disposal scenario proposed by ANDRA predicts glass alteration in an unsaturated or transitory medium for tens of thousands of years before groundwater from the surrounding clay medium completely saturates the repository [187]. Therefore, it can be expected that a vapor hydrated or "pre-hydrated" glass will react with groundwater. As described in section 1.3, research on glass corrosion by water has been rather extensive in the field of nuclear waste management in several countries in order to predict the rate of release of radionuclides from HLW glass packages and to ensure environmental safety of geological disposal concepts [41, 47, 188-191]. Some differences between aqueous alteration of pristine glasses and pre-hydrated glasses can be possible. The main questions with regards to the differences are:

(i) Is the alteration of a pre-hydrated glass in aqueous medium different than the aqueous alteration of a pristine glass? If the pre-hydrated glass has developed a gel layer, it will be the first material to be in contact with water. Is the gel dissolution similar to glass dissolution?

(ii) Does the gel layer that formed during vapor hydration have a passivating effect during subsequent aqueous alteration? Although there are no studies that concretely prove that the gel layer formed during vapor hydration has a passivating nature against further glass corrosion, inflexion of vapor hydration rate over time has been noticed in a few studies in literature [27, 53], as well as in our study as discussed in chapter 2.

(iii) Are the surface secondary precipitates that are formed soluble? Several vapor hydration studies have shown that secondary precipitates form quite rapidly while glass is exposed to vapor phase due to the very small volume of water that can quickly attain thermodynamically favorable conditions. Some of these phases are capable of incorporating radionuclides. Therefore, the solubility of these phases during subsequent aqueous alteration could have significant impact on the safety of the environment. As discussed earlier in section 1.7, some studies have shown an increase in release of radioactivity due to dissolution of phases and formation of colloids [11, 91].

In order to gain insights on some of the above mentioned questions, the 6 glasses that were hydrated in vapor phase as described in chapter 2 were then altered in aqueous medium.

The leachate was analyzed using Inductively-coupled Plasma (ICP-OES) and the immersed glasses were characterized using SEM to observe the fate of the altered layer formed during vapor hydration during subsequent aqueous alteration. The obtained results are compared with literature and aqueous alteration of pristine glasses for interpretation. The three simplified glasses Q, QCa and QMg that were fabricated specially for this work (as described in chapter 2) were also altered under the same conditions as the pre-hydrated samples for comparison.

This chapter also deals with a second axis of study which concerns the comparison of glass alteration in aqueous medium and vapor phase. A few studies have considered that vapor hydration of glasses is equivalent to aqueous alteration at a very high SA/V ratio. Some authors conducted experiments at a very high SA/V ratio to predict the secondary phases that might precipitate during long-term aqueous alteration [19]. However, this line of thought has been questioned. We have probed further into this association by comparing aqueous alteration at low SA/V ratio and high SA/V ratio and vapor phase of the three simple glasses at the same temperature.

Geochemical modelling of the experiments described in this chapter based on GRAAL model [190] has been attempted to understand the mechanisms of glass alteration under given conditions.

5.2 Materials and methods

5.2.1 Experiments

1. Experiments to study the aqueous alteration of vapor hydrated glasses:

The six glasses AVM6, AVM10, AVMV4, Q, QCa and QMg were altered in vapor phase at 50°C and 95% RH for 180 days and 557 days respectively (described in detail in chapter 2). Afterwards, they were altered in aqueous medium by immersion in DI water at 50°C for 28 days at an SA/V ratio of 19.4 m^{-1}. This ratio was achieved by using a quarter of the vapor-hydrated glass monoliths (of 1.25x1.25x0.1 cm^3 dimensions) and 20 mL of water. The leachate was periodically sampled and analyzed by ICP-OES to measure the concentration of the glass elements leached. At the end of the experiment, the glasses were characterized by SEM to study the fate of the altered layer formed during vapor hydration when immersed in water. Samples of pristine Q, QCa and QMg glasses were also altered in exactly the same conditions as described above, in order to be compared with the aqueous alteration of the pre-hydrated samples.

2. Experiments to compare vapor hydration of glasses and aqueous alteration at a very high SA/V ratio:

The three simple glasses Q, QCa and QMg were altered in DI water at a very high SA/V ratio of 193186, 189533, 198876 m^{-1} respectively at 50°C for 91 days. This SA/V ratio was achieved by using 3 g of glass powders of particle size 2-5 µm in 27 mL of water. The specific surface areas of the Q, QCa and QMg glass powders are 1.72 m^2/g, 1.69 m^2/g and 1.77 m^2/g respectively.

The protocol for aqueous alteration is described in detail in chapter 4 (figure 4-1). The samples along with the DI water were taken in a Teflon container known as “savillex” of required volume. The water-loss from the savillex was reduced by using a double envelope with water and Teflon ribbons to tighten the cap of the container.

5.2.2 Solution analysis and sample characterization

The concentrations of the elements of interest (Si, B, Na, Ca, Mg, Li, Mo or Cs) were analyzed by ICP-OES.

The rate of glass alteration corresponds to the slope of the evolution of the Normalized mass Loss of elements (usually boron is considered as a tracer since it is not retained in gel layer or in secondary phases) (NL in g/m^2) with respect to time [192].

NL is calculated using the equation 5.2.2.1 as shown below:

$$NL(i) = \frac{C(i)}{\frac{SA}{V} * x(i)} \qquad \text{Equation 5.2.2.1}$$

i denotes the element; C denotes the concentration of the element at a given time in g/m^3; SA/V is the surface area of glass to solution volume ratio in m^{-1}; x denotes the mass fraction of the element in glass. Equation 5.2.2.1 was slightly modified as shown in equation 5.2.2.2 to correct for the volume of leachate that was sampled periodically.

$$NL(i)_t = NL(i)_{t-1} + \frac{C(i)_t * V\ (before\ sampling)_t - C(i)_{t-1} * V\ (after\ sampling)_{t-1}}{SA * x(i)} \qquad \text{Equation 5.2.2.2}$$

The equivalent thickness of altered glass (E_{eq}) can be calculated depending on sample geometry. For monoliths, it can be calculated from the NL of elements using equation 5.2.2.3.

$$E_{eq} = \frac{NL(i)_t}{\rho} \qquad \text{Equation 5.2.2.3}$$

ρ is the density of glass in g/m^3. For glass powders, (E_{eq}) can be calculated using the equation 5.2.2.4.

$$E_{eq} = \left(1 - (1 - AGf)^{\frac{1}{3}}\right) * R_0 \qquad \text{Equation 5.2.2.4}$$

$$R_0 = \frac{3}{\rho * S_S} \qquad \text{Equation 5.2.2.5}$$

$$AGf = \frac{C(B)_t * V_t + \sum_{j=1}^{t-1} C(B)_j * V_{s_j}}{m_0 * x(B)} \qquad \text{Equation 5.2.2.6}$$

AGf is the fraction of altered glass calculated from boron concentration; R_0 is the initial glass grain radius in m; S_S is the specific surface area of glass powders in m^2/g; V_t is the leachate volume at time t in m^3; V_{s_j} is the volume sampled at time j in m^3; m_0 is the initial mass of glass powders in g.

The altered monolith samples were characterized using SEM (refer Appendix A for apparatus details).

5.3 Results and discussion

5.3.1 Aqueous alteration of vapor hydrated glasses

From here on, the samples that were pre-hydrated for 180 days are referred to as pre-hydrated for 6 months (denoted as “6m”) and the samples that were pre-hydrated for 557 days are referred to as pre-hydrated for 18 months (denoted as “18m”). The pristine samples are referred to as “pg”. The concentrations of elements that would be present in the leachate, if the entire gel layer formed during vapor hydration dissolved after immersion in water, were calculated based on the thickness of the gel layer formed on the monoliths and the gel layer composition (data from chapter 2). This concentration is referred to as “max from gel” in the figures. The glass alteration rates are calculated by linear regression of the evolution of NL(B) as function of time. All the figures and tables referred to in this chapter whose caption starts with A5 are given in Appendix 5.

Simplified glasses (Q, QCa and QMg):

The concentration of glass elements in the leachate that was analyzed by ICP-OES, the calculated NL and E_{eq} values and the thickness of the altered layer observed in SEM images are provided in tables A5-1, 2 & 3. Figures A5-1, 2 & 3 describe the NL(i)=f(t) curves for the glasses Q, QCa & QMg glasses respectively. Figure A5-4 shows the SEM images of the pristine and

pre-hydrated Q, QCa and QMg glasses after aqueous alteration. Table 5-3 in section 5.3.2 provides the thicknesses of the gel layers formed in vapor phase.

Effect of pre-hydration: In this section, a comparison of the "pg" sample, "6m" sample and "18m" sample of all three simplified glasses are discussed in terms of pH, concentration of glass elements in leachate, normalized mass losses (NL), the release rates of elements and glass alteration rates.

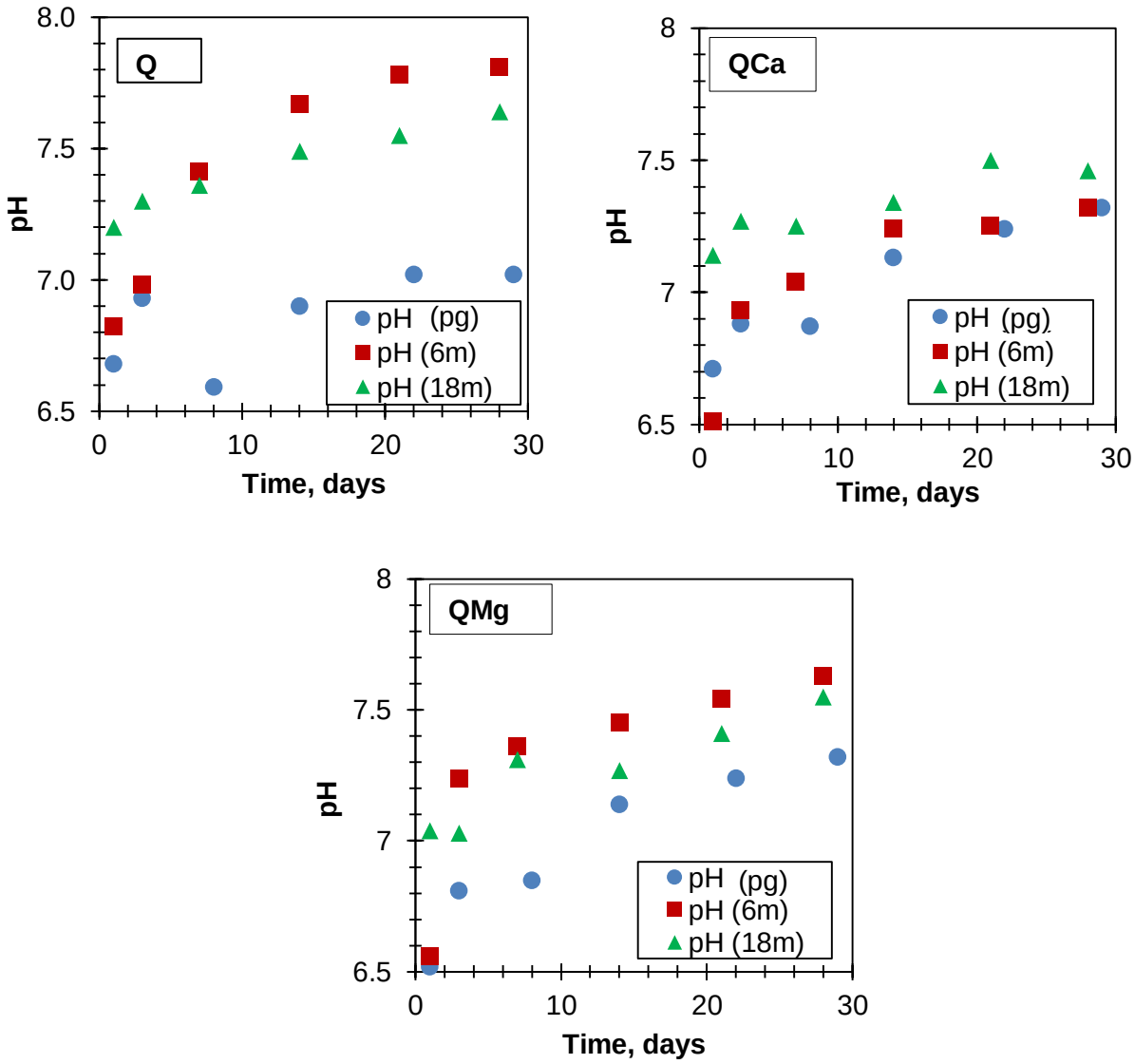

Figure 5- 1 The evolution of the pH of the simplified glasses Q (top-left), QCa (top-right) and QMg (bottom) with time; In each graph, the pH evolution for the pristine glass (pg), glass pre-hydrated for 6 months (6m) and the glass pre-hydrated for 18 months (18m) is provided

pH: Figure 5-1 shows the evolution of pH with time for all 9 samples (pg, 6m and 18m samples of Q, QCa and QMg glasses).

For the Q glass, the difference in pH between the pristine glass (Q-pg) and the pre-hydrated glasses (Q-6m and Q-18m) is the highest (0.5-0.8 unit) after 7 days of immersion. This could be due to the glass alteration rates of Q-6m and Q-18m higher by a factor of 1.5-1.8 times than the Q-pg glass (see table 5-1 release rates of boron of Q-pg, Q-6m and Q-18m). On the first day after immersion, the pH of the Q-18m glass is the highest, followed by the Q-6m glass. The pH of the Q-18m glass is 0.4 & 0.5 unit higher than the Q-6m glass and Q-pg glass respectively. The Q-18m glass contains more secondary phases that instantaneously dissolve when immersed in water, resulting in an increased pH.

For the QCa glass, the difference in pH between the pristine glass (QCa-pg) and the pre-hydrated glasses (QCa-6m and QCa-18m) is much lesser. For the QCa glass as well, the pH on the first day of immersion is higher by 0.4 & 0.6 unit for the QCa-18m glass than the QCa-pg and QCa-6m glasses respectively.

For the QMg glass, the difference in pH between the pristine glass (QMg-pg) and the pre-hydrated glasses (QMg-6m & QMg-18m) is between 0.2-0.4 units. As in Q and QCa glass, the pH of the QMg-18m glass is 0.5 unit higher than the pH of the QMg-6m and QMg-pg glasses on the first day of immersion.

For all three glasses, the samples vapor hydrated for a longer duration (18m) have a higher quantity of secondary phases. It seems that some of these phases might dissolve instantaneously, resulting in a higher pH for these samples on the first day of immersion.

Concentration of glass elements in leachate: The size of the glass monoliths altered (1.25x1.25 cm^2) and the water volume (20.0 mL) were similar in all 9 samples. Therefore, their concentrations can be directly compared.

Q glass: Figure 5-2 shows the comparison of the concentrations of B, Na and Si for the Q-pg, Q-6m and Q-18m glasses. The first point to note is that the B and Na concentrations for the Q-6m and Q-18m glasses are above the “max from gel” limit (indicated as red and green lines in the graphs). This means that water has access to the pristine glass from the beginning of immersion of the pre-hydrated glasses, probably because the gel layer formed in vapor phase dissolved within the first day of immersion or due to cracks and pores in the gel layer formed in vapor phase. The B concentration of the Q-pg glass is lower than the B concentration of the Q-6m and Q-18m glasses. But inversely, the Na concentration of the Q-pg glass is higher than the Q-6m and Q-18m glasses. The Si concentration of the Q-6m glass is almost in the same range as the “max from gel” value and does not increase with time. The Si concentration of the Q-18m sample increases very slowly with time and is higher than the Q-6m sample. The Si

concentration of the Q-pg sample increases with time and is higher than the Q-6m and Q-18m samples after 14 days. The B and Na concentrations of the Q-6m and Q-18m samples are very similar unlike the Si concentrations for these two samples.

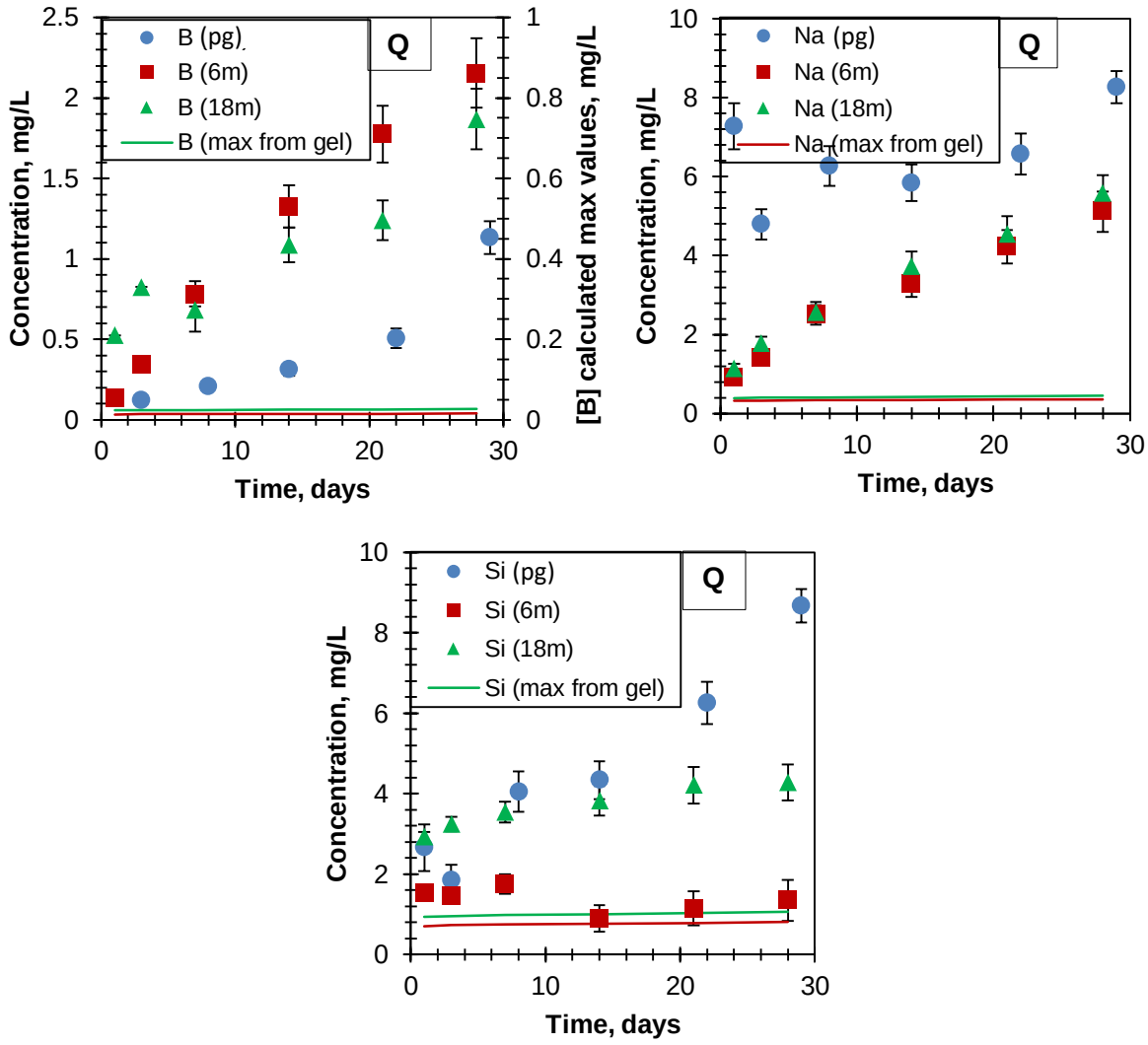

Figure 5- 2 Concentration of glass elements (B (top-left); Si (top-right); Na (bottom)) in the leachate of the pristine Q glass (Q-pg), pre-hydrated Q glasses (Q-6m and Q-18m); The red line in each graph corresponds to the calculated maximum concentration of the element in the leachate if the entire gel formed in vapor phase during 6 months dissolved after immersion; The green line corresponds to the same calculated maximum concentration if the gel formed in vapor phase during 18 months dissolved

QCa glass: Figure 5-3 shows the comparison between QCa-pg, QCa-6m and QCa-18m glasses for the concentrations of B, Na, Si and Ca in the leachate. As in the Q glasses, the B and Na concentrations of the QCa-6m and QCa-18m samples are higher than the “max from gel” value. Other similarity between Q and QCa glasses is that, the B and Na concentrations of the QCa-6m

and QCa-18m glasses are very similar and the Si concentration of the QCa-18m glass is higher than the QCa-6m glass.

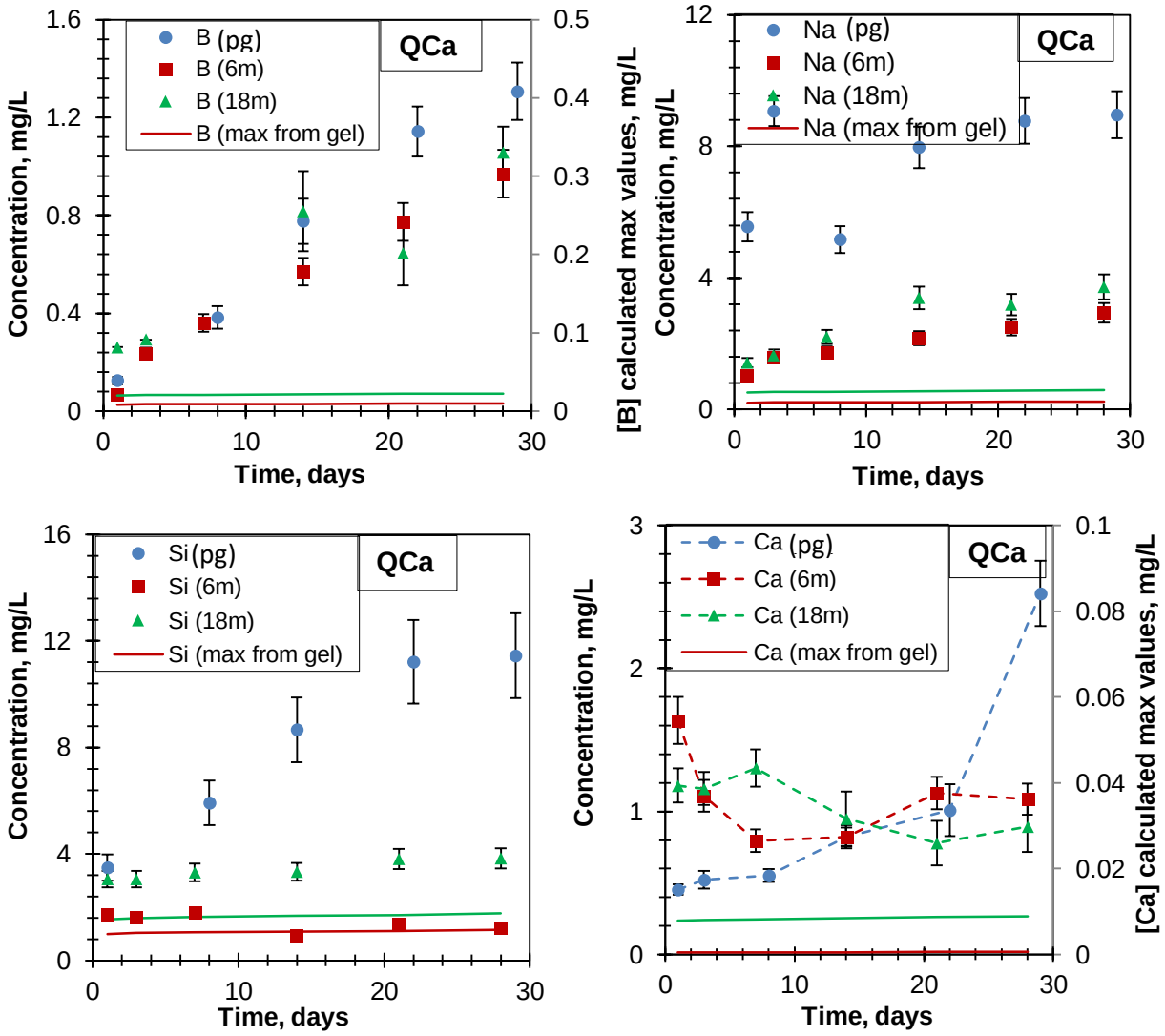

Figure 5- 3 Concentration of glass elements (B (top-left); Si (bottom-left); Na (top-right); Ca (bottom-right)) in the leachate of the pristine QCa glass (QCa-pg), pre-hydrated QCa glasses (QCa-6m and QCa-18m); The red line in each graph corresponds to the calculated maximum concentration of the element in the leachate if the entire gel formed in vapor phase during 6 months dissolved after immersion; The green line corresponds to the same calculated maximum concentration if the gel formed in vapor phase during 18 months dissolved

Unlike Q glass, in the QCa glasses, the B concentration of QCa-pg, QCa-6m and QCa-18m are very similar. The Na and Si concentrations of the QCa-pg glass are however higher than the QCa-6m and QCa-18m glasses. The evolution of the Ca concentration with time of the QCa-pg glasses is opposite of the pre-hydrated QCa-6m and QCa-18m glasses. For the QCa-6m and QCa-18m glasses, the instantaneous dissolution of calcite, which was formed during vapor hydration of the QCa glass, resulted in an initially higher Ca concentration. This concentration

reduced with time either due to precipitation of secondary phases or incorporation of Ca in the gel layer (formed during aqueous alteration) of the QCa-6m and QCa-18m samples. Given the pH of the study, which is around 7.2, it is more likely that Ca is incorporated in the gel layer of QCa-6m and QCa-18m samples.

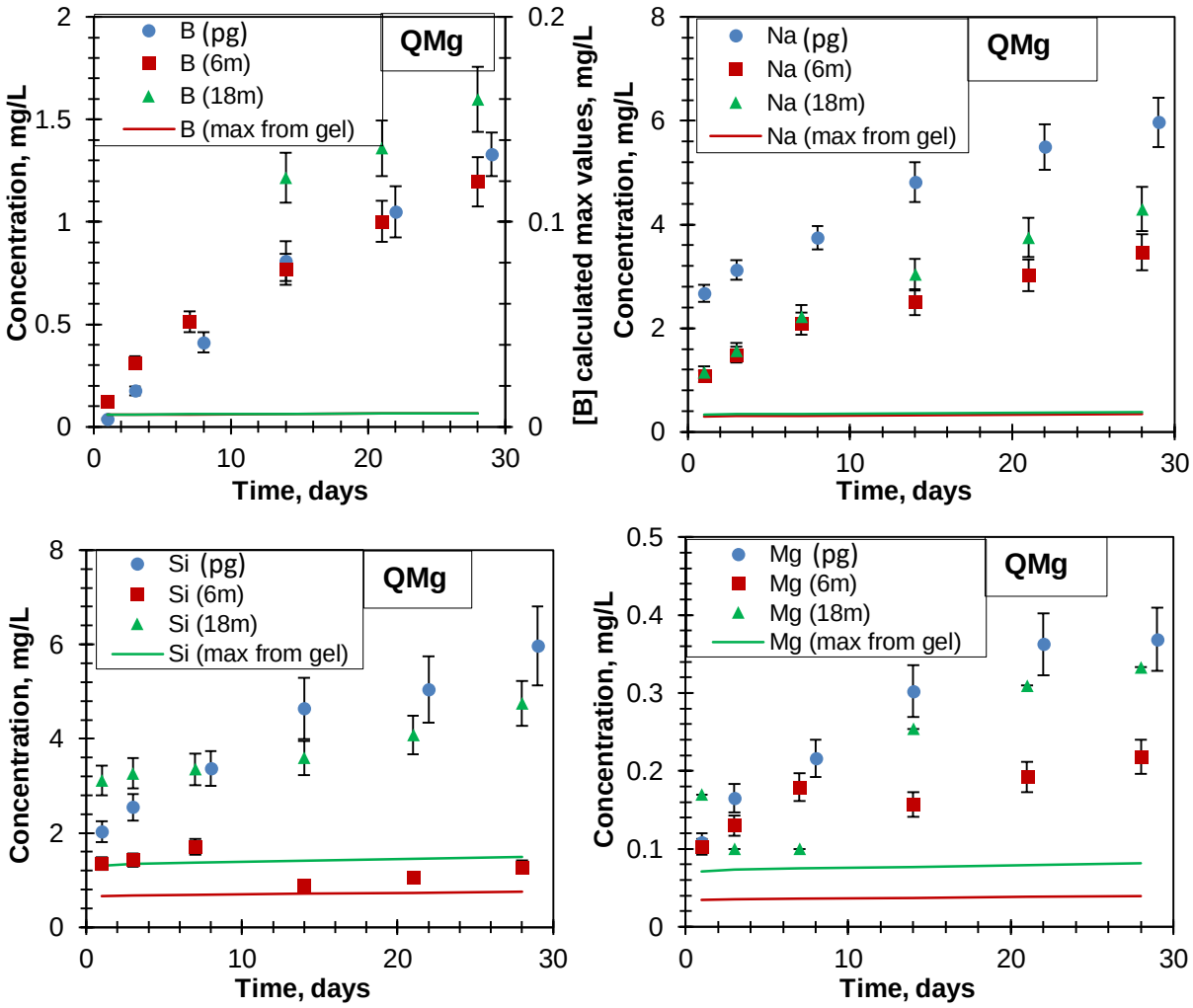

Figure 5- 4 Concentration of glass elements (B (top-left); Si (bottom-left); Na (top-right); Mg (bottom-right)) in the leachate of the pristine QMg glass (QMg-pg), pre-hydrated QMg glasses (QMg-6m and QMg-18m); The red line in each graph corresponds to the calculated maximum concentration of the element in the leachate if the entire gel formed in vapor phase during 6 months dissolved after immersion; The green line corresponds to the same calculated maximum concentration if the gel formed in vapor phase during 18 months dissolved

QMg glass: Figure 5-4 shows the comparison of B, Na, Si and Mg concentrations between the glasses QMg-pg, QMg-6m and QMg-18m glasses. Similar to the Q and QCa glasses, the Na concentrations of the two pre-hydrated glasses (QMg-6m and QMg-18m) were very similar to each other and were higher than the “max from gel” value. The Si concentration of the QMg-6m glass was in the range of the “max from gel” value and did not increase with time. The Si

concentration of the QMg-18m glass was higher than the Si concentration of the QMg-6m glass. The Si concentration of the QMg-pg glass increased with time and was close to the QMg-18m glass. The evolution of Mg concentration with time of the QMg-pg, QMg-6m and QMg-18m glasses are similar to the evolution of Si concentration, except, Mg concentration of QMg-6m slightly increased with time. The B concentration of the QMg-pg was similar to the QMg-6m glass. The B concentration of the QMg-18m glass was higher than the QMg-6m glass. The Na concentration of the QMg-pg glass evolved similarly with time with the QMg-6m and QMg-18m glasses. However, the concentration values were offset (higher by 1.4 - 2.5 times) in the QMg-pg sample. This offset could be due to initially predominant inter-diffusion mechanism during glass alteration in aqueous medium, resulting in a significant release of Na (higher than B) during the premier instants of glass alteration.

Summary:

From the comparison of concentration of elements in the leachate for the “6m” glasses and “18m” glasses, we have learnt that the leached concentration of Si (in the case of Q, QCa and QMg) and the concentration of Mg (in the case of QMg) depend on the duration of vapor hydration of glasses. This suggests that the release of Si and Mg must be due to the dissolution of gel or secondary phases, since the glass vapor hydrated for a longer duration contains a higher quantity of gel/secondary phases. On the other hand, irrespective of the duration of the vapor hydration (6m or 18m), the leached B and Na concentrations are very similar (between 6m and 18m glasses for Q, QCa and QMg). Therefore, they are leached from the glass. A Ca containing phase that formed during vapor hydration of the QCa glasses (mostly calcite since other phases were not detected) dissolved rapidly within the first day of immersion.

The notable differences from the comparison of the pristine glasses with the pre-hydrated glasses are: B concentration of Q-pg, which was lower than the B concentration of the Q-6m and Q-18m glasses, the higher pH (by 0.5-0.8 unit) of the Q-6m and Q-18m glasses than the Q-pg glass, the offset in the Na concentration of the QMg-pg glass with respect to QMg-6m and QMg-18m glasses and the increasing Ca concentration for the QCa-pg glass while the Ca concentration decreases with time for the QCa-6m and QCa-18m glasses.

Normalized mass losses (NLs) of elements and their release rates: The surface areas of the pre-hydrated glasses (6m and 18m) is higher than that of the pristine glasses due to the secondary phases and the porosity of the gel layer formed in vapor phase. However, the exact values of the surface areas are unknown. For the purpose of data analysis, the geometrical surface area of

the sample was used to calculate SA/V ratio and NL(i) (by ignoring the fact that surface roughness might be greater than 1 µm for the pre-hydrated samples). The release rate of boron is considered as the glass alteration rate. It is justified to use boron as glass alteration tracer even in the case of the pre-hydrated glasses, despite the fact that boron is retained to a small extent in the gel layer formed in vapor phase, because the thickness of the gel layer formed in vapor phase is relatively small. Also, as can be seen from the comparison of leachate B and Na concentrations and calculated "max from gel" values, the gel layer formed during vapor hydration apparently does not prevent water-pristine glass contact from the first day of immersion.

From the calculation of the NL values (appendix 5, figures A5-1,2 and tables A5-1,2), it was noticed that for the Q-pg and QCa-pg glasses, the initial NL of Na and Si were higher than the NL of B. The release rates of these elements over 28 days were also almost twice that of the B release rates. This cannot be explained by the generally accepted glass alteration mechanism in aqueous medium in the given conditions and duration. Since, B concentration for the Q-pg, Q-6m and Q-18m glasses and the B concentration of the QCa-pg, QCa-6m and the QCa-18m samples are in the same order of magnitude, it was concluded that the measured B concentrations are correct. It was considered that the measured Na and Si concentrations of Q-pg and QCa-pg are incorrect (either contamination or analysis error). Therefore, NL(Na, Si)=f(t) curves for the Q-pg and QCa-pg have not been discussed below.

Q glass: Figure A5-1 shows the NL(i)=f(t) & NL(i)=f(√t) graphs for Q-pg, Q-6m and Q-18m glasses for the elements Si, B and Na. Looking at the Q-6m glass first, the NLs of B and Na increase parabolically with time. The NL(B, Na)=f(√t) curves are however linear, suggesting the formation of gel layer and a diffusive mechanism of glass alteration since the first day. The NL of Si does not increase with time. Table 5-1[20] shows that the release rate of Na is slightly lower than the release rate of B in the Q-6m glass. The fact that Si does not increase with time indicates that it precipitates to form the layer. As can be seen from the SEM image shown in figure A5-4, a gel layer of approximately 400 nm thickness is present on the Q-6m sample surface. The SEM characterization did show any surface precipitates on the Q-6m surface after aqueous alteration.

For the Q-18m glass, the NL and release rate of Na is slightly higher than the NL and the release rate of B (see table 5-1 for release rates). While the B release rate of Q-18m glass is

[20] It is to be noted that the release rates were calculated by linear regression of the NL(i)=f(t) curves and a few aberrant points were omitted. The line is not made to pass through zero since the rate of glass alteration between 0-1 days can be expected to be higher than the rate of glass alteration between 1-28 days.

slightly lower than the B release rate of the Q-6m glass, the Na release rate of the Q-18m glass is slightly higher than the Na release rate of the Q-6m glass. Similar to the Q-6m glass, NL(Na, B)=f(√t) is linear. While, the NL(Si) of the Q-6m glass did not increase with time, NL(Si) of the Q-18m glass increased slowly with time. The Si release rate in the Q-18m glass is 4-6 times lower than the B and Na release rates. This suggests the formation of a Si-rich gel layer. The SEM image in figure A5-4 also confirms the presence of a gel layer of approximately 600 nm thickness. The thickness measured by SEM images is only approximate since the sample was tilted.

From table 5-1, it can be seen that the B release rate of the Q-pg sample is lower than the B release rate of the pre-hydrated samples (Q-6m and Q-18m). From figure A5-1, there is no rate drop in the NL(B) with time. NL(B)=f(√t) is linear from the third day of alteration.

QCa glass: Figure A5-2 shows the NL(i)=f(t) and NL(i)=f(√t) curves for the QCa-pg, QCa-6m and QCa-18m glasses. Looking at the pre-hydrated glasses first, the behavior of the QCa-6m and QCa-18m glasses are very similar to the Q-6m and Q-18m glasses in the following ways: (i) NL(Na, B) increase with time is parabolic and NL(Na, B)=f(√t) evolution is perfectly linear for QCa-6m glass and more or less linear for QCa-18m glass; (ii) B release rate of QCa-6m was higher than the B release rate of the QCa-18m glass and Na release rate of QCa-6m was lower than the Na release rate of the QCa-18m glass (see table 5-1 for release rates); (iii) In the QCa-6m glass, Na release rate was lower than the B release rate, whereas in the QCa-18m glass, Na release rate was higher than the B release rate; (iv) NL(Si) of the QCa-6m glass did not increase with time, while the NL(Si) of the QCa-18m glass increased at a rate that was 4-5 times slower than the Na and B release rates. The NL(Ca) of the QCa-6m and the QCa-18m samples glasses decreased with time due to the initially high Ca concentration released in solution by calcite dissolution and then its incorporation in the gel layer.

The NL(B) of the QCa-pg glass increased linearly with time (non-parabolic evolution). Unlike the Q glasses, the B release rate of the QCa-pg glass was higher than the B release rates of the QCa-6m and QCa-18m samples. NL(Ca) of the QCa-pg glass increased linearly with time at a rate lower than that of B.

QMg glass: Figure A5-3 shows the NL(i)=f(t) and NL(i)=f(√t) curves for the QMg-pg, QMg-6m and the QMg-18m glasses. The trends of release of B, Na and Si of the pre-hydrated QMg glasses (QMg-6m and QMg-18m) show the same 4 similarities listed in the above passage for

the QCa pre-hydrated glasses (QCa-6m and QCa-18m). The evolution of NL(Mg)=f(t) is quite similar to NL(Si)=f(t) in both QMg-6m and QMg-18m.

The B release rate of the QMg-pg glass was higher than the B release rate of the QMg-6m and QMg-18m glasses (see table 5-1 for release rates). Among the three pristine glasses (Q-pg, QCa-pg & QMg-pg), only QMg-pg showed a parabolic evolution of NL of all four elements (Si, B, Na, Mg) with time. The initial magnitude of NL(Na) was higher than the NL(B) in the QMg-pg glass. This initial offset is an indication of inter-diffusion mechanism which occurred predominantly during the initial stages of glass alteration. This kind of offset is absent in the pre-hydrated QMg glasses. This suggests that pre-hydration in vapor phase has limited the predominant inter-diffusion phase at the beginning of glass alteration in aqueous medium. NL(Si)=f(t) behavior is also different between the pristine and the pre-hydrated glasses.

Summary:

The study of evolution of NL(i)=f(t) of the pristine glasses and the pre-hydrated glasses has shown that the glass alteration rates are in the same order of magnitude whether the glass is pristine or pre-hydrated for 6 months or 18 months. However, among the Q glasses, the Q-pg glass alters slightly slower than the pre-hydrated Q-6m and Q-18m glasses. Among the QCa and QMg glasses, the pre-hydrated glasses alter at a slower rate than the pristine glasses. This may be because the release rates of Ca and Mg in the pristine glasses are higher than in the pre-hydrated glasses. In the pre-hydrated glasses, they may be incorporated more in the gel layer (precipitation of Ca/Mg secondary phases is less likely at the near neutral pH in this study), leading to a more passivating gel layer [97, 101].

Another difference between pristine glasses and pre-hydrated glasses is that in the pristine Q and QCa glasses, the evolution of NL was linear between 1-28 days whereas, the NL of the pre-hydrated samples showed a parabolic evolution. For the QMg glass, the evolution of NL with time was parabolic for both the pristine glass and the pre-hydrated glasses, but slight differences in the magnitude of NL was noticed, especially for Na. Therefore, the glass alteration mechanism at a given duration seems to be affected by pre-hydration of the samples.

Among the two different pre-hydrated glasses (6m and 18m), an increased duration of vapor hydration seems to have resulted in a lower glass alteration rate (release rate of B), but a higher release rate of Si and Na. This once again suggests the dissolution of secondary phases.

Influence of pre-hydration on the effect of Ca and Mg:

Figure 5-5 below shows a comparison of glass alteration rates (NL(B)=f(t)) of Q, QCa and QMg glasses that are pristine (top-left), pre-hydrated for 6m (top-right) and pre-hydrated for 18m (bottom).

Among the pristine glasses, Ca and Mg have a negative effect on glass alteration. Among the 6m glasses, Ca and Mg have a positive effect. Among the 18m samples, Ca clearly has a positive effect. Mg on the other hand, has a positive effect compared to Q, if the alteration rates are compared. The reason for this difference in the influence of elements between pristine and pre-hydrated samples could be the changing glass alteration mechanisms as discussed earlier. The pg glasses (especially Q-pg and QCa-pg) must be in the initial glass alteration regime (since NL(B, Na)=f(t) is linear). In this regime, network hydrolysis is the dominant glass alteration mechanism. Since the Q glass has a lesser NBO fraction than QCa and QMg (chapter 2), it alters at a lower rate. The pre-hydrated glasses, on the other hand, are in a rate-drop regime (glass alteration controlled by diffusion through gel layer since NL(B, Na)=f(t) is slightly parabolic and NL(B, Na)=f($\sqrt{t}$) is linear). The gel layer of QCa has begun to incorporate Ca from 3 days of alteration, thereby making the gel more passivating than that of the Q glass. It was also mentioned earlier that the release rate of Mg is also lower in the pre-hydrated glasses than the pristine glasses, suggesting that it is also retained in the gel layer and makes it more passivating than the Q-glass.

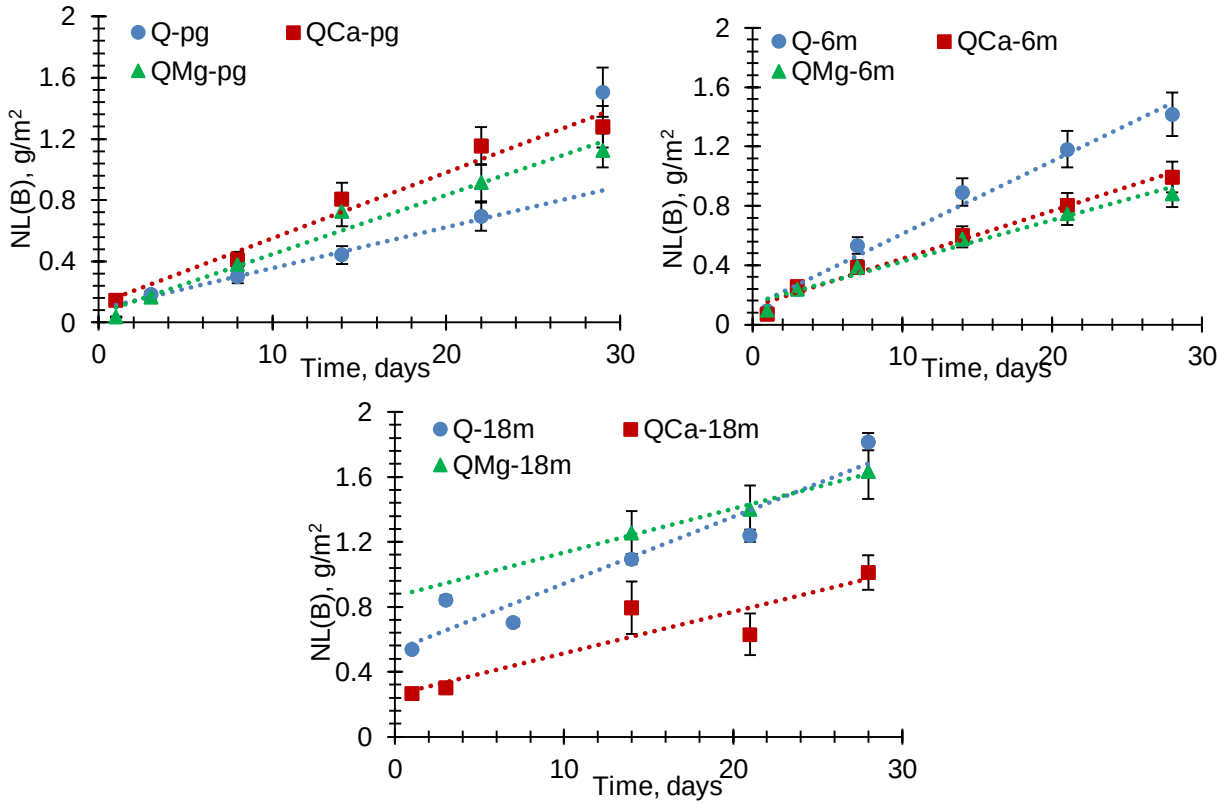

Figure 5- 5 Evolution of Normalized mass Losses (NL) of boron for the three simplified glasses that were pristine (top-left) and pre-hydrated for six months (top-right) and pre-hydrated for 18 months (bottom); The dotted lines represent the linear regression of the NL(B)=f(t) curves that were used to calculate glass alteration rate;

Table 5- 1 Release rates of elements in DI water at 50°C and SA/V ratio of 20 m^{-1} for a period between 1-28 days; Rate calculated by the linear regression of the NL(i)=f(t) curves; The rates are provided for three glasses Q, QCa and QMg, whose samples were pristine (pg), pre-hydrated for 6 months (6m) and pre-hydrated for 18 months (18m);

	Rate, g/m²day		
	Q-pg	**Q-6m**	**Q-18m**
B	$(2.67\pm0.32).10^{-2}$	$(4.9\pm0.59).10^{-2}$	$(4.1\pm0.49).10^{-2}$
Na		$(3.7\pm0.44).10^{-2}$	$(5.7\pm0.68).10^{-2}$
Si			$(0.97\pm0.17).10^{-2}$
	QCa-pg	**QCa-6m**	**QCa-18m**
B	$(4.3\pm0.52).10^{-2}$	$(3.2\pm0.38).10^{-2}$	$(2.6\pm0.31).10^{-2}$
Na		$(2.3\pm0.28).10^{-2}$	$(3\pm0.36).10^{-2}$
Si			$(0.6\pm0.07).10^{-2}$
Ca	$(3.1\pm0.37).10^{-2}$		
	QMg-pg	**QMg-6m**	**QMg-18m**
B	$(3.9\pm0.47).10^{-2}$	$(2.8\pm0.34).10^{-2}$	$(2.7\pm0.32).10^{-2}$
Na	$(3.3\pm0.4).10^{-2}$	$(2.3\pm0.28).10^{-2}$	$(4.5\pm0.54).10^{-2}$
Si	$(2.3\pm0.28).10^{-2}$		$(1.3\pm0.17).10^{-2}$
Mg	$(1.7\pm0.2).10^{-2}$	$(0.6\pm0.07).10^{-2}$	$(1.4\pm0.17).10^{-2}$

Complex glasses (AVM6, AVM10 & AVMV4):

The concentration of major glass elements in the leachate that was analyzed by ICP-OES, the calculated NL and E_{eq} values and the thickness of the altered layer observed in SEM images are provided in tables A5-4 & 5. Figures A5-8, 9 & 10 describe the NL(i)=f(t) curves for the glasses AVM6, AVM10 and AVMV4 glasses respectively. Figure A5-11 describes the NL(i)=f(√t) curves for the three glasses. Figures A5-5, 6 & 7 show the SEM images of the pre-hydrated complex glasses after aqueous alteration. Table 5-3 provides the thicknesses of the gel layers formed during vapor hydration.

AVM6: The AVM6 glasses that were pre-hydrated in vapor phase for 6 months and 18 months had altered to a much larger extent than the simplified glasses. As described in chapter 2, these vapor hydrated glasses had a substantial quantity of secondary precipitates on the surface and the altered layer was extremely irregular. In certain zones, the altered layer was only a few tens of nm thick and in other zones, irregularly shaped altered zones that could be up to a few µm

thick were discontinuously present. Therefore, the interpretation of the aqueous alteration results of these pre-hydrated glasses could be complicated. The alteration rates of these pre-hydrated glasses are compared with the initial glass dissolution rates of the pristine AVM glasses under similar conditions that are available in literature, to understand the effect of vapor hydration during subsequent aqueous alteration.

The pHs of the leachates are the highest on the first day of immersion of the pre-hydrated glasses in DI water ($pH_{50°C}$ 8.2 for AVM6-6m and 8.8 for AVM6-18m). The pH gradually reduces with time until 7 days and then it stabilizes between 7 and 28 days (figure 5- 6). Such initially high pH values were also obtained during the aqueous alteration of other vapor hydrated glasses (SON68 glass, $pH_{50°C}$ values between 8-9.5) [53, 68]. This initially high pH suggests the instantaneous dissolution of some of the secondary phases formed during vapor hydration when they come in contact with sufficient volume of water. The pH of the sample pre-hydrated for a longer duration (18 months) is higher (by 0.6 unit) than the sample that was pre-hydrated in vapor phase for a shorter duration (6 months). As discussed in chapter 2, the sample that was vapor hydrated for 18 months had noticeably higher quantity of secondary precipitates. The decrease in pH with time could be due either due to a gradual dissolution of carbonates that might have formed during vapor hydration or the formation of hydrated aluminosilicates during aqueous alteration.

In order to determine if the elements found in the leachate were a result of gel dissolution or glass dissolution, we calculated a threshold concentration of elements that could be found in the leachate if the entire gel formed during vapor hydration dissolved. This was complex since the alteration during vapor hydration was heterogeneous. Therefore we considered an average gel layer thickness of 1 µm, based on ToF-SIMS results and calculated the threshold concentrations by using the gel composition estimated using ToF-SIMS profiles (chapter 2). If the actual measured concentration of elements in the leachate was below this maximum value, elements may be released either from the gel or glass; if they are higher than the threshold concentration, it is certain that at least a fraction of the elements are released due to glass dissolution. In the case of AVM6, the concentrations of mobile elements such as B, Na and Li exceeded this threshold value 3 days after immersion in water (figure 5-7). Hence, it is more likely that these elements are released due to both gel and glass dissolution at least for short duration. The concentration of the elements Si and Mg were however within this threshold limit. Therefore, it could be either due to the dissolution of gel or secondary precipitates or glass. The SEM images provided in figure A5-5 show the presence of the leafy secondary precipitates on

the surface of the pre-hydrated samples after alteration in aqueous medium for 28 days. This shows that the phyllosilicates formed during vapor hydration are either not easily soluble or dissolve very slowly. However, the SEM images of the vapor hydrated AVM6 samples showed the presence of clusters of needle shaped secondary precipitates (chapter 2). These needle-shaped phases were not present in the SEM images of the samples taken after aqueous alteration. Therefore, these precipitates might have dissolved. The SEM images also show the presence of a continuous gel layer beneath the secondary precipitates of around 700-1000 nm. This was not present on the vapor hydrated samples before aqueous alteration. These observations lead to the following conclusions; when the vapor hydrated AVM6 samples were immersed in water, some secondary phases dissolved; it also seems that it is not necessary for the gel to dissolve completely for the water to have access to the pristine glass; the presence of a "new" gel layer beneath the secondary precipitates (figure A5-5) suggests that water can access the pristine glass surface through cracks or open pores in the gel layer formed during vapor hydration.

Figure A5-8 shows the evolution of the NL of various elements with time for the AVM6 samples pre-hydrated for 6 months and 18 months. The NL was calculated using the mass fraction of elements in the glass and the surface area of the glass. It can be seen that the NL of all the major elements (B, Na, Li, Si and Mg) is slightly higher in the sample pre-hydrated for 18 months than the sample pre-hydrated for 6 months. This can also be verified from the table 5-2 below (except Mg, whose release rate is lower in the 18m sample, even though value of NL is higher), where the release rates of the major elements over a period of 28 days is provided. For both the samples (AVM6-6m and AVM6-18m), the NL(B, Na, Li)=f(t) evolution is parabolic and the NL(B, Na, Li)=f($\sqrt{t}$) evolution is linear, suggesting that the glass alteration is controlled by a diffusive mechanism.

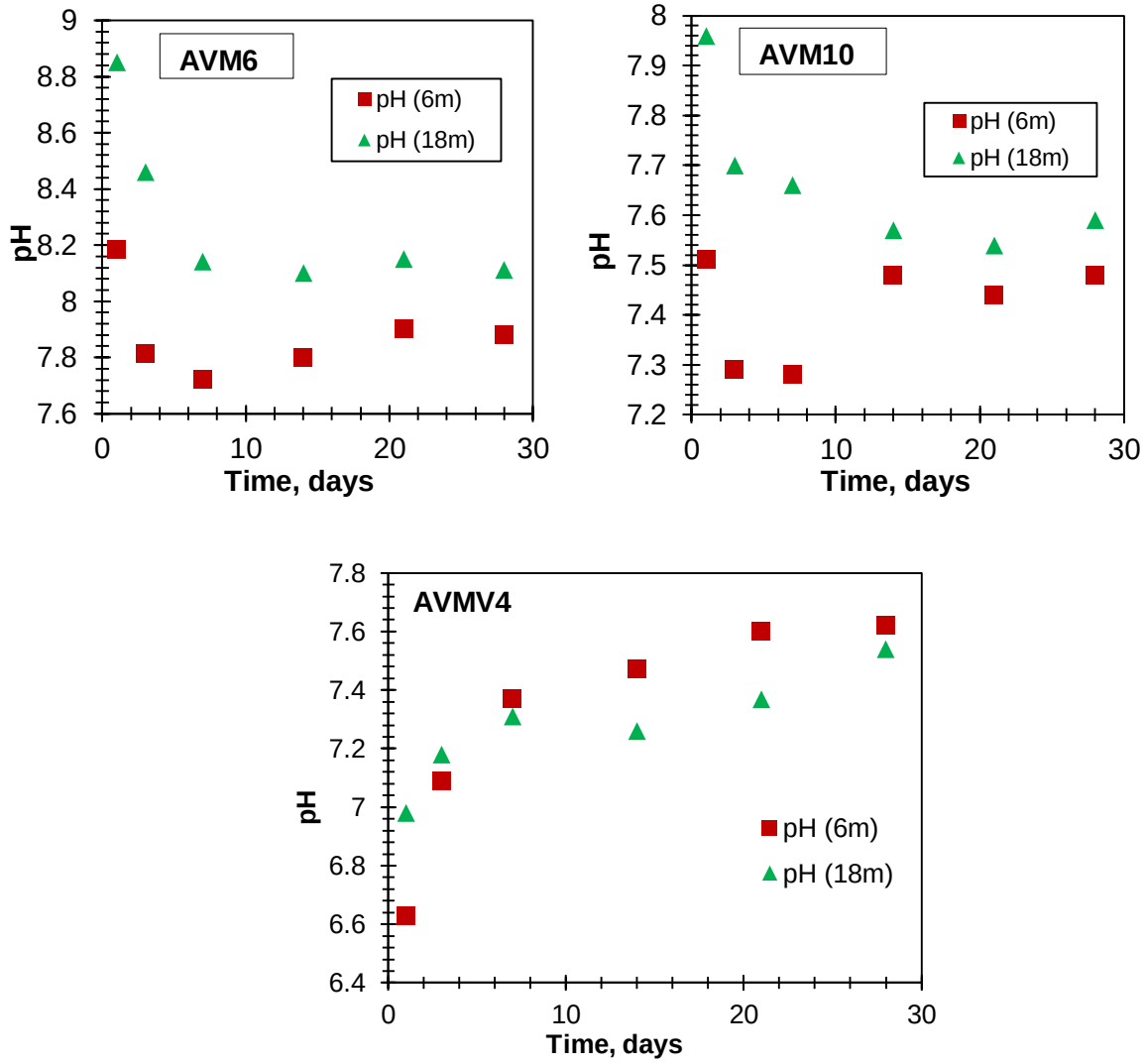

Figure 5- 6 Evolution of the pH of the complex glasses AVM6, AVM10 and AVMV4; In each graph, the pH evolution during aqueous alteration in DI water at 50°C and SA/V of 20 m^{-1} for 28 days in the glass pre-hydrated for 6 months (6m) and the glass pre-hydrated for 18 months (18m) is provided

For the purpose of comparison with aqueous alteration of pristine glasses, the release rate of Si between 1 and 3 days of immersion of the pre-hydrated samples (0.073 & 0.076 g/m^2day for AVM6-6m and AVM6-18m respectively) was compared with the initial glass dissolution rate (based on concentration of Si released into the leachate) of a pristine glass sample of AVM6 under similar conditions (50°C, 0.1 cm^{-1} SA/V) (0.078 g/m^2day) (personal communication-internship work of Nicolas Bisbrouck). The values were in the same order of magnitude.

It is difficult to make a reasonable comparison in terms of NL of pre-hydrated and pristine samples in this case since the concentrations of elements in the leachate are within the range of the “max from gel” values. The surface areas of the pre-hydrated samples are also unknown and

they are higher than the surface area of the pristine sample. Therefore, the actual NL values could be lower than the calculated ones. An agreeable comparison can only be made between the samples pre-hydrated for six months and the samples pre-hydrated for 18 months, which shows clearly that the concentration of elements increases with the increase of the duration of vapor-hydration. Therefore, as far as the AVM6 glass is concerned, the gel layer formed during vapor hydration does not have a passivating effect during subsequent aqueous alteration.

AVM10: The case of the AVM10 glass is similar to that of AVM6 glass, in the sense that this glass too had altered extensively and in a heterogeneous manner during vapor hydration. Therefore, the data treatment of the aqueous alteration of the vapor hydrated samples is handled in a similar manner to the AVM6 samples. The threshold concentration, which is used to get an idea if the concentration of glass elements in leachate is due to dissolution of gel or glass, was calculated by assuming an average thickness of the gel formed during vapor hydration. This value was taken to be 630 nm for the gel formed during vapor-hydration for 6 months (based on ToF-SIMS profiles and statistical calculation-chapter 2) and 900 nm for the gel formed during vapor-hydration for 18 months (based on ToF-SIMS profiles in chapter 2).

Except Li, the concentrations of the other elements in the leachate are in the same order of magnitude as that of the calculated threshold concentration (figure 5-8). From SEM images in Appendix 5 (figure A5-6), it can be seen that the surface of the pre-hydrated samples have been strongly modified during aqueous alteration. However, a gel layer is not clearly visible beneath the secondary phases as it was the case in AVM6 glass samples. Therefore, it could most probably be the gel layer and/or secondary phases rather than the pristine glass that first dissolves during the aqueous alteration of a pre-hydrated AVM10 glass.

Similar to AVM6, the concentration and the normalized mass loss of elements for the sample pre-hydrated for 18 months is greater than the sample pre-hydrated for 6 months. It is true that the surface area of the pre-hydrated samples is unknown. But we know from SAXS data in chapter 2 that the surface area of the gel is lower at 18 months than at 6 months. Therefore, the NL of the samples pre-hydrated for 18 months may be higher than the calculated values.

Table 5- 2 Release rates of elements (g/m^{2}day) in DI water at 50°C and SA/V ratio of 20 m^{-1} for a period between 1-28 days, before and after an apparent rate drop; Rates are calculated by the linear regression of the NL(i)=f(t) curves; The rates are provided for three glasses AVM6, AVM10 & AVMV4, whose samples were pre-hydrated for 6 months (6m) and pre-hydrated for 18 months (18m)

	Rate (1-28 days)	Rate before rate drop (1-3 or 7 days)	Rate after rate drop (3 or 7-28 days)	Rate drop factor
		B		
AVM6-6m	$(4.5\pm0.54).10^{-2}$			
AVM6-18m	$(7.4\pm0.88).10^{-2}$			
AVM10-6m	$(0.8\pm0.1).10^{-2}$			
AVM10-18m	-			
AVMV4-6m	$(3.4\pm0.4).10^{-2}$			
AVMV4-18m	-			
		Na		
AVM6-6m	$(3.74\pm0.45).10^{-2}$			
AVM6-18m	$(11.12\pm1.33).10^{-2}$			
AVM10-6m	$(0.62\pm0.07).10^{-2}$			
AVM10-18m	$(2.5\pm0.3).10^{-2}$			
AVMV4-6m	$(3.03\pm0.36).10^{-2}$			
AVMV4-18m	$(5.31\pm0.64).10^{-2}$			
		Si		
AVM6-6m	$(3.22\pm0.39).10^{-2}$	$(7.28\pm0.87).10^{-2}$	$(2.37\pm0.28).10^{-2}$	3
AVM6-18m	$(4.54\pm0.54).10^{-2}$	$(7.63\pm0.92).10^{-2}$	$(1.48\pm0.18).10^{-2}$	5
AVM10-6m	$(0.75\pm0.09).10^{-2}$	$(5.39\pm0.65).10^{-2}$	$(0.88\pm0.11).10^{-2}$	6
AVM10-18m	$(3.37\pm0.40).10^{-2}$	$(8.95\pm1.1).10^{-2}$	$(0.84\pm0.1).10^{-2}$	11
AVMV4-6m	$(0.38\pm0.05).10^{-2}$	$(3.25\pm0.39).10^{-2}$	$(0.52\pm0.06).10^{-2}$	6
AVMV4-18m	$(1.91\pm0.23).10^{-2}$	$(2.99\pm0.36).10^{-2}$	$(0.86\pm0.1).10^{-2}$	4
		Mg		
AVM6-6m	$(2.89\pm0.35).10^{-2}$	-	-	
AVM6-18m	$(1.34\pm0.16).10^{-2}$	-	-	
AVM10-6m	$(1.16\pm0.14).10^{-2}$	$(4.39\pm0.53).10^{-2}$	$(0.54\pm0.06).10^{-2}$	8
AVM10-18m	$(2.38\pm0.29).10^{-2}$	$(4.16\pm0.5).10^{-2}$	$(1.96\pm0.24).10^{-2}$	2
AVMV4-6m	$(1.51\pm0.18).10^{-2}$	$(3.92\pm0.47).10^{-2}$	$(1.04\pm0.12).10^{-2}$	4
AVMV4-18m	$(3.2\pm0.38).10^{-2}$	$(4.41\pm0.53).10^{-2}$	$(2.02\pm0.24).10^{-2}$	2
		Li		
AVM6-6m	$(3.99\pm0.48).10^{-2}$			
AVM6-18m	$(9.56\pm1.15).10^{-2}$			
AVM10-6m	$(0.61\pm0.07).10^{-2}$			
AVM10-18m	$(2.02\pm0.24).10^{-2}$			
AVMV4-6m	$(2.68\pm0.32).10^{-2}$			
AVMV4-18m	-			

The main difference between the aqueous alteration of the pre-hydrated AVM6 and AVM10 glasses is that, in the case of the AVM10 glass, the NL of Si is higher than the NL of B (table A5-4&5). This is the case for both the pre-hydrated AVM10 glasses (6m and 18m). In addition, the NL of Si of the glass pre-hydrated for 18 months is 3 times higher than the NL of Si of the glass pre-hydrated for 6 months. This is a strong indicator that this is due to the dissolution of the gel or secondary phases (which were present in a higher quantity in the sample pre-hydrated for 18 months) and not the glass. If glass dissolved, a higher NL(B) can be expected. Even the release rates of Si & Mg are higher than the release rates of B. Another point that supports the argument that it must be either the secondary phases or gel layer that dissolves is the significant rate drop in the release rates of Si and Mg after 3-7 days of aqueous alteration (refer to table 5-2, rate before rate drop & after rate drop).

The extremely high concentration of Li released into solution after the first day of immersion in aqueous medium also suggests dissolution of secondary phases. In the Tof-SIMS profiles of vapor hydrated AVM10 glasses shown in chapter 2, Li was enriched in the zone considered to be phyllosilicates, similar to Mg.

The pH evolution of the samples (figure 5-6) also suggests that instantaneous dissolution of some secondary precipitates occurred when the pre-hydrated samples were immersed in water. Due to this the pH of the sample on the first day of immersion is higher by 0.2 to 0.4 units than the pH measured during higher immersion times.

In terms of comparison with the initial glass dissolution rate of the pristine AVM10 sample (0.037 g/m^2day) (personal communication-internship work of Nicolas Bisbrouck), there is no concrete conclusion since the unknown surface area of the altered samples is higher than the pristine sample and therefore even though the calculated NL values are slightly higher in the pre-hydrated samples, they might have been over-estimated.

These results do not signal any passivating effect of the gel layer formed during vapor hydration. As in AVM6, they only suggest that some of the secondary phases formed during vapor hydration dissolve rapidly during initial contact with aqueous medium.

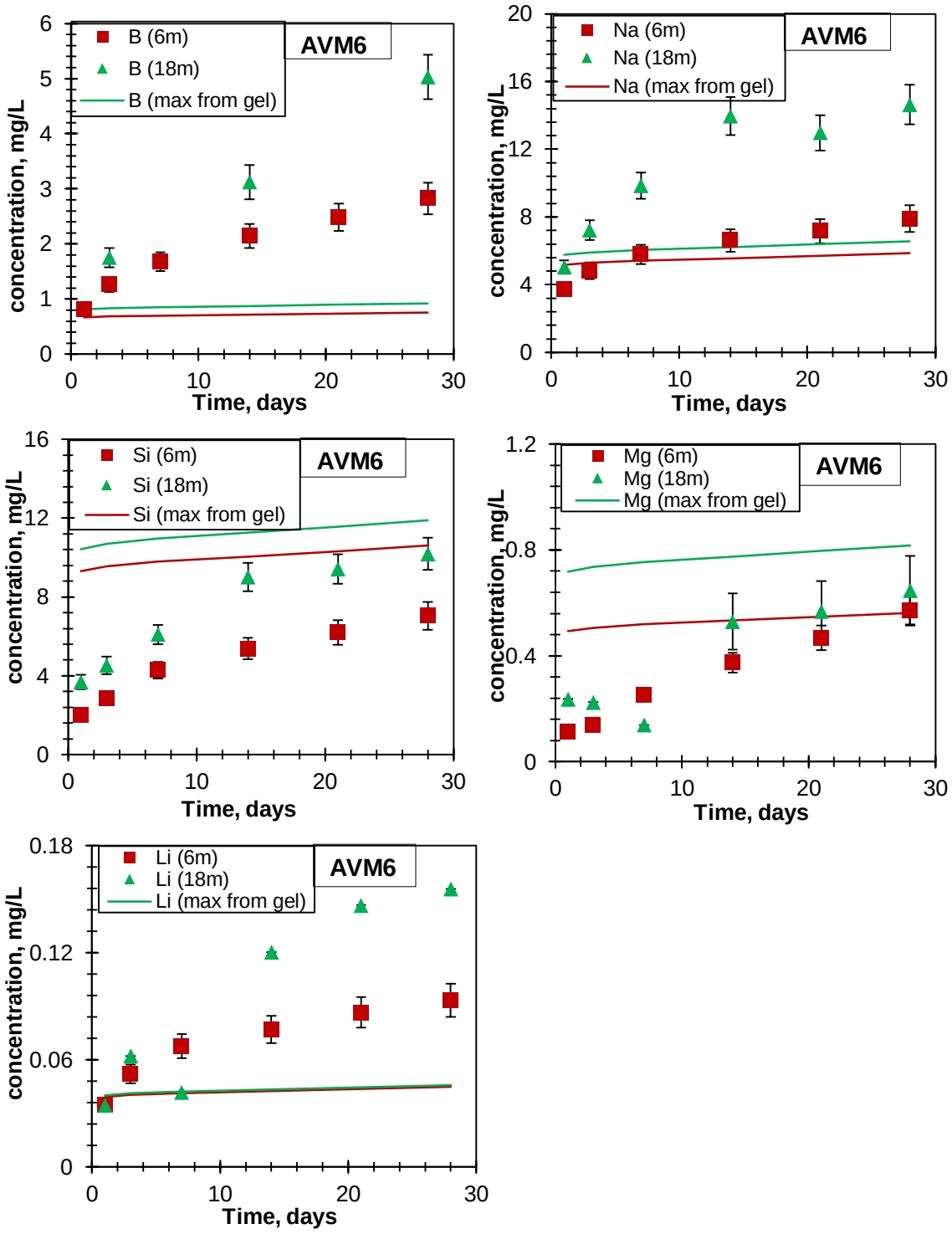

Figure 5- 7 Evolution of B, Na, Si, Mg and Li concentrations with time for the AVM6 glasses that were pre-hydrated for 6 months (6m) and 18 months (18m); The calculated "max from gel" values are given as red lines for the 6m sample and as green line for the 18m samples

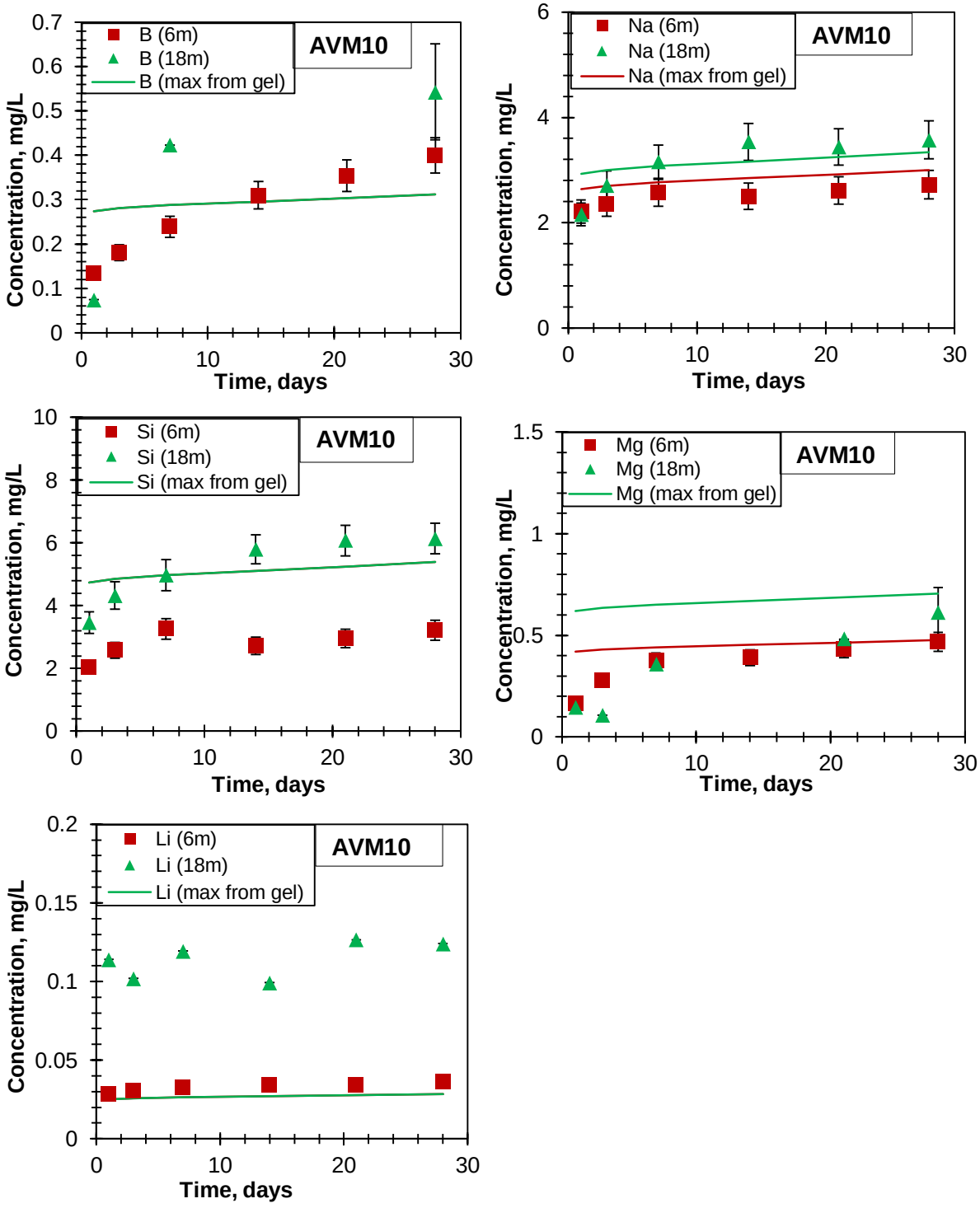

Figure 5- 8 Evolution of B, Na, Si, Mg and Li concentrations with time for the AVM10 glasses that were pre-hydrated for 6 months (6m) and 18 months (18m); The calculated "max from gel" values are given as red lines for the 6m sample and as green line for the 18m samples

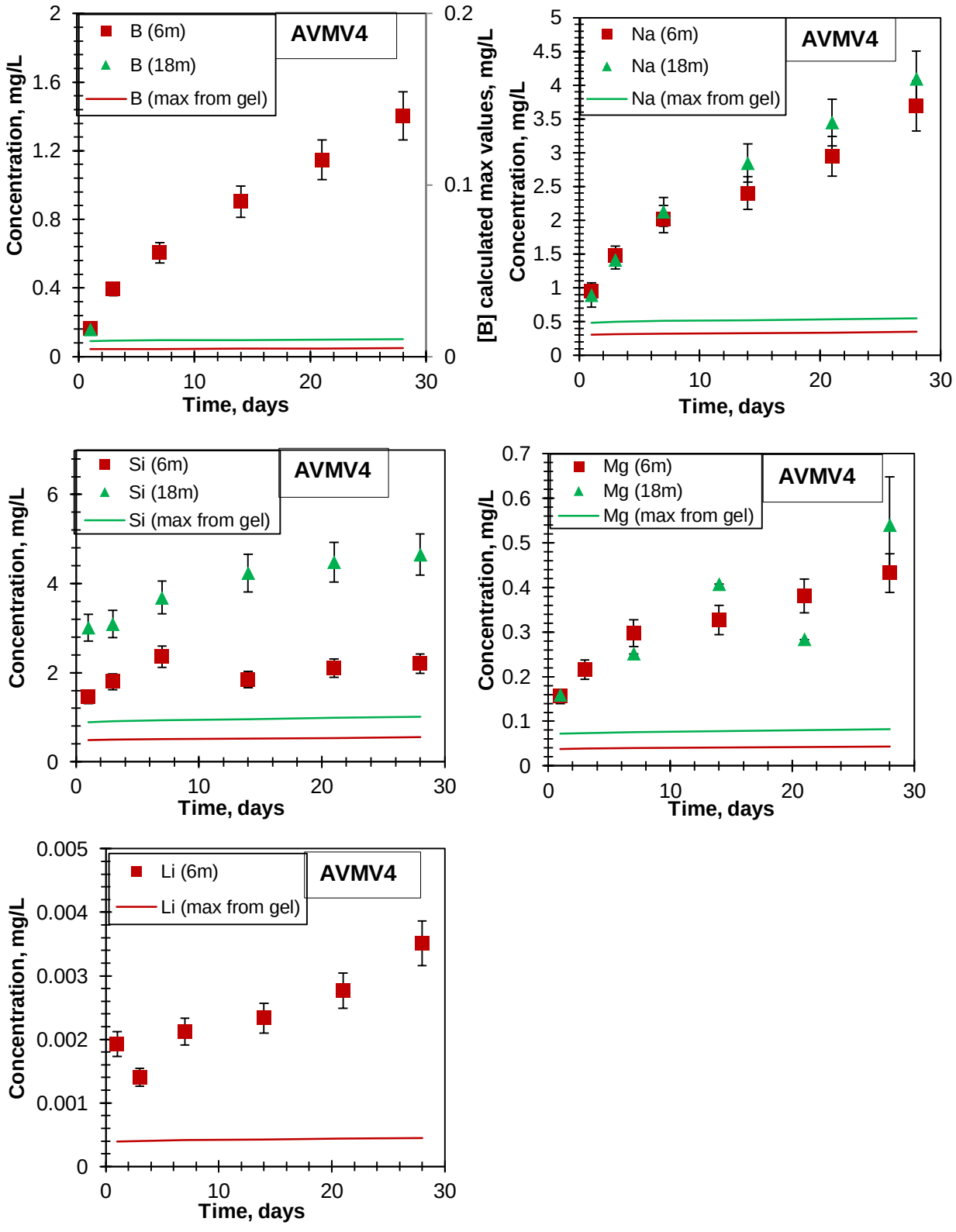

Figure 5- 9 Evolution of B, Na, Si, Mg and Li concentrations with time for the AVMV4 glasses that were pre-hydrated for 6 months (6m) and 18 months (18m); The calculated "max from gel" values are given as red lines for the 6m sample and as green line for the 18m samples

AVMV4: The behavior of the pre-hydrated AVMV4 samples during aqueous alteration is comparable to that of the simplified glasses. Like the simplified glasses, the pre-hydrated AVMV4 samples too had a relatively thin and homogeneous gel layer (of a few tens of nm thickness) formed during vapor hydration. The pH on the first day of immersion of the sample pre-hydrated for 18 months was higher by 0.4 units than that of the sample pre-hydrated for 6 months (figure 5-6). However, the pH of the sample pre-hydrated for 6-months was higher by 0.1-0.4 unit from 14-28 days, with evolution in time.

The concentrations of the B, Na, Si and Mg in the leachate suggest that the quantity of the pre-hydrated glass dissolved during the first day of aqueous immersion was higher than the total quantity of gel available in the pre-hydrated sample (figure 5-9). Therefore, the concentrations of elements in the leachate are due to glass dissolution as well.

Looking at the release rates of Na, Si and Mg (between 1-28 days), the samples pre-hydrated for 18-months alter faster than the samples pre-hydrated for 6-months (table 5-2). This suggests that the gel layer formed during vapor hydration does not possess any passivating properties.

The initial glass dissolution rate of the pristine AVMV4 sample is 0.057 g/m^{2}day (personal communication). The release rates of B and Na between 1-3 days are higher than this value, leading to think that there may be a negative effect of vapor hydration of glasses. However, considering that the real surface areas of the pre-hydrated samples are higher than that of the pristine samples, the calculated NL values are overestimated.

There was a reversal of glass durability between the glasses AVM10 and AVMV4 in vapor phase and aqueous medium. (i. e.) in aqueous medium AVM10 glass dissolves at a slower rate than AVMV4; in vapor phase, the vapor hydration rate of AVMV4 is 10 times slower than AVM10. During the aqueous alteration of pre-hydrated glasses, it is logical to expect that AVM10 dissolves at a slower rate than AVMV4. This is true if the release rates of B and Na are compared for both the samples pre-hydrated for 6 months and 18 months (table 5-2). However, the release rate of Si of the AVM10 glass is higher than the release rate of Si of AVMV4 glass. The NL of Mg of AVM10 is also comparable to that of the AVMV4 glass. This again goes on to demonstrate that although the AVM10 glass has shown itself to be relatively more durable than AVMV4 in aqueous medium since the glass alteration rate of AVM10 is lower, the dissolution of the Mg-silicate phases formed during vapor hydration results in a higher concentration of Si and Mg in the leachate for the AVM10 glass.

In summary, for the AVM glasses,

(i) None of the gel layers formed during vapor hydration has shown any significant passivating properties during subsequent aqueous alteration.

(ii) The NL of elements over 28 days of samples pre-hydrated for 18 months is higher than the NL of elements of samples pre-hydrated for 6 months for all the elements. This shows a negative effect of increasing duration of vapor hydration or it could be because the surface area of the older gel (18m) is lower than the newer gel (6m), resulting in higher NL values for the older gel.

(iii) Some of the secondary phases formed during vapor hydration readily dissolve during subsequent aqueous alteration. This raises some concerns since radioactive elements could be incorporated into some of the phases formed during vapor hydration. If the phases dissolve rapidly during contact with water, environmental contamination would be facilitated.

5.3.2 Comparison of vapor hydration of glasses with aqueous alteration at a very high SA/V ratio

Aqueous alteration at a very high SA/V ratio: In this section, the results of the 'experiment 2' that was described in section 5.2.1 are presented and discussed. The three simplified glasses Q, QCa and QMg were altered at 50°C and an SA/V ratio of 200000 m^{-1} for 91 days. The leachate was sampled periodically and the concentrations of glass elements were measured by ICP-OES.

Figure 5-10 presents the evolution of pH and the normalized mass loss of boron with time in the three simplified glasses altered at a very high SA/V ratio. The pH of the QCa glass is the highest (around 9.7 and 9.9), followed by the QMg glass (around 9.5) and Q glass (around 9.3). This can be explained by the Na, Ca and Mg concentrations in the leachates of QCa and QMg respectively. The NL(B) values (see figure 5-10) and the E_{eq}(B) values (see table A5-6) indicate a positive effect of Ca and a negative effect of Mg when compared to the glass Q under conditions of high SA/V ratio (see figure 5-10). At a pH around 9.5, Mg-silicates are susceptible to form, which may consume Si and destabilize the gel or decrease its passivation properties [97-100, 193]. This may be the reason for the slightly higher alteration of the QMg glass, although precipitation of these phases could not be verified by XRD or SEM images.

Even at a pH close to 10.5 under given conditions, Ca-Silicate-Hydrates (CSHs) may not form during aqueous alteration at a low reaction progress [101]. At higher reaction progress

(residual rate regime) CSHs and zeolites precipitate at a basic pH for certain glass compositions [174, 194]. The NL(B)=f(t) curve of the glass QCa (figure 5-10) shows a step like increase in NL(B) between 28 and 42 days. This sudden increase could have been due to precipitation of CSHs. But, as can be seen, after 42 days, the NL(B)=f(t) curve stabilizes and the glass alteration rate between 42-91 days is still lower than that of the glass Q. Under the given pH conditions and duration in this study, it seems likely that CSHs did not precipitate extensively, and therefore, most of the Ca is most likely retained in the gel layer. Retention of Ca in the gel layer increases its passivation properties [143, 195], which may explain the slightly lower alteration of the QCa glass than the Q glass.

Table A5-6 lists the concentration of the glass elements in the leachate as measured by ICP-OES, the calculated NL values and E_{eq} values for all three glasses. Figure A5-12 shows the graphs depicting the NL(i)=f(t) and NL(i)=f(√t) curves for all the glass elements. In the glass Q, the NL of Si and Al increase until 14 days and then drops by a factor of 2 to a stable concentration value until 91 days. This drop in the Si and Al concentration could be due to the formation of gel layer and/or precipitation of secondary phases. In the case of the glasses QCa and QMg, the concentration of Si and Al is stable from the first leachate sampling done at 8 days, suggesting that the gel layer must have started to form before 8 days and consumes Si, Al, Ca and Mg. Unlike Si, the NL of boron and Na increase continually with time until 91 days for all three glasses. The NL of Na increases at a slower rate than boron in all three cases. This suggests that a fraction of Na is retained in the gel layer. The retention factor of an element can be calculated by considering boron as a tracer for glass alteration using the formula $Retention\ Factor\ (RF) = 1 - \frac{NL(i)}{NL(B)}$, where i corresponds to any element. Using this formula, the retention of Na in the gel layer of Q was calculated to be 45%, in the gel layer of QCa 37% and in the gel layer of QMg 40%. All the other elements in these three glasses such as Si, Al, Ca and Mg were 98-100% retained in the gel layer. In the QCa and QMg glasses, the retention of Na, Ca and Mg indicated that the fraction of positive charges ($1*Na^{+}+2*Ca^{2+}$ or Mg^{2+}) was 40% excessive of the total negatively charged $[AlO_4]^-$ units. Therefore, either solubility of Ca and Mg might have been reduced at the basic pH of this experiment and/or secondary phases incorporating these elements might have precipitated.

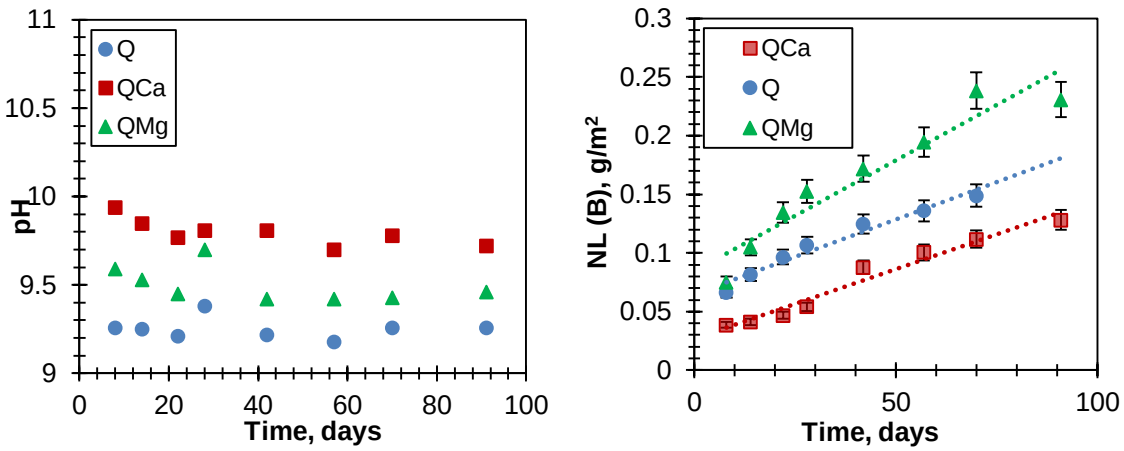

Figure 5- 10 (Left) The evolution of pH with time and (right) the evolution of NL of boron with time of the three simplified glasses altered in aqueous medium at a high SA/V ratio of 200000 m^{-1} at 50°C for 91 days

The evolution of NL with time of Na and boron is linear with the square root of time from 8 to 91 days of aqueous alteration for the glasses Q and QMg. This suggests that glass alteration is controlled by diffusive transport of soluble species through the gel layer. In this time duration, the glass alteration is in a rate drop regime. Comparing the glass alteration rates between 8-28 days given in table 5-4 and the glass alteration rates between 8-91 days (0.0013 g/m^2day for the glass Q, 0.0012 g/m^2day for the glass QCa and 0.0019 g/m^2day for the glass QMg, calculated by linear regression of the slopes of the NL(B)=f(t) curve shown in figure 5-10), it can be seen that the glass alteration rate has reduced after 28 days. For the glass QCa, the evolution of NL with the square root of time is only linear after 42 days, suggesting a change in the rate-controlling glass alteration mechanism between 28 and 42 days. However, this change is not accompanied by a change in the pH and the rate of increase in NL is equal between 8-28 days and 42-91 days (0.0008 g/m^2day), while the overall rate of increase in NL between 8-91 days is 0.0012 g/m^2 day. The glass alteration of the QCa glass is not yet in a rate drop regime.

Vapor hydration: In this section, a recapitulation of the vapor hydration study described in the chapter 2 is given. The three simplified glasses Q, QCa and QMg were hydrated in vapor phase at 50°C and 95% RH for 6 months and 18 months. The relevant results are recalled in the below passages.

Briefly, the glasses QCa and QMg had altered to the same extent (52 nm thick altered layer measured by ToF-SIMS analysis) after 6 months of vapor hydration, which was around 60% higher than that of the glass Q (31 nm thick altered layer measured by ToF-SIMS analysis). The FTIR spectroscopy results indicated that the evolution of glass alteration was linear, considering

uncertainties, until 6 months. After 18 months of vapor hydration, the glasses Q and QMg had altered to the same extent (66 nm thick altered layer), which was around 50% lower than that of the glass QCa (121 nm thick altered layer). The FTIR spectroscopy analysis indicated that the rate of increase in the absorbance of SiOH molecules from 6 months to 18 months of vapor hydration was 15 times lower than that from 0 to 6 months for the Q glass. For the QCa glass, this rate was lower by a factor of 10. The increase in absorbance of the QMg glass fluctuated, and the overall rate between 6 to 18 months was negative (believed to be artefact due to uncertainties).

Table 5-3 recapitulates the thicknesses of the gel layers formed and the retention factors of the soluble elements in the gel layer as measured by ToF-SIMS (data from chapter 2). The depletion of elements such as Ca, Mg, Al and a fraction of Na could be due to the formation of secondary precipitates while the depletion of boron could either be due to condensation of water and surface run-off or due to the evaporation of the boron species. Boron can form precipitates at extremely high pH (>13), but the pH in the gel layer formed during vapor hydration is not known.

This difference in the effect of the addition of Ca and Mg between glasses altered for different duration highlights the well-known fact that the role played by an element, which can either ameliorate or deteriorate glass durability, depends on the rate-controlling mechanism at the time of glass alteration. For example, in aqueous medium, Zr can have a very favorable effect on glass durability when glass alters at the initial glass dissolution rate. At this stage, the rate-controlling mechanism is network hydrolysis and Zr reinforces the glass's resistance to network hydrolysis. During the rate drop regime of glass alteration, a high concentration of Zr in the glass (≥4 mol%) has an unfavorable effect on the reduction of glass dissolution rate since it prevents rapid reorganization of gel that permits to increase the passivation properties of the gel layer [37, 165].

Table 5- 3 Thicknesses of the gel layer formed during vapor hydration at 50°C and 95% RH in the "pre-hydrated" samples and the retention factors of elements in the gel layer calculated from ToF-SIMS profiles (data from chapter 2)

	Thickness of gel layer formed during vapor hydration, nm	Retention factors of elements in the gel layer (from ToF-SIMS)			
		B	Na	Ca	Mg
Q-6m	32	0.12	0.62		
Q-18m	66	0.09	1		
QCa-6m	52	0.04	0.36	0.003	
QCa-18m	120	0.06	0.57	0.03	
QMg-6m	52	0.02	0.39		0.57
QMg-18m	66	0.04	0.87		0.55
AVM6-6m	~1000	0.22	1		0.43
AVM6-18m	~1000	0.3	1		0.7
AVM10-6m	~600	0.2	1		0.44
AVM10-18m	~900	0.2	0.9		0.65
AVMV4-6m	52	0.018	0.86		0.63
AVMV4-18m	66	0.07	1		0.61

Similarly, in the case of vapor hydration, as discussed in detail in chapter 2, the effect of Ca and Mg seems to vary between the first 6 months and between 6-18 months. The lower durability of the glasses containing Ca and Mg during the first six months may in fact be due to the higher fraction of non-bridging oxygen atoms (because of lower Si content) and not really an effect of the presence of Ca or Mg. During this period, it seems that network-hydrolysis is the rate-limiting mechanism. From 6 months to 18 months, based on the FTIR results, the vapor hydration rate has dropped. It seems reasonable to suppose that this rate drop could be due to a transport barrier posed by the gel layer formed during the initial six months of vapor hydration. This assumption could explain the highest alteration of the glass QCa at the end of 18 months, since according to ToF-SIMS analysis, the gel layer of QCa is the most depleted in terms of modifier cations and therefore could be less passivating. At 18 months, it seems that Mg has no effect on vapor hydration of glasses since Q and QMg have the same thickness of gel layer. This could be due to the retention of Mg in the gel layer which might have made the gel more

passivating than that of the Q glass. Therefore, after 6 months, the rate drop in the glass QMg might have been higher than the rate drop of the glass Q.

Effect of varying SA/V ratio: This section discusses the effect of varying SA/V ratio during aqueous alteration and analyzes if these effects can explain the differences observed between aqueous alteration and vapor hydration. The main effects of increasing SA/V ratio are: decrease in the quantity of glass altered to achieve saturation conditions for reducing chemical affinity of Si dissolution; increasing pH of solution due to smaller volume of water; quicker achievement of residual glass alteration rates; and varying influence of elements depending on the regime of glass alteration and conditions favorable for secondary phase precipitation [101, 172, 196]. These effects have been observed during the comparison of the low SA/V ratio and high SA/V ratio alteration of simplified glasses in this study as well.

Table 5- 4 below shows the release rates of B and Na calculated between 7-28 days in the case of the pristine glasses altered at low SA/V (20 m^{-1}) (the same experiment discussed in section 5.3.1 of the samples Q-pg, QCa-pg and QMg-pg) and 8-28 days in the case of the pristine glasses altered at a high SA/V ratio (200000 m^{-1}). The duration for the calculation of the rate was chosen to facilitate the comparison of the two cases. As can be seen, the increase in the SA/V ratio has reduced the glass alteration rates by at least an order of magnitude. While the effect of Ca and Mg is negative during 28 days in the low SA/V experiment, Mg has a negative effect and Ca has a positive effect on glass alteration in the high SA/V experiment. Similarly, the pH values of the solution of the high SA/V experiments are at least two units higher than those in the low SA/V experiments.

Table 5- 4 Release rates of soluble glass elements during aqueous alteration of the glasses Q, QCa and QMg at 50°C in conditions of low SA/V (20 m^{-1}) and high SA/V (200000 m^{-1}) for a period of 29 days and 91 days respectively; The rates have been calculated between 8-28 days to facilitate comparison between the two experiments;

	Alteration rates g/m²day calculated between 8-28 days			**Equivalent thickness of altered glass, nm**
	SA/V, m-1	**B**	**Na**	**E_{eq} (B)**
Q	**20**	$(2.82\pm0.34).10^{-2}$		617
	200000	$(0.2\pm0.02).10^{-2}$	$(0.1\pm0.01).10^{-2}$	116
QCa	**20**	$(4.15\pm0.5).10^{-2}$		512
	200000	$(0.08\pm0.01).10^{-2}$	$(0.03\pm0.004).10^{-2}$	56
QMg	**20**	$(3.38\pm0.41).10^{-2}$		460
	200000	$(0.38\pm0.05).10^{-2}$	$(0.21\pm0.03).10^{-2}$	176

The known main differences between the samples altered in aqueous medium at a very high SA/V ratio and in vapor phase are: slower kinetics of formation of the altered layer in the vapor phase; and influence of Ca, which is positive in the aqueous alteration experiment and negative in the vapor hydration experiment.

If we consider that vapor hydration of glasses is indeed an extrapolation of aqueous alteration at a very high SA/V ratio, then we would expect to see a lower quantity of glass altered in vapor phase. This is true for all three glasses altered in vapor phase. The rate of formation of the altered layer[21] in vapor phase is 0.18 nm/day for the glass Q, 0.29 nm/day for the glasses QCa and QMg. In aqueous alteration at a high SA/V, it is 2.4 nm/day for Q, 1.5 nm/day for QCa and 4.3 nm/day for the glass QMg.

In terms of the differences observed on the effect of Ca, the differences can be explained by the dominant rate controlling mechanism. As long as hydrolysis is the rate controlling mechanism, QCa will alter faster than Q, since Q glass has lesser NBO fraction than QCa. In chapter 2, it has already been discussed that up until 6 months, network hydrolysis seems to be rate controlling mechanism and therefore the higher alteration of QCa than Q is coherent. The glass QCa alters at a higher rate than the glass Q in the low SA/V aqueous alteration experiment as well. It is well-established that hydrolysis is the dominant glass alteration mechanism during the initial stages of glass alteration. It is only during the formation of gel layer in the rate drop regime that Ca begins to have a positive effect due to its retention in the gel layer (as is the case in the high SA/V ratio experiment).

At a low SA/V ratio, a longer time is necessary to reach equilibrium between gel and solution, which would result in diffusion through the gel becoming the rate-controlling mechanism [179]. In aqueous medium, as the SA/V ratio increases, the duration of the initial glass alteration regime controlled by network hydrolysis decreases. In this line of thought, the duration of vapor hydration that is controlled by network hydrolysis must be very small. However, network hydrolysis is the dominant rate controlling mechanism for 4-6 months of vapor hydration at this temperature. This difference strongly suggests that vapor hydration phenomenon is rather particular and glass behavior in vapor phase cannot be considered as aqueous alteration in a very high SA/V ratio. In aqueous medium, the saturation of the leaching solution results in the

[21] The rate of formation of the altered layer in vapor phase was calculated by dividing the thickness of the altered layer measured by ToF-SIMS in chapter 2 by the total duration of vapor hydration (6 months). Similarly the rate of formation of altered layer in high SA/V aqueous alteration experiment was calculated by dividing the E_{eq} by the duration. This was done to facilitate the comparison of the two experiments that were carried out for different durations. This makes the assumption that the rate up to 6 months in the vapor hydration and 91 days in the case of aqueous alteration is linear. While this is more or less true for vapor hydration, the rate is linear from 8-91 days, but not from 0-91 days for aqueous alteration.

formation of a gel layer, which in turn results in the change in rate-controlling mechanism to diffusion through the passivating gel layer. In vapor phase, while the formation of gel layer results in change in rate-controlling mechanism to most likely a diffusive phenomenon, the formation of gel layer (controlled by network-hydrolysis) is a much slower and a more local process. Eventually, a comparison between vapor hydration and aqueous alteration at a very high SA/V ratio and a very slow renewal rate can be envisaged [179]. But untangling the complicities of the influence of various parameters in such an aqueous alteration seems complicated for the moment.

The results obtained in chapter 4 also provide very strong arguments to the point of view that vapor hydration is not equivalent to aqueous alteration at a very high SA/V ratio. Firstly, while in this chapter, at 50°C, the quantity of glass altered in vapor phase after six months was lower than the quantity of glass altered in aqueous medium at a very high SA/V ratio after three months, in chapter 4, at 90°C, the quantity of QCa glass altered in vapor phase was much higher than the quantity of glass altered in aqueous medium for the same duration. This also shows that there are differences in the thermal activation of the glass alteration mechanisms in these two different media.

Another important difference is the protective nature of the gel layer. During glass alteration in aqueous medium, especially as the SA/V ratio increases, the gel layer becomes protective more rapidly resulting in a rapid drop in the glass alteration rates and the residual glass alteration rate is reached more quickly. This has been observed in this thesis work as well. For example, in chapter 4, the glass alteration rate of the Q glass at 90°C and 500000 m^{-1} SA/V ratio drops to almost zero after 8 days of aqueous alteration, suggesting the very protective nature of the gel layer. In vapor phase however, the gel layer is not as protective. Even though in chapter 2, it was shown that the gel layer that was formed resulted in an inflexion of the vapor hydration rate, it has been shown that this gel layer has no protective properties while immersed in aqueous medium.

Figure 5-11 is a schematic representation of a global understanding of vapor hydration phenomenon, based on various studies. Initially when pristine glasses are exposed to humid atmosphere, water molecules physically adsorb onto glass surface due to intermolecular forces depending on intrinsic and extrinsic alteration parameters. A thin water film might form on the glass surface due to cohesion of adsorbed water molecules that result from Van der Waals forces. The pH of this solution might become basic due to the release of modifier cations as a result of formation of a hydrated layer by means of inter-diffusion and hydrolysis reactions. With

time, the thickness of the hydrated layer may increase and this hydrated layer may reorganize within itself due to increase in SiOH content and trapped modifier ions released into the gel network, which may further participate in depolymerisation of the silicate network, as evidenced in the work of Alloteau et al. [33]. While local network hydrolysis and inter-diffusion reactions during vapor hydration studies have been evidenced, complete dissolution and precipitation mechanism for the formation of the gel layer in vapor phase has not been reported. Meanwhile, due to atmospheric composition and pH of the surface film, carbonates and/or silicates may form depending on thermodynamic conditions.

Beyond the formation of the gel layer, there are many uncertainties related to the continuation of glass alteration in a vapor phase. Is there a difference in the adsorption of water on a pristine surface and an altered surface? If yes, is the adsorption enhanced or diminished on the altered surface? As explained in the figure 5-11, there is a dynamic nature associated with vapor hydration due to the constant supply of water molecules from the alteration environment. For certain glasses, if the thermodynamic state of the altered surface is less conducive to physical adsorption, or if the gel is passivating and decreases the diffusion of water molecules to the pristine glass, the vapor hydration may be similar to a static alteration of glass at a very high SA/V ratio (no solution renewal). In other cases, vapor hydration may be dynamic in nature (due to condensation and run-off of water films and continuous vapor availability). This may most likely be determined by the glass composition and nature of the alteration products formed.

To summarize this section, many differences have been observed between aqueous alteration and vapor hydration of glasses; some of the differences such as rapid and extensive precipitation of secondary phases and lower quantity of altered glass can be explained by the much higher SA/V ratio in vapor phase; But the duration of vapor hydration rate controlled by network hydrolysis cannot be explained if we consider vapor hydration as aqueous alteration of glasses in a very high SA/V ratio. A certain dynamic nature is associated with vapor hydration due to the constant supply of water molecules from the vapor phase. The rate at which water film on glass surface gets renewed depends on intrinsic parameters of the glass, and it remains complicated to predict. To conclude, vapor hydration of glasses cannot be considered equivalent to glass alteration in very high SA/V ratio (especially if the comparison is made with a static experiment; Even in the case of dynamic experiments, the flow rate which is equivalent to vapor hydration phenomenon is unknown).

Experiments such as “Pressurized Under Flow (PUF)” tests for glass alteration in unsaturated medium may be attempted in the future to quantify the dynamic nature of vapor hydration phenomenon [197].

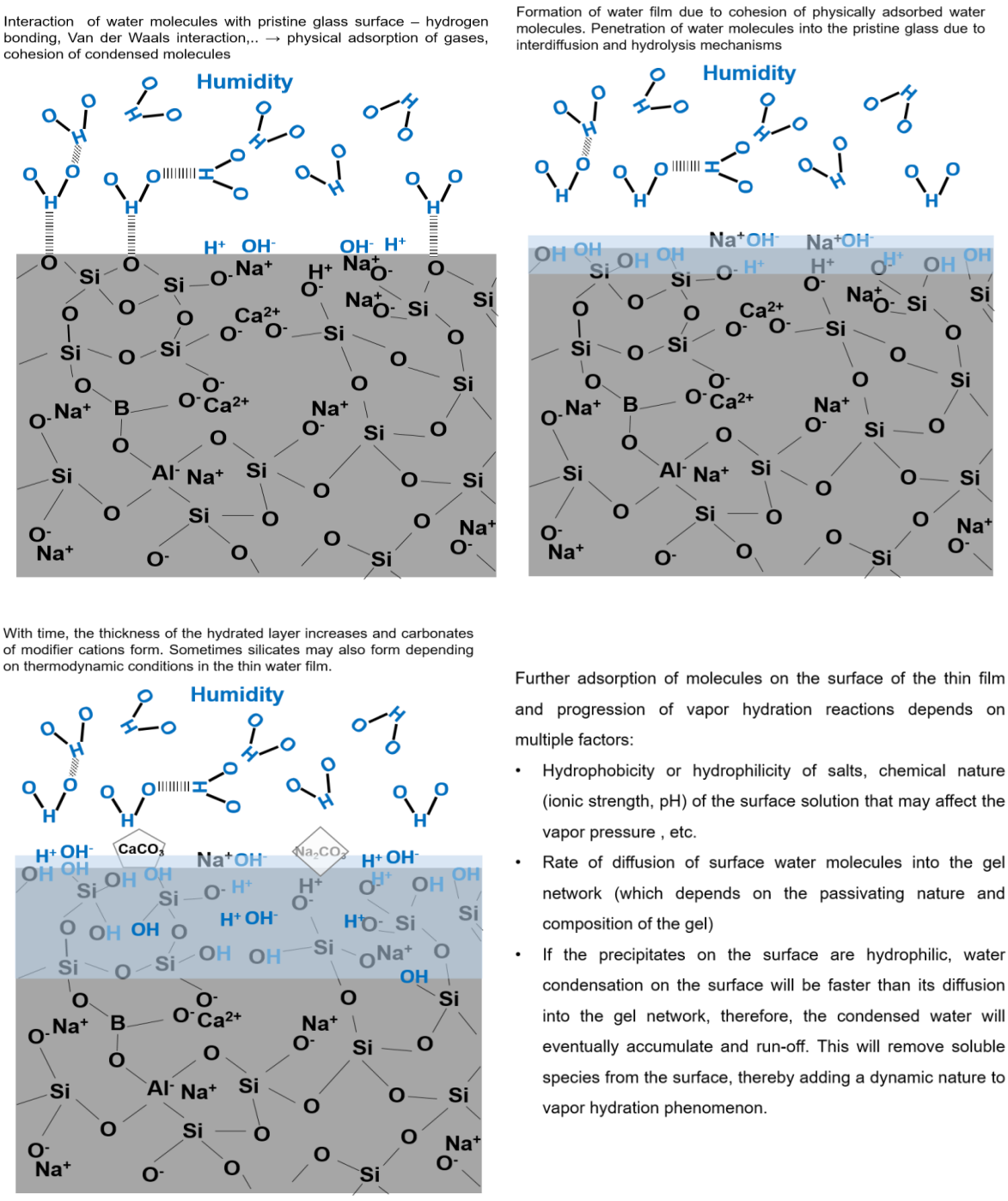

Figure 5- 11 Schematic representation of vapor hydration phenomenon constructed based on the literature survey

5.4 Geochemical modelling

The three simplified glasses Q, QCa and QMg were altered in DI water at a high SA/V ratio (191100 m^{-1}, 187700 m^{-1} & 196600 m^{-1} respectively) and 50°C for 91 days (experiment 2 in section 5.2.1). The evolution of concentration of the elements in the leachate over time was simulated using GRAAL model with HYTEC (version 4.32) computational code [198-200].

GRAAL model:

The model for glass alteration used in this study was based on the GRAAL model constructed by Frugier et al. [190, 201].

Note: A very simple description of the model is provided below to highlight the different model parameters. All the equations cited below are based on the document cited above.

The glass is described as an infinite media in contact on one side with a semi-infinite fluid. Based on the experiment in this study, the fluid is pure water at 50°C. The glass, referred to as a 'primary solid', is described as a mineral in the geochemical code. The composition of the mineral is defined according to the stoichiometric composition of the glass. The rate of dissolution (r_1, m/s) of this primary solid, under the given temperature and pH conditions, is controlled by a diffusion coefficient D (m^2/s) and the thickness of a 'protective layer' x_{PL} (m), referred to hereafter as Passivating Reactive Interphase (PRI).

$$r_1 = \frac{D\frac{\pi}{2}}{x_{PL}} \qquad \text{(Equation 5.4.1)}$$

Equation 5.4.1 is derived by following Fick's second law with the hypothesis that the driving force for diffusion of elements is the concentration gradient between the pristine glass and the glass/fluid interface and by considering a constant diffusion coefficient in the fluid.

The PRI is a silica rich amorphous layer ($SiAl_{0.0833}O_{2.125}$) with a diffusion coefficient that determines the transport properties of this layer. The rate of formation of this layer is usually equal to or slightly lower than the rate of dissolution of the primary solid.

The rate of dissolution of the primary solid will determine the concentration in solution of glass tracer elements such as boron, which are not retained in the gel layer.

The rate of dissolution of the PRI, r_2 is defined as:

$$r_2 = k_+(H^+)^n e^{\frac{-E_a}{RT}}(1-\frac{Q}{K}) \qquad \text{(Equation 5.4.2)}$$

In the above equation, k_+ is the dissolution rate of the PRI in pure water (m/s), n is the pH dependence coefficient of the initial rate, E_a is the activation energy of the initial rate (J/mol), Q is the activity product of the PRI, K is the activity product at the saturation of the PRI.

The model also gives allowance for the formation of one or multiple "Non-Protective Layers-NPL" or depleted gel, whose formation is controlled by thermodynamic equilibrium with the solution in contact. These NPLs, sometimes referred to as 'poles'/'end-members', describe an amorphous layer, whose composition is determined based on a vast database of experimental observations and glass composition. In the geochemical code, they are described as amorphous silicates or alumino-silicates with Ca or Na for charge compensation of $[AlO_4]^-$ units.

Thus, with these set of equations and description of amorphous secondary phases, the geochemical code is able to take into account both transport properties and chemical affinity to describe glass alteration. The implementation of this model in a reactive transport code is described in detail in Frugier et al. 2018 [202].

Modelling of alteration of glass Q in DI water at high SA/V conditions:

Parameters: The fixed parameters (experimental values) applied in the model include the glass composition, molar density, SA/V, initial leachate concentration, initial pH and temperature.

The global kinetic model to describe reaction rates used in HYTEC takes into account several kinetic laws and the one used in the GRAAL model is a Monod type equation with non-competitive inhibition [198]. Model parameters such as correction coefficient for linear gradient hypothesis, the "w-term power" parameter that describes the dependence of the reaction rate to the concentration of species in the solution are also used in the model. The standard values for these parameters calculated earlier by P. Frugier for the aqueous alteration modelling of simplified glasses at 50°C were used in this model as well.

The rate of dissolution of the PRI was based on the glass dissolution rate at 50°C and pH 7 (0.05 g/ m^2.day) for the Q glass approximately calculated from the experiment described in section 5.3.1). The diffusion coefficient used in the model is 6.3×10^{-22} m^2/s. The determination of the diffusion coefficient in the protective layer is complex. The value of D retained for a similar quaternary glass altered at 50°C was 4.3×10^{-22} m^2/s. This value was estimated from experiments

conducted at different SA/V ratios and pH conditions [203]. The experimental value of D that was calculated from our study using the below formula is between $4x10^{-22}$ m^2/s to $9x10^{-22}$ m^2/s.

$$C_i = 2(\sqrt{\frac{Dt}{\pi}})\rho X_i \frac{SA}{V} \qquad \text{(Equation 5.4.3)}$$

Since the average of D calculated experimentally using equation 5.4.3 was in the same order of magnitude as the value estimated by Y. Minet for similar simplified glasses altered at 50°C and low SA/V [203], this value was used for the model.

The amorphous poles used for the model are:

	Log K at 50°C
$SiAl_{0.0833}Na_{0.0833}O_{2.16666}$ (SiAl) (PRI)	2.0
$SiAlNaO_2(OH)_4$ (SiAlNa)	-12

The values of the solubility constants were also chosen based on the compilation of data and estimation of model parameters carried out by P. Frugier and Y. Minet [203].

Results:

A comparison of the model prediction with experimental values is presented in figures 5-12. This model was able to simulate the evolution of concentration of all the four glass elements in the leachate to an appreciable extent. The glass dissolution rate is initially higher until the solution is saturated with respect to Si and the pole SiAl begins to precipitate. Once the altered layer begins to precipitate, the glass dissolution occurs at a slower and steady rate. This is reflected in the evolution of the concentrations of Si and Al as well, which remain more or less constant with time experimentally. The model reproduces the evolution of the concentration of Al much better than Si. The evolution of Si concentration increases continually at a slower rate than boron in the model, whereas experimentally, the concentration of Si is constant with time. Since boron is not retained in the gel layer, its concentration continually increases. Na is a mobile element with high solubility. The quantity of Na retained in the gel is dependent on the stoichiometry of Al, as it is retained as charge compensating atom for $[AlO4]^-$ units. Since the mol% of Na is 2-3 times higher than Al in the glass, its concentration also continually increases with time.

The model does not reproduce the pH values correctly. There is a difference of about 0.5 pH units between the model values and experimental values. However, when the same solution concentrations of elements as calculated by the model, are entered in PHREEQC, and the solution is equilibrated with atmosphere, the calculated pH value is similar to the experimental value (±0.05 units). The difference in pH between PHREEQC and HYTEC calculations could be due to the different databases used.

The experimental values and the model results show a classic evolution of concentration of elements with time that is observed for high SA/V experiments.

Modelling of alteration of glass QCa in DI water at high SA/V conditions:

Parameters: The variable parameter influencing the results of the model are the diffusion coefficient associated with the PRI. Sufficient experimental data for similar glass composition was not available in the literature for choosing this parameter. Therefore, this value was chosen based on experimental results using equation 5.4.3. The value chosen is 3.1×10^{-22} m2/s. The initial glass dissolution rate chosen for the dissolution rate of the PRI is the same value as that was used for Q glass (0.05 g/m^{2}day).

The poles chosen to describe the formation of the altered layer are:

	Log K (50°C)
$SiAl_{0.08333}Na_{0.08333}O_{2.16666}$ (SiAl)	1.8[22]
Si_2CaO_5 (SiCa)	-9.8
$SiAlCa_{0.5}O_2(OH)_4$ (SiAlCa)	-30
$SiAlNaO_2(OH)_4$ (SiAlNa)	-12

These poles were chosen based on the composition of the glass and the studies conducted in the past for the modelling of similar glasses [203].

[22] The log K of the pole SiAl slightly varies with glass composition. This shows the need to adapt the composition and solubility of the protective layer depending on glass composition.

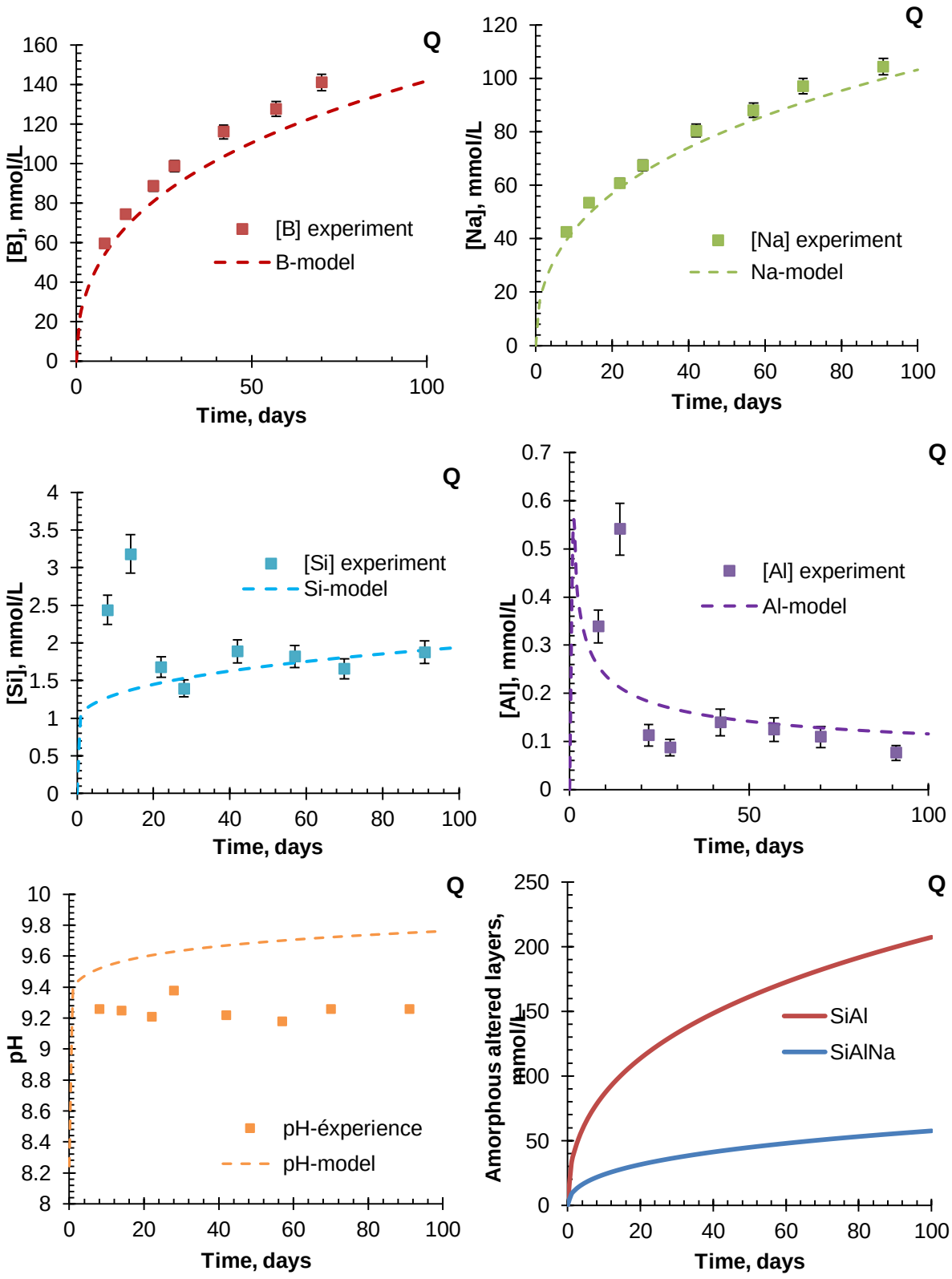

Figure 5- 12 A comparison of the model and experimental results of Q glass altered at a high SA/V ratio of 191100 m^{-1} at 50°C for 91 days

Results:

Figure 5-13 shows that the model predicts the experimental solution chemistry of the QCa glass reasonably well. For Al, it is also correctly able to reproduce the evolution of concentration over time. The experimental values of Ca are scattered. But the model reproduces the slightly decreasing concentration towards 90 days. This decrease is due to its incorporation in the altered layer. The evolution of the concentrations of boron and Na over time is correctly reproduced. The concentration of Si in the solution is saturated since day 7 experimentally, and does not show an increasing trend. However, the concentration of Si predicted by the model slightly increases with time. The assemblage of the amorphous phases in the model indicates that the gel layer is a silica-rich layer. Al is well-retained in the gel layer and it retains Ca and Na in the gel layer according to its stoichiometry. It is to be noted here that although Ca is preferentially retained for charge compensation of $[AlO_4]^-$ units experimentally, the model reproduces solution chemistry better if it precipitates the poles SiAlNa rather than SiAlCa. This discrepancy between the model and experiment remains unexplained at this moment. The pH of the solution is however correctly reproduced. The evolution of the rate of glass dissolution over time (calculated by the model) is a classic evolution observed in high SA/V ratio experiments. The glass dissolution occurs at a relatively high rate in the beginning and arrives at a steady lower rate after the solution is saturated with respect to the concentration of Si (depending on the solubility of the PRI 'SiAl').

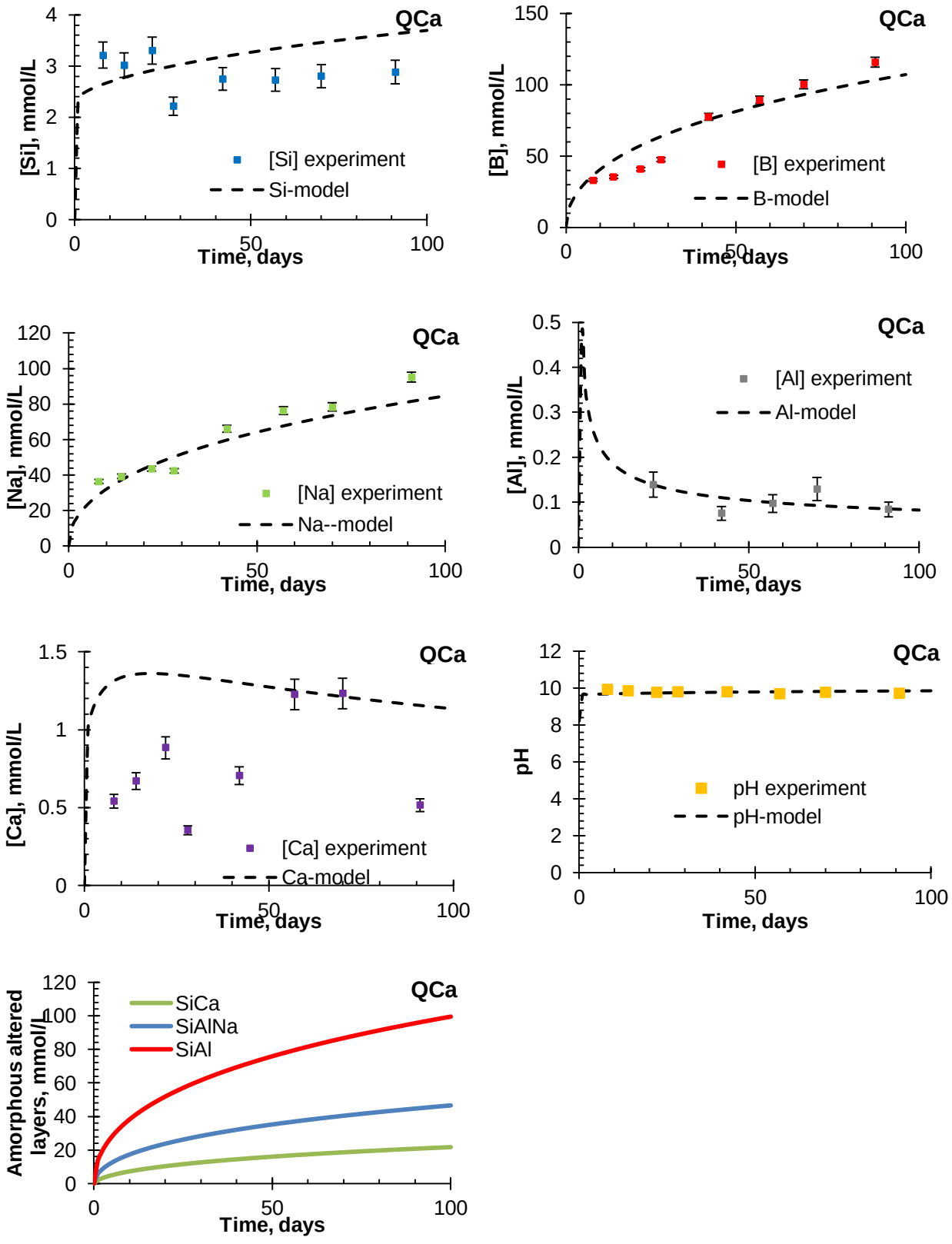

Figure 5- 13 A comparison of the model and experimental results of QCa glass altered at a high SA/V ratio of 187700 m^{-1} at 50°C for 91 days

Modelling of alteration of glass QMg in DI water at high SA/V conditions:

Parameters: The approach to modelling of the alteration of the QMg glass in a high SA/V ratio and 50°C for 91 days was similar to the ones used for the glasses Q and QCa. The parameters varied for the model are the diffusion coefficient through the protective layer and the experimental parameters such as glass composition and SA/V ratio. The amorphous layers described as 'protective layer' and 'non-protective layers' in the GRAAL model were also changed according to glass composition. The Ca in the phases is replaced with Mg. A few crystalline Mg-silicate phases were also allowed to precipitate, since they have been recurrently noticed in literature [96, 99].

	Log K (50°C)
$SiAl_{008333}O_{2.125}$ (SiAl)	2.6[23]
Si_2MgO_5 (SiMg)	-9.8
$SiAlMg_{0.5}O_2(OH)_4$ (SiAlMg)	-28
$SiAlNaO_2(OH)_4$ (SiAlNa)	-12
$Si_6Mg_4O_{16}$ (Silicate_Mg)	-44

Results: (Figures 5-14) The model is able to reproduce to an acceptable degree the evolution of the concentrations of B, Na and Al. The concentration of Mg at short times and pH are slightly over-estimated. The concentration of Si is over-estimated by a factor of 2-6 times.

The amorphous protective (passivating) and non-protective layers that precipitate are SiAl, SiAlNa and Silicate_Mg. The amorphous phases SiMg and SiAlMg do not precipitate under the given conditions. Since Na is more soluble than Mg, experimentally, it has been remarked that Mg is preferentially retained for charge compensation by $[AlO_4]^-$ units than Na [96]. But according to the model, Mg does not precipitate in the altered layer along with Al, but rather forms magnesium silicates. The model does not reproduce the concentration of Si accurately despite several attempts at fitting model parameters within a realistic range and influencing reaction affinity by varying the solubility of the possible amorphous phases that can precipitate.

[23] The log K of the pole SiAl was adjusted to obtain satisfactory results and prevent equilibrium failure in the model calculations. This shows the need to adapt the composition and solubility of the protective layer depending on glass composition.

Based on the work done by N. Godon and P. Frugier on the Mg-containing glasses AVM6 and AVM10, a different approach needs to be adapted to correctly reproduce the aqueous alteration experiment of Mg-containing glasses. It was noted that the model that was used to describe aqueous alteration of the SON68 glass needed to be adjusted for passivation properties of the PRI and its composition. With an advanced version of HYTEC (version 5), the authors developed a new approach to model AVM glasses alteration [201]. This new approach permits to describe the kinetic formation of two altered layers. A Mg-containing layer, which has a slightly lower effective diffusion coefficient than the other Na-containing layer. According to their model, during the aqueous alteration of Mg-containing glasses, initially a Mg-containing altered layer is formed (i.e. $[AlO_4]^-$ units are charge compensated by Mg ions); As the solution gets saturated with respect to secondary Mg-containing phases such as smectites, the Mg-containing altered layer dissolves and the Na-containing altered layer forms. In reality, the Mg ions are removed from the gel layer to form Mg-silicates and Na ions from the solution become part of the altered layer to compensate the charge of the $[AlO_4]^-$ units.

Evidently, the model used to describe the QMg glass needs to be improved to achieve a mass balance between the concentration of elements in solution, quantity of glass altered and the composition of the altered layer. Since the model does not quantitatively reproduce the chemistry of the leachate, hypotheses to explain the mechanism of alteration of these glasses are not proposed.

Possibility of geochemical modelling of glass alteration in vapor phase:

Geochemical modelling of glass alteration in vapor phase would be invaluable to predict its long term durability in the framework of a geological disposal scenario. The approach that was initially considered was to increase the glass surface area in the model to the highest value possible and compare the rate of glass alteration between vapor hydration experiments and the simulation. As shown in the three previous sub-sections, the GRAAL model successfully simulated the evolution of solution concentrations with time for two of the three glasses (Q and QCa) at 200000 m^{-1} SA/V ratio and 50°C. When the glass surface area of the same model was increased to simulate vapor phase, we encountered a few problems. Firstly, we were unable to increase the SA/V ratio beyond 800000 m^{-1} due to problems with the code which crashed as a result of equilibrium failure (presumably due to high ionic strengths of the solution). We expect that in vapor phase the SA/V ratio will be at least two orders of magnitude higher than this value. Another problem is that until the highest SA/V ratio that we were able to simulate, Ca always had

a positive effect in the model that reduced the glass alteration of QCa by 20-30% compared to that of Q, whereas in vapor phase, experiments have shown that Ca either has no significant effect or it has a negative effect. The attempts that were made so far by allowing secondary phase precipitation in the model were unsuccessful to simulate the negative effect of Ca. The third issue is that as the SA/V ratio was increased, the model calculated lower NL(B) values, which is coherent with experimental observations. However, considering the results of chapter 4, more glass was altered in vapor phase than in immersed conditions at 500000 m^{-1} SA/V ratio and 90°C. It is not clear how the model would succeed in simulating this inverse trend at a higher temperature. Recent literature studies suggest that the accelerated alteration at higher temperature is not always linked to secondary phase precipitation as was initially supposed in chapter 1 [54]. More effort, thought and time needs to be dedicated to be able to successfully do geochemical modelling vapor phase hydration. The approach that was adapted also inherently assumed that vapor phase hydration is equivalent to aqueous alteration at a very high SA/V ratio, which we have already discussed to be rather false. Therefore, there is a necessity to rethink the modelling approach.

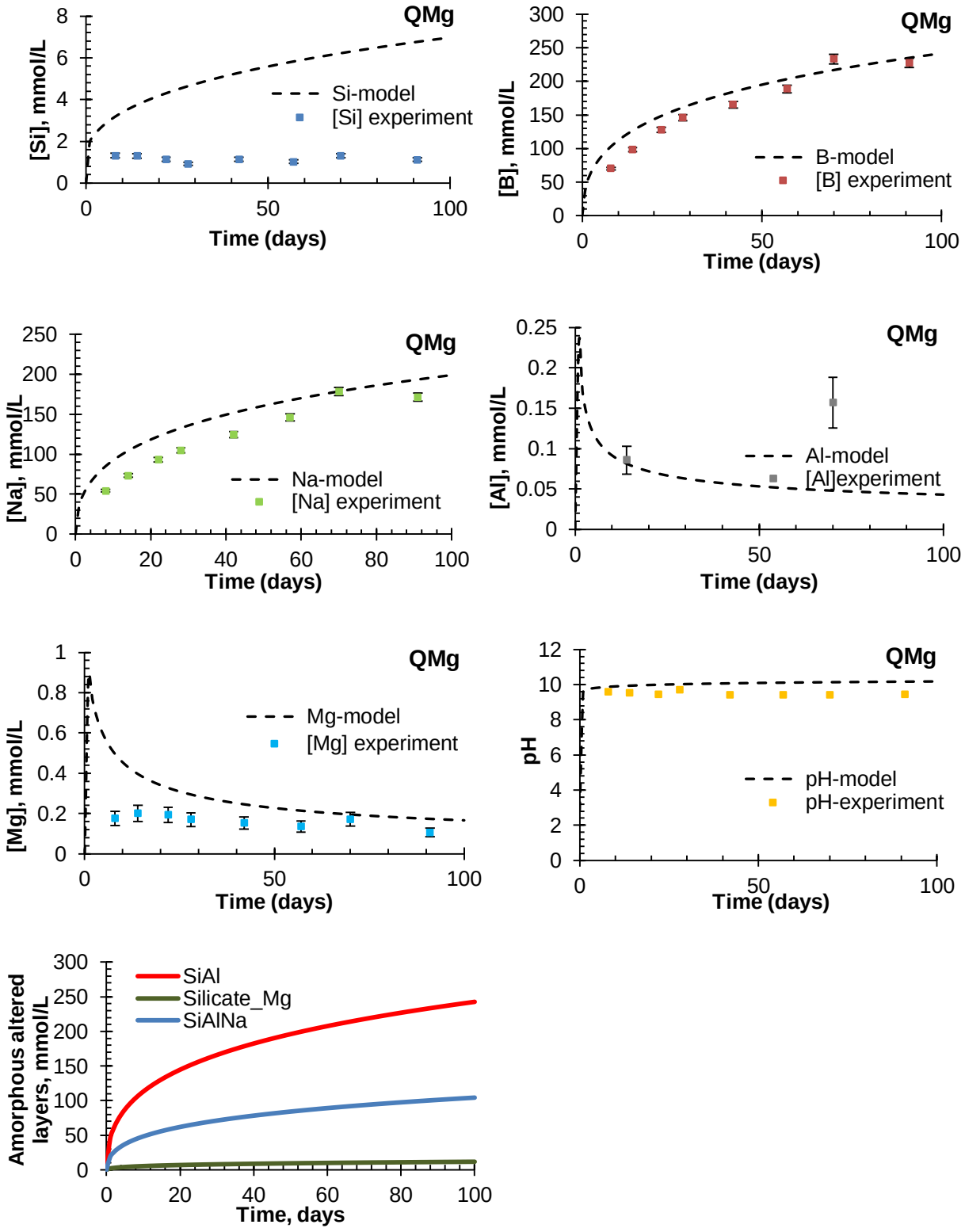

Figure 5- 14 A comparison of the model and experimental results of QMg glass altered at a high SA/V ratio of 196600 m^{-1} at 50°C for 91 days

5.5 Conclusion

In one part of this chapter, the aqueous alteration of vapor hydrated samples was investigated. It was concluded that the gel layer formed during vapor hydration did not have any significant passivating effect during subsequent aqueous alteration for any of the six glasses studied. The aqueous alteration mechanism of the simplified pre-hydrated glasses seemed to be modified in comparison to the aqueous alteration mechanism of the simplified pristine glasses. The normalized mass losses of glass elements was higher for the glasses that were pre-hydrated for 18 months than the glasses that were pre-hydrated for only 6 months. This could mean that higher the duration of glass alteration in vapor phase, higher the quantity of secondary phases and higher the release of elements from the vapor hydrated glass into the leachate. While there was strong evidence for the instantaneous dissolution of some of the secondary phases formed in vapor phase hydration, the phyllosilicates formed on one of the complex glasses are either insoluble or poorly soluble. These experiments suggest that the most noteworthy effect of vapor hydration of glasses during subsequent aqueous alteration is during the initial instants of immersion due to secondary phase dissolution. Future studies can focus the attention on the initial glass dissolution rates of pre-hydrated glasses and try to identify soluble and non-soluble phases. This could be useful for studying the fate of secondary phases incorporating radionuclides.

Another part of this chapter deals with the comparison of vapor hydration phenomenon to aqueous alteration of glasses at a very high SA/V ratio. An inter-comparison of the results of aqueous alteration of the simplified glasses at low SA/V ratio, high SA/V ratio and vapor phase was carried out. It was concluded that vapor hydration phenomenon is not simply equivalent to aqueous alteration at a very high SA/V ratio since vapor hydration of glasses have a dynamic nature associated with them due to the continuous availability of water vapor that can physically adsorb onto the vapor hydrated surface. The renewal of the surface water film depends on intrinsic and extrinsic parameters that seem complicated at the moment to unravel. This unpredictability of the progression of reaction in vapor phase does not seem to justify comparison with aqueous alteration experiments at a high SA/V ratio (especially static tests). To further examine this question, new vapor hydration protocols that would permit to quantify condensing water should be developed.

The last part of this chapter deals with the geochemical modelling of the aqueous alteration experiments of the simplified glasses Q, QCa and QMg at a very high SA/V ratio, with a goal to study the possibility of extending the model to simulate vapor hydration experiments.

Experiments have established that glass alteration is not always a stoichiometric dissolution followed by precipitation of an amorphous layer rich in Si and other glass elements with low solubility as described by GRAAL (i.e. glass exhibits non-congruent dissolution). However, the model has successfully been able to replicate the evolution of solution chemistry in two of the three glasses at high SA/V ratio. It helps to understand better the chemical interactions and validate hypotheses made on glass dissolution mechanisms. However, the attempt to extend the model to simulate vapor hydration mechanisms was unsuccessful.

Conclusions and perspectives

Principal results and conclusions

The core of this thesis revolves around the vapor hydration of glasses with special focus on the influence of glass composition of the inactive AVM nuclear glasses. In this framework, AVM6, AVM10 and AVMV4 are the three inactive complex (made of >20 oxides) borosilicate AVM glasses chosen for the study. Three simplified glasses made of 4 (Q) or 5 oxides (QCa and QMg), whose composition was based on the Si/Al stoichiometry of the AVMV4 glass, were also chosen for the study.

Influence of glass composition on vapor hydration: In the first part of the thesis, all six glasses were altered in a climatic chamber at 50°C and 95% RH for 6 months and 18 months, in order to study the influence of glass composition on vapor hydration rates and mechanisms. Along with characterization of vapor hydrated samples after 6 months and 18 months using SEM, TEM, XRD, ToF-SIMS and SAXS, the vapor hydration kinetics was also studied until 18 months using FTIR spectroscopy.

The results from this study highlighted the high sensibility of vapor hydration rates of glasses to small changes in glass stoichiometry. According to literature, we expected that the alkaline-earth elements such as Ca and Mg would have a negative effect on glass alteration due to their tendency to easily form secondary precipitates in vapor phase. All three AVM glasses studied in this work contain a significant amount of Mg. However, the vapor hydration rates of two of the three AVM glasses were at least an order of magnitude higher than the third glass. After careful analysis of the results, we came to the conclusion that in the more durable AVM glass (AVMV4), the negative effect of Mg was suppressed by the presence of equal quantities of MgO and Al_2O_3. In case of the other two glasses, the quantity of MgO is higher than that of Al_2O_3, thus leading to the acceleration of hydration rates due to the formation of Mg-rich smectites.

The vapor hydration rates of the three simplified glasses studied, whose Si/Al molar ratio was based on that of the more durable AVM glass, was in the same order of magnitude as the more durable AVM glass. One of these glasses did not contain any alkaline-earth elements (Q) and the other two glasses contained higher quantity of Al_2O_3 than CaO (QCa) or MgO (QMg). The quantity of secondary phases formed on the four more durable glasses was scarce in comparison to the two less durable glasses.

While looking at the morphology of the vapor hydrated glasses, all six glasses showed the presence of a gel layer of few tens of nm thickness. In case of the two less durable glasses, their accelerated alteration in vapor phase has led to irregular-cup shaped highly porous zones of a few hundred nm to a few µm depth that were discontinuously present beneath the gel layer.

Comparing the thickness of the gel layer formed on the more durable glasses after six months of vapor hydration to the fraction of NBO in the pristine glass structure, network-hydrolysis is identified as the rate-controlling vapor hydration mechanism. The dependence of the overall glass durability on the ratio of Al_2O_3/(MgO or CaO) also supports the idea that network-hydrolysis must be the predominant vapor hydration mechanism, at least until six months of vapor hydration at low temperature (50°C).

The study of vapor hydration kinetics until 18 months shows an inflexion of increase in SiOH quantity in altered glass with time between 120-200 days of vapor hydration for all six glasses. The inflexion suggests that the vapor hydration rate must have dropped by a factor of 5 to 15 after 120-200 days. This suggests the presence of a passivating mechanism by the gel layer formed in vapor phase. A comparison of the factor by which the rate drops to the retention of elements in the gel layer implies that after approximately six months, the predominant vapor hydration mechanism (network-hydrolysis) changes to water diffusion through the gel layer into the pristine glass.

This is also in a way supported by the results of measurement of porosity and pore-sizes on some of the vapor hydrated glasses. The glass that had the smallest rate-drop factor during vapor hydration kinetics had the largest measured pore-size.

Complementary studies to gain further insights on vapor hydration of glasses: Vapor hydration of nuclear waste glasses is a relatively recent domain of study in the field of chemical durability of nuclear waste glass in France. Literature review also suggested that glass response to extrinsic parameters such as temperature and relative humidity could also be composition dependent. Therefore, Other complementary vapor hydration studies were also conducted, which investigated (i) the effect of temperature on the influence of glass composition using the three simplified glasses Q, QCa and QMg; (ii) the effect of temperature and relative humidity on AVM6 glass; and (iii) vapor hydration mechanisms using vapor phase enriched in isotopic tracers (D_2O+$H_2{}^{18}O$).

The study of the effect of temperature on the influence of glass composition using the three simplified glasses showed that for some glasses, the rate-controlling vapor hydration

mechanism changed with temperature (probably between network hydrolysis and secondary phase precipitation) and as a result, the influence of Ca and Mg also varied.

The isotopic tracer study conducted at 20°C on four of the six glasses suggested that the predominant vapor hydration mechanism changed depending on glass composition too (interdiffusion or network hydrolysis) along with temperature.

The study of effect of temperature on the AVM6 glass showed that with temperature, the nature of the secondary phases that precipitated varied, and consequently, the behavior of elements in the gel layer also varied. However, the altered glass morphology was similar. While in general vapor hydration rate increased with temperature, only two of the four glasses, whose temperature dependence was studied, followed Arrhenius law for temperature dependence.

In case of the effect of relative humidity on AVM6 glass, the vapor hydration rate also increased exponentially with increasing relative humidity. Some secondary phases incorporating transition metals and rare-earth elements were identified only at low relative humidity values. Decreasing pH with increasing relative humidity was postulated as the most reasonable hypothesis to explain change in element behavior in the gel layer and secondary phase precipitation with relative humidity. Nevertheless, it was not possible to measure/calculate the pH values as a function of RH.

Comparison of structure of gel formed in vapor phase and in aqueous medium: A comparative study of the gel layers enriched in ^{17}O that were formed at 90°C in vapor phase and in aqueous medium was conducted by probing the local environment of ^{17}O, ^{11}B, ^{29}Si, ^{27}Al and ^{23}Na using NMR spectroscopy. ^{17}O is an isotope that permits to probe the global structure of gel and pristine glass and it has been used for the first time to probe the structure of a gel layer formed in vapor phase.

The results showed some underlying differences in the mechanism of formation of the gel layer in both media at 90°C. For the first time, it was shown that in vapor phase boron from the gel layer recondenses with ^{17}O coming from the alteration medium like Si and Al. In aqueous medium, although boron was present in the gel layer due to the extremely high SA/V ratio, there was no evidence for boron recondensation with ^{17}O coming from the alteration medium. The results also suggested that in vapor phase, Al bonds seem to be less hydrolysable than in aqueous medium, suggesting that network-hydrolysis is a more selective/local phenomenon in vapor phase than in aqueous medium.

Aqueous alteration of glasses: The first objective of studying aqueous alteration of glasses is to investigate the effect and fate of the alteration products formed during vapor hydration during subsequent aqueous alteration. For this purpose, the samples that were vapor hydrated for 6 months and 18 months at 50°C and 95% RH were then immersed in pure water at 50°C and a surface are to solution volume ratio of 20 m^{-1} for 28 days.

The results show that the gel layer formed in vapor phase has no passivating properties against glass alteration in aqueous medium. The passivation mechanism in the gel layer that was discussed earlier is only against further degradation in vapor phase and it has no effect in aqueous medium. Some of the secondary phases formed during vapor hydration were also readily soluble when immersed in water. The results also seem to suggest that the gel layer itself might be soluble/unstable.

The second objective was to study if vapor hydration of glasses is equivalent to aqueous alteration at a very high SA/V ratio. The alteration kinetics of glasses altered at 50°C in vapor phase and aqueous medium at a very high SA/V ratio was compared. According to our results, more glass is altered in aqueous medium than in vapor phase for a given duration at 50°C, while at 90°C, the contrary is observed. This result seems important since it suggests that the gel layer formed in vapor phase is much less passivating than that formed in aqueous medium. Another significant difference between the two alteration mediums is the influence of Ca on glass durability. Despite the very high SA/V ratio used, the influence of Ca on glass alteration was positive in aqueous medium and negative in vapor phase. One more strong argument provided by the results in this manuscript is the change in the relative durability of the AVM glasses in the two alteration media. The structural and kinetic studies show clearly that vapor hydration of glasses is not comparable to its alteration in aqueous medium at a very high SA/V ratio.

Geochemical modelling of aqueous alteration experiments at a very high SA/V ratio was also attempted with a goal to study the possibility of extending the model to vapor hydration experiments by changing the SA/V ratio in the model.

Consequences of the results to geological disposal of HLW glasses

In terms of the implications of the results obtained in this manuscript in the context of geological disposal of HLW AVM nuclear waste glasses, our study has demonstrated that the vapor hydration rate could vary over large ranges spanning a couple of orders of magnitudes depending on glass composition. It has to be kept in mind that although the temperature and relative humidity were chosen to be representative of the actual conditions when glass packages are expected to be exposed to vapor phase, several factors such as composition of vapor

phase, radioactivity of the glasses, fractures in the glass blocks, contact of glass blocks with immediate environment, possibility of glass exposure to alternating unsaturated and saturated medium etc. have not been taken into account in this study. Therefore, caution needs to be exercised while applying the data from this research to safety assessment studies and waste glass package lifetime estimation.

Another implication is that our results have shown that secondary phases form rather rapidly in vapor phase. Some of these phases also seem readily soluble. In our study the glasses that were used were inactive simulants. If radioactive elements were incorporated in the alteration products formed during vapor hydration, a sudden release of radioactivity could be expected when the vapor hydrated glasses come in contact with aqueous medium. Past studies in literature have also shown that the radioactivity released during aqueous alteration of a glass pre-hydrated in vapor phase was higher than that released by a pristine glass.

Perspectives

Auto-irradiation in glasses results in structural changes and it needs to be investigated if this results in changes in the predominant vapor hydration mechanisms. Studies in the literature suggest possible changes in the pH of the small volume of water that is adsorbed on glass surface due to radiolysis of water and this may also contribute to changes in predominant vapor hydration mechanism.

One of the important perspectives in the vapor hydration study of the radioactive AVM nuclear waste glasses is the study of release of radionuclides from a vapor hydrated glass into aqueous medium. Some of the aspects of this study are: (1) the characterization of the radionuclide incorporating secondary phases that may form, (2) the stability/solubility of these phases when in contact with aqueous medium and (3) also the radionuclide retention capacity of the gel layer during subsequent aqueous alteration of the vapor hydrated glasses.

Another axis of research that needs to be part of a future work is the presence of fractures and fissures in the glass block, which could result in increased quantity of altered glass due to increased surface area of the glass block. Small fissures could promote water condensation due to capillary effect locally or may become preferential zones for secondary phase precipitation and accelerated alteration.

In this work, it has been considered that the duration of vapor hydration is uninterrupted. In a realistic scenario, if a transitory environment exists where the glass comes into contact with

saturated medium intermittently, the vapor hydration rates could be affected significantly and an earlier release of radioactivity due to dissolution of alteration products would be possible. Therefore, studies on the impact of cycles of vapor hydration and aqueous alteration need to be conducted.

A major handicap of the current vapor hydration studies is the inability to measure pH in the porewater of the gel layer or the layer of water adsorbed on the glass surface. Knowledge of the pH value is key to understand the vapor hydration mechanisms without making a significant number of assumptions. It would also help to understand the different secondary phases that precipitate at different temperatures and assist in geochemical modelling. Imbibing altered glasses in pH sensitive fluorophores or the use of optical/advanced pH sensors could be envisioned as early steps towards developing a protocol for surface pH measurement and pH measurement in nano-pores.

While our results show that network-hydrolysis could be the rate-controlling vapor hydration mechanism for until the first six months of vapor hydration, the change in predominant vapor hydration mechanisms with time needs to be investigated further. The passivation mechanism that results in vapor hydration rate drop needs to be assessed further as well. The phenomenon of heterogeneous alteration in vapor phase has also not been studied deeply in this work, which could be probed further. The significance of the molar ratio of Al_2O_3 to oxides of alkaline-earth elements to glass durability could also be investigated further for different glass compositions and temperatures. The structural role of Mg in the glass and gel and its capability to compensate negative charge of $[AlO_4]^-$ units needs to be investigated to understand the positive effect of Al that prevails over the negative effect of Mg on glass durability. Aqueous alteration of the same glasses at very basic pH ($pH_{50°C}$>11) that may provoke the precipitation of similar secondary phases could be conducted in order to observe the relative durability of these glasses.

Vapor adsorption isotherm studies on pristine glass monolith surfaces and glass powders and altered and porous gel layers could also be conducted to gain information on the SA/V ratio in vapor phase and its evolution with glass alteration. Literature survey suggests that the adsorption of water vapor on glasses could also be affected by glass composition and secondary phase precipitation.

Finally, there is a strong need to make advances in the geochemical modelling of the vapor hydration phenomenon in order to be able to predict vapor hydration rates over geological

time scales. In this thesis, a small demonstration of one of the modelling approaches was briefly discussed. The presence of a small layer of water on glass surface is recognized. Therefore, the GRAAL model could be useful. However, we were not able to overcome the problem of thermodynamic equilibrium failure in high ionic strength conditions. Another approach could be to also take into account the interaction between gas phase (rich in H_2 and CO_2) and the thin water film and study its impact. Geochemical modelling could be used to study the effect of SA/V, temperature, thickness of water film, glass composition and pH separately during aqueous alteration and understand how these parameters change the predominant alteration mechanisms. The results could be compared to glass alteration in vapor phase to understand the difference between glass alterations in these two media. For example, geochemical modelling of aqueous alteration could be used to understand why despite such a high SA/V ratio, Ca has a negative effect in vapor phase, even though precipitation of CSHs was not identified explicitly. Dynamic alteration of glasses at a very high SA/V ratio could also be attempted to better understand the dynamic nature of glass alteration in vapor phase.

References

1. Friedman, I. and W.D. Long, *Hydration rate of obsidian.* Science, 1976. **191**: p. 347-352.
2. Anovitz, L.M., D.R. Cole, and L.R. Riciputi, *Low-temperature isotopic exchange in obsidian: Implications for diffusive mechanisms.* Geochimica and Cosmochimica Acta, 2009(73): p. 3795-3806.
3. Friedman, I. and R.L. Smith, *A new dating method using obsidian: Part I, The Development of the Method.* American Antiquity, 2017. **25**(4): p. 476-493.
4. Anovitz, L.M., D.R. Cole, and M. Fayek, *Mechanisms of rhyolitic glass hydration below the glass transition.* The American mineralogist, 2008. **93**(7): p. 1166-1178.
5. Hull, K.L., *Reasserting the Utility of Obsidian Hydration Dating: A Temperature-Dependent Empirical Approach to Practical Temporal Resolution with Archaeological Obsidians.* Journal of Archaeological Science, 2001. **28**(10): p. 1025-1040.
6. Anovitz, L.M., et al., *The Failure of Obsidian Hydration Dating: Sources, Implications, and New Directions.* Journal of Archaeological Science, 1999. **26**(7): p. 735-752.
7. Mazer, J.J., et al., *The experimental hydration of obsidian as a function of relative humidity and temperature.* American Antiquity, 1991. **56**(3): p. 504-513.
8. Bates, J.K., et al., *Issues affecting the prediction of glass reactivity in an unsaturated environment.* Journal of Nuclear Materials, 1992. **190**: p. 198-227.
9. Bates, J.K., L.J. Jardine, and M.J. Steindler, *Hydration aging of nuclear waste glass.* Science, 1982. **218**: p. 51-53.
10. Bates, J.K., M.J. Steindler, and P.L. McDaniel, *Hydration of stressed nuclear waste glass.* Materials Letters, 1984. **2**(4, Part A): p. 296-300.
11. Bates, J.K., M.G. Seitz, and M.J. Steindler, *The relevance of vapor phase hydration aging to nuclear waste isolation.* Nuclear and Chemical Waste Management, 1984. **5**: p. 63-73.
12. Bates, J.K., et al., *The hydration alteration of a commercial nuclear waste glass.* Chemical Geology, 1985. **51**(1): p. 79-87.
13. Abrajano, T., J.K. Bates, and C.D. Byers, *Aqueous corrosion of natural and nuclear waste glasses I. Comparative rates of hydration in liquid and vapor environments at elevated temperatures.* Journal of Non Crystalline Solids, 1986. **84**: p. 251-257.
14. Abrajano, T.A., Jr., J.K. Bates, and J.J. Mazer, *Aqueous corrosion of natural and nuclear waste glasses. II. Mechanisms of vapor hydration of nuclear waste glasses.* Journal of Non-Crystalline Solids, 1989. **108**: p. 269-288.
15. Biwer, B.M., et al., *Comparison of the layer structure of vapor phase and leached SRL glass by use of AEM.* Materials research Society Symposium proceedings, 1989. **176**: p. 255-263.
16. Bates, J.K., et al., *Issues affecting the prediction of glass reactivity in an unsaturated environment.* Journal of Nuclear Materials, 1992. **190**: p. 198-227.
17. Bates, J.K., T.J. Gerding, and A.B. Woodland, *Parametric effects of glass reaction under unsaturated conditions*, in *Scientific Basis for Nuclear Waste Management XIII*, V.M. Oversby and P.W. Brown, Editors. 1990, Mater. Res. Soc.: Pittsburgh, PA. p. 347-354.
18. Ebert, W.L. and J.K. Bates, *The reaction of synthetic nuclear waste glass in steam and hydrothermal solution*, in *Scientific Basis for Nuclear Waste Management XIII*, V.M. Oversby and P.W. Brown, Editors. 1990, Mater. Res. Soc: Pittsburgh, PA, USA. p. 339-346.
19. Ebert, W.L., J.K. Bates, and W.L. Bourcier, *The hydration of borosilicate waste glass in liquid water and steam at 200° C.* Waste Management, 1991. **11**: p. 205-221.
20. Gong, W.L., et al., *Analytical electron microscopy study of surface layers formed on the French SON68 nuclear waste glass during vapor hydration at 200°C.* Journal of Nuclear Materials, 1998. **254**(2): p. 249-265.

21. Mazer, J.J., et al., *Water diffusion in tektites: An example of the use of natural analogues in evaluating the long-term reaction of glass with water.* Journal of Nuclear Materials, 1992. **190**: p. 277-284.
22. Luo, J.S., et al., *Simulation of natural corrosion by vapor hydration test: seven-year results*, in *Scientific Basis for Nuclear Waste Management XX Symposium*, W.J. Gray and I.R. Triay, Editors. 1996, Mater. Res. Soc: Pittsburgh, PA, USA. p. 157-163.
23. Luo, J.S., T.A. Abrajano, Jr., and W.L. Ebert, *Natural analogues of nuclear waste glass corrosion.*, A.N. Laboratory, Editor. 1998. p. 1-179.
24. Abdelouas, A., et al., *A Preliminary Investigation of the ISG Glass Vapor Hydration.* INTERNATIONAL JOURNAL OF APPLIED GLASS SCIENCE, 2013. **4**(4): p. 307-316.
25. Chaou, A.A., et al., *The French SON68 glass vapor hydration under different atmospheres.* Procedia Materials Science, 2014. **7** p. 179 – 185.
26. Neeway, J., et al., *Vapor hydration of SON68 glass from 90 °C to 200 °C: A kinetic study and corrosion products investigation.* Journal of Non Crystalline Solids, 2012. **358**(21): p. 2894-2905.
27. Chaou, A., et al., *Vapor hydration of a simulated borosilicate nuclear waste glass in unsaturated conditions at 50 °C and 90 °C.* RSCC Advances, 2015. **5**(64538).
28. Chaou, A., et al., *The role of pH in the vapor hydration at 175 °C of the French SON68 glass.* Applied Geochemistry, 2017. **76**: p. 22-35.
29. Bouakkaz, R., A. Abdelouas, and B. Grambow, *Kinetic study and structural evolution of SON68 nuclear waste glass altered from 35 to 125 °C under unsaturated H_2O and D_2O^{18} vapour conditions.* Corrosion Science, 2018. **134**: p. 1-16.
30. Sterpenich, J. and G. Libourel, *Using stained glass windows to understand the durability of toxic waste matrices.* Chemical Geology, 2001. **174**: p. 181-193.
31. Lombardo, T., et al., *Characterisation of complex alteration layers in medieval glasses.* Corrosion Science, 2013. **72**: p. 10-19.
32. Sessegolo, L., et al., *Long-term weathering rate of stained-glass windows using H and O isotopes.* npj Materials Degradation, 2018. **2**(1): p. 17.
33. Alloteau, F., et al., *New insight into atmospheric alteration of alkali-lime silicate glasses.* Corrosion Science, 2017. **122**: p. 12-25.
34. Bellendorf, P., et al. *Archaeological Glass: The Surface and Beyond*. in *Glass and Ceramics Conservation 2010*. 2010. Corning, New York.
35. Papadopoulos, N. and C.A. Drosou, *Influence of weather conditions on glass properties.* Journal of the University of Chemical Technology and Metallurgy, 2012. **47**(4): p. 429-439.
36. Verney-Carron, A., S. Gin, and G. Libourel, *A fractured roman glass block altered for 1800 years in seawater: Analogy with nuclear waste glass in a deep geological repository.* Geochimica et Cosmochimica Acta, 2008. **72**(22): p. 5372-5385.
37. Gin, S., et al., *Effect of composition on the short-term and long-term dissolution rates of ten glasses of increasing complexity from 3 to 30 oxides.* Journal of Non-Crystalline Solids, 2012. **358**(18-19): p. 2559-2570.
38. Bunker, B.C., *Molecular mechanisms for corrosion of silica and silicate glasses.* Journal of Non-Crystalline Solids, 1994. **179**: p. 300-308.
39. De Echave, T., et al., *Effect of clayey groundwater on the dissolution rate of SON68 simulated nuclear waste glass at 70 °C.* Journal of Nuclear Materials, 2018. **503**: p. 279-289.
40. De Echave, T., et al., *Influence of iron on the alteration of the SON68 nuclear glass in the Callovo-Oxfordian groundwater.* Applied Geochemistry, 2019. **100**: p. 268-278.
41. Gin, S., et al., *Atom-Probe Tomography, TEM and ToF-SIMS study of borosilicate glass alteration rim: A multiscale approach to investigating rate-limiting mechanisms.* Geochimica et Cosmochimica Acta, 2017. **202**: p. 57-76.

42. Suzuki-Muresan, T., et al., *Alteration of vitrified intermediate level nuclear waste in alkaline media: effects of cementitious materials, pH and temperature.* RSC Advances, 2018. **8**(66): p. 37665-37680.
43. Rieke, P.C., et al., *Adaptation of the GRAAL model of Glass Reactivity to accommodate non-linear diffusivity.* Journal of Nuclear Materials, 2018. **512**: p. 79-93.
44. Gin, S., et al., *The controversial role of inter-diffusion in glass alteration.* Chemical Geology, 2016. **440**: p. 115-123.
45. Frugier, P., et al., *Modeling glass corrosion with GRAAL.* npj Materials Degradation, 2018. **2**(1): p. 35.
46. Grambow, B. and R. Muller, *First-order dissolution rate law and the role of surface layers in glass performance assessment.* Journal of Nuclear Materials, 2001. **298**(1,2): p. 112-124.
47. Gin, S., Abdelouas, A., Criscenti, L.J., Ebert, W.L., Ferrand, K., Geisler, T., Harrison, M.T., Inagaki, Y., Mitsui, S., Mueller, K.T., Marra, J.C., Pantano, C.G., Pierce, E.M., Ryan, J.V., Schofield, J.M., Steefel, C.I., Vienna, J.D., *An international initiative on long-term behavior of high-level nuclear waste glass.* Materials Today, 2013. **16**(6): p. 243-248.
48. Gin, S., et al., *Origin and consequences of silicate glass passivation by surface layers.* Nature Communications, 2015. **6**.
49. Jollivet, P., et al., *Investigation of gel porosity clogging during glass leaching.* Journal of Non-Crystalline Solids, 2008. **354**(45): p. 4952-4958.
50. Fournier, M., S. Gin, and P. Frugier, *Resumption of nuclear glass alteration: State of the art.* Journal of Nuclear Materials, 2014. **448**(1-3): p. 348-363.
51. Estevenon, P., *Altération des verres en phase vapeur*. 2015.
52. Vienna, J.D., et al., *Hanford Immobilized LAW Product Acceptance: Initial Tanks Focus Area Testing Data Package*. 2000, United States Department of Energy.
53. Bouakkaz, R., *Altération aqueuse et hydration en phase vapeur du verre SON68 à basse température (35-90°C)*. 2014, L'Université Nantes Angers Le Mans.
54. Alloteau, F., et al., *Temperature-dependent mechanisms of the atmospheric alteration of a mixed-alkali lime silicate glass.* Corrosion Science, 2019: p. 108129.
55. Moriya, Y. and M. Nogami, *Hydration of silicate glass in steam atmosphere.* Journal of Non-Crystalline Solids, 1980. **38**: p. 667-672.
56. Kudriavtsev, Y., et al., *Water vapor interaction with borosilicate glass.* Solid State Ionics, 2018. **321**: p. 122-125.
57. Kudriavtsev, Y., R. Asomoza-Palacio, and L. Manzanilla-Naim, *Interaction of water vapor with silicate glass surfaces: Mass-spectrometric investigations.* Technical Physics Letters, 2017. **43**(5): p. 447-449.
58. Gentaz, L., et al., *Role of secondary phases in the scaling of stained glass windows exposed to rain.* Corrosion Science, 2016. **109**: p. 206-216.
59. Gong, W.L., et al., *Analytical electron microscopy study of surface layers formed on the French SON68 nuclear waste glass during vapor hydration at 200°C.* Journal of Nuclear Materials, 1998. **254**(2-3): p. 249-265.
60. Cunnane, J.C., et al., *High-level waste borosilicate glass : a compendium of corrosion characteristics, Volume II*, U.S.D.o. Energy, Editor. 1994. p. 324.
61. Alloteau, F., *Contribution à la compréhension des mécanismes de l'altération atmosphérique des verres et étude d'un traitement de protection à base de sels de zinc. Application à la conservation des objets en verre du patrimoine culturel.* 2017, l'Université de recherche Paris Sciences et Lettres PSL Research University.
62. Biron, I., *Émaux sur Métal – du IXe au XIXe Siècle. Histoire, Technique et Matériaux*. 2015: Faton edition.

63. France Commissariat à l'énergie, a., V. Centre de, and I.I.S.e.t.d.L. Université Montpellier, *Actes des journées sur le Verre: Université d'été CEA/VALRHÔ = CEA/VALRHÔ Summer Session proceedings Glass ; Recherche scientifique pour un confinement de haute performance = Scientific research for high performance containment, 31 août-7 septembre 1997 = 31 august-7 september 1997, Méja*. Commissariat à l'énergie atomique 1997.
64. Sterpenich, J., *Altération des vitraux médiévaux - Contribution à l'étude du comportement à long terme des verres de confinement*. 1998, Université Henri Poincaré. p. 440.
65. Barger, M.S., D.K. Smith, and W.B. White, *Characterization of corrosion products on old protective glass, especially daguerreotype cover glasses.* Journal of Materials Science, 1989. **24**(4): p. 1343-1356.
66. Wronkiewicz, D.J., et al., *Effects of radiation exposure on glass alteration in a steam environment*, in *Scientific Basis for Nuclear Waste Management XVI*, C.G. Interrante and R.T. Pabalan, Editors. 1992, Mater. Res. Soc: Pittsburgh, PA. p. 183-190.
67. Wronkiewicz, D.J., et al., *Effects of radiation exposure on SRL 131 composition glass in a steam environment*, in *Scientific Basis for Nuclear Waste Management XVII*, A. Barkatt and R.A. Van Konynenburg, Editors. 1994, Mater. Res. Soc: Pittsburgh, PA, USA. p. 259-267.
68. Neeway, J., *The alteration of the SON68 reference waste glass in silica saturated conditions and in the presence of water vapor*. 2010, Université de Nantes. p. 205.
69. Jollivet, P., et al., *Caractérisation du premier échantillon de verre altéré en phase vapeur au LCLT*. 2014.
70. Sessegolo, L., *Utilisation de traceurs isotopiques pour l'étude des mécanismes et des cinétiques d'altération des verres de vitraux en milieu atmosphérique*. 2018, Université Paris-Est Créteil Val-de-Marne.
71. Burns, P.C., et al., *$KNa_3(UO_2)_2(Si_4O_{10})_2(H_2O)_4$, a new compound formed during vapor hydration of an actinide-bearing borosilicate waste glass.* Journal of Nuclear Materials, 2000. **278**: p. 290-300.
72. Byers, C.D., R.C. Ewing, and M.J. Jercinovic, *Experimental alteration of basalt glass applied to the alteration of nuclear waste glass.*, CEA, Editor. 1986. p. 1-9.
73. Ebert, W.L., R.F. Hoburg, and J.K. Bates, *The sorption of water on obsidian and nuclear waste glass.* Phys. Chem. Glasses, 1991. **32**(4): p. 133-137.
74. Sing, K.S.W., et al., *REPORTING PHYSISORPTION DATA FOR GAS/SOLID SYSTEMS with Special Reference to the Determination of Surface Area and Porosity.* Pure and Applied Chemistry, 1985. **57**(4): p. 603-619.
75. Bartholomew, R.F., P.A. Tick, and S.D. Stookey, *Water/glass reactions at elevated temperatures and pressures.* Journal of Non-Crystalline Solids, 1980. **38&39**: p. 637-642.
76. Jannot, Y., *Isothermes de sorption : modèles et détermination*. 2008: Université Bordeaux I, laboratoire TREFLE.
77. Razouk, R.I. and A.S. Salem, *The Adsorption of Water Vapor on Glass Surfaces.* The Journal of Physical and Colloid Chemistry, 1948. **52**(7): p. 1208-1227.
78. Nishioka, G.M., *Adsorption/desorption of water on glass fiber surfaces.* Journal of Non-Crystalline Solids, 1990. **120**(1): p. 34-39.
79. Leed, E.A. and C.G. Pantano, *Computer modeling of water adsorption on silica and silicate glass fracture surfaces.* Journal of Non-Crystalline Solids, 2003. **325**(1): p. 48-60.
80. Cunnane, J.C., et al., *High-level nuclear-waste borosilicate glass : a compendium of characteristics.*, in *Scientific Basis for Nuclear Waste Management XVI*, C.G. Interrante and R.T. Pabalan, Editors. 1993, Mater. Res. Soc.: Pittsburgh, PA. p. 225-232.
81. Cassingham, N.J., et al., *Alteration layer formation of Ca- and Zn-oxide bearing alkali borosilicate glasses for immobilisation of UK high level waste: A vapour hydration study.* Journal of Nuclear Materials, 2016. **479**: p. 639-646.

82. Wronkiewicz, D.J., J.E. Young, and J.K. Bates, *Effects of alpha and gamma radiation on glass reaction in an unsaturated environment*, in *Scientific Basis for Nuclear Waste Management*. 1991, Mater. Res. Soc. p. 99-106.
83. Wronkiewicz, D.J., et al., *Radiation effects in moist-air systems and the influence of radiolytic product formation on nuclear glass corrosion*. 1997, Argonne National Laboratory.
84. Sevigny, G.J., et al., *Iron Phosphate Glass- Containing Hanford Waste Simulant*. 2012, Pacific Northwest National Laboratory.
85. Bates, J.K., M.J. Steindler, and P.L. McDaniel, *Hydration of stress nuclear waste glass.* Materials letters, 1984. **2**(4A): p. 296-300.
86. Michalske, T.A. and S.W. Freiman, *A molecular mechanism for stress corrosion in vitreous silica.* Journal of the American Ceramic Society, 1983. **66**(4): p. 284-288.
87. Kim, D., et al., *Development and Testing of ICV Glasses for Hanford LAW*. 2003, Pacific Northwest National Laboratory.
88. Friedman, I., R.L. Smith, and W.D. Long, *Hydration of natural glass and formation of perlite.* Geological Society of America Bulletin, 1966. **77**: p. 323-328.
89. Friedman, I. and F.W. Trembour, *Obsidian: The dating stone: The depth of water penetration on a surface of this stone reveals the dates of geologic and archeologic events.* American Scientist, 1978. **66**(1): p. 44-51.
90. Mazer, J.J., et al., *Alteration of tektite to form weathering products.* Nature, 1992. **357**(6379): p. 573-576.
91. Bates, J.K., W.L. Ebert, and T.J. Gerding. *Vapor hydration and subsequent leaching of transuranic-containing SRL and WV glasses*. in *International topical meeting on high-level radioactive waste management*. 1990.
92. Feng, X., et al., *Effects of S/V on secondary phase formation on waste glasses*, in *Ceramic Transactions - Environmental and Waste Management Issues in the Ceramic Industry II*, D. Bickford, et al., Editors. 1994, The American Ceramic Society: Westerville, OH. p. 243-254.
93. Gin, S., et al., *New insight into the residual rate of borosilicate glasses: effect of S/V and glass composition.* submitted to International Journal of Applied Glass Science, 2013. **4**(4): p. 371-382.
94. Ebert, W.L. and J.K. Bates, *The reaction of synthetic nuclear waste glass in steam and hydrothermal solution*. 1990, United States: Materials Research Society.
95. Godon, N., *Reference document on the long-term behaviour of nuclear glass*, CEA, Editor. 2005.
96. Thien, B., *Développement des bases théoriques nécessaires à la modélisation de la vitesse résiduelle d'altération en milieu aqueux des verres nucléaires AVM*. 2010, Université Montpellier II. p. 244.
97. Thien, B., et al., *The dual effect of Mg on the long-term alteration rate of AVM nuclear waste glasses.* Journal of Nuclear Materials, 2012. **427**: p. 297-310.
98. Arena, H., et al., *Impact of Zn, Mg, Ni and Co elements on glass alteration: Additive effects.* Journal of Nuclear Materials, 2016. **470**: p. 55-67.
99. Aréna, H., et al., *Impact of iron and magnesium on glass alteration: Characterization of the secondary phases and determination of their solubility constants.* Applied Geochemistry, 2017. **82**: p. 119-133.
100. Aréna, H., et al., *Impact of Fe, Mg and Ca elements on glass alteration: Interconnected processes.* Geochimica et Cosmochimica Acta, 2018. **239**: p. 420-445.
101. Mercado-Depierre, S., et al., *Antagonist effects of calcium on borosilicate glass alteration.* Journal of Nuclear Materials, 2013. **441**(1-3): p. 402-410.
102. Jollivet, P., et al., *Effect of clayey groundwater on the dissolution rate of the simulated nuclear waste glass SON68.* Journal of Nuclear Materials, 2012. **420**: p. 508-518.

103. Jegou, C., S. Gin, and F. Larche, *Alteration kinetics of a simplified nuclear glass in an aqueous medium: effects of solution chemistry and of protective gel properties on diminishing the alteration rate.* Journal of Nuclear Materials, 2000. **280**(2): p. 216-229.
104. Trotignon, L., et al., *The compared aqueous corrosion of four simple borosilicate glasses: Influence of Al, Ca, and Fe on the formation and nature of secondary phases.* Journal of Nuclear Materials, 1992. **190**: p. 228-246.
105. Collectif, *Référentiel du comportement des colis de déchets HA-MAVL - Tome 2 - Déchets vitrifiés*, ANDRA and CEA, Editors. 2012. p. 1-548.
106. Collin, M., et al., *Impact of alkali on the passivation of silicate glass.* npj Materials Degradation, 2018. **2**(1): p. 16.
107. Angeli, F., et al., *Structure and Chemical Durability of Lead Crystal Glass.* Environmental Science & Technology, 2016. **50**(21): p. 11549-11558.
108. Spalla, O., S. Lyonnard, and F. Testard, *Analysis of the small-angle intensity scattered by a porous and granular medium.* Journal of Applied Crystallography, 2003. **36 part 32**: p. 338-347.
109. Spalla, O., et al., *Influence of insoluble elements on the nanostructure of water altered glasses.* Journal of Non-Crystalline Solids, 2004. **347**(1-3): p. 56-68.
110. Cailleteau, C., *Influence de la morphologie du gel sur la cinétique d'altération des verres nucléaires: rôle du calcium et du zirconium.* 2008, Thèse de l'école polytechnique de Paris.
111. Thien, B.M.J., *A simple way to constrain the stoichiometry of secondary smectites upon aqueous glass alteration.* Applied Geochemistry, 2014. **42**: p. 45-46.
112. Jolyon, R. and I. Chau, *Mindat : base de données minéralogiques*, in *http://www.mindat.org/*. 2013.
113. Bailey, S.W., *Crystal Structures of Clay Minerals and Their X-ray Identification.* Mineralogical Society, London, 1980. **Monograph 5**: p. 1-123.
114. Brindley, G.W. and G. Brown, *Crystal Structures of Clay Minerals and their X-ray identification.* Mineralogical Society, London, 1980. **Monograph 5**: p. 169-180.
115. Kloprogge, J.T., S. Komarneni, and J.E. Amonette, *Synthesis of smectite clay minerals a critical review.* Clays and Clay Minerals, 1999. **47**(5): p. 529-554.
116. Harder, H., *The role of magnesium in the formation of smectite minerals.* Chemical Geology, 1972. **10**(1): p. 31-39.
117. Pascua, C.S. and H. Yamada, *LOW-TEMPERATURE FORMATION OF CLAY MINERALS : CORRELATING LABORATORY EXPERIMENTS WITH NATURAL FIELD-SCALE PROCESSES.* Clay Science, 2012. **16**(2): p. 25-32.
118. Joly, J.-F., et al., *Phyllosilicates 2:1 trioctaédriques et leur procédé de préparation*, E.P. Office, Editor. 1991, IFP Energies Nouvelles France.
119. Py, M., *Study of interfaces and nanometric structures by ToF-SIMS : upon a spatially resolved quantitative analysis*, in *Micro and nanotechnologies/Microelectronics*. 2011, Université de Grenoble.
120. Romanos, G.E., et al., *Methods of evaluating pore morphology in hybrid organic–inorganic porous materials.* Microporous and Mesoporous Materials, 2009. **120**(1): p. 53-61.
121. Rebiscoul, D., et al., *Protective properties and dissolution ability of the gel formed during nuclear glass alteration.* Journal of Nuclear Materials, 2005. **342**(1): p. 26-34.
122. Rebiscoul, D., et al., *Morphological evolution of alteration layers formed during nuclear glass alteration: new evidence of a gel as a diffusive barrier.* Journal of Nuclear Materials, 2004. **326**(1): p. 9-18.
123. Cailleteau, C., et al., *Why Do Certain Glasses with a High Dissolution Rate Undergo a Low Degree of Corrosion?* The Journal of Physical Chemistry C, 2011. **115**(13): p. 5846-5855.

124. Le Guillou, C., et al., *New experimental approach to study aqueous alteration of amorphous silicates at low reaction rates.* Chemical Geology, 2015. **412**: p. 179-192.
125. Balasubramanian, R., et al., *Investigation of the vaporization of boric acid by transpiration thermogravimetry and knudsen effusion mass spectrometry.* J. Phys. Chem. B, 2008. **112**: p. 13873-13884.
126. Gaillardet, J., et al., *Evaporation and Sublimation of Boric Acid: Application for Boron Purification from Organic Rich Solutions.* Geostandards Newsletter, 2001. **25**(1): p. 67-75.
127. Siboni, S. and C. Della Volpe, *Some mathematical aspects of the Kelvin equation.* Computers & Mathematics with Applications, 2008. **55**(1): p. 51-65.
128. Sicard, L., et al., *Study of the kinetics of glass alteration by small-angle X-ray scattering.* Journal of Physical Chemistry B, 2004. **108**: p. 7702-7708.
129. Girard, L., M. Arab, and O. Spalla, *Time resolved alteration process of oxide glasses.* Journal of Colloid and Interface Science, 2008. **319**(1): p. 214-225.
130. Toquer, G., et al., *Effect of leaching concentration and time on the morphology of pores in porous glasses.* Journal of Non-Crystalline Solids, 2011. **357**(6): p. 1552-1557.
131. Kanehashi, K., *Structural roles of calcium in alkaline and alkaline-earth aluminosilicate glasses by solid-state ^{43}Ca, ^{17}O and ^{27}Al NMR.* Solid State Nuclear Magnetic Resonance, 2017. **84**: p. 158-163.
132. Guo, R., et al., *The effect of magnesium on the local structure and initial dissolution rate of simplified UK Magnox waste glasses.* Journal of Non-Crystalline Solids, 2018. **497**: p. 82-92.
133. Angeli, F., et al., *Influence of glass composition and alteration solution on leached silicate glass structure : a solid-state NMR investigation.* Geochimica et Cosmochimica Acta, 2006. **70**(10): p. 2577-2590.
134. Thien, B., et al., *Structural identification of a trioctahedral smectite formed by the aqueous alteration of a nuclear glass.* Applied Clay Science, 2010. **49**: p. 135-141.
135. Godon, N. and M. Fenart, *Vitesses d'altération de verres R7T7 et AVM en régime résiduel et en eaux de site influencées par le matériau de remplissage seul (S2) et avec l'eau du COx (S3)*. 2019: CEA/DEN/MAR/DE2D/SEVT/DIR.
136. Sicard, L., et al., *Dissolution of Oxide Glasses: A Process Driven by Surface Generation.* The Journal of Physical Chemistry C, 2008. **112**(5): p. 1594-1603.
137. Verney-Carron, A., et al., *Understanding the mechanisms of Si–K–Ca glass alteration using silicon isotopes.* Geochimica et Cosmochimica Acta, 2017. **203**: p. 404-421.
138. Gin, S., et al., *The fate of silicon during glass corrosion under alkaline conditions: A mechanistic and kinetic study with the International Simple Glass.* Geochimica et Cosmochimica Acta, 2015. **151**: p. 68-85.
139. Pitzer, K.S., et al. *Thermodynamics of high temperature brines*. in *American Society for testing and materials symposium*. 1979.
140. Mazer, J.J., *Temperature effects on waste glass performance*. 1991: United States.
141. Vienna, J.D., et al., *Impacts of glass composition, pH, and temperature on glass forward dissolution rate.* npj Materials Degradation, 2018. **2**(1): p. 22.
142. Jollivet, P., S. Gin, and S. Schumacher, *Forward dissolution rate of silicate glasses of nuclear interest in clay-equilibrated groundwater.* Chemical Geology, 2012. **330**: p. 207-217.
143. Chave, T., et al., *Glass-water interphase reactivity with calcium rich solutions.* Geochimica and Cosmochimica Acta, 2011. **75**(15): p. 4125-4139.
144. Rajmohan, N., P. Frugier, and S. Gin, *Composition effects on synthetic glass alteration mechanisms: Part 1. Experiments.* Chemical Geology, 2010. **279**(3-4): p. 106-119.
145. Utton, C.A., et al., *Dissolution of vitrified wastes in a high-pH calcium-rich solution.* Journal of Non-Crystalline Solids, 2013. **435**: p. 112-122.

146. Debure, M., et al., *Dolomite effect on borosilicate glass alteration.* Applied Geochemistry, 2013. **33**: p. 237-251.
147. Bruker. *EVA software for phase analysis*. Available from: https://www.bruker.com/products/x-ray-diffraction-and-elemental-analysis/x-ray-diffraction/xrd-software/eva/overview.html.
148. Cummings, K., W.A. Lanford, and M. Feldmann, *Weathering of glass in moist and polluted air.* Nuclear Instruments and Methods in Physics Research Section B: Beam Interactions with Materials and Atoms, 1998. **136-138**: p. 858-862.
149. Anovitz, L.M., et al., *The effect of changes in relative humidity on the hydration rate of Pachuca obsidian.* Journal of Non-Crystalline Solids, 2006. **352**(52): p. 5652-5662.
150. Altmaier, M., V. Neck, and T. Fanghänel, *Solubility of Zr(IV), Th(IV) and Pu(IV) Hydrous Oxides in CaCl2 Solutions and the Formation of Ternary Ca-M(IV)-OH Complexes.* Radiochimica Acta, 2008. **96**(9-11): p. 541-550.
151. Brendebach, B., et al., *EXAFS study of aqueous Zr-IV and Th-IV complexes in alkaline CaCl2 solutions: Ca-3[Zr(OH)(6)](4+) and Ca-4[Th(OH)(8)](4+).* Inorganic Chemistry, 2007. **46**(16): p. 6804-6810.
152. Collin, M., *Géochimie en milieu nanoporeux : Application aux verres nucléaires*, in *Physique*. 2018, Université de Montpellier.
153. Bray, P.J. and W.J. Dell, *NMR studies of the structure of glass.* 1982. **43**: p. 131-42.
154. Angeli, F., et al., *Influence of glass chemical composition on the Na-O bond distance: a (23)Na 3Q-MAS NMR and molecular dynamics study.* Journal of Non Crystalline Solids, 2000. **276**(1-3): p. 132-144.
155. Aujla, R., et al., *A Magic angle spinning NMR study of the vitreous silica prepared in different ways.* Defect data, 1987. **53-54**: p. 99-104.
156. Irwin, A.D., J.S. Holmgren, and J. Jonas, *Al and Si NMR study of sol gel derived alumunosilicates and soduim aluminosilicates.* Journal of Materials Science, 1988. **23**: p. 2908-2912.
157. Massiot, D., et al., *Structure and dynamics of oxide melts and glasses: A view from multinuclear and high temperature NMR.* Journal of Non-Crystalline Solids, 2008. **354**(2): p. 249-254.
158. Moustafa, Y.M., H. Doweidar, and G. El Damrawi, *Utilisation of infrared spectroscopy to determine the fraction of the four coordinated borons in borate glasses.* Physics and Chemistry of Glasses, 1994. **35**(2): p. 104-107.
159. Du, L.-S. and J.F. Stebbins, *Site Preference and Si/B Mixing in Mixed-Alkali Borosilicate Glasses: A High-Resolution 11B and 17O NMR Study.* Chemistry of Materials, 2003. **15**(20): p. 3913-3921.
160. Quintas, A., et al., *NMR Study of a Rare-Earth Aluminoborosilicate Glass with Varying CaO-to-Na2O Ratio.* Applied Magnetic Resonance, 2007. **32**(4): p. 613-634.
161. Angeli, F., et al., *Boron Speciation in Soda-Lime Borosilicate Glasses Containing Zirconium.* Journal of the American Ceramic Society, 2010. **93**(9): p. 2693-2704.
162. Park, S.Y. and S.K. Lee, *Probing the structure of Fe-free model basaltic glasses: A view from a solid-state 27Al and 17O NMR study of Na-Mg silicate glasses, Na2O-MgO-Al2O3-SiO2 glasses, and synthetic Fe-free KLB-1 basaltic glasses.* Geochimica et Cosmochimica Acta, 2018. **238**: p. 563-579.
163. Kelsey, K.E., J.R. Allwardt, and J.F. Stebbins, *Ca–Mg mixing in aluminosilicate glasses: An investigation using 17O MAS and 3QMAS and 27Al MAS NMR.* Journal of Non-Crystalline Solids, 2008. **354**(40): p. 4644-4653.
164. Angeli, F., et al., *O-17 3Q-MAS NMR characterization of a sodium aluminoborosilicate glass and its alteration gel.* Chemical Physics Letters, 2001. **341**(1-2): p. 23-28.
165. Angeli, F., et al., *Influence of zirconium on the structure of pristine and leached soda-lime borosilicate glasses: Towards a quantitative approach by 17 17 MQMAS NMR.* Journal of Non-Crystalline Solids, 2008. **354**(31): p. 3713-3722.

166. Doret, A., et al., *Influence of Alteration Solutions on the Chemical Durability of the Zerodur® Glass-Ceramic: Structural Investigation.* International Journal of Applied Ceramic Technology, 2015. **12**(4): p. 811-822.
167. Collin, M., et al., *Structure of International Simple Glass and properties of passivating layer formed in circumneutral pH conditions.* npj Materials Degradation, 2018. **2**(1): p. 4.
168. Angeli, F., et al., *Effect of thermally induced structural disorder on the chemical durability of International Simple Glass.* npj Materials Degradation, 2018. **2**(1): p. 31.
169. Angeli, F., et al., *Influence of zirconium on the structure of pristine and leached soda-lime borosilicate glasses: Towards a quantitative approach by 17O MQMAS NMR.* Journal of Non-Crystalline Solids, 2008. **354**(31): p. 3713-3722.
170. Mercier, C., et al., *Surface alteration of zinc ultraphosphate glass in humid air at 140°C.* Journal of Non-Crystalline Solids, 1999. **256-257**: p. 124-129.
171. Feng, X. and I.L. Pegg, *A glass dissolution model for the effects of S/V on leachate pH.* Journal of Non-Crystalline Solids, 1994. **175**(2): p. 281-293.
172. Gin, S., et al., *New insight into the residual rate of borosilicate glasses: effect of S/V and glass composition.* International Journal of Applied Glass Science, 2013. **4**: p. 371-382.
173. Fournier, M., et al., *Contribution of zeolite-seeded experiments to the understanding of resumption of glass alteration.* npj Materials Degradation, 2017. **1**(1): p. 17.
174. Ribet, S. and S. Gin, *Role of neoformed phases on the mechanisms controlling the resumption of SON68 glass alteration in alkaline media.* Journal of Nuclear Materials, 2004. **324**(2): p. 152-164.
175. Massiot, D., et al., *Two-dimensional magic-angle spinning isotropic reconstruction sequences for quadrupolar nuclei.* Solid State Nuclear Magnetic Resonance, 1996. **6**(1): p. 73-83.
176. Bertmer, M., et al., *Short and Medium Range Order in Sodium Aluminoborate Glasses. 2. Site Connectivities and Cation Distributions Studied by Rotational Echo Double Resonance NMR Spectroscopy.* The Journal of Physical Chemistry B, 2000. **104**(28): p. 6541-6553.
177. Janssen, M. and H. Eckert, *11B{23Na} Rotational echo double resonance NMR: a new approach for studying the spatial cation distribution in sodium borate glasses.* Solid State Ionics, 2000. **136-137**: p. 1007-1014.
178. Hopf, J., et al., *Glass–water interaction: Effect of high-valence cations on glass structure and chemical durability.* Geochimica et Cosmochimica Acta, 2016. **181**: p. 54-71.
179. Frugier, P., et al., *Application of the GRAAL model to leaching experiments with SON68 nuclear glass in initially pure water.* Journal of Nuclear Materials, 2009. **392**(3): p. 552-567.
180. NIETO, P., et al., *Study by Ca-43 NMR-Spectroscopy of the sol-gel transformation or the calcium-silicate complex.* Comptes Rendus de l'Academie des Sciences, 1995. **320**(9): p. 485-488.
181. Fleury, B., *Étude de la sensibilité de la Vitesse Résiduelle d'altération et de ses paramètres de modélisation à la composition des verres*. 2013, Université Montpellier II. p. 307.
182. Arena, H., *Effets cumulatifs et compétitifs des éléments chimiques sur l'altération des verres nucléaires*, in *Chimie et Physico-chimie des matériaux*. 2016, Université de Montpellier. p. 248.
183. Engelhardt, G. and D. Michel, *High Resolution Solid State NMR of Silicates and Zeolites*. 1987, New York.
184. Oglesby, J.V., P. Zhao, and J.F. Stebbins, *Oxygen sites in hydrous aluminosilicate glasses: the role of Al-O-Al and H2O.* Geochimica et Cosmochimica Acta, 2002. **66**(2): p. 291-301.
185. Angeli, F., et al., *Contribution of 43Ca MAS NMR for probing the structural configuration of calcium in glass.* Chemical Physics Letters, 2007. **440**(4): p. 324-328.
186. Jones, A.R., et al., *23Na, 29Si, and 13C MAS NMR Investigation of Glass-Forming Reactions between Na2CO3 and SiO2.* The Journal of Physical Chemistry B, 2005. **109**(49): p. 23154-23161.
187. ANDRA-Collectif, *Dossier d'options de sûreté - Partie après fermeture (DOS-AF)*. 2016, ANDRA. p. 1-467.

188. Grambow, B., *Nuclear Waste Glasses - How durable ?* Elements, 2006. **2**: p. 357-364.
189. Conradt, R., *Chemical Durability of oxide glasses in aqueous solutions: A Review.* J. Am. Ceram. Soc, 2008. **91**(3): p. 728-735.
190. Frugier, P., Gin, S., Minet, Y., Chave, T., Bonin, B., Godon, N.,Lartigue, J.E., Jollivet, P., Ayral, A., De Windt, L., Santarini, G., *SON68 Nuclear glass dissolution kinetics: Current state of knowledge and basis of the new GRAAL model.* Journal of Nuclear Materials, 2008. **380**(1-3): p. 8-21.
191. Vienna, J.D., et al., *Current Understanding and Remaining Challenges in Modeling Long-Term Degradation of Borosilicate Nuclear Waste Glasses.* International Journal of Applied Glass Science, 2013. **4**(4): p. 283-294.
192. Isabelle, R. and G. Nicole, *Altération par l'eau des verres borosilicatés - Exemple des verres nucléaires*. 2014.
193. Jollivet, P., et al., *Effect of clayey groundwater on the dissolution rate of the simulated nuclear waste glass SON68.* Journal of Nuclear Materials, 2012. **420**(1): p. 508-518.
194. Muller, I.S., et al. *Characterization of alteration phases on HLW glasses after 15 years of PCT leaching*. in *American Ceramic Society*. 2005.
195. Oka, Y. and M. Tomozawa, *Effect of alkaline earth ion as an inhibitor to alkaline attack on silica glass.* Journal of Non-Crystalline Solids, 1980. **42**: p. 535-543.
196. Pederson, L.R., C.Q. Buckwalter, and G.L. McVay, *The effects of surface area to solution volume on waste glass leaching.* Nuclear Technology, 1983. **62**: p. 151-158.
197. McGrail, B.P., et al., *Application of the Pressurised Unsaturated Flow (PUF) Test for Accelerated Ageing of Waste Forms*, in *Ageing Studies and Lifetime Extension of Materials*, L.G. Mallinson, Editor. 2001, Springer US: Boston, MA. p. 313-320.
198. De Windt, L., et al., *Modélisation couplée chimi-transport avec HYTEC - Application à la migration de polluants et aux géomatériaux*. 2017, Centre de Géosciences MINES ParisTech.
199. Van der Lee, J., et al., *Presentation and application of the reactive transport code HYTEC*, in *Developments in Water Science - Computational Methods in Water Resources, Proceedings of the XIVth International Conference on Computational Methods in Water Resources (CMWR XIV)*, S.M. Hassanizadeh, Editor. 2002, Elsevier. p. 599-606.
200. van der Lee, J., *Reactive transport modelling with HYTEC Users guide and tutorial*, E.d.M.d. Paris, Editor. 2005. p. 1-114.
201. Godon, N. and P. Frugier, *Modélisation de l'altération des verres AVM6 et AVM10 en eau initialement pure et solutions magnésiennes*. 2018, CEA. p. 76.
202. Frugier, P., et al., *Modelling glass corrosion with GRAAL.* npj Materials Degradation, 2018. **in press**.
203. Minet, Y., et al., *Modélisation GRAAL dans le domaine de température 25-90°C*. 2017, CEA. p. 82.
204. Peña, F.d.l., et al., *hyperspy/hyperspy v1.4.1*. 2018.
205. Deloule, E., et al., *Trace element and isotope analysis using Secondary Ion Mass Spectrometry*, in *Mineral reaction kinetics: Microstructures, textures, chemical and isotopic signatures*. 2017, Mineralogical Society of Great Britain and Ireland. p. 0.
206. Estevenon, P., *Etude bibliographique: Altération des verres en phase vapeur*. 2015, ENSCM CHIMIE Montpellier & CEA Marcoule.
207. Feng, X., et al., *Glass optimization for vitrification of hanford site low-level Tank Waste*, PNL, Editor. 1996.
208. Gong, W.L., et al., *Secondary phase formation and the microstructural evolution of surface layers during vapor phase alteration of the French SON68 nuclear waste glass at 200°C*, in *Scientific Basis for Nuclear Waste Management XIX*, W.M. Murphy and D.A. Knecht, Editors. 1996, Mater. Res. Soc: Philadephia, PA, USA. p. 197-204.

209. McKeown, D.A., et al., *Tc and Re Behavior in Borosilicate Waste Glass Vapor Hydration Tests.*, in *Scientific Basis for Nuclear Waste Management XXX*, D. Dunn, C. Poinssot, and B. Begg, Editors. 2007, Materials Research Society: Boston, Massachussetts, USA. p. 199-204.
210. Buechele, A.C., et al., *Tc and Re behavior in borosilicate waste glass vapor hydration tests II.* Journal of nuclear materials, 2012. **429**(1-3): p. 159-165.
211. Bates, J.K., et al., *The hydration alteration of a Commercial Nuclear Waste Glass.* Chemical Geology, 1985. **51**: p. 79-87.

Appendix A Materials and methods

Characterization techniques

SEM: Morphological analysis of the altered samples were carried out using a field emission Scanning Electron Microscope (SEM) Zeiss Gemini Supra 55, JEOL JSM 6330F with an Energy Dispersive Spectroscopy (EDS) system. The gel layer is identified visually through density differences between pristine glass and gel layer. The spatial resolution of the SEM does not permit to detect the presence of gel layers lower than 100 nm in thickness. EDS analysis can be used to identify secondary precipitates using compositional analysis, but the minimum specimen size required for EDS analysis is 1 to 2 µm (laterally and perpendicularly) to avoid signals from surrounding material. All samples were observed directly (after metallization using carbon) by titling the altered sample at an angle to observe the altered surface and the presence of an altered layer. All samples were also enrobed in an epoxy resin, and polished to surface roughness < 1 µm to be observed in SEM for cross-section images.

TEM (only for chapter 2): FEI TECNAÏ G2 Transmission Electron Microscope (TEM) was used for morphological and chemical analysis. The 80 kV to 200 kV TEM permits to do conventional imaging and analytics, disposes of bright-field and dark-field imaging, EDS and Scanning TEM (STEM) to probe chemical composition of materials. The spatial resolution is 0.27 nm. Ultra-thin samples for observation by TEM (the length of the sample is approx. 5 µm and it is about one hundred nm thick) were prepared using Dual Beam FIB (FEI Helios 600 NanoLab). The uncertainty associated with the quantitative STEM-EDX analyses was estimated to be around 12% relative error. Scanning transmission electron microscopy (STEM) and EDS mapping were performed on QMg sample altered for 180 days using a Thermofisher Titan Themis 300 microscope operated at 300 keV, located at the “Centre Commun de Microscopie – CCM” at the university of Lille. Hyperspectral EDS data were obtained using the super-X detector system equipped with four windowless silicon drift detectors. The probe current was set at 50 pA. The analysis of the hyperspectral data was performed using the Hyperspy python-based package [204]. The signal was first denoised using Principal Component Analysis (PCA). Then, the EDS spectra at each pixel were fitted by a series of Gaussian functions and a physical model for background/bremsstrahlung. Quantification was performed thanks to the Cliff-Lorimer method, using experimentally determined k-factors and absorption correction routines.

XRD: The presence of crystalline secondary phases was analysed using a Philips X’Pert diffractometer X-Ray Diffraction (XRD) apparatus equipped with a copper tube ($\lambda_{K\alpha1}$=1.542 Å,

tension 40 kV and intensity 40 mA) and a goniometer (4-80° 2θ, step size 0.01744°). Each glass monolith was analyzed for 12 h on a multiple purpose sample stage (MPSS). The resulting peaks (if present) in the XRD pattern was treated with EVA software to identify the secondary phases corresponding to the peak [147].

ToF-SIMS: The behavior of elements in the altered layer was characterized using ToF-SIMS (SSIMS on TOF 5 (IONTOF)).

Principle: Secondary Ion Mass Spectrometry (SIMS) is useful to determine the distribution of chemical species at solid surface. Figure AA 1 is a schema describing the simplified principle of SIMS surface analysis drawn based on descriptions in reference [205]. The sample surface is placed in a vacuum chamber and it is bombarded by accelerated primary ions. The collision dislodges atoms from the sample surface and ejects secondary ions into the sample chamber, which are extracted normal to their surface as a secondary ion beam by acceleration by an electrostatic field and analyzed in a mass spectrometer. Since SIMS analysis is destructive, it removes the atoms from the surface analyzed giving access to the inner regions of the sample. Thus the composition of the sample can be analyzed layer by layer, permitting us to obtain depth profiles. The advantage of the SIMS technique is that it is capable of analyzing hydrogen, differentiating isotopes and detecting the presence of elements in trace quantities as well.

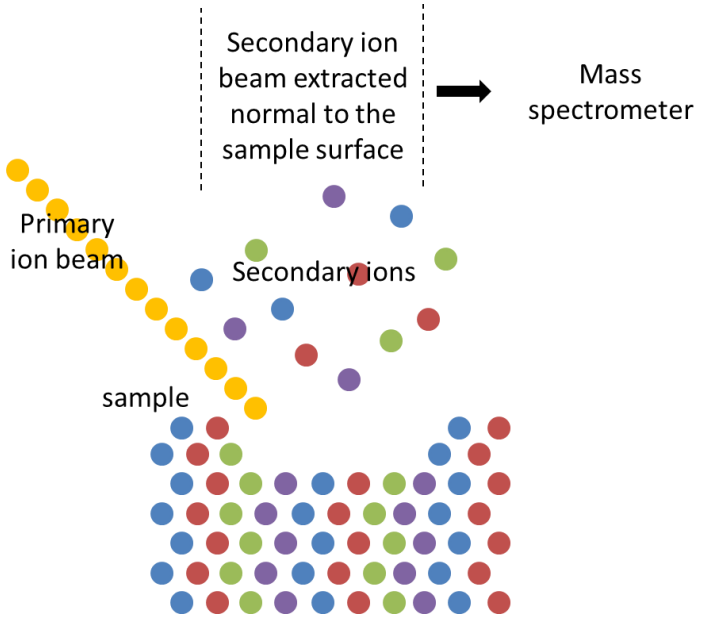

Figure AA 1 Schema describing the simplified principle of Secondary Ion Mass Spectrometry.

Usually the sample does not require any preparation before analysis. The spatial resolution is a few tens of μm^2 but the vertical resolution can be less than 1 nm. Below, the experimental parameters of data acquisition for ToF-SIMS characterization for different chapters are provided.

Data acquisition parameters:

For secondary positive ion analysis (for chapter 2): Depth profiles of secondary positive ions were obtained by alternating analysis and abrasion cycles. 25 keV Bi_1^+ primary ions at 2 pA current were used for analysis cycles. 1 keV primary O_2^+ ions at 250 nA current were used for the abrasion cycles. The eroded area was 200x200 μm^2. The analyzed area was 60x60 μm^2 for the samples altered for 180 days (for chapter 2) and 50x50 μm^2 for the samples altered for 557 days (for chapter2). The surface charge was neutralized on the monoliths by a pulsed low-energy (<20 keV) electron flux. The depth calibration was carried out using the abrasion rate and a mechanical profilometer to measure the crater depth at the end of the analysis. It is to be noted that the same abrasion rate was used for analyzing the gel layer and the pristine glass. This choice was justified by the good correspondence between thickness of altered layer measured by SEM and ToF-SIMS in other works [29].

For secondary positive ion analysis (for chapter 3 & chapter 4): Similar protocol and parameters as described in the passage above. 25 keV Bi_1^+ primary ions at 1.5 pA current were used for analysis cycles; 1 keV primary O_2^+ ions at 300 nA current were used for the abrasion cycles. The area analyzed was 50x50 μm^2.

For secondary negative ion analysis (for chapter 3, section 3.4.2 and for chapter 4, section 4.2.2.1): For the ToF-SIMS analysis of the secondary negative ions adapted to profile $^{18}O/^{16}O$ isotopes, the primary ions used for analysis cycles are 25 KeV Bi_3^{++} ions at 0.03 pA current and the primary ions used for abrasion cycles were 1 KeV Cs^+ ions at 60 nA. The area analyzed was 50x50 μm^2 at a resolution of 32x32 pixels. For the ToF-SIMS analysis of the secondary negative ions adapted to profile D/H isotopes, the primary ions used for analysis cycles are 25 KeV Bi_1^+ ions at 1.5 pA current and the primary ions used for abrasion cycles were 1 KeV Cs^+ ions at 60 nA. The area analyzed was 50x50 μm^2 at a resolution of 256x256 pixels.

At the end of the analysis, the depth of the crater (portion of the sample analyzed) is measured using a mechanical profilometer and is used for depth calibration. Thus at the end of the analysis, we obtain the intensities of different elements as a function of the depth of the sample analyzed (depth profiles).

The profiles were normalized with respect to the intensity of each element (C) in the pristine glass (denoted as PG) and with respect to the intensity of Si (C_{Si}) at given depth as shown in the equation AA-1 below.

$$Normalized\ intensity = \frac{\frac{C}{C_{Si}}}{(\frac{C}{C_{Si}})_{PG}} \quad \text{Equation AA-1}$$

$$Altered\ layer\ depth = \ x_0\ at\ which \left(0.5 - \frac{\frac{C_B}{C_{Si}}}{\left(\frac{C_B}{C_{Si}}\right)_{PG}} = 0 \right) \quad \text{Equation AA-2}$$

In most of the vapor hydration studies, boron is the element that is the most depleted in the altered layer (in depth and in quantity), although it is surprising. Retention of boron in the gel layer is often less than 10-20%. Therefore, it is used as a tracer to calculate the depth of the altered layer using equation AA-2.

Often, the depth of hydrogen penetration is compared to the thickness of boron depletion during vapor hydration. The hydrogen penetration depth is calculated from the ToF-SIMS profiles using equation AA-3 as shown below. Similarly, the depth of penetration of deuterium and ^{18}O are also studied and compared in chapter 3. These depths are also calculated using AA-3 by replacing $C_{H_{(gel\ layer)}}$ with $C_{D_{(gel\ layer)}}$ or $C_{18_{O\,(gel\ layer)}}$.

$$Depth\ of\ hydrogen\ penetration = \frac{C_{H\,(gel\ layer)}+1}{2} \quad \text{Equation AA-3}$$

Appendix 1

Table A1- 1 Vapor hydration experimental conditions of the glasses studied and the hydration layer thickness, secondary precipitates and behavior of elements in the altered layer for the references cited [206]

Ref	Glass	T °C	RH%	Time, days	Hydration layer thickness	Secondary phases	Elements enriched in the gel layer	Elements enriched in the phyllosilicates	Elements depleted in the gel layer	Elements depleted in the phyllosilicates layer
[9]	SRL211	120	100%	92	5,5 µm	analcime	Mn, Fe, Ni	Al, Si, Ca, Fe	Al, Si, Ca	Na, Mn, Ni
		202	100%	8	82 µm	tobermorite				
		240	100%	2	41 µm	analcime, tobermorite				
	SRL131	120	100%	92	7,2 µm		Ca, Ni, Mn, Fe	Si, Fe	Al	Na, Ca, Ti, Mn, Ni
		202	100%	10	27 µm	analcime, tobermorite				
		240	100%	2	25 µm	analcime, tobermorite				
[11]	PNL76-68	240	100%	7	too little	no surface alteration or layer formation				
		260	100%	14	10µm	Pollucite, analcime, polyaugite, a monoclinic pyroxene type pattern				
	SRL211	240	100%	7						
		260	100%	14						
	SRL165	202	100%	4		Analcime, gyrolite, tobermorite, weeksite				
	SRL131	240	100%	7						
		260	100%	14						

[13]	SRL165	190		91	16µm	Analcime, gyrolite, tobermorite, weeksite				
	SRL211	90	90%	3 yrs	1,5-2Mm					
	PNL76-68	90	90%	3 yrs						
		120	100%	3 months						
		150	100%	3 months						
		202	100%	3 months						
		240	100%	3 months						
		260	100%	3 months						
	verre basaltique	190	100%	95	1 µm	Ca-aluminosilicate & Ca-silicate				
	tektite	202	100%	14						
	obsidian	202	100%	14						
	SRL131	202	100%	25						
		202	95%	10						
		202	80%	10						
		202	58%	10	No measurable layer					
		202	47%	10	No measurable layer					
[14]	PNL76-68	188	100%	8	No measura	no alteration phases	Ca, Fe,	Na, Ca,	B, Na, Si	B, Si

					ble layer	evident	U	Fe		
		81	95%	240						
		187	100%	92	40µm					
	SRL165	81	95%	180						
		202	100%	61	20µm	tobermorite, analcime, gyrolite				
		202	95%	14						
		202	80%	14						
		202	58%	61	No measura ble layer					
		202	47%	61	No measura ble layer					
		81	95%	180						
		75	100%	360						
	SRL131	75	95%	360						
[18]	WVCM44	200	100%	40	90µm	Li3PO4and Hydroxy apatite precipitates, Analcime, Gyrolite, Orthoclase, OH-apatite, Weeksite				
	WVCM50	200	100%	14	250µm	Li3PO4and Hydroxy apatite precipitates, Analcime, Gyrolite, Orthoclase, OH-apatite, Weeksite				
	SRL165	200	100%	70	40µm	Analcime, gyrolite, tobermorite, weeksite				
	SRL202	200	100%	70	70µm	Analcime, gyrolite, tobermorite, weeksite, orthoclase				
[91]	SRL+Np,P	200	100%	10	12					

	u, Am	200	100%	16	17					
		200	100%	22	22					
		200	100%	44	35	Apatite, weeksite, Li3Po4, orthoclase, analcime				
		150	100%	30	<1					
		150	100%	80	<1					
		150	100%	98	<1					
		150	100%	143	<1					
		90	100%	37	<1					
		90	100%	101	<1					
		90	100%	180	<1					
	WV-U, Th, Np, Pu, Am, Tc	200	100%	10	20					
		200	100%	16	25					
		200	100%	22	15					
		200	100%	44	70	Analcime, weeksite, gyrolite				
		150	100%	30	<1					
		150	100%	80	<1					
		150	100%	98	<1					
		150	100%	143	<1					
		90	100%	37	<1					
		90	100%	101	<1					
		90	100%	180	<1					
[15]	SRL131	75	100%	365	15-35µm	Smectite	Ca, Fe, Ti	Si, Mn, Ni	Si	Ca, Ti, Fe

		75	95%	731	7µm	Analcime, Calcite				
		75	60%	365	750Å					
	SRL131U	75	100%	365						
		75	95%	365	5µm	smectite, Calcite				
		75	60%	365						
[19]	WVCM44	200	100%	40	90-100µm	Apatite, weeksite, Li3Po4, orthoclase, analcime, Ca-Silicate, K-substituted zeolites, gyrolite	Mg, Si, Ti, Mn, Fe, Ni, Th, U		Zr, K, Al, Na, B, Li	
	WVCM50	200	100%	15	250µm	crystalline smectite clay, nontronite, montmorillonite, tincalconite, K-substituted zeolites, gyrolite	Mg, Ca, Ti, Mn, Fe, Ni, Th, U		Li, B, Na, Al, Si, K, Zr, Ba	
[66]	SRL202U	200	100%	56	130µm	smectite, illite, nontronite, saponite	Mg, Ca, Ti, Fe		Na, K	
	SRL202A	200	100%	35	600µ	Ca, Si crystals, tobermorite, adularia, haiweeite, Na-U-Silicates, smectite or smectite/illite clay, nontronite, saponite				
	SRL165U	200	100%	56						
	SRL165A	200	100%	56						
	SRL131U	150	100%	182						
	SRL131A	150	100%	56						
[67]	SRL131U	150	100%	720	70µm	Zeloite, smectite, calcium and sodium silicates, phosphae, evaporitic salts, uranyl silicate phases	Al, Ti, Mn, Fe, Ni	Mg, Al, Ti, Mn, Fe, Ni	Na, Mg, K, Ca	Na, K, Ca
	SRL131A	150	100%	56	40µm	Zeloite, smectite, calcium and sodium				

						silicates, phosphae, evaporitic salts, uranyl silicate phases				
[207]	Reference composition-Hanford waste glass	70	100%	56	No measurable layer					
		120	100%	28	No measurable layer	Gobbinsite				
		15	100%	11	>200µ	Gobbinsite, Phillipsite, Analcime, Na-Al-silicate				
		175	100%	5	>800µ	Analcime, philipsite, Na-Al-silicate				
		200	100%	3	fully altered	Analcime, philipsite, Na-Al-silicate				
[208]	SON68	200	100%	1021	26µm	Analcime, tobermorite, apatite, weeksite, Na-SI phase, Ca-Mo phase, Ag-Te phase				
[22]	Synthetic basaltic glass	70	100%	7 years	0,5µm	Clay	Ti, Fe		Ca	
	SRL165	70	100%	7 years	Not mentioned	Clay	Al, Mn, Ni		Ca	
[52]	Reference composition-Hanford waste glass	150	100%	250	different thickness for different compositions	Analcime, Na-Ti-silicate, Na-Al-Silicate hydrate, Na-Al-silicate B hydroxide hydrate, tincalconite, spinel, Gobbinsite, phillipsite, pinakiolite, Ca-Si-hydroxide hydrate, Na-Zr silicate, hydroxycancrinite				
		175	100%	79						
		200	100%	150						
		250	100%	12						
		275	100%	12						
		300	100%	3						
[71]	U-dop BS	200	100%	60	100-	KNAURSI-KNa3(UO2)2(Si4O1				

	glass				300µm	0)2(H2O)4 , Na-bearing zeolites, weeksite, Ca & Fe phosphosilicates, Ca & Fe silicates, alkali bearing Ca-silicate, CaOH				
[209]	Tc and Re containing reference glasses	238	100%	24,8	100% to upto 60-70% of glass was reacted	Analcime, Na, Ca, Zn-silicate crystalline phases				
[68]		90	92%	512		tobermorite, analcime, Fe-rich phase, powellite, calcite	Si	Si	Na, Al, Ca, Fe, Zn, Zr, Mo, Cs	Na, Al, Ca, Fe, Zn, Zr, Mo, Cs
		125	92%	154	2-2,5 µ					
		150	92%	99	1-3,4 µ					
		175	92%	99	3,8-4,3 µ					
		200	92%	57	4-6,4 µ					
		175	80%	99	2,8-1,2 µ					
		175	85%	90	2,5-2,3 µ					
	SON68	175	95%	99	8,3-8,5 µ					
[84]	Iron phosphate glass-CCC treated	200	100%	7	80-290 µm					
	Iron phosphate glass-quenched	200	100%	7	<14µm					
[210]	6 reference compositions of LAW glass	200	100%	23-30 days	50-150 µm	Analcime, (Na, Zn)-silicate and (na, Ca)-silicate crystalline phases	Tc, Fe, Slightly enriched Re		Na, B, Al, Ca	
[24]	ISG	175°C	60%	65	~1 µm	Tobermorite				

				days						
		175°C	80%	65 days	~1 µm	Tobermorite				
		175°C	98%	2.3, 5.6, 7.9, 65 days	~1 µm	Tobermorite, Analcime, Calcite				
[53]			92%	766	1,6 µm	Calcite, powellite, apatite				
			95%	832	2,3 µm	Calcite, powellite, apatite				
			98%	653	2,4-2,7µm	Calcite, powellite, apatite				
		90	99,90%	653	2,5-2,8 µm	Calcite, powellite, apatite				
		125	95%	766	2,57-5,2µm	Tobermorite, calcite, powellite, apatite				
		35	95%	766	0,31-0,6 µm	Calcite				
			92%	490	0,4-0,7 µm	Calcite				
	SON68	50	98%	490	0,6-0,9 µm	Calcite				
	SON68-D218O	125	95%	593	4,7-5µm	Tobermorite, calcite, powellite, apatite	Si, Al, Fe, Ca	Na, B, Li, Zn, Ni	Zn, Ni, Si, Al, Fe, Ca	
[25]	SON68-under H2S 1% Ar	175	98%	1 hr-1 yr	4 µm		Si, Al	Na, Ca, Fe		
	SON68-under NH3 8% Ar	175	98%	1 hr-1 yr	15 µm	Analcime, tobermorite, honeycomb alteration phase	Fe, RE, Ca	Na, Cs, Mo, Al		
[69]	SON68	150	91%	101	2 µm	Parallelopiped shaped crystals, needle like crystals	Mo, Si, Al, Fe, Cr, Ni	B, alkaline earths,	Fe, Mn, Zn	

								RE		
[27]			92%		65-85 nm					
			95%	35	80-90 nm					
			92%							
		50	95%	365	>1 µm		Si	Na, Ca		
			92%		209-230 nm					
			95%	35	225-250 nm	Apatite, calcite				
			92%							
	CSD-B	90	95%	365	>1 µm	Apatite, calcite, ruthenium				
[28]	SON68-H2S	175	98%	365	4 µm	No precipitates				
	SON68-CO2	175	98%	365	5,8 µm	No precipitates	Fe, Zn, La, Ce, Nd	Na, Al, Si		
	SON68-Ar	175	98%	290	9 µm	tobermorite, analcime, apatite and gyrolite				
	SON68-NH3	175	98%	98	15 µm	Analcime, tobermorite, apatite	Ca, Cr, Mn, Fe, Zn, Ni	Na, Al		

Table A1- 2 Formula of minerals for references cited in the report [206]

Mineral	Formula
Analcime	$Na(AlSi_2O_6).H_{2O}$
Gyrolite	$Ca_2Si_3O_7(OH)_2.H_2O$
Tobermorite	$Ca_5Si_6O_{16}(OH)_2.4H_2O$
Jennite	$Ca_9Si_6O_{18}(OH)6.8H_2O$
Afwillite	$Ca_3(SiO_3OH)_2.2H_2O$
Nekoite	$Ca_3Si_6O_{15}.7H_2O$
Weeksite	$K_2(UO_2)_2Si_6O_{15}.4H_2O$
Na-weeksite	$Na_2(UO_2)_2Si_6O_{15}.4H_2O$
KNAURSI	$KNa_3(UO_2)_2(Si_4O_{10})_2.4H_2O$
Apatite	$Ca_{10}(PO_4)_6(OH)_2$
Calcite	$CaCO_3$
GIbbsite	$Al(OH)_3$
Powellite	$(Ca, Sr)MoO_4$
Phases Ag-Te	Ag_2TeO_3
Pollucite	$CaAlSi_2O_6.H_2O$
Orthoclase	$KAlSI_3O_8$
Phillipsite	$(K,Na)_2(Si,Al)_8O_{16}.4H_2O$
Montmorillonite	$(Na,Ca)_{0.3},(Al,Mg)_2Si_4O_{10}(OH)_2.nH_2O$
Gobbinsite	$(Na_2,Ca)_2K_2Al_6Si_{10}O_{32}.12H_2O$
Herschelite	$Na_4Al_4Si_8O_{24}.12H_2O$
Cancrinite	$Na_6Ca_2Al_6Si_6(CO_3)O_{24}.2H_2O$
Sodalite	$Na_8(SiAlO_4)_6(ClO_3)_2$
Nosean	$Na_8Al_6Si_6O_{24}(SO_4)$
Adularia	$KAlSi_3O_8$
Lithium phosphate	Li_3PO_4
Haiweeite	$K_2(UO_2)_2Si_6O_{15}.4H_2O$
Soddyite	$(UO_2)_2SiO_4.2H_2O$
Tincalconite	$Na_2B_4O_7.5H_2O$
Augite	$Ca(Mg,Fe)Si_2O_6$
Acmite	$NaFeSi_2O_6$
Pinakiolite	$(Mg,Mn^{2+})_2(Mn^{3+},Sb^{5+})BO_5$
Catapleite	$Na_2ZrSi_3O_9.2H_2O$

Table A1- 3 Composition of glasses cited in the report (weight %) – a-[9], b-[11, 211], c-[13], d-[18], e-[59],f-[53], g-[24], h-[27]

Glass	SRL131[a]	SRL211[a]	Obsidian[a]	PNL 76-68[b]	Tektite[c]	Basalt[c]	SRL165[c]
SiO_2	44	42,9	62-81	41,5	70	50,7	51,6
B_2O_3	10,9	7,9		8,89			6,8
Na_2O	13,7	15,2	3-4	15,3	1	4,5	10,8
Al_2O_3	3,5	3,8	1-12	0,42	14	11,7	4,3
MgO	1,6		0,05-0,2		3	6,7	0,3
CaO	1,4	5,2	0,2-2	2,15	2	10,6	1,6
Li_2O	4,2	3,2		0,02			4,8
Fe_2O_3	14,3	14,2	0,1-3	10,26	5	13,1	11,7
NiO	1,8	1,7	<0,01	0,22			0,8
Cr_2O_3				0,3			
ZnO				4,76			
P_2O_5				0,54			
SrO		0,4	<0,01	0,38			
ZrO_3/ZrO_2	0,4		<0,01	1,77			0,7
MoO_3				1,81			
MnO	3,1	3,2	<0,01		0,1	0,2	2,8
CoO							
Cs_2O		0,1		0,69			
BaO		0,06	<0,1	0,43			
Y_2O_3				0,23			
La_2O_3/La_2O	0,4		<0,01	0,5			
CeO_2/Ce_2O_3		0,8	<0,01	1,03			
Nd_2O_3		0,9	<0,01	4,08			
Pr_6O_{11}/Pr_2O_3				0,56			
Gd_2O_3							
UO_2							
ThO_2							
K_2O			4-5	0,15	3	0,6	0,2
Ag_2O				0,03			
CdO				0,02			
SnO_2							
Sb_2O_3				0,07			
TeO_2				0,11			
RuO_2		0,5		0,37			
Rh_2O_3				0,18			
PdO				0,56			
CuO				0,08			
TiO_2	0,7		0,1-0,2	2,88	1	1,9	0,2
Eu_2O_3		0,1	<0,01	0,07			
Ge_2O_3				0,05			
Rb_2O				0,13			
Sm_2O_3				0,35			

Glass	WVCM44[d]	WVCM50[d]	SRL165U[d]	SRL202U[d]	R7T7[e]	SON68[f]	ISG[g]	CSD-B[h]
SiO_2	45,8	39,6	52,86	51,22	45,48	45,85	56,18	50,33
B_2O_3	8,42	12,27	6,76	8,06	14,02	14,14	17,34	14,44
Na_2O	9,1	9,79	10,85	6,75	9,86	10,22	12,17	12,58
Al_2O_3	6,14	9,86	4,08	4,76	4,91	5	6,06	8,7
MgO	1,38	0,79	0,7	1,47				
CaO	0,99	0,82	1,62	0,79	4,04	4,07	4,98	3,1
Li_2O	2,8	2,22	4,18	4,69	1,98	1,99		2,17
Fe_2O_3	11,4	11,93	11,74	12,05	2,91	3,03		2,84
NiO	0,42	0,3	0,85	1,03	0,74	0,43		0,33
Cr_2O_3	0,03	0,14	<0,01		0,51	0,53		0,07
ZnO					2,5	2,53		
P_2O_5	2,2	2,47	0,02		0,28	0,29		0,42
SrO		0,02	0,11	0,13	0,33	0,35		
ZrO_3/ZrO_2	0,29	0,39	0,66		2,65	2,75	3,28	1,99
MoO_3					1,7	1,78		0,69
MnO	1,29	1,21	2,79	3,47	0,72			0,19
CoO					0,12			0,27
Cs_2O	0,07	0,07	0,07	0,07	1,42	1,12		
BaO	0,05	0,19	0,06		0,6	0,62		0,36
Y_2O_3					0,2	0,2		
La_2O_3/La_2O					0,9	0,93		
CeO_2/Ce_2O_3	0,06	0,7	<0,05		0,93	0,97		
Nd_2O_3					1,59	2,04		
Pr_6O_{11}/Pr_2O_3					0,44	0,46		
Gd_2O_3								
UO_2	0,7	0,61	0,92	1,08	0,52			
ThO_2	3,3	3,52			0,33			
K_2O	3,63	1,6		3,21				
Ag_2O					0,03	0,03		
CdO					0,03	0,03		
SnO_2					0,02	0,02		
Sb_2O_3					0,01			
TeO_2					0,23	0,23		
RuO_2								0,12
Rh_2O_3								
PdO								
CuO								
TiO_2	0,88	0,82	0,14	1,32				
Eu_2O_3								
Ge_2O_3								
Rb_2O								
Sm_2O_3								

Appendix 2

Section 1 SAXS data acquisition parameters and data treatment

Characterization techniques:

SAXS:

Principle: Small angle X-ray Scattering (SAXS) is an experiment useful to identify the size, shape, density and surface area of a substance of a particular electronic density dispersed in a medium of a different electronic density. Figure A2(A) 1 shows the basic principle of SAXS methodology and the sample configuration used in our study . Looking at the image on the right, a monochromatic beam of X-rays is passed though the sample. The scattered X-rays are collected on a detector at an angle 2θ. The scattered intensity, I(q) is the Fourier Transform of g(r), which gives information about the electronic density. SAXS experiments measure the scattered intensity at very small scattering vectors (q) to investigate systems with sizes ranging from a few Å to a few µ. The data treatment of the scattered intensity to convert it into absolute intensity in order to extract information on density, size shape and internal structure is described below.

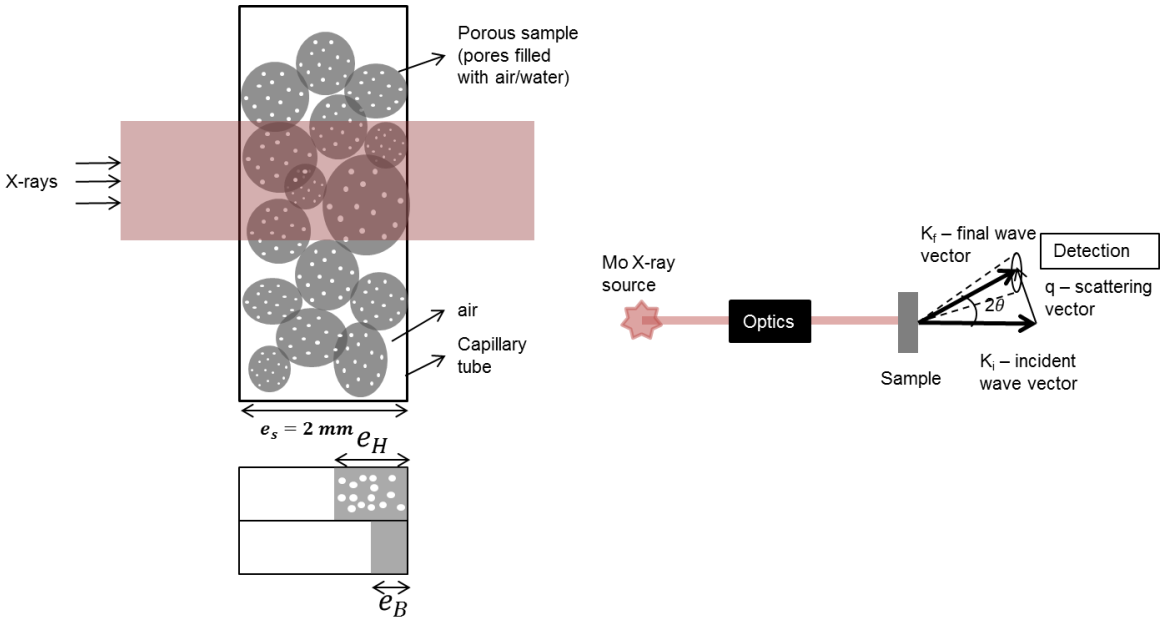

Figure A2(A) 1 Schematic representation of the basic principle of the SAXS methodology (right) and the sample configuration in the capillary tube to demonstrate the different sample thicknesses; the macroscopic sample thickness e_S, the equivalent thickness of the grains (powder+inner pores) e_H and the equivalent solid thickness e_B

The apparatus used is a SAXS-Mo apparatus emitting monochromatic X-ray beam at λ 0.709 Å and the photon flux is $3x10^6$ photons.s^{-1} approximately. The q-range covered is 0.2 to 30 nm^{-1}. The distance scale D is related to the scattering vector q by the formula D = 2π/q. The sample was filled in a glass capillary tube of 2 mm (e_s) diameter and approximately 10 µm wall thickness. In the section of the sample analyzed, the inter-grain porosity is filled with air. The inner porosity of each grain could be filled with air or water. The data treatment for a porous or granular medium with special attention to the case of glass leaching by water was handled by Spalla et al. 2003 [108]. The data treatment was based on previous works [108-110] and is explained in detail in the Appendix 2-section1.

The absolute intensity of the SAXS signal in cm^{-1} was calculated based on the formula given below.

$$I_{abs} = \left(\frac{1}{C * e_B}\right) * \left(\frac{I'_{sample}}{T_{sample} * t_c} - \frac{I'_{ec}}{T_{ec} * t_c}\right) \quad \text{(Equation A2-1)}$$

Where, C is the correction coefficient (1.33) characteristic of the apparatus, e_B is the apparent average solid thickness in the path of the X-ray beam (cm), I' is the measured intensity (after integration) of the sample or empty capillary (denoted as ec) (detector counts), T is the transmission by either the sample or the ec, which is calculated as the ratio of flux of photons after traversing the sample to the flux of photons hitting the sample and t_c is the time of acquisition of each diagram (1800 seconds for the samples).

For the experimental set-up used and for alteration in vapor phase, two cases are possible: air in the inter-grains porosity and (i) air in the inner pores or (ii) water in the inner pores (or possibly a combination of both). The difference between the data treatment of the two cases lies in the calculation of the apparent sample thickness. In case (i), e_B is used as mentioned above in equation A2-1. In case (ii), e_H is used to calculate the absolute intensity. The differences and the relation between these sample thicknesses are as follows:

$$e_B = \frac{-\ln(T)}{\mu_{solid}} \quad \text{(Equation A2-2)}$$

$$e_B = e_s * \emptyset^* * (1 - \emptyset) \quad \text{(Equation A2-3)}$$

μ_{solid} is the X-ray mass attenuation coefficient calculated from the composition of the altered glass. $\emptyset^*$ is the compactness of the sample defined by the ratio of the total volume of the grain envelopes and the volume of the sample and Ø is the inner porosity of the solid.

$$e_H = \frac{-\ln(T)}{\mu_{grain}} \quad \text{(Equation A2-4)}$$

$$\mu_{grain} = \mu_{solid} * (1 - \emptyset) + \mu_{solvent} * \emptyset \quad \text{(Equation A2-5)}$$

$$; e_H = e_s * \emptyset^* \quad \text{(Equation A2-6)}$$

$\mu_{solvent}$ is the X-ray mass attenuation co-efficient of water. In this study, it is considered that the pores are filled with water. The plot of the scaled intensity (cm^{-1}) as a function of q (cm^{-1}) gives information on the physical parameters of the sample such as the characteristic pore size, internal particle structure, porosity in the particles, and specific surface area of the grains and the inner pores of the particles.

The particle structure, i.e. the interface between two phases of different electronic densities in the sample can be deduced based on a power law dependence of the intensity and q, given by equation A2-7.

$$I(q) \alpha\ q^{-D} \quad \text{(Equation A2-7)}$$

D is a factor which indicates the characteristics of the interface between two phases. For cylinders or filaments, D = 1; for discs or plate like shapes, D = 2 [110]. When 3 ≤ D ≤ 4, porod's law becomes applicable (equations A2-10 to A2-12) for well-defined pores with smooth interface. In the field of glass alteration, when D varies between 3 and 4, the scattering is considered to be due to the surface of pores and when D<3, it is considered to be due to a ramified pore network

created due to the loss of soluble elements from the glass matrix during alteration. The typical pore size in this case is considered to be less than 1 nm [123].

The absolute intensity calculated from equation A2-1 is scaled to the solid content in the sample by dividing it by the solid fraction $\emptyset_s$ calculated using equation A2-8, in the case of air in pores, or it is simply equal to $\emptyset^*$ in the case of water in the inner porosity.

$$\emptyset_s = \emptyset^* * (1 - \emptyset) \quad \text{(Equation A2-8)}$$

The normalized solid intensity of the pristine glass sample is the intensity scattered by the glass layer. The intensity scattered by the gel layer, denoted as I_g, is calculated by subtracting the solid intensity of the pristine glass sample from the solid intensity of the altered glass sample. I_g contains signals coming from both the grain envelopes and the inner pores of the material. The scattering from the grain envelopes should be subtracted from the intensity using the equations described below:

$$I(corr) = I_g(q) - I_g(q_*)\frac{q_*^4}{q^4} \quad \text{(Equation A2-9)}$$

Where q_* is a fixed value of q in the low-q domain. $I(corr)$ contains information about the scattering of X-rays in the high q domain or the pores of the gel layer and is therefore used to calculate the pore characteristics in the gel layer.

The porosity, the specific surface area of the grains and the inner pores can be calculated from the equations A2-10 to A2-12 when D=4:

$$\emptyset = \frac{\int_0^\infty I(corr)q^2 dq}{2\pi^2 \Delta\rho^2} \quad \text{(Equation A2-10)}$$

$$\Sigma_P = \frac{\lim_{q\to\infty} I(corr)q^4}{2\pi\Delta\rho^2\rho_{gel}} \quad \text{(Equation A2-11)}$$

$$\Sigma_G = \frac{\lim_{q \to 0} I_{abs} q^4}{2\pi \Delta\rho^2 \rho_v} \quad \text{(Equation A2-12)}$$

$\emptyset$ is the porosity, $\Delta\rho$ is the difference in the average scattering length of the two phases, Σ_P is the specific surface area of the pores calculated from the intensity in the high-q domain and Σ_G is the specific surface area of the grains calculated from the intensity in the low-q domain [108]. The porosity and specific surface area of the pores thus calculated are normalized to the volume fraction of gel in the grains. This volume fraction is assumed based on the ToF-SIMS analysis on glass monoliths. The other assumptions made for the SAXS data treatment include the scattering length of the altered layer (ρ_{e^-}) (cm^{-2}) and its density (assumed to be 2 g/cm^3). ρ_{e^-} of the altered layer is calculated based on a composition estimated from the ToF-SIMS profiles. Similarly, the X-ray mass attenuation co-efficient of the gel layer (μ_{solid}) was also calculated based on the ToF-SIMS profiles.

Section 2 SEM/TEM images of AVM6 and AVM10 samples

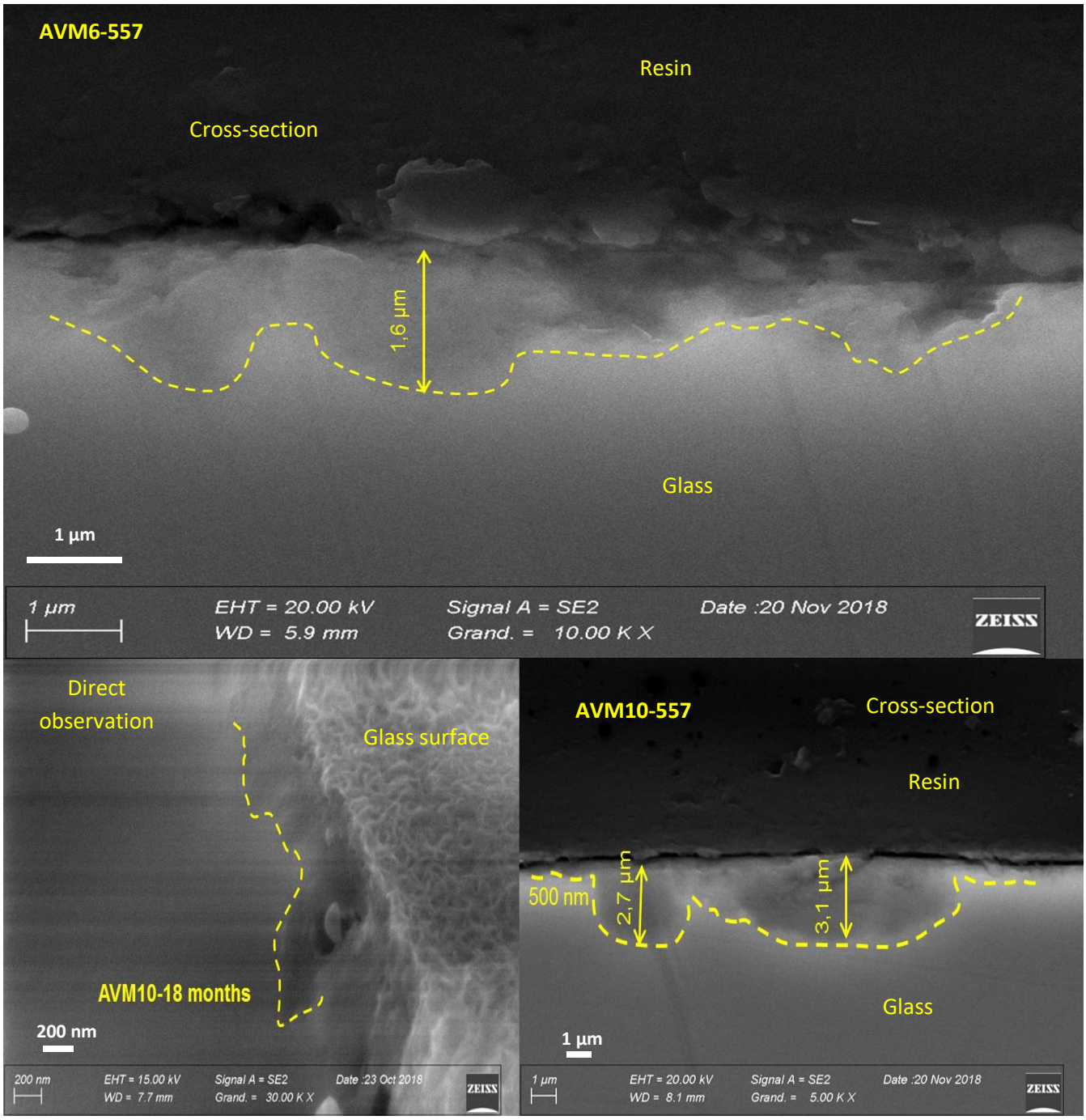

Figure A2- 1 SEM images of AVM6 and AVM10 altered at 50°C and 95% RH for 557 days ; These glasses have irregular altered zones present punctually in the altered sample surface

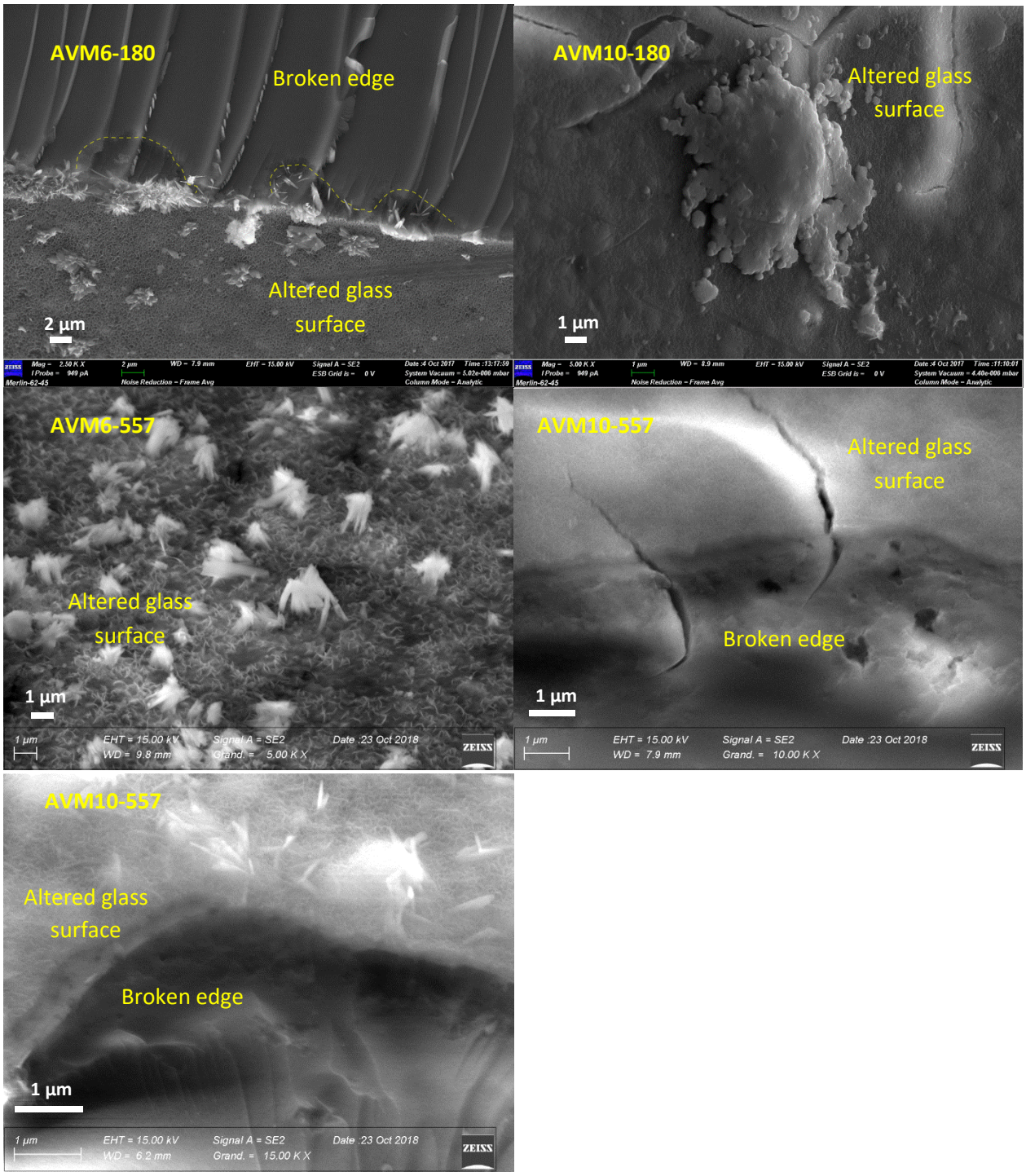

Figure A2- 2 SEM images of AVM10-180 and AVM10-557; The leafy precipitates were better developed in the sample altered for 557 days than 180 days and that they are visually different than the leafy precipitates formed on AVM6 samples; The third image in left column shows that more needle like crystalline phases were present on AVM10 sample altered for 557 days; All the five images above are a direct observation of the surface of the altered sample;

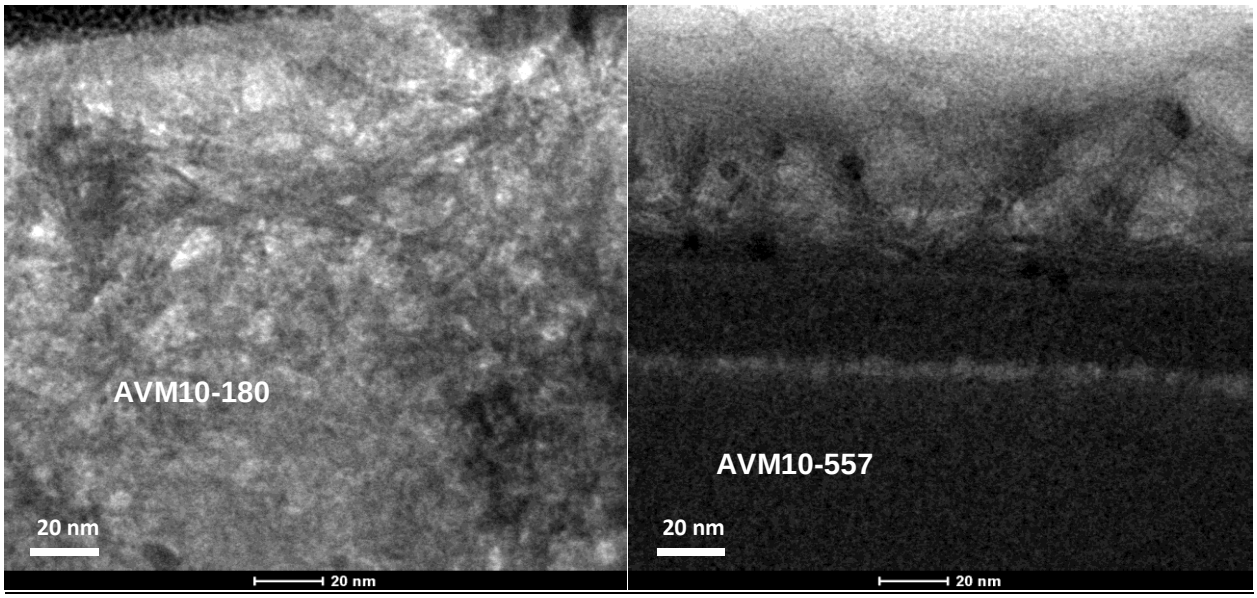

Figure A2- 3 TEM image of phyllosilicates formed on AVM10-180 and AVM10-557 (cross-sections); The phyllosilicates are better developed in AVM10-557

STEM EDS mapping of AVM6-180: Ca seems enriched in the porous zone. Al is depleted in the smectite layer. Mg is enriched in the smectite layer. Na is enriched in the smectite layer and seems depleted in the porous zone.

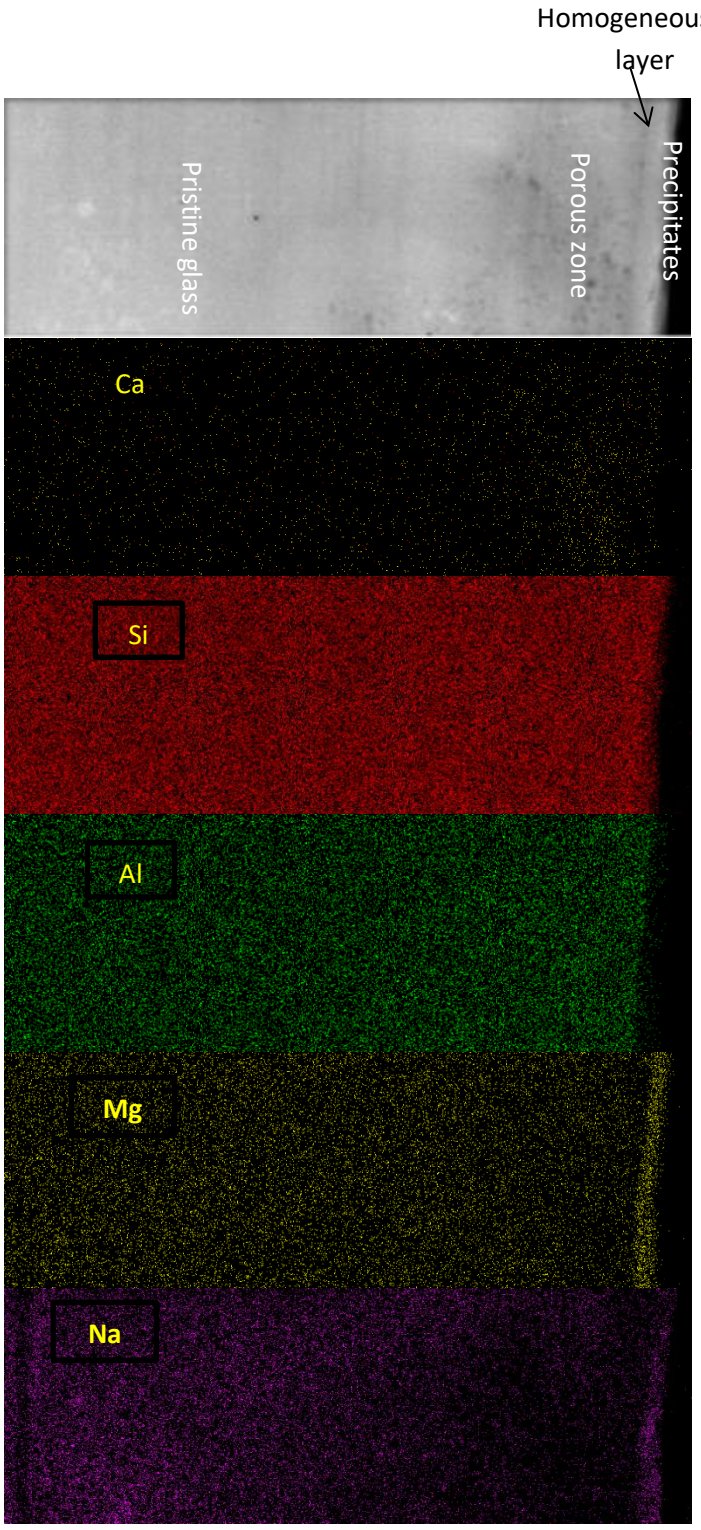

Figure A2- 4 STEM EDS mapping of AVM6-180 (AVM6 altered for 180 days at 50°C and 95% RH)

STEM-EDS mapping of AVM6-557: Si is enriched in the homogeneous gel layer. Mg is enriched in the smectite layer (phyllosilicates). Al is depleted in the smectite layer. Ca is enriched towards the extreme surface.

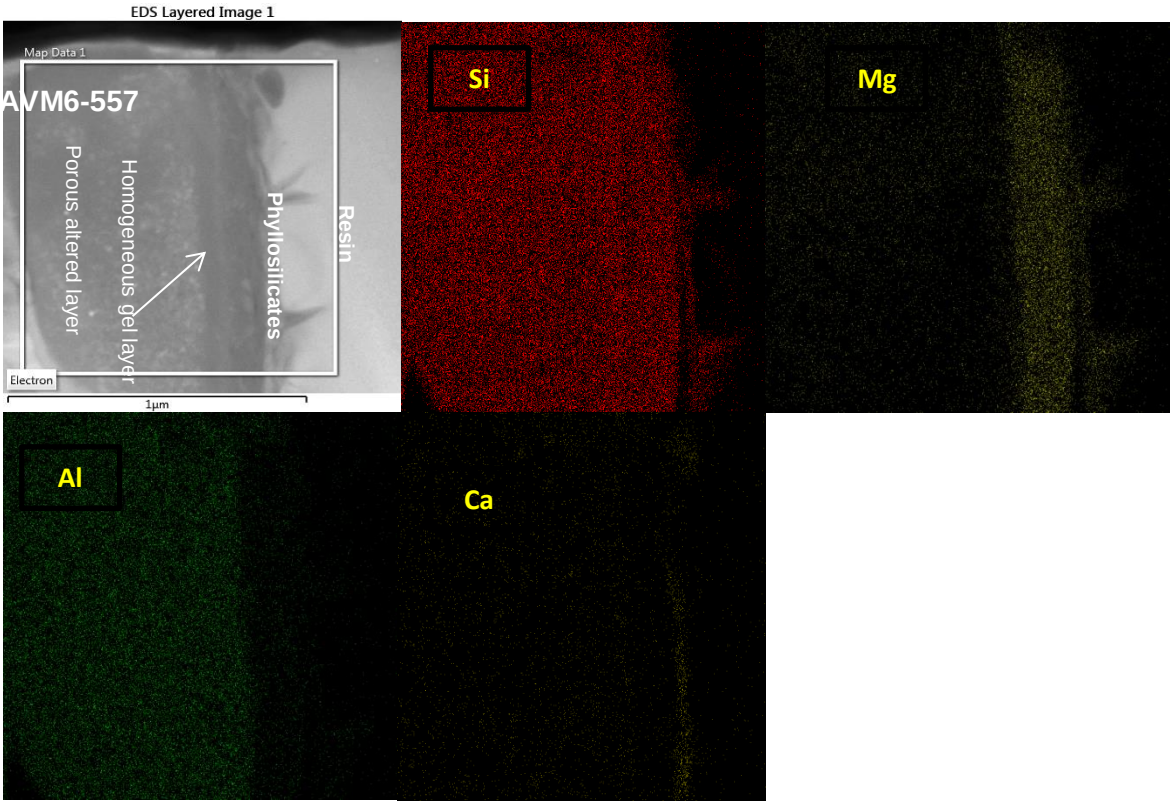

Figure A2- 5 STEM-EDS mapping of AVM6-557 (AVM6 altered for 557 days at 50°C and 95% RH)

Section 3 STEM-EDX analysis and composition of altered layer

Gel composition of AVM6-180 (STEM EDX)

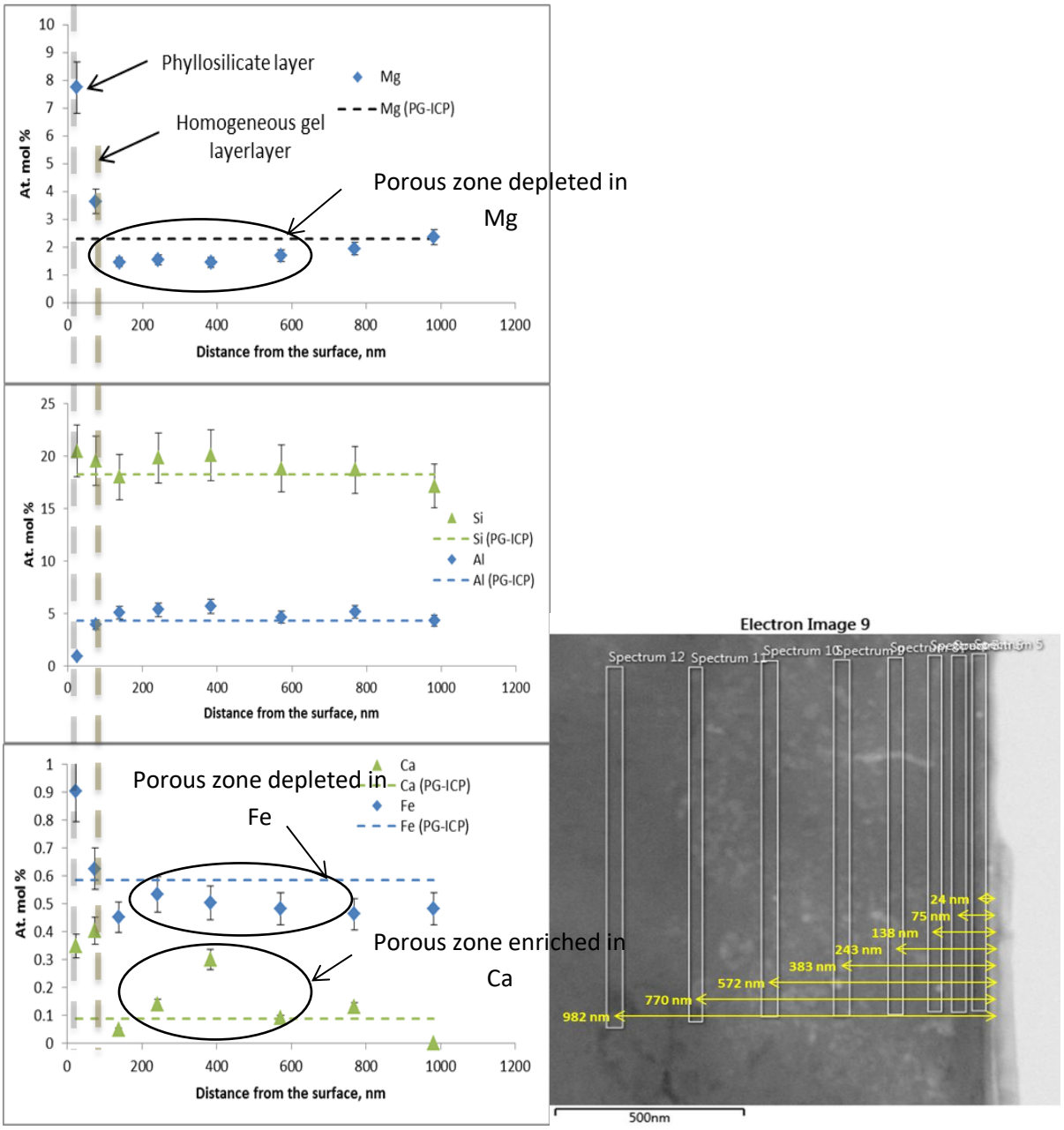

Figure A2- 6 STEM-EDX analysis of a micro-section of AVM6 sample altered at 50°C and 95% RH for 180 days; The analyzed zones are marked as rectangle in the left side image. The distance from the glass surface-resin interface to the zone analyzed is marked in the image and the analyzed compositions are presented as a function of the distance from the interface on the right. The dotted lines in the graphs represent the composition of pristine glass measured by ICP

Gel composition of AVM6-557 (STEM-EDX)

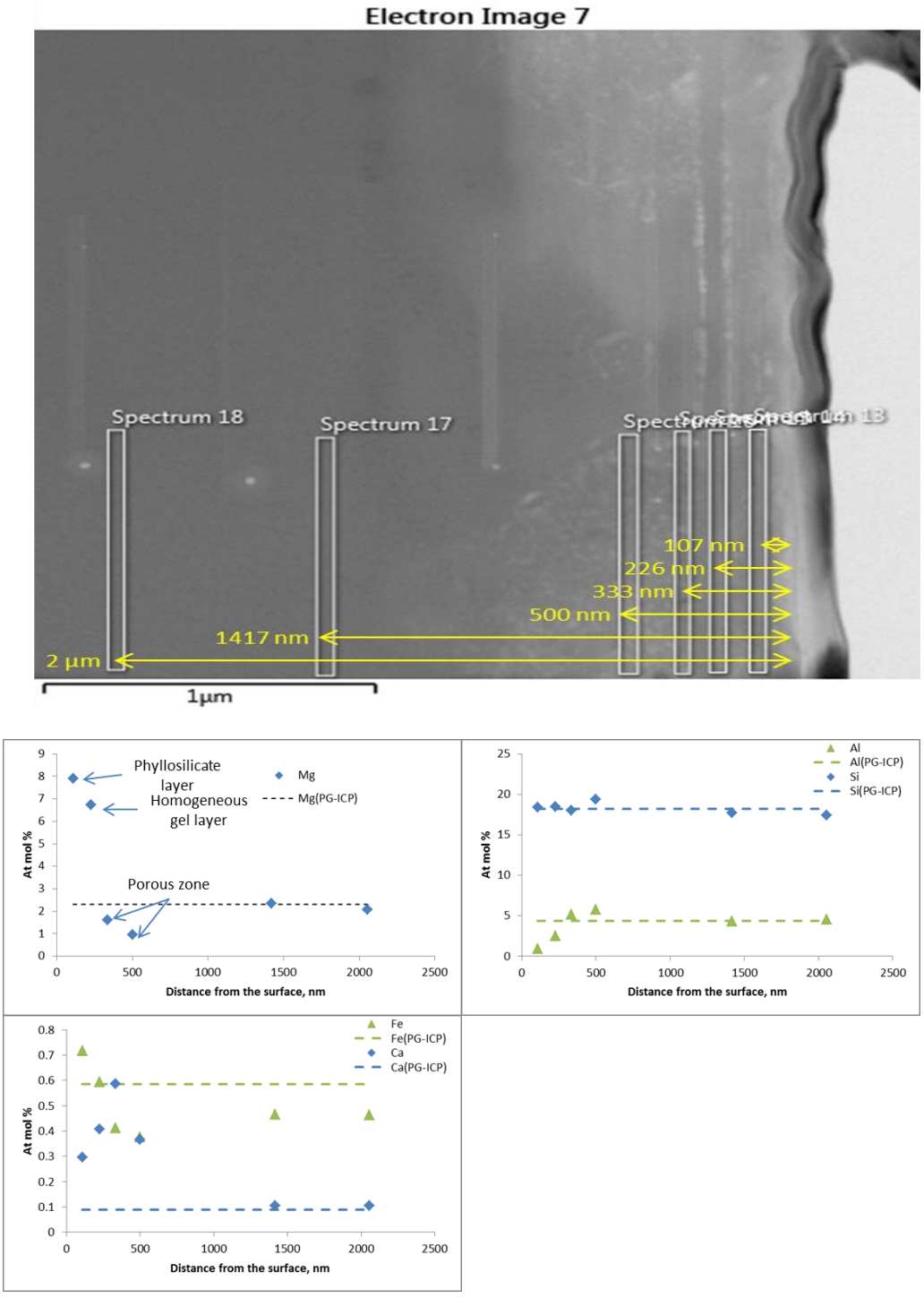

Figure A2- 7 STEM-EDX analysis of a micro-section of AVM6 sample altered at 50°C and 95% RH for 557 days; the analyzed zones are marked as rectangle in the top image. The distance from the glass surface-resin interface to the zone analyzed is marked in the image and the analyzed compositions are presented as a function of the distance from the interface on the graphs beneath. The dotted lines in the graphs represent the composition of pristine glass measured by ICP. It can be seen that the porous zones are depleted in Mg, Fe and enriched in Ca. The relative error associated with the concentration measured by STEM-EDX analysis is at least 12%

Gel composition AVM10-180 (STEM-EDX)

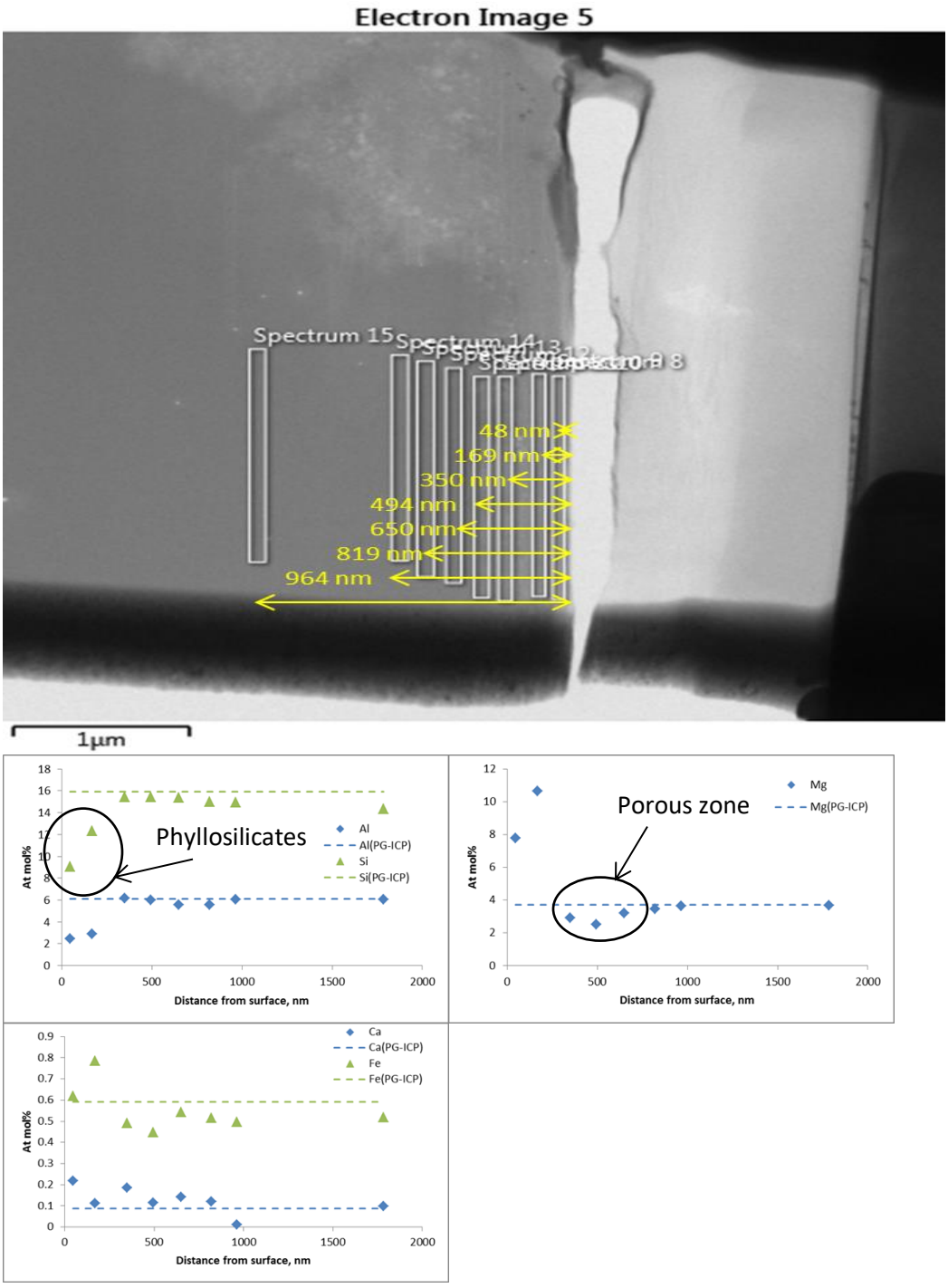

Figure A2- 8 STEM-EDX analysis of a micro-section of AVM10 sample altered at 50°C and 95% RH for 180 days; the analyzed zones are marked as rectangle in the top image. The distance from the glass surface-resin interface to the zone analyzed is marked in the image and the analyzed compositions are presented as a function of the distance from the interface on the graphs beneath. The dotted lines in the graphs represent the composition of pristine glass measured by ICP. It can be seen that the porous zones are depleted in Mg, Fe and enriched in Ca. The relative error associated with the concentration measured by STEM-EDX analysis is at least 12%

Gel composition AVM10-557 (STEM-EDX)

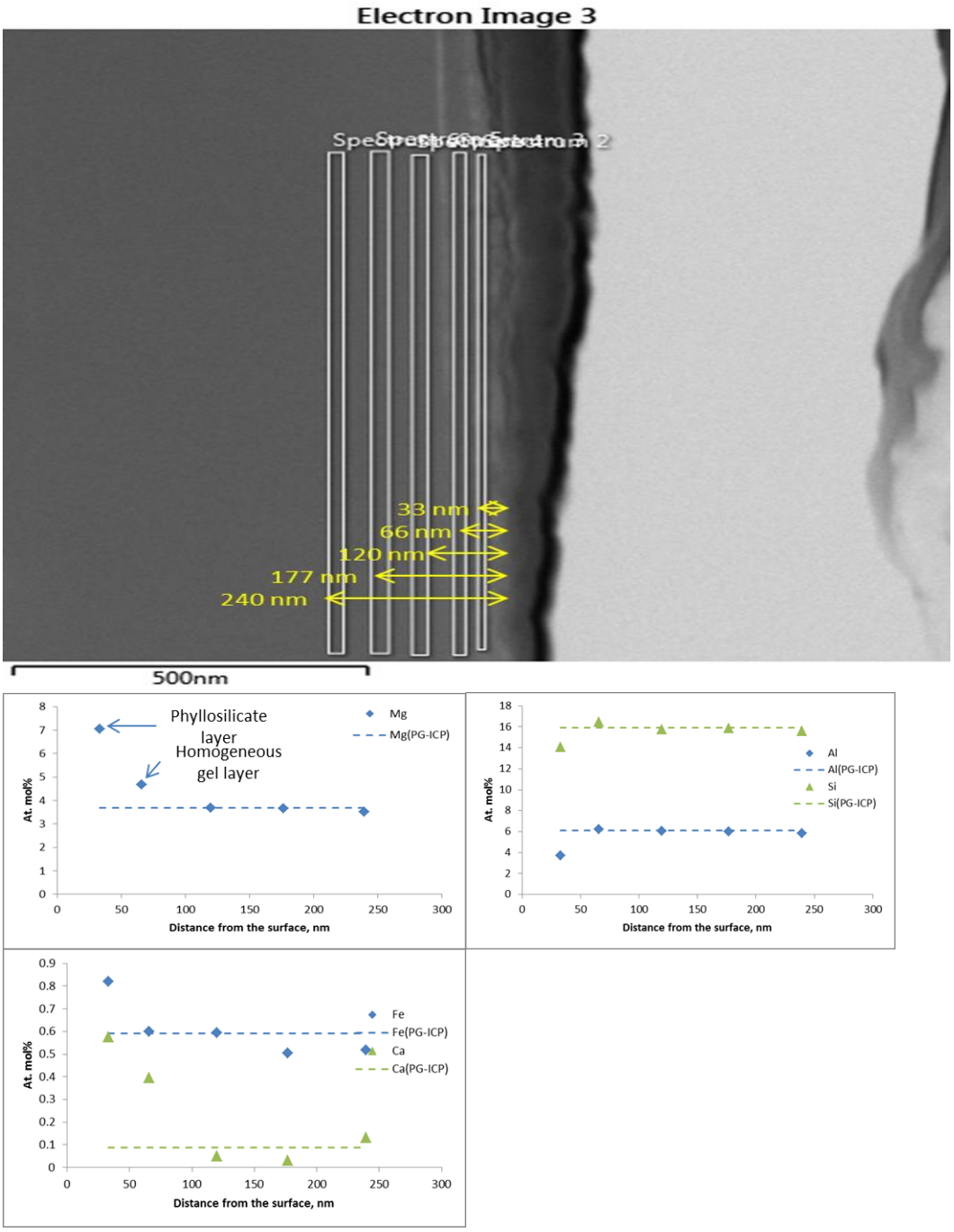

Figure A2- 9 STEM-EDX analysis of a micro-section of AVM10 sample altered at 50°C and 95% RH for 557 days; The analyzed zones are marked as rectangle in the top image. The distance from the glass surface-resin interface to the zone analyzed is marked in the image and the analyzed compositions are presented as a function of the distance from the interface on the graphs beneath. The dotted lines in the graphs represent the composition of pristine glass measured by ICP. . It can be seen that the homogeneous gel layer is enriched in Mg and Ca, with respect to the pristine glass. The relative error associated with the concentration measured by STEM-EDX analysis is at least 12%

Section 4 XRD patterns

XRD pattern of AVM6 sample altered for 180 days and 557 days at 50°C and 95% RH (AVM6-180 and AVM6-557 respectively)

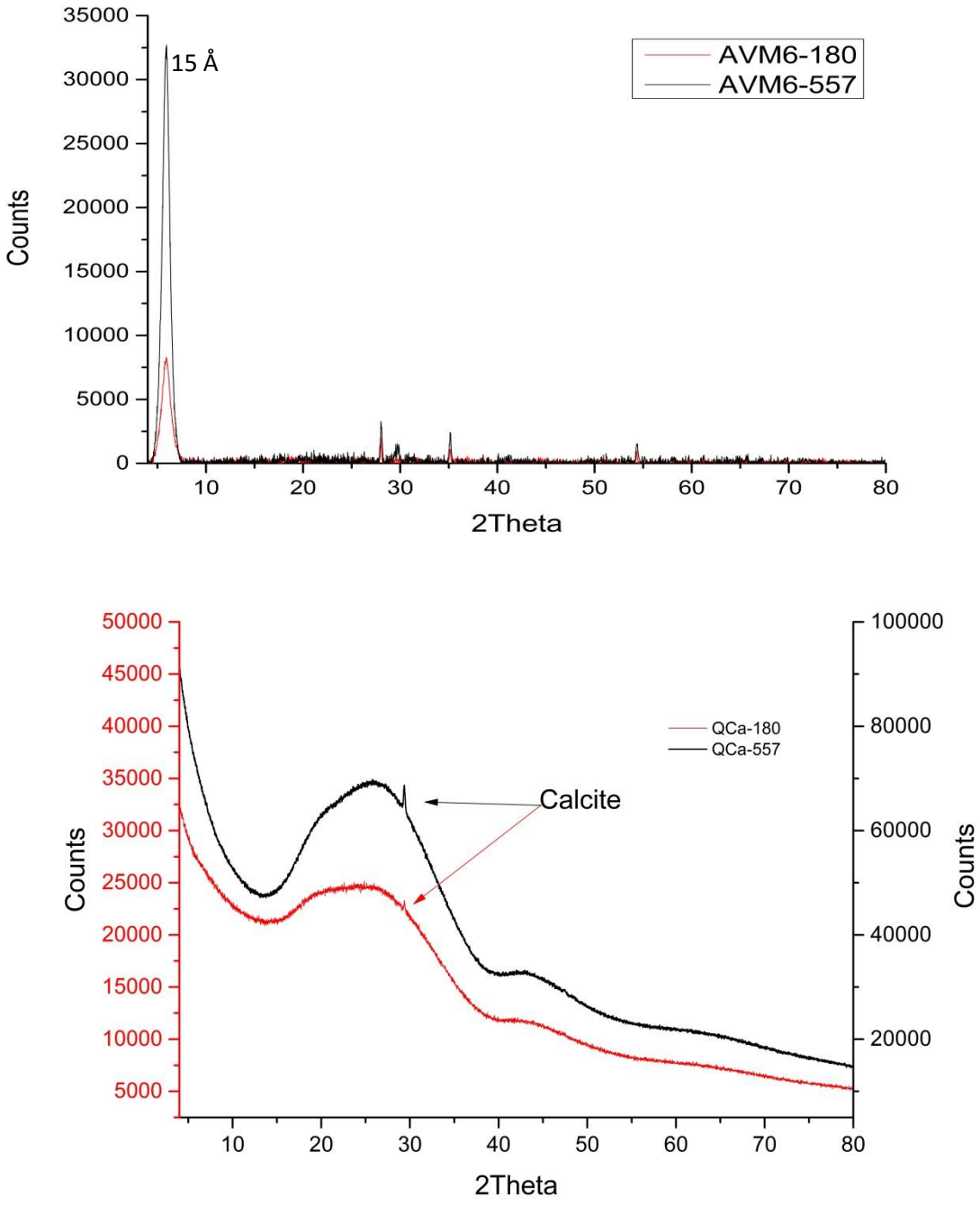

Figure A2- 10 (Top) XRD pattern of AVM6 glass altered at 50°C and 95% RH for 180 days (AVM6-180) (red line) and 557 days (AVM6-557) (black line); (Bottom) XRD pattern of QCa glass altered altered at 50°C and 95% RH for 180 days (QCa-180) (red line) and 557 days (QCa-557) (black line);

Section 5 TEM images of AVMV4

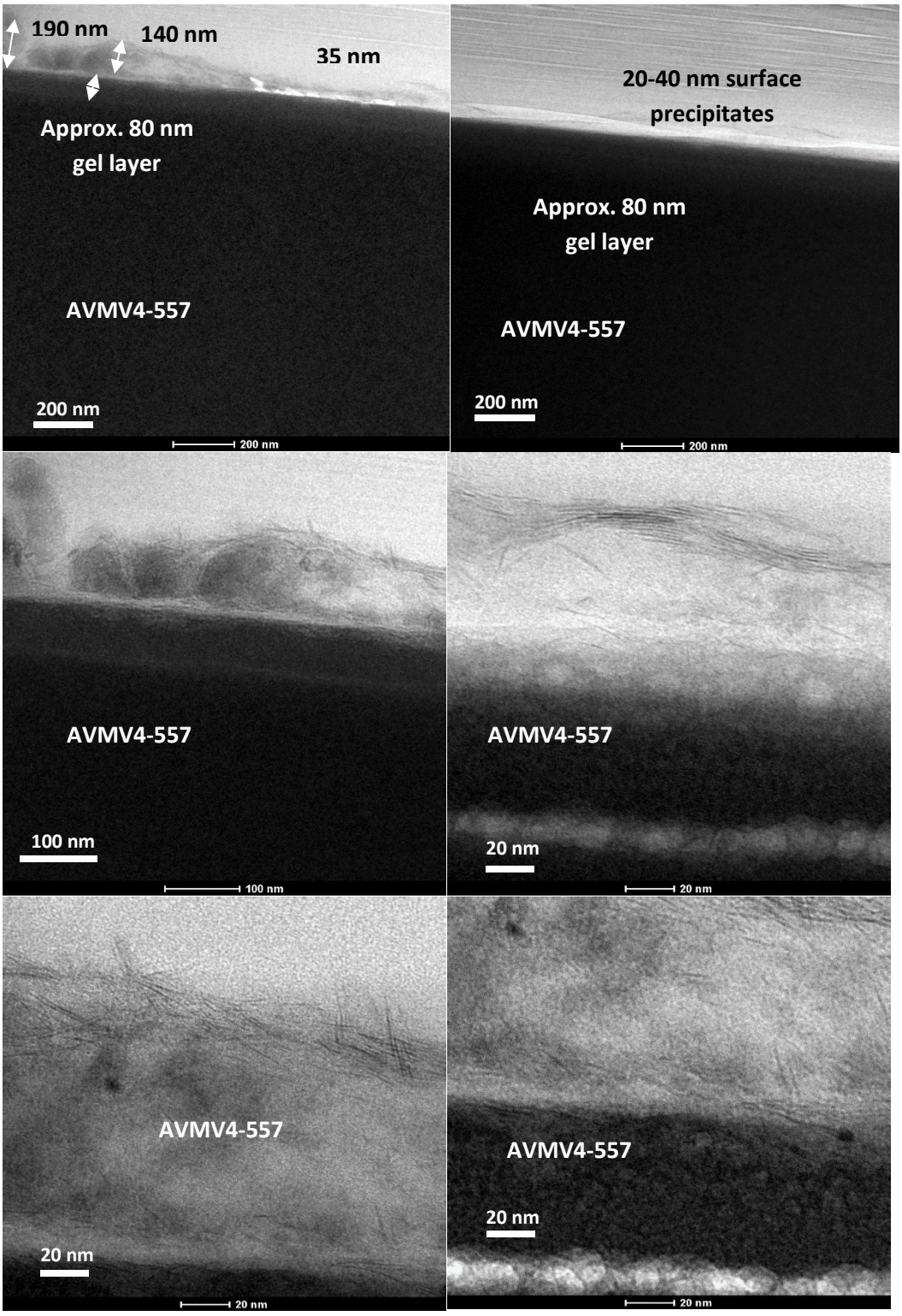

Figure A2- 11 TEM images (cross-sections) of AVMV4 sample altered at 50°C and 95% RH for 557 days

Section 6 STEM-EDX analysis of QMg

Altered layer composition of QMg-180 (STEM-EDX) (Analysis done by C. Le Guillou from University of Lille, France)

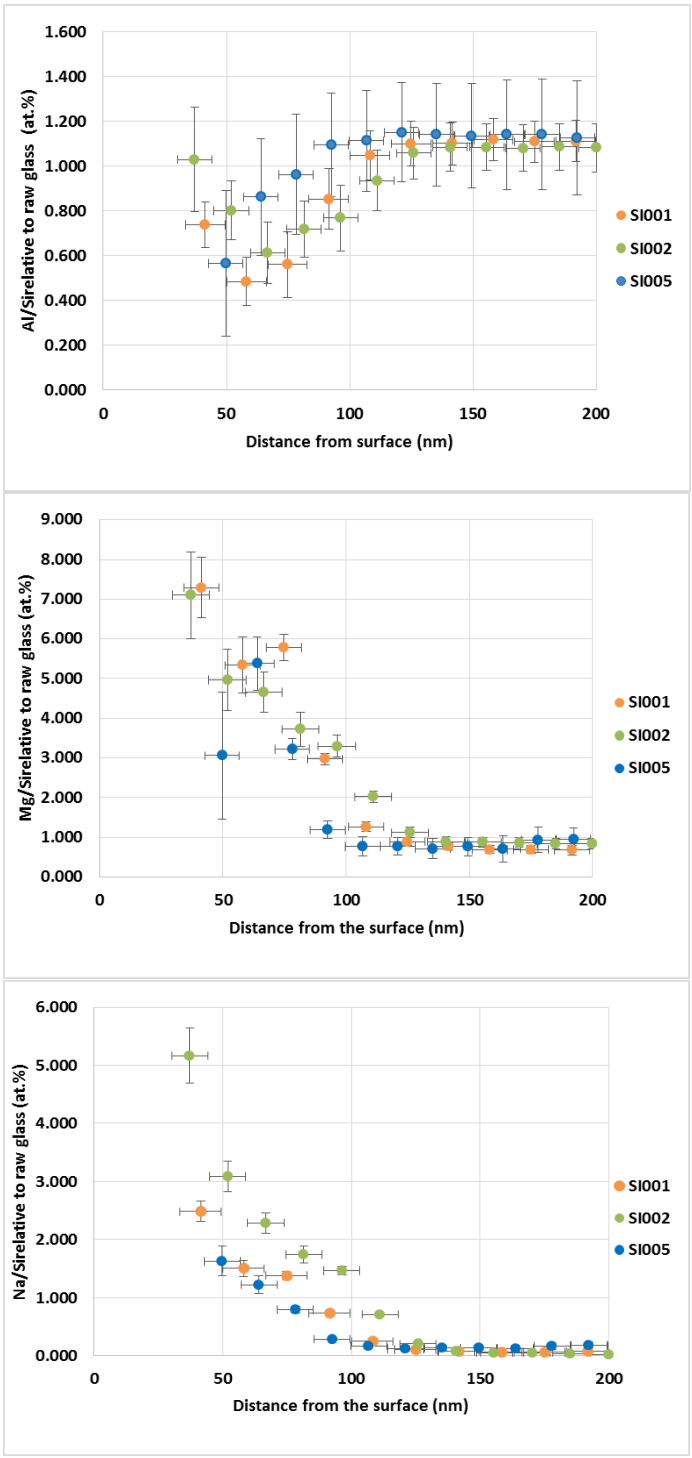

Figure A2- 12 Plots of molar ratios of Al, Mg and Na over Si as a function of distance from the surface of the sample QMg altered at 50°C and 95% RH for 180 days; SI001, SI002 and SI005 correspond to different measurements carried out at different regions of the sample micro-section.

Section 7 ToF-SIMS profiles

ToF-SIMS profiles of AVM6-180 (sample altered for 180 days at 50°C and 95% RH)

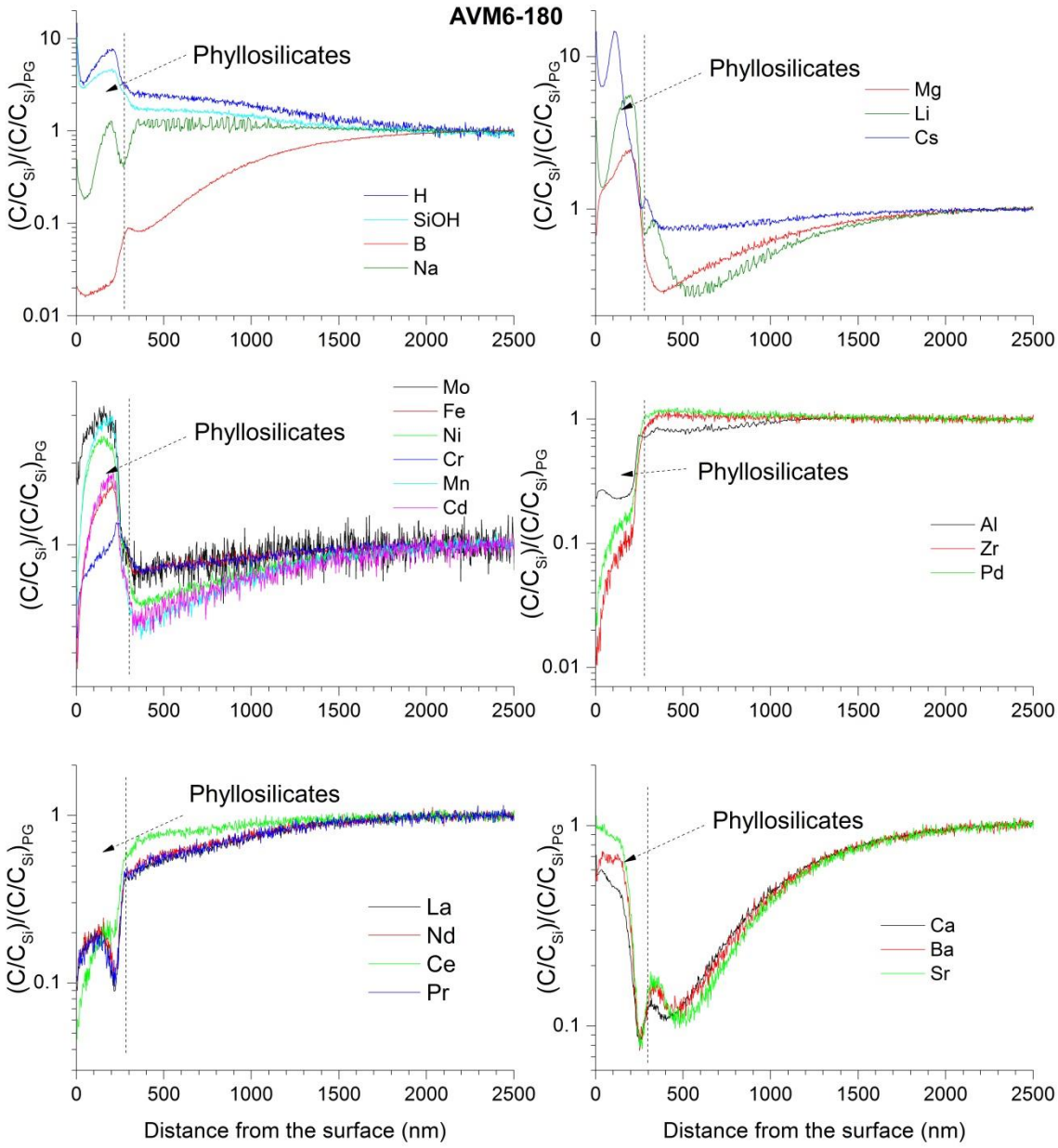

Figure A2- 13 ToF-SIMS profiles of AVM6 sample altered at 50°C and 95% RH for 180 days; the y-axis is the normalized intensity calculated from equation AA-1 in Appendix A

ToF-SIMS profiles of AVM6-557 (sample altered for 557 days at 50°C and 95% RH)

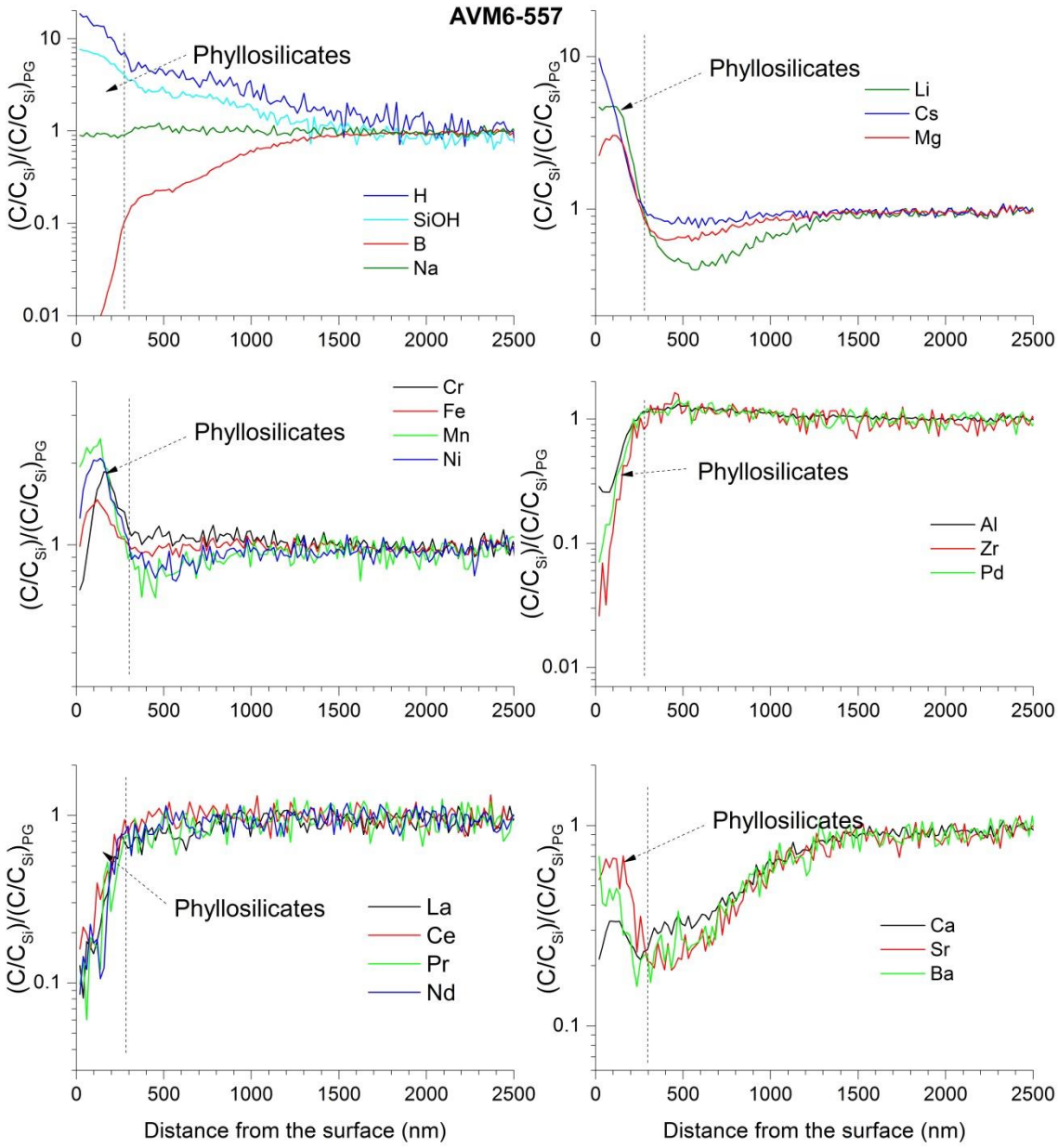

Figure A2- 14 ToF-SIMS profiles of AVM6 sample altered at 50°C and 95% RH for 557 days; the y-axis is the normalized intensity calculated from equation AA-1 in Appendix A

ToF-SIMS profiles of AVM10-180 (sample altered for 180 days at 50°C and 95% RH)

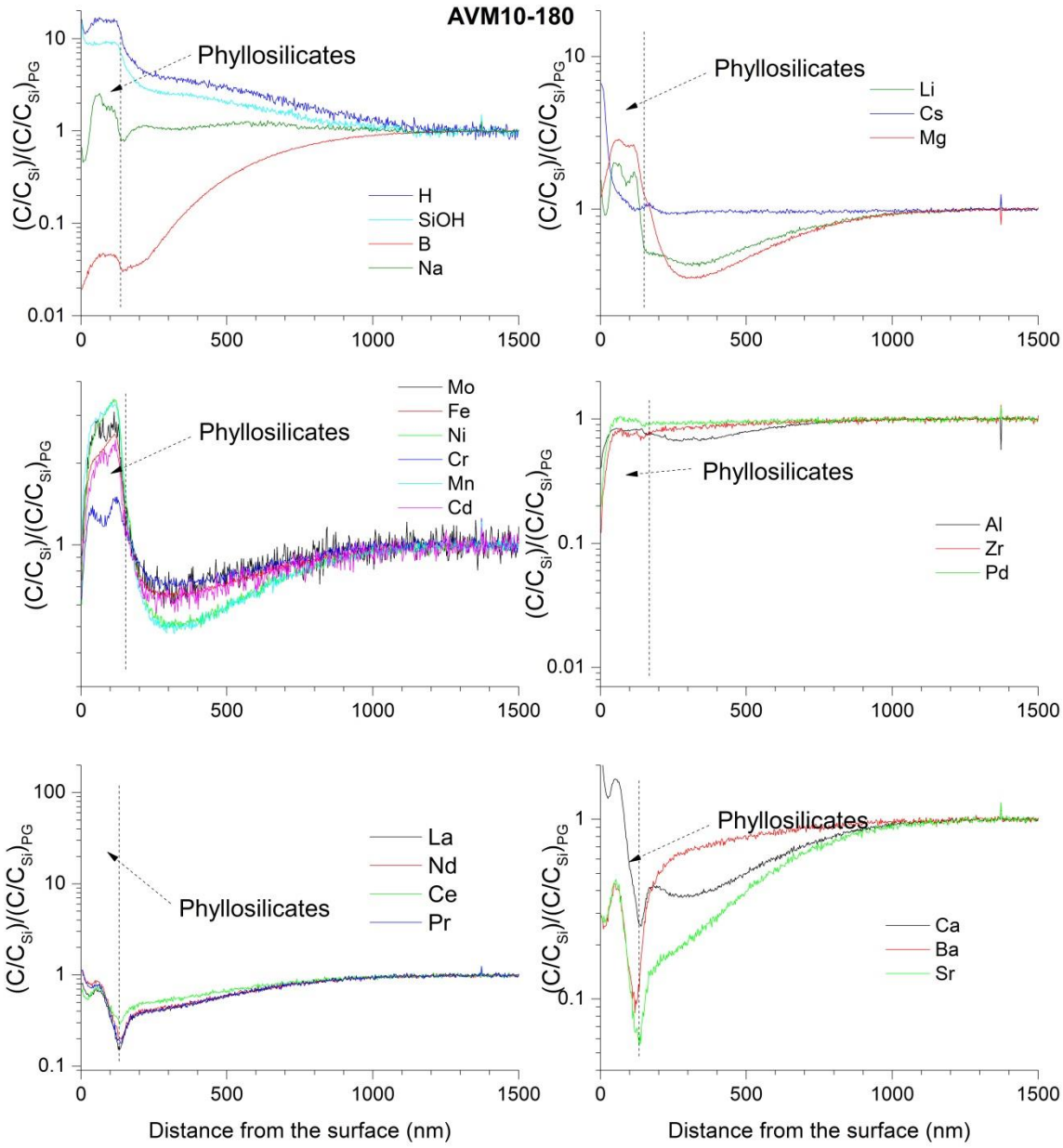

Figure A2- 15 ToF-SIMS profiles of AVM10 sample altered at 50°C and 95% RH for 180 days; the y-axis is the normalized intensity calculated from equation AA-1 in Appendix A

ToF-SIMS profiles of AVM10-557 (sample altered for 557 days at 50°C and 95% RH)

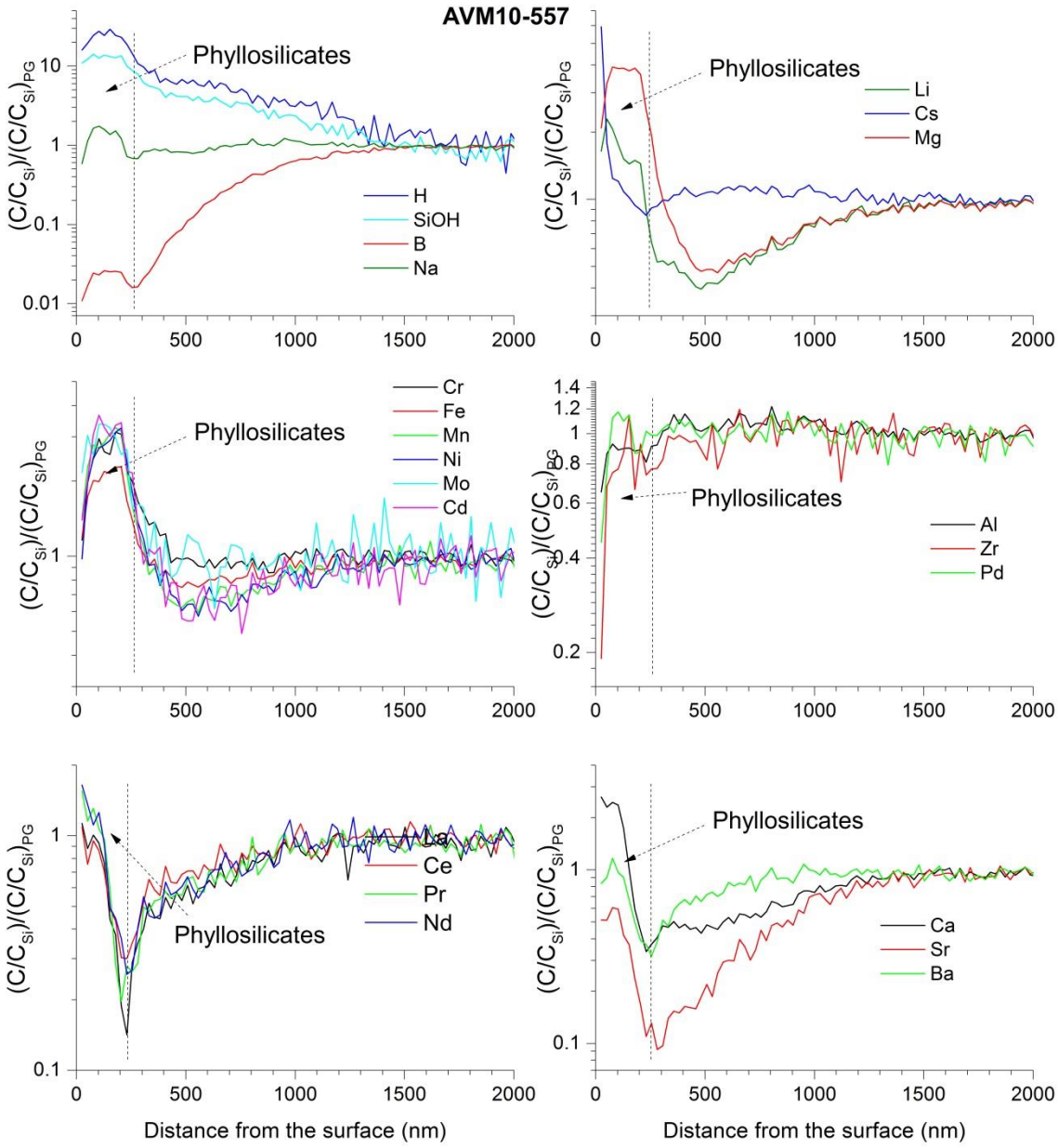

Figure A2- 16 ToF-SIMS profiles of AVM10 sample altered at 50°C and 95% RH for 557 days; the y-axis is the normalized intensity calculated from equation AA-1 in Appendix A

ToF-SIMS profiles of AVMV4-180 (sample altered for 180 days at 50°C and 95% RH)

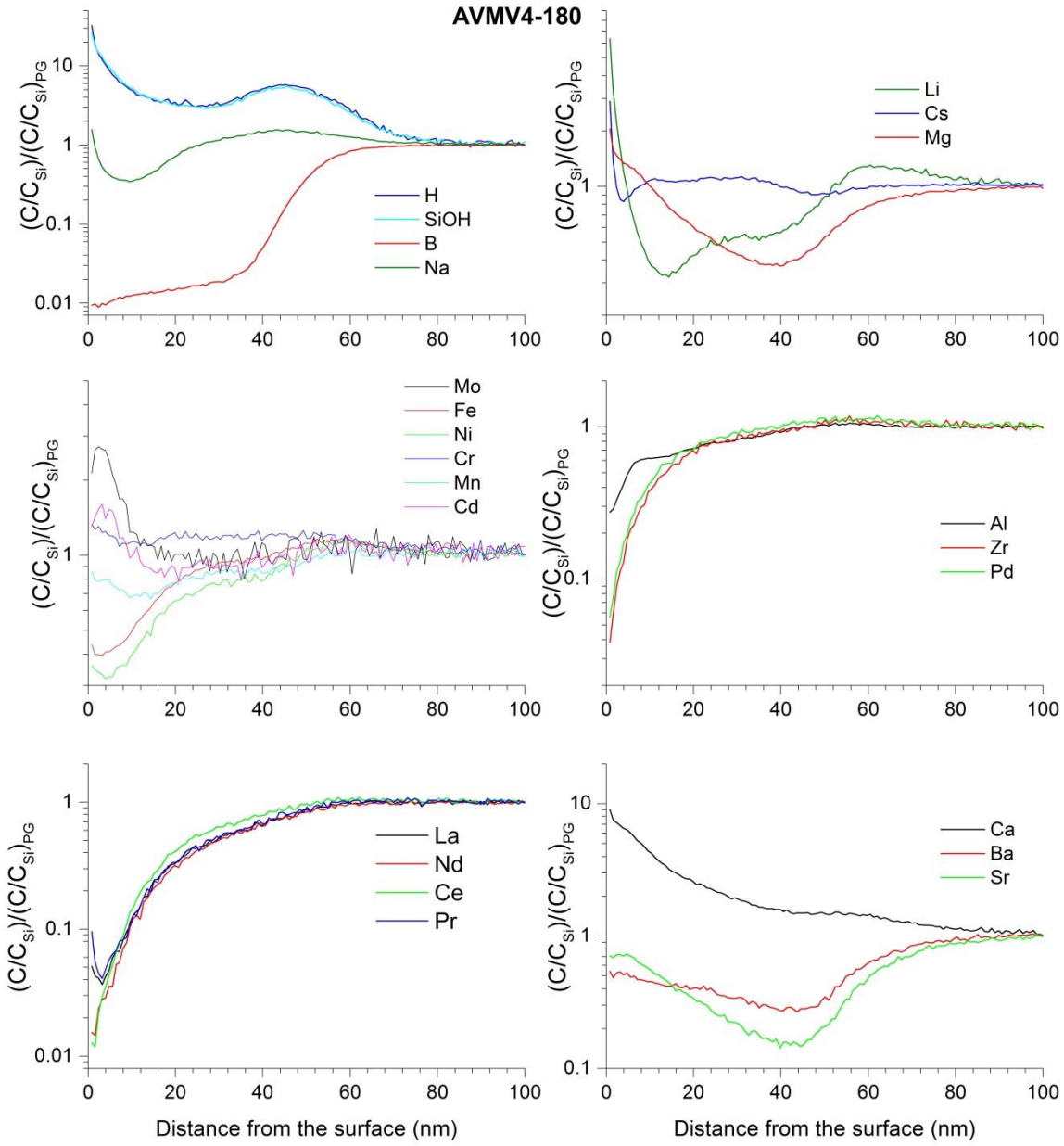

Figure A2- 17 ToF-SIMS profiles of AVMV4 sample altered at 50°C and 95% RH for 180 days; the y-axis is the normalized intensity calculated from equation AA-1 in Appendix A

ToF-SIMS profiles of AVMV4-557 (sample altered for 557 days at 50°C and 95% RH)

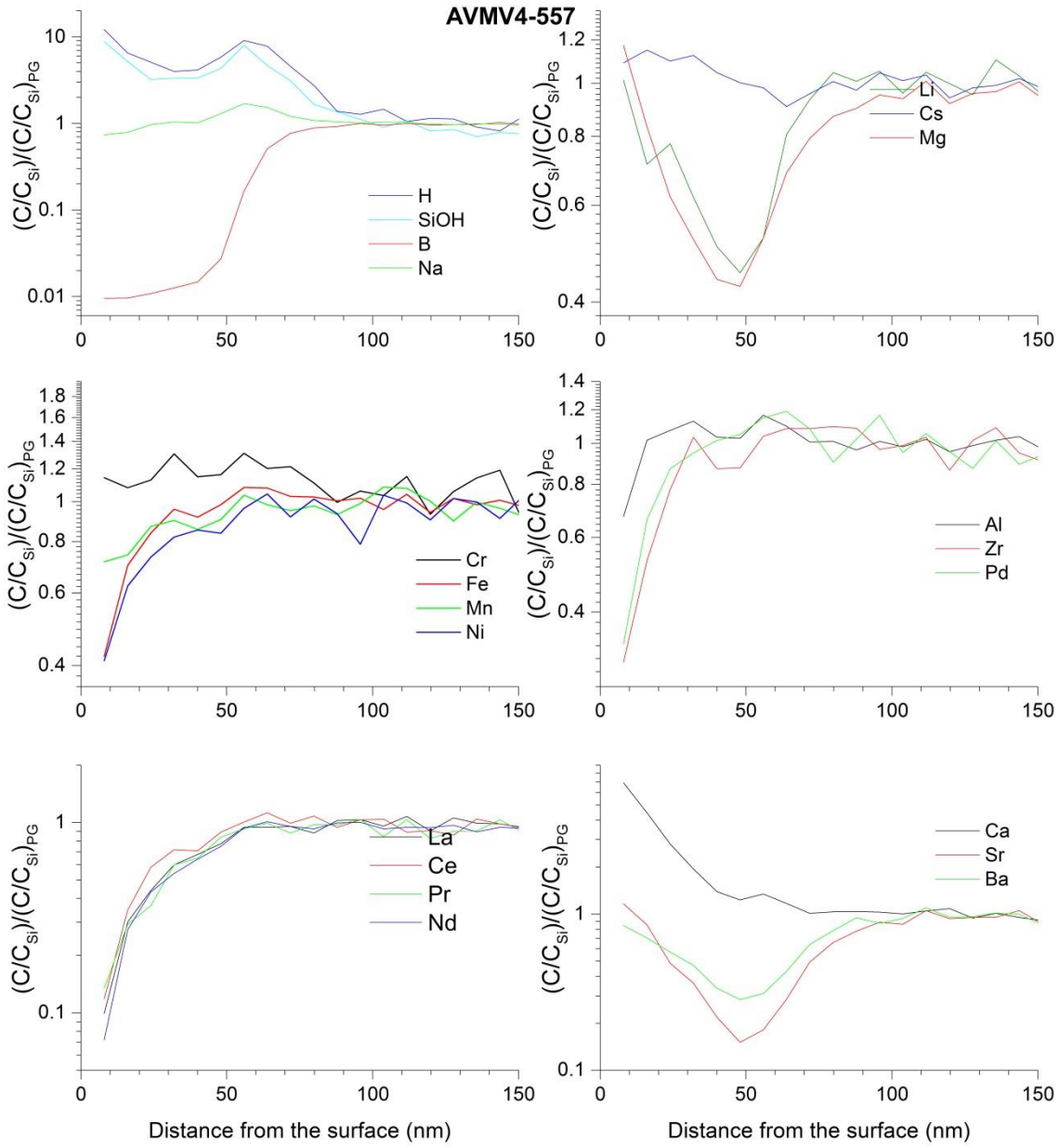

Figure A2- 18 ToF-SIMS profiles of AVMV4 sample altered at 50°C and 95% RH for 557 days; The y-axis is the normalized intensity calculated from equation AA-1 in Appendix A

ToF-SIMS profiles of Q, QCa and QMg altered for 180 days and 557 days at 50°C and 95% RH (Q-180, QCa-180, QMg-180, Q-557, QCa-557 and QMg-557 respectively)

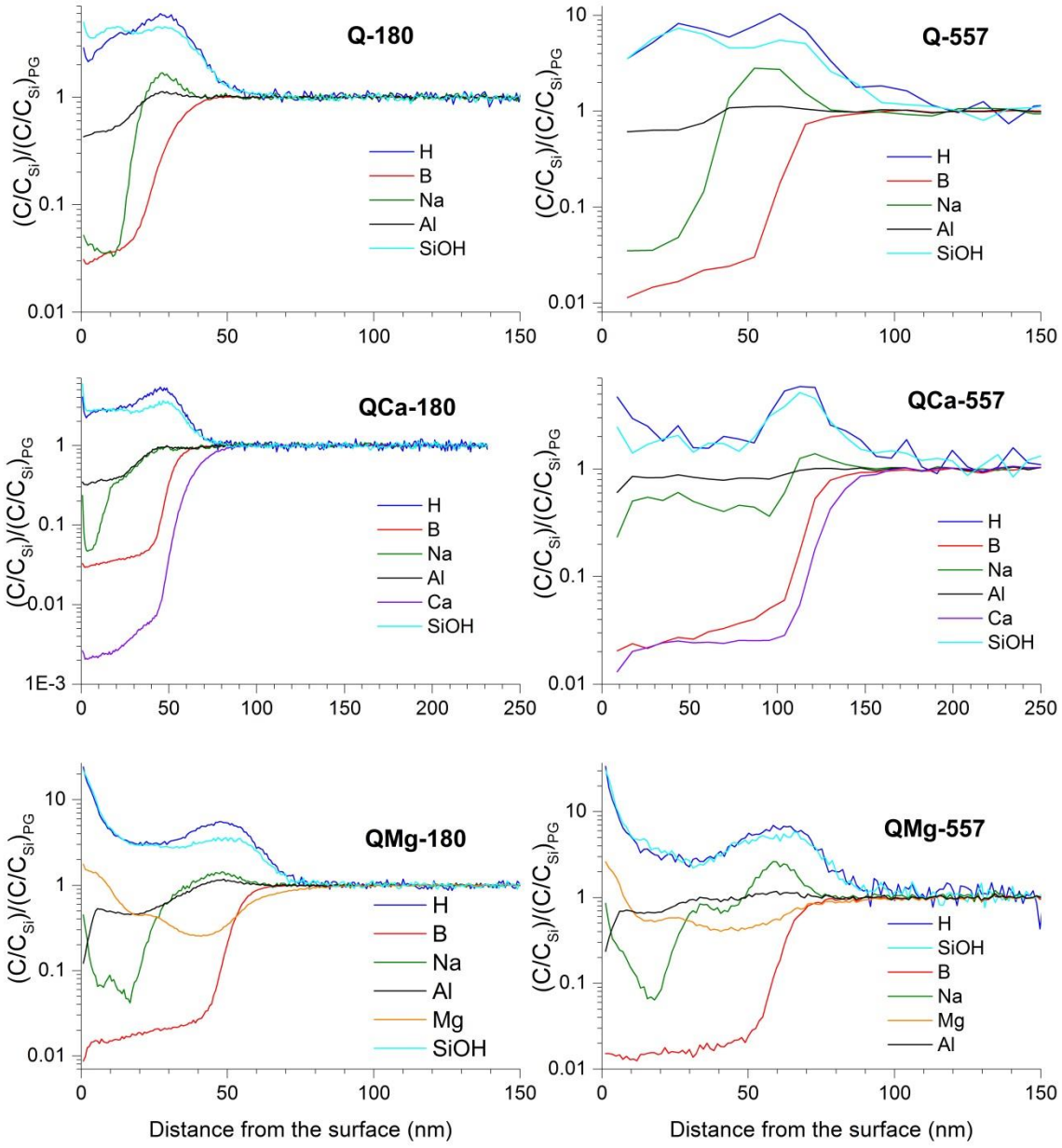

Figure A2- 19 ToF-SIMS profiles of Q, QCa and QMg altered for 180 days and 557 days at 50°C and 95% RH (Q-180, QCa-180, QMg-180, Q-557, QCa-557 and QMg-557 respectively); The y-axis is the normalized intensity calculated from equation AA-1 in Appendix A

A comparison of the ToF-SIMS profiles of Na, Mg, Al , B and H of the glasses AVMV4 and QMg altered for 180 days to show the similarity in their behavior

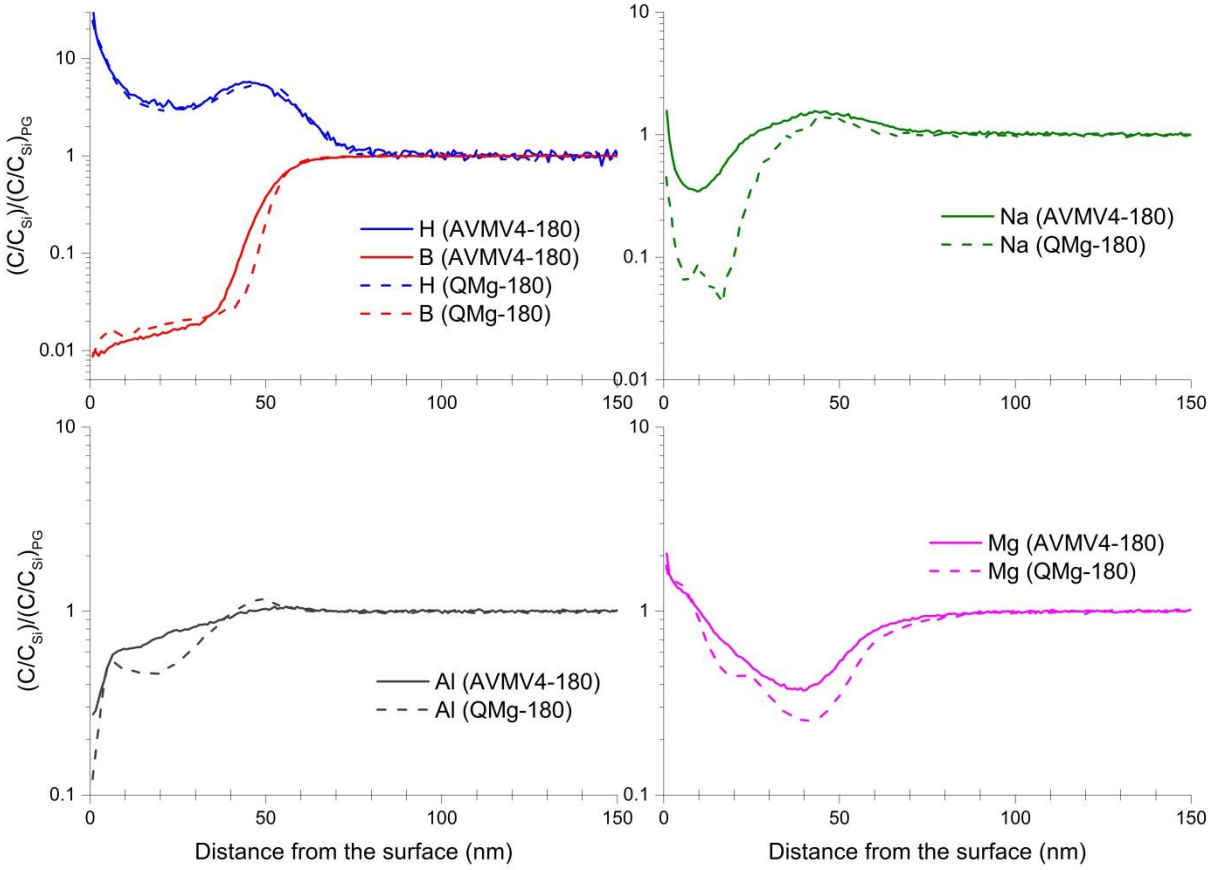

Figure A2- 20 ToF-SIMS profiles of the elements H, B, Na, Al and Mg in the samples of AVMV4 and QMg, altered at 50°C and 95% RH for 180 days

Section 8 SAXS diagrams

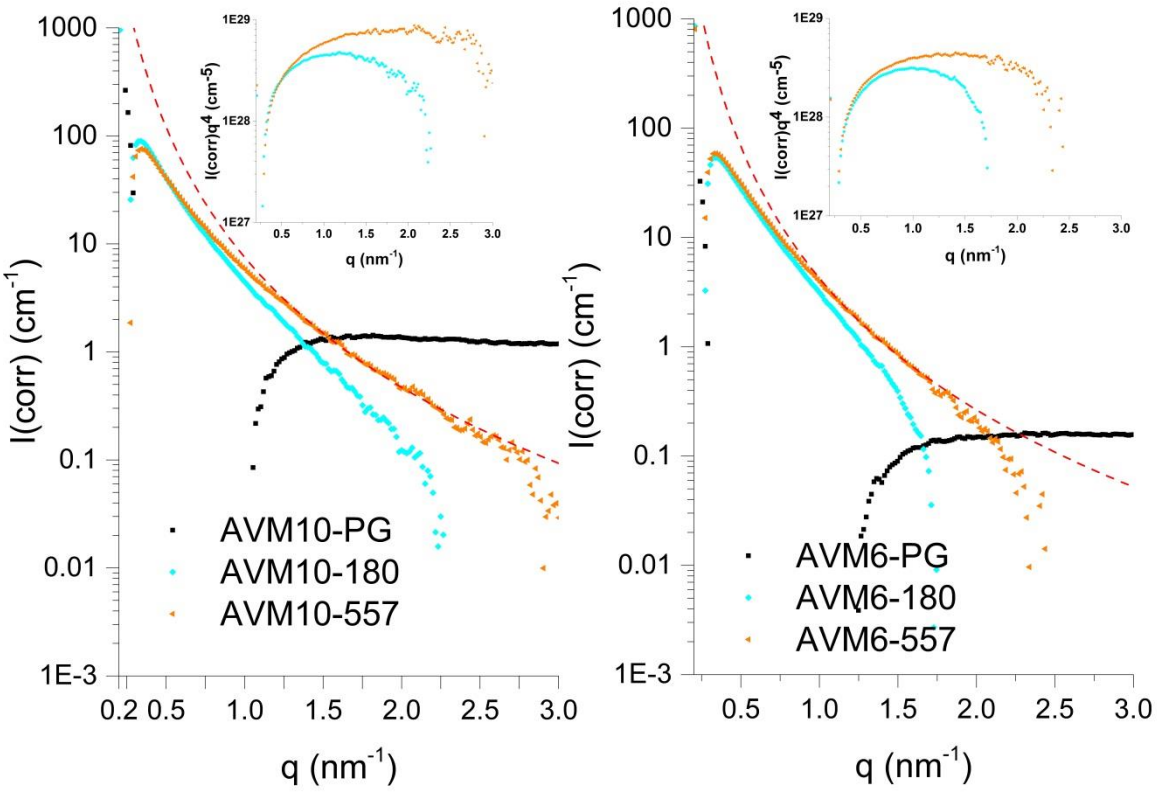

Figure A2- 21 SAXS diagrams of AVM10 (left) and AVM6 (right) glass powders that were altered at 50°C and 95% RH for 180 days (AVM10-180 and AVM6-180) and 557 days (AVM10-557 and AVM6-557); AVM10-PG and AVM6-PG signify the SAXS diagrams of pristine glasses. I(corr) is a result of the data treatment used to separate the intensity scattered by the grain envelopes and the intensity scattered by the inner pores of the gel layer; The red dotted lines represent the $I \alpha q^{-4}$ relation

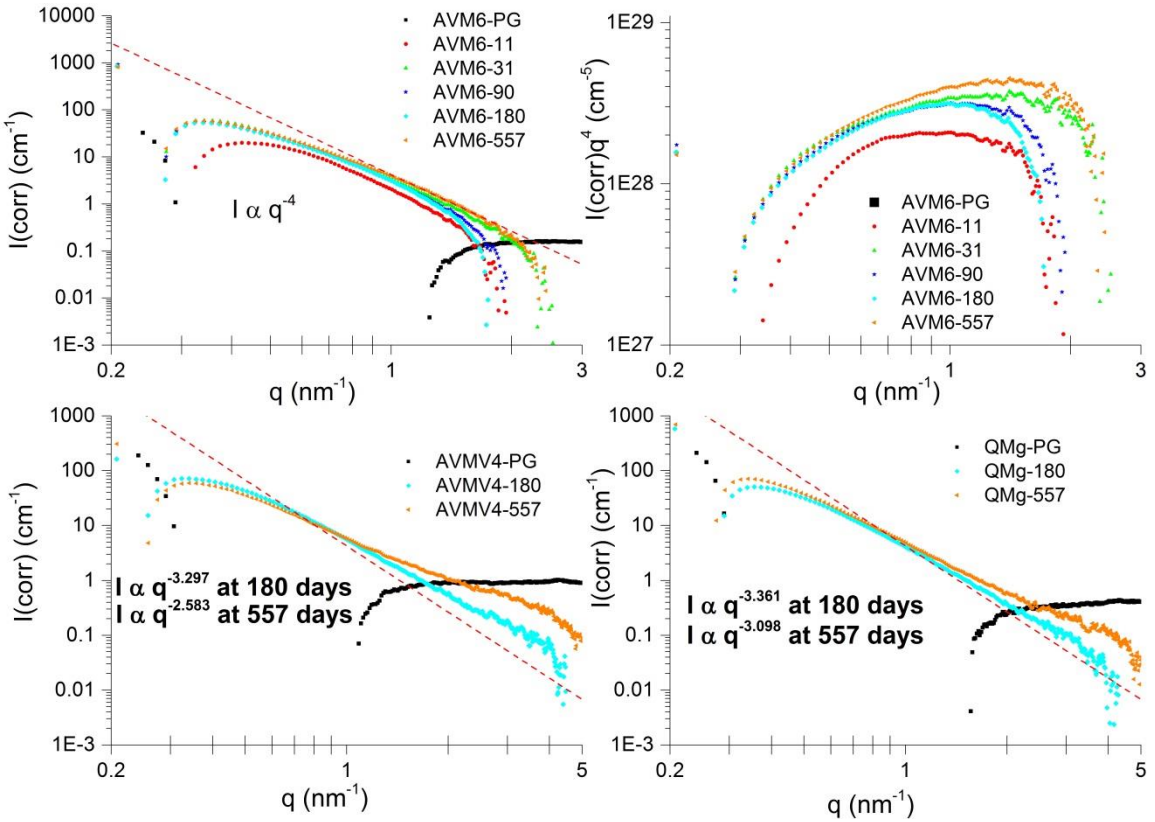

Figure A2- 22 (Top) SAXS diagrams of AVM6 glass powders altered at 50°C and 95%RH for 11 days, 31 days, 90 days, 180 days and 557 days (AVM6-11, AVM6-31, AVM6-90, AVM6-180 and AVM6-557) to study the evolution of porosity of the altered layer over time; (bottom) SAXS diagrams of AVMV4 (left) and QMg (right) glass powders that were altered at 50°C and 95% RH for 180 days (AVMV4-180 and QMg-180) and 557 days (AVMV4-557 and QMg-557); AVMV4-PG and QMg-PG signify the SAXS diagrams of pristine glasses. I(corr) is a result of the data treatment used to separate the intensity scattered by the grain envelopes and the intensity scattered by the inner pores of the gel layer; The red dotted lines represent the relation I α q^{-4}

Calculation of a theoretical porosity

$$Theoretical\ porosity = \sum_{i=B,Na,Ca,Mg,..}(\emptyset_i - (R_{ToF-SIMS} * \emptyset_i)) \qquad \text{Equation A2-13}$$

$$\emptyset_i = \frac{x_i * no.of\ oxygen\ atoms\ per\ cation}{\sum_{j=Si,B,Na,Al,Ca,Mg\ etc.} x_j * no.of\ oxygen\ atoms\ per\ cation} \qquad \text{Equation A2-14}$$

x_i is the mol fraction of oxide in the pristine glass.

Table A2- 1 Calculated theoretical porosity values

	AVM6	AVM10	AVMV4	Q	QCa	QMg
Theoretical porosity-180 days	0.17	0.19	0.22	0.17	0.25	0.23
Theoretical porosity-557 days	0.13	0.17	0.18	0.14	0.21	0.17

Section 9 Relation between thickness of altered layer and NBO fraction

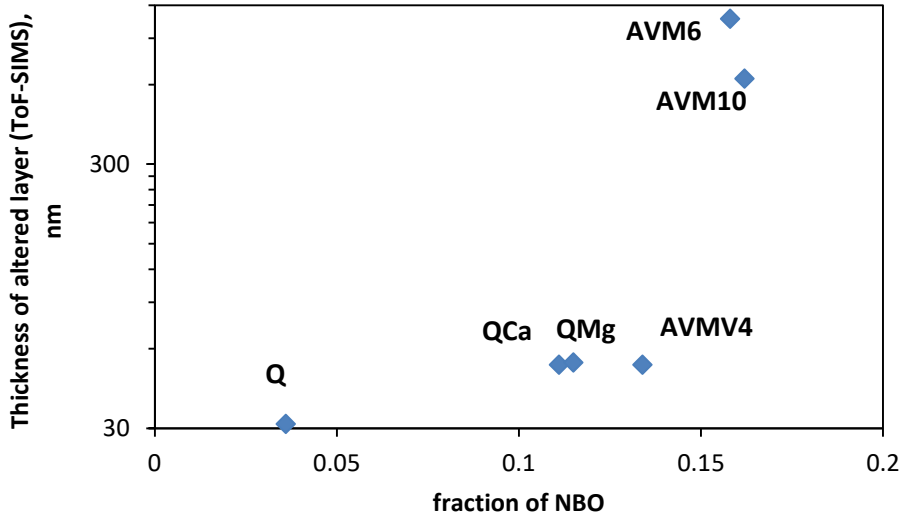

Figure A2- 23 Thickness of the altered layer formed on the six glasses after vapor hydration at 50°C and 95% RH for 180 days plotted as a function of the fraction of non-bridging oxygen atoms (NBO) in the pristine glass structure. Although the evolution is not linear, it is noticeable that the thickness of the altered layer varies significantly with the fraction of NBO.

The correlation shown in figure A2-23 indicates that the vapor hydration mechanism could be network hydrolysis. The plot of the thickness of the altered layer formed on the six glasses after vapor hydration at 50°C and 95% RH for 557 days as a function of the NBO fraction does not seem to indicate any correlation. This attests to the conclusion that the vapor hydration mechanism changes with time.

Section 10 Composition of the gel layer

Composition of the gel layer formed during vapor hydration at 50°C and 95% RH for 180 days

Retention factors of elements in the gel layer are estimated from ToF-SIMS analysis. After normalization of the ToF-SIMS profiles using equation AA-1 in appendix 2, the average of the normalized intensity values in the region considered to be as gel is taken as the retention factor of the element in the gel. Therefore, if the retention factor is 1, this means the same number of atoms is present in the gel layer and the pristine glass. If the retention factor is 0.4, for example, then 40% of the number of atoms in the pristine glass is present in the gel layer.

Table A2- 2 Retention factors of elements in the gel layer formed in vapor phase alteration at 50°C and 95% RH (calculated from ToF-SIMS profiles)

	Retention factors-180 days					
	AVM6	**AVM10**	**AVMV4**	**Q**	**QCa**	**QMg**
Si	1	1	1	1	1	1
Al	0.85	0.74	0.75	0.75	0.48	0.59
B	0.22	0.2	0.018	0.12	0.04	0.02
Na	1	1	0.86	0.62	0.36	0.39
Ca	0.23	0.45	1		0.003	
Li	0.42	0.51	1			
Zr	1	0.88	0.69			
Fe	0.85	0.7	0.77			
Ni	0.69	0.57	0.64			
Cr	0.85	0.75	1			
P		1	1			
Sr	0.2	0.31	0.33			
Y	1	1	1			
Mo	1	1	1			
Mn	0.31	0.56	0.79			
Ag	1	1	1			
Cd	1	1	1			
Te	1	1	1			
Cs	0.79	0.96	1			
Ba	0.22	0.72	0.34			
La	0.6	0.5	0.38			
Ce	0.79	0.6	0.46			
Pr	0.61	0.51	0.39			
Nd	0.63	0.52	0.36			
Ru	1	1	1			
Pd	1	1	1			
Mg	0.43	0.44	0.63			0.57

The retention factors given above are multiplied with the mole fraction of elements (excluding oxygen) in the pristine glass and then normalized to 1 in order to obtain the gel composition

Table A2- 3 Mole fraction of elements in the gel layer (excluding oxygen & after normalization);

	Normalized cation mol fr. Of elements in gel (formed during 180 days) (without oxygen)					
	AVM6	**AVM10**	**AVMV4**	**Q**	**QCa**	**QMg**
Si	0.46	0.41	0.49	0.59	0.70	0.65
Al	0.09	0.11	0.11	0.12	0.1	0.11
B	0.08	0.06	0.0061	0.04	0.02	0.01
Na	0.31	0.31	0.321	0.25	0.18	0.18
Ca	0.0005	0.001	4.4E-04		2.5E-04	
Li	0.007	0.009	8.7E-04			
Zr	0.001	0.002	0.002			
Fe	0.01	0.01	0.006			
Ni	0.002	0.001	8.4E-04			
Cr	0.003	0.003	0.002			
P		0.03	0.003			
Sr	5.3E-05	2.1E-04	1.9E-04			
Y	1.3E-04	4.1E-04	2.9E-04			
Mo	0.001	0.004	0.003			
Mn	1.2E-04	6.8E-04	8.1E-04			
Ag	2.7E-04	5.4E-04	4.4E-04			
Cd	0.002	0.002	5.8E-04			
Te	1.3E-04	2.7E-04	2.9E-04			
Cs	5.3E-04	0.002	0.001			
Ba	5.9 E-05	5.9E-04	2 E-04			
La	2.4E-04	6.1E-04	3.9E-04			
Ce	3.2E-04	7.3E-04	4.7E-04			
Pr	8.2 E-05	2.8E-04	1.7E-04			
Nd	4.2E-04	9.9E-04	0.001			
Ru	6.7E--04	0.002	0.002			
Pd	5.4E-04	0.001	0.001			
Mg	0.03	0.04	0.05			0.04

Table A2- 4 Mole fraction of oxides in the gel layer formed in vapor phase at 50°C and 95% RH

	Normalized Mol fr. Of oxides in gel (formed during 180 days)					
	AVM6	**AVM10**	**AVMV4**	**Q**	**QCa**	**QMg**
SiO2	0.62	0.55	0.63	0.74	0.83	0.77
Al2O3	0.062	0.08	0.07	0.08	0.06	0.07
B2O3	0.052	0.04	0.004	0.02	0.009	0.004
Na2O	0.21	0.21	0.21	0.15	0.11	0.11
CaO	0.001	0.001	0.001		2.9E-04	
Li2O	0.005	0.006	0.001			
ZrO2	0.002	0.003	0.002			
Fe2O3	0.009	0.007	0.004			
NiO	0.002	0.002	0.001			
Cr2O3	0.002	0.002	0.001			
P2O5		0.02	0.002			
SrO	7.2E-05	2.8E-04	2.5E-04			
Y2O3	7.9E-05	2.5E-04	1.7E-04			
MoO3	0.002	0.005	3.8E-04			
MnO	1.7E-04	0.00	0.001			
Ag2O	1.8E-04	3.7E-04	2.8E-04			
CdO	0.003	0.003	0.001			
TeO2	1.8E-04	3.7E-04	3.8E-04			
Cs2O	3.6E-04	0.001	0.001			
BaO	7.9E-05	0.001	2.6E-04			
La2O3	1.6E-04	4.2E-04	2.5E-04			
Ce2O3	2.1E-04	0.001	3.0E-04			
Pr2O3	5.5E-05	1.9E-04	1.1E-04			
Nd2O3	2.8E-04	0.001	0.001			
RuO2	0.001	0.003	0.002			
PdO	0.001	0.002	0.00			
MgO	0.03	0.06	0.06			0.05

Composition of the gel layer formed during vapor hydration at 50°C and 95% RH for 557 days

Table A2- 5 Retention factors of elements in the gel layer formed in vapor phase alteration at 50°C and 95% RH for 557 days (calculated from ToF-SIMS profiles)

	Retention factors-557 days					
	AVM6	**AVM10**	**AVMV4**	**Q**	**QCa**	**QMg**
Si	1	1	1	1	1	1
Al	1	1	1	0.88	0.84	0.9
B	0.3	0.2	0.07	0.09	0.06	0.04
Na	1	0.9	1	1	0.57	0.87
Ca	0.37	0.51	1		0.03	
Li	0.48	0.51	0.64			
Zr	1	0.97	0.83			
Fe	0.97	0.85	0.89			
Ni	0.87	0.78	0.79			
Cr	1	1	1			
P		1	1			
Sr	0.3	0.28	0.42			
Y	1	1	1			
Mo	1	1	1			
Mn	0.83	0.77	0.88			
Ag	1	1	1			
Cd	1	1	1			
Te	1	1	1			
Cs	0.85	1	1			
Ba	0.33	0.74	0.47			
La	0.8	0.61	0.6			
Ce	1	0.7	0.7			
Pr	0.84	0.63	0.6			
Nd	0.89	0.64	0.59			
Ru	1	1	1			
Pd	1	1	1			
Mg	0.7	0.65	0.61			0.55

Table A2- 6 Mole fraction of elements in the gel layer (excluding oxygen & after normalization);

	Normalized cation mol fr. Of elements in gel (formed during 557 days) (without oxygen)					
	AVM6	**AVM10**	**AVMV4**	**Q**	**QCa**	**QMg**
Si	0.43	0.39	0.44	0.51	0.59	0.51
Al	0.10	0.15	0.13	0.13	0.14	0.13
B	0.1	0.06	0.02	0.02	0.02	0.01
Na	0.29	0.27	0.34	0.34	0.24	0.32
Ca	0.001	0.001	3.9E-04		0.002	
Li	0.008	0.008	0.001			
Zr	0.001	0.003	0.002			
Fe	0.01	0.01	0.006			
Ni	0.002	0.002	0.001			
Cr	0.004	0.004	0.002			
P		0.03	0.003			
Sr	7.5E-05	1.8E-04	2.2E-04			
Y	1.3E-04	3.9E-04	2.6E-04			
Mo	0.001	0.004	0.003			
Mn	3.1E-04	0.001	0.001			
Ag	2.5E-04	0.001	3.9E-04			
Cd	0.002	0.002	0.001			
Te	1.3E-04	2.6E-04	2.6E-04			
Cs	0.001	0.002	0.001			
Ba	8.3E-05	0.001	2.5E-04			
La	3.0E-04	0.001	0.001			
Ce	3.8E-04	0.001	0.001			
Pr	1.0E-04	3.3E-04	2.4E-04			
Nd	0.001	0.001	0.002			
Ru	0.001	0.002	0.002			
Pd	0.001	0.001	0.001			
Mg	0.04	0.06	0.04			0.03

Table A2- 7 Mole fraction of oxides in the gel layer formed in vapor phase at 50°C and 95% RH

	Normalized Mol fr. Of oxides in gel (formed during 557 days)					
	AVM6	**AVM10**	**AVMV4**	**Q**	**QCa**	**QMg**
SiO2	0.58	0.53	0.59	0.68	0.74	0.66
Al2O3	0.07	0.10	0.09	0.08	0.09	0.09
B2O3	0.07	0.04	0.01	0.02	0.01	0.008
Na2O	0.2	0.18	0.23	0.23	0.15	0.21
CaO	0.001	0.002	0.001		0.003	
Li2O	0.005	0.006	3.4E-04			
ZrO2	0.001	0.003	0.002			
Fe2O3	0.009	0.008	0.004			
NiO	0.003	0.003	0.001			
Cr2O3	0.002	0.003	0.001			
P2O5		0.02	0.002			
SrO	1.0E-04	2.5E-04	3.0E-04			
Y2O3	7.5E-05	2.4E-04	1.6E-04			
MoO3	0.002	0.005	0.004			
MnO	4.2E-04	0.001	0.001			
Ag2O	1.7E-04	3.6E-04	2.6E-04			
CdO	0.003	0.003	0.001			
TeO2	1.7E-04	3.6E-04	3.5E-04			
Cs2O	3.6E-04	0.001	0.001			
BaO	1.1E-04	0.001	3.3E-04			
La2O3	2.0E-04	4.9E-04	3.7E-04			
Ce2O3	2.5E-04	0.001	4.3E-04			
Pr2O3	7.1E-05	2.3E-04	1.6E-04			
Nd2O3	3.8E-04	0.001	0.001			
RuO2	0.001	0.003	0.002			
PdO	0.001	0.002	0.001			
MgO	0.05	0.08	0.05			0.04

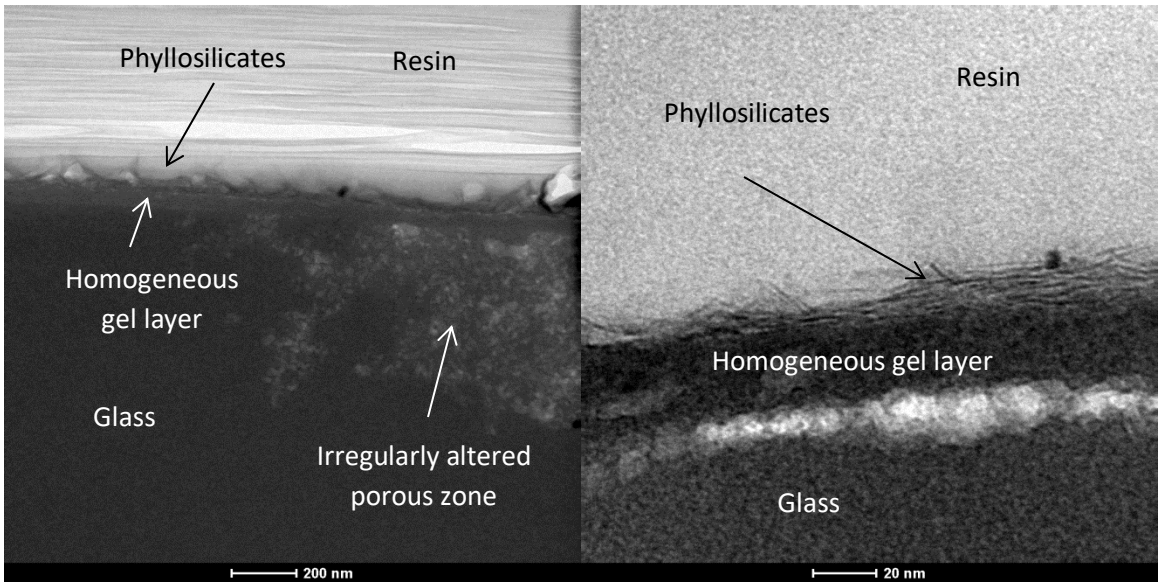

Figure A2- 24 (left) TEM image of AVM6 sample altered in vapor phase for 90 days at 50°C and 95% RH; (right) TEM image of AVMV4 sample altered in vapor phase for 90 days at 50°C and 95% RH;

Section 11 Hydration kinetics

Infrared spectra of the AVM6 samples (dimensions 2.5x2.5x0.08 cm^3) vapor hydrated at 50°C and 95% RH until 557 days:

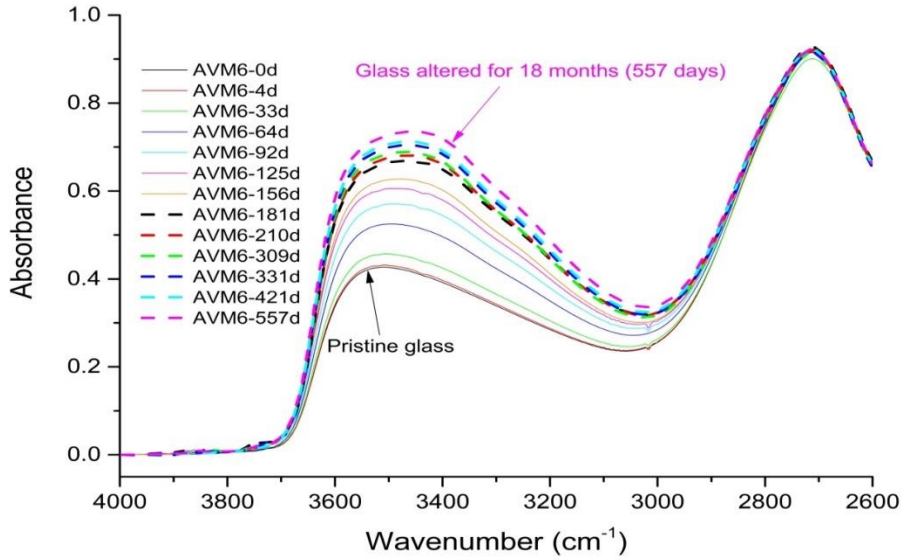

Figure A2- 25 Infrared spectra of the AVM6 glass vapor hydrated for various duration (0d indicates pristine glass, 4d indicates 4 days duration and so on) at 50°C and 95% RH

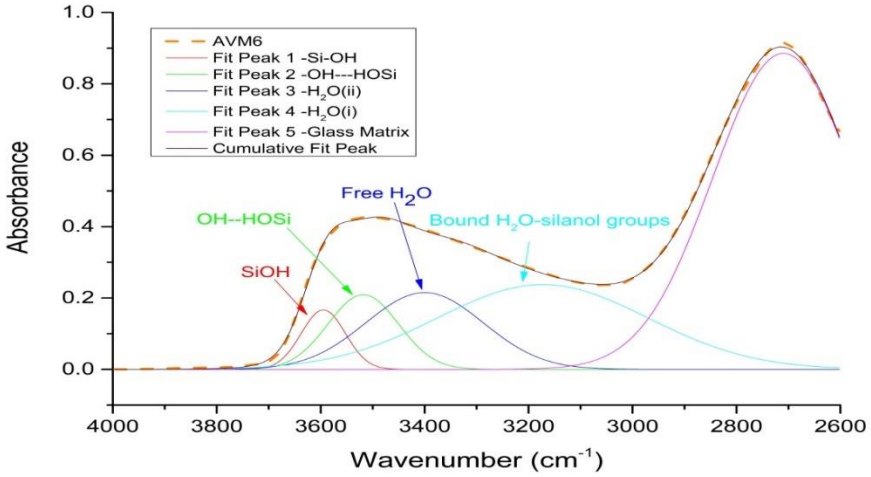

Figure A2- 26 Deconvolution of the infrared spectrum into five Gaussian bands attributed to the vibration of the OH stretching mode in SiOH molecules (3595 cm^{-1}), bound water-silanol groups (3518.14 cm^{-1} & 3172.84 cm^{-1}), symmetrical OH stretching mode in the free water molecule (3400.12 cm^{-1}) and the glass matrix (≈ 2700 cm^{-1})

Table A2- 8 Centroid of the five Gaussian bands used for deconvolution of the infrared spectra for all the six glasses (cm^{-1})

	AVM6	AVM10	AVMV4	Q	QCa	QMg
OH stretching mode in SiOH molecules	3595	3595	3595	3600	3599.84	3600.6
Bound water-silanol group	3518.14	3517	3518.3	3517	3516.16	3517
Symmetrical OH stretching mode in the free water molecule	3400.12	3400	3400	3400	3400	3400
Bound water-silanol group	3172.84	3175	3170	3170	3170	3170
Glass matrix	2709.6	2673.69	2697	2717.61	2708.99	2707.54

Evolution of the increase in absorbance of the Gaussian bands associated with stretching mode of water molecules in the deconvolution of the FTIR spectra

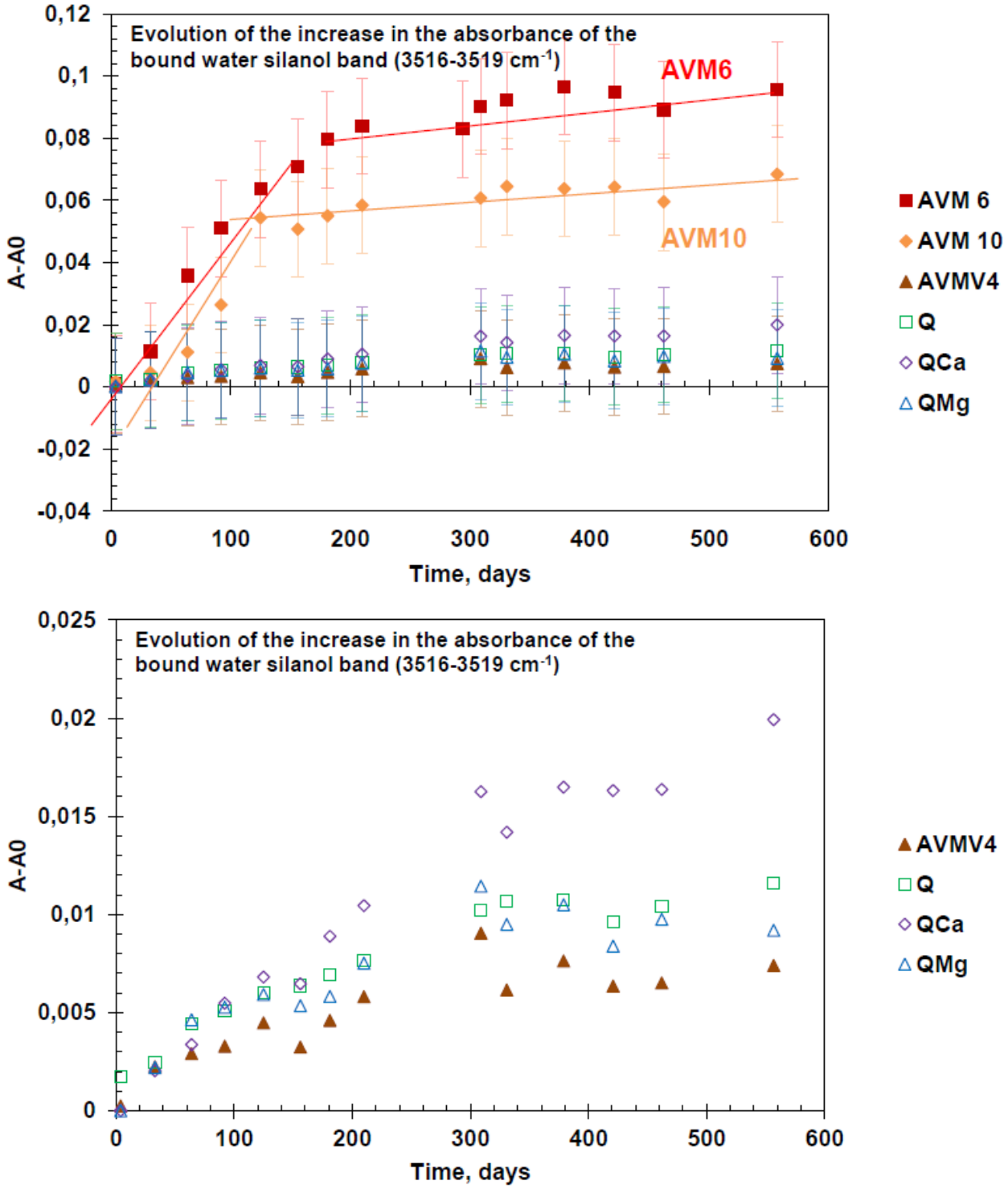

Figure A2- 27 Evolution of the increase in the absorbance of the bound water silanol band (3516-3519 cm^{-1})

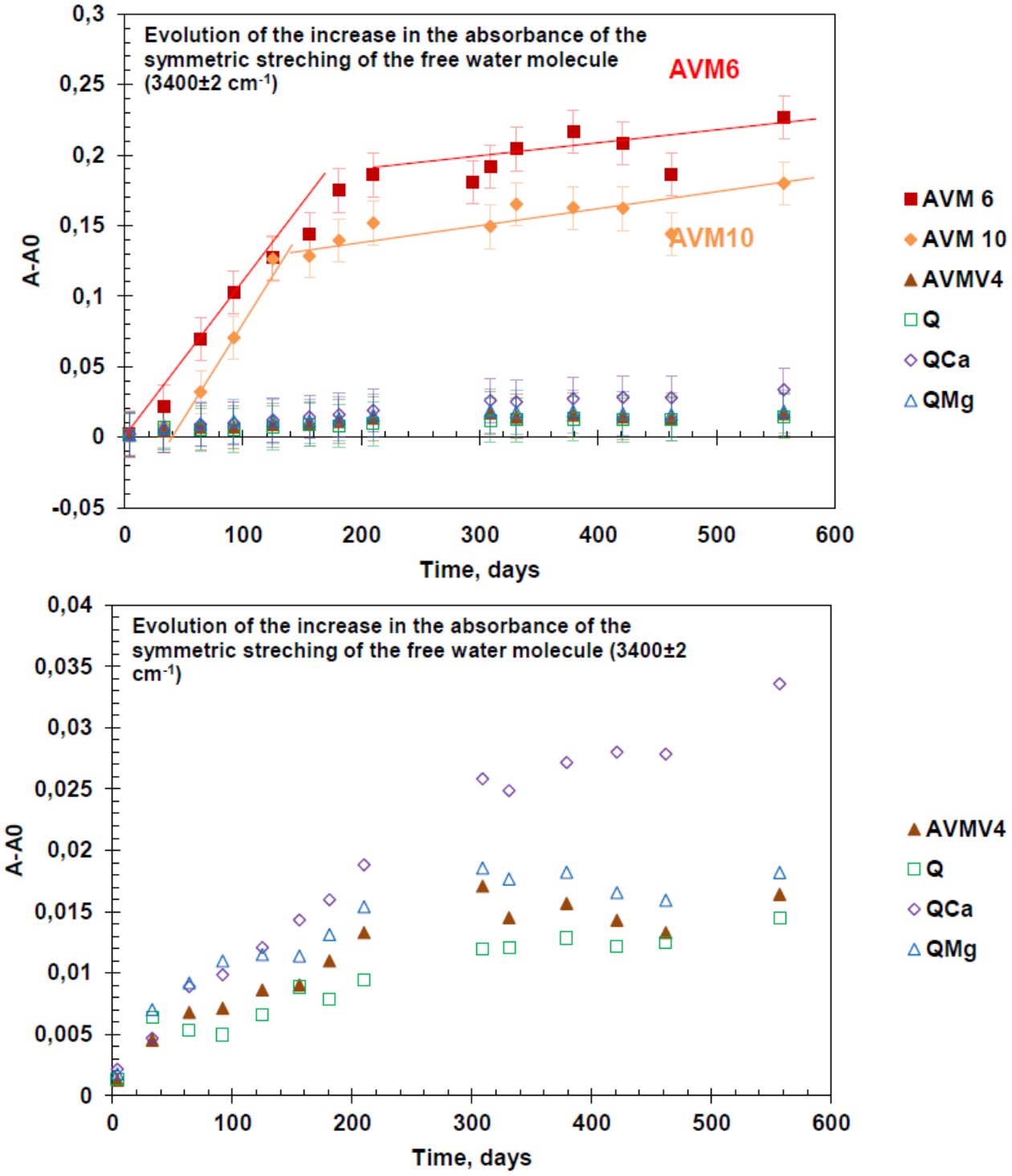

Figure A2- 28 Evolution of the increase in the absorbance of the symmetric stretching of the free water molecule (3400±2 cm^{-1})

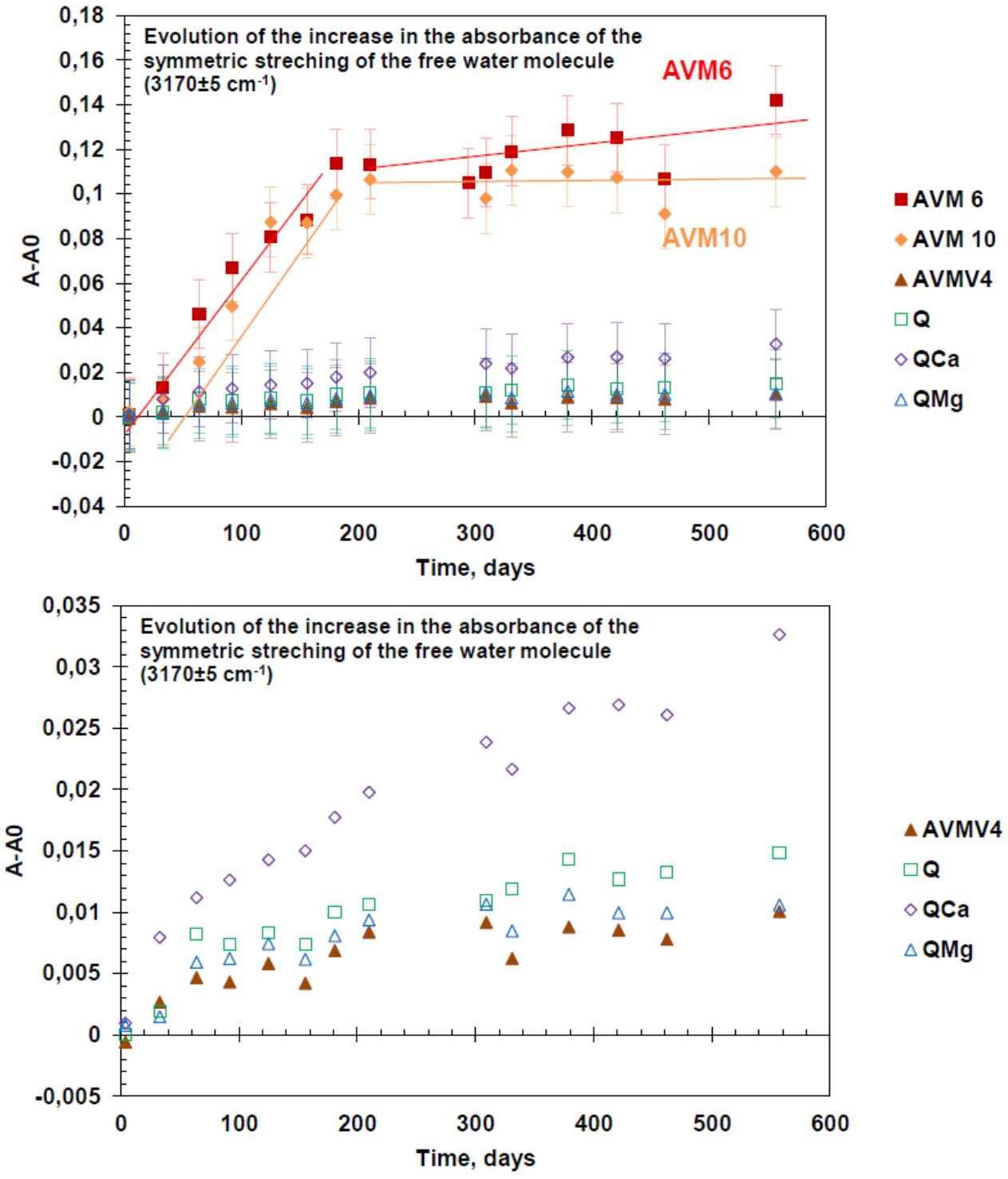

Figure A2- 29 Evolution of the increase in the absorbance of the symmetric stretching of the bound water-silanol groups (3170±5 cm^{-1})

Appendix 3

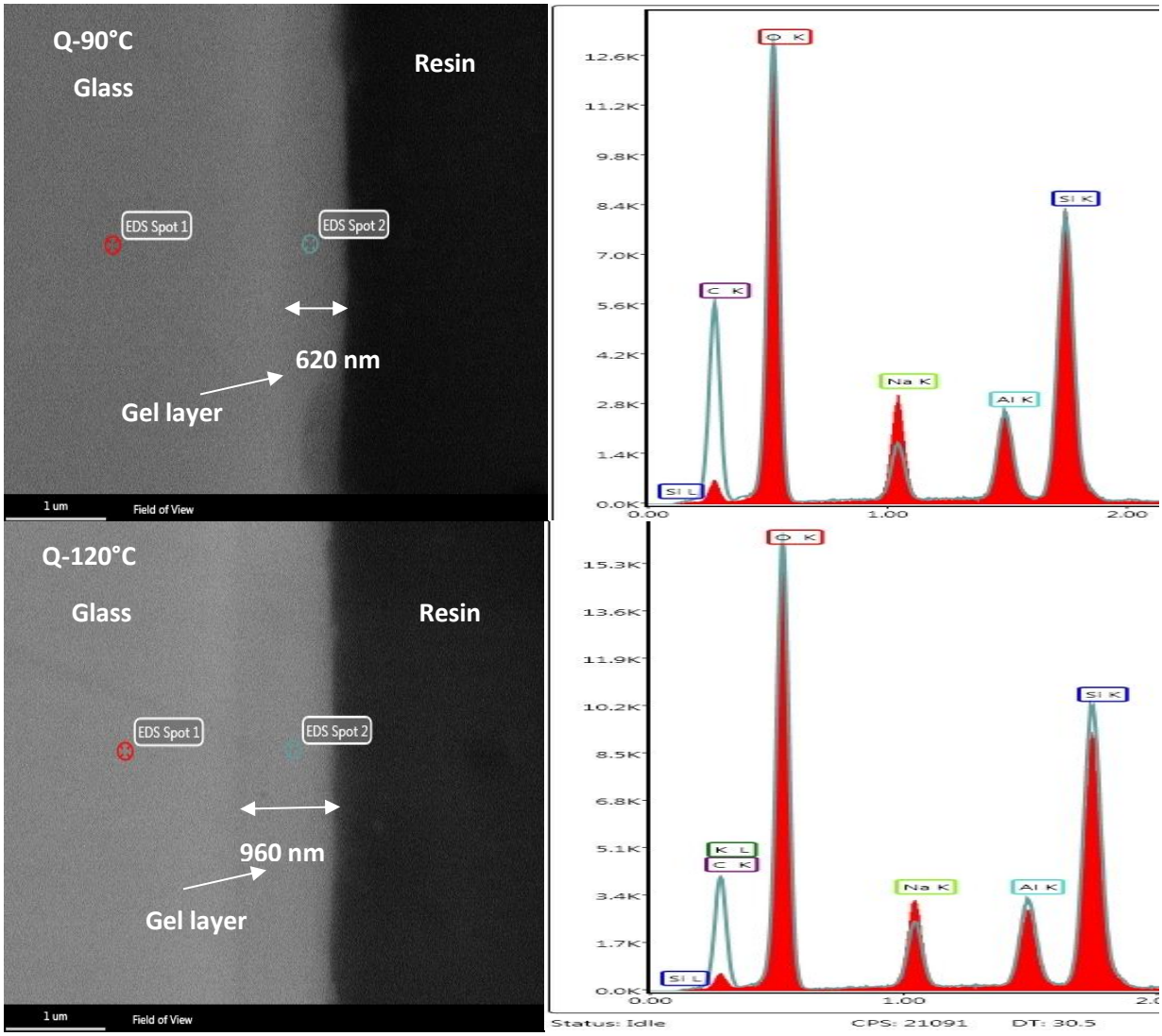

Figure A3- 1 SEM images of cross-sections of Q glass altered in vapor phase at 95% RH and 90°C (top-left) and 120°C (bottom-left) for 91 days; (Top-right and bottom-right) EDS spectra recorded on pristine glass (spot 1) and gel layer (spot 2) for both the glass samples; The red spectra corresponds to spot 1 and the green lines correspond to spot 2;

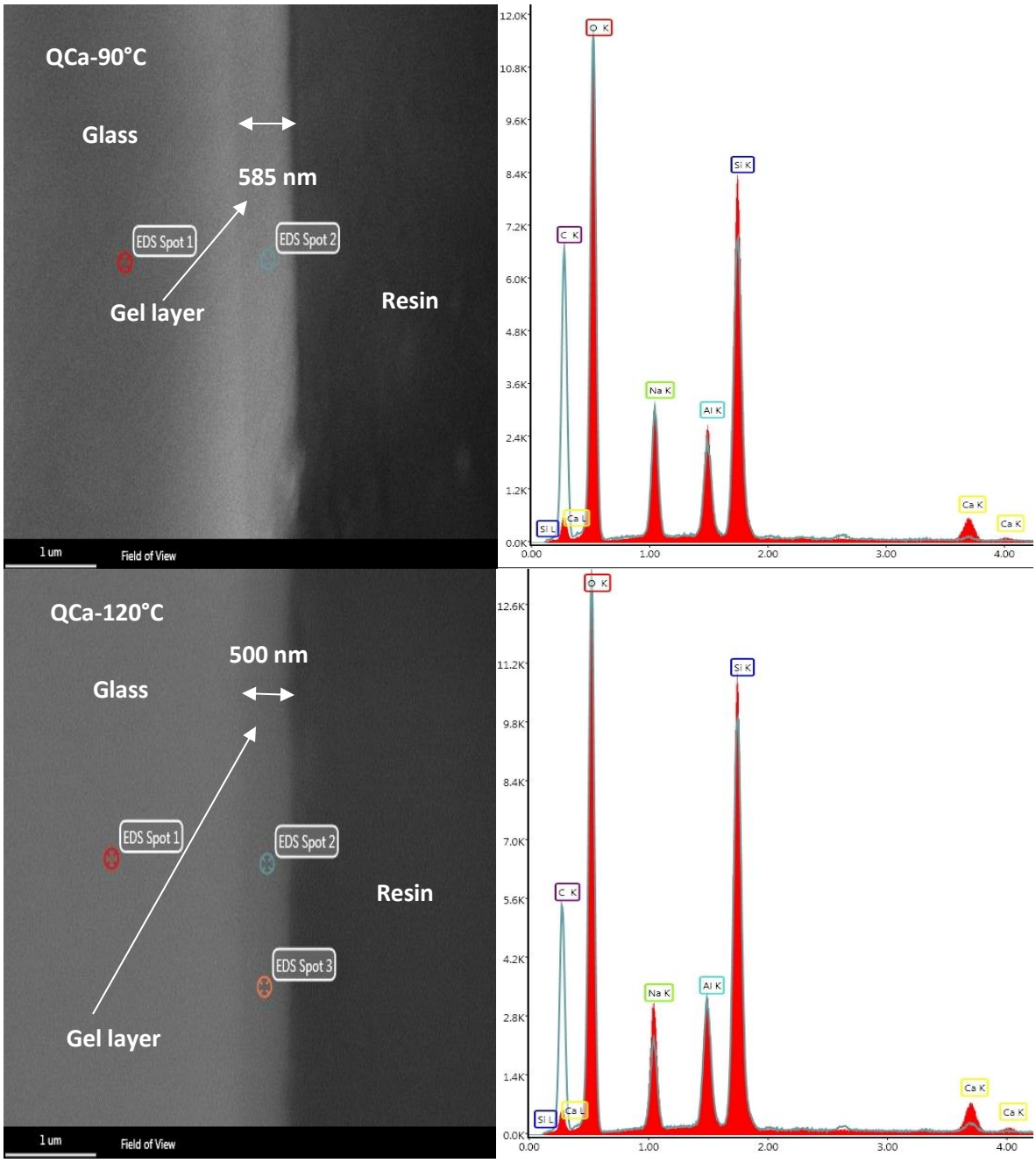

Figure A3- 2 SEM images of cross-sections of QCa glass altered in vapor phase at 95% RH and 90°C (top-left) and 120°C (bottom-left) for 91 days; (Top-right and bottom-right) EDS spectra recorded on pristine glass (spot 1) and gel layer (spot 2) for both the glass samples; The red spectra corresponds to spot 1 and the green lines correspond to spot 2;

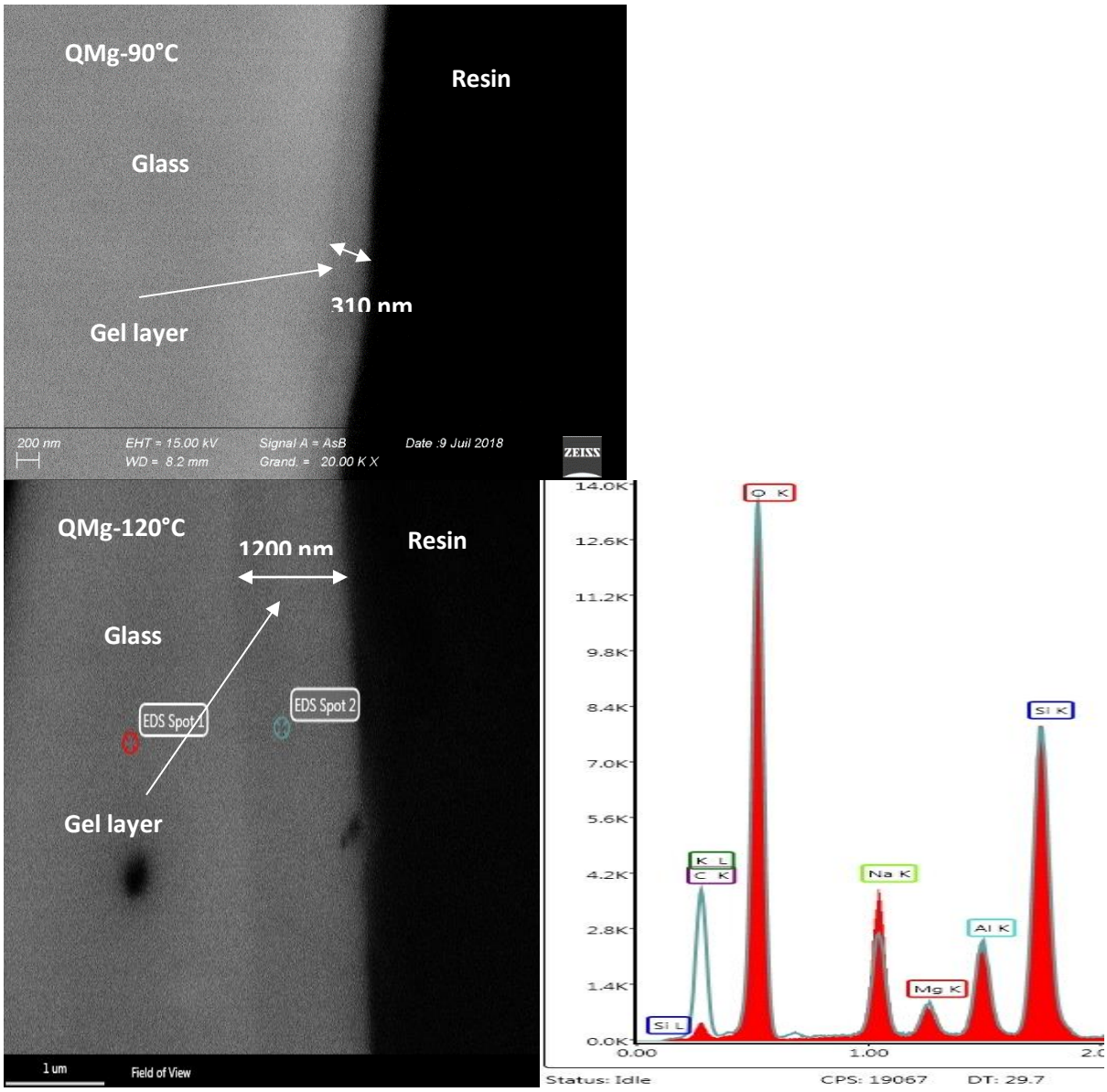

Figure A3- 3 SEM images of cross-sections of QMg glass altered in vapor phase at 95% RH and 90°C (top) and 120°C (bottom-left) for 91 days; (Bottom-right) EDS spectra recorded on pristine glass (spot 1) and gel layer (spot 2) for the QMg sample altered at 120°C; The red spectra corresponds to spot 1 and the green lines correspond to spot 2;

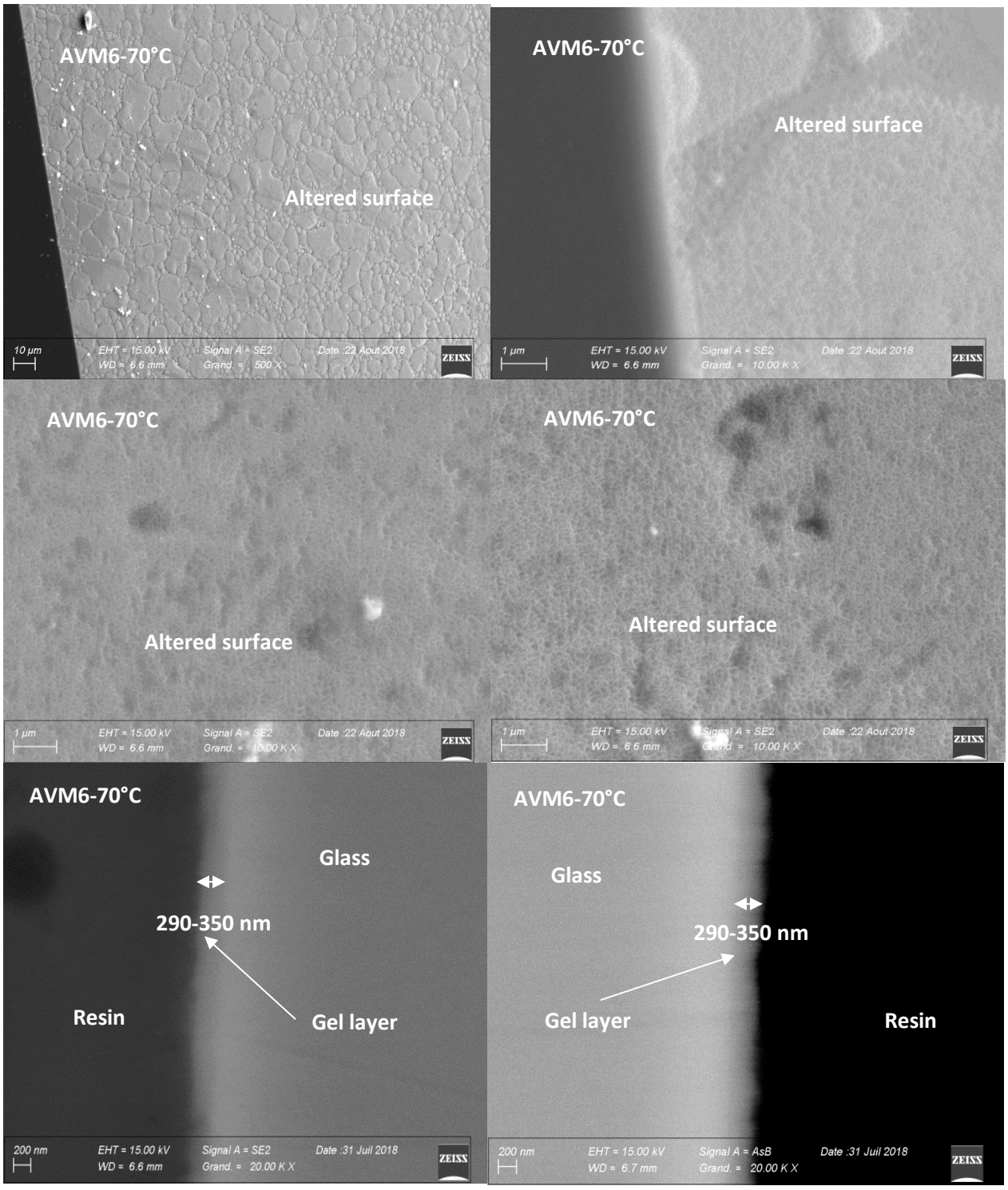

Figure A3- 4 SEM images of AVM6 glass altered in vapor phase at 97% RH and 70°C for 1 year. The top and middle images are the direct observations of the altered surface. The bottom two images are cross-sections of the altered sample.

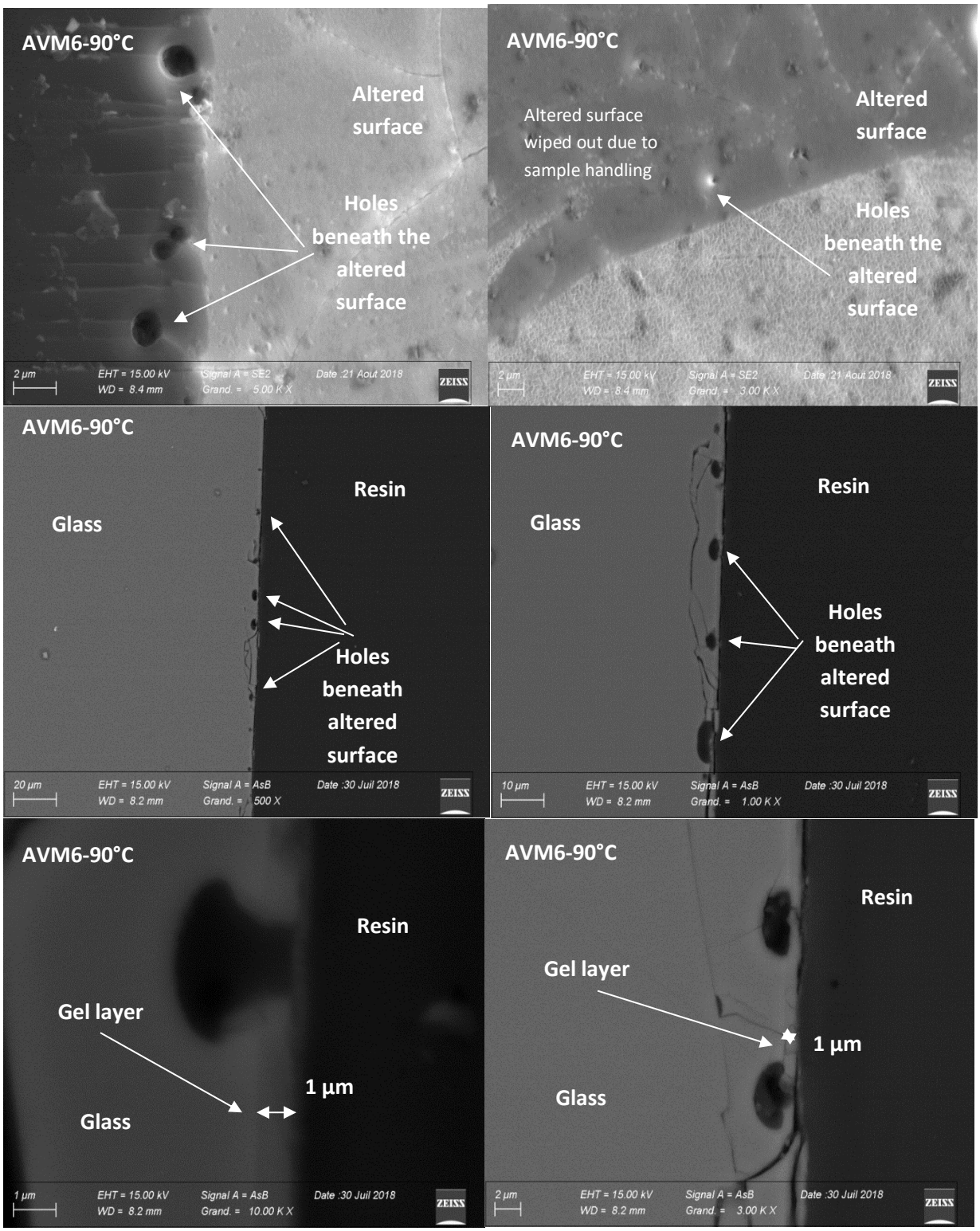

Figure A3- 5 SEM images of AVM6 glass altered in vapor phase at 97% RH and 90°C for 1 year. The top and middle images are the direct observations of the altered surface. The bottom two images are cross-sections of the altered sample.

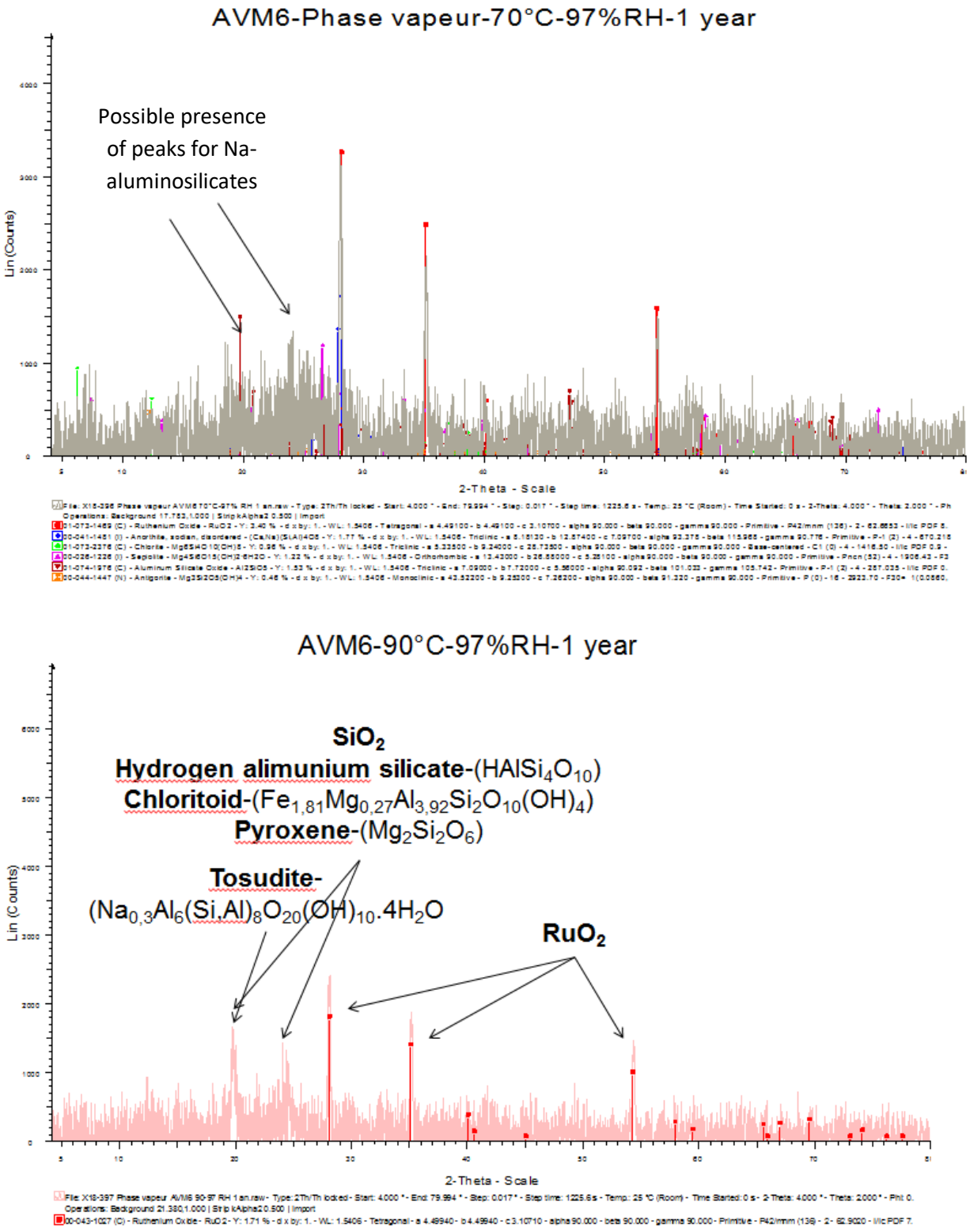

Figure A3- 6 XRD patterns of the AVM6 glass altered at 97% RH and 70°C (top) and 90°C (bottom) for 1 year

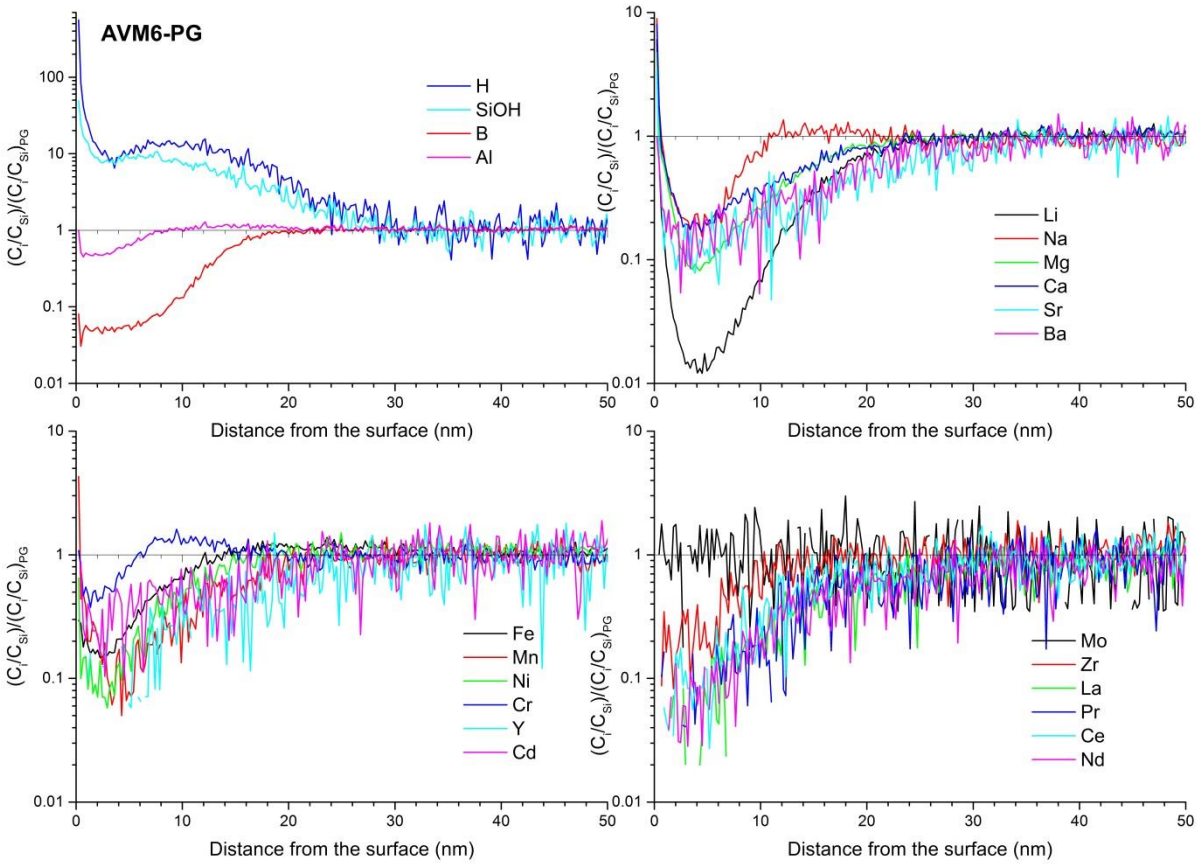

Figure A3- 7 ToF-SIMS profiles (normalized with respect to the intensity of Si and pristine glass) for the pristine AVM6 glass

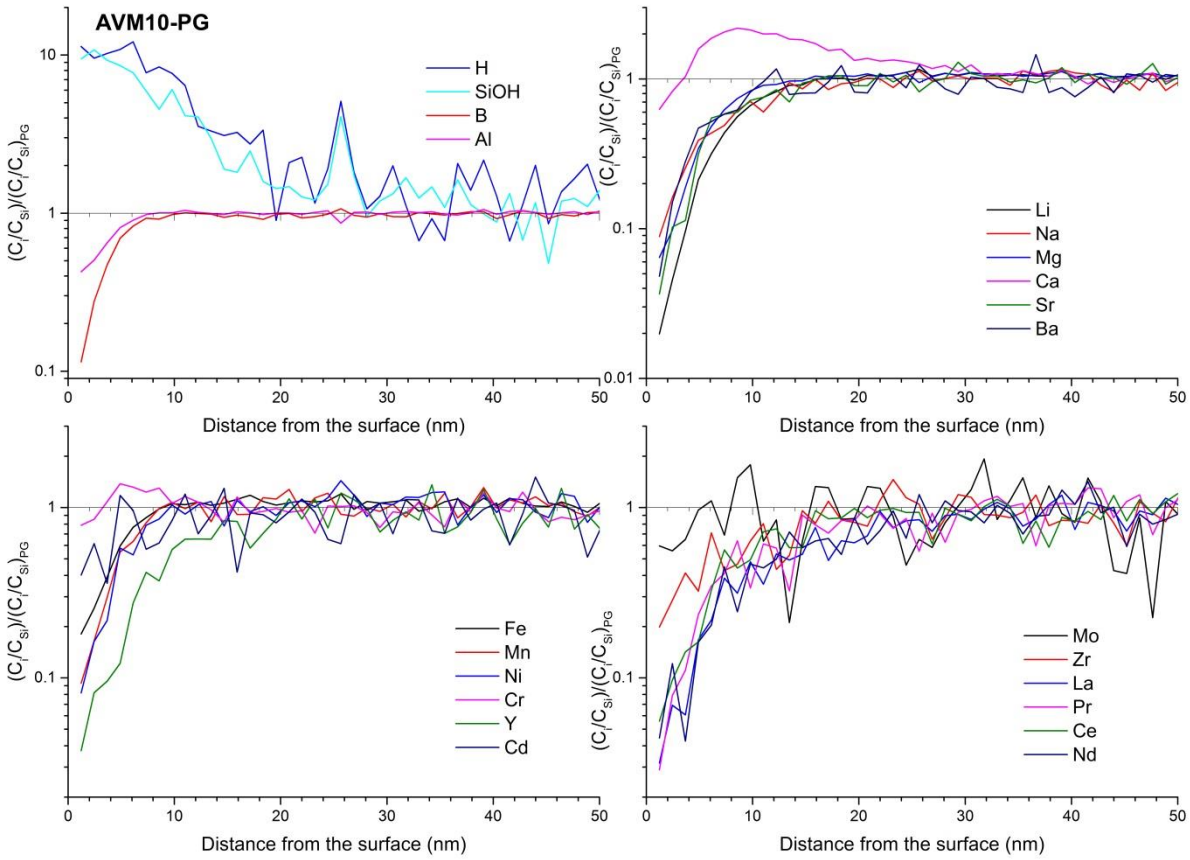

Figure A3- 8 ToF-SIMS profiles (normalized with respect to the intensity of Si and pristine glass) for the pristine AVM10 glass

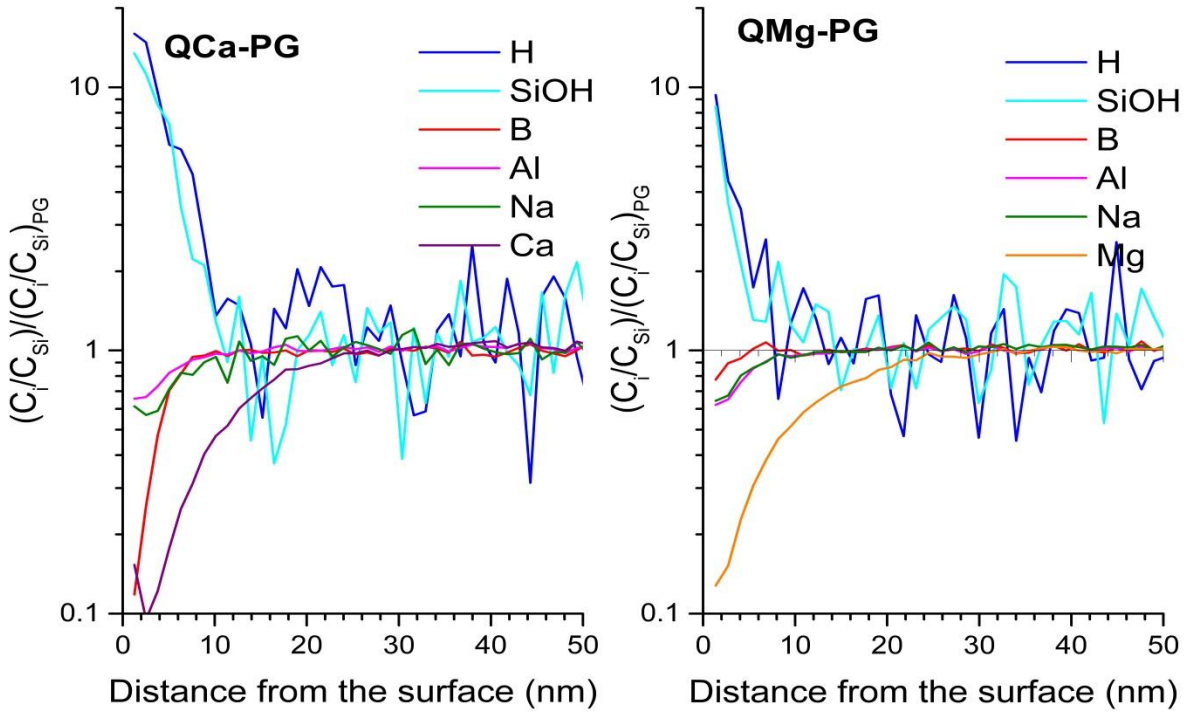

Figure A3- 9 ToF-SIMS profiles (normalized with respect to the intensity of Si and pristine glass) for the pristine QCa glass (left) and QMg glass (right)

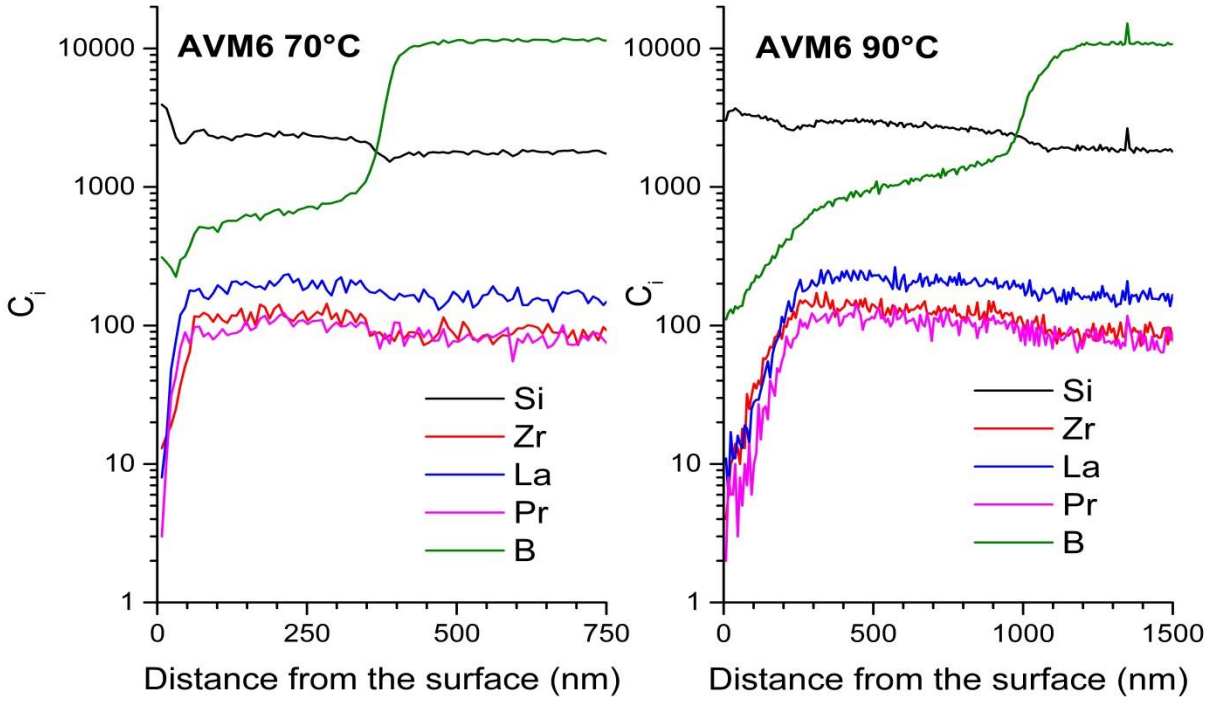

Figure A3- 10 ToF-SIMS profiles (raw data) of the AVM6 glass altered in vapor phase at 97% RH and 70°C and 90°C for 1 year;

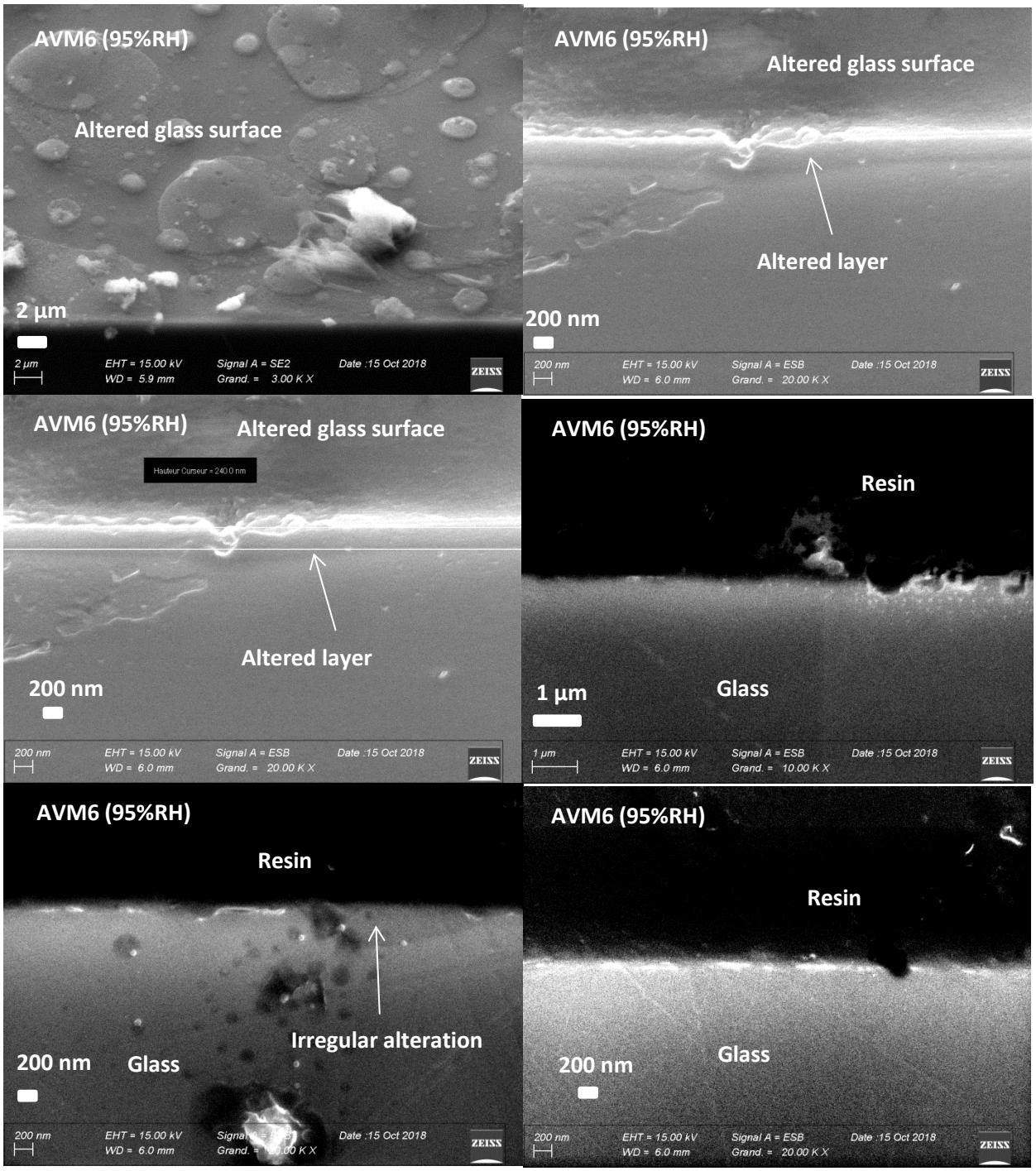

Figure A3- 11 SEM images of AVM6 glass altered in vapor phase at 50°C and 95% RH for 1 year; The center-right and bottom images are cross-sections of altered glass, whereas the remaining images are direct observations of the altered surface of the samples

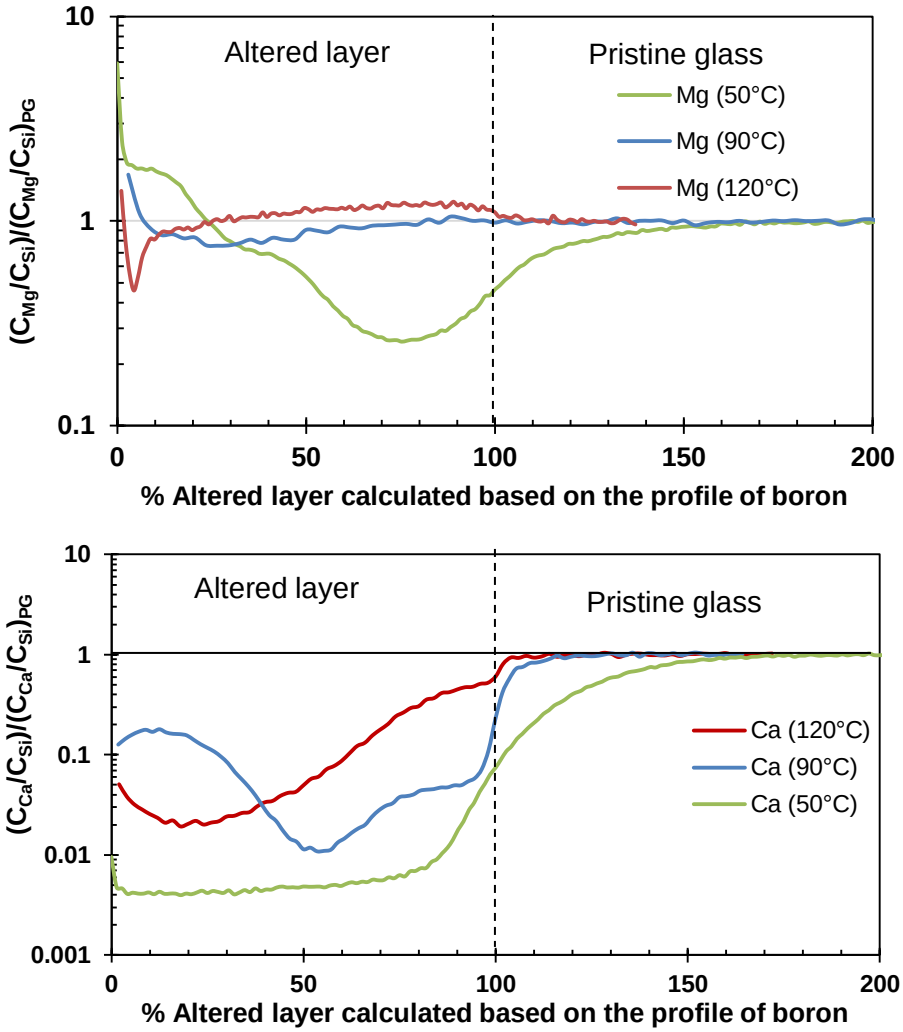

Figure A3- 12 (Top) ToF-SIMS profiles of Mg in the QMg glass altered in vapor phase at 95% RH and 50°C for 181 days and 90°C and 120°C for 91 days; (Bottom) ToF-SIMS profiles of Ca in the QCa glass altered in vapor phase at 95% RH and 50°C for 181 days and 90°C and 120°C for 91 days; The profiles normalized with respect to the intensity of Si and the intensity in the pristine glass are plotted as a function of "percent of altered layer"[24]

[24] "Percent of altered layer" is calculated by considering that the depth at which the intensity of boron is 50% of its intensity in the pristine glass equals 100% of the altered layer. It is a normalization method that permits to facilitate the visual comparison of the shapes of element profiles in the altered layer.

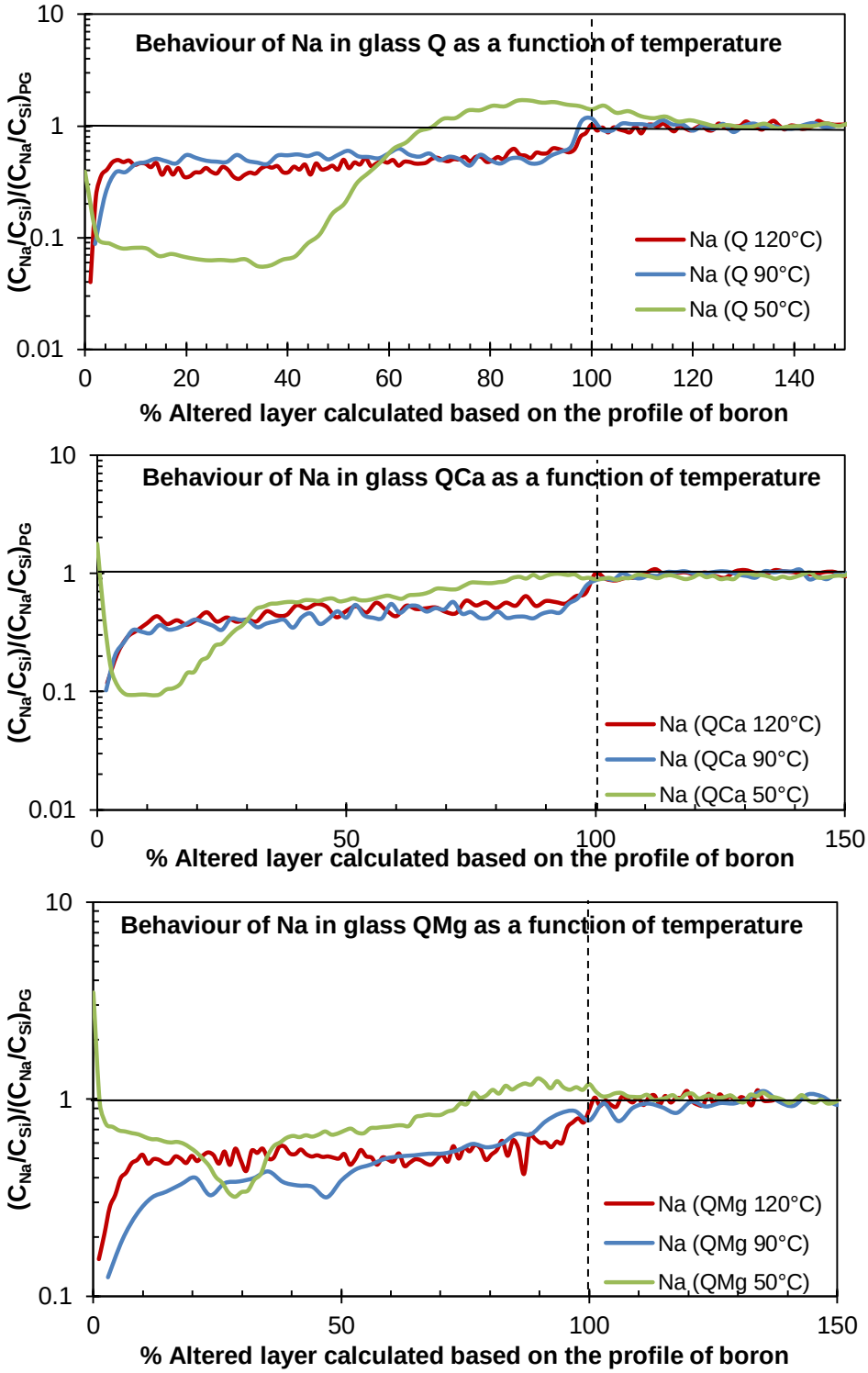

Figure A3- 13 ToF-SIMS profiles of Na in the glasses Q (top), QCa (center) and QMg (bottom) altered in vapor phase at 95% RH and 50°C for 180 days and 90°C and 120°C for 91 days; The profiles normalized with respect to the intensity of Si and the intensity in the pristine glass are plotted as a function of "percent of altered layer"[24]

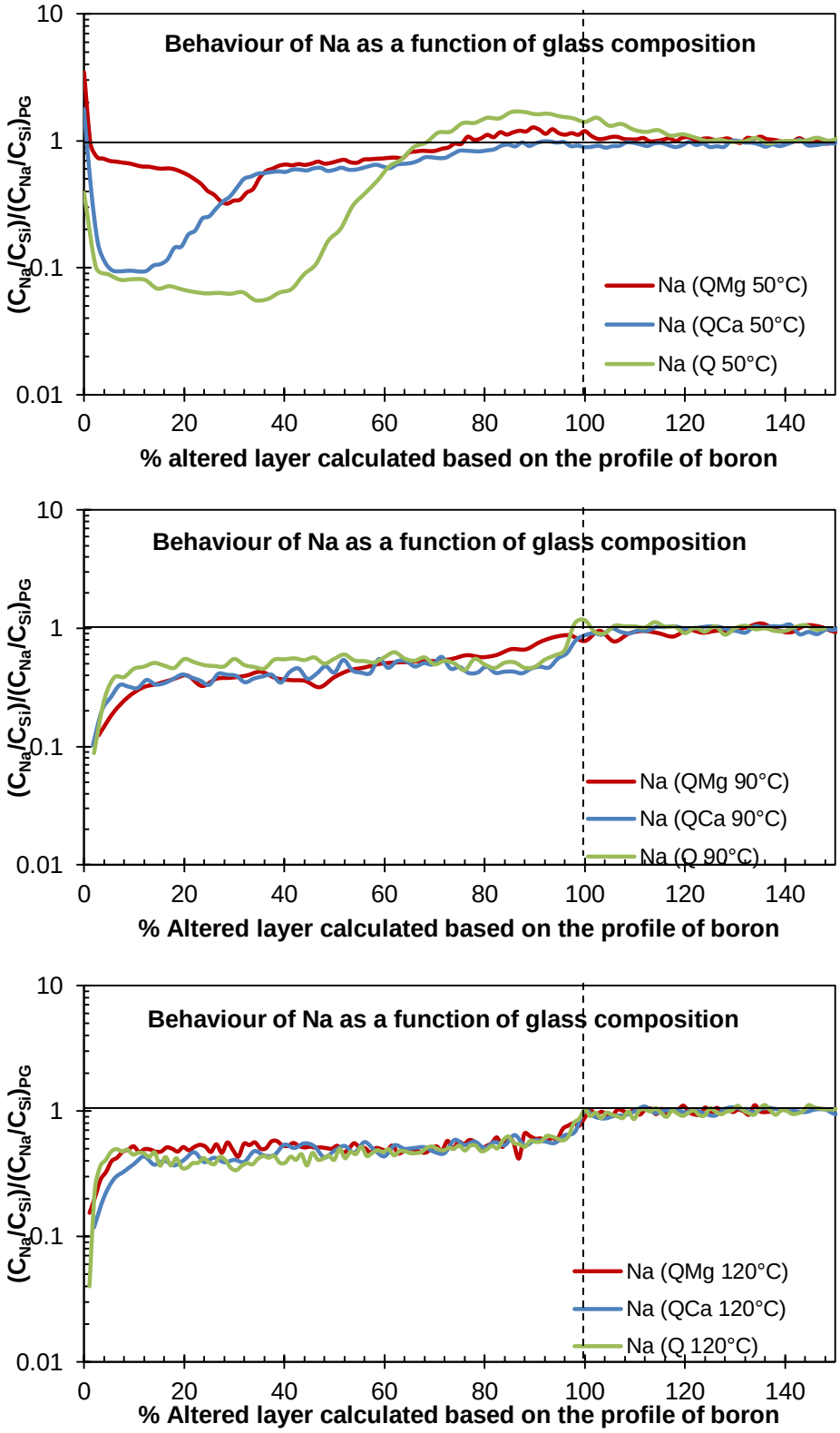

Figure A3- 14 ToF-SIMS profiles of Na in the glasses Q, QCa and QMg altered in vapor phase at 95% RH and 50°C for 180 days (top) and 90°C (center) and 120°C (bottom) for 91 days; The profiles normalized with respect to the intensity of Si and the intensity in the pristine glass are plotted as a function of "percent of altered layer"[24]

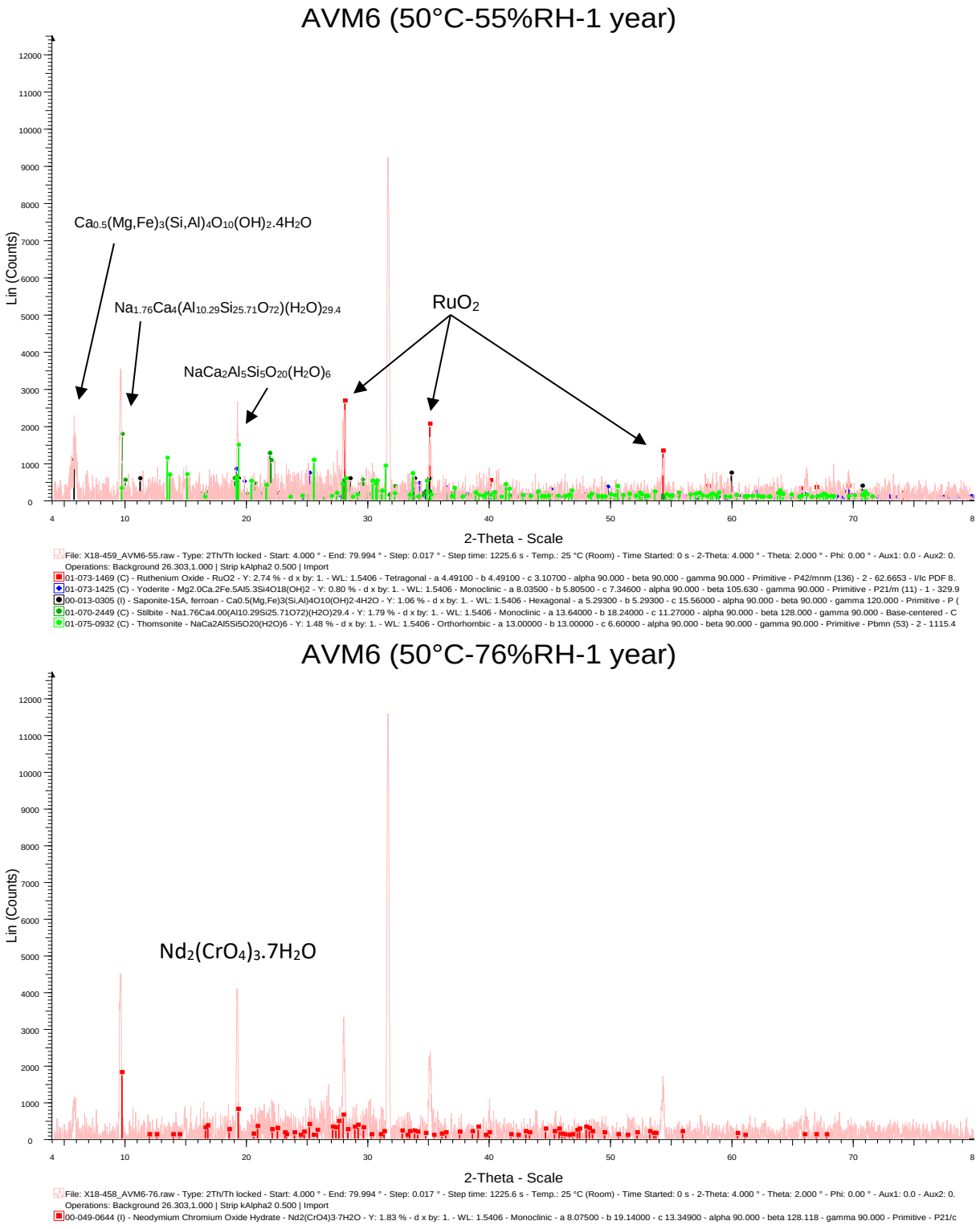

Figure A3- 15 XRD patterns of the AVM6 glass altered in vapor phase at 50°C and 55% RH (top) and 76% RH (bottom) for 1 year

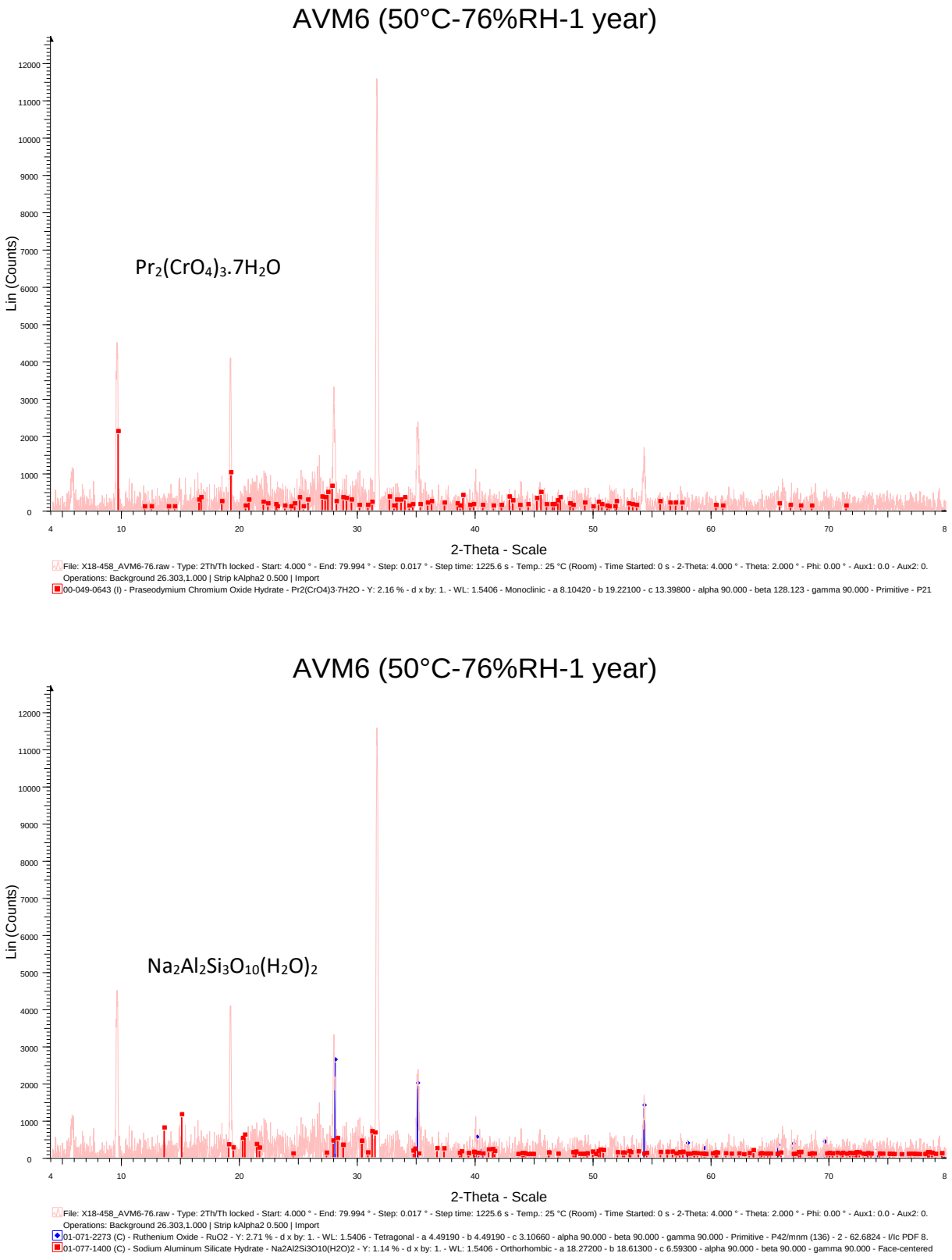

Figure A3- 16 XRD patterns of the AVM6 glass altered in vapor phase at 50°C and 76% RH for 1 year

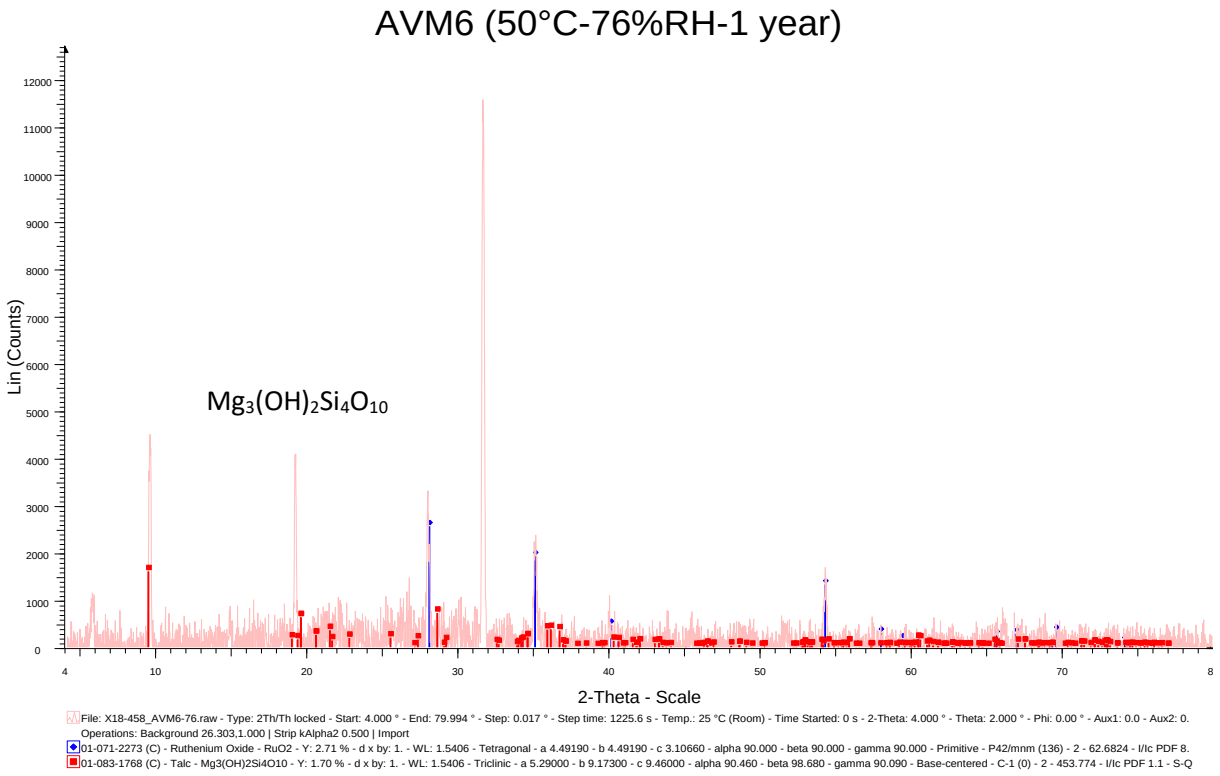

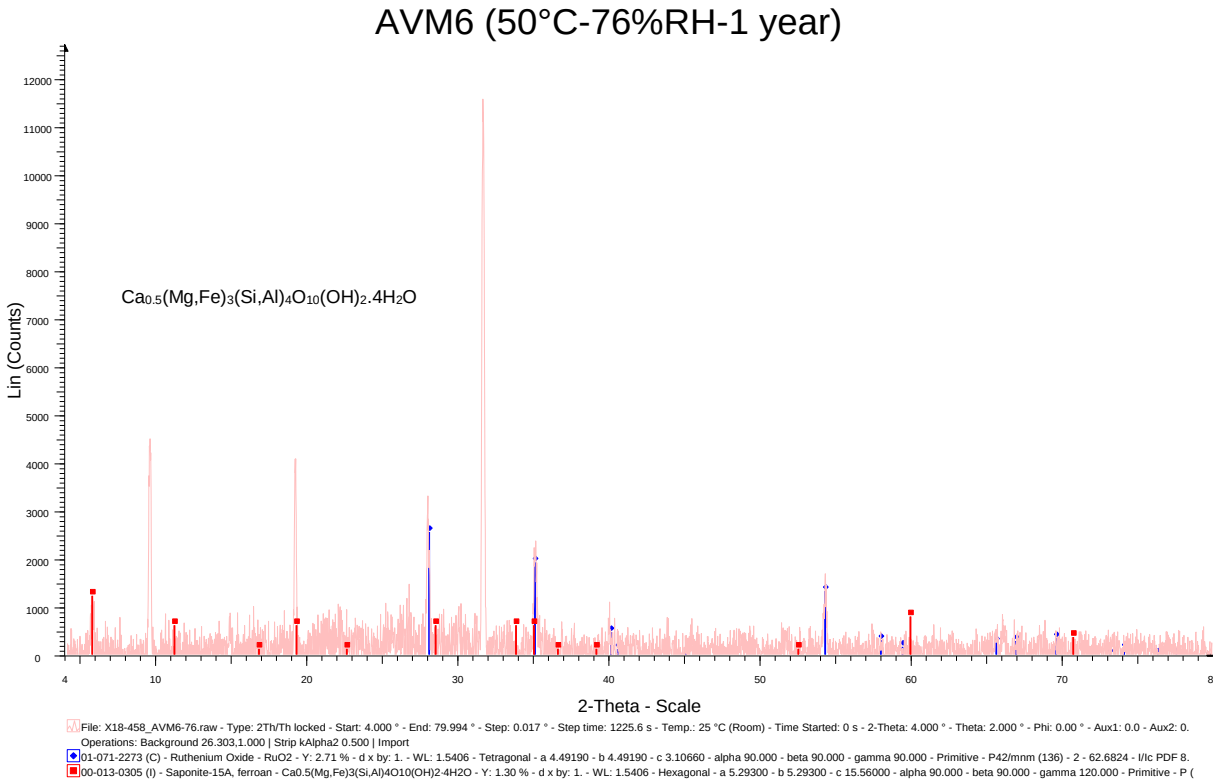

Figure A3- 17 XRD patterns of the AVM6 glass altered in vapor phase at 50°C and 76% RH for 1 year

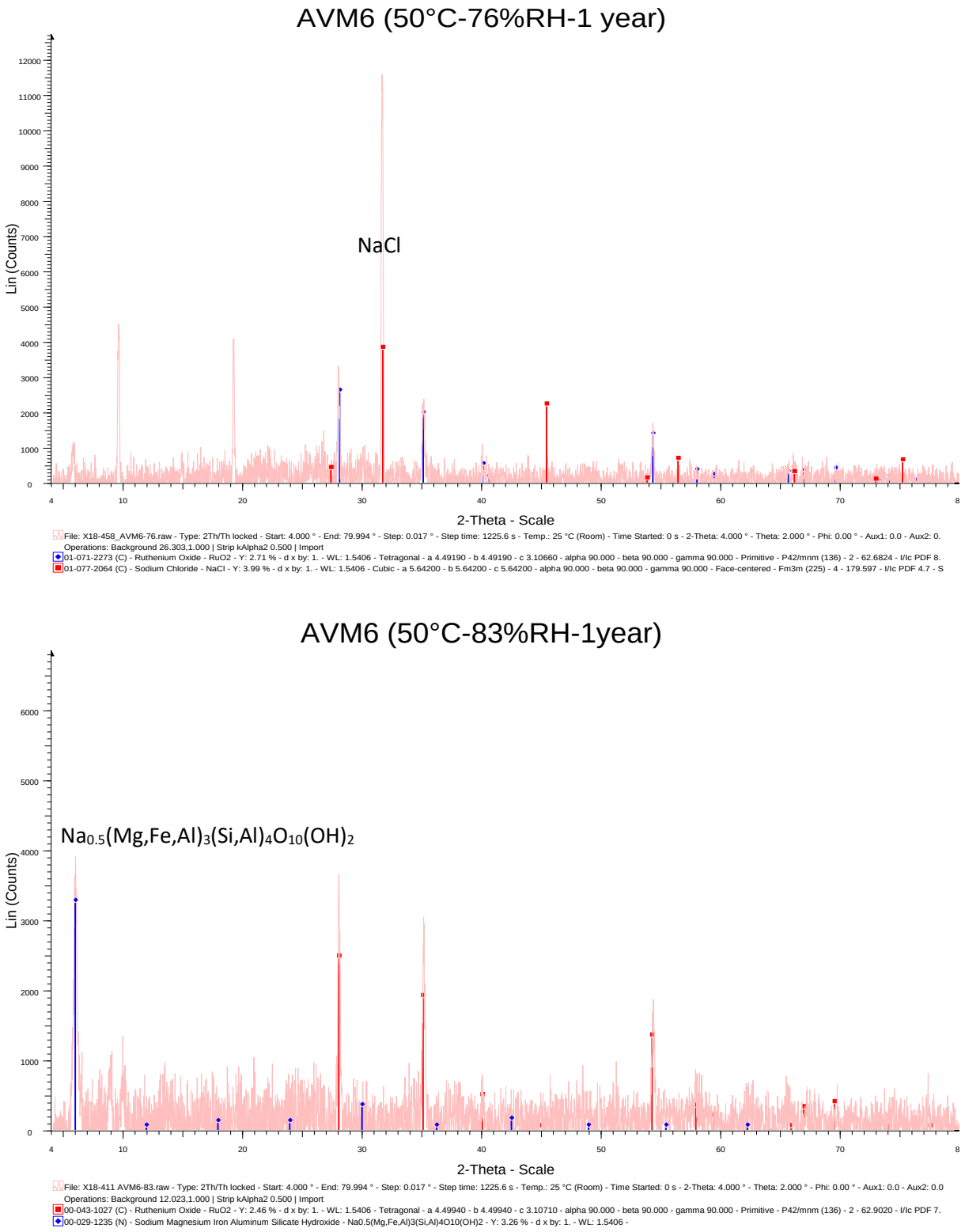

Figure A3- 18 XRD patterns of the AVM6 glass altered in vapor phase at 50°C and 76% RH (top) and 83% RH (bottom) for 1 year

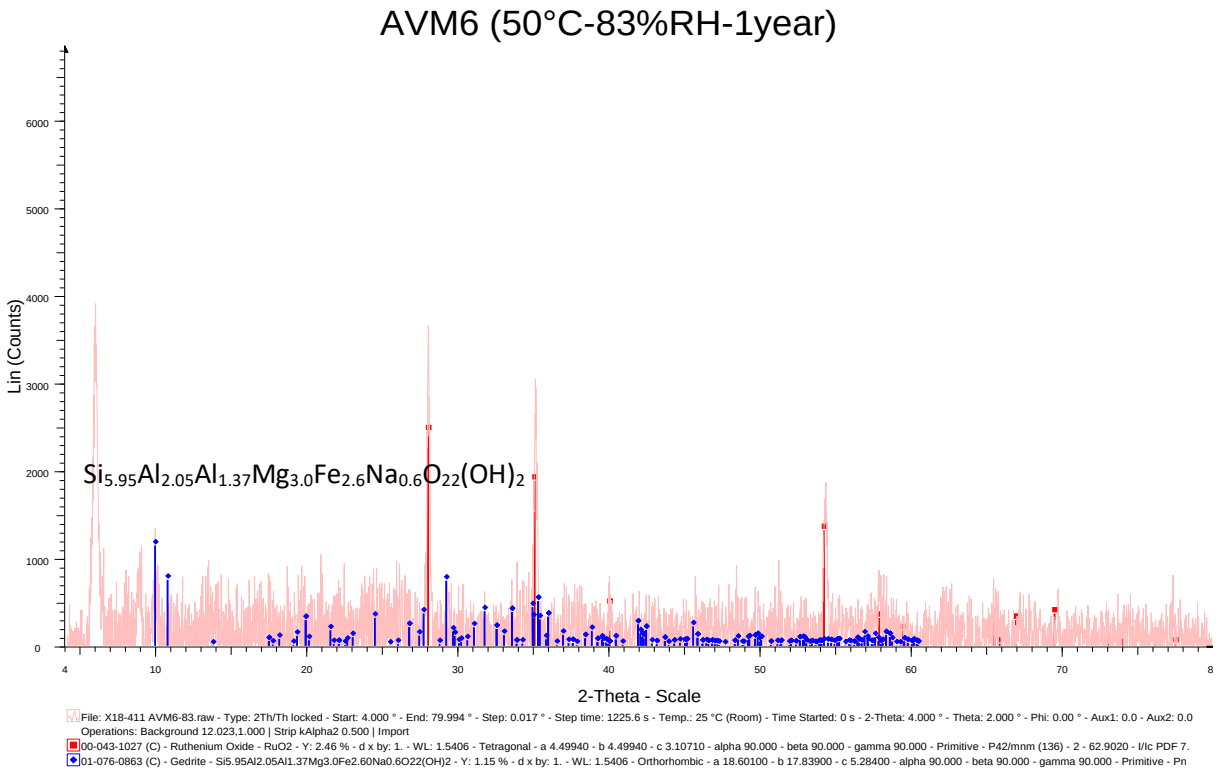

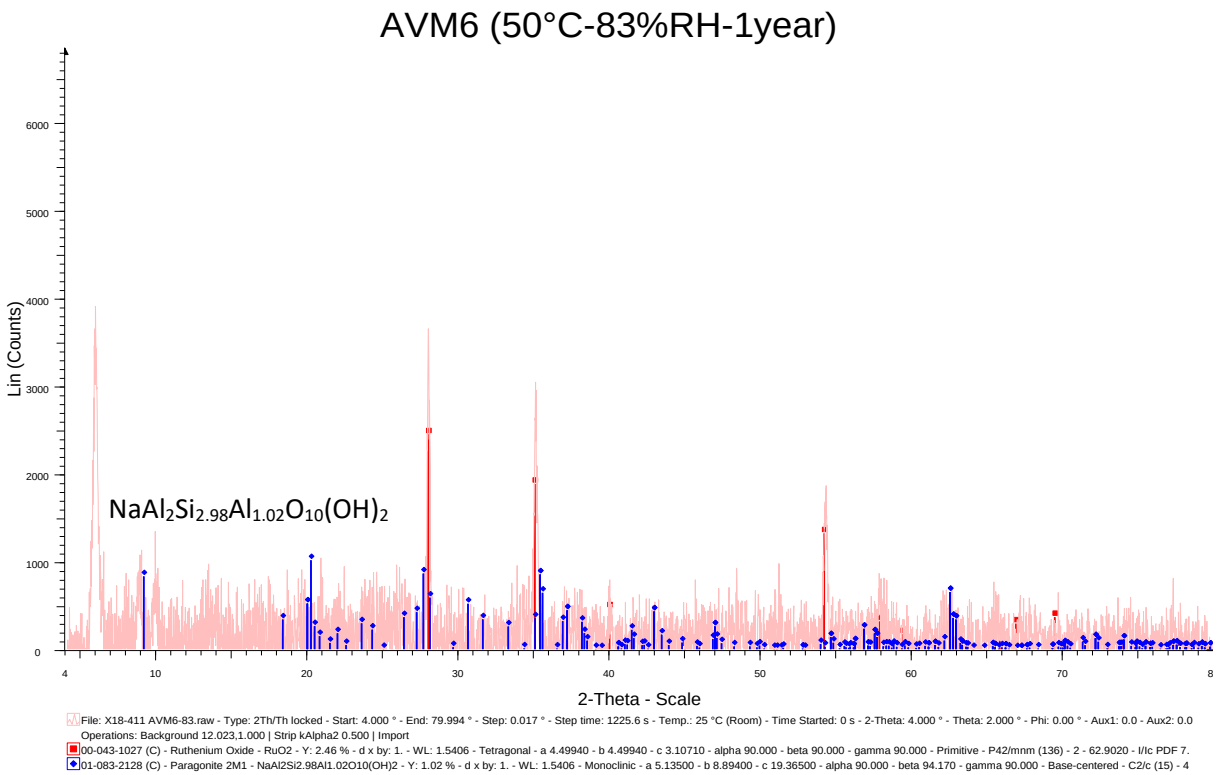

Figure A3- 19 XRD patterns of the AVM6 glass altered in vapor phase at 50°C and 83% RH for 1 year

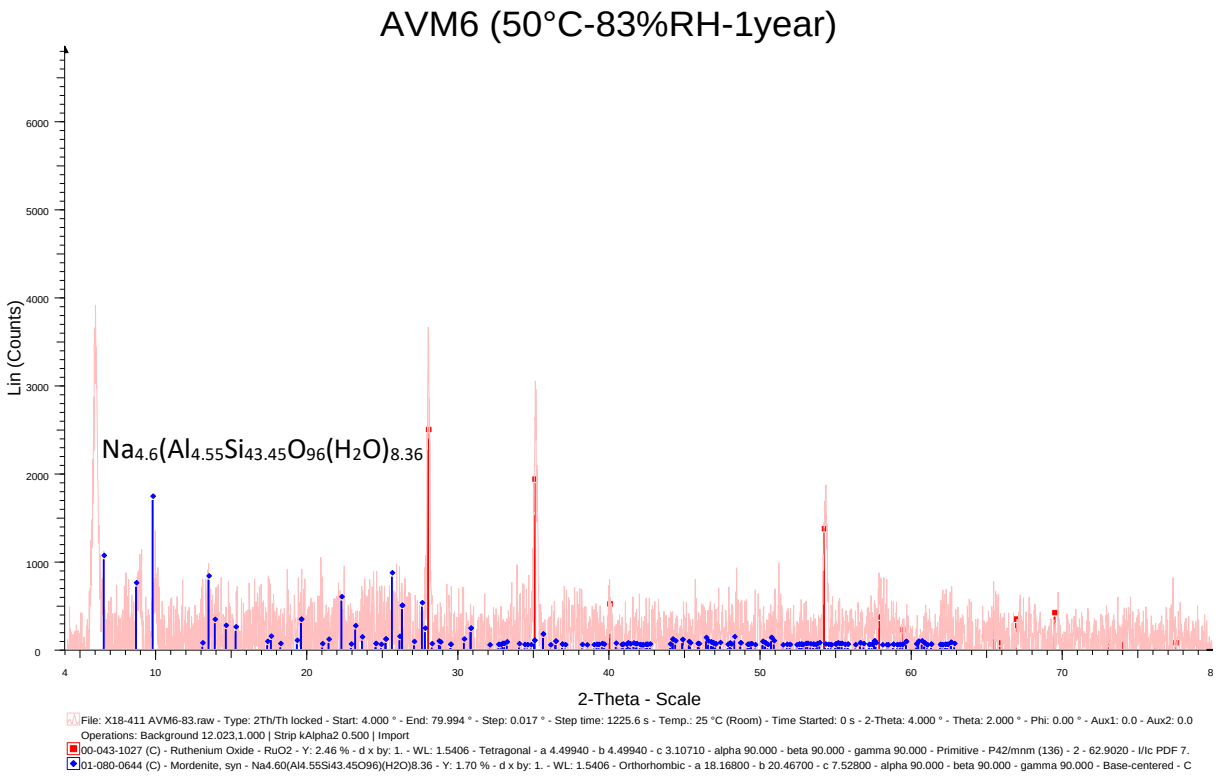

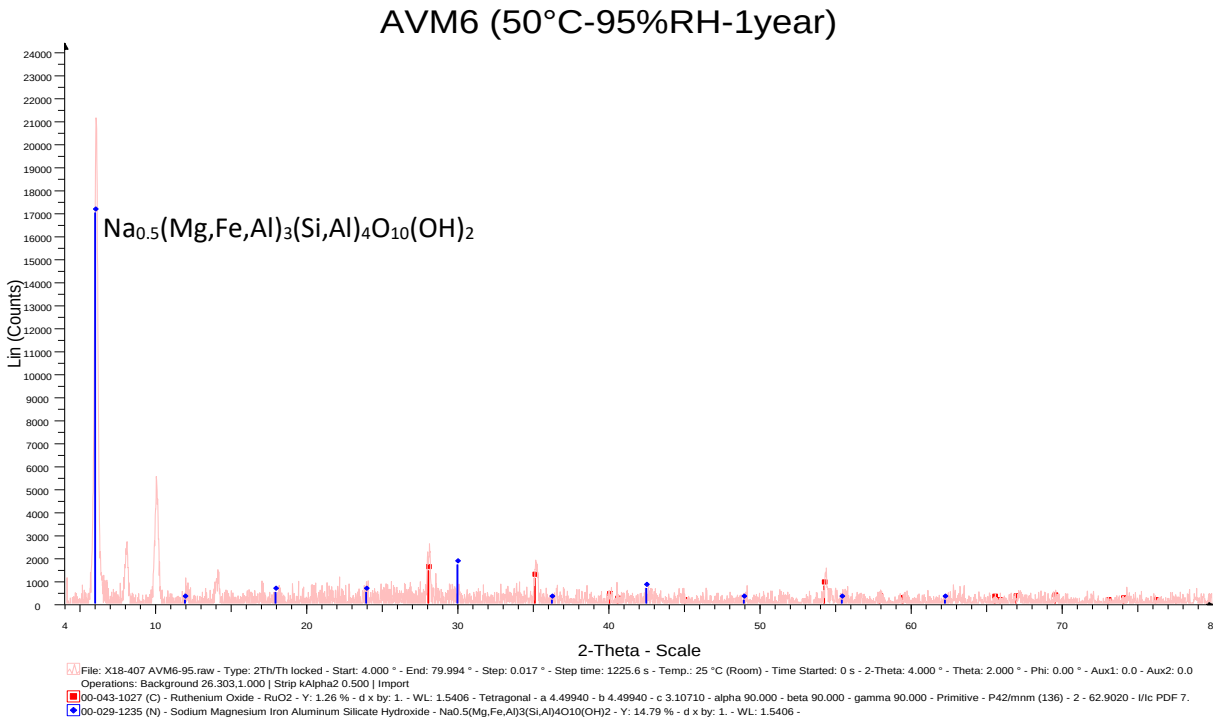

Figure A3- 20 XRD patterns of the AVM6 glass altered in vapor phase at 50°C and 83% RH (top) and 95% RH (bottom) for 1 year

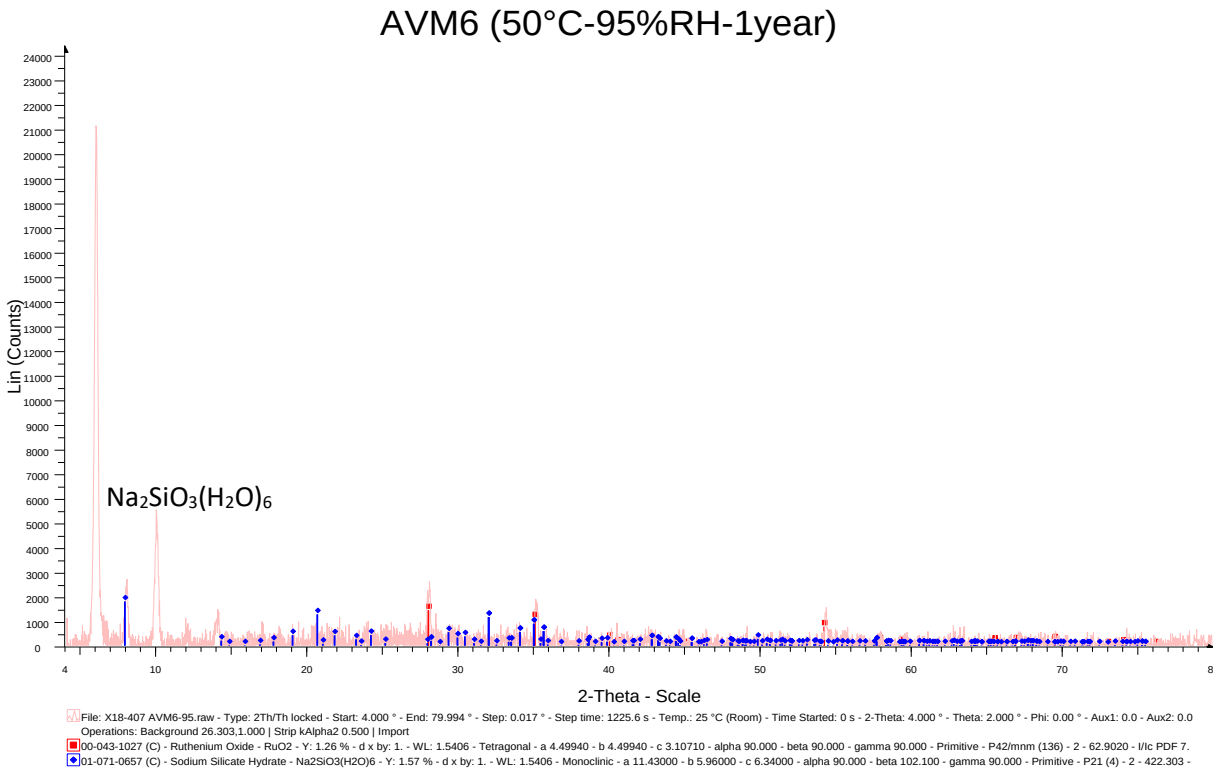

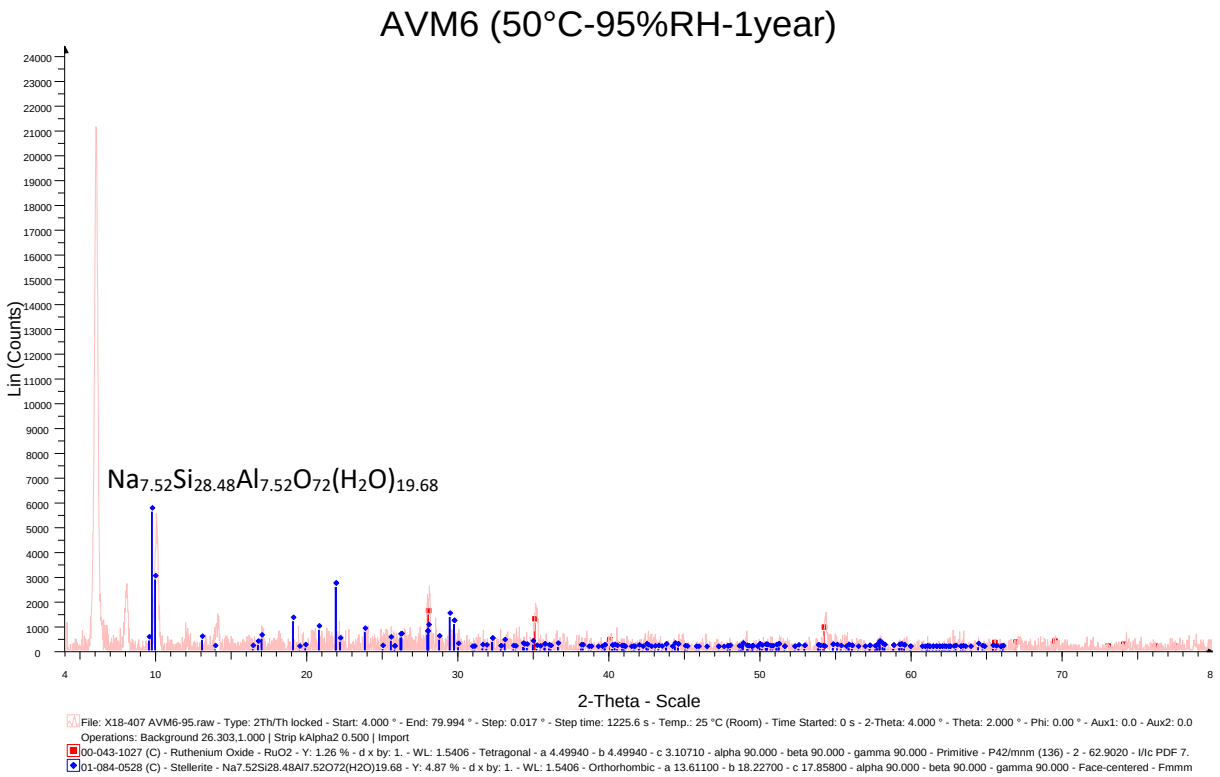

Figure A3- 21 XRD patterns of the AVM6 glass altered in vapor phase at 50°C and 95% RH for 1 year

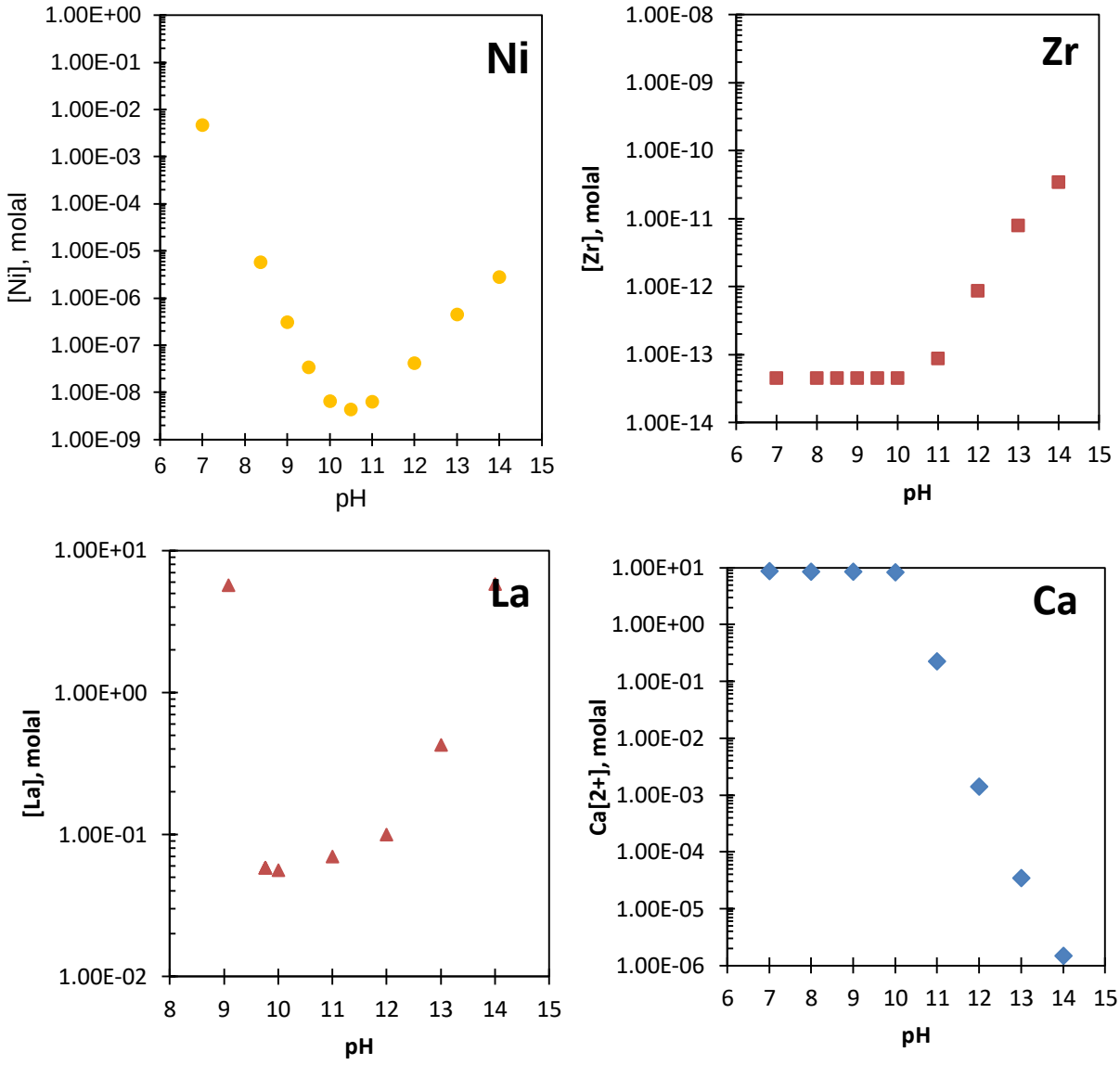

Figure A3- 22 Evolution of calculated concentrations of Ni (top-left), Zr (top-right), La (bottom-left) and Ca (bottom-right) in solution as a function of pH; The concentrations were calculated by PHREEQC software by modelling the dissolution of $Ni(OH)_2$, zircon, $La(OH)_3$ and $Ca(OH)_2$ respectively in water at 50°C and using HCl and NaOH to fix the pH values.

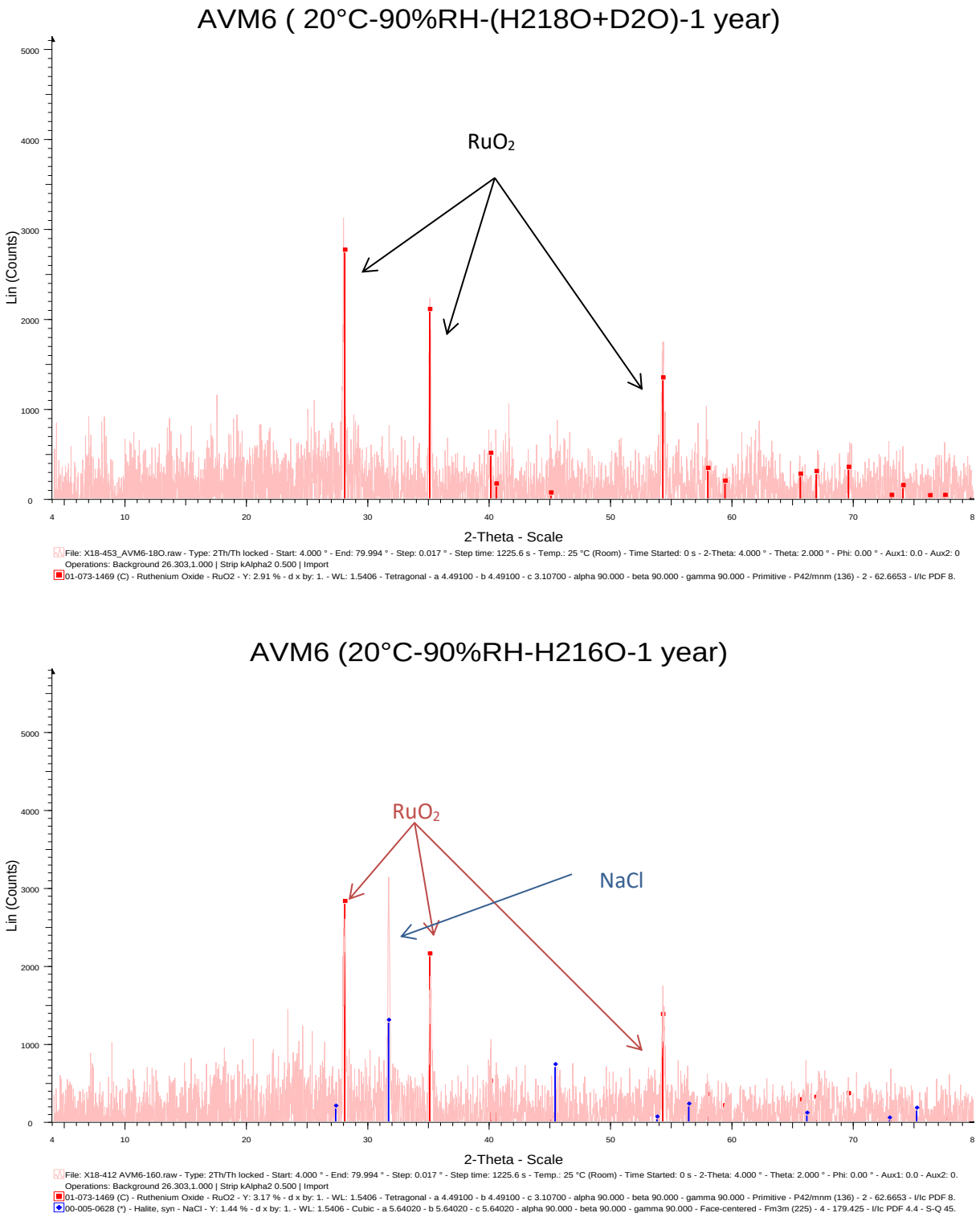

Figure A3- 23 XRD patterns of AVM6 glass altered in vapor phase at 20°C and 90% RH in the presence of enriched fraction of D and ^{18}O isotopes (top) and at natural isotopic abundance (bottom)

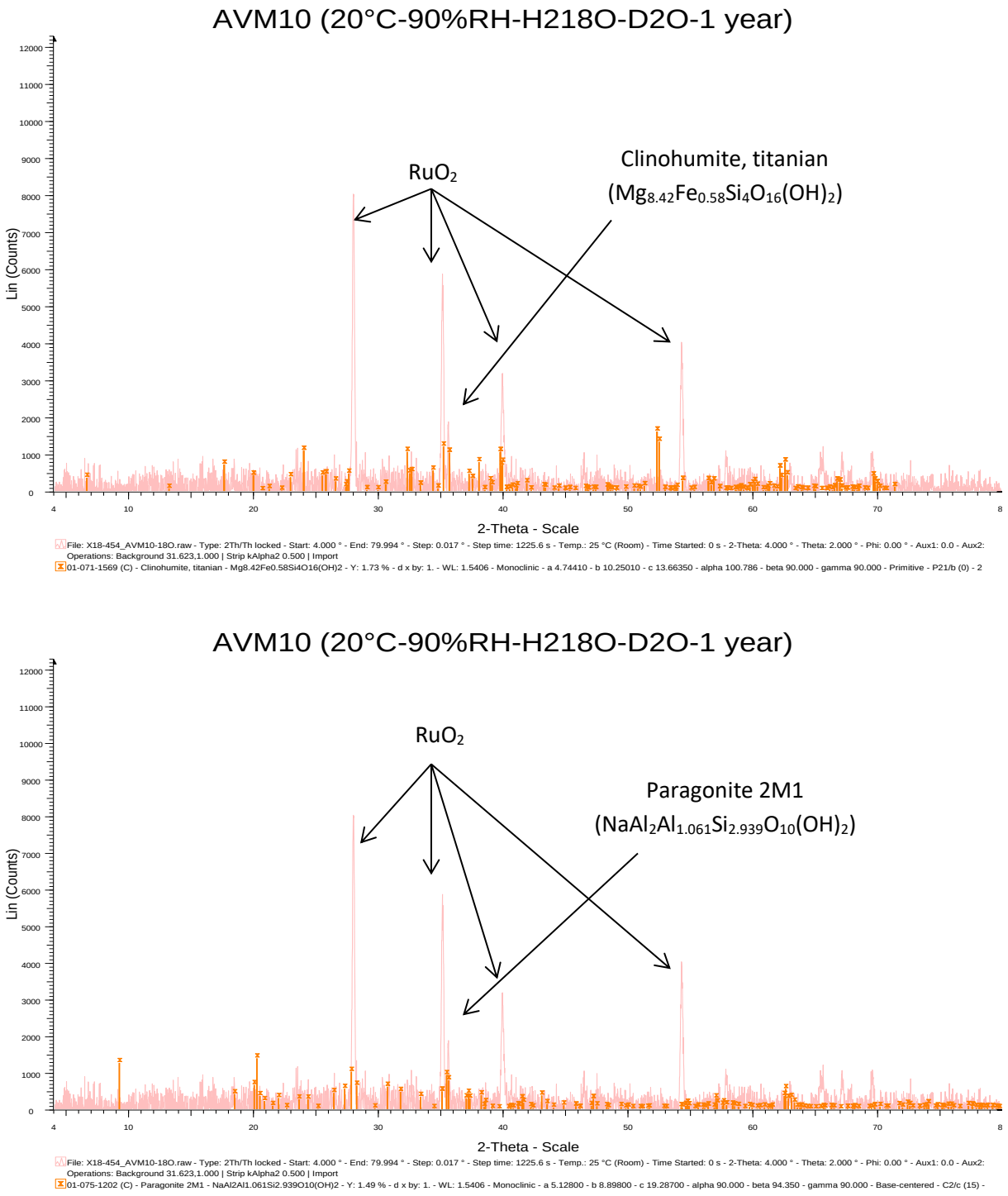

Figure A3- 24 XRD patterns of AVM10 glass altered in vapor phase at 20°C and 90% RH in the presence of enriched fraction of D and ^{18}O isotopes

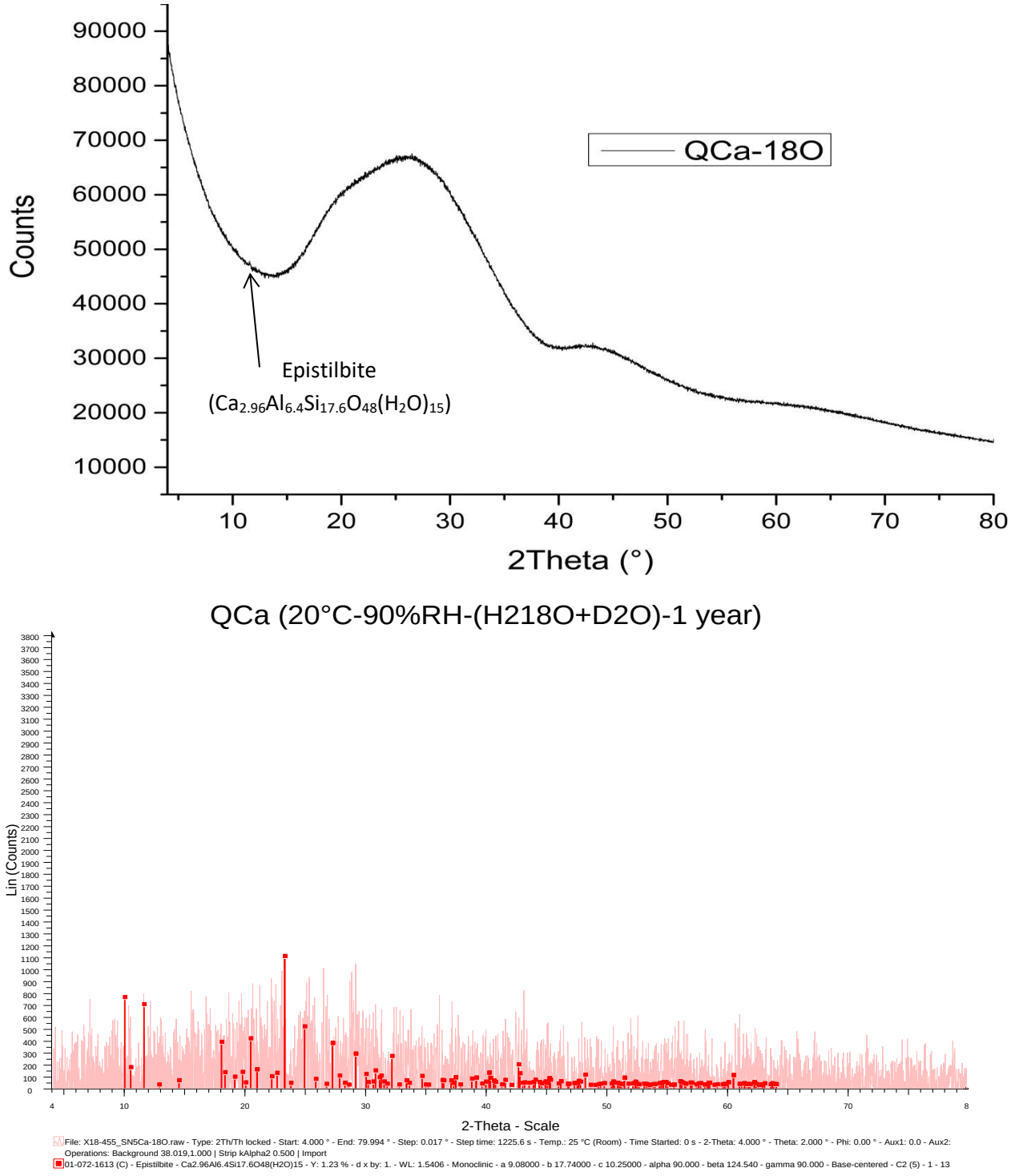

Figure A3- 25 XRD patterns of QCa glass altered in vapor phase at 20°C and 90% RH in the presence of enriched fraction of D and ^{18}O isotopes

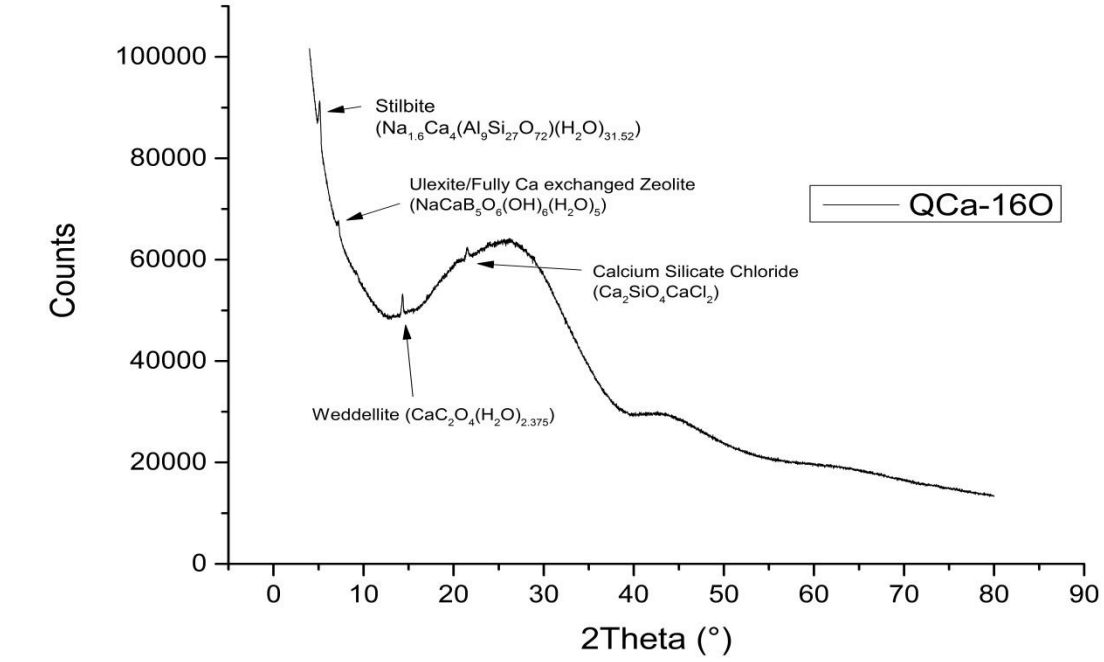

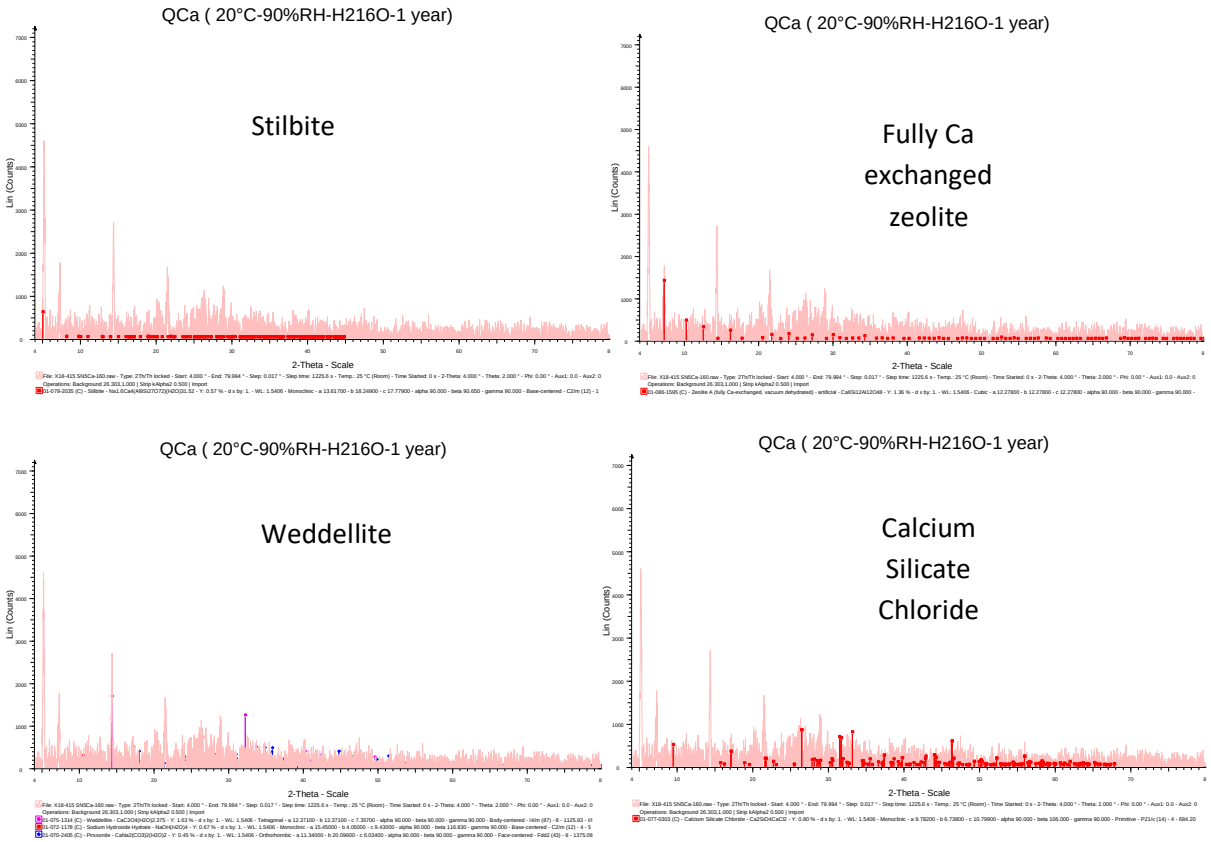

Figure A3- 26 XRD patterns of QCa glass altered in vapor phase at 20°C and 90% RH at natural isotopic abundance

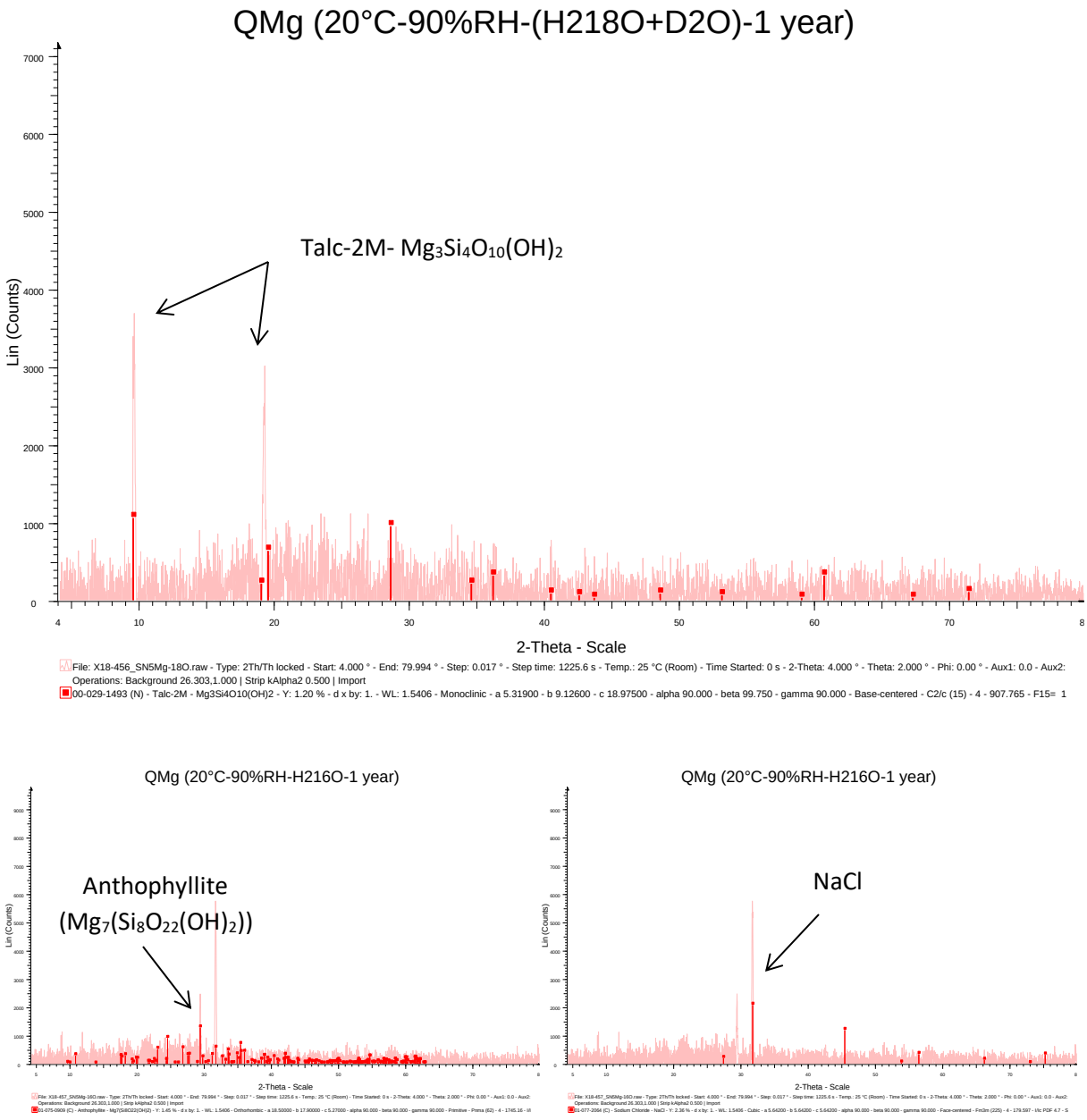

Figure A3- 27 XRD patterns of QMg glass altered in vapor phase at 20°C and 90% RH in the presence of enriched fraction of D and ^{18}O isotopes (top) and at natural isotopic abundance (bottom)

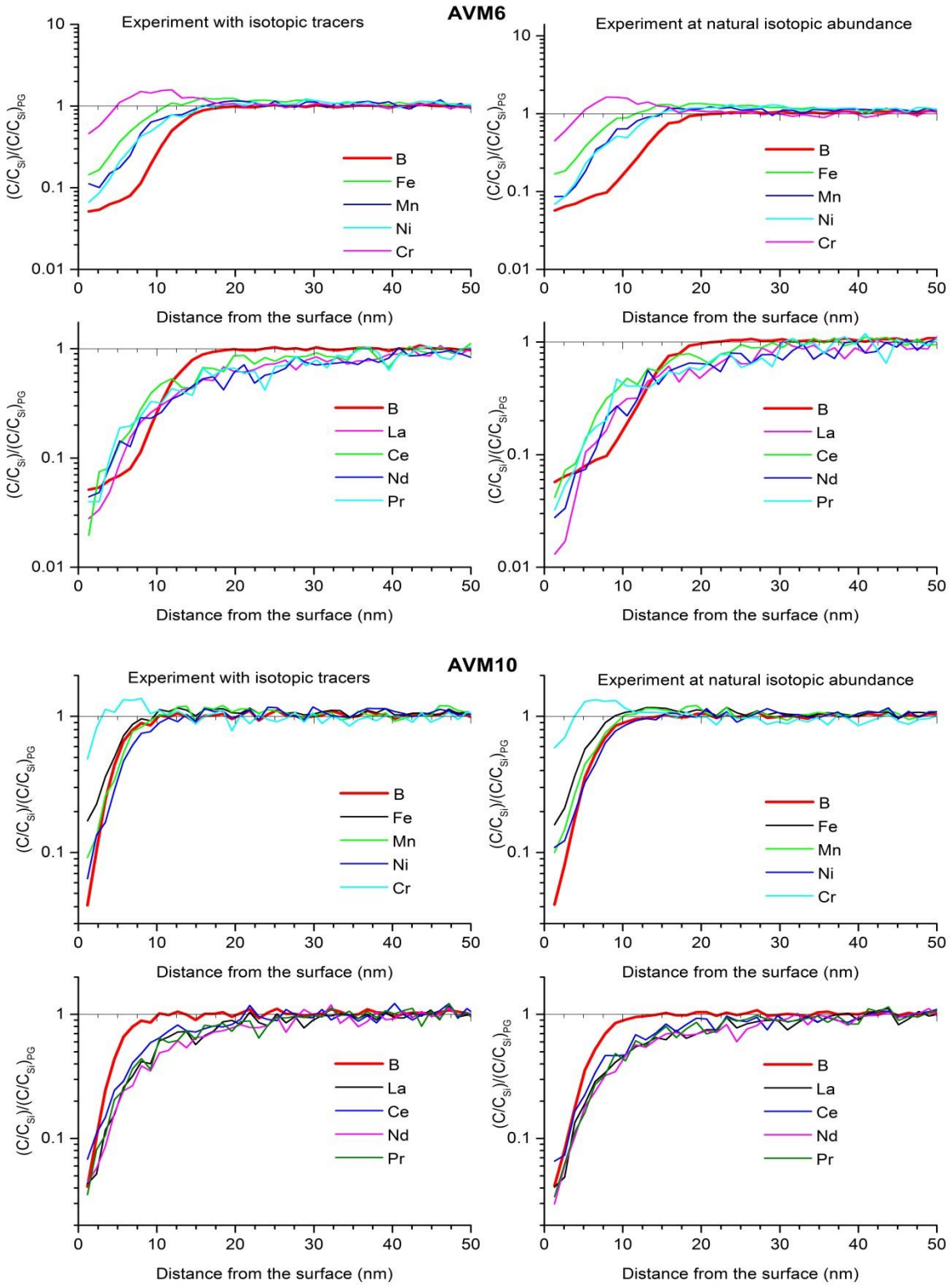

Figure A3- 28 Normalized ToF-SIMS profiles of the transition metals and rare-earth elements for the AVM6 (top) and AVM10 (bottom) samples altered in vapor phase at 20°C and 91% RH for 1 year; The profiles on the left side correspond to the experiment conducted with enriched isotopic tracers D and ^{18}O; The profiles on the right side for the same elements correspond to the experiment conducted at natural isotopic abundance.

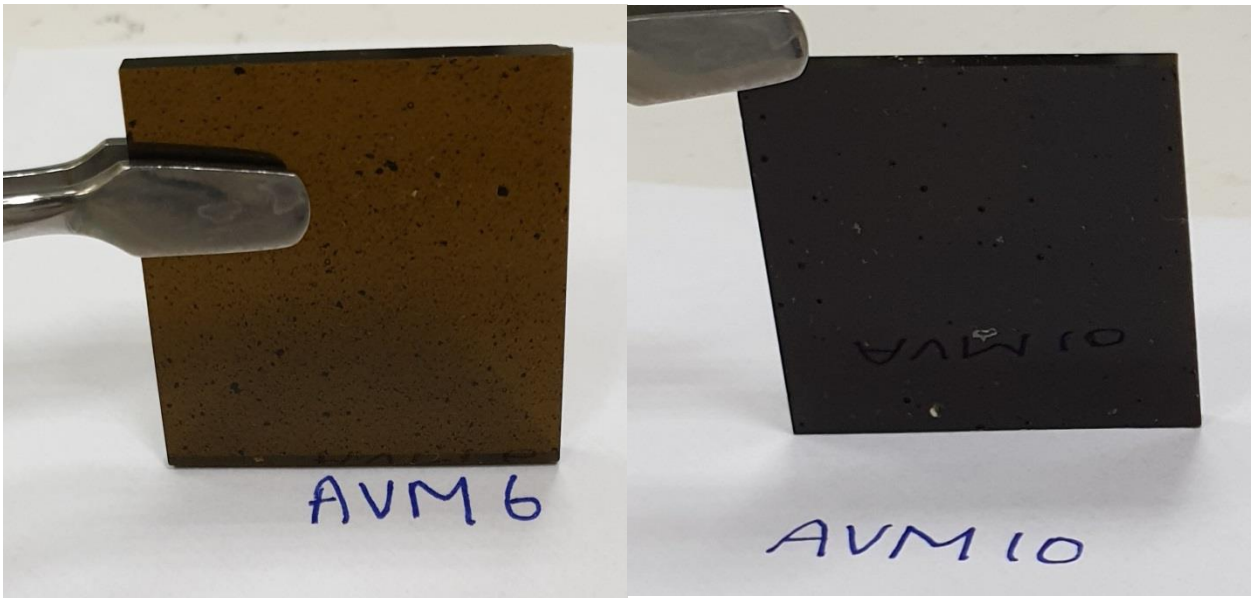

Figure A3- 29 (left) Photo of pristine AVM6 glass monolith; (right) photo of pristine AVM10 glass monolith after polishing to surface roughness <1 µm and cutting to dimensions 2.5x2.5x0.1 cm^3; AVM6 is more transparent than AVM10, but it is clear that both glasses contain heterogeneities due to the presence of insoluble elements such as ruthenium and the formation of platinoids; AVMV4 glass monolith also has similar heterogeneities but the photo is currently unavailable.

Appendix 4

For solution analysis after the concentrations have been measured by ICP-OES *(section 4.2.2.2)*:

$$Altered\ glass\ percentage\ (AG\%) = \frac{C_t(B)*V_t + \sum_{j=1}^{t-1} C_j(B)*V_{sj}}{m_0*x_B}\ x\ 100 \qquad \text{Equation A4-1}$$

$$Normalized\ mass\ loss\ (NL), g/m^2 = \frac{C(i)}{\frac{SA}{V}*x_i} \qquad \text{Equation A4-2}$$

AG%- altered glass percentage; $C_t(B)$ – concentration of boron at time t (g/m^3); V_t – solution volume at time t (m^3); V_{sj} – volume of solution sampled at time j (m^3); m_0 – initial mass of glass (g); x_B – mass fraction of boron in unaltered glass; $C(i)$ – Concentration of element in solution (g/m^3); $\frac{SA}{V}$ – glass surface area to solution volume ratio (m^{-1}); x_i – mass fraction of element i in the glass;

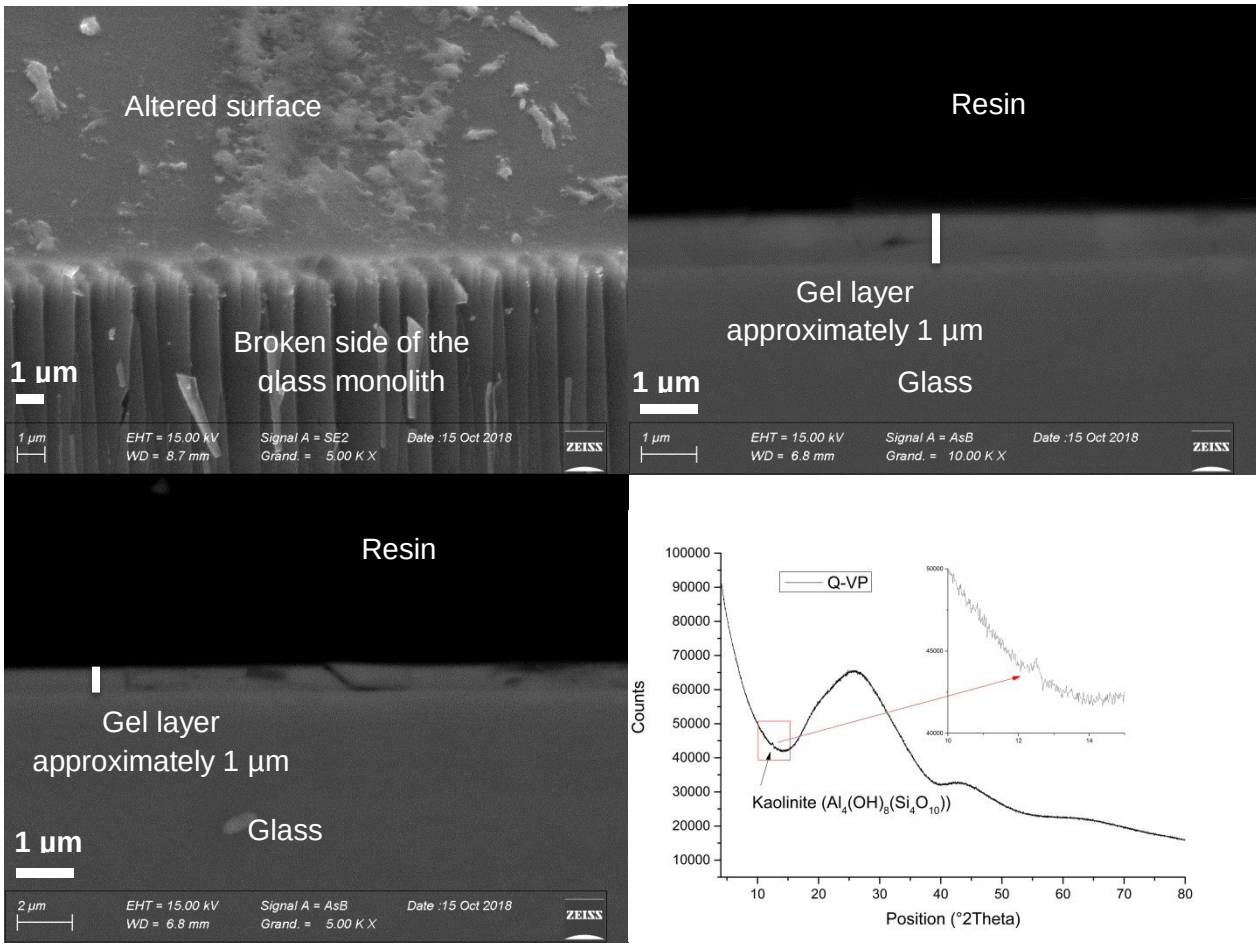

Figure A4- 1 (Top-left) SEM image of the Q monolith sample altered in vapor phase at 90°C and 98% RH for 213 days ; (Top-right & bottom-left) SEM image of cross-section of the Q monolith sample; (Bottom-right) XRD pattern of the Q monolith sample;

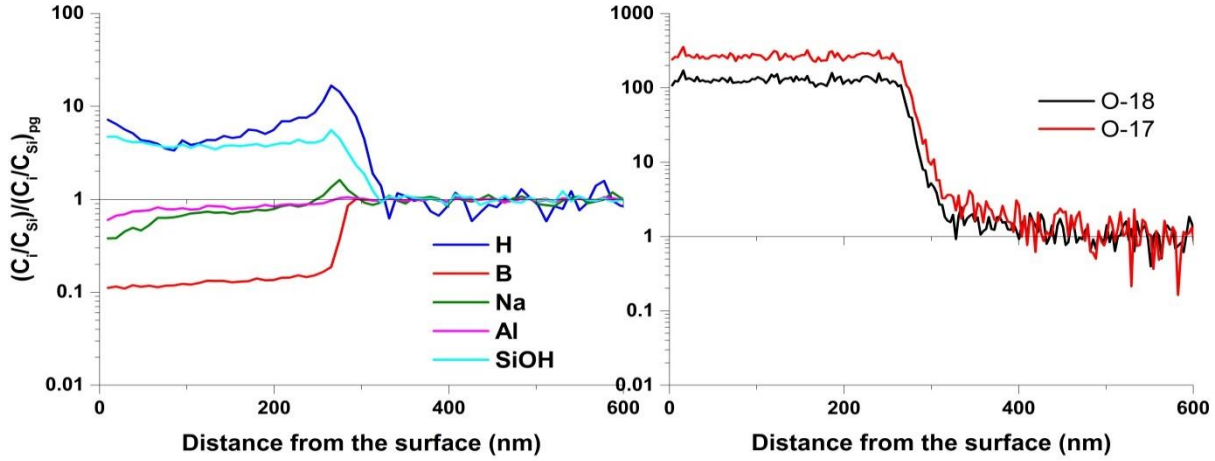

Figure A4- 2 ToF-SIMS profiles of the Q monolith sample altered in vapor phase at 90°C and 98% RH for 213 days; (left) Profiles of the secondary positive ions normalized with respect to the intensity of Si and to the intensity of element "i" in pristine glass (pg); (right) Profiles of the secondary negative oxygen ions normalized with respect to the intensity of Si and to the intensity of element "i" in pristine glass (pg);

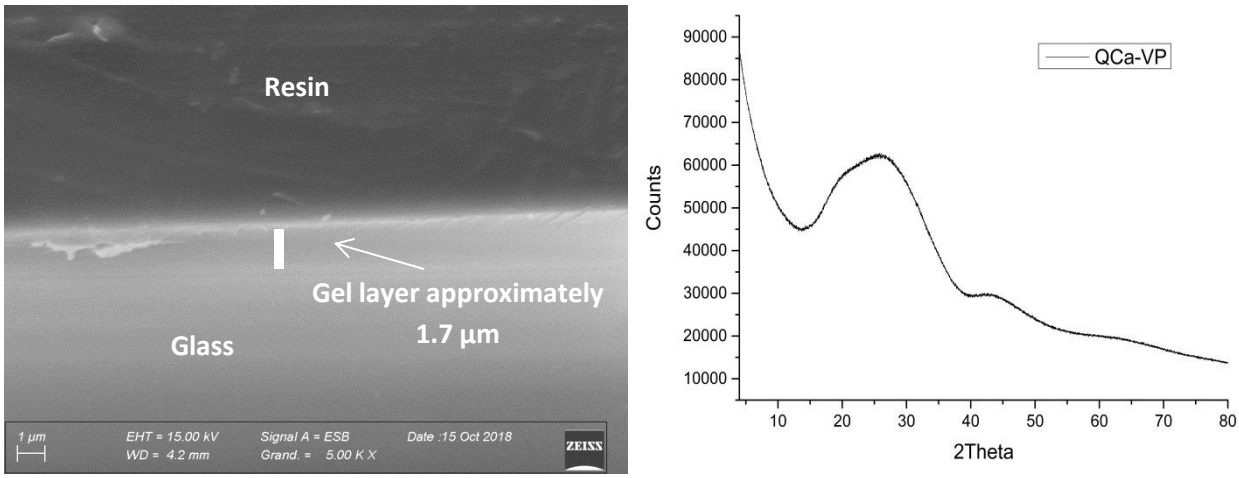

Figure A4- 3 SEM image of a cross-section of the QCa monolith sample altered in vapor phase at 90°C and 98% RH for 213 days; XRD pattern of the same monolith

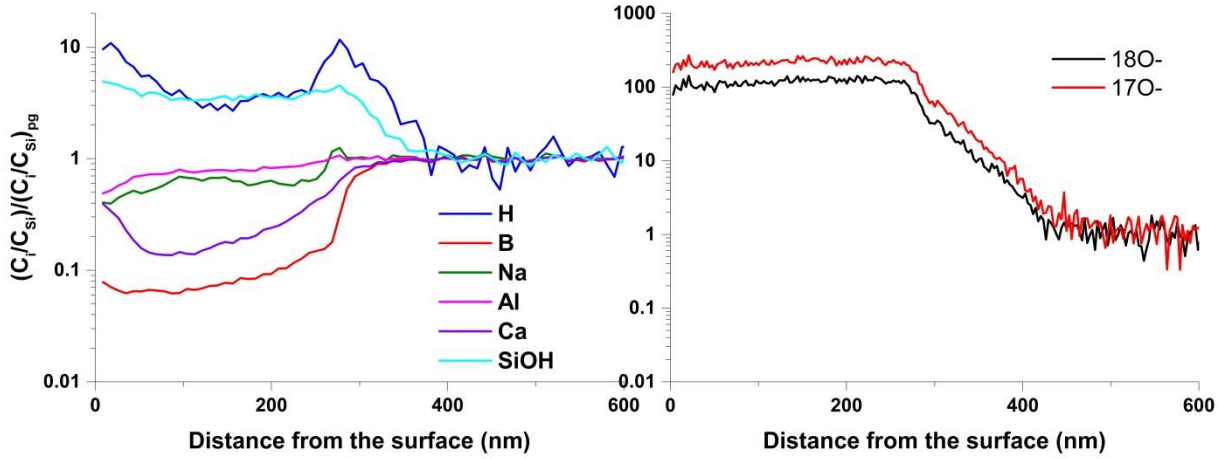

Figure A4- 4 ToF-SIMS profiles of the QCa monolith sample altered in vapor phase at 90°C and 98% RH for 213 days; (left) Profiles of the secondary positive ions normalized with respect to the intensity of Si and to the intensity of element "i" in pristine glass (pg); (right) Profiles of the secondary negative oxygen ions normalized with respect to the intensity of Si and to the intensity of element "i" in pristine glass (pg);

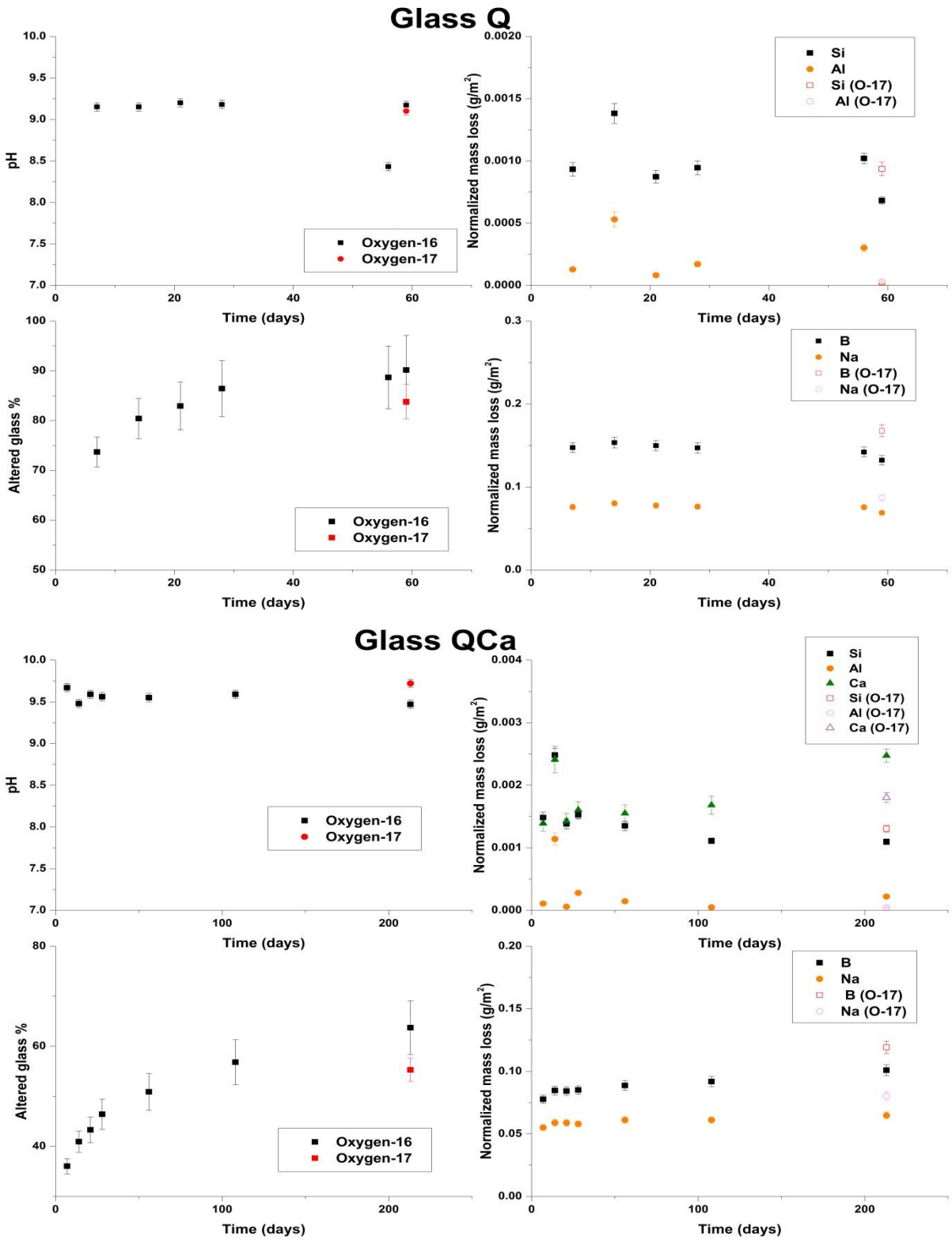

Figure A4- 5 Evolution of pH (top-left), % altered glass (bottom-left) and normalized mass loss (right) with time of the glasses Q (top) and QCa (bottom) altered in aqueous medium at 90°C and a very high SA/V ratio (around 600000 m^{-1})

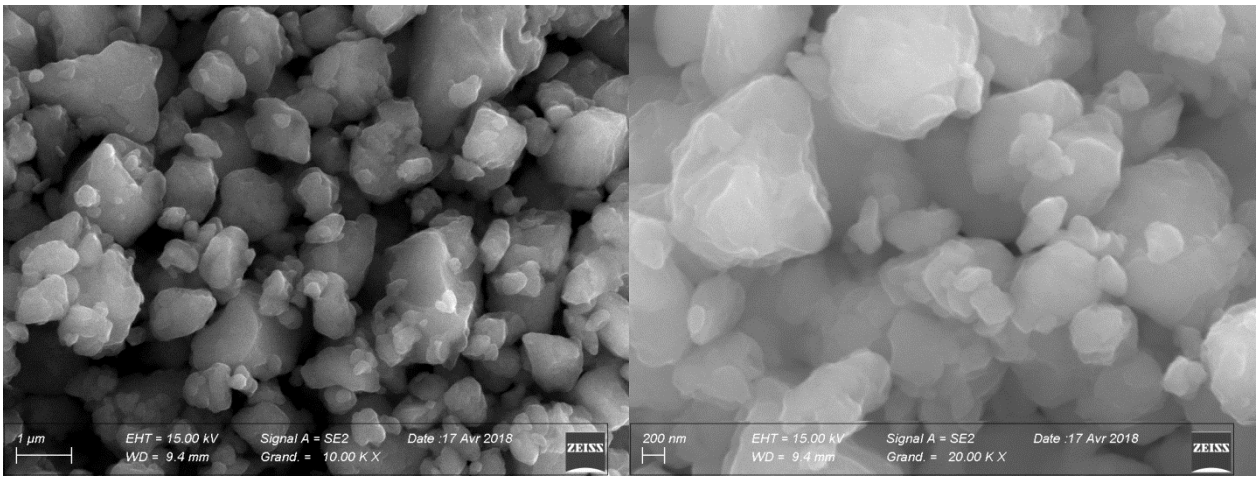

Figure A4- 6 SEM images of the Q glass powders (of grain size < 2 µm) altered in aqueous medium at 90°C and an SA/V ratio of 570438 m^{-1} for 59 days

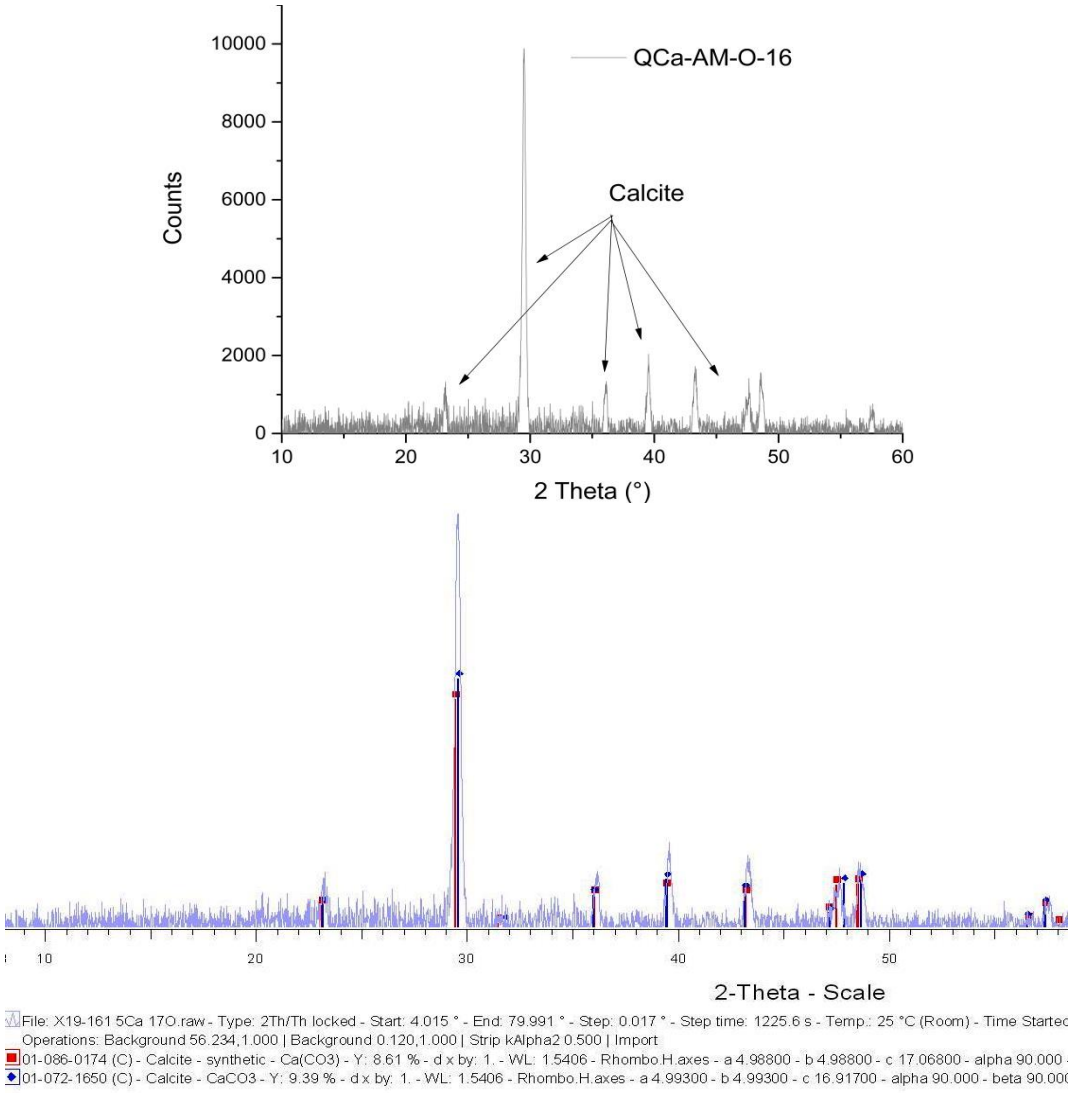

Figure A4- 7 XRD pattern of the QCa sample altered in aqueous medium at 90°C and a very high SA/V ratio of 563708 m^{-1} for 213 days

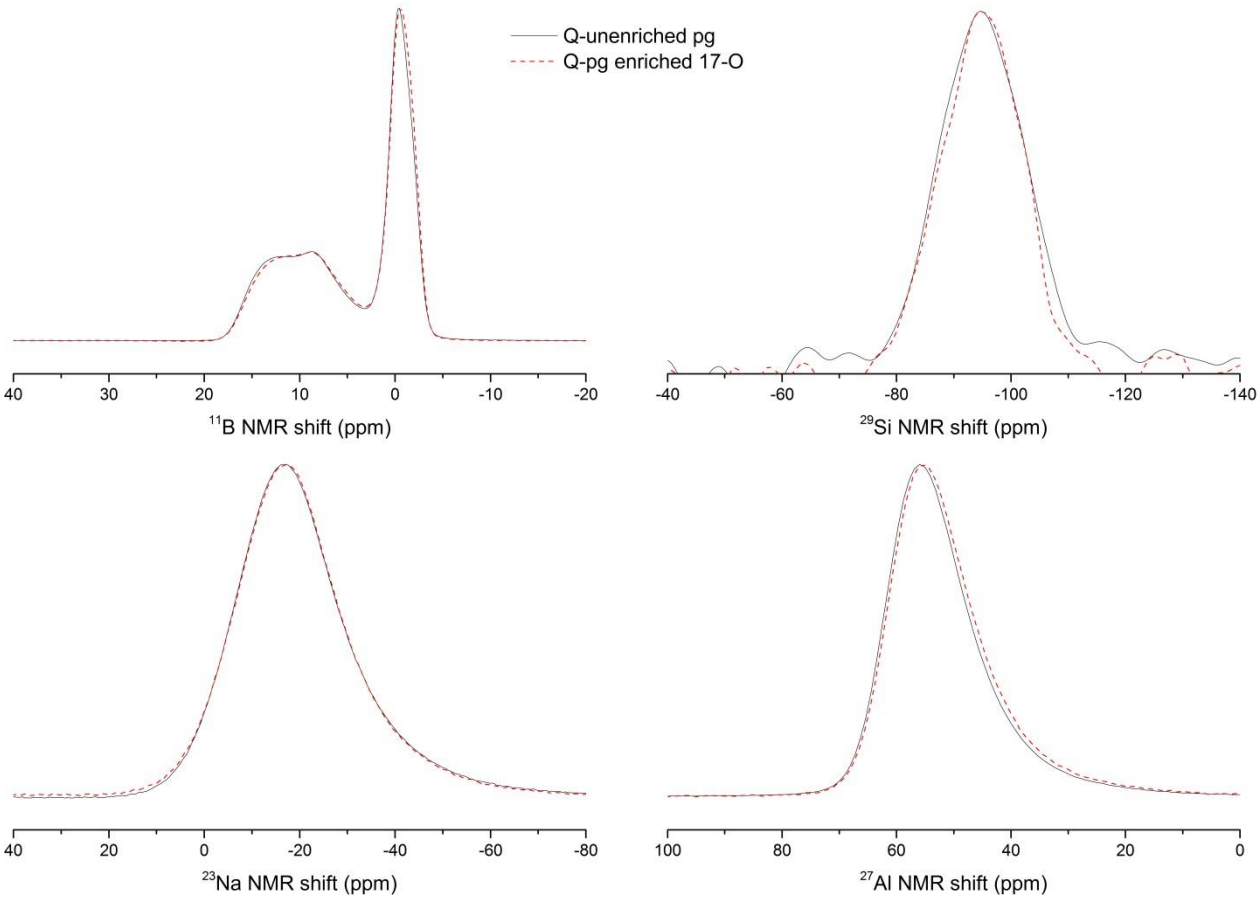

Figure A4- 8 ^{11}B (top-left), ^{29}Si (top-right), ^{23}Na (bottom-left) and ^{27}Al (bottom-right) MAS NMR spectra of the pristine Q glass (unenriched) (solid lines: Q-unenriched pg) and the pristine Q glass that is enriched in ^{17}O (80%) (red dotted lines: Q-pg enriched 17-O)

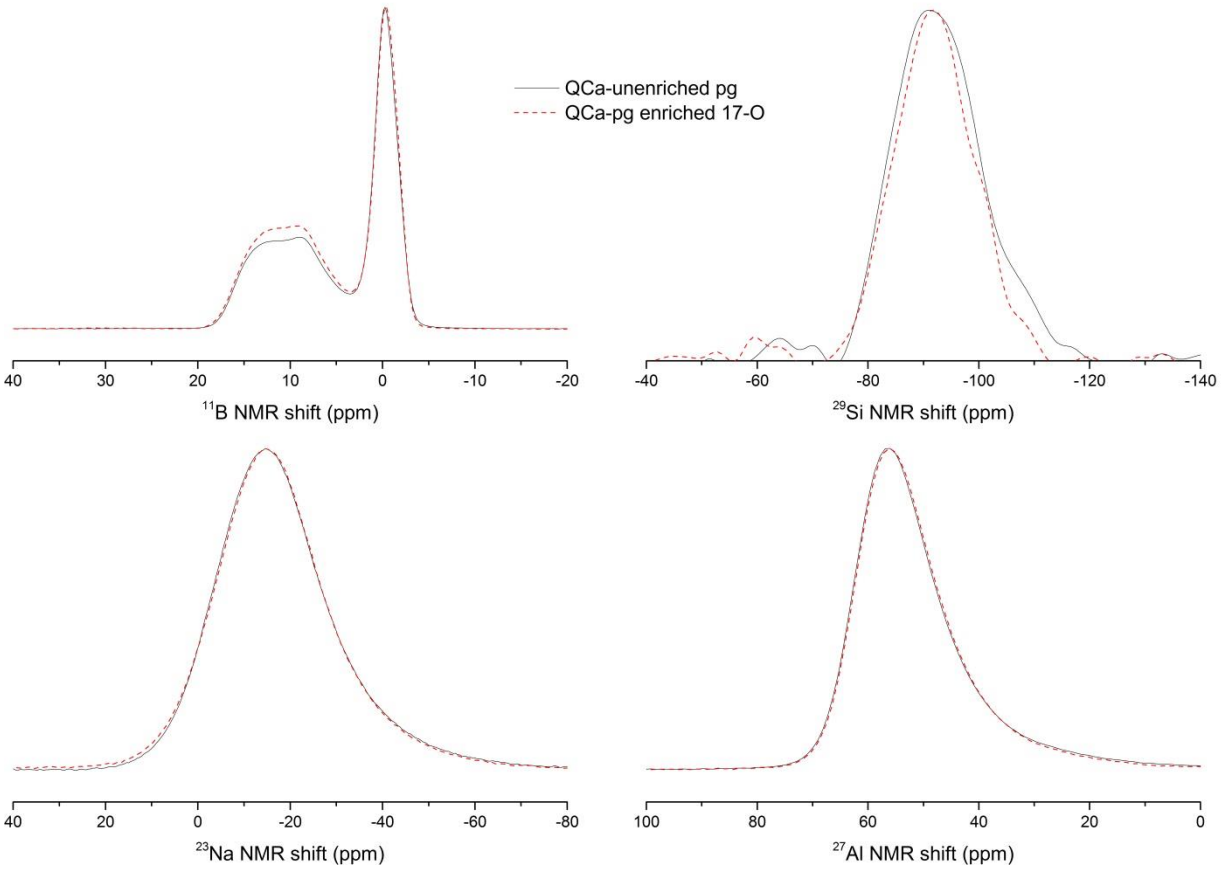

Figure A4- 9 ^{11}B (top-left), ^{29}Si (top-right), ^{23}Na (bottom-left) and ^{27}Al (bottom-right) MAS NMR spectra of the pristine QCa glass (unenriched) (solid lines: QCa-unenriched pg) and the pristine QCa glass that is enriched in ^{17}O (80%) (red dotted lines: QCa-pg enriched 17-O)

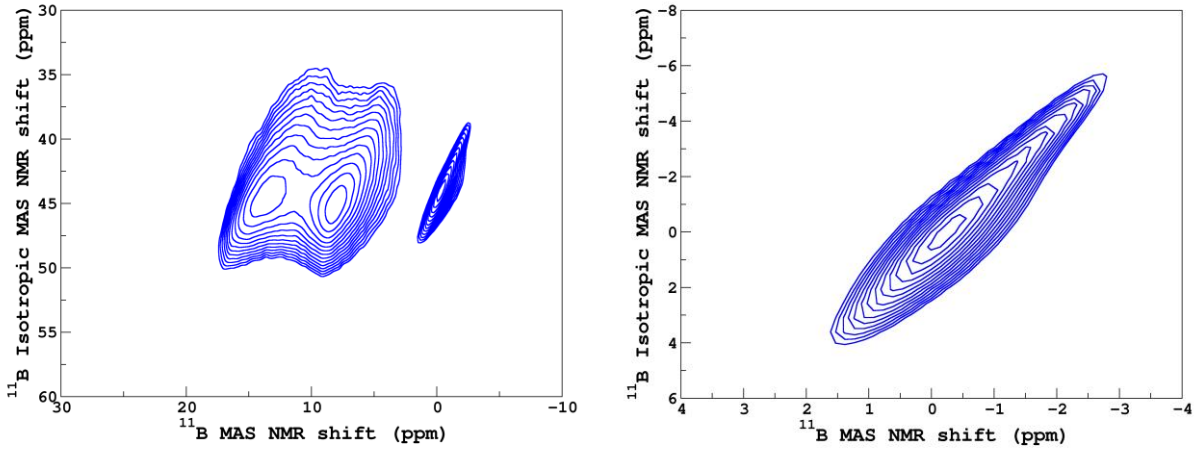

Figure A4- 10 ^{11}B MQMAS NMR spectra of tricoordinate boron (left) and tetrahedral boron in the pristine Q glass (unenriched)

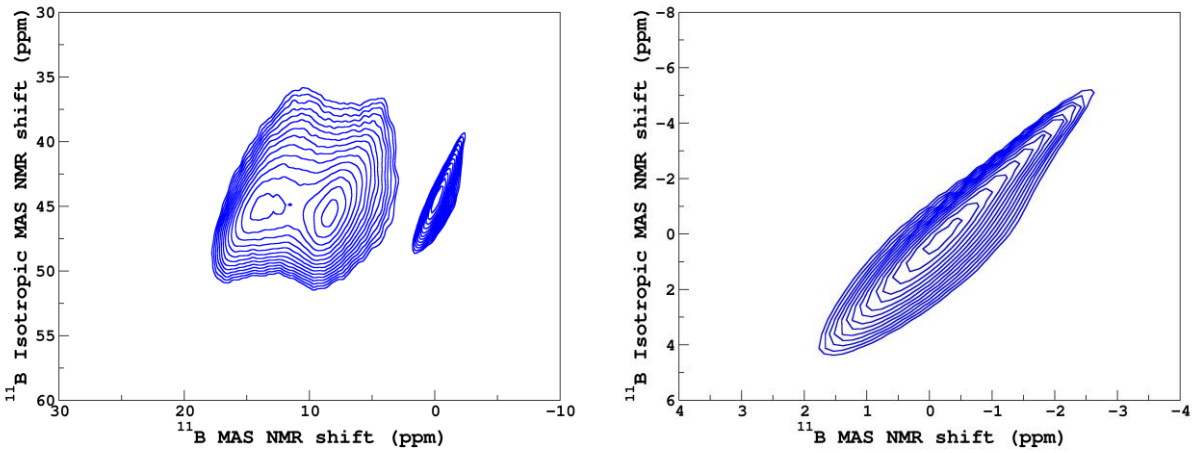

Figure A4- 11 ^{11}B MQMAS NMR spectra of tricoordinate boron (left) and tetrahedral boron in the pristine QCa glass (unenriched)

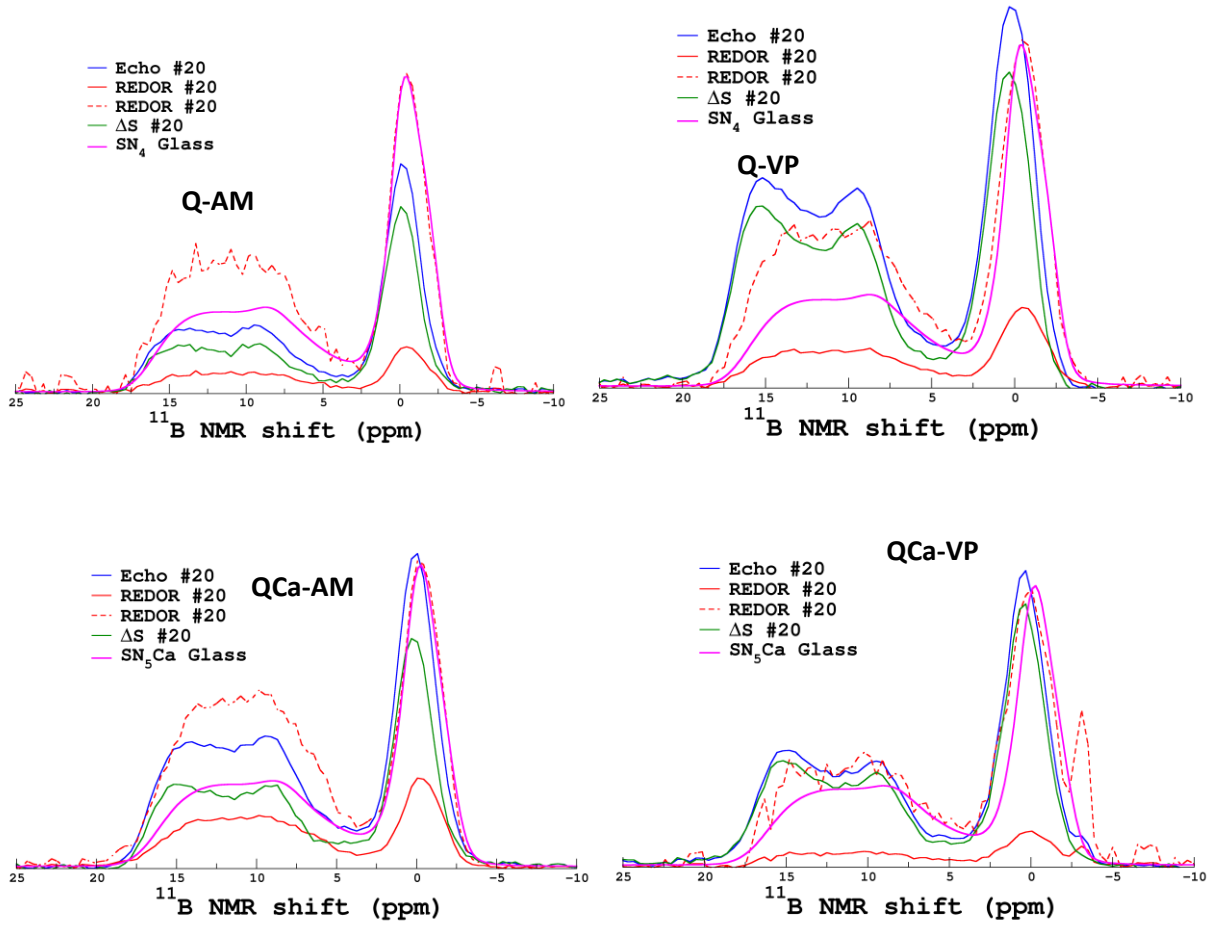

Figure A4- 12 ^{11}B NMR spectra from MAS, echo and ^{11}B{^{1}H} REDOR experiments for the glasses Q and QCa altered in aqueous medium (AM) and in vapor phase (VP)

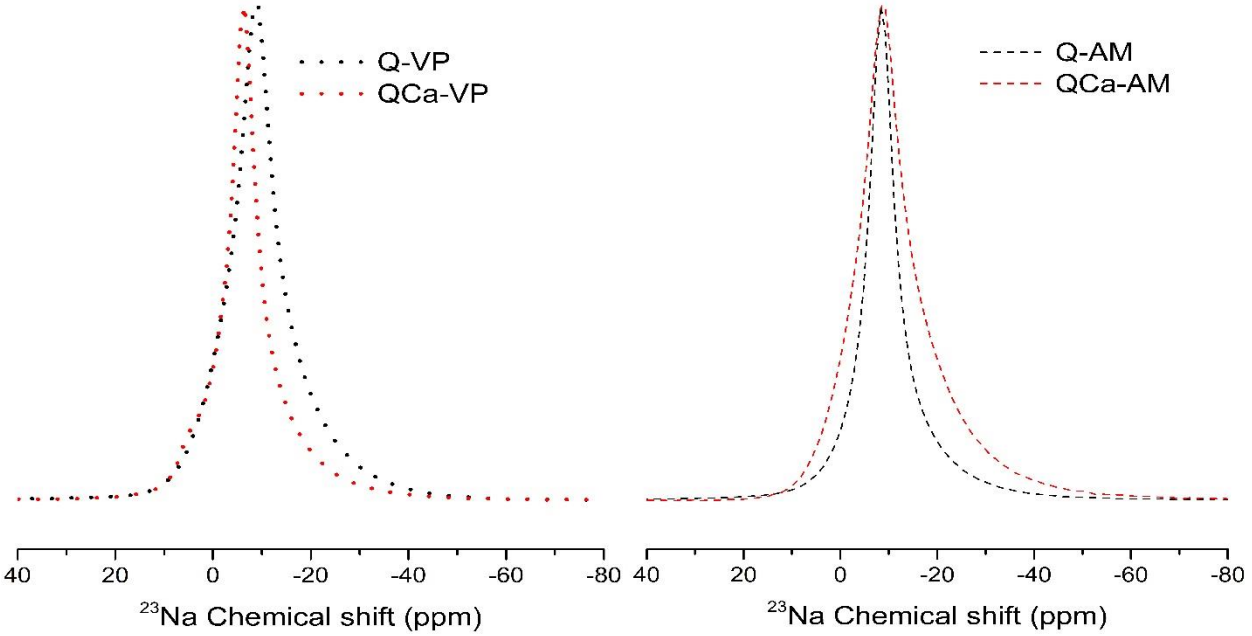

Figure A4- 13 ^{23}Na MAS NMR spectra of the Q and QCa glasses altered in vapor phase (left) and in aqueous medium (right)

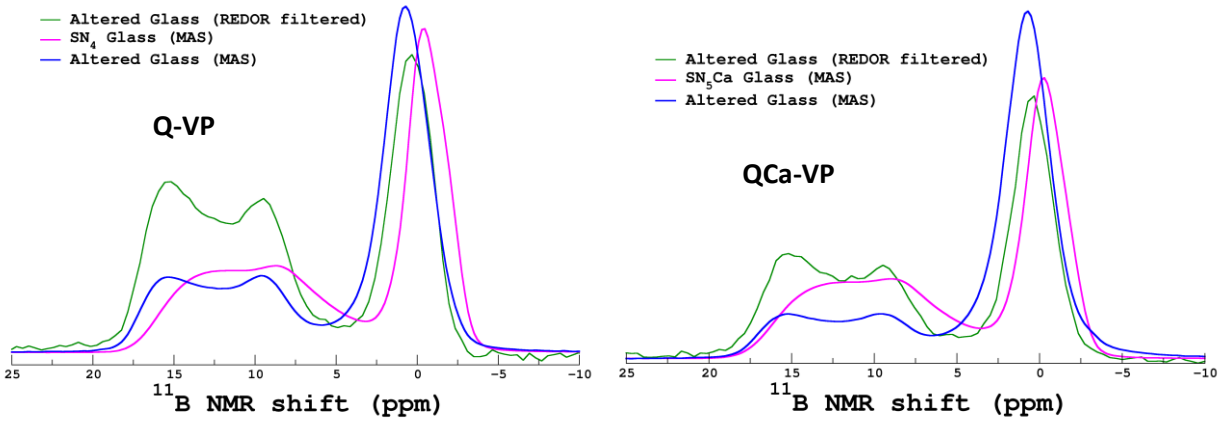

Figure A4- 14 Comparison of the ^{11}B MAS NMR spectra of the pristine glass (pink line) and altered glass (blue line) with the ^{11}B echo signal from the altered glass after ^{11}B{^{1}H} REDOR filtration (green line) for the glasses Q (left) and QCa (right) altered in vapor phase (VP)

Table A4- 1 $pH_{50°C}$, normalized mass losses (NL) of elements and altered glass percentage based on element concentrations measured in the leachates from the aqueous alteration of Q and QCa glasses at 90°C and a very high SA/V ratio (around 600000 m^{-1})

	Experiment conducted with water in…	Time, days	pH	NL(B), g/m²	NL(Na), g/m²	NL (Si), g/m² (x10⁻⁵)	NL (Al), g/m² (x10⁻⁵)	NL (Ca), g/m² (x10⁻⁴)	Altered glass%	Equivalent thickness of altered layer (NL(B)/ρ), nm
Q	Natural abundance	7	9.15	0.1474 ± 0.006	0.0758 ± 0.0033	93±5.4	13±1.3		73.7 ± 3	61
		14	9.15	0.1534 ±0.0065	0.0802 ± 0.0033	138±8	53±6.3		80.4 ± 4.1	66
		21	9.2	0.1497 ± 0.0062	0.0775 ± 0.0033	87±5.1	81±1.6		82.9 ± 4.8	68
		28	9.18	0.1470 ± 0.0062	0.0762 ± 0.0032	94±5.6	17±2		86.4 ± 5.6	71
		56	8.43	0.1420 ± 0.0059	0.0755 ± 0.0032	102±4.3	30±3.2		88.7 ± 6.3	73
		59	9.17	0.1321 ± 0.0056	0.0688 ± 0.0029	68±2.9	1.4 ± 0.6		90.1 ± 6.9	74
	Enriched in ^{17}O	59	9.1	0.1676 ± 0.0067	0.0871 ± 0.0037	9.4±5.5	2.8±0.8		83.8 ± 3.5	69
QCa	Natural abundance	7	9.67	0.0777 ± 0.0034	0.0551 ± 0.0024	148±8.7	11±2.2	13.9 ±1.2	36 ± 1.5	31
		14	9.48	0.0847 ± 0.0036	0.0590 ± 0.0026	24.8±1.1	114±9.5	24.1±2.1	40.9 ± 2.1	35
		21	9.59	0.0842 ± 0.0035	0.0588 ± 0.0025	138±8.1	58±1.9	14.3±1.2	43.3 ± 2.6	37
		28	9.56	0.0851 ± 0.0034	0.0579 ± 0.0024	153±6.4	28±3.1	16±1.3	46.4 ± 3	40
		56	9.55	0.0887 ± 0.0039	0.0611 ± 0.0026	135±7.9	14±1.7	15.5±1.3	50.9 ± 3.7	44
		108	9.59	0.0919 ± 0.0040	0.0611 ± 0.0026	111±4.7	4.9±0.9	16.8±1.5	56.8 ± 4.5	49
		213	9.47	0.1009 ± 0.0048	0.0647 ± 0.0028	110±4.6	22±1.9	24.7±1.1	63.7 ± 5.4	55
	Enriched in ^{17}O	213	9.72	0.1192 ± 0.0051	0.0802 ± 0.0034	130±5.5	4.4±0.4	1.8±0.8	55.3 ± 2.3	48

Appendix 5

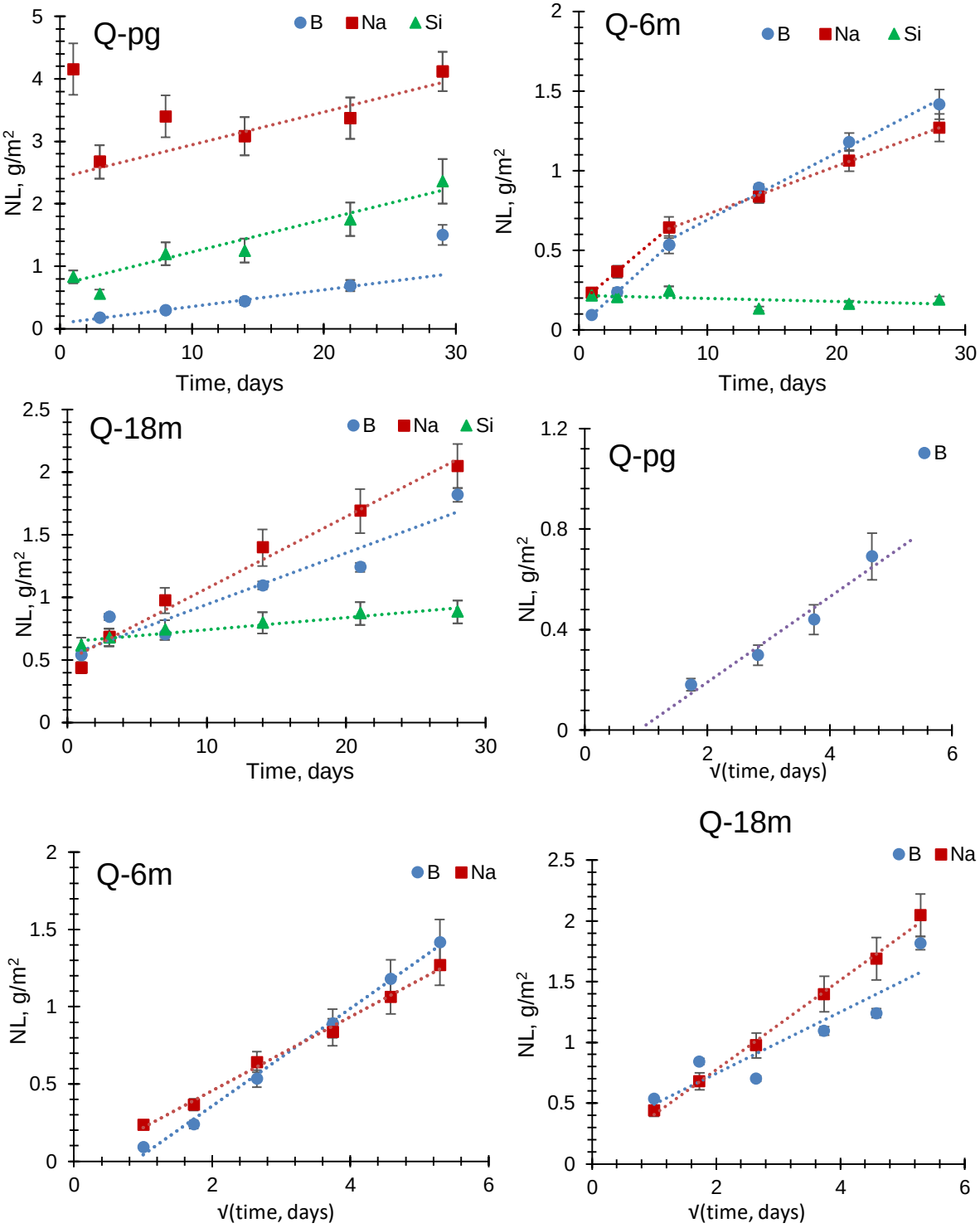

Figure A5- 1 Evolution of NL of the glass elements of Q that was initially pristine (pg), pre-hydrated for 6 months (6m) and pre-hydrated for 18 months (18m) (top and center-left); (center-right and bottom) NL=f(√t) curves of the elements B and Na for the glasses Q-pg, Q-6m and Q-18m.

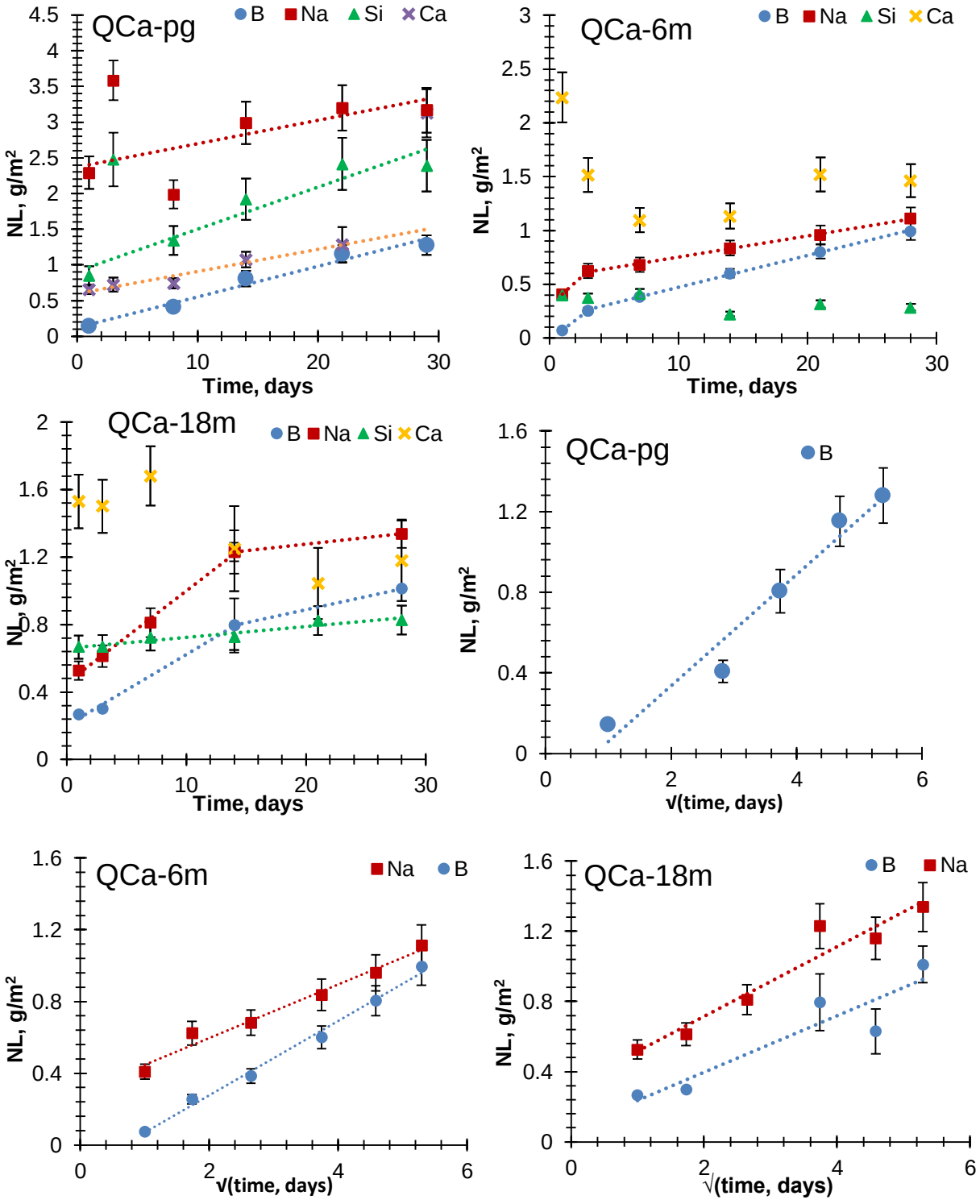

Figure A5- 2 Evolution of NL of the glass elements of QCa that was initially pristine (pg), pre-hydrated for 6 months (6m) and pre-hydrated for 18 months (18m) (top and center-left); (center-right and bottom) NL=f(√t) curves of the elements B and Na for the glasses QCa-pg, QCa-6m and QCa-18m.

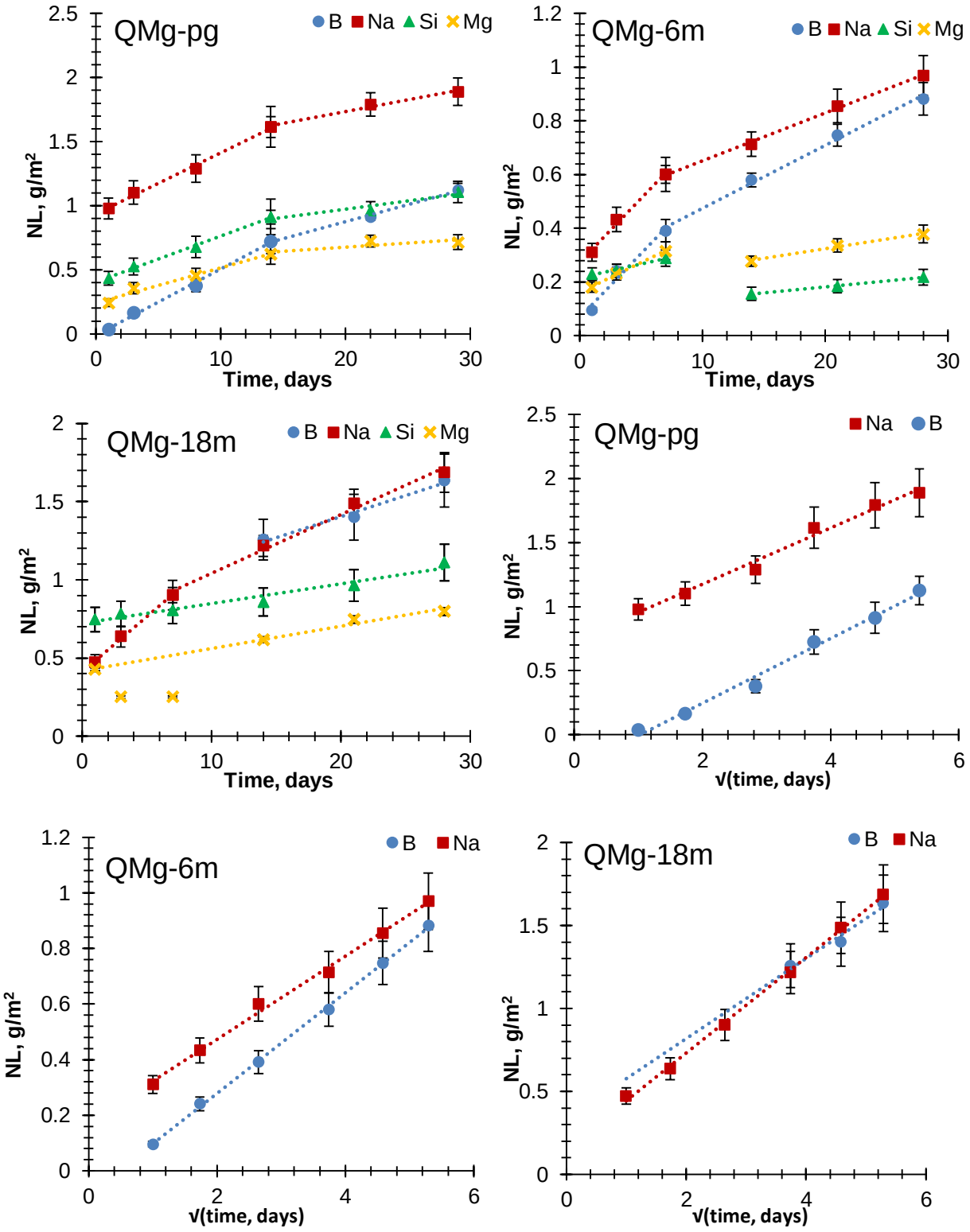

Figure A5- 3 Evolution of NL of the glass elements of QMg that was initially pristine (pg), pre-hydrated for 6 months (6m) and pre-hydrated for 18 months (18m) (top and center-left); (center-right and bottom) NL=f(√t) curves of the elements B and Na for the glasses QMg-pg, QMg-6m and QMg-18m.

SEM images of the simplified glasses after aqueous alteration in DI water at 50°C and 20 m^{-1} SA/V for 28 days

**The indicated gel layer thicknesses measured on SEM images have a large uncertainty since the sample was tilted during image acquisition

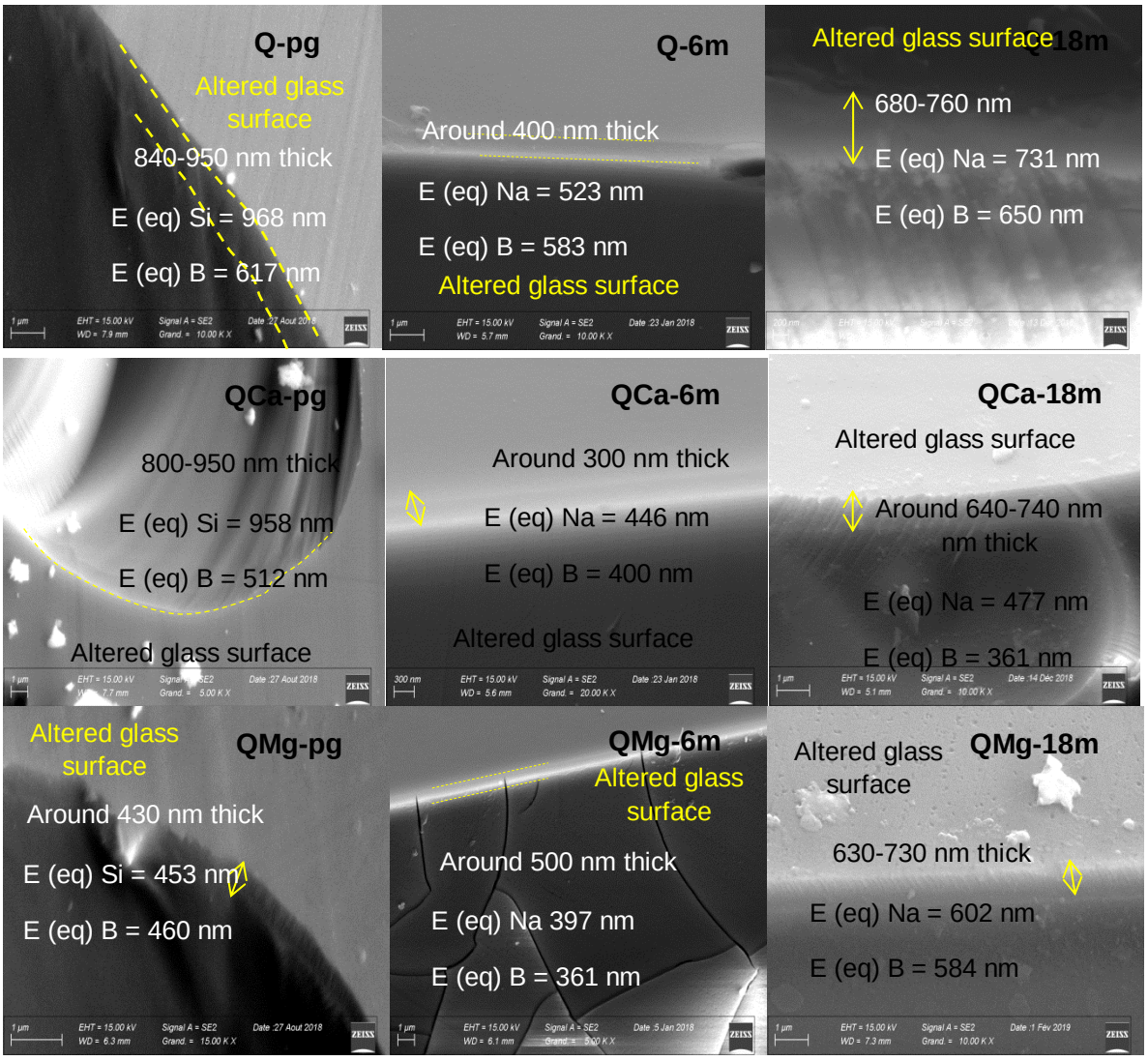

Figure A5- 4 SEM images of pristine Q (first row), QCa (second row) & QMg (third row) glasses (pg), and glasses pre-hydrated for 6 months and 18 months (6m & 18m) after aqueous alteration in DI water for 28 days at 50°C and 20 m^{-1} SA/V ratio; E (eq) denotes the equivalent thickness of glass altered, calculated based on normalized mass loss of the indicated elements.

SEM images of the complex glasses after aqueous alteration in DI water at 50°C and 20 m^{-1} SA/V for 28 days

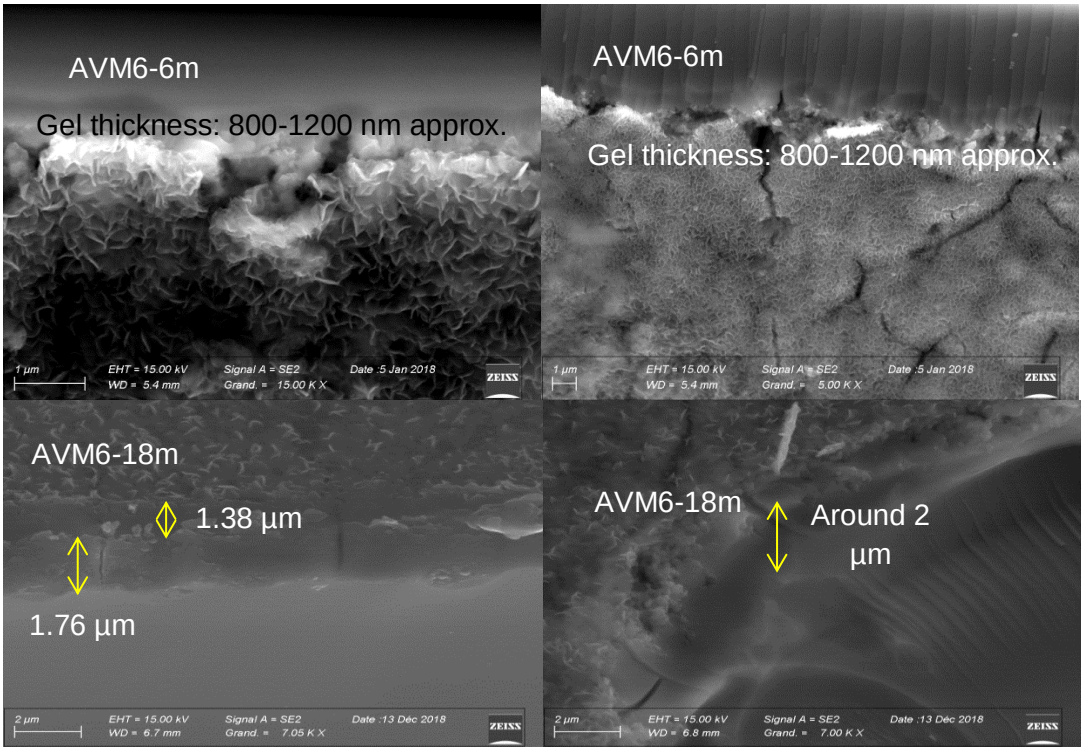

Figure A5- 5 SEM images of AVM6 glass pre-hydrated for 6 months (top) and 18 months (bottom) after aqueous alteration in DI water for 28 days at 50°C and 20 m^{-1} SA/V ratio;

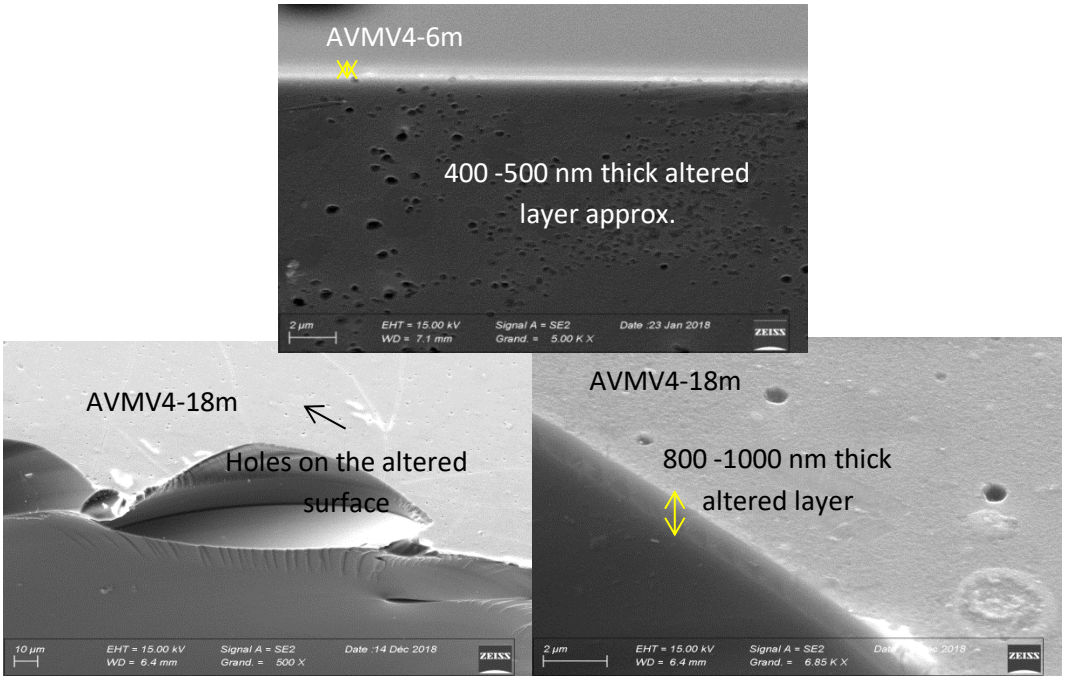

Figure A5- 6 SEM images of AVMV4 glass pre-hydrated for 6 months (top) and 18 months (bottom) after aqueous alteration in DI water for 28 days at 50°C and 20 m^{-1} SA/V ratio;

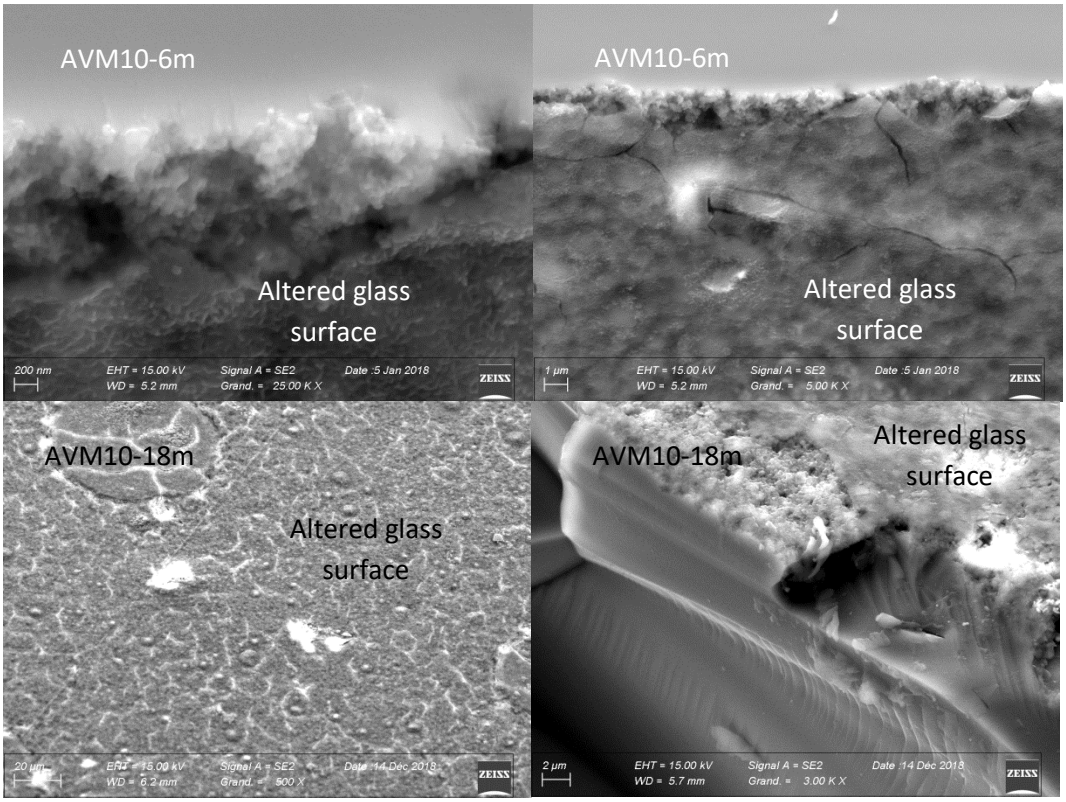

Figure A5- 7 SEM images of AVM10 glass pre-hydrated for 6 months (top) and 18 months (bottom) after aqueous alteration in DI water for 28 days at 50°C and 20 m^{-1} SA/V ratio; The thickness of altered layer for these glasses is unclear /irregular;

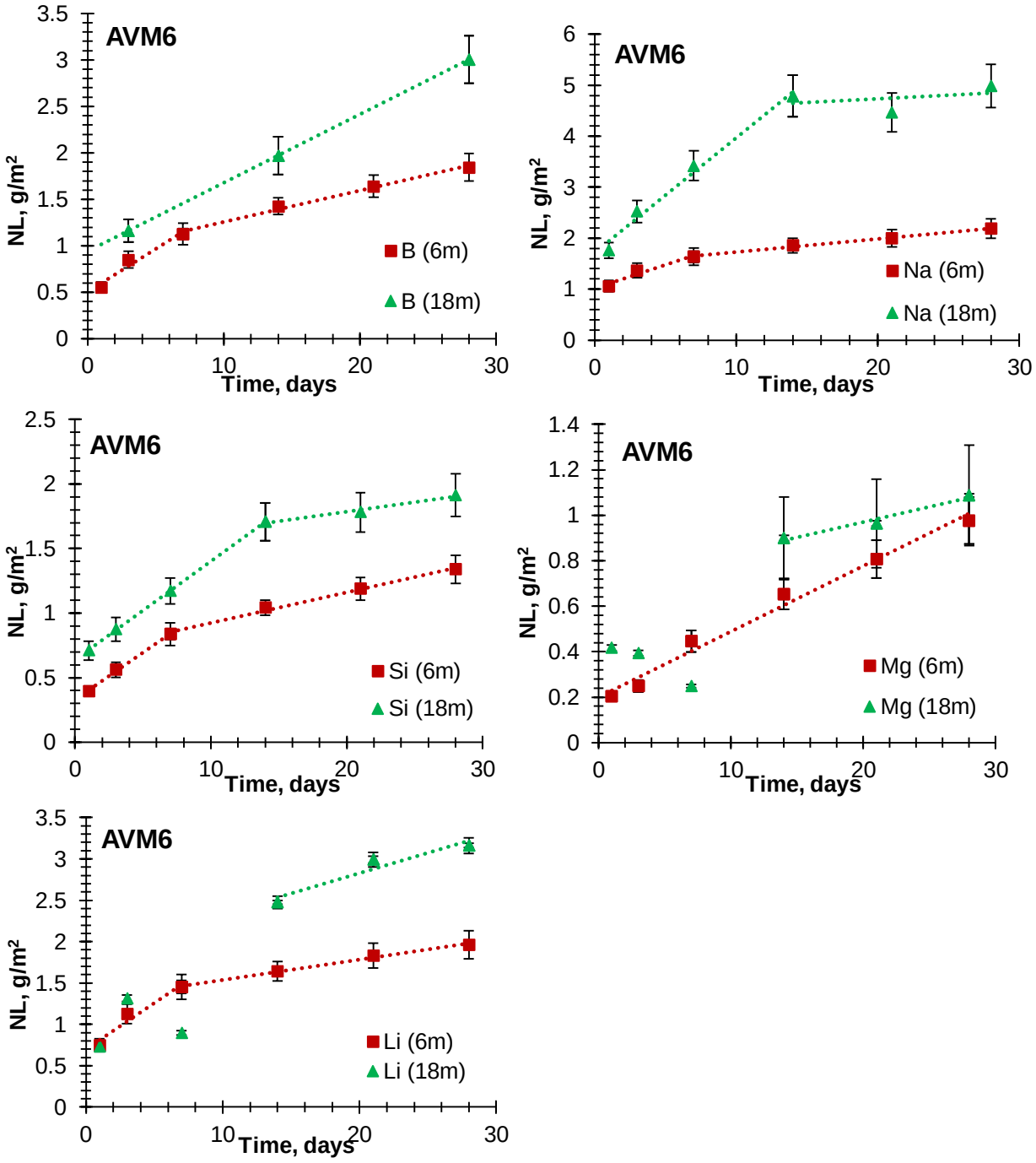

Figure A5- 8 Evolution of normalized mass losses (NL) of B, Na, Si, Mg and Li for the AVM6 glass samples pre-hydrated for 6 months (6m) and for 18 months (18m); the dotted lines represent the linear regression by which the release rates of the elements were calculated

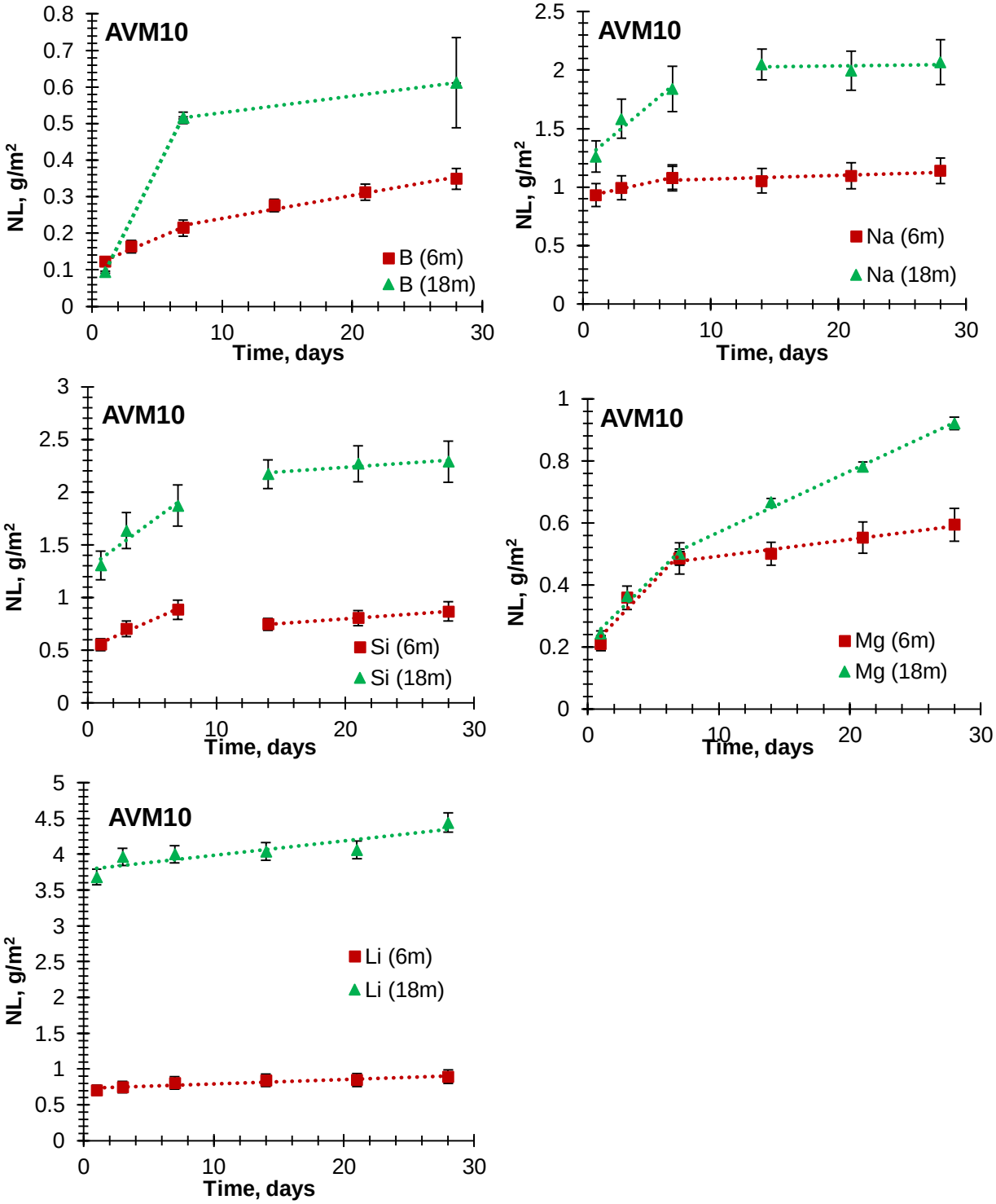

Figure A5- 9 Evolution of normalized mass losses (NL) of B, Na, Si, Mg and Li for the AVM10 glass samples pre-hydrated for 6 months (6m) and for 18 months (18m); the dotted lines represent the linear regression by which the release rates of the elements were calculated

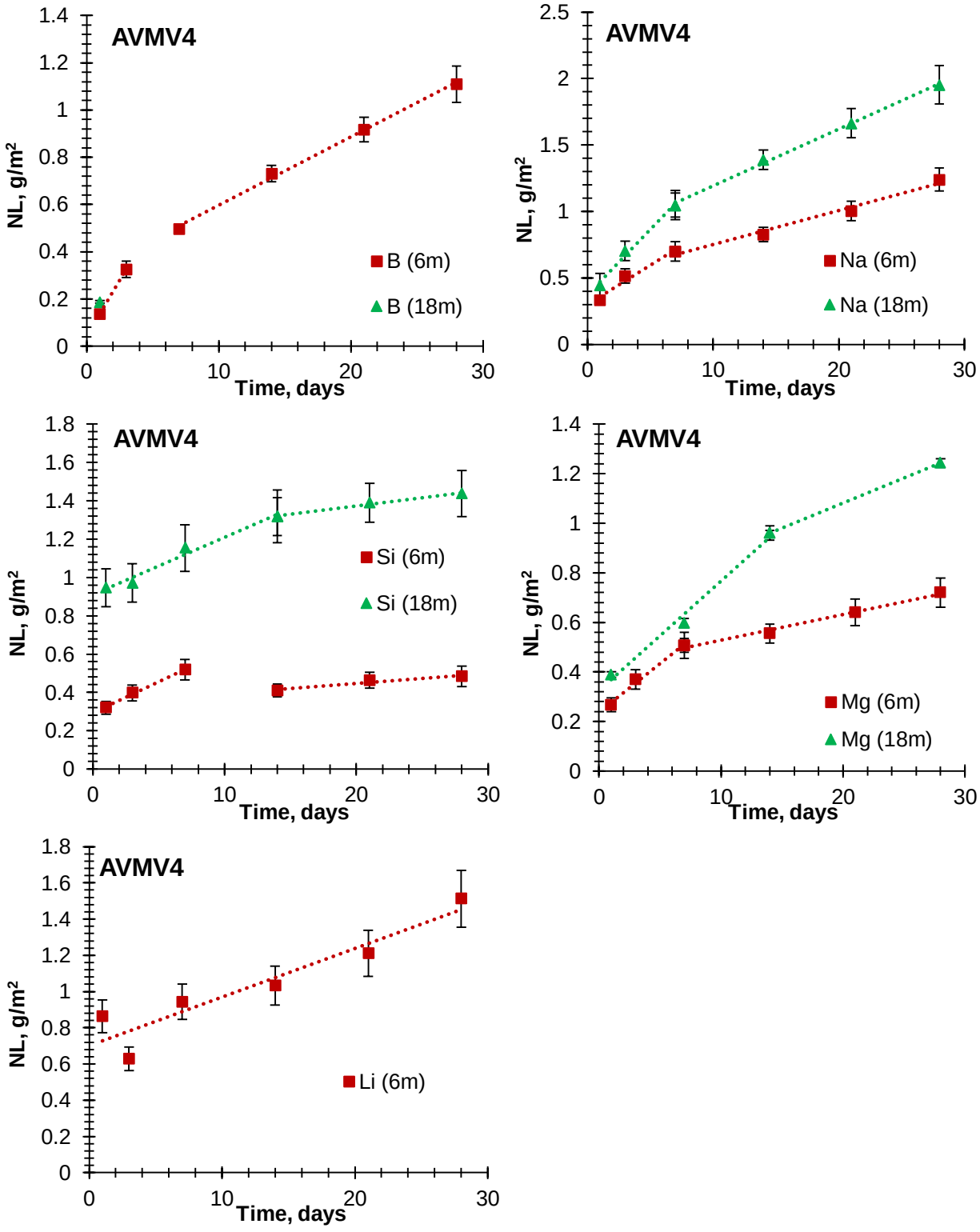

Figure A5- 10 Evolution of normalized mass losses (NL) of B, Na, Si, Mg and Li for the AVMV4 glass samples pre-hydrated for 6 months (6m) and for 18 months (18m); the dotted lines represent the linear regression by which the release rates of the elements were calculated

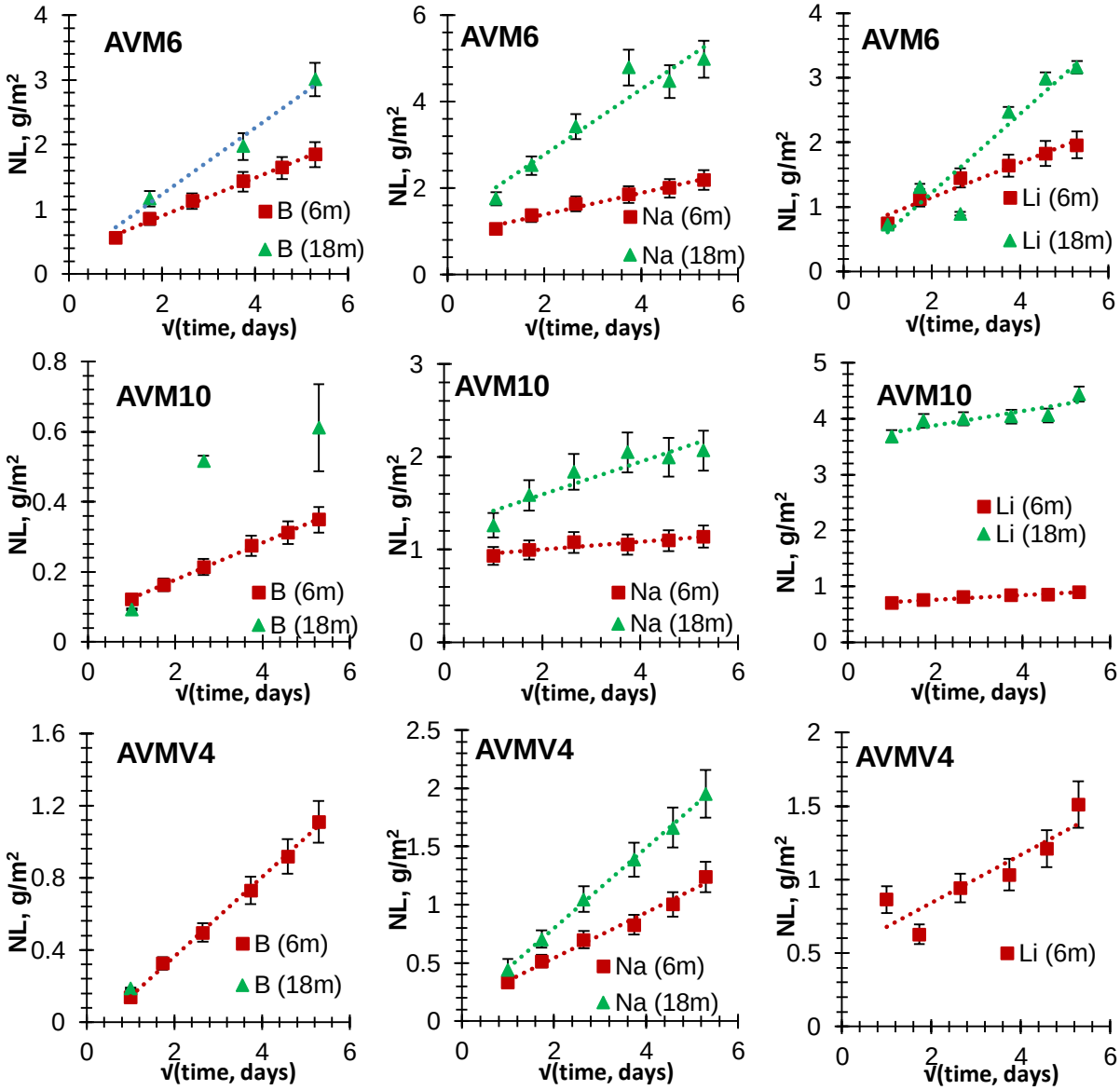

Figure A5- 11 NL(i)=f(√time) curves for i= B, Na and Li for the glasses AVM6 (top), AVM10 (center) and AVMV4 (bottom) that were pre-hydrated in vapor phase for 6 months (6m) (in red) and 18 months (18m) (in green)

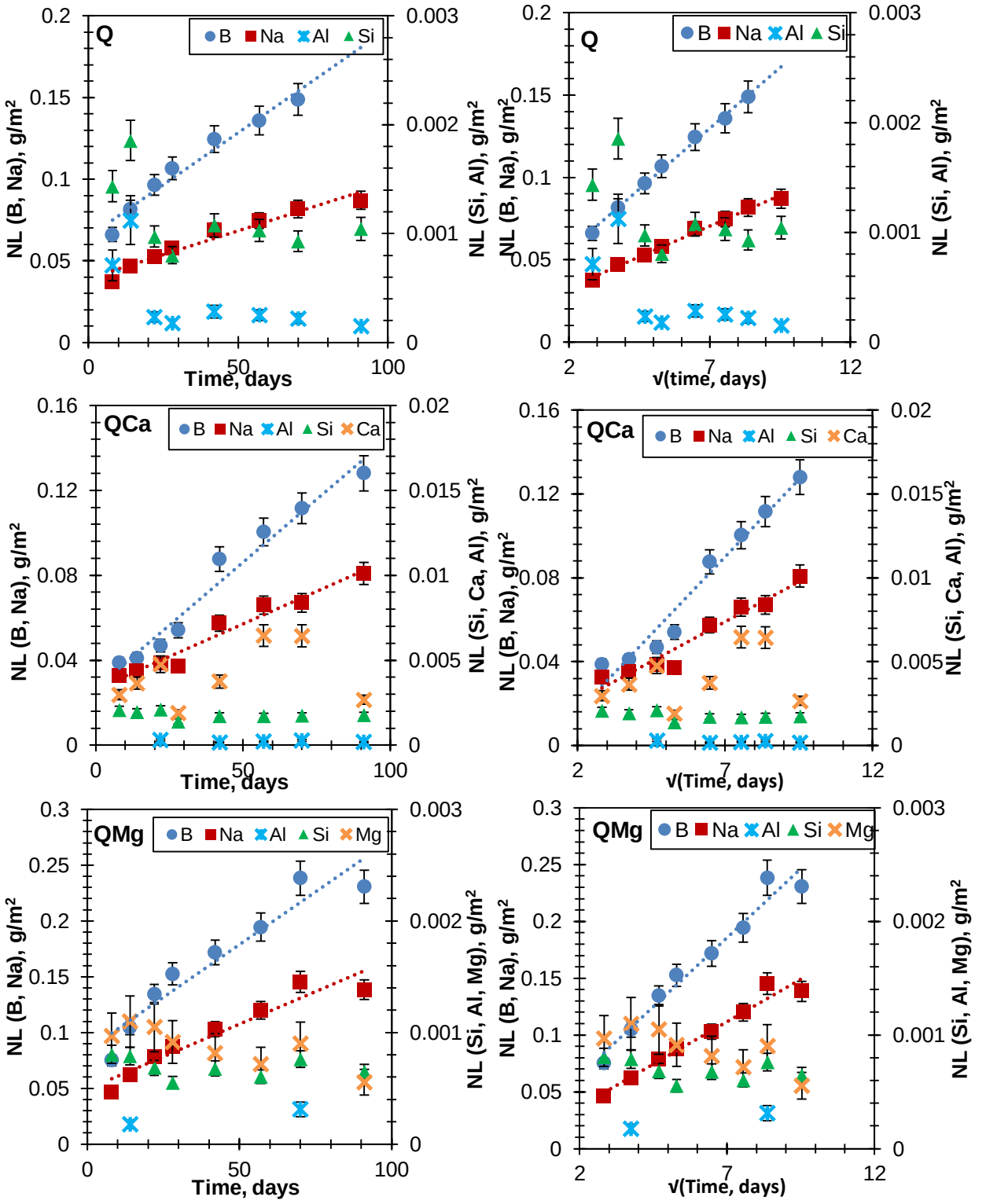

Figure A5- 12 Evolution of the normalized mass losses of the glass elements in the leachate during the aqueous alteration of the glasses Q, QCa and QMg at 50°C and SA/V ratio of 200000 m^{-1} during 91 days; (lefft side) evolution of NL with time; (right side) evolution of NL with square root of time;

Appendix 5

Table A5- 1 Solution analysis of the leachate that was used to alter the three simplified pristine glasses at 50°C and a low SA/V of 20 m^{-1} for 29 days; The uncertainties associated with the concentration, NL and equivalent thickness are around 10% for Al & Na, 13% for B, Mg & Ca and 15% for Si;

Glass	Time, days	$pH_{50°C}$	Concentration, mg/L						NL, g/m2						Equivalent thickness of altered glass, nm						Thickness (MEB), nm
			Si	B	Na	Al	Ca	Mg	Si	B	Na	Al	Ca	Mg	Si	B	Na	Al	Ca	Mg	
Q	1	6.68	2.66		7.28	0.13			0.83		4.16	0.14			339		1705	59.3			840-950 nm approx.
	3	6.93	1.85	0.12	4.80	0.12			0.56	0.18	2.67	0.14			230	74.2	1095	56.3			
	8	6.59	4.05	0.21	6.26	0.53			1.20	0.30	3.40	0.58			492	122	1394	238			
	14	6.90	4.34	0.31	5.84	0.07			1.25	0.44	3.08	0.08			512	180	1265	32.0			
	22	7.02	6.26	0.50	6.57	0.11			1.75	0.69	3.37	0.12			718	283	1383	47.6			
	29	7.02	8.68	1.13	8.27	0.84			2.36	1.50	4.12	0.85			968	617	1689	348			
QCa	1	6.71	3.49	0.13	5.56	0.06	0.45		0.85	0.14	2.29	0.06	0.65		340	57.2	918	22.4	261		800-950 nm approx.
	3	6.88	10.62	1.53	9.08	1.71	0.52		2.48	1.67	3.59	1.46	0.72		993	669	1437	585	289		
	8	6.87	5.92	0.38	5.17	0.11	0.55		1.34	0.41	1.99	0.09	0.74		538	163	796	38.1	297		
	14	7.13	8.67	0.78	7.97	0.22	0.82		1.92	0.81	2.99	0.18	1.08		769	323	1198	72.3	431		
	22	7.24	11.21	1.14	8.77	0.30	1.01		2.41	1.15	3.20	0.24	1.28		966	462	1282	95.1	515		
	29	7.32	11.45	1.31	8.96	0.29	2.52		2.39	1.28	3.17	0.23	3.12		958	513	1270	90.2	1252		
QMg	1	6.52	2.02	0.04	2.67	0.02		0.11	0.43	0.04	0.98	0.02		0.24	178	15.1	401	7.3		99.5	Around 430 nm approx.
	3	6.81	2.55	0.18	3.12	0.07		0.16	0.53	0.17	1.10	0.05		0.36	216	67.6	452	20.1		146	
	8	6.85	3.36	0.41	3.75	0.11		0.22	0.68	0.38	1.29	0.08		0.46	278	155	528	33.1		187	
	14	7.14	4.64	0.81	4.82	0.17		0.30	0.91	0.72	1.62	0.12		0.62	374	297	662	48.7		255	
	22	7.24	5.05	1.05	5.50	0.23		0.36	0.96	0.91	1.79	0.15		0.72	395	374	734	63		297	
	29	7.32	5.97	1.33	5.97	0.28		0.37	1.11	1.12	1.89	0.19		0.72	454	461	774	76.0		293	

Table A5- 2 Solution analysis of the leachate that was used to alter the three simplified glasses pre-hydrated for 6 months at 50°C and a low SA/V of 20 m^{-1} for 28 days; The uncertainties associated with the concentration, NL and equivalent thickness are around 10% for all elements; The uncertainty of pH measurement is ±0.05 units

Glass	Time, days	$pH_{50°C}$	Concentration, mg/L					NL, g/m2					Equivalent thickness of altered glass, nm					Thickness (MEB), nm
			Si	B	Na	Ca	Mg	Si	B	Na	Ca	Mg	Si	B	Na	Ca	Mg	
Q	1	6.82	1.53	0.13	0.91			0.22	0.09	0.24			89.2	38.1	96.8			Around 500 nm thick
	3	6.98	1.46	0.34	1.41			0.21	0.24	0.37			85.4	97.8	150			
	7	7.41	1.76	0.78	2.50			0.25	0.53	0.64			102	219	264			
	14	7.67	0.90	1.32	3.29			0.13	0.89	0.84			54.7	366	344			
	21	7.78	1.15	1.78	4.23			0.17	1.18	1.06			68.0	486	437			
	28	7.81	1.35	2.15	5.12			0.19	1.42	1.27			78.4	583	523			
QCa	1	6.51	1.72	0.07	1.05	1.64		0.40	0.07	0.41	2.24		159	29.2	164	898		Around 300 nm thick
	3	6.93	1.62	0.24	1.60	1.11		0.37	0.26	0.62	1.51		150	103	250	608		
	7	7.04	1.80	0.36	1.75	0.79		0.41	0.39	0.68	1.10		166	155	274	440		
	14	7.24	0.93	0.57	2.17	0.82		0.22	0.60	0.84	1.13		89.7	241	336	455		
	21	7.25	1.37	0.77	2.51	1.13		0.32	0.80	0.96	1.52		127	323	386	611		
	28	7.32	1.22	0.97	2.94	1.08		0.29	1.00	1.11	1.46		115	400	447	588		
QMg	1	6.56	1.35	0.12	1.07		0.10	0.23	0.10	0.31		0.18	94	39.2	127		74.5	Around 400 nm thick
	3	7.24	1.42	0.31	1.49		0.13	0.24	0.24	0.43		0.23	99	98.9	178		94.7	
	7	7.36	1.71	0.51	2.09		0.18	0.29	0.39	0.60		0.32	119	160	246		129	
	14	7.45	0.88	0.77	2.50		0.16	0.16	0.58	0.71		0.28	64	237	293		114	
	21	7.54	1.07	1.00	3.02		0.19	0.18	0.75	0.86		0.34	75.7	306	350		138	
	28	7.63	1.28	1.20	3.46		0.22	0.22	0.88	0.97		0.38	89.4	361	397		155	

Table A5- 3 Solution analysis of the leachate that was used to alter the three simplified glasses pre-hydrated for 18 months at 50°C and a low SA/V of 20 m^{-1} for 28 days; The uncertainties associated with the concentration, NL and equivalent thickness are around 10% for Na and Si, boron, Li, Mg and Al concentrations are mostly indicative and the uncertainty could be more than 10%; The uncertainty of pH measurement is ±0.05 units

Glass	Time, days	$pH_{50°C}$	Concentration, mg/L						NL, g/m2						Equivalent thickness of altered glass, nm						Thickness (MEB), nm
			Si	B	Na	Al	Ca	Mg	Si	B	Na	Al	Ca	Mg	Si	B	Na	Al	Ca	Mg	
Q	1	7.20	2.93	0.52	1.14	0.08			0.61	0.54	0.44	0.07			219	192	156	23.6			680-760 nm approx.
	3	7.30	3.24	0.82	1.77	0.13			0.68	0.84	0.68	0.10			243	301	243	36.2			
	7	7.36	3.54	0.68	2.56				0.74	0.70	0.97				264	251	348				
	14	7.49	3.82	1.09	3.72	0.08			0.80	1.09	1.40	0.07			284	391	499	23.2			
	21	7.55	4.21	1.24	4.54	0.03			0.87	1.24	1.69	0.02			311	443	603	8			
	28	7.64	4.28	1.87	5.59	0.32			0.88	1.82	2.05	0.23			315	649	731	81.2			
QCa	1	7.14	3.05	0.26	1.42	0.18	1.18		0.67	0.27	0.53	0.14	1.53		238	95.4	188	51.6	546		640-740 nm approx.
	3	7.27	3.06	0.29	1.66	0.12	1.16		0.67	0.30	0.61	0.10	1.50		239	107	219	35.5	535		
	7	7.25	3.32		2.21		1.30		0.72		0.81		1.68		258		290		600		
	14	7.34	3.33	0.82	3.40	0.18	0.95		0.73	0.80	1.23	0.14	1.25		259	284	439	49.3	446		
	21	7.50	3.81	0.64	3.19	0.16	0.78		0.82	0.63	1.16	0.13	1.04		294	225	414	45.2	372		
	28	7.46	3.83	1.06	3.73	0.24	0.90		0.83	1.01	1.34	0.18	1.18		295	361	478	65.0	421		
QMg	1	7.04	3.11		1.15	0.16		0.17	0.75		0.47	0.14		0.43	266		168	48.4		152	630-730 nm approx.
	3	7.03	3.27		1.56			0.10	0.78		0.64			0.25	280		228			89.3	
	7	7.31	3.35		2.22			0.10	0.80		0.90			0.25	287		322			89.6	
	14	7.27	3.59	1.22	3.04	0.15		0.25	0.86	1.26	1.22	0.12		0.62	306	449	435	44.3		220	
	21	7.41	4.08	1.36	3.75	0.22		0.31	0.97	1.40	1.49	0.17		0.74	345	501	531	62.2		266	
	28	7.55	4.75	1.60	4.30	0.24		0.33	1.11	1.63	1.69	0.19		0.80	396	584	603	68.1		285	

Table A5- 4 Solution analysis of the leachate that was used to alter the three complex glasses pre-hydrated for 6 months at 50°C and a low SA/V of 20 m^{-1} for 28 days; The uncertainties associated with the concentration, NL and equivalent thickness are around 10%; The uncertainty of pH measurement is ±0.05 units

Glass	Time, days	$pH_{50°C}$	Concentration, mg/L					NL, g/m2					Equivalent thickness of altered glass, nm					Thickness (MEB), nm
			Si	B	Na	Mg	Li	Si	B	Na	Mg	Li	Si	B	Na	Mg	Li	
AVM6	1	8.2	2.01	0.82	3.73	0.11	0.03	0.40	0.55	1.06	0.20	0.75	141	197	378	72.6	268	880-1200 nm approx.
	3	7.8	2.85	1.26	4.82	0.14	0.05	0.56	0.85	1.37	0.25	1.12	200	304	488	89	401	
	7	7.7	4.28	1.68	5.79	0.25	0.07	0.84	1.13	1.64	0.45	1.45	299	403	584	159	518	
	14	7.8	5.38	2.15	6.61	0.37	0.08	1.04	1.43	1.86	0.65	1.64	372	510	664	233	586	
	21	7.9	6.19	2.49	7.15	0.47	0.09	1.19	1.64	2.00	0.81	1.83	425	586	714	288	654	
	28	7.9	7.04	2.82	7.89	0.57	0.09	1.34	1.85	2.19	0.98	1.96	478	659	782	349	701	
AVM10	1	7.5	2.02	0.13	2.21	0.16	0.03	0.55	0.12	0.93	0.21	0.70	197	43.5	333	75.0	251	Irregular / unclear
	3	7.3	2.58	0.18	2.36	0.28	0.03	0.70	0.16	0.99	0.36	0.75	252	58.3	355	128	268	
	7	7.3	3.26	0.24	2.56	0.38	0.03	0.88	0.21	1.08	0.49	0.81	316	76.6	385	173	288	
	14	7.5	2.72	0.31	2.50	0.39	0.03	0.75	0.28	1.05	0.50	0.84	266	98.4	377	179	300	
	21	7.4	2.96	0.35	2.61	0.43	0.03	0.81	0.31	1.10	0.55	0.85	288	111	391	197	303	
	28	7.5	3.22	0.40	2.72	0.47	0.04	0.87	0.35	1.14	0.59	0.89	310	125	407	212	319	
AVMV4	1	6.6	1.45	0.17	0.95	0.16	1.93E-03	0.32	0.14	0.33	0.27	0.86	115	49.1	119	95.2	308	400-500 nm approx.
	3	7.1	1.80	0.39	1.47	0.22	1.40E-03	0.40	0.33	0.51	0.37	0.63	142	116	184	132	224	
	7	7.4	2.36	0.61	2.02	0.30	2.12E-03	0.52	0.50	0.70	0.51	0.94	185	177	250	181	337	
	14	7.5	1.84	0.90	2.40	0.33	2.33E-03	0.41	0.73	0.83	0.56	1.03	146	261	296	198	369	
	21	7.6	2.10	1.15	2.95	0.38	2.76E-03	0.46	0.92	1.00	0.64	1.21	165	328	359	229	432	
	28	7.6	2.20	1.40	3.69	0.43	3.51E-03	0.48	1.11	1.24	0.72	1.51	173	396	443	257	540	

Table A5- 5 Solution analysis of the leachate that was used to alter the three complex glasses pre-hydrated for 18 months at 50°C and a low SA/V of 20 m^{-1} for 28 days; The uncertainties associated with the concentration, NL and equivalent thickness are around 10% for Na and Si, boron, Li, Mg and Al concentrations are mostly indicative and the uncertainty could be more than 10%; The uncertainty of pH measurement is ±0.05 units

Glass	Time, days	$pH_{50°C}$	Concentration, mg/L						NL, g/m2						Equivalent thickness of altered glass, nm						Thickness (MEB), nm
			Si	B	Na	Al	Mg	Li	Si	B	Na	Al	Mg	Li	Si	B	Na	Al	Mg	Li	
AVM6	1	8.9	3.67		5.04	0.06	0.24	0.03	0.71		1.76	0.05	0.42	0.73	254		629	19.4	149	261	Around 2 µm with irregularities
	3	8.5	4.53	1.76	7.22	0.40	0.22	0.06	0.88	1.17	2.53	0.34	0.39	1.32	313	416	902	121	141	470	
	7	8.1	6.09		9.85	0.00	0.14	0.04	1.17		3.42	0.01	0.25	0.90	418		1222	3.0		320	
	14	8.1	9.01	3.12	13.96	0.94	0.53	0.12	1.71	1.97	4.79	0.77	0.90	2.48	610	704	1711	274	321	884	
	21	8.2	9.42		12.97	0.07	0.57	0.15	1.78		4.47	0.09	0.96	2.99	636		1596	30.6	344	1068	
	28	8.1	10.19	5.03	14.63	1.22	0.65	0.16	1.91	3.01	4.99	0.96	1.09	3.16	683	1074	1782	342	388	1130	
AVM10	1	8.0	3.45	0.07	2.16	0.27	0.14	0.11	1.31	0.09	1.26	0.27	0.26	3.90	466	33.2	451	95.7	92.2	1394	unclear
	3	7.7	4.32		2.71		0.11	0.10	1.63		1.58		0.19	3.49	584		566		68.7	1246	
	7	7.7	4.97	0.42	3.16	0.57	0.36	0.12	1.87	0.52	1.84	0.55	0.63	4.07	669	184	657	195	226	1455	
	14	7.6	5.80		3.53			0.10	2.17		2.05		0.02	3.41	776		731			1219	
	21	7.5	6.08		3.44	0.17	0.48	0.13	2.27		2.00	0.17	0.82	4.28	810		713	59.2	293	1529	
	28	7.6	6.14	0.54	3.57	0.53	0.61	0.12	2.29	0.61	2.07	0.49	1.03	4.20	818	218	738	175	369	1502	
AVMV4	1	7.0	3.01	0.16	0.89	0.17	0.16		0.95	0.19	0.44	0.19	0.39		338	67.0	158	66.6	139		800-1000 nm thickness
	3	7.2	3.09		1.42		0.01		0.97		0.70		0.04		347		252		13		
	7	7.3	3.69		2.13		0.25		1.15		1.05		0.60		412		374		214		
	14	7.3	4.24		2.85		0.41		1.32		1.39		0.96		471		496		343		
	21	7.4	4.48		3.45		0.28		1.39		1.66		0.68		496		594		243		
	28	7.5	4.65		4.09		0.54		1.44		1.95		1.24		513		697	5.4	444		

Table A5- 6 Solution analysis of the leachate that was used to alter the three simplified pristine glasses at 50°C and a high SA/V of 200000 m^{-1} for 91 days; The uncertainties associated with concentration, NL and equivalent thickness are around 20% for Al & Mg, 6.5% for B & Na, and 10% for Si & Ca; The uncertainty of pH measurement is ±0.05 units

Glass	Time, days	$pH_{50°C}$	Concentration, mg/L						NL, g/m2						Equivalent thickness of altered glass, nm					
			Si	B	Na	Al	Ca	Mg	Si	B	Na	Al	Ca	Mg	Si	B	Na	Al	Ca	Mg
Q	8	9.26	68.51	645.37	976.41	9.14			0.0014	0.0660	0.0374	0.0007			1.4	68.9	38.4	0.71		
	14	9.25	89.38	805.09	1228.90	14.59			0.0019	0.0817	0.0467	0.0011			1.9	86.4	48.2	1.1		
	22	9.21	47.15	957.93	1399.90	3.04			0.0010	0.0965	0.0529	0.0002			0.98	103	54.7	0.23		
	28	9.38	39.22	1068.27	1550.59	2.34			0.0008	0.1068	0.0581	0.0002			0.81	116	60.3	0.18		
	42	9.22	53.02	1255.34	1850.10	3.76			0.0011	0.1245	0.0688	0.0003			1.1	137	71.9	0.28		
	57	9.18	51.14	1380.97	2025.08	3.36			0.0010	0.1359	0.0747	0.0003			1.0	151	78.4	0.25		
	70	9.26	46.53	1525.85	2231.64	2.95			0.0009	0.1489	0.0816	0.0002			0.93	167	86.1	0.22		
	91	9.26	52.66		2399.65	2.05			0.0010		0.0871	0.0002			1.1		92.1	0.15		
QCa	8	9.94	90.28	358.10	837.68		21.69		0.0021	0.0387	0.0327		0.0030		2.1	39.0	32.8	0.00	2.9	
	14	9.85	84.83	382.91	904.38		26.93		0.0019	0.0411	0.0351		0.0036		1.9	41.6	35.3	0.00	3.6	
	22	9.77	92.77	440.70	1004.03	3.75	35.43		0.0021	0.0469	0.0386	0.0003	0.0048		2.1	47.8	38.9	0.31	4.7	
	28	9.81	62.32	512.82	976.86		14.24		0.0014	0.0541	0.0373		0.0019		1.4	55.6	37.6	0.00	1.9	
	42	9.81	77.21	836.63	1517.23	2.03	28.30		0.0017	0.0876	0.0574	0.0002	0.0037		1.7	91.8	58.6	0.16	3.7	
	57	9.7	76.72	966.07	1755.99	2.61	49.09		0.0017	0.1004	0.0659	0.0002	0.0064		1.7	106	67.6	0.21	6.4	
	70	9.78	78.77	1083.17	1800.66	3.48	49.38		0.0017	0.1116	0.0671	0.0003	0.0064		1.7	119	68.8	0.28	6.4	
	91	9.72	81.00	1252.67	2188.23	2.26	20.63		0.0018	0.1280	0.0809	0.0002	0.0027		1.7	139	83.6	0.18	2.6	
QMg	8	9.59	36.93	758.58	1246.74			4.26	0.0008	0.0752	0.0463			0.0010	0.83	81.3	49.2	0.00		1.0
	14	9.53	36.45	1065.71	1684.86	2.32		4.86	0.0008	0.1047	0.0621	0.0002		0.0011	0.81	116	66.6	0.18		1.1
	22	9.45	31.92	1378.86	2141.45			4.68	0.0007	0.1345	0.0783			0.0010	0.71	152	84.9	0.00		1.1
	28	9.70	25.96	1576.37	2416.26			4.11	0.0006	0.1525	0.0876			0.0009	0.57	176	95.6	0.00		0.94
	42	9.42	32.13	1789.02	2862.94			3.70	0.0007	0.1717	0.1030			0.0008	0.70	202	114	0.00		0.84
	57	9.42	28.88	2042.82	3361.27			3.28	0.0006	0.1945	0.1200			0.0007	0.62	233	134	0.00		0.74
	70	9.43	36.69	2522.87	4101.65	4.24		4.16	0.0008	0.2383	0.1452	0.0003		0.0009	0.79	297	165	0.32		0.93
	91	9.46	31.46	2459.85	3937.62			2.57	0.0006	0.2306	0.1384			0.0006	0.67	287	156	0.00		0.57

UNIVERSITE MATIERE BRETAGNE MOLECULES LOIRE ET MATERIAUX

IMT Atlantique
Bretagne-Pays de la Loire
École Mines-Télécom

Titre : Influence de la composition des verres nucléaires type AVM lors de son altération en phase vapeur

Mots clés : Hydratation, phase vapeur, verres, effet composition, couche altérée, mécanismes

Résumé : L'hydratation en phase vapeur des verres inactif (simples et complexes) du domaine AVM *(Atelier de Vitrification de Marcoule)* a été étudiée en se focalisant sur l'influence de la composition du verre. Dans la première partie, les échantillons de verre ont été altérés à 50°C et 95% d'humidité relative, et les couches altérées (gel) ont été caractérisés par SEM, TEM, XRD, ToF-SIMS et SAXS. Les résultats montrent que la teneur en aluminium par rapport à celle des alcalino-terreux joue un rôle clé dans la durabilité du verre. Lorsque le rapport molaire Al_2O_3/MgO<1, la vitesse d'hydratation en phase vapeur est augmentée de 10 à 20 fois par la formation des précipités riches en Mg. Dans d'autres cas, l'hydrolyse du réseau vitreux a été identifiée comme le mécanisme contrôlant la vitesse d'hydratation en phase vapeur. Des études complémentaires sur l'effet de la température et de l'humidité relative ont montré que le mécanisme prédominant d'hydratation en phase vapeur varie en fonction de la température et de la composition du verre. Dans la deuxième partie, des expériences avec des verres hydratés en phase vapeur puis immergés dans de l'eau pure ont montré que le gel n'avait pas d'effet passivant vis-à-vis l'altération aqueuse et que des phases secondaires formées pendant l'hydratation en phase vapeur pouvaient être solubles. Deuxièmement, une étude comparative de la structure des gels enrichies en ^{17}O formées lors d'hydratation en phase vapeur (à 90 °C) et de l'altération aqueuse à très fort S/V par la spectroscopie RMN a montré pour la première fois, de la recondensation du bore avec de l'oxygène provenant de la phase vapeur. Les résultats suggèrent que l'altération du verre en phase vapeur n'est pas équivalente à l'altération en milieu aqueux à très fort S/V.

Title : Influence of composition on vapor hydration of AVM nuclear waste glasses

Keywords : Vapor hydration, glasses, composition, gel layer, mechanisms, structure

Abstract : The vapor hydration of inactive surrogates of AVM *(Atelier de Vitrification de Marcoule)* glasses (simple and complex) has been studied in this thesis work with a special focus on the influence of glass composition. In the first part of the thesis, multiple glass samples were altered at 50°C and 95% RH and the altered samples were characterized using SEM, TEM, XRD, ToF-SIMS and SAXS to study the altered (gel) layer. The results show that aluminum plays a key role in glass durability under the given conditions, especially in relative proportions to alkaline-earth elements. When the molar ratio of Al_2O_3/MgO<1, the overall vapor hydration rate was accelerated by 10-20 times due to the formation of Mg-rich smectites. In other cases, network-hydrolysis was identified as the rate controlling vapor hydration mechanism for the first six months. Complementary studies on the effect of temperature and relative humidity gave further insights into secondary phase precipitation, behavior of elements in the gel layer and altered layer morphology. These studies show that the predominant vapor hydration mechanism varies with temperature and glass composition as well. In the second part of the thesis, aqueous alteration experiments are discussed in two contexts. First, vapor hydrated glasses immersed in pure water showed that the gel layer did not have a passivating effect against aqueous alteration and that some of the secondary phases formed during vapor hydration are readily soluble. Secondly, comparative structural study of ^{17}O-enriched gel layers that were formed during vapor hydration (at 90°C) and aqueous alteration at a very high SA/V ratio using NMR spectroscopy showed for the first time, evidence of recondensation of boron with oxygen from the vapor phase. The results suggest that glass alteration in vapor phase is not equivalent to alteration in aqueous medium at a very high SA/V ratio.